

# Oil & Natural Gas Technology

DOE Award No.: DE-FC26-06NT42877

## Final Technical Report

**HYDRATE RESEARCH ACTIVITIES THAT BOTH SUPPORT AND  
DERIVE FROM THE MONITORING STATION/SEA-FLOOR  
OBSERVATORY,  
MISSISSIPPI CANYON 118, NORTHERN GULF OF MEXICO**

Submitted by:

CENTER FOR MARINE RESOURCES AND ENVIRONMENTAL TECHNOLOGY  
111 BREVARD HALL, UNIVERSITY, MS 38677

Principal Author: Carol Lutken, PI

Prepared for:  
United States Department of Energy  
National Energy Technology Laboratory

December, 2013



**Office of Fossil Energy**

**HYDRATE RESEARCH ACTIVITIES THAT BOTH SUPPORT AND  
DERIVE FROM THE MONITORING STATION/SEA-FLOOR  
OBSERVATORY,  
MISSISSIPPI CANYON 118, NORTHERN GULF OF MEXICO**

FINAL TECHNICAL REPORT  
1 JULY, 2006 THROUGH 31 JULY, 2013

PREPARED BY THE MANAGEMENT TEAM  
Carol Blanton Lutken and Dianne R. Welch  
CENTER FOR MARINE RESOURCES AND ENVIRONMENTAL TECHNOLOGY  
111 BREVARD HALL, UNIVERSITY, MS 38677  
(CONTACT: CAROL LUTKEN)

DECEMBER, 2013

**DOE AWARD NUMBER DE-FC26-06NT42877**

**FOLLOWING DOE AWARD NUMBERS  
DE-FC26-00NT40920 and DE-FC26-02NT41628**

**DISCLAIMER:**

This report was prepared as an account of work sponsored by an agency of the United States Government. Neither the United States Government nor any agency thereof, nor any of their employees, makes any warranty, express or implied, or assumes any legal liability or responsibility for the accuracy, completeness, or usefulness of any information, apparatus, product, or process disclosed, or represents that its use would not infringe privately owned rights. Reference herein to any specific commercial product, process, or service by trade name, trademark, manufacturer, or otherwise does not necessarily constitute or imply its endorsement, recommendation, or favoring by the United States Government or any agency thereof. The views and opinions of authors expressed herein do not necessarily state or reflect those of the United States Government or any agency thereof.

## **PHASE 1 Subcontractors and Tasks for FY 2006:**

Paul Higley, Specialty Devices, Inc., 2905 Capital Street, Wylie, TX 75098

Task 1: Design and Construction of four Horizontal Line Arrays.

Bob A. Hardage, Bureau of Economic Geology, John A. and Katherine G.

Jackson School of Geosciences, University of Texas at Austin, University Station, Box X, Austin, TX 78713

Task 2: Seismic Data Processing at the Gas Hydrate Sea-floor Observatory: MC118.

Jeffrey Chanton, Department of Oceanography, Florida State University, Tallahassee, FL 32306

Task 3: Coupling of Continuous Geochemical and Sea-floor Acoustic Measurements.

Peter Gerstoft, Marine Physical Laboratory, University of California at San Diego, 9500 Gilman Drive, La Jolla, CA 92093

Task 4: Noise-Based Gas Hydrates Monitoring.

## **PHASE 2 Subcontractors and Tasks for FY 2008:**

Camelia Knapp, Department of Geological Sciences, University of South Carolina, 701 Sumter Street, Columbia, SC 29208.

TASK 2: Processing and Interpretation of TGS-NOPEC Industry Seismic Data and Integration with Existing Surface-Source/Deep-Receiver (SSDR) High Resolution Seismic Data at MC118, Gulf of Mexico.

Bob A. Hardage, Bureau of Economic Geology, John A. and Katherine G. Jackson School of Geosciences, the University of Texas at Austin, University Station, Box X, Austin, TX 78713-8924.

TASK 3: Seismic Data Processing at the Gas Hydrate Sea-Floor Observatory: MC118.

Laura Lapham and Jeff Chanton, Department of Oceanography, Florida State University, Tallahassee, Florida, 32306-4320.

TASK 4: Geochemical investigations at MC 118: Pore fluid time series and gas hydrate stability.

John Noakes, Scott Noakes, and Chuanlun Zhang, The University of Georgia, Athens, Georgia, and Tim Short, SRI International, St. Petersburg, Florida.

TASK 5: Automated Biological/Chemical Monitoring System (ABCMS) for Offshore Oceanographic Carbon Dynamic Studies.

Rudy Rogers, Department of Chemical Engineering, Mississippi State University, PO Drawer 9595, Mississippi State, MS 39762.

TASK 6: Microbial techniques to extract carbon from stored hydrocarbon gases.

Ira Leifer, Marine Science Institute, University of California at Santa Barbara, Bldg. 2, Room 3357, Santa Barbara, CA 93103-5080.

TASK 7: Scoping study using Spatio-Temporal Measurement of Seep Emissions by Multibeam Sonar at MC118.

Paul Higley, Specialty Devices, Inc., 2905 Capital Street, Wylie, TX 75098

TASK 8: Validate high-frequency scatter on SSDR data by acquisition of targeted cores and velocity profiles at MC118 Hydrate Mound.

Sabodh Garg, Science Applications International Corporation, 10260 Point Campus Drive, MS A-3, San Diego, CA 92121.

TASK 9: Recipient shall model carbonate/hydrate mound in Mississippi Canyon 118 using modified version of (THROBS).

### **PHASE 3 Subcontractors and Tasks for FY 2009:**

Camelia Knapp and James H. Knapp, Department of Geological Sciences, University of South Carolina, 701 Sumter Street, Columbia, SC 29208.

TASK 2: Geological and Geophysical Baseline Characterization of Gas Hydrates at MC118, Gulf of Mexico.

Bob A. Hardage, Bureau of Economic Geology, John A. and Katherine G. Jackson School of Geosciences, the University of Texas at Austin, University Station, Box X, Austin, TX 78713-8924.

TASK 3: Near seafloor geology at MC118 using converted shear-waves from 4C seafloor sensor data.

Laura Lapham and Jeff Chanton, Department of Oceanography, Florida State University, Tallahassee, Florida, 32306-4320.

TASK 4: Geochemical investigations at MC 118: Pore fluid time series and gas hydrate stability.

John Noakes, Scott Noakes, and Chuanlun Zhang, The University of Georgia, Athens, Georgia, and Tim Short, SRI International, St. Petersburg, Florida.

TASK 5: Automated Biological/Chemical Monitoring System (ABCMS) for Offshore Oceanographic Carbon Dynamic Studies.

Ira Leifer, Marine Science Institute, University of California at Santa Barbara, Bldg. 2, Room 3357, Santa Barbara, CA 93103-5080.

TASK 6: Quantification of Seep Emissions by Multibeam Sonar at MC118.

Sabodh Garg, Science Applications International Corporation, 10260 Point Campus Drive, MS A-3, San Diego, CA 92121.

TASK 7: Modeling a carbonate/hydrate mound in Mississippi Canyon 118 using modified version of (THROBS).

### **PHASE 4 Subcontractors and Tasks for FY 2010**

Leonardo Macelloni, Carol Lutken and Ken Sleeper, Mississippi Mineral Resources Institute, University of Mississippi, University, MS, 38677.

TASK 2: Integration of Multiple Methods of Geological and Geophysical investigations to advance Shallow Subsurface Characterization at MC118.

Sabodh Garg, Science Applications International Corporation, 10260 Point Campus Drive, MS A-3, San Diego, CA 92121.

TASK 3: Modeling a carbonate/hydrate mound in Mississippi Canyon 118 using modified version of (THROBS).

Laura Lapham and Jeff Chanton, Department of Oceanography, Florida State University, Tallahassee, Florida, 32306-4320.

TASK 4: Geochemical investigations at MC 118: Pore fluid time series and gas hydrate stability.



John Noakes, Scott Noakes, and Chuanlun Zhang, The University of Georgia,  
Athens, Georgia, and Tim Short, SRI International, St. Petersburg, Florida.  
TASK 5: Automated Biological/Chemical Monitoring System (ABCMS) for  
Offshore Oceanographic Carbon Dynamic Studies.

Ira Leifer, Marine Science Institute, University of California at Santa Barbara,  
Bldg. 2, Room 3357, Santa Barbara, CA 93103-5080.  
TASK 6: Quantification of Seep Emissions by Multibeam Sonar at MC118.

# TABLE OF CONTENTS

PAGE

DISCLAIMER.....	ii
PHASE 1 Subcontractors and Tasks for FY 2006.....	iii
PHASE 2 Subcontractors and Tasks for FY 2008.....	iii
PHASE 3 Subcontractors and Tasks for FY 2009.....	iv
PHASE 4 Subcontractors and Tasks for FY 2010.....	iv
TABLE OF CONTENTS.....	vi
LIST OF GRAPHICAL MATERIALS.....	vii
ABSTRACT.....	x
INTRODUCTION.....	1
EXECUTIVE SUMMARY.....	2
MONITORING STATION SYSTEMS STATUS SUMMARY.....	19
Geophysical Sensor Systems/Geology.....	19
Geochemical Sensor Systems.....	29
Biological Experiments and Monitoring.....	34
Vehicle/Support Systems.....	38
REFERENCES.....	45
EXPERIMENTAL/RESULTS AND DISCUSSION.....	47
PHASE 1.....	47
PHASE 2.....	58
PHASE 3.....	84
PHASE 4.....	133
CONCLUSIONS.....	225
LIST OF ACRONYMS AND ABBREVIATIONS.....	227
COST STATUS.....	228
MILESTONE STATUS.....	235
ACCOMPLISHMENTS.....	237
PROBLEMS/DELAYS.....	239
PRODUCTS.....	239
RECENT PUBLICATIONS BY CONSORTIUM MEMBERS.....	240
APPENDIX A: Jumbo Piston Coring Cruise aboard the TDI Brooks, R/V <i>Brooks</i> <i>McCall</i> , GULF OF MEXICO HYDRATES RESEARCH CONSORTIUM SUMMARY OF ACTIVITIES FOR JANUARY, 2011.....	257
APPENDIX B: Report on the Lithostratigraphy of the Jumbo Piston Cores taken from MC118 in January 2011. C. Brunner, Department of Marine Science, University of Southern Mississippi.....	267
APPENDIX C: Heat-Flow Interpretive Report (TDI Brooks, International, Inc.).....	274

## LIST OF GRAPHICAL MATERIALS

- Figure 1.** MC118 is located ~30 miles off the toe of Birdsfoot Delta in the edge of a massive slump.....3
- Figure 2.** Woolsey Mound at MC118 has 3 distinct crater complexes. The image on the left shows bathymetry and acoustic backscatter (hardgrounds) at the site. To the right, “master faults” – blue, violet, yellow – and shallower, radiating faults – orange – are plotted with this same bathymetry to illustrate surface expression of the fault system.....4
- Figure 3.** While the Pelican motors to the target, the SSD, complete with upgrades, resides in its cage, ready to dive.....6
- Figure 4.** The ABIL is deployed using the Pelican’s crane. Note the compact, central, arrangement of instruments - CTD, acoustic releases, battery, transponder - protected by the glass floats in hard-hats. Scanning sonar – red – is located above the other lander components for greater access to its surroundings.....6
- Figure 5.** As part of the pre-dive preparations, the SSD undergoes a dunk test prior to its initial dive. This test will determine what adjustments need to be made to the vehicle’s ballast and trim, so that its travel in the water-column will be stable and its responses predictable.....7
- Figure 6.** The SSD feeds back a variety of information to the vessel via fiber-optic cable feed: photographic data from multiple cameras, sonar, and information about its location and attitude. Its power comes from a battery built into the vehicle which doubles as a clump-weight.....8
- Figure 7.** The ECOGIG lander, built by the MMRI/CMRET shop, was located 115m from the location given the navigation. Using the SSD’s sonar and multiple camera capabilities, we were able to locate the lander, then survey its position, document the orientations of the instruments and remove the chimneys (grey cylinders in the front of the image on the right) and place them on the seafloor where the seafloor showed signs of gas emissions (bacterial mat, pitted surfaces).....8
- Figure 8.** The SSD feeds back a variety of information to the vessel via fiber-optic cable feed: photographic data from multiple cameras, sonar, and information about its location and attitude. Its power comes from a battery built into the vehicle which doubles as a clump-weight.....9
- Figure 9.** Multibeam image of Mississippi Canyon 118. Data acquired by C&C technologies and reprocessed by The University of Mississippi and University of Rome, La Sapienza.....19
- Figure 10.** Backscatter intensity draped over bathymetry over the Woolsey Mound, MC118, reveals hardgrounds, crater complexes and scarps (Caruso, 2007).....20
- Figure 11.** Improving resolution reveals different features as shown in this pair of images of the same section of seafloor. A. Regional multibeam can be used quite effectively to target locations that display features associated with seeps, benthic communities, slumping, etc. B. Higher resolution AUV surveys can then be used to extract the detail needed to conduct focused study (Lutken, et al., 2013).....20

<b>Figure 12. Changes in morphology over four years that elapsed between successive AUV surveys (From Lutken, et al., 2010).....</b>	<b>21</b>
<b>Figure 13. Profiles through some areas exhibiting greatest changes between two AUV surveys (From Lutken, et al., 2010).....</b>	<b>22</b>
<b>Figure 14. Methane anomalies recorded by AUV-borne mass spectrometer (left) with location of anomalies on the mound at MC118, right. (From Lutken et al., 2010, modified from Camilli, et al., 2009).....</b>	<b>22</b>
<b>Figure 15. Rock slabs on the seafloor as revealed in a A) 50m altitude AUV Eagle Ray [Flag: italicize Eagle Ray] survey (~1.2m resolution) and B) a 15m altitude survey (raw data ~.5m resolution) (From Lutken, et al., 2013).....</b>	<b>23</b>
<b>Figure 16. Example of combination of criteria used to evaluate a site for possible hydrate occurrence in the shallow subsurface. Note high frequency backscatter on SSSR data, lower left (UM and USC).....</b>	<b>24</b>
<b>Figure 17. JPC1 was cored and found to host slabs, chunks and grains of hydrate as well as a 2cm thick slab. Samples were collected from this core, evaluated for hydrocarbon species content (FSU) and the results plugged into the SAIC hydrate simulator.....</b>	<b>25</b>
<b>Figure 18. Three resolutions of seismic data were used to evaluate the subsurface at Woolsey Mound. The top profile was acquired using a chirp subsystem profiler of ~8kHz frequency and 10cm resolution. The middle profile was acquired using a shallow- source-deep- receiver system of ~1.5kHz frequency and 1m resolution. The bottom profile was extracted from industry 3D data of ~50Hz frequency and 50m resolution. Note difference in scales and coverage highlighted by the boxed areas. (variation of Simonetti et al., 2011 and Macelloni et al., 2012).....</b>	<b>27</b>
<b>Figure 19, left, the ROVARD, with CSA, as seen from the ROV, Holiday, during an October, 2012, NRDA cruise.....</b>	<b>30</b>
<b>Figure 20. Water-column data collected with the CSA over a six-month deployment on the seafloor at Woolsey Mound.....</b>	<b>30</b>
<b>Figure 21. The pore-fluid sampling array (PFA). (Figures from Lapham et al., 2008).....</b>	<b>31</b>
<b>Figure 22. Newly designed PFA system with a smaller footprint designed to be deployed and retrieved by ROV. This image shows the PFA box deployed at Cascadia Margin. (Figure from Lapham et al., 2013).....</b>	<b>32</b>
<b>Figure 23. Peeper device for collecting sediment porewater (Figure from Lapham et al., 2010).....</b>	<b>32</b>
<b>Figure 24. Flux map developed from gravity and push cores and 4 Jumbo Piston Cores collected across Woolsey Mound. (Figure from Wilson et al., in press).....</b>	<b>33</b>
<b>Figure 25. Bacterial mats and clams form part of a complex community on the seafloor at MC118.</b>	
<b>Figure 26. Deep Sea Corals at MC118. Reefs provide habitat, recruitment and nursery functions for a range of deep-water organisms including commercial fish species. Deep sea corals may provide windows into past environmental/ecological conditions. This colony of <i>Madrepora oculata</i>, or zig-zag coral, is a rare find in the Gulf.....</b>	<b>35</b>

**Figure 27. Abundant life is found at the crater complexes on Woolsey Mound. Fish, crabs, echinoderms, chemoautotrophic snails and abundant bacterial mat have been and continue to be reported, and where possible, mapped over the mound.....36**

**Figure 28. A conceptual model of the spatial distribution of biogeological process throughout the Woolsey Mound. Major morphological units, sediment types and biological habitat are mapped, based upon video data, classes of acoustic backscatter anomalies and, where available, sediment core data. The model provides regionalization of the biogeological processes occurring at the mound and highlights significant differences within the three complexes (from Macelloni et al., 2013).....37**

**Figure 29. A fully loaded lander about to be deployed via the I-SPIDER.....39**

**Figure 30. The SSD undergoes a series of ondeck tests prior to every dive. Note the new camera on the manipulator arm, center of image.....40**

**Figure 31. The SSD team effects a smooth vehicle recovery.....41**

**Figure 32. The SSD being rigged for deployment via the I-SPIDER (left). The I-SPIDER “watches” as the SSD flies from its cage to service a lander on the seafloor. (photos from Lowe, et al., 2013).....42**

**Figure 33. The AUV team prepares to launch the Eagle Ray AUV from the Pelican’s main deck via the launch and recovery system (LARS), designed and built specifically for it.....44**

**Figure 34. The AUV team prepares to launch the Mola Mola photo-AUV from the Pelican’s upper deck.....44**

## **ABSTRACT**

A permanent observatory has been installed on the seafloor at Federal Lease Block, Mississippi Canyon 118 (MC118), northern Gulf of Mexico. Researched and designed by the Gulf of Mexico Hydrates Research Consortium (GOM-HRC) with the geological, geophysical, geochemical and biological characterization of in situ gas hydrates systems as the research goal, the site has been designated by the Bureau of Ocean Energy Management as a permanent Research Reserve where studies of hydrates and related ocean systems may take place continuously and cooperatively into the foreseeable future.

The predominant seafloor feature at MC118 is a carbonate-hydrate complex, officially named Woolsey Mound for the founder of both the GOM-HRC and the concept of the permanent seafloor hydrates research facility, the late James Robert "Bob" Woolsey. As primary investigator of the overall project until his death in mid-2008, Woolsey provided key scientific input and served as chief administrator for the Monitoring Station/ Seafloor Observatory (MS-SFO).

This final technical report presents highlights of research and accomplishments to date. Although not all projects reached the status originally envisioned, they are all either complete or positioned for completion at the earliest opportunity. All Department of Energy funds have been exhausted in this effort but, in addition, leveraged to great advantage with additional federal input to the project and matched efforts and resources. This report contains final reports on all subcontracts issued by the University of Mississippi, Administrators of the project, *Hydrate research activities that both support and derive from the monitoring station/sea-floor Observatory, Mississippi Canyon 118, northern Gulf of Mexico*, as well as status reports on the major components of the project. All subcontractors have fulfilled their primary obligations.

Without continued funds designated for further project development, the Monitoring Station/Seafloor Observatory is in danger of lapsing into disuse. However, for the present, interest in the site on the continental slope is healthy and The Center for Marine Resources and Environmental Technology continues to coordinate all activity at the MS/SFO as arranged through the BOEM in 2005.

Field and laboratory research projects and findings are reviewed, new technologies and tests described. Many new sensors, systems and two custom ROVs have been developed specifically for this project. Characteristics of marine gas hydrates are dramatically more refined than when the project was initiated and include appear in sections entitled *Accomplishments, Products and Publications*.

## **INTRODUCTION/ PROJECT SUMMARY**

The Gulf of Mexico Gas Hydrates Research Consortium (GOM-HRC) was organized in 1999, with the goal of establishing a monitoring station/sea-floor observatory (MS/SFO) to investigate the hydrocarbon system within the hydrate stability zone (HSZ) of the northern Gulf of Mexico. The intention has been to consolidate research effort and to equip the MS/SFO with a variety of sensors that will enable more-or-less continuous monitoring of the near-seabed hydrocarbon system and to determine the steady-state description of physical, chemical and biological conditions in its local environment as well as to detect temporal changes of those conditions.

The purpose of the GOM-HRC is to oversee the development and emplacement of such a facility to provide a better understanding of this complex hydrocarbon system, particularly hydrate formation and dissociation, fluid venting to the water column, and associated microbial and/or chemosynthetic communities. Models developed from these studies are intended to provide researchers with an improved understanding of gas hydrates and associated free gas as: 1) a geo-hazard to conventional deep oil and gas activities; 2) a future energy resource of considerable significance; and 3) a source of hydrocarbon gases, venting to the water column and eventually the atmosphere, with global climate implications.

Initial funding for the MS/SFO was received from the Department of Interior (DOI) Minerals Management Service (MMS, now the Bureau of Ocean Energy Management, BOEM) in FY1998. Funding from the Department of Energy (DOE) National Energy Technology Laboratory (NETL) began in FY2000 and from the Department of Commerce (DOC) National Oceanographic and Atmospheric Administration's National Undersea Research Program (NOAA-NURP, now NOAA/OER (Ocean Exploration and Research)) in 2002 via their National Institute for Undersea Science and Technology (NIUST) Seabed Technology Research Center (STRC). Some nineteen industries and an even greater number of universities have been actively involved in Consortium/Observatory research; the United States Geological Survey (USGS), the US Navy, Naval Meteorology and Oceanography Command, Naval Research Laboratory (NRL) and NOAA's National Data Buoy Center are involved at various levels of participation. Funded investigations include a range of physical, chemical, and biological studies. Studies of the benthic fauna as a proxy for seafloor hydrocarbon venting comprise a recent addition to the emphasis areas of the Consortium.

Since 2005, the MS/SFO has been functioning as a test-bed for a great variety of projects relating to *in situ* hydrates research; the site continues to function in that capacity. The acquisition of a significant and diverse body of data and the designation of MC118/Woolsey Mound as the sole Research Reserve in the GOM make the site a target for continued successful research, both long and short-term.

The project is administered by the Center for Marine Resources and Environmental Technology (CMRET), the marine arm of the Mississippi Mineral Resources Institute (MMRI) of The University of Mississippi (UM).

## EXECUTIVE SUMMARY

In 1999, a consortium of leaders in gas hydrates research in the Gulf of Mexico was assembled for the purpose of consolidating both laboratory and field efforts. The Consortium, established at and administered by the University of Mississippi's Center for Marine Resources and Environmental Technology (CMRET), has, as its primary objective, the design and emplacement of a remote monitoring station on the seafloor in the northern GOM. The primary purpose of the station is to monitor activity within the zone of hydrate stability in an area where gas hydrates are known to be present and stable or meta-stable at, or just below, the sea-floor. In order to meet this goal, the Consortium has developed and assembled components for a station that will monitor physical and chemical parameters of the sea water, seafloor sediments, and shallow sub-seafloor sediments on a more-or-less continuous basis over an extended period of time. Study of chemosynthetic and other benthic communities and their interactions with geologic processes is a component of the Observatory; results provide an assessment of environmental health in the area of the station – and by extension, in areas sharing similar provenance and geochemical conditions - including the effects of deep sea activities on world atmosphere and, therefore, weather and climate.

Central to the establishment of the Consortium is the need to coordinate activities, avoid redundancies and promote effective and efficient communication among researchers. Complementary expertise, both scientific and technical, has been assembled; collaborative research and coordinated research methods have grown out of the Consortium and design and construction of a large suite of instruments, sensor systems, remotely operated vehicles and other devices has resulted.

In October, 2004, Mississippi Canyon 118 (MC118) (Figure 1) was selected by unanimous consensus of the GOM-HRC at their semiannual fall meeting as the location likeliest to fulfill the research needs and goals of the group. Criteria for selection included evidence of gas hydrates on the sea-floor, active venting and availability. Based upon roughly five years of site evaluations, sensor design, fabrication, testing and data collection and evaluation, selection of the site was followed by MMS placing a research restriction on the unleased block so Observatory research might continue even if the block should subsequently be leased, as is now the case. ***MC118 is the only research reserve in the Gulf of Mexico and the Seafloor Observatory is the only such facility in the Gulf.***

Since changes in the hydrate stability zone must in some way be measured against an established baseline, a significant effort has been devoted to establishing the baseline geology and chemistry at the site of the MS/SFO at MC118. Characterization and determination of baseline geophysical, geochemical and biological conditions commenced in spring 2005. The First Phase Sea-floor Probe (SFP) installation was completed, successfully, with two sub-sea-floor arrays emplaced in the sea-floor at MC118; a thermistor array, and a geochemical, pore-fluid chemistry, and pressure sensor array were deployed using the MMS/BOEM gravity-driven SFP. In spite of a variety of delays, including the effects of several severe hurricanes, follow-up surveys and deployments, continue to take place. Geophysicists and geologists at the



University of Mississippi and the University of South Carolina (USC) have established that Woolsey Mound, a hydrate-carbonate feature and site of the observatory, lies directly over a rising salt dome, that “master faults” extend from the salt body to the seafloor, that the three crater complexes on the mound reside each on the hanging wall of one of these master faults, that swarms of radial faults intersect these master faults providing a conduit system sufficient to supply hydrocarbon fluids from depth to the seafloor and water column (Figure 2). Moreover, resistivity data, heat-flow and additional geophysical findings suggest that these conduits are alternately open and closed – possibly by hydrate dissociation or dissolution and formation – and that each crater complex appears to represent a different fluid flux regime and a different stage in mound development (Macelloni et al., submitted JGR, 2013).

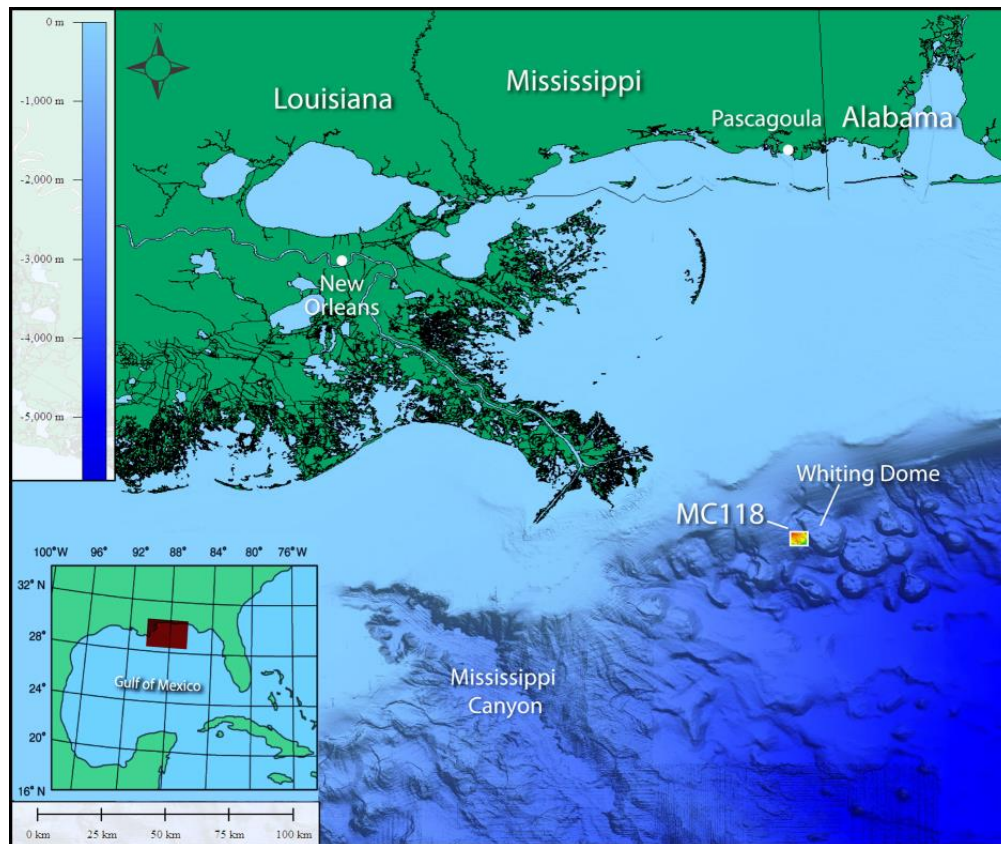


**Figure 1. MC118 is located ~30 miles off the toe of Birdsfoot Delta on the edge of a massive slump.**

Experiments designed to assess water-column geochemistry, microbial communities and activities, hydrate host materials, and composition of pore-fluids have been designed and built, and tests run at MC118. Sediments collected from Mississippi Canyon have been studied for effects of parameters possibly involved in hydrate formation. Laboratory analyses show that smectite clays promote hydrate formation when basic platelets slough off the clay mass. These small platelets act as nuclei for hydrate formation. Experiments show an increasing importance of microbial activities

surrounding active vents in promoting the formation and stability of seafloor gas hydrates. Rogers (2001) **established a connection between the microbial communities and hydrate formation and recently found through experimental analyses of MC118 microbial consortia that *microbial cell wall material inhibits hydrate formation***, a necessary occurrence for the bacterial cell's survival preventing hydrate formation-heats from being liberated directly onto cell surfaces. Microbes inhibit hydrate formation, thus enhancing their ability to survive the extreme conditions of the deep sea HSZ.

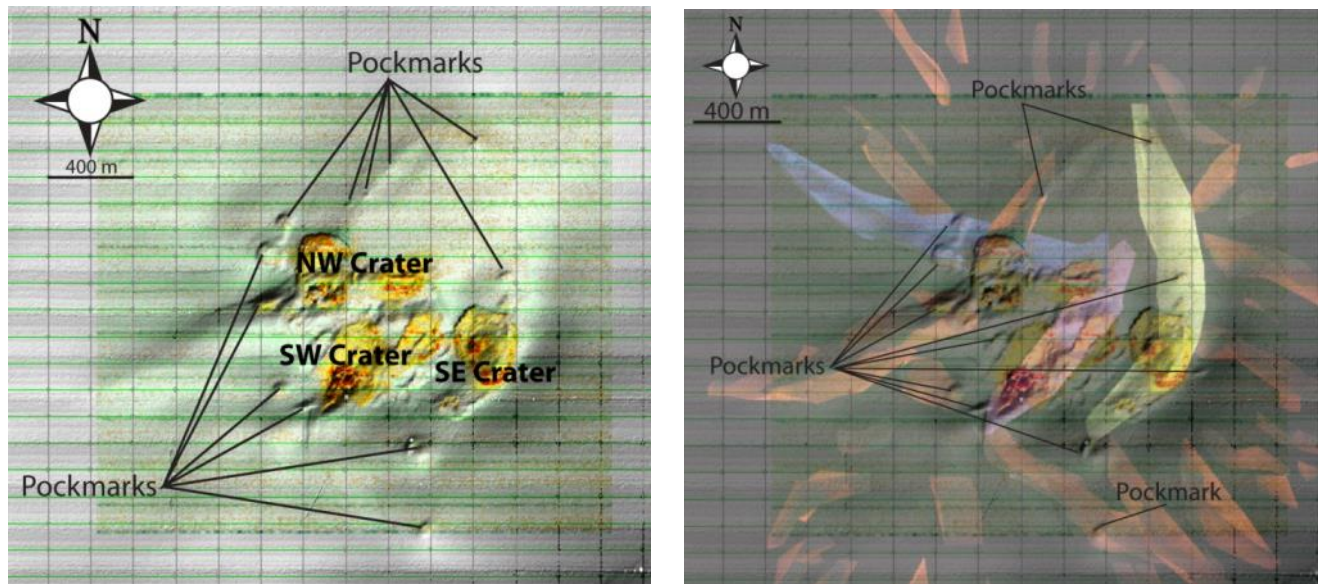


**Figure 2. Woolsey Mound at MC118 has 3 distinct crater complexes. The image on the left shows bathymetry and acoustic backscatter (hardgrounds) at the site. To the right, “master faults” – blue, violet, yellow – and shallower, radiating faults – orange – are plotted with this same bathymetry to illustrate surface expression of the fault system.**

During the life of this award, the CMRET planned and directed 30 cruises to MC118 and participated in others including those sponsored by the US Navy, BOEM, NOAA and NRDA (National Resource Damage Assessment). The Consortium has participated in all NIUST Autonomous Underwater Vehicle (AUV) cruises to map the seafloor and to collect and mosaic photo-images of Woolsey Mound, directed by the Underwater Vehicles Technology Center (UVTC). A 2009 Eagle Ray AUV survey collected multibeam and chemical data via mass spectrometer, revealing a new vent that has led to a number of additional studies and deployments. AUV surveys in 2013 recovered multibeam and polarity-preserved chirp data that, although not all completely processed, have revealed an extremely complex shallow subsurface at the observatory site connected directly to deep salt structures. These datasets will be processed and analyzed by scientists at the CMRET/STRC. The multibeam data will be used to produce bathymetry and backscatter images while the chirp data allow us to image, in great detail, the shallowest portion of the subsurface.

Ship time, a major expense incurred in the conduct of marine research, was generally covered with BOEM funding to the CMRET. DOE-funded researchers and their projects were frequent participants. A major contribution of the CMRET has always been as facilitator, organizing cruises, coordinating projects, reserving ships/facilities and providing shop and at-sea support for Consortium projects. This has been the case since 1999 but the discussion here is limited to activities that post-date the selection of the observatory site and developments that resulted from research focused on the cold-seep and carbonate-hydrate complex, Woolsey Mound, at MC118. This time corresponds almost exactly with the life of this Cooperative Agreement. Although much outstanding research precedes this award and is related directly to it, it has been reported previously in Final Reports for those awards: DE-FC26-00NT40920 and DE-FC26-02NT41628.

Cruise reports are posted at

<http://www.mmri.olemiss.edu/Home/Publications/Cruise.aspx>.

Highlights of cruise activities facilitated and supervised by CMRET in support of hydrates research and seafloor observatory activities are listed. Projects' funding sources are noted in parentheses and final reports for DOE projects are included in the section entitled EXPERIMENTAL/RESULTS AND DISCUSSION.

#### MAJOR CRUISE ACCOMPLISHMENTS:

1. CMRET deploys vehicles as well as landers and other instruments using a 4000m armored fiber-optic cable (BOEM) that enables us to communicate directly from a surface vessel to instruments on the seafloor;
2. For all cruises, CMRET performed calibration for HyPack navigation and USBL locating of instruments, vehicles, coring devices, etc.
3. A complete surface-source/deep-receiver (SSDR) survey (BOEM) targeting the HSZ at Woolsey Mound, MC118, has been made. The resultant 109 profiles of very high resolution seismic data have undergone processing to create a 3-D model of the mound, including the application of Empirical Mode Decomposition (EMD) described by Battista et al., 2007.
4. Over 30 hours of direct current resistivity (DCR) data from the Woolsey Mound area at MC118 were recovered using the CMRET's Remotely Operated Vehicle, the Station Service Device (SSD), Figure 3 (STRC), and Baylor's 1100m DCR streamer (DOE- separate contract).
5. We have made multiple deployments of the University of Georgia/SRI Lander (DOE). This system has been developed to include a MIMS (membrane induction mass spectrometer) as well as a downward-facing camera and lights, and surface-controlled high-throughput sampling system so that water samples can be filtered on demand from areas of visual or chemical interest. This system has been used to locate/select sites for many instrument deployments.
6. We have imaged bubble streams with multibeam instruments (DOE) and added locations to terrestrial background methane data (DOE).
7. We have deployed and recovered a CMRET-designed and built calibration mooring (BOEM), ABIL (Autonomous Benthic Instrument Lander), Figure 4, with



Ultra-short Baseline (USBL) transponder, CTD (conductivity-temperature-depth instrument), and the University of Southern Mississippi's (USM's) sonar scanner (BOEM) aboard.

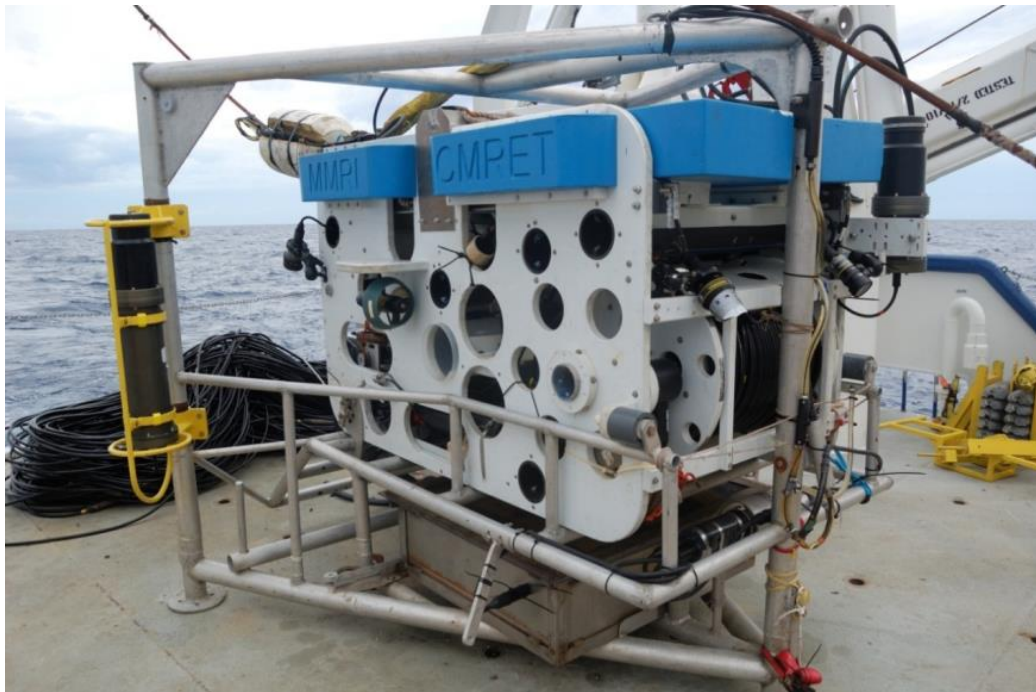


**Figure 3. While the Pelican motors to the target, the SSD, complete with upgrades, resides in its cage, ready to dive.**



**Figure 4. The ABIL is deployed using the Pelican's crane. Note the compact, central, arrangement of instruments - CTD, acoustic releases, battery, transponder - protected by the glass floats in hard-hats. Scanning sonar - red - is located above the other lander components for greater access to its surroundings.**

8. CMRET performed lander operations with the SSD (NOAA), Figures 5, 6, for ECOGIG (Ecosystem Impacts of oil and gas inputs to the Gulf - Gulf Recovery Initiative). Major accomplishments include:
  - a. video-ing the location and disposition of a lander (Figure 7);
  - b. video-ing the instruments on the lander;
  - c. video-ing surroundings for potential instrument/CSA (Chimney Sampler Array) (NOAA) deployment sites – bubble streams, bacterial mat, exposed hydrate;
  - d. remove a probe from a lander and place it in mud (on-target);and
  - e. placing chimneys on the seafloor (remove each from the lander and place at a suitable site for determining flux of gas from seafloor sediments, i.e. where bacterial mats are abundant or bubble streams are visible).

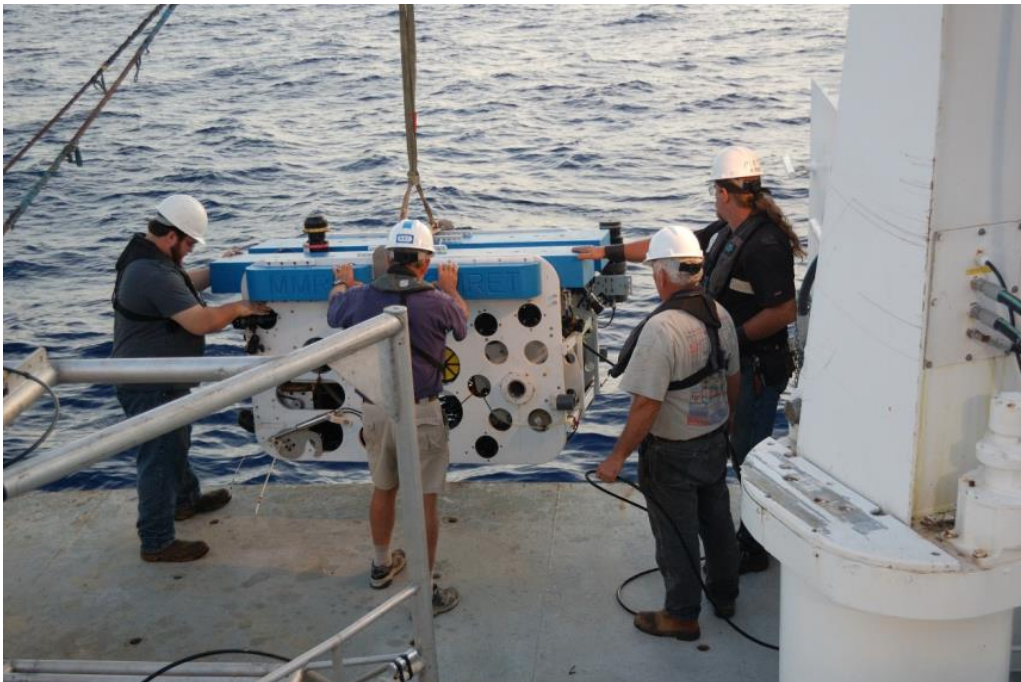


***Figure 5. As part of the pre-dive preparations, the SSD undergoes a dunk test prior to its initial dive. This test will determine what adjustments need to be made to the vehicle's ballast and trim, so that its travel in the water-column will be stable and its responses predictable.***

9. With the NIUST AUV team, CMRET researchers recovered multibeam and chirp data from 50m above seafloor for MC118. CMRET/STRC has begun to process and interpret the data: the multibeam data will be used to produce bathymetry and backscatter images while the chirp data allow us to image, in great detail, the shallowest (~60m) portion of the subsurface (see *MONITORING STATION SYSTEMS STATUS SUMMARY Geophysical Sensor Systems/Geology*).
10. With the NIUST AUV team, CMRET recovered – and is processing - multibeam data from 15m above the seafloor, Figure 8, over the Woolsey Mound at MC118 for a ***very high resolution bathymetry study***, unlike traditional AUV surveys.

11. With the NIUST AUV team, CMRET/STRC recovered high resolution photo data from several sites, including MC118, using the *Mola Mola* AUV (see *MONITORING STATION SYSTEMS STATUS SUMMARY Vehicle/Support Systems*). ***This is the first survey conducted with the Mola Mola with proper navigation.***



***Figure 6. The SSD feeds back a variety of information to the vessel via fiber-optic cable feed: photographic data from multiple cameras, sonar, and information about its location and attitude. Its power comes from a battery built into the vehicle which doubles as a clump-weight.***



***Figure 7. The ECOGIG lander, built by the MMR/CMRET shop, was located 115m from the location given the navigation. Using the SSD's sonar and multiple camera capabilities, we were able to locate the lander, then survey its position, document the orientations of the instruments and remove the chimneys (grey cylinders in the front of the image on the right) and place them on the seafloor where the seafloor showed signs of gas emissions (bacterial mat, pitted surfaces).***



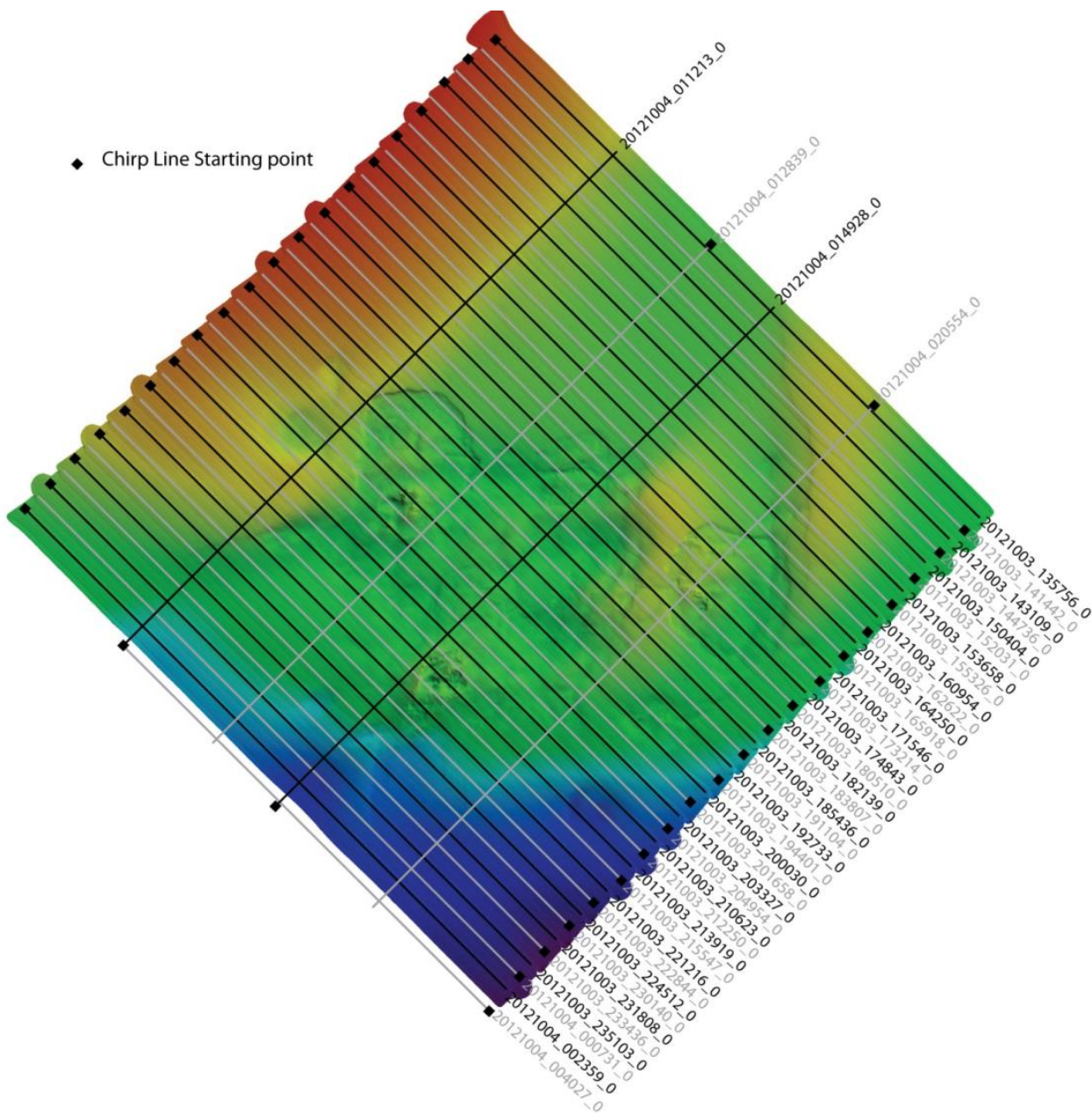


**Figure 8. The plot of the high resolution multibeam survey conducted from the Eagle Ray AUV. Polarity-preserving chirp sonar was run simultaneously with multibeam (plotted here over the unprocessed resulting bathymetry). The AUV flew 15m above the seafloor. Survey line spacing is ~60m; resolution is 50cm.**

12. CMRET made an extremely successful debut of the I-SPIDER ROV (see MONITORING STATION SYSTEMS STATUS SUMMARY Vehicle/Support Systems) using it to reconnoiter potential lander deployment sites and to deploy the MMRI-constructed landers from the *Pelican's* main winch via our fiber-optic cable.

13. Routine cruise activities include making acoustic contact with the Integrated Data Power Unit or IDP (master data-logger for the Observatory), communicating with it successfully and regularly throughout a cruise, diving the SSD to locate the IDP and/or other instruments on the seafloor using the SSD's sonar and visuals, landing the SSD within 5-10m of a target, confirming the location and orientation of an instrument or seafloor feature and determining its direction and disposition, surveying an area for instrument deployment possibilities, investigating the habitats along an active fault scarp, and collecting push cores and oil/water slurpers of sediment and oil samples for microbial and chemical analysis;
14. With the NIUST AUV team, CMRET/STRC effected a single dive of the Mola Mola AUV over AT357 that resulted in 4666 images that will be mosaicked to produce a single image of very diverse benthic assemblage.
15. The CMRET shop team completed the consolidation of electronics into a single "topside system" that greatly increases our ability to control and monitor at-sea operations;
16. The CMRET shop team installed Ultra-short Baseline (USBL) transponders in the hull of the R/V *Pelican* to maintain exceptional navigation/locating capabilities at sea;
17. CMRET contracted with TDI Brooks, International, and Sidney Geophysical Consultants, Ltd. to collect, extrapolate, and interpret heat-flow data from Woolsey Mound in order to investigate the presence, circulation and effects of hydrocarbon – and other – fluids within the HSZ. A paper, Macelloni, et al., reports findings of this study and has been submitted to the Journal of Geophysical Research.
18. Consortium scientists planned, contracted for and executed a research cruise aboard the R/V *Pelican*, during which the WHOI optic modem was deployed, established contact with the Benthic Boundary Layer Array (BBLA) and transferred three months' worth of data, remotely, ***the first instance of real data being retrieved, optically, from the seafloor.*** This method enables data recovery without risk of collision, entanglement, etc. of instruments to the sea surface. A full data download – 3.5 months of data - was completed in just over an hour's time. From the deck to the site in the water-column and maintaining a 75m watch circle with the vessel, establishing communication with the BBLA, downloading data and returning to the deck all occupied less than two hours. ***This was the first use of this method to recover real data.***
19. The MMR/CMRET shop designed, built, deployed, recovered, evaluated and redesigned several landers to serve the needs of this project. One, the Remotely Operated Vehicle-assisted recovery device (ROVARD) has been used to deploy numerous geochemical systems, returning them and their data-loggers safely to the sea's surface after lengthy or short periods. The ROVARD's downward-facing camera functions to identify targets such as bubble streams in the water-column, sea creatures, chemosynthetic communities, coral beds, etc. and to use visual data to select a site.
20. Consortium scientists participated in and directed the efforts of a Jumbo Piston coring (JPC) cruise aboard the M/V *Brooks McCall*, January 25-31, 2011. Five JPCs each ~12-15m in length, were recovered from a variety of environments at



MC118. Core targets were selected using an integrated approach that included three different resolution seismic datasets as well as multibeam, backscatter and core data from gravity coring efforts and previous findings of the geochemical and microbial biology groups. Prioritization of target coring locations was based on the importance of maximum expected core penetration (64ft, or ~20m), likelihood of penetrating the high frequency scatter zone suspected of being indicative of hydrates in the shallow subsurface, the potential to ground-truth shallow seismic data already collected at MC118, and the potential to constrain lithologic, paleontologic and stratigraphic parameters at the observatory site. Hydrates were documented in the subsurface, ~ 10-12m subseafloor, **verifying both resistivity and shallow-source-deep-receiver findings that indicated the possibility of hydrate in the shallow subsurface.** A more detailed report of these activities is included here as Appendix A;

21. Using the ship's rosette and some reconfigured lander components/instruments, we redirected our efforts on a June, 2010 SSD cruise to water chemistry. Our instruments – mass spectrometer and follow up gas chromatography - **verified the presence of methane plumes at depth - ~600m and ~800m, apparently as a result of the Deep Water Horizon spill** in April. We have never seen readings this high and certainly not up in the water column that far, so distant from the seafloor and any possible vent;
22. Visiting scholar, Michela Ingrassia was able to participate in the BOEM and NOAA-sponsored *Lophelia* II cruise in the northern Gulf in October-November, 2010; Woolsey Mound was added to the cruise's list of dive sites. PI Chuck Fisher reported the highest diversity of benthic fauna of all sites they visited and installed permanent markers for use in future documentation of change at MC118;

### **Summary of Accomplishments, by Project**

This cooperative Agreement includes 12 subcontracts for which final reports appear in *Experimental/Results and Discussion* section. Highlights of these are summarized below and form a major component of the achievement record for this award. Many figure prominently in the summary report; some have served to guide the progress of research at the MS/SFO.

#### ***Design and Construction of four Horizontal Line Arrays***

- Four 500m-long hydrophone only seafloor arrays with data-loggers have been designed, built, tested successfully at 1000m depth equivalency and await a suitable opportunity for deployment at the observatory.

#### ***Seismic Data Processing at the Gas Hydrate Sea-floor Observatory: MC118***

- Seismic Data Processing at the Gas Hydrate Sea-floor Observatory: MC118. The University of Texas' Bureau of Economic Geology (BEG) investigated the utility of alterations in seismic response and how the hydrate system beneath the observatory site varies as a function of calendar-time events such as thermal cycles in the water column and local microseisms. They investigated a phenomenon that is unique to 4C seismic data – P-SV images made with

positive-offset source stations often differ from P-SV images made with data collected from negative-offset source stations. They found that, indeed, there are some differences in images made from these two offset domains. This research finding will be helpful as we use P-SV data to build a model of the near-seafloor geology across Block MC118.

***Noise-Based Gas Hydrates Monitoring: Monitoring gas hydrates by extracting Green's functions from noise***

- As data were not readily available from the site of the MS/SFO, the University of California – San Diego (UCSD) team began by monitoring storms in the Pacific using seismics: Nonlinear wave-wave interactions generate double-frequency (DF) microseisms, which include both surface waves (mainly Rayleigh-type) and compressional (*P*) waves.
- DF *P* waves generated by severe storms far offshore are detected by beamforming of land-based seismic array data, allowing storms to be well-tracked, seismologically. Two distinct spectral bands associated with different microseismic *P*-wave source locations are observed: short-period DF band, dominated by *P* waves generated in the deep ocean by local wind seas near the storm, and *P* waves in the long-period DF band that are weaker and generated closer to the coast from swell interactions. The accurate identification of DF *P*-wave microseism source areas is necessary to image Earth structure using ambient noise.
- The UCSD team then focused on processing ambient noise using noise cross-correlation to recover surface wave Green's functions between receivers, rarely attempted using surface waves. They built a 1D velocity model showing very low shear wave-speed in the uppermost model, consistent with local geology.
- In April, 2011, CMRET collected weak seismic Ocean Bottom Seismometer (OBS) data from MC118 and UCSD found that with a single day of data, the use of ambient noise demonstrated its utility as a monitoring approach (Carriere and Gerstoft, 2013).

***Geochemical investigations at MC 118: Coupling of Continuous Geochemical and Sea-floor Acoustic Measurements and Pore fluid time series and gas hydrate stability.***

- 1<sup>st</sup> Pore fluid Array - PFA - box designed and built by Florida State University researchers was deployed at MC118 5/05 and serviced 9/06. Data were recovered and analyzed (previous grant).
- Second PFA redesigned based on lessons learned from 1<sup>st</sup>. Deployed April 2008. Not recovered.
- Peepers, small osmosamplers, were designed, built, deployed and recovered. The recovered data reflected challenges of deployment. 6 peepers deployed Sept, 2006 produced the somewhat unexpected finding that methane concentrations increased away from buried hydrate toward the seafloor.
- Methane spikes at 10 days and 120 days were correlated with nearby earthquakes confirming FSU's hypothesis that seismic events influence geochemical parameters.

- Core 9 (5/05) microbial “hot spot” supports the hypothesis that thermogenic methane supplied from a deep reservoir is influencing subsurface geochemistry and fueling microbial activity at the site;
- Researchers defined 3 regimes of microbial activity in shallow subsurface:
  - High sulfate concentrations at depth coincide with low concentrations of thermogenic methane, that nevertheless exhibited an advective profile; methane isotopes decoupled from DIC isotope values were characterized as a low microbial activity site; methane supply has not been present long enough for the establishment of an active chemosynthetic community;
  - Cores that exhibited high methane concentrations and sulfate depletion with depth signified a more robust microbial community, hence an active vent that had been established for some time. These areas were characterized as a ‘middle stage’ vent;
  - Late stage vents were characterized by low methane concentrations and high sulfate concentrations, but with carbonate isotopes significantly different from DIC values.
- Methane collected from JPCs was analyzed and fed into the multi-gas hydrate simulator developed under this award (See Final Report for Phase 4 Task 3).
- Methane was the dominant gas (79%) followed by ethane (11%), propane (9%), and butane (1%). The  $\delta^{13}\text{C}_{\text{methane}}$  was  $-40.4\text{‰} \pm 0.7$  (n=9). Cumulatively, the relatively high proportion of ethane and propane, as well as the heavy methane carbon isotopes confirm that the source for the hydrate is thermogenic.
  - In JPCs, we saw a range of microbial activities and evidence of both biogenic and thermogenic methane sources across the mound complex.
  - In general, areas that had faults but little acoustic backscatter showed little influence of thermogenic methane suggesting that transported hydrocarbons are constrained within the fault itself and not affecting surrounding sediment geochemistry.
  - On the other hand, areas near faults with high acoustic backscatter do show evidence of thermogenic sources contributing to the methane pool and generally have higher methane fluxes and microbial activity rates (as inferred from sulfate reduction rates).
- Measurements of methane and other hydrocarbons in concert with geochemical gradients suggest that saturated methane conditions are not obligatory for natural hydrate occurrence. However, experimentally, we have shown that artificial hydrates will continue to dissolve until the surrounding water reaches saturation. Further investigation is needed to determine whether natural conditions are contributing to the stability of hydrate outcrops as observed at MC118.

***Modeling a carbonate/hydrate mound in Mississippi Canyon 118 using modified version of (THROBS)***

- The SAIC-developed hydrate simulator, THROBS, restricted to one-dimension and Structure I methane hydrate was expanded/generalized in several respects in order to treat the multigas hydrate typical of MC118. Goals were to

- Incorporate the stability curve and other hydrate properties (heat of melting, hydration number, and thermomechanical properties) for structure II hydrates.
- Replace methane gas equation-of-state (EOS) and gas solubility relationship by an EOS and solubility curve that reflects the gas composition.
- Develop a multi-dimensional version of THROBS.
- SAIC incorporated structure II hydrate stability curve and relevant properties (previous point) into THROBS simulator. The gas mixture forming the hydrate was represented as a single gas. The modified THROBS simulator was used to model (1) the hydrate distribution above the shallowest BSR, (2) presence of high salinity fluids within the hydrate stability zone, and (3) gas venting at the sea-floor.
- A “compositional” (i.e. multi-gas) simulator is needed to account for the various gas components present in MC118 hydrates and for modeling phenomena such as molecular fractionation and multiple BSRs. SAIC initiated the development of a multi-component (methane, ethane, and propane) simulator that included (1) development of a computationally efficient multi-component equation-of-state (i.e. PVT behavior of 3-gas components, water, and salt; phases will include hydrate and precipitated salt as solid phases, water with dissolved gases and salt as a liquid phase, and a gas phase), and (2) modification of the simulator to accommodate the new equation –of-state.
- In preparation for the extension of the approach to treat multidimensional problems, SAIC completed the adoption of the existing (single gas) THROBS equation-of-state for use in the multidimensional STAR simulator. Test calculations have verified that, with the new STAR/HYDCH4 constitutive description, the two codes (THROBS and STAR) produce identical results when used to solve 1-D problems. Since the MC118 site analysis will eventually require a multidimensional treatment, this is a necessary step in the development. With the existing THROBS constitutive description incorporated into STAR, it is now possible to carry out preliminary multidimensional studies and we are in a better position to proceed toward the final goal of a multidimensional, multi-component modeling capability.
- In June 2012, SAIC was informed by the University of Mississippi that recently very accurate heat flow data were collected at 15 sites in and around MC118. SAIC used the completed HYDGAS correlations to compute the base of the hydrate stability zone (for 100% methane gas, and a mixture of methane, ethane and propane) at these 15 sites. This work is included in a multi-author paper recently submitted to the Journal of Geophysical Research (Macelloni et al.).

***Microbial techniques to extract carbon from stored hydrocarbon gases***

- Mississippi State University (MSU) conducted investigations into the influence of indigenous microbes on the mechanisms and kinetics of seafloor hydrate formations and dissociations. They found that many sediments that proliferate microbial activities around MC-118 hydrates play an important part in the nucleation, accumulation, and dissociation of near-surface hydrates.

- Additional investigations were made into the possibility of utilizing microbial techniques to extract carbon from stored hydrocarbon gases—i.e., to assist in the production of the occluded hydrocarbon gases.
- MSU researchers made the intriguing finding that microbial cell wall material inhibits hydrate formation—a necessary occurrence for the bacterial cell’s survival, as it prevents hydrate formation-heats from being liberated directly onto cell surfaces. Further, they found the hydrate inhibitor to be peptidoglycan, a chemical common in microbial cell walls: ***This constitutes the first report of hydrate inhibition by bacterial cell wall material.*** Data were gathered showing this peptidoglycan polymeric compound, which is water-insoluble, to be increasingly effective as an inhibitor by increasing its surface area through cell lysing.
- A smaller, water-soluble, molecular component of the peptidoglycan polymer was tested and shown to retain hydrate-inhibiting properties. In tests comparing with a methanol standard, this water-soluble, glycan strand performed better in delaying gas hydrate formation (i.e., longer induction times) than similar amounts of methanol.

#### ***Automated Biological/Chemical Monitoring System (ABCMS) for Offshore Oceanographic Carbon Dynamic Studies***

- The team integrated a high throughput deep water filtration system (DWFS) for microbiological sampling and a membrane introduction mass spectrometer (MIMS) for chemical analysis. The package was also equipped with a CTD sensor and altimeter. This integrated capability allowed for a rapid survey of large areas in the water column for detecting methane and measuring a variety of other chemical and physical components such as temperature, dissolved CO<sub>2</sub> and nitrogen above a hydrate mound. The DWFS can be activated any time for biomass and surficial sediment collection associated with methane gas.
- A first of its kind experiment was accomplished in which the instrument package was lowered to deliberately perturb the sediment. The MIMS detected a strong methane signal upon impact with the seafloor and the DWFS immediately collected a filter sample containing biomass and sediment particles.
- A next-generation lander, the Automated Biological/Chemical Monitoring System (ABCMS) was designed and built following lessons learned with the DWFS/MIMS experiments. The ABCMS is capable of collecting multiple filter samples at operator-programmed seawater volume, and at depths exceeding 1000 meters. The filtered samples can be used to study the microbial community thriving in the water column and in the sediment pore water as well as to study the surficial sediment associated with the methane seeps. The multi-filter capability allows the ABCMS to be deployed for an extended duration and to survey for potential methane “hot spots”, facilitated by its video, positioning, photography capabilities, coupled with its ability to perform real time measurements of water chemistry.
- The ABCMS is capable of landing where a methane anomaly is detected and can perform physical and chemical measurements while collecting samples for biological and sediment analysis.

- The filter packs are prefilled with distilled water to prevent contamination from surrounding water during deployment. Once deployed and upon pump activation, the distilled water is displaced with seawater at the desired depth and location. Upon activation, the pump will continue to move seawater through the filter until the desired volume is reached or the filter has been clogged.
- The new MIMS system was designed for deployment to a depth of 2000 m. Initial tests have demonstrated a power consumption of 50 Watts (24 VDC), without running the sample pump and membrane probe heaters. These components will add up to 20 Watts additional power consumption, depending on the set point of the membrane probe heater system and the initial temperature of water being analyzed. The instrument has a length of 64 cm (without considering connectors) and a diameter of 24 cm. Its weight in air is approximately 25 kg and has close to neutral buoyancy in water.
- During one of the field methane detection tests, in June 2010, SRI deployed the MIMS at MC118 to investigate potential changes in dissolved gas and volatile organic concentrations in the water column that may be due to the Deepwater Horizon spill. Data from three vertical profiling casts were collected, and in each case the data indicate elevated concentrations of methane (over previous profiling casts performed before the spill in approximately the same area) at approximately 600 m and 800 m depths.
- July 2013, the ABCMS was again deployed at MC118 seafloor. During decent, the MIMS continuously streamed realtime data back to the surface and recorded two strong methane peaks. Mass spectrometry data, video and filter samples were collected for approximately two hours during the deployment.

***Validate high-frequency scatter on SDR data by acquisition of targeted cores and velocity profiles at MC118 Hydrate Mound Development of a Shallow Sediment Velocity Probe (SSVP) for use in the Gas Hydrates Research - Consortium Sea Floor Observatory Program at MC118***

- The successful installation of the Pore Fluid Array and Temperature Array with sensors to depths of nearly 10 m subseafloor at MC118 (2005) opened the possibility of installing acoustic sensors on a similar probe as a method of measuring sediment velocity.
- Inclusion of the sediment probe with imbedded hydrophones and an electronics package as an attachment to a 10m MMRI gravity sediment coring device designed to collect core samples of gas Hydrates or Hydrate bearing sediments affords the opportunity to collect a vertically graduated sample of the speed of sound, temperature and shear strength of Hydrate bearing sediments simultaneously with the collection of a core sample of this material.
- An acoustic sound source for the speed of sound measurements and an accelerometer to detect bottom contact and measure the deceleration rate are included in the sediment probe electronics housing. The bottom contact triggers a time series of temperature measurements and a time delayed series of speed of sound measurements. The deceleration rate is used to determine the shear strength of the material through which the probe penetrates.

- The software and hardware for this probe are completed and have been bench tested to verify operation. The battery pack is included in the electronics housing eliminating the need for an external battery pack but sufficient to allow multiple insertions and retrievals prior to recovery; however adding an external battery is possible should longer-term stand-alone use be desired.
- The sediment probe electronics package is positioned with the acoustic source transducer installed on the end plate of the electronics package. This provides a line of sight for the acoustic source to the sensors in the receiving array in the seafloor adjacent to the core barrel. The sediment probe electronics package includes the controller/data logger, a sensor interface and A/D converter an accelerometer sensor, the battery power supply and the acoustic source.

***Geological and Geophysical Baseline Characterization of Gas Hydrates at MC118, Gulf of Mexico – time-lapse seismic monitoring***

- Repeat seismic surveys through time – 4D seismic monitoring – was accomplished through acquisition, processing and evaluation of multiple datasets from the observatory site, MC118, to determine time-scale at which hydrates form, accumulate and/or dissociate.
- Temporal changes in shallow subsurface anomalies were clearly detected over the time-span of the datasets: 3 years. These include interpreted venting of gas, changes in pockmarks and craters, fractures plugged/subsequently unplugged by hydrates, biodiversity at the seafloor and presence/disappearance of “bright spots.”

***Scoping study using Spatio-Temporal Measurement of Seep Emissions by Multibeam Sonar at MC118***

- Landers were equipped with commercially available sonars and rotators. Two such assemblages were bench tested then field tested in a variety of marine environments in which the effects of temperature as well as pressure, depth (travel distance), gas composition, currents, bubble size, bubble stream density and configuration were investigated and analyzed.
- In July 2013, the sonar rotators were mounted to a lander that also carried multiple lights and cameras as well as USBL and navigated to multiple seep sites at MC118 where repeat crossings of bubble streams were made and recorded.
- Terrestrial methane data were recovered via “air ram” set up in the roof of a recreational vehicle over a period of weeks on three different occasions and plotted like seep data.
- Marine data have been placed in a broader context alongside terrestrial data collected before, during and after the collection of the marine data. These gas data are compared in a qualitative manner and reflect broad trends.
- Data are plotted within a satellite data context.

***Near seafloor geology at MC118 using converted shear-waves from 4C seafloor sensor data using Ocean Bottom Seismometer data***

- An ocean bottom seismometer (OBS) experiment was conducted at MC118. The primary goal of this study is to process seismic recordings to isolate both P-wave

and converted S-wave data over the Woolsey Mound. Of special interest are spatial changes in the ratio of P-wave to S-wave interval velocity, which may indicate changes in methane hydrate concentration across the study area.

- The initial processing task is to recover just those time segments of the receiver data that correspond to source firing times, and organizing that subset of data into SegY formatted files. This processing creates a SegY file for each OBS station that contains all five source lines, with four channels (one hydrophone and three geophones) for each source firing on each source line.
- Processing these SegY files then shows that a combination of hydrophone (pressure sensor) and geophone (velocity sensor) responses may be manipulated to separate P-wave and converted S-wave arrivals at each OBS station.
- In addition, comparison of the Gas Injection (GI) Gun source to the Water Gun source may influence the choice of sources for future surveys.
- Results of the OBS study were compared favorable though inconclusively with an SDR profile approximating the same survey line.
- Includes innovative solutions for dealing with data of marginal value.

#### ***Integration of Multiple Methods of Geological and Geophysical investigations to advance Shallow Subsurface Characterization at MC118***

- A heat-flow study was designed and heat-flow data were collected from key locations on and off Woolsey Mound, site of the Seafloor Observatory.
- Heat-flow data from MC118 were interpreted, a report written and a paper written integrating results from this study with those from the SAIC hydrate simulating model, core data, and geophysical surveys.
- Jumbo piston cores were collected from locations considered key to ground-truthing shallow geophysical data including a high frequency seismic anomaly suspected of representing hydrates.
- A processing protocol has been established for the polarity-preserving chirp (PPchirp) system now installed and working on the NIUST AUV, *Mola Mola*.
- The PPchirp files can now be converted to .sgy and processed using standard processing software to produce analyses of sediment properties and the production of 3D surfaces.
- A lithological interpretation of MC118 has been produced.
- A 15-site Ocean Bottom Seismometer data survey was run utilizing two sources – an airgun and a water gun - over the site of the major known subsurface hydrate occurrence and seismic anomaly on Woolsey Mound. Though the recovered data are not ideal an in-depth analysis has been made and appears as a component report.



## MONITORING STATION SYSTEMS STATUS SUMMARY

### Geophysical and Geological Systems

Geophysical studies as well as coring efforts have been used to investigate the baseline geology at the MS/SFO site. Multibeam swath bathymetry and chirp sonar systems on the C&C Hugin 3000 AUV were employed to recover the first survey of MC118 in 2005. The multibeam data were used to define seafloor morphology and bottom reflectivity (see Figures 9, 10 and 11); the high resolution chirp sub-bottom profiling data were used to reveal the structure of the shallow subseafloor, both on and off the mound. Together these datasets have guided much of the subsequent chemical and biological study at MC118 as well as defining the direction of further geological investigations.

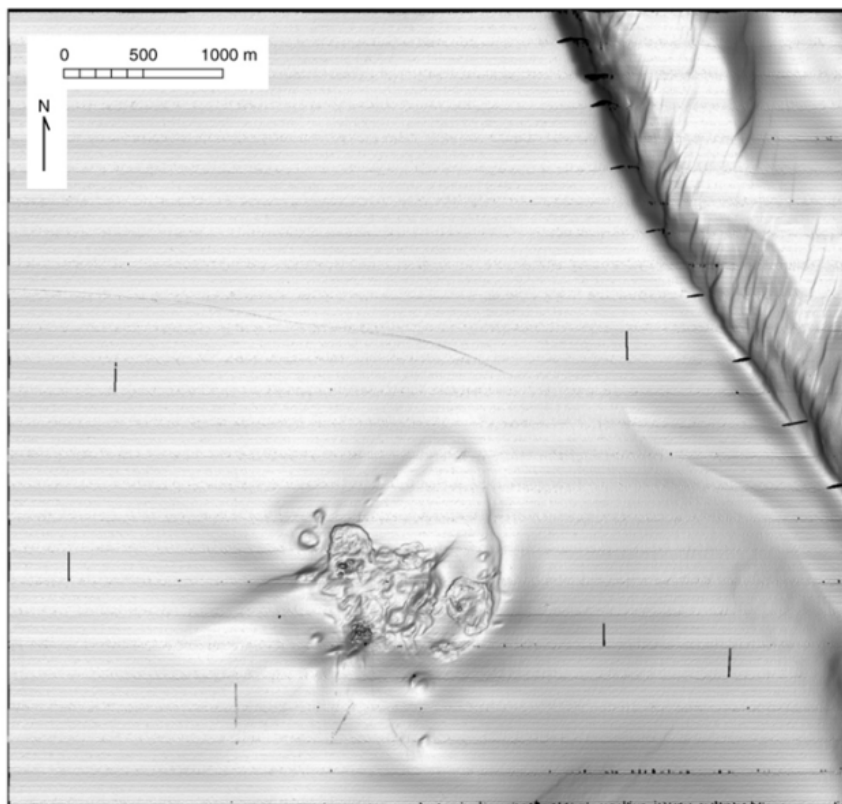


**Figure 9. Multibeam image of Mississippi Canyon 118. Data acquired by C&C technologies and reprocessed by The University of Mississippi and University of Rome, La Sapienza.**

With meticulous reprocessing of the data, extremely detailed images of the seafloor and ~60-70m profiles of the subseafloor have been made. These very high resolution images are placed in a regional context that we have now updated using the *Okeanos Explorer* multibeam data acquired late in 2011 (an example appears as Figure 11). (<http://oceanexplorer.noaa.gov/okeanos/explorations/ex1105/welcome.html>).

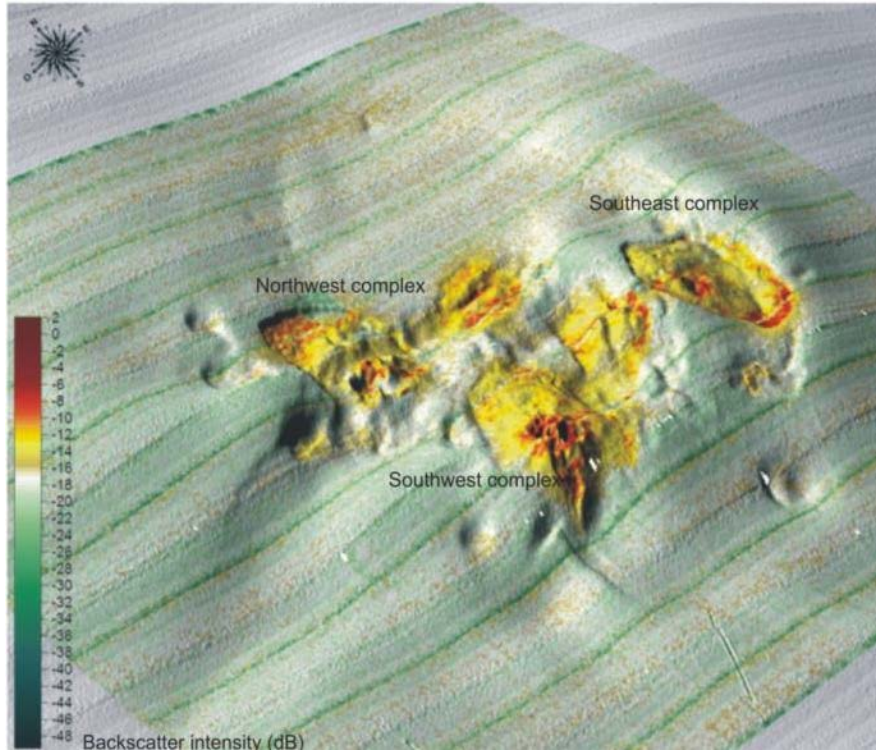


**Figure 10. Backscatter intensity draped over bathymetry over the Woolsey Mound, MC118, reveals hardgrounds, crater complexes and scarps (Caruso, 2007).**

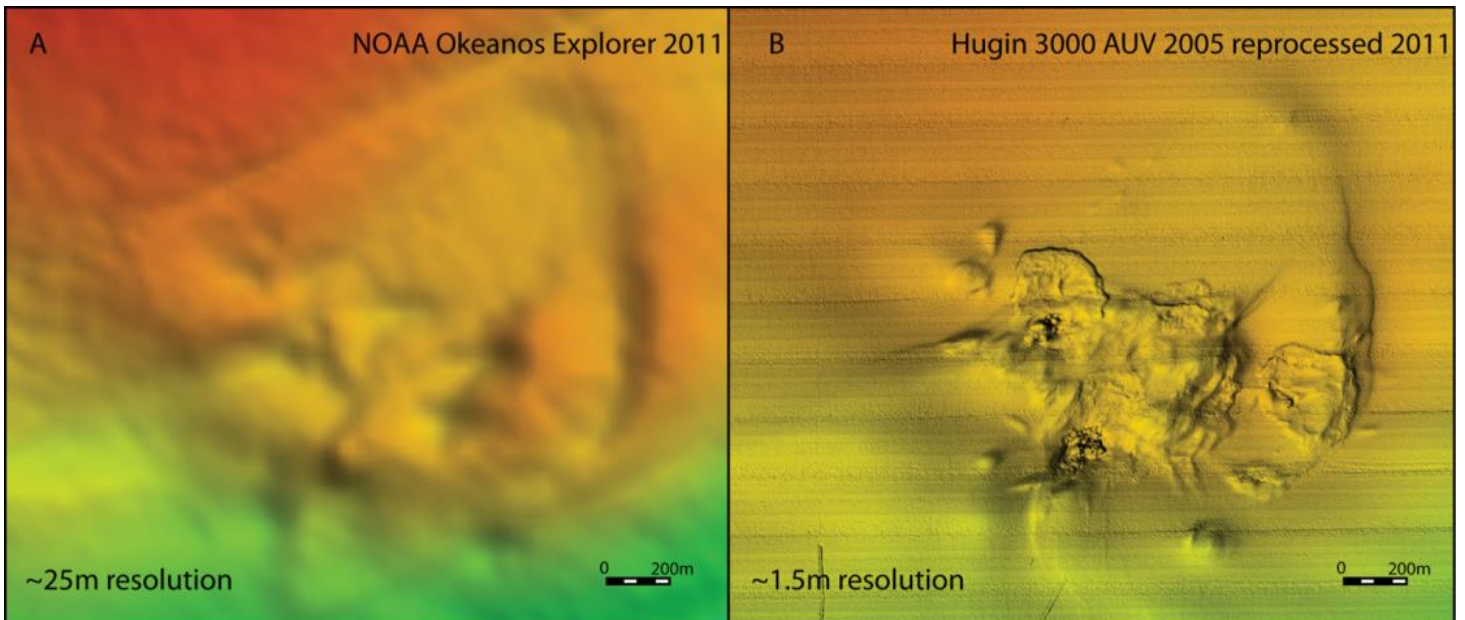


**Figure 11. Improving resolution reveals different features as shown in this pair of images of the same section of seafloor. A. Regional multibeam can be used quite effectively to target locations that display features associated with seeps, benthic communities, slumping, etc. B. Higher resolution AUV surveys can then be used to extract the detail needed to conduct focused study (Lutken, et al., 2013).**

In 2009, a multibeam survey was acquired using the NIUST *Eagle Ray* AUV and similar survey parameters. In addition, however, a near seafloor high resolution survey was also run with the Woods Hole Oceanographic Institute's (WHOI) Tethys mass spectrometer mounted in the vehicle and chemical surveying accomplished at 6m from the seafloor. From this survey, researchers were able to define changes in seafloor morphology over time (4 years), Figures 12 and 13 (Lutken et al., 2010; Macelloni, et al., 2010) and identify areas of anomalous methane concentrations in the near seafloor (Camilli et al., 2010), Figure 14.

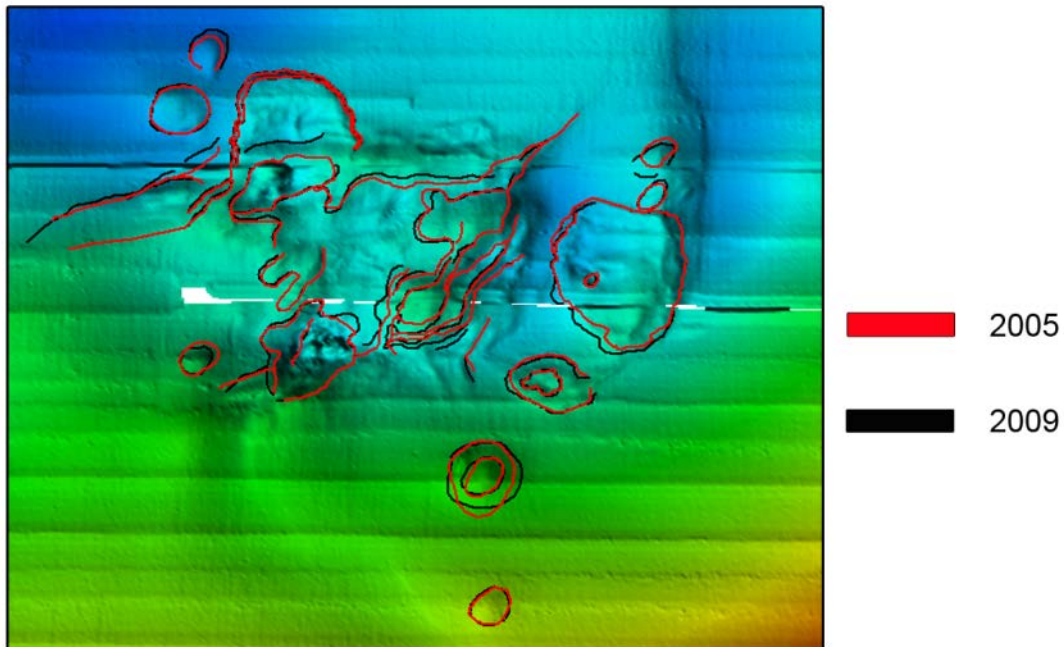


**Figure 12. Changes in morphology over four years that elapsed between successive AUV surveys (From Lutken, et al., 2010).**

New NIUST UVTC *Eagle Ray* AUV surveys have been acquired that include multibeam (from which new bathymetry and backscatter images are being generated by MMR/CMRET/STRC) and a new polarity-preserving chirp subbottom survey (NOAA/DOE) (see Phase 4, Task 2 of this report). These include a high resolution survey run 15m from the seafloor that reveals 50cm detail in the multibeam and 10cm detail in the profiles (an example appears as Figure 15). Although these data have yet to be thoroughly processed and interpreted, we believe this resolution will improve researchers' ability to distinguish hydrate/structures associated with hydrate in the subsurface.



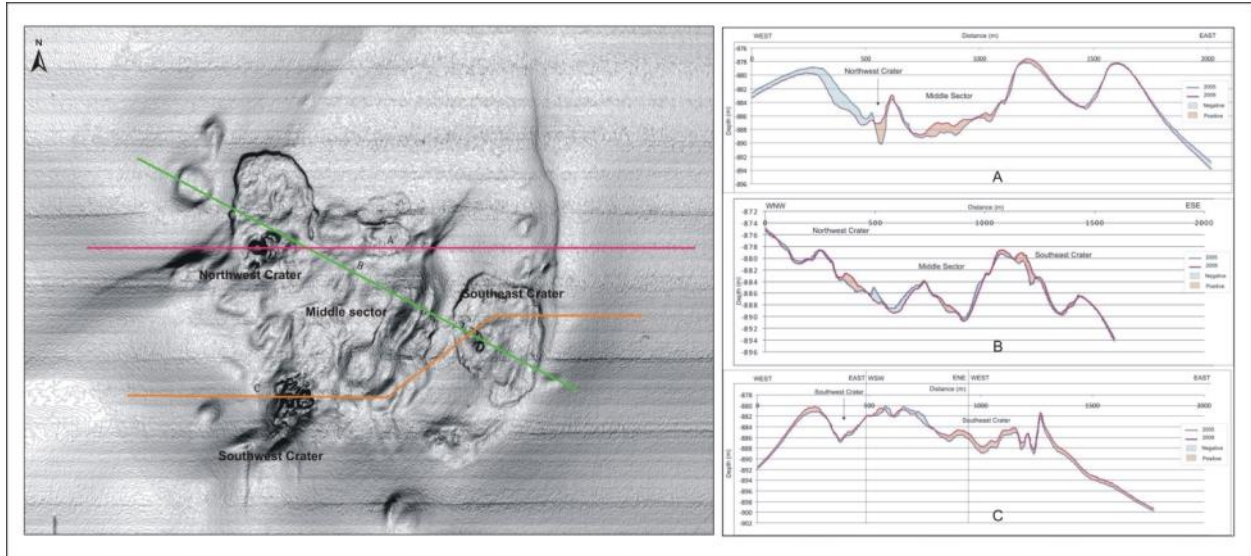


Figure 13. Profiles through some areas exhibiting greatest changes between two AUV surveys (From Lutken, et al., 2010).

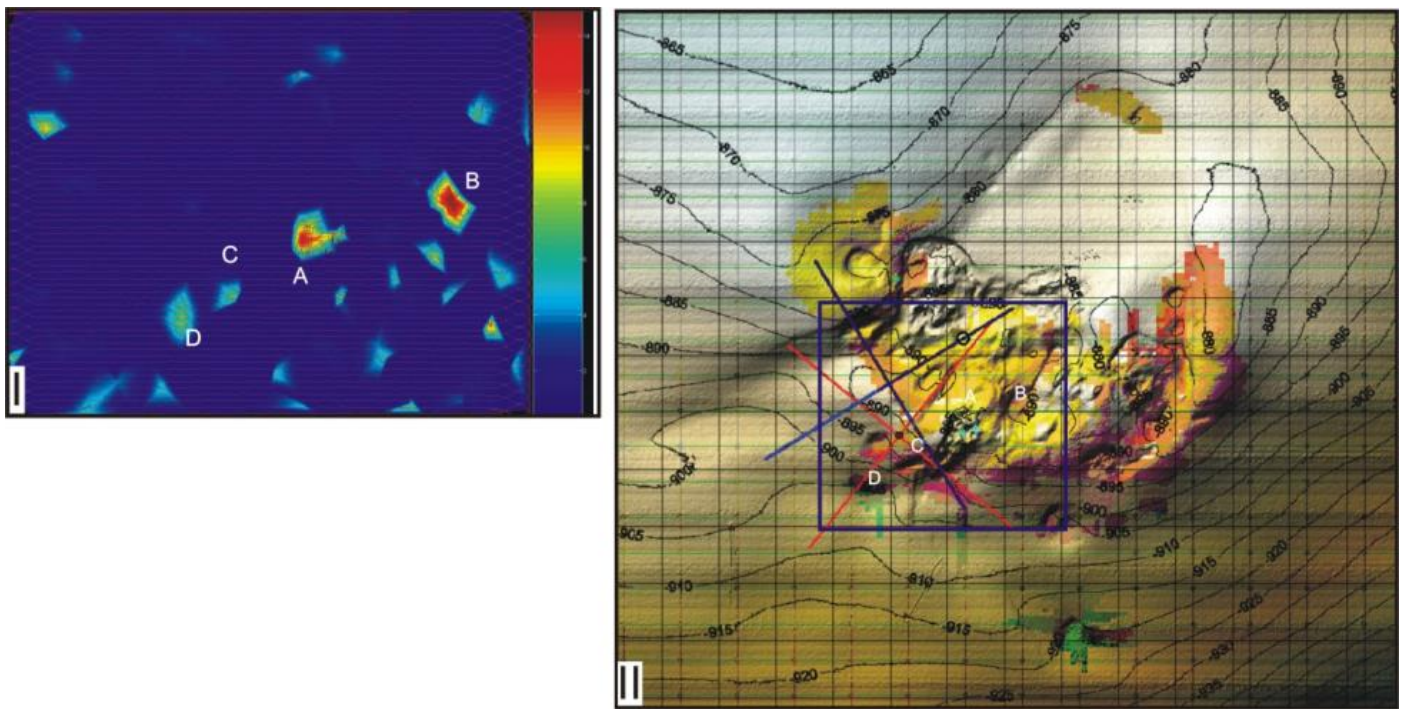
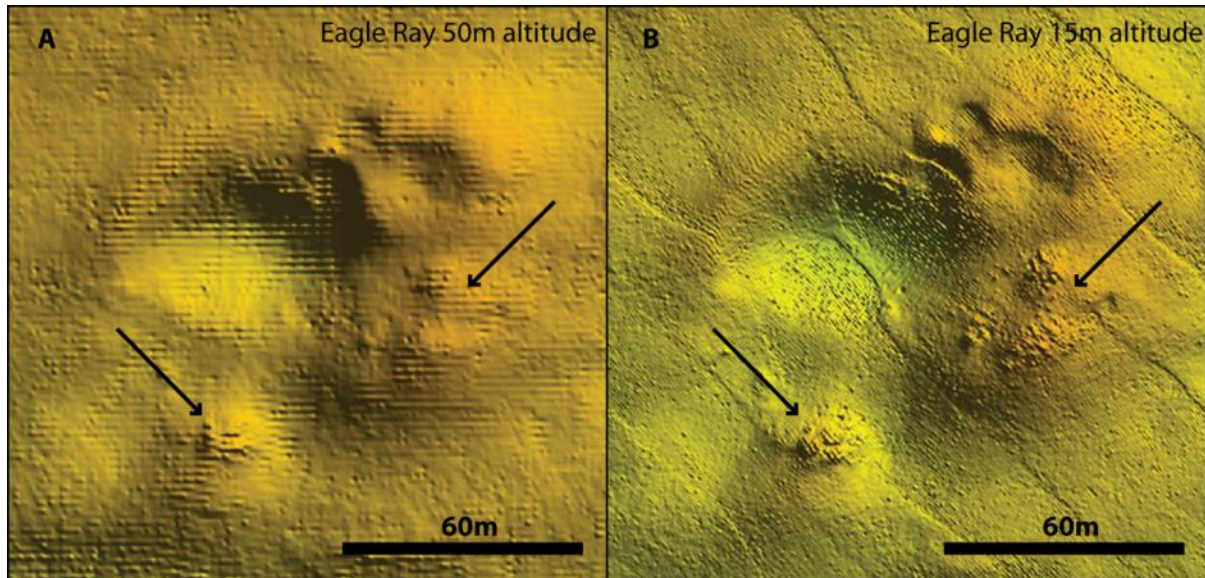


Figure 14. Methane anomalies recorded by AUV-borne mass spectrometer (left) with location of anomalies on the mound at MC18, right. (From Lutken et al., 2010, modified from Camilli, et al., 2009).



**Figure 15. Rock slabs on the seafloor as revealed in a A) 50m altitude AUV Eagle Ray [Flag: *italicize Eagle Ray*] survey (~1.2m resolution) and B) a 15m altitude survey (raw data ~.5m resolution) (From Lutken, et al., 2013).**

By integrating different data types and different resolution profiling data, we have **succeeded in predicting areas of hydrated sediments and proven these speculations by coring target locations**. Although not yet 100% accurate, these methods were used to select targets for the 2008 gravity coring cruise and chemical sensor emplacements as well as for the Jumbo Piston Coring (JPC) (Simonetti, et al., 2013) and Heat-flow cruises (Macelloni, et al., submitted).

A 2006 surface-source deep-receiver system or SSSDR (single channel seismic profiling with resolution improved via source-signature processing), has been used to complete a 3x3km survey of the hydrate/carbonate mound at MC118 (officially named after the late Dr. J. R. "Bob" Woolsey, MMR/CMRET Director, and founder of the Consortium and of the Hydrates Monitoring Station/Seafloor Observatory project). The resultant 109 profiles of very high resolution seismic data have undergone processing - including the application of Empirical Mode Decomposition (EMD) described by Battista et al. (2007) - to create a 3-D model of the mound. This dataset is capable of imaging features associated with gas hydrates – chimneys, fractures, fracture porosity, etc. – hundreds of meters below the seafloor (Macelloni et al., 2012). An industry dataset, acquired by TGS-NOPEC (top 3 sec donated to this project) has been evaluated by geophysicists and geologists in the Consortium in order to extend the range of baseline information from the MS/SFO site to the deeper subsurface and the source(es) of hydrocarbons and fracturing at depth (Knapp et al., 2010). In addition, Consortium geophysicists have acquired Controlled-source Electro-Magnetic (CSEM) data adjusted for shallow hydrate targets and a Direct Current Resistivity data set to produce high resolution images beneath the mound. Although the CSEM data have not yet been processed and evaluated, they are expected to show distribution of hydrates and 3-D structures such as dipping faults to ~200m beneath the seafloor. Results of the analyses of the



resistivity data show likely hydrate concentrations associated with areas of faulting and fractures (conduits for migrating fluids) and suggest that these pathways for hydrocarbon migration open but, at least in some cases, subsequently fill with hydrate and become blocked to further fluid migration and perhaps reopen or open elsewhere, forming seafloor features such as pockmarks and seafloor seeps and vents. These findings were corroborated by a 2011 jumbo piston coring effort that recovered hydrate from sites identified from the survey (Simonetti et al., 2013). In preparation for the JPC cruise in 2011, Consortium geoscientists collaborated in making use of all in-hand data to select the 5 sites (and 3 alternates) to core. The goal was to satisfy as many of the Consortium's questions as would be possible with a very limited number of long cores. As shown in Figure 17, the group was successful in predicting the occurrence of hydrate in the lower portions of JPC1. Additional resistivity studies are planned that will improve the resolution of the initial efforts and may identify areas of greater/lesser hydrate concentrations.

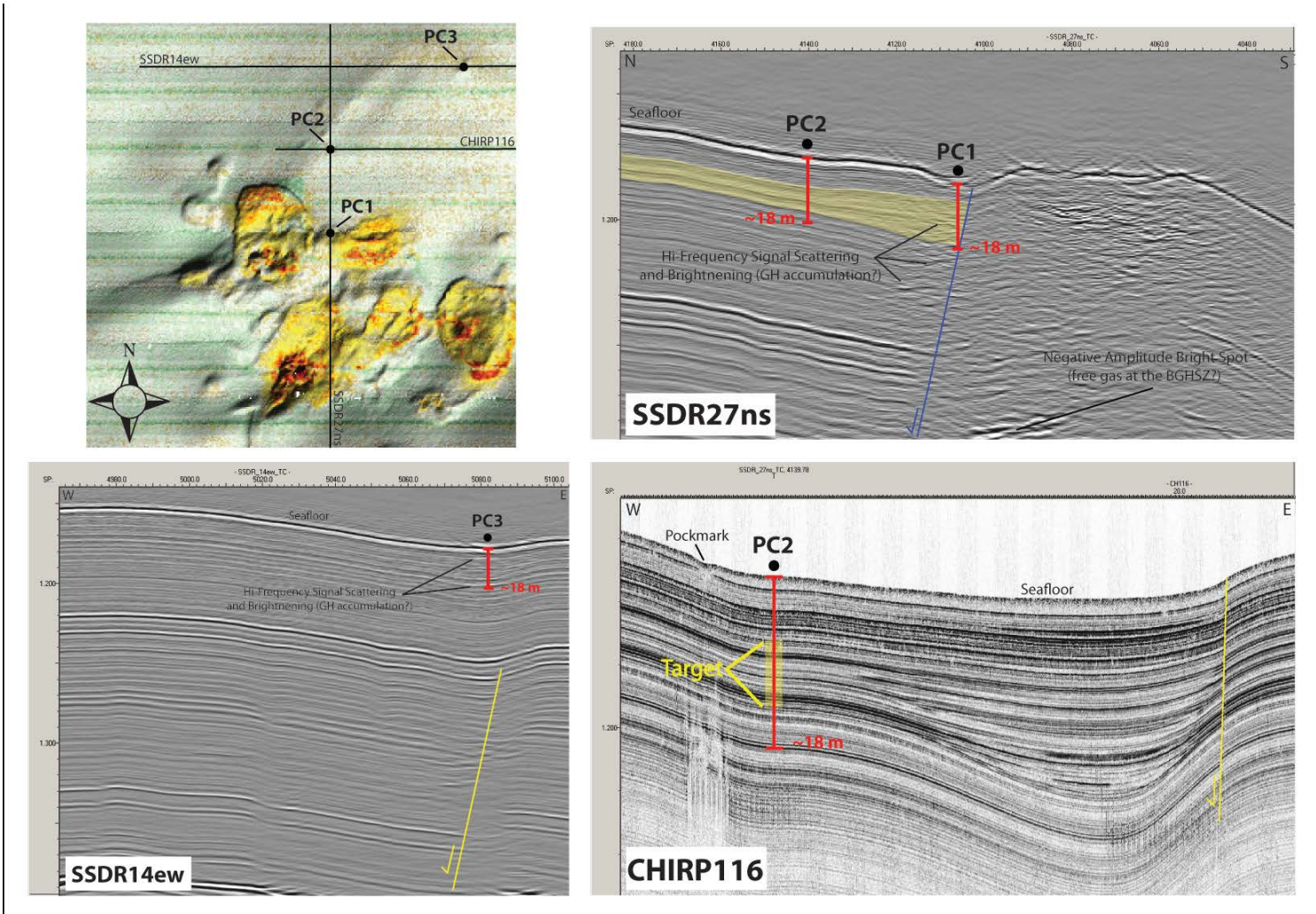


**Figure 16. Example of combination of criteria used to evaluate a site for possible hydrate occurrence in the shallow subsurface. Note high frequency backscatter on SSDR data, lower left (UM and USC).**

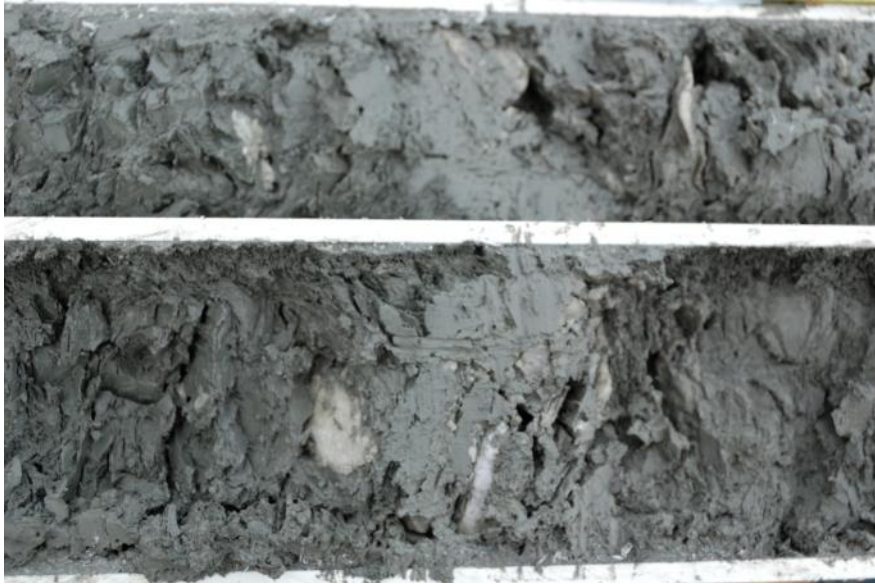


*Figure 17. JPC1 was cored and found to host slabs, chunks and grains of hydrate as well as a 2cm thick slab. Samples were collected from this core, evaluated for hydrocarbon species content (FSU) and the results plugged into the SAIC hydrate simulator.*

In the spring of 2012, a heat-flow study was conducted across the mound that also supports these findings. In addition, polarity-preserved chirp data from the 2005 AUV survey have been extracted by C&C Technologies and provided to the UM team for incorporation into the existing geophysical data library. With multiple resolution datasets and meticulous processing and interpretation, we have been able to construct a continuous record that extends from the salt structures – and deep petroleum reservoir potential - at depth through the shallow section and on to the seafloor. An example of this approach appears as Figure 18 and is explored in detail in Simonetti et al., 2011 and Macelloni et al., 2012.

Geophysical systems designed and built for permanent installation at the Observatory include a vertical water-column array (VLA) of sensors to determine sub-bottom structure and materials and an orthogonal cross of horizontal line arrays (HLAs) of sensors. Advantages of the HLAs include utilization of surface noise produced by noise-generating ships of opportunity providing P-wave energy for the hydrophones of the vertical and horizontal arrays. Further, the composite vertical and horizontal arrays can be used in experimental work with natural ambient sound, such as ship noise or wind-driven wave noise, as a passive seismic energy source (see Experimental/Results and Discussion, Phase 1, Task 4). The planned addition of accelerometers to the suite of seafloor sensors would enable passive monitoring via microseisms. These events, known to occur frequently in the region, are produced by ubiquitous salt movements as well as by deeper, basement-related seismic events. They can be recorded and possibly related to various observed phenomena at the study site such as pore-fluid migration and large scale episodic fluid venting.

Seismic data-processing software has been developed at Exploration Geophysics Laboratory (EGL) of the Texas Bureau of Economic Geology (BEG) that is structured to optimize P-P and P-SV image resolution in the immediate vicinity of 4-component (4C) seafloor-based seismic sensors. In April, 2011, an Ocean Bottom Seismometer (OBS)

experiment was conducted over a portion of Woolsey Mound to collect 4C data, an effort to enable researchers to establish the shear features/characteristics of the shallow subsurface (This task is discussed in more detail in the section, Experimental/Results and Discussion; Phase 2, Task 3). Passive data were also collected via the OBSs and have been evaluated by the University of California-San Diego (UCSD) for their utility in monitoring the HSZ (Carriere and Gerstoft, 2013). Additional 4C work is planned following the deployment of the HLAs. Software has already been written but is being modified for this experiment. In addition, inversion of the seismic data with the resistivity data is anticipated as a possible next step in geophysical characterization of this site.

Currently the completed water-column VLA, with the seabed HLA horizontal cross, is awaiting installation. The HLA's are complete and were successfully pressure-tested at Southwestern Research Institute in February, 2010, to 1000m water depth equivalents. Several attempts to deploy these ponderous arrays have not been successful and the recovery of the ROV (Remotely Operated Vehicle)-Assisted Recovery Device or ROVARD and the pop-up buoy, April, 2012, have been made in an effort to explore a lander-deployment of at least one of the arrays as a test of the concept, though this will necessarily happen beyond the end-date of this award.

Additional geophysical and geological studies are either complete or are underway or in the planning stages. Recent AUV multibeam surveys present the possibility of performing additional time-series analyses of seafloor changes at the Observatory site, including the evolution of chimneys, gas vents, sediment accumulations and changes in hydrate outcroppings. The June 2009 multibeam survey was run simultaneously with Woods Hole Oceanographic Institution's (WHOI) Mass spectrometer, *Tethys*. During this survey, *Tethys* detected methane spikes in areas where multibeam data indicated the possible presence of a seep that had not been evident in the 2005 survey. This critical find verifies the utility of these systems, particularly when used in concert as well as the transitory nature of cold seep sites. A new SDR survey would serve the same purpose but would address changes in the subsurface, including the HSZ. Mounting a hydrophone on the *Eagle Ray* and placing the receiver nearer the seafloor would eliminate cable strum, improving the data as well as extending the range of usable data deeper into the subsurface by increasing the arrival time of the surface ghost.

Reaching no resolution with GeoAcoustics to problems in the software that supports the Polarity Preserving/Discriminating Chirp sub-bottom profiler system (PPchirp), we tackled this problem internally. As can be seen in the more detailed discussion section, Experimental/Results and Discussion, Phase 4, Task 2, results of the initial successfully navigated survey are promising. CMRET and UVTC scientists have worked together to translate the GeoAcoustics code into segy so that the PPchirp data can be processed using standard, commercially available software. The goal of this technology is to enable researchers to discern reflectors related to near-bottom geologic features - including shallow gas horizons - to depths of approximately 50m. A particular benefit is its frequency compatibility with the AUV multibeam swath bathymetry mapping system, permitting simultaneous operation.



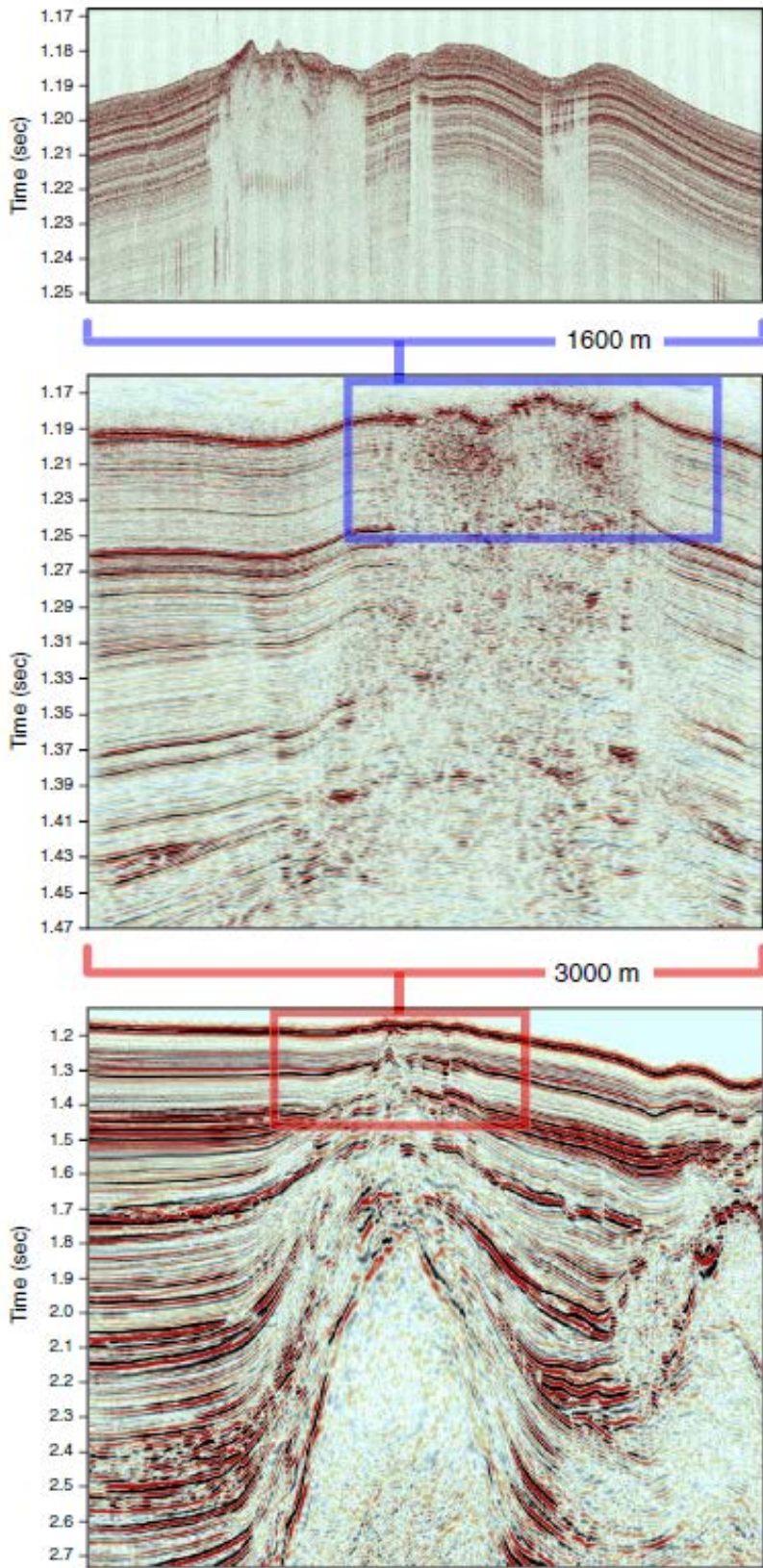


**Figure 18.** Three resolutions of seismic data were used to evaluate the subsurface at Woolsey Mound. The top profile was acquired using a chirp subsystem profiler of ~8kHz frequency and 10cm resolution. The middle profile was acquired using a shallow- source-deep- receiver system of ~1.5kHz frequency and 1m resolution. The bottom profile was extracted from industry 3D data of ~50Hz frequency and 50m resolution. Note difference in scales and coverage highlighted by the boxed areas. (variation of Simonetti et al., 2011 and Macelloni et al., 2012.

An additional industry data set acquired by Western Geophysical Company was purchased in 2010 and delivered in early 2011. Researchers at the USC and the UM have worked together to unravel the complex deep geology of Woolsey Mound; this additional dataset has already allowed these teams to identify previously unidentified structures and features, such as gas pockets that do not appear in the other data - adding a time-series component to study of the areas of vertical overlap. Amplitude variation with offset (AVO) can be applied to this data set to discriminate between fluid and solid material in pore fluids, the latter providing evidence of hydrate. This survey, which includes 12 sec records, also includes about 30% of the data into bordering blocks for full lateral coverage of the observatory block. Western Geco (2003) data were analyzed with the TGS data (2000) to perform time-lapse seismic monitoring. This time-lapse seismic (or 4-D seismic) analysis was conducted to detect the short-term dynamics that drive hydrate dissociation and seepage at Woolsey Mound. The approach consisted of quantifying changes in subsurface amplitude anomalies through time (i.e. 3-year time scale) that could indicate changes in the pore-fluid content (e.g. more vs. less gas accumulated at the BHSZ) (Simonetti et al., 2012b, and 2013).

Construction of speed of sound probes to accompany CMRET's 10m coring capability is underway and will be used at targeted locations in an attempt to further define a seismic signal for hydrate, something that has eluded hydrate workers to the present. Target locations have been identified based on the noise/scatter of signal noted in SSSR data collected from particular locations at MC118, from identification of resistivity anomalies and from detailed study of the morphologic features apparent in the extremely detailed seafloor images produced by meticulous processing of the multibeam backscatter and bathymetry, and corroborated in the chirp data. CMRET has also constructed a site reconnaissance camera (or I-SPIDER, described in the section Support Systems/Vehicles) to inspect seafloor locations of interest prior to coring and/or deployment of landers and sensors on the seafloor.

Jumbo Piston Cores (JPCs) were collected by Consortium geologists and geochemists working with TDI Brooks, International aboard the R/V *Brooks McCall* (Simonetti et al., 2013; Wilson et al., in press). Five cores of roughly 12-15m length were collected from sites selected using a combination of geophysical surveys from the area and core histories (refer to Figure 16 and Appendix A). Sites of high resistivity readings were given priority as were sites where seafloor expression of gas expulsion and faulting are evident on multibeam images. Hydrates were recovered in the bottom 2 meters of the core (Simonetti et al., 2013) from the site of highest resistivity readings. A newly acquired IR camera (NOAA) was used for the first time on this cruise and proved to be quite successful in predicting both high and low heat within unopened cores. This technique is being explored further and refined for use in future coring efforts as hydrate is known to dissociate rapidly upon recovery while temperature gradients may remain for longer periods. This area was targeted in the heat-flow study and found to have the highest heat-flow of the 13 measured sites on Woolsey Mound, a clear indication of warm fluids migrating through the fracture and to the seafloor.

## Geochemical Sensor Systems

Experiments designed to assess water-column geochemistry, microbial communities and activities, hydrate host-materials, bubble streams and composition of pore-fluids have been designed, built and tests run at MC118. Sediments collected from Mississippi Canyon have been studied for effects of parameters possibly involved in hydrate formation. Laboratory analyses show that smectite clays promote hydrate formation when basic platelets slough off the clay mass. These small platelets act as nuclei for hydrate formation. Experiments show an increasing importance of microbial activities surrounding active vents in promoting the formation and stability of seafloor gas hydrates. Experimental analyses of MC118 microbial consortia (Phase 3, Task 6) have shown the intriguing finding that *microbial cell wall material inhibits hydrate formation*, a necessary occurrence for the bacterial cell's survival, as it prevents hydrate formation-heats from being liberated directly onto cell surfaces. Microbes inhibit hydrate formation, thus enhancing their ability to survive the extreme conditions of the deep sea HSZ.

Evolution of geochemical sensor systems has helped define the baseline as well as the direction of geochemical research at MC118. Early in the history of the Observatory project, a 200m water-column oceanographic line array (OLA) was planned to monitor hydrocarbon pore-fluids venting from the surficial sediments in the vicinity of hydrate mounds and transiting the lower water column. As experience and an improved understanding of the hydrocarbon system and hydrography of the lower water column have emerged, a more comprehensive approach developed. The OLA (NETL/NOAA), was modified to a 60m length and designed to monitor the benthic boundary layer, hence the designation Benthic Boundary Layer Array (BBLA) (NOAA). This array was deployed successfully in March of 2009 and recovered in June. Three months of water-column chemistry were recovered. The BBLA was refitted to include a Contros methane sensor on the bottom node and redeployed at MC118 in September, 2010 and recovered in April, 2011. This dataset has been evaluated and appears to include water-column indications of the Deepwater Horizon spill of April, 2010. Unfortunately, the Contros methane sensor failed after less than 24 hours at depth (1000m). The BBLA was redeployed in June, 2011; in October, 2011, the WHOI optic modem was used successfully to *transfer data remotely from the BBLA to the ship*. This is the first instance of remote data transfer via optic modem and demonstrates the potential of this system. The BBLA was again recovered in April, 2012 for re-batterying and instrument maintenance. The newest dataset, collected over nearly a full year are being evaluated by a visiting scholar, hired to evaluate, process and interpret the geochemical data from the MS/SFO, primarily that recovered using the BBLA.

A small barrel-like, chimney sampler array (CSA), (NOAA/NIUST), outfitted with sensors that collect chemical data related to hydrate formation/dissociation, was fabricated by STRC subcontractors and tested in shallow water. The prototype unit was deployed and tested at MC118 in September, 2006, using the Johnson SeaLink (JSL) manned submersible submarine. A modified and expanded version of this sensor system was deployed on the MMR/CMRET-designed ROVARD at MC118 in September, 2010 and was recovered in June, 2011. Failure of the METS (methane sensor) truncated collection after 3 weeks. An upgraded system was deployed in October (Figure 19) and

collected in April, 2012. Although the METS again failed, it had been routed to a different circuit, allowing the other sensors to continue to collect very high resolution geochemical data, as displayed in Figure 20. Once the BBLA data-evaluation is complete, an attempt will be made to merge the datasets from these two arrays. In addition, the CSA is a major component of ECOGIG's time-series geochemical evaluation of seeps – both natural and anthropogenic – and continues collecting data from key sites in the northern GOM.



*Figure 19, left, the ROVARD, with CSA, as seen from the ROV, Holiday, during an October, 2012, NRDA cruise.*

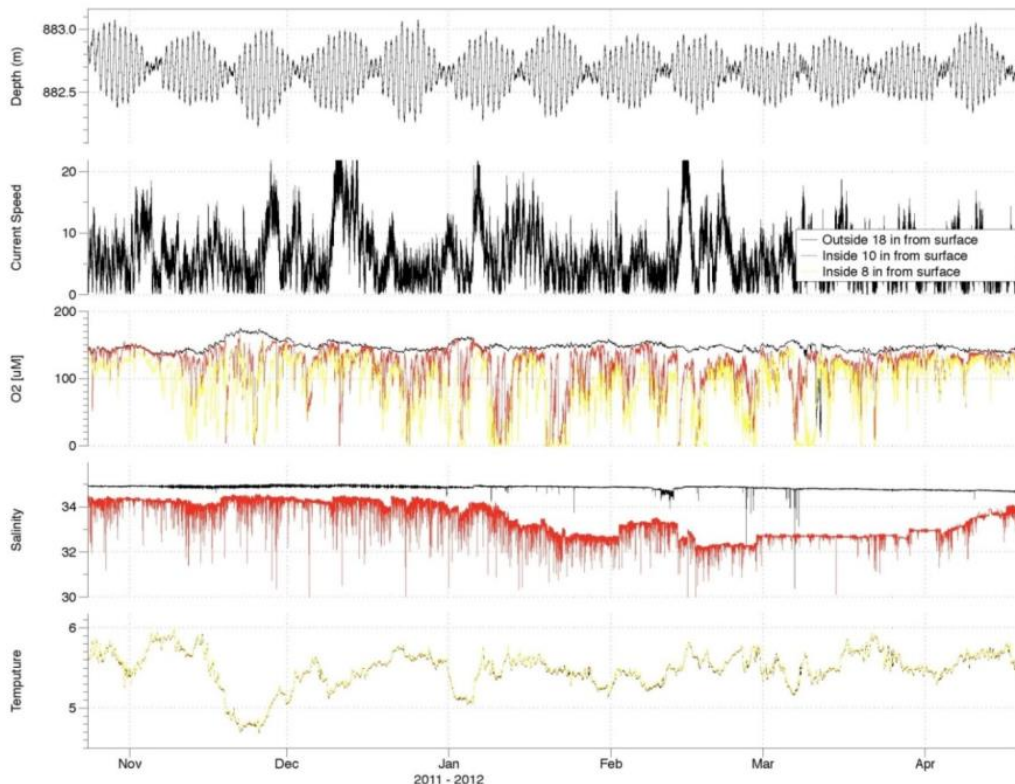


*Figure 20. Water-column data collected with the CSA over a six-month deployment on the seafloor at Woolsey Mound.*



The pore-fluid sampling array (PFA, Figure 21) was designed to sample and analyze pore-fluid chemistry of the shallow, near-seabed HSZ (Lapham et al., 2008). The first PFA was completed in time for deployment during a May, 2005 cruise using a 10m SFP in much the same way as the thermistor array (TA) was emplaced. The osmo-sampler retrievable section was recovered on the September 2006 JSL dive along with the TA data-logger.

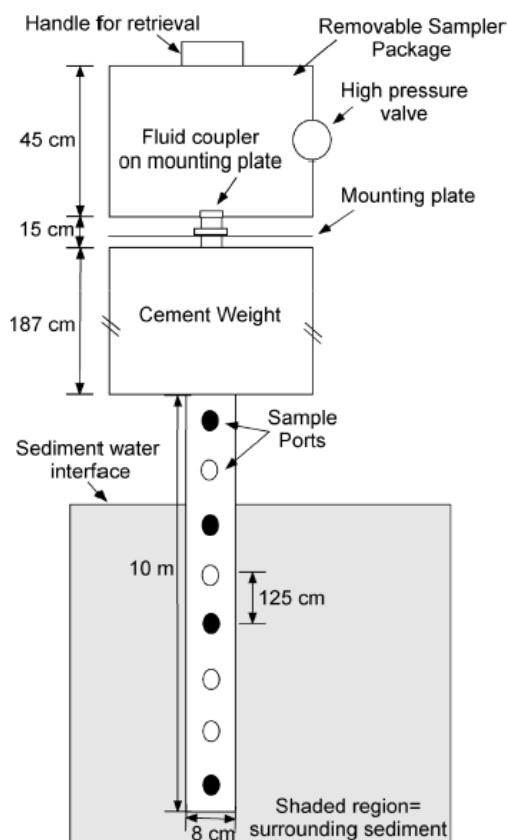


**Figure 21. The pore-fluid sampling array (PFA). (Figures from Lapham et al. 2008)**

Smaller pore-fluid samplers have been deployed using a variety of methods and expand the lateral coverage of pore-fluid geochemistry at the Observatory. Recovered water samples have since been processed yielding valuable data on the pore fluid chemistry representative of its location (Lapham et al., 2008b; 2010). Laboratory experiments demonstrate the pure structure I and structure II hydrate dissolve until conditions reach saturation (Lapham et al. 2012; 2014). Cumulatively, the laboratory and field results suggest that natural products may shield the hydrate surface preventing dissolution *in situ* (Lapham et al., 2014). The PFA design and its sampling success prompted the fabrication of a second PFA to expand the lateral coverage of the pore fluid investigation to additional areas of interest (Lapham et al., 2013). A second unit was installed during the April 2008 cruise, penetrating a fracture zone within 3m of a 10m gravity core site which yielded significant hydrates (gravity corer and PFA precision

guided by ultra-short base-line (USBL) navigation system). Smaller pore-fluid collecting devices, or landers (Figure 22), and “peepers” (Figure 23) were among the sensors deployed on the MMR/CMRET-designed ROVARD that was recovered in June, 2011. Additional replacement osmoboxes as well as smaller pore-fluid sampling units - landers and peepers – have been deployed at MC118 and elsewhere (see Final Report for Phase 4, Task 4, *Experimental Results and Discussion*).

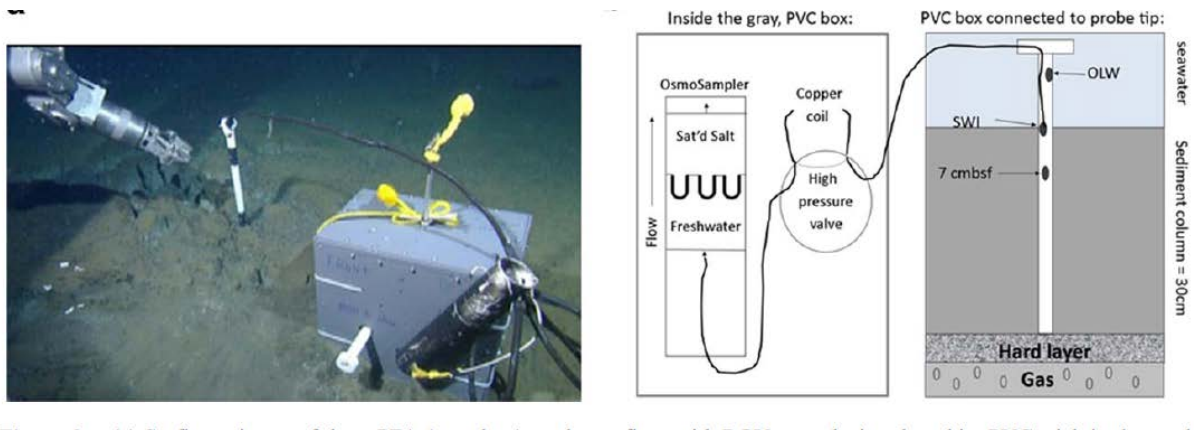


**Figure 22. Newly designed PFA system with a smaller footprint designed to be deployed and retrieved by ROV. This image shows the PFA box deployed at Cascadia Margin. (Figure from Lapham et al., 2013)**

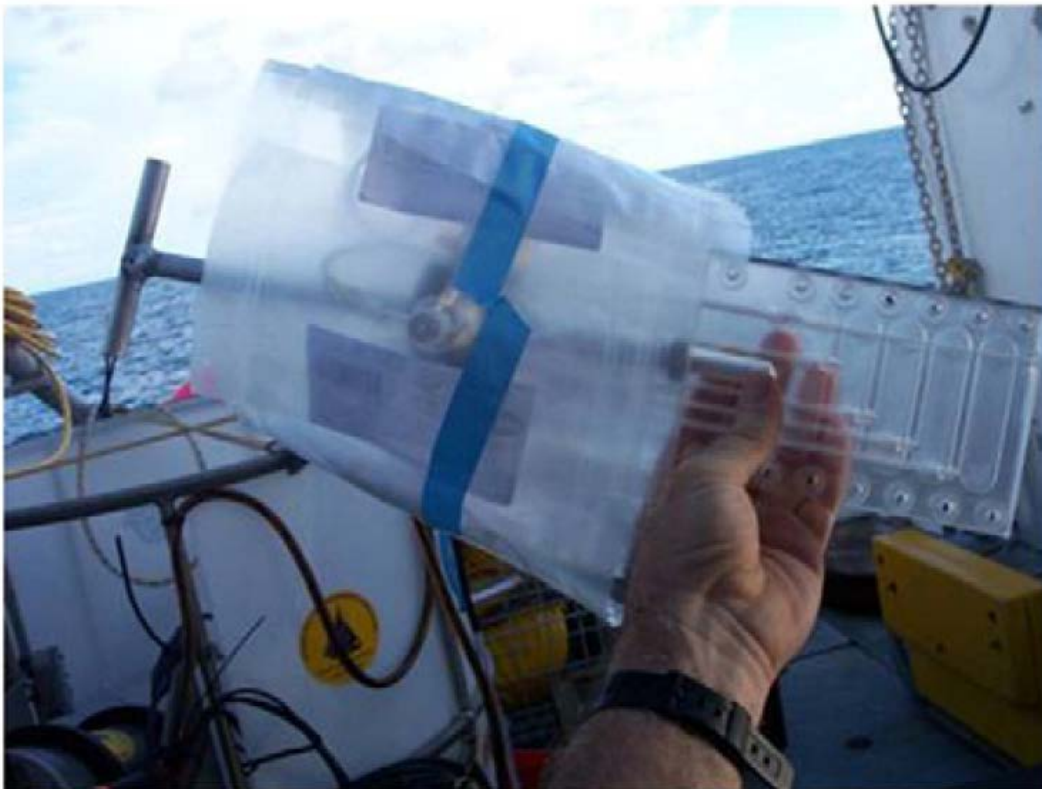


**Figure 23. Peeper device for collecting sediment porewater (Figure from Lapham et al., 2010).**

This device is also under consideration for adaptation to collect microbial growth information. Over fifty gravity and push cores have been collected across the site and their porewaters analyzed. This information contributed to the development of a seep evolution model (Lapham et al. 2008) and eventually a methane flux map (Wilson et al. *in press*), Figure 24.

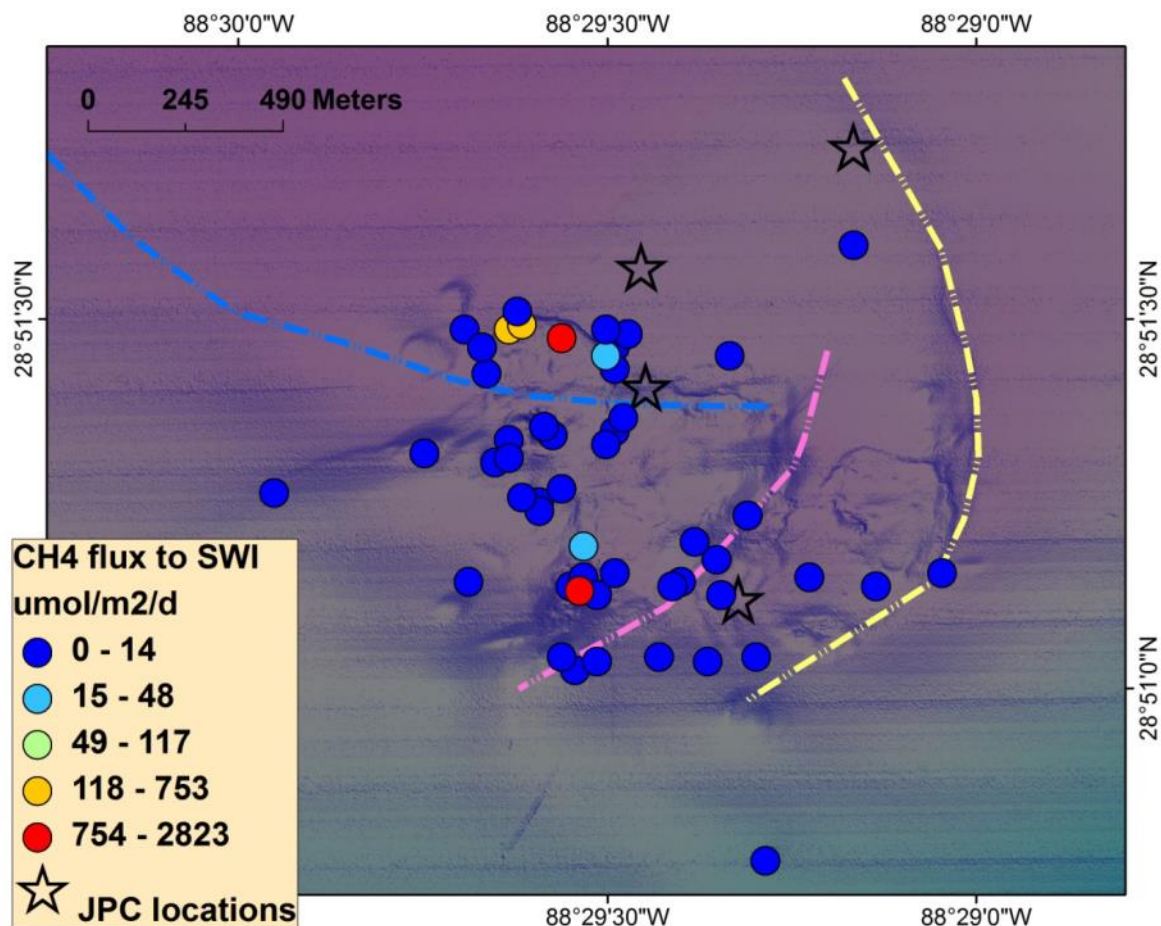


**Figure 24. Flux map developed from gravity and push cores and 4 Jumbo Piston Cores collected across Woolsey Mound. (Figure from Wilson et al., *in press*).**

The Noakes Lander with Automated Biological/Chemical Monitoring System (ABCMS) was used quite successfully in October, 2011, to evaluate several sites under consideration for installment of the CSA. The Noakes system - which now includes a downward-looking camera - operated for 9 hours recovering visual data continuously and samples of water-column suspended material, on demand. Although the membrane induction mass spectrometer (MIMS) did not function, the electronics to and from it did. The system was taken out again on the final cruise for this project with a newly fabricated reduced-in-size MIMS. Although the system's battery had to be replaced, it worked as hoped. The camera was able to locate a bubble plume, the MIMS recorded two methane peaks and the software communicated the command to collect data via the high throughput filter (see Phase 4, Task 5, *Experimental/Results and Discussion*).

The University of California, Santa Barbara (UCSB) 3-D sonar rotator was also included on the final cruise for this project. Plagued with difficulties and especially electronics failures in the past, this system was finally successful. Researchers were able to image bubble streams and to distinguish them from the tether and from instrument signals. This system had been used successfully in shallow water (<200m) but this was its first use in deep water. A complete report appears as Phase 4 Task 6 in the *Experimental/Results and Discussion* section.

### **Biological Experiments and Monitoring**

The importance of microbial activity to the production and stability of hydrates has been acknowledged by Consortium researchers since the early discussions of the MS/SFO. The possibility of adding a microbial component to the station was discussed for several years prior to the addition of microbial researchers to the Observatory project via NIUST. Four projects were funded and provided ship time with the Consortium beginning in September, 2006, with deployment of experiments on the seafloor with the JSL. Their work continues using the NOAA/NIUST specially designed ROV, station service device (SSD), for deployment and recovery. The Consortium (via NIUST) has provided the microbial team with access to the site by making a portion of Consortium-requested ship time and ROV/SSD submersible time available for their use. Microbial collectors have been deployed and several sampling efforts have succeeded in beginning to elucidate the microbial activities at the observatory site. In this way, the MS/SFO becomes a three-way observatory providing geophysical, bio-geochemical, and microbial data from the sea-floor, eventually on a continuous, near real-time basis. This additional dimension has greatly expanded the utility of this multi-disciplinary facility and improved our ability to investigate and model the interrelated physical, chemical and biological processes at work at this active carbonate - hydrate mound complex, complete with dynamic hydrocarbon fluid venting.

In 2009, serious attention began to be given to the macrofauna at MC118. Through collaborations with other researchers and the efforts of new student interns, we are beginning to unravel the history of the fauna on the seafloor, their ecology and history and how these factors reveal the venting history at MC118. Four submersible cruises to MC118 in 2010-11 revealed much more diversity and complexity on the seafloor than previously known. Additional cruises and projects, mostly carried out through affiliates of the CMRET, occurred through the end of 2011 with the CMRET providing maps, bathymetry, locations of seafloor instruments, hazards, etc. to researchers from a variety of institutions, participating in Deep Water Horizon recovery work at MC118. In 2012, UVTC and STRC cooperated on a *Mola Mola* AUV cruise that included a photo-survey of the western craters at MC118. The high definition photos reveal the seafloor and its inhabitants in incredible detail, as illustrated in Figures 25, 26, 27. Figure 28 illustrates the distribution of seafloor types - as determined from video and sampling - including hardground at MC118, where biota are found in abundance.





**Figure 25.** *Bacterial mats and clams form part of a complex community on the seafloor at MC118.*

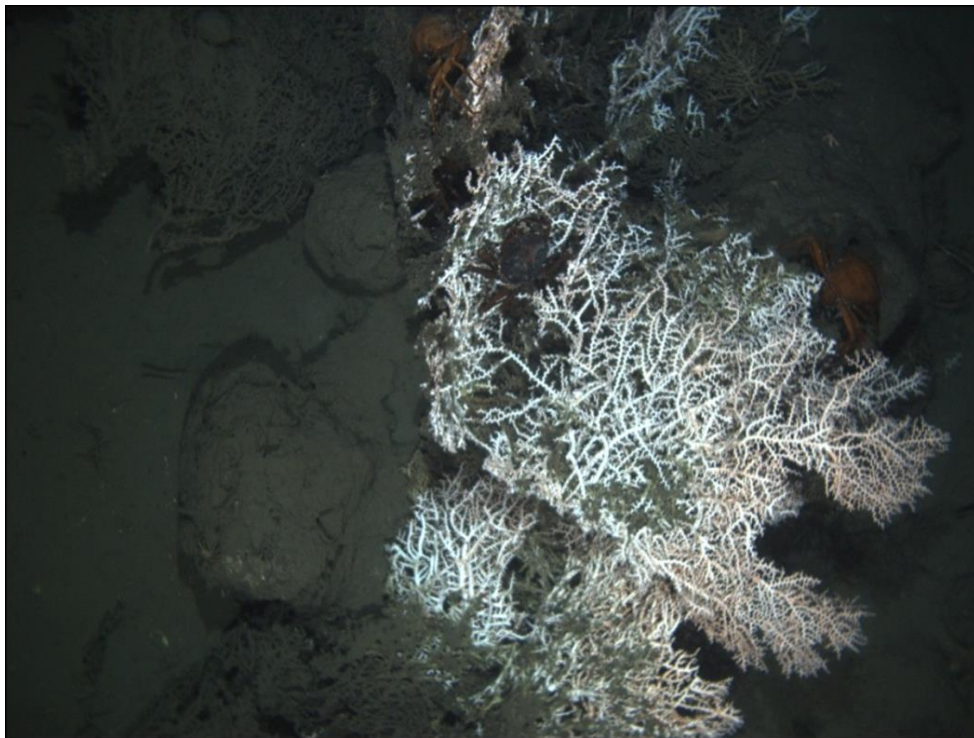


**Figure 26.** *Deep Sea Corals at MC118. Reefs provide habitat, recruitment and nursery functions for a range of deep-water organisms including commercial fish species. Deep sea corals may provide windows into past environmental/ecological conditions. This colony of Madrepora oculata, or zig-zag coral, is a rare find in the Gulf.*

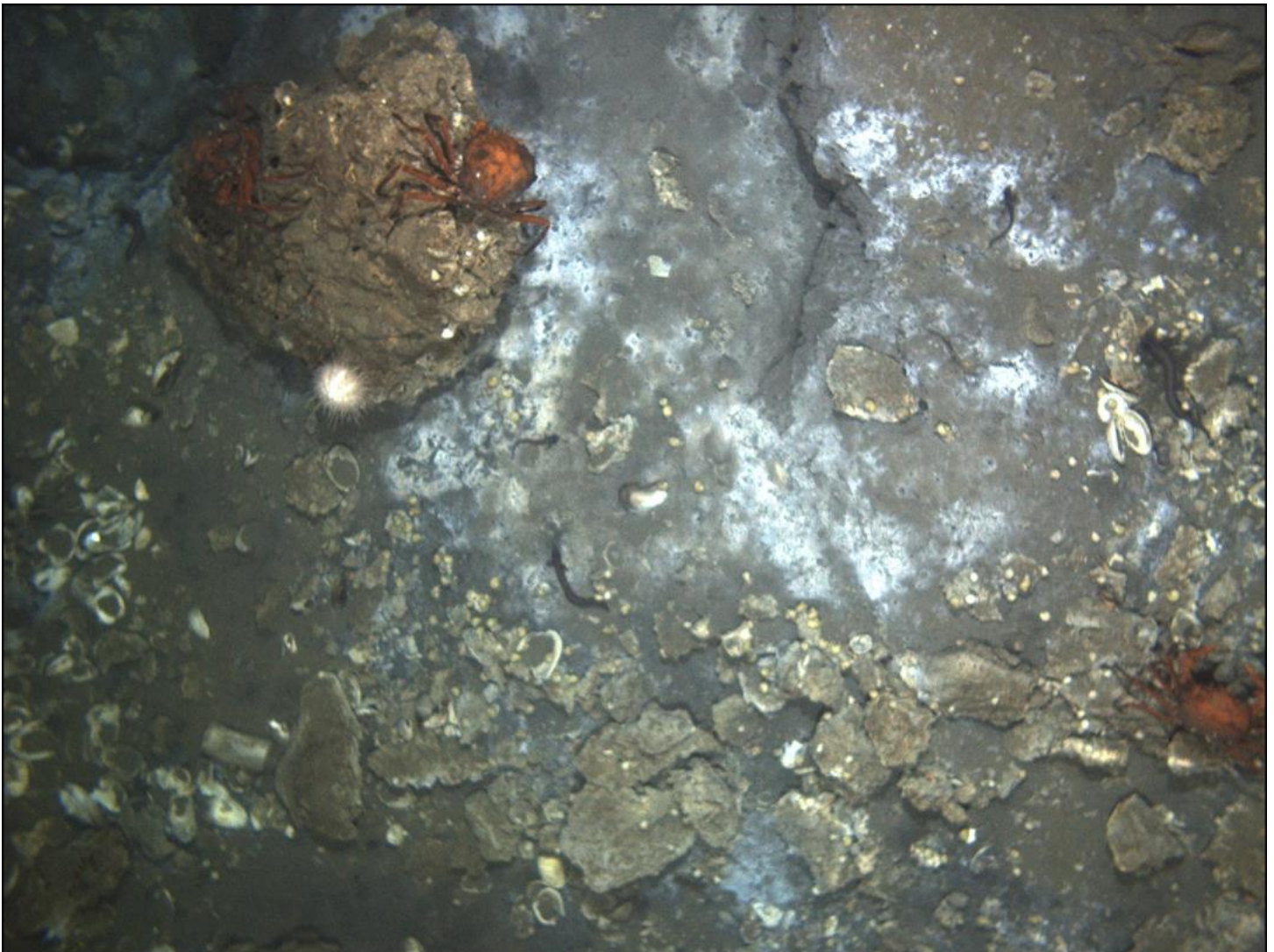


*Figure 27. Abundant life is found at the crater complexes on Woolsey Mound. Fish, crabs, echinoderms, chemoautotrophic snails and abundant bacterial mat have been and continue to be reported, and where possible, mapped over the mound.*



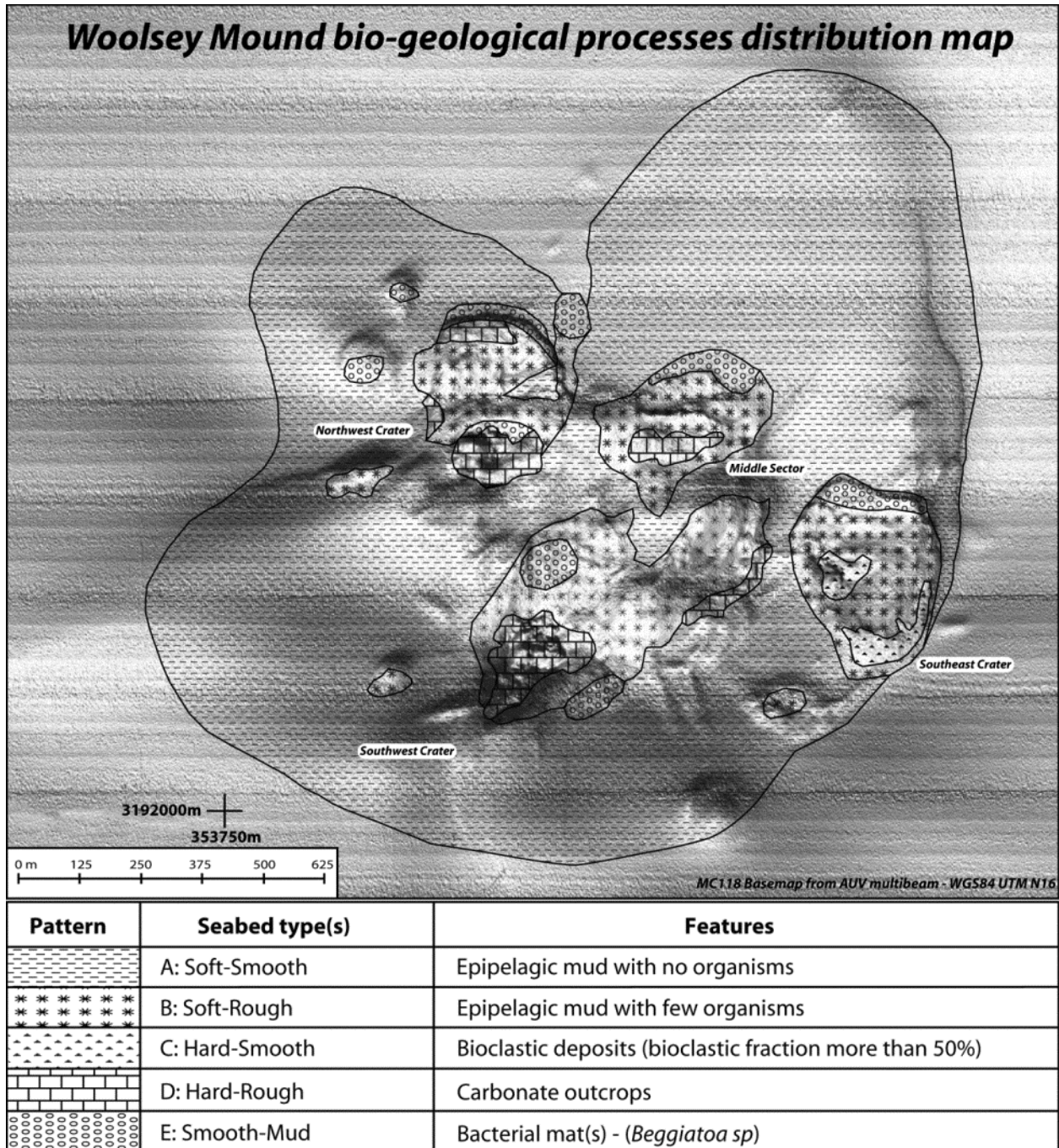


**Figure 28.** A conceptual model of the spatial distribution of biogeological process throughout the Woolsey Mound. Major morphological units, sediment types and biological habitat are mapped, based upon video data, classes of acoustic backscatter anomalies and, where available, sediment core data. The model provides regionalization of the biogeological processes occurring at the mound and highlights significant differences within the three complexes (from Macelloni et al., 2013).

## Vehicle/Support Systems

Several vehicles and other support systems serve to make deployments and recoveries possible at the MS/SFO. The SSD, I-SPIDER, landers including the ROVARD and ABIL, Rochester fiber-optic cable, pop-up system and probes are included in this category. The integrated data power unit (IDP) and the data-recovery system (DRS), designed primarily to facilitate data-recovery, are being redesigned to accommodate the HLAs. In addition, CMRET has been involved in every cruise that the UVTC has executed with the AUVs *Eagle Ray* and *Mola Mola*. The vehicles are described, briefly, below.

*The I-SPIDER* or Integrated Scientific Platform for Instrumental Deployment and Emergency Recovery is a battery-powered, tethered system that communicates to the surface control station via fiber optic cable. In its standard format, it holds lights and video cameras outstretched on eight arms. It contains systems for navigation, payload interface, and precision instrument deployment. The I-SPIDER is capable of carrying a lander to a seafloor target (Figure 29) and holding it until an ideal location or specific target is confirmed, visually.

The *I-SPIDER* features include:

- 6 real time video cameras, arrayed in a pattern to give a near-hemisphere of visual coverage of the seafloor and near-seafloor water-column,
- 7 high output LED lights to combat the complete darkness of depths greater than 200 meters beneath the sea's surface and down to more than 2000 meters operating depth,
- Ultra-short baseline (USBL) navigation providing extreme accuracy and repeatability in a variety of deployment and recovery schemes,
- Altimeter (Benthos) for low altitude bottom reconnaissance,.
- High-resolution sonar (Kongsberg) for obstacle-avoidance and to obtain target lock long before visual contact is made,
- Modular battery packs for quick turn-around between deployments as well as stack-ability for high-power draw or long duration missions,
- Customized surface-controlled release mechanism for deployment operations,
- Large payload area for the addition of specially requested devices and sensor arrays,
- Electronic Control Unit/Payload Interface with internal compass and attitude sensor (OceanServer) as well as systems health monitoring with communication to the surface by means of a single mode fiber-optic uplink,
- Payload support, i.e. auxiliary fiber-optic channel, six serial channels (four RS232, two RS422 or 485), 10/100/1000 Ethernet line and custom power feeds,
- Utilizing high-strength, armored cable connected to the ship's winch to meet the challenges of extreme snap-loads in ever-changing sea states as well as heavy payloads and large profile instruments with a working load near 10,000lbs and a breaking strength of near 40,000 lbs.,
- User-friendly surface control/navigation system contained in a single armored case providing rapid mobilization and demobilization,

- Auxiliary large-screen monitor for real-time visualization and judgment of areas of opportunity,
- 4 TB 16 channel high-resolution DVR system for archiving dive operations and device placement.

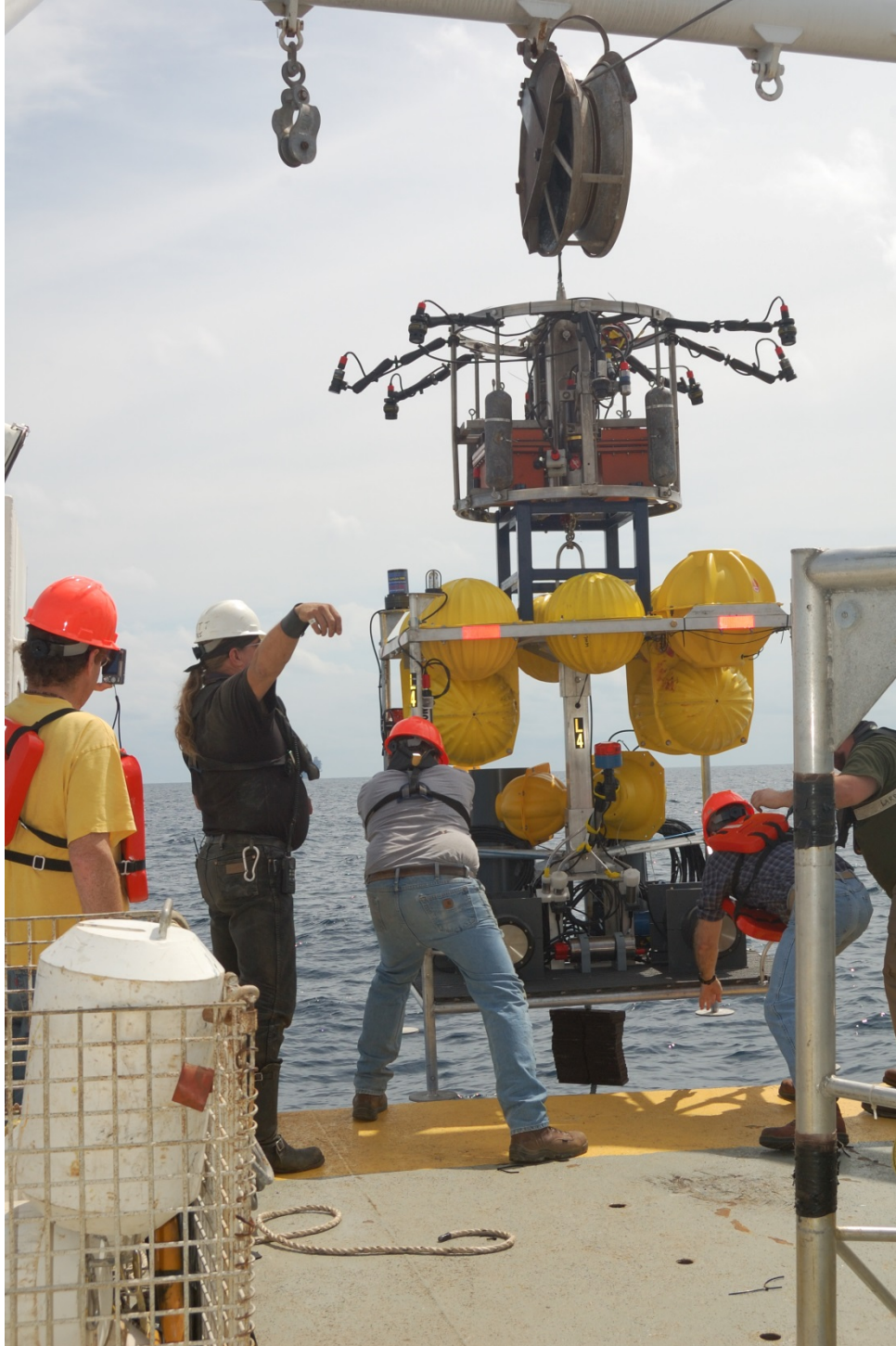


*Figure 29. A fully loaded lander about to be deployed via the I-SPIDER.*



The *Station Service Device (SSD)*, NOAA/NIUST; The SSD is a specially designed ROV system for use on level-two-equipped, non-dynamically positioned vessels (available at a much lower day rate than a level one) for the purpose of deploying station sensors and support equipment (see Figures 3, 30 and 31). Battery change-out and general maintenance are also among the tasks of the SSD. The system differs from conventional ROVs in that, instead of being suspended in the usual manner, it works off a clump-weight/pressure compensated battery (its power supply), lowered to the seafloor. A small, specially designed ROV is maneuvered from the clump-weight platform, powered by the battery and controlled *via* an umbilical, within a limited working radius (50m), but sufficient to carry out the required tasks of the station. Significant development of this system has taken place and its versatility continues to be apparent: From its first mission in 2007 - when it recovered microbial experiments from the seafloor - to its current capability of collecting targeted push cores and seafloor samples, by virtue of its navigation capabilities and multiple cameras the SSD continues to be adapted to Consortium researchers' needs. During the June, 2009 cruise, ***over 30 hours of resistivity data were acquired using the SSD as the transport for the 1100m towed cable (the first time such a survey has ever been attempted with an ROV).*** In April, 2010, the SSD successfully carried equipment on the seafloor to the node designed to accommodate the HLA data-loggers, deployed an array spool, collected push-cores and collected many hours of seafloor video images. In September, 2010, the ROV worked in tandem with the ROVARD lander to install geochemical chimney sampler arrays at specific, high value sites on the seafloor.

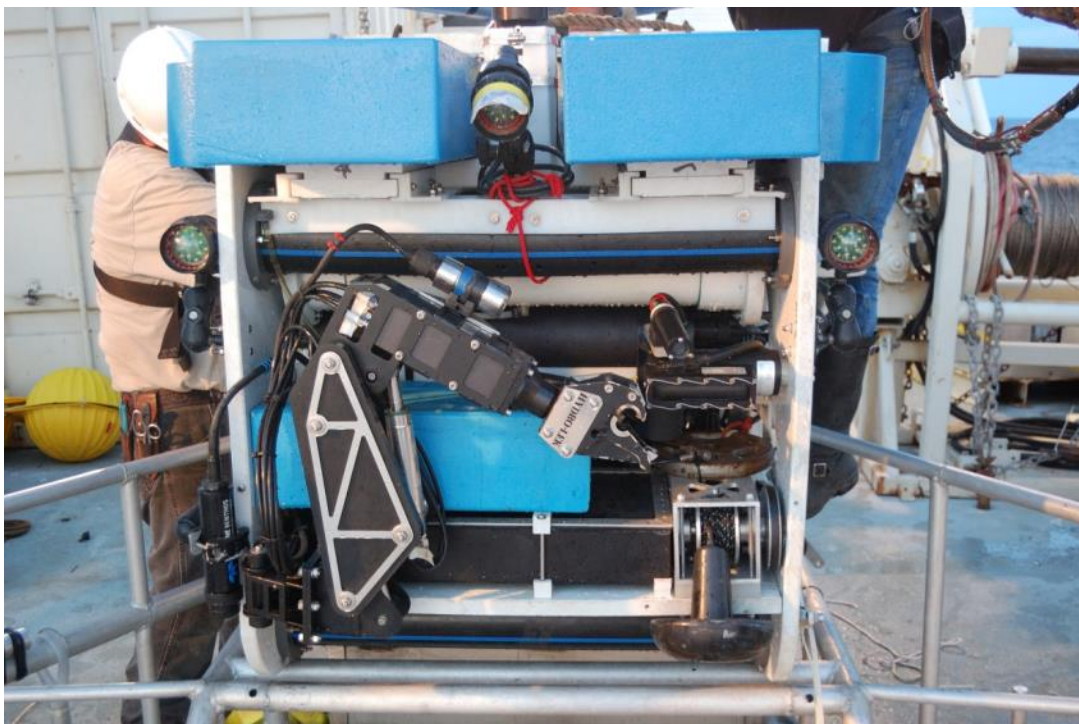


***Figure 30. The SSD undergoes a series of ondeck tests prior to every dive. Note the new camera on the manipulator arm, center of image.***

Extensive upgrades to the SSD were designed to enable it to function at greater depths (up to 2,000m) and with increased maneuverability. A new camera, lights and optical multiplexers for improved imaging and reconnaissance capabilities have been installed. As mentioned earlier, the July, 2012 cruise tested these systems at 1,600+m and the vehicle functioned nearly flawlessly.

*The Station Service Device features include*

- 3 real time video cameras, including forward, arm-cam, and vehicle-tether-directed,
- high output LED lights to combat the complete darkness of depths greater than 200 meters beneath the sea's surface and down to more than 2000 meters operating depth,
- Ultra-short baseline (USBL) navigation providing extreme accuracy and repeatability in a variety of deployment and recovery schemes,
- Altimeter (Benthos) for low altitude bottom reconnaissance,
- High-resolution sonar (Kongsberg) for obstacle-avoidance and to obtain target lock long before visual contact is made,
- 5-function manipulator arm,
- Additional hydraulic payload capabilities,
- Push-coring capability and rack,
- Wire-cage transport capability,
- Ballast and trim, operated by the hydraulic system,
- syntactic foam for increased buoyancy and payload capacity,
- retrievable drop-weight system (the yo-yo) added for lifting and repositioning heavier payloads on the seafloor,
- User-friendly surface control/navigation system contained in a single armored case providing rapid mobilization and demobilization,
- Auxiliary large-screen monitor for real-time visualization and judgment of areas of opportunity,
- 4 TB 16 channel high-resolution DVR system for archiving dive operations and device placement; captures and displays multiple video feeds simultaneously.



**Figure 31. The SSD team effects a smooth vehicle recovery.**

### *The ROV Combination*

The SSD is used for manipulating lander systems, completing/fine-tuning deployment configurations, throwing switches, and preparing landers and/or instrument packages for recovery. This ROV consists of several thrusters, cameras, and a hydraulic manipulator. When used in concert with the I-SPIDER (Figure 32), the latter provides an overview of the work area. Upon deploying a lander, the I-SPIDER-SSD combo can sample the surroundings by pushing probes into the seafloor, carrying samplers over targets of interest, i.e. seeps, bacterial mats. Landers have been deployed, serviced, and recovered successfully - with their months' of data - by the SSD and I-SPIDER.

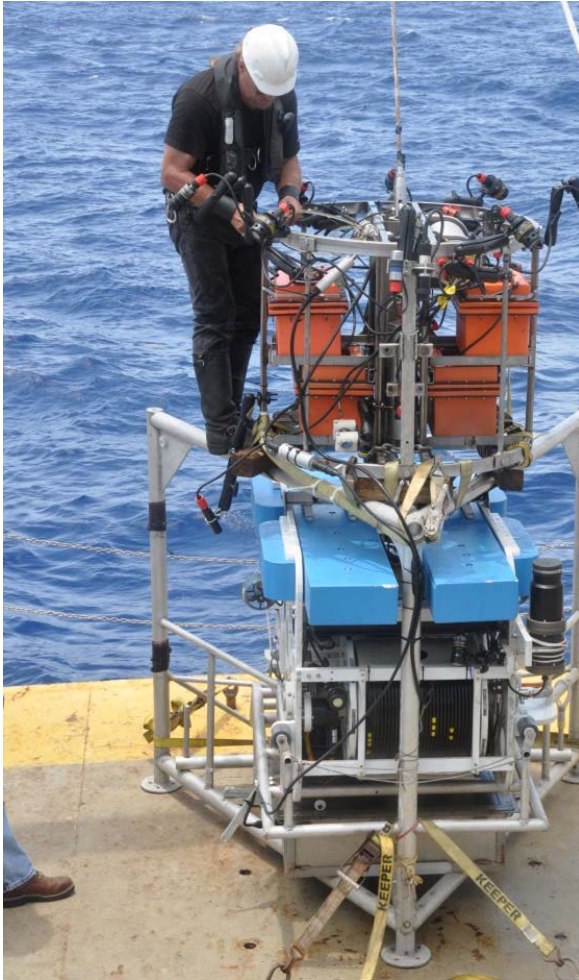
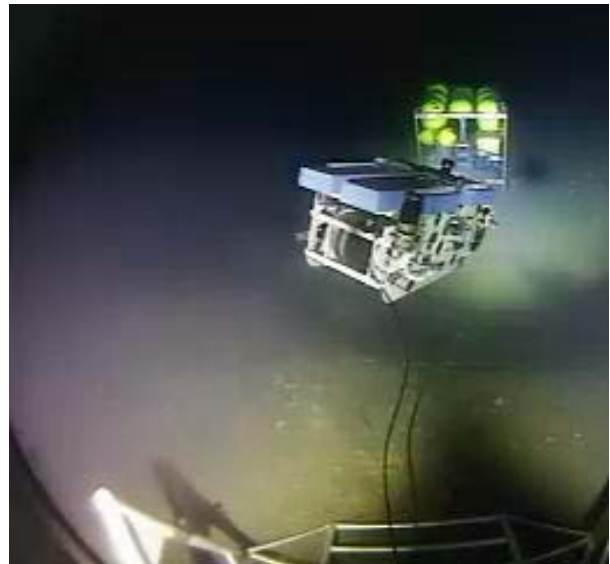


**Figure 32. The SSD being rigged for deployment via the I-SPIDER (left). The I-SPIDER “watches” as the SSD flies from its cage to service a lander on the seafloor. (photos from Lowe, et al., 2013).**



*Landers (BOEM, NOAA, DOE):* Landers are one of the areas of primary expertise for the CMRET shop. Depending on the task(s) to be performed on the seafloor or in the water-column, the lander team can build or rebuild a lander of their own design or of another's. The ABIL (Figure 4), and ROVARD (Figure 19) were designed by the MMR/CMRET shop and the ECOGIG landers adapted to perform specific functions for researchers while lending themselves to servicing by the MMR/CMRET ROVs. From task through design, construction, testing, operation, deployment, servicing, documentation of performance and recovery, landers have made many, many of the tasks of this project possible.



*Autonomous Underwater Vehicle (AUV), NOAA/NIUST:* The AUV “*Eagle Ray*”, Figure 33, acquired from ISE (International Submarine Engineering) and operated via a cooperative venture between NOAA, and NIUST, has completed sea trials of its basic operating, navigation and seafloor mapping systems and has progressed to working vehicle status. UVTC has now conducted several seabed mapping projects, which have included MC118. The ISE design is capable of operating to depths of 2200m and is equipped with a large instrument pay load capacity, making the vehicle ideal as a test platform for a variety of sensors. The MMRI division of NIUST, STRC, is responsible for, among other things, developing new tools and sensors for the AUV, particularly systems applicable to the exploration of seafloor occurrences of gas hydrates and hydrocarbon seeps and vents. In June, 2009, the *Eagle Ray* carried the Woods Hole Oceanographic Institute’s (WHOI) mass spectrometer during its survey of the near-seabed (6m above seafloor) water column geochemistry at the MC118 test site. In progress, is the adaptation of the CMRET, shallow-source/deep-receiver (SSDR; BOEM) high resolution seismic system (deep receiver component) for installation on the AUV. This innovation is expected to greatly improve stability, near seafloor operation, data acquisition to subbottom depths of 500-700m, navigation accuracy, noise reduction and reduction of survey time by a factor of four. A PPchirp system, has been designed, built and installed on the *Eagle Ray*. A test cruise was executed in July, 2011, data recovered and evaluated for performance of the software (Phase 4, Task 2). A landmark cruise was conducted in September-October, 2012 during which ***complete multibeam and polarity-preserving chirp surveys – including a high-resolution survey conducted at 15m above seafloor – returned data of unparalleled detail*** (see Phase 4, Task 2.3). The MMRI-NIUST team continues to work with UVTC to improve the PPchirp software and processing development.

*Mola Mola AUV, NOAA/NIUST:* This vehicle (Figure 34) is designed primarily as a visual survey tool. The *Mola Mola*’s primary capability is to photograph the seafloor on a continuous basis. Mosaics of the seafloor can then be made from the series of still photographs. In 2012, The *Mola Mola* performed photosurveys, complete with superior navigation (necessary for mosaicking as well as population and ecological studies) over two blocks in Mississippi Canyon. Four missions returned photos of extraordinary detail. A complete photomosaic of the Woolsey Mound was made in 2012.

*The Rochester fiber-optic cable.* This piece of equipment is vital to all our operations that require live-streaming of information from the seafloor to the support vessel. The functions of the SSD, for example, depend upon the live connection to the lab for operations: lights, cameras, ballast, pitch, roll, manipulator arm, etc. Since the failure of the original Rochester Cable in September, we have acquired a new, three-fiber replacement, .750” diameter and 3600m in length, for access to 2,000m water depth. Several subcontractors have developed their systems to function with this powerful system: University of Georgia’s lander, UCSB’s sonar scanner, the SSD, the I-SPIDER all depend upon this vital component of our at-sea “tool box” for performance of their basic functions.



*Figure 33. The AUV team prepares to launch the Eagle Ray AUV from the Pelican's main deck via the launch and recovery system (LARS), designed and built specifically for it.*

*Figure 34. The AUV team prepares to launch the Mola Mola photo-AUV from the Pelican's upper deck.*



## REFERENCES

(References for individual reports follow the appropriate section directly)

- \*Battista, Bradley, Camelia Knapp, Tom McGee and Vaughn Goebel, 2007: Application of the Empirical Mode Decomposition and Hilbert-Huang Transform to seismic reflection data. *Geophysics*, 72(2), pp. H29-H37.
- Camilli, R., L. Macelloni, V. Asper, M. Woolsey, J. Williams, A. Diercks, C.B. Lutken, K. Sleeper, 2009, Discovery and characterization of cold seeps using a mass spectrometer operating aboard an autonomous underwater vehicle, AGU fall meeting, San Francisco, CA, December, 17, 2009.
- \*Carrière, Olivier and Peter Gerstoft, 2013, *Deepwater subseafloor imaging using active seismic interferometry*, *Geophysics* 78,Q15-Q24. [.dx.doi.org/10.1190/geo2012-0241.1](https://doi.org/10.1190/geo2012-0241.1)
- Caruso, Simona, M.S. theses, 2007, *Definition of Mississippi Canyon Block 118 Seafloor bio-geological processes, combining acoustic, video, and geological data*. University of Rome, La Sapienza.
- Knapp, James H., Camelia C. Knapp, Leonardo Macelloni, Antonello Simonetti, Carol Lutken, 2010, *Subsurface Structure and Stratigraphy of a Transient, Fault-Controlled Thermogenic Hydrate System at MC-118, Gulf of Mexico* AAPG 2010 Annual Convention Oral Presentation, Abstracts Volume, p.134.
- Lapham, LL, JP Chanton, CS Martens, PD Higley, HW Jannasch, and JP Woolsey (2008) Measuring temporal variability in pore-fluid chemistry to assess gas hydrate stability: development of a continuous pore-fluid array. *Environmental Science and Technology* **42**: 7368-7373
- Lapham, LL, JP Chanton, CS Martens, K Sleeper, and JR Woolsey (2008b) Microbial activity in surficial sediments overlying acoustic wipeout zones at a Gulf of Mexico cold seep. *Geochemistry Geophysics Geosystems* **9**(6): 1-17
- Lapham, LL, JP Chanton, R Chapman, and CS Martens (2010) Methane under-saturated fluids in deep-sea sediments: implications for gas hydrate stability and rates of dissolution. *Earth and Planetary Science Letters* **298**(3-4):275-285
- Lapham, LL, RM Wilson, and JP Chanton (2012) Pressurized laboratory experiments show no stable carbon isotope fractionation of methane during gas hydrate dissolution and dissociation. *Rapid Comm Mass Spec* **26**: 32-36
- Lapham L. L., Wilson R. M., MacDonald I. R., and Chanton J. P. (submitted 2013) Gas hydrate dissolution rates quantified with laboratory and seafloor experiments. *Geochimica et Cosmochimica Acta* in review.
- Lapham, L., R. Wilson, J. P. Chanton, C. Paull, and M. Riedel, Temporal variability of in situ methane concentrations in gas hydrate bearing sediments near Bullseye Vent, In preparation for *Global Biogeochem. Cycles*.
- Lowe, P. M., M. Woolsey, R. Jarnagin, C. B. Lutken, B. Noakes, L. Overstreet, S. Tidwell, Development of I-SPIDER: a towed platform for video survey and instrument placement, Proc. OCEANS Conf. 2013.
- Lutken, Carol B., Leonardo Macelloni, Laura Lapham, Simona Caruso, Mariangela Lodi, Richard Camilli, Vernon Asper, Arne Diercks, Camelia Knapp, Jim Knapp, 2010, *Monitoring Seafloor Morpho-Geological Evolution of the MC118 Hydrate/Carbonate Mound via Multiple AUV Missions*, AAPG 2010 Annual Convention Poster Presentation, Abstracts Volume, p.155.

\*Lutken, Carol B., Marco D'Emidio, Leonardo Macelloni, Michela Ingrassia, Martina Pierdomenico, Vernon Asper, Arne Diercks, Max U. Woolsey, Roy Jarnagin, 2013, *Challenges in imaging the deep seabed: examples from Gulf of Mexico cold seeps*, Transactions of the GCAGS, New Orleans, 2013.

\*Macelloni, L., S. Caruso, L. Lapham, C. Lutken, C. Brunner, and A. Lowrie, 2010, *Spatial distribution of seafloor biogeological and geochemical processes as proxy to evaluate fluid-flux regime and time evolution of a complex carbonate/hydrates mound, northern Gulf of Mexico*: Gulf Coast Association of Geological Societies Transactions, v. 60, p. 461-480.

\*Macelloni L., Simonetti, A., Knapp, J.H., Knapp, C.C., and Lutken, C.B., 2012. *Multiple-Resolution Seismic Imaging of a Shallow Hydrocarbon Plumbing System, Woolsey Mound, Northern Gulf of Mexico*. Marine and Petroleum Geology 38: 128-142.

Macelloni, L., Lutken, C. B., Garg, S., Simonetti, A., D'Emidio, M., Wilson, R., Sleeper, K., Lapham, L., Lewis, T., Pizzi, M., Knapp, J., Knapp, C., Brooks, J. and McGee T.M., submitted to JGR, *Geothermal regime and hydrate stability zone of Woolsey Mound (northern Gulf of Mexico): A transient, thermogenic, fault-controlled hydrate system*.

\*Macelloni, Leonardo, Charlotte Brunner, Simona Caruso, Carol Lutken, Marco D'Emidio, Laura Lapham, 2013, *Spatial distribution of seafloor biogeological and geochemical processes as proxies of fluid flux regime and evolution of a carbonate/hydrates mound, northern Gulf of Mexico*, Deep Sea Research, Part 1, Manuscript Number: DSR1-D-12-00118R1.

Rogers, R.E., and Lee, M.S., 2001: *Biosurfactant from Microbial Activity in Ocean Sediments Enhances Gas Hydrate Formation*. Presented at The Geological Society Earth System Processes- Global Meeting, Sponsored jointly by the Geological Society of London and Geological Society of America, Edinburgh, Scotland, June 24- 28, 2001.

Simonetti, Antonello, James H. Knapp, Camelia C. Knapp, Leonardo Macelloni, Carol B. Lutken, 2011, *Defining the hydrocarbon leakage zone and the possible accumulation model for marine gas hydrates in a salt tectonic driven cold seep: examples from Woolsey Mound, MC118, northern Gulf of Mexico*, Proceedings of the 7th International Conference on Gas Hydrates (ICGH 2011), Edinburgh, Scotland, United Kingdom, July 17-21, 2011.

Simonetti, Antonello, James H. Knapp, Camelia C. Knapp, Carol B. Lutken, 2012, *4d seismic imaging of a thermogenic gas hydrate system in the northern Gulf of Mexico (Woolsey Mound, MC118)*, The Gordon Research Conference on Natural Gas Hydrate Systems, Ventura, California, March 18<sup>th</sup>-23<sup>rd</sup>

Simonetti, Antonello, James H. Knapp, Michael Riedel, Camelia C. Knapp, 2012b, *Short and long-term dynamics of a thermogenic gas hydrate system in a cold seep area in the Gulf of Mexico deep waters (Woolsey Mound, MC118)*, 15th Annual AAPG-SEG Student Expo in Houston, Texas, USA, 17-18 September 2012.

\*Simonetti A., 2013, *Spatial and Temporal Characterization of a Cold Seep-Hydrate System (Woolsey Mound, Deep-Water Gulf of Mexico)*, PhD Dissertation, University of South Carolina, Columbia, South Carolina, USA, 14 November 2013, 100p.

\*Wilson, Rachel, Leonardo Macelloni, Antonello Simonetti, Jeffrey Chanton, Jim Knapp, Laura Lapham, Carol Lutken, Ken Sleeper, Charlotte Brunner, Chris Martens, Marco D'Emidio, 2013, in press, *Integrating geochemical profiles with seismic surveys to identify subsurface methane sources and migration pathways*, G-Cubed, (DOI: 10.1002/2013GC004888).

## **EXPERIMENTAL/RESULTS AND DISCUSSION**

(Note: Figures are numbered consistently within individual reports)

### **PHASE 1 Tasks for FY 2006:**

#### **Task 1: Design and Construction of four Horizontal Line Arrays**

Evolution of Horizontal Array development for Installation in the Gas Hydrates Research Consortium Sea Floor Observatory at MC118.

(Subcontractor, Specialty Devices, Inc., Wiley, Texas; Paul Higley, PI)

##### **Introduction**

The Horizontal Line Array (HLA) design evolved from the original 2007 concept as an experiment to generate shear waves in the seafloor and record them with a horizontal array. This concept was to utilize shear wave sensor platforms developed for the 3-D seismic industry. These sensors had extreme shear sensitivity and included a hydrophone making a 4C element that in theory was ideal for the desired gas hydrate monitoring plan at the time. The sensors were to be deployed as 4 of the 4C sensors in each of two long horizontal arrays with the possibility of adding 4 hydrophones between the 4C sensors. The sensors were tested in Mobile Bay on an MMRI sled system in shallow water. This test proved the capabilities of these sensors. It also highlighted the difficulty of adapting these sensors for use in our application. The sensors were well integrated into the rest of the seismic industry application and were not easily adaptable for use as nearly stand-alone sensors. The separation of the sensors from the intended seismic package was being addressed both by the manufacturer and by SDI. Considerable software and electronics were needed to adapt these sensors for use in a long term deployment. During this time, the determined needs of the observatory were changing.

The project plan for the HLAs had included building 2 arrays of 4C sensors, each 400 meters long to be arranged as an "L" pattern. This plan was modified to include more than 2,000 meters of hydrophone arrays in the form of four hydrophone arrays arranged as an "X" pattern. Each array was to be at least 500 meter long and contain 16 hydrophones in each of the four arrays for a total of 64 hydrophones deployed. New cable designs were developed to meet these program needs and a deployment concept developed. Four new all hydrophone arrays were built. Several deployment techniques were developed and prototype deployments tested. The deployment centered about a four array set of cables which would utilize the SSD ROV to connect each to the IDP; individually deployed cables were lowered to the IDP, connected and then deployed in the desired pattern with the SSD. This final approach was used during the 1<sup>st</sup> installation of the HLAs at MC118. Unfortunately this deployment was spoiled by severe weather.

##### **Evolution of the HLA array development**

The Horizontal Line Array (HLA) design was contracted in April 2007 with the plan to build two horizontal 4C arrays utilizing technology developed for these 4C sensors

during the Borehole Line Array (BLA) development project. The project plan for the HLAs included building two 400m arrays of 4C sensors. This plan was modified to include more than 2,000 meters of arrays in the form of four all hydrophone arrays arranged as an "X" pattern of 500 meter per leg.

In addition to building these arrays, efforts have continued to develop a method to deploy these arrays. The planned deployment method has evolved based on available installation vehicles. The original deployment plan for the HLAs included using a sled but has evolved into the use of the Sea Floor Observatory's SSD ROV. The preliminary concept for the deployment had all of these arrays simultaneously deployed on a HLA POD. The connections were to be made between the arrays and the Sea Floor Observatory's IDP using the SSD.



*The HLA spools and POD were built along with four hydrophone arrays. These arrays were built as two 500 meter long arrays and two 550 meter long arrays, each equipped with 16 hydrophone/preamplifier/driver elements.*



*The HLA spools fit into the "Pod" for deployment as a single unit.*





*A total of 64 hydrophones with the pre amplifier driver units (top) were built with a few spare units (center) included in the production.*

*The hydrophones were installed on the arrays (bottom).*





The hydrophone arrays were wound on the deployment spools and all arrays were pressure-tested at the SouthWestern Research Institute (SWRI) in San Antonio Texas. Some array problems were detected during these tests which were corrected and the arrays retested at SWRI.



*550 m HLA Cable on deployment Spool Arrives at SWRI (left).*

*HLA Cable in the Pressure Vessel at SWRI (right).*

### **Hydrophone Installation and Testing**

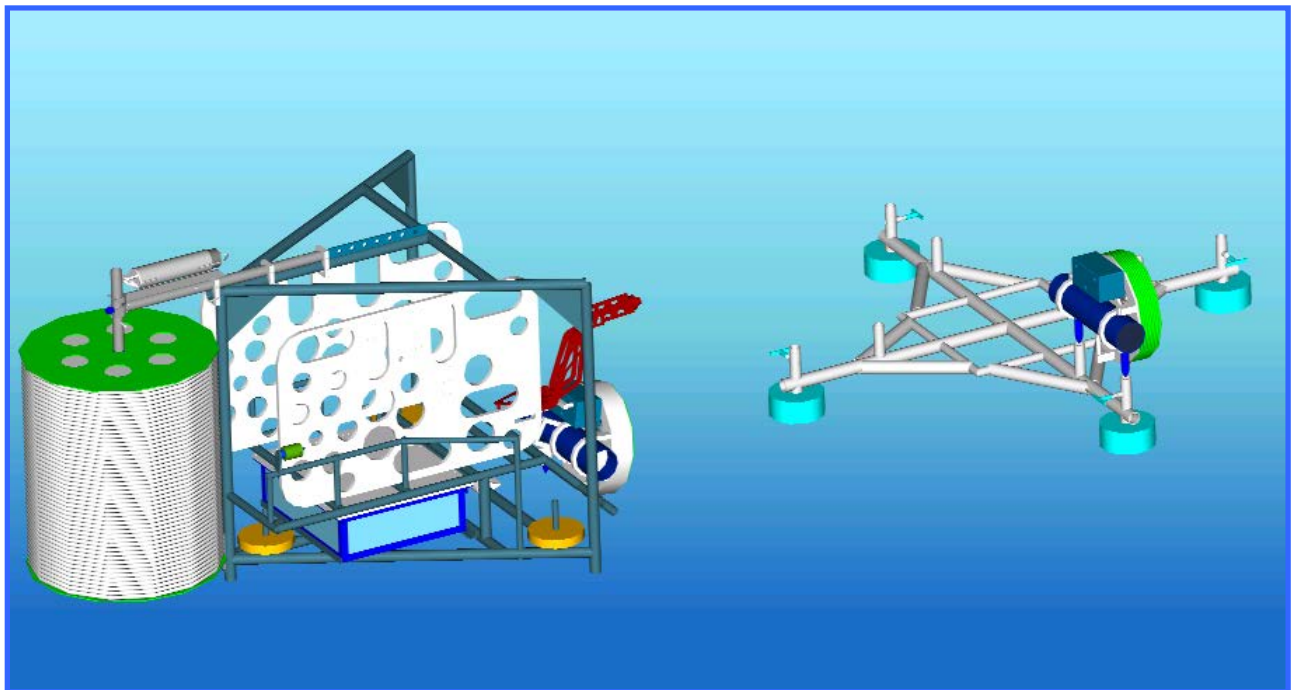
Hydrophone installation and testing of the HLA cables with the HLA Data Acquisition and Telemetry Systems (DATS) electronics packages has been underway at SDI.

### **Deployment Method**

The planned method to deploy these arrays evolved based on available installation vehicles. The original plan was to use a sled method and this later was changed to the HLA POD method using the SSD to release each cable spool from the pod and deploy the cable. A concern over the ability of the SSD to perform the associated tasks including safe release of the spool from the POD and pickup of this large an object along with a concern over deploying all four arrays at once, lead to investigation of other methods. The possible availability of the Johnson Sea Link appeared to be a better method but this option has been removed as a possibility with the retirement of the SeaLink. Industry standard work class ROV's were discussed as a possibility but this task was determined to be outside the reasonable scope of work addressed by these vehicles.

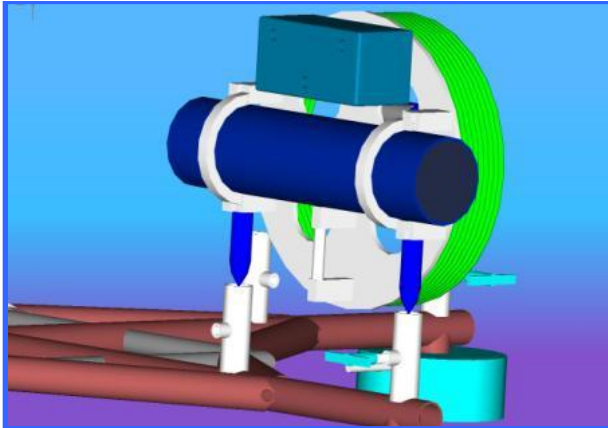
A new plan was developed to use the SSD with the SSD cage used to carry one array to the sea floor at a time and a new HLA DATS carrier that allows the SSD to swim from its cage carrying the DATS and install the HLA DATS, with HLA cable attached, to a modification of the previous HLA POD as a receptacle for the HLA DATS. The SSD could then return to its cage and trigger a release of the HLA spooled cable from the SSD Cage. The SSD would then be used to tow the cable spool away from the HLA POD, deploying the cable. This approach was pursued with a shallow water feasibility test which was conducted in Pensacola Bay.

This new deployment method includes the deployment on the seafloor of a modified HLA POD in the proximity of the Interconnection and Data Recovery (IDP) device. This HLA POD is designed to accept one HLA array Data Logger (HLA DATS) at a time in the form of an HLA Transporter. The HLA transporter included an HLA DATS and a spool of cable which allowed it to be connected to the IDP. This transporter was designed to be carried down to the seafloor by the SSD ROV with a full HLA cable carried on the back of the SSD deployment cage. This deployment operation is depicted below. The HLA POD is shown to the right with one HLA transporter in place. The SSD ROV cage with a full HLA cable on its deployment spool and an HLA Transporter mounted to the front of the SSD cage ready to be installed on the HLA POD.



***HLA deployment method: HLA POD is shown to the right with one HLA transporter in place. The SSD ROV cage with a full HLA cable on its deployment spool and an HLA Transporter mounted to the front of the SSD cage ready to be installed on the HLA POD.***

The final transporters have been designed and built. The transporter includes the make and break underwater ROV compatible connector which mates the HLA DATS to the IDP. The SSD cage was modified to include an HLA array spool deployment capability.



*The concept design of the Transporter. The design (left) is illustrated along with the actual transporter (right).*



*The HLA Spool on the SSD Cage (left) and loaded with cable (right).*

### **Deployment Attempt**

Two closely timed cruises occurred in September 2010. The later cruise included an inspection dive to verify the location and condition of the previously deployed IDP and HLA POD assemblies at MC118.



## Inspection Dive Recovery

With all sea floor equipment in good condition and the operation status of the IDP checked via acoustic modem, the 1<sup>st</sup> HLA array to be deployed was assembled on the SSD ROV. Along with the HLA array, the HLA DATS “transporter”, the HLA DATS, and the interconnect for the IDP were installed on the SSD.



*SSD Dive 37: HLA POD and IDP Inspection Dive*

The deployment configuration has the HLA array wound on a deployment spool which is mounted on the back of the SSD deployment cage. The array cable extends to the front of the SSD deployment cage and terminates at the HLA DATS which is mounted in its “transport.” This transport carries both the DATS and the interconnect cable and connector to interface the DATS to the IDP. A set of syntactic floats on the “transporter” make the weight in water nearly neutral.

Due to the large size of the HLA array spool and associated equipment the weather conditions need to be good for successful deployment. When the HLA array cable and its deployment spool are mounted on the back of SSD and the complete assembly is submerged, the total weight and entrained mass of the water within the array and the SSD make the assembly susceptible to rough sea conditions.

The weather did not cooperate and the dive was delayed. With the available cruise time running out, an attempt was made in less than ideal conditions. When the SSD and its HLA equipment entered the water, the boat heaved in response to a large wave. The heave was sufficient to cause the lifting line to the SSD to become slack. With the reversal of the heave the lifting line went taut and the resulting shock load was severe. This was repeated through a few ship heave cycles and the result was a fracture in the HLA Spool mounts on the SSD cage. The array pulled from of this mount

and was suspended below the SSD cage as if ready to be laid on the sea floor. Unfortunately this was premature and the deployment could not be continued in this manner. The weather conditions did not improve to an acceptable level during the remainder of the cruise. The deployment of these arrays was reserved for better weather. Alternates for the array mounts were investigated to extend the acceptable weather conditions.



*HLA Deployment Attempt, R/V Pelican, September, 2010.*

### **Conclusion**

The horizontal array development has been completed and the equipment is in storage awaiting another deployment opportunity.

This task is complete. Although the HLAs are still not deployed at the Observatory site, they are complete and ready for deployment, thus satisfying the obligation of SDI, the subcontractor. However, SDI has agreed to continue to work with MMRI toward the eventual goal of deployment of all arrays.



## **TASK 2: Seismic Data Processing at the Gas Hydrate Sea-floor Observatory: MC118.**

This task was extended into Phase 2 and has now been completed: software has been written, tested on data from another hydrates location, and awaits data from the MS/SFO. For the Final Report, see Phase 2, Task 3.

## **Task 3: Coupling of Continuous Geochemical and Sea-floor Acoustic Measurements**

This task was continued into all four Phases of the MS/SFO/Hydrates project. A Final Report appears in Phase 4, task 4 and covers work from

**Phase 1, TASK 3:** Coupling of Continuous Geochemical and Sea-floor Acoustic Measurements.

**Phase 2, 3, and 4, all TASK 4:** Biogeochemical investigations at MC 118: Pore fluid time series and gas hydrate stability.

## **Task 4: Noise-Based Gas Hydrates Monitoring.**

(Subcontractor: The University of California – San Diego; Peter Gerstoft, PI)

### **Abstract**

Monitoring of gas hydrates at Mississippi Canyon 118 is possible using ambient noise as a sound source. The goal is to attempt to apply passive methods to supply information similar to that supplied by active sources, but on a continuous basis, as passive sources, such as wave-noise, are ever-present at MC118.

### **Introduction**

By using ambient noise-based methods with dense networks, passive monitoring of gas hydrates is possible. Making use of ambient-noise cross correlation function of diffuse fields between two receivers, information can be recovered that is similar to that recovered using an active source.

### **Executive summary**

In the first half of 2011, we have focused on collecting data from MC118 and we are currently working on these data. We have five papers published on this analysis in the Journal of Society of America and Geophysical Research Letters.

### **Hurricane monitoring**

We have a paper [Zhang et al., 2010] showing how we can monitor storms in the Pacific using seismics: Nonlinear wave-wave interactions generate double-frequency (DF) microseisms, which include both surface waves (mainly Rayleigh-type) and compressional ( $P$ ) waves. Although it is unclear whether DF surface waves generated in deep oceans are observed on land, we show that DF  $P$  waves generated under Super Typhoon Ioke far offshore are detected by beamforming of land-based seismic array data, allowing tropical cyclones to be well-tracked seismologically. Two distinct spectral

bands associated with different microseismic *P*-wave source locations are observed. The short-period DF band (0.16– 0.35 Hz) is dominated by *P* waves generated in the deep ocean by local wind seas near the storm. In contrast, *P* waves in the long-period DF band (0.1–0.15 Hz) are weaker and generated closer to the coast of Japan from swell interactions. The accurate identification of DF *P*-wave microseism source areas is necessary to image Earth structure using ambient noise.

### **Noise cross correlation**

In the second half of 2010, we have focused on noise processing of ambient noise in the East Pacific Rise (see AGU abstract). Noise cross-correlation has been used to recover surface wave Green's functions between receivers. However, most noise cross-correlation studies are restricted to land seismic stations and few studies have observed higher-mode surface waves. We apply noise cross-correlation on three-component broadband data recorded by 30 ocean bottom seismometers (OBSs) around the Gofar/Discovery/Quebrada transform faults on the Eastern Pacific Rise. On the vertical component, the cross-correlation functions (CFs) reveal clear Rayleigh wave propagation between each station pair for both the fundamental mode in the 2-30s period band and the first-higher mode in the 2-10 s band. However, on the radial component CFs, the first-higher mode Rayleigh waves dominate within 2-10s band and the fundamental mode Rayleigh waves appear mainly in 10-20s band. On the transverse component CFs, Love waves are observed within 2-10s band. The directionality of CFs is different for the fundamental mode and the first higher-mode surface waves, and is also frequency dependent. This infers different mechanisms for each mode, probably due to ocean wave activities and ocean bottom scattering. The dispersion characteristics of the vertical component CFs are analyzed using the time-frequency analysis for group velocities and a time-variable filter technique for phase velocities. We obtain inter-station dispersion curves within 2-30s period for the fundamental mode and within 2-8s period for the first higher-mode. These dispersion curves are averaged over station pairs and used to invert for the 1-D shear wavespeed structure in the crust and uppermost mantle in the study region. The obtained 1-D velocity model shows very low shear wavespeed in the uppermost mantle (4.25 and 4.0 km/s within 10-25 km and 25-45 km depth ranges, respectively), consistent with the local geology with hot upper mantle material upwelling to the surface through the ridges of the Eastern Pacific Rise.

### **Seismic noise in MC118**

In early April 2011 we collected a week of seismic noise data from MC-118 in the Gulf of Mexico. We are currently analyzing the OBS data from the experiment.

Results of the work can be found in Carriere and Gerstoft (2012).

While only one day of ambient noise data was available, the data demonstrated hope for further good results.

### **Published papers:**

- Carriere, O, Gerstoft, P. 2012. [Deep-water subsurface imaging using OBS interferometry](#). *Geophysics*. 78:Q15-Q24. [10.1190/geo2012-0241.1](#)
- Zhang, Jian, Peter Gerstoft, and Peter D. Bromirski (2010), Pelagic and coastal sources of P-wave microseisms: Generation under tropical cyclones, *Geophys. Res. Lett.*, 37, L15301, doi:10.1029/2010GL044288.
  - Brooks, Laura A, Peter Gerstoft (2009), Green's function approximation from cross-correlation of active sources in the ocean, *J Acoust. Soc. Am.*, 126, 46-55.
  - Brooks, Laura A, Peter Gerstoft (2009), Green's function approximation from cross-correlations of 20–100 Hz noise during a tropical storm, *J Acoust. Soc. Am* 125, 723-734.
  - Traer, James, Peter Gerstoft, Peter D Bromirski, WS Hodgkiss, and Laura A Brooks (2008), Shallow-water seismo-acoustic noise generation by Tropical Storms Ernesto and Florence, *J Acoust. Soc. Am EL*, 124, EL170-176, DOI:10.1121/1.2968296.
  - Brooks, Laura A, Peter Gerstoft, and David P Knobles (2008), Multichannel array diagnosis using noise cross-correlation, *J Acoust. Soc. Am EL*, 124, EL203-EL209, DOI:10.1121/1.2960937.

### **Abstract**

H. Yao, P. Gouedard, P. Gerstoft, J. McGuire, J. A. Collins, R. van der Hilst, Analysis of fundamental and higher mode surface waves from noise correlation near Eastern Pacific Rise, AGU fall meeting 2010.

### **Conclusions**

Several papers demonstrate the utility of passive monitoring. The analysis shows promise of providing a true monitoring capability at MC118.

## **PHASE 2 Tasks for FY 2008:**

### **TASK 1: Project Management Plan (complete)**

### **TASK 2: Processing and Interpretation of TGS-NOPEC Geophysical Company Industry Seismic Data and Integration with Existing Surface-Source/Deep-Receiver (SSDR) High Resolution Seismic Data at MC118, Gulf of Mexico.**

(Subcontractor: The University of South Carolina; Camelia Knapp, PI)

This task includes processing and interpreting industry seismic data collected and provided by TGS-NOPEC, Inc. Geophysical Company and integrating them with existing Surface-source/ Deep-receiver (SSDR) high resolution seismic data at from Mississippi Canyon Block 118, Gulf of Mexico (GOM), in order to image and understand the complex geologic structures at the Observatory site and how they relate to gas hydrate formation and dissociation. This work has been focused on the (1) refinement of the structural interpretation of the TGS-NOPEC seismic data, (2) interpretation and mapping of the high-amplitude reflectors identified as possible bottom simulating reflectors (BSRs), (3) integration of this dataset with the high-resolution SSDR single-channel seismic data, (4) preparation and submission of a proposal to the Integrated Ocean Drilling Program (IODP), and (5) initiation of a thorough analysis of the rock physics properties of the inferred gas hydrates at the study site.

The characterization of the subsurface geology – particularly the structure of the carbonate-hydrate mound and how it relates to and impacts hydrate formation and dissociation – has been completed. Integration of the data from the nearby ARCO-1 deep well was a major accomplishment of this phase. The proposal submitted to the IODP supports this effort and has progressed to the full proposal stage but the time at which it might develop into a full project is unknown. The proposal is to drill borehole(s) to define the subsurface geology at MC118 and to provide the ability to monitor the subsurface at the site, continuously, into the future.

To date, findings of this effort support the inferences that the structure, stratigraphy and thermal and fluid-flow architecture at MC118 are dominated by salt structures, the mound having evolved in association with a crestal fault system that formed over a domed salt body. Depth conversions have been performed and horizons on TGS records correlated with picked horizons in the ARCO-1 well. Amplitude vs. offset (AVO) analysis was performed on one of the TGS inlines. The results included the identification of an interpreted accumulation of free gas beneath the base of gas hydrates. A request for an additional seismic line in raw form – one that crosses the middle of the mound - was made to substantiate this find and to determine how wide-spread the reflector might be. TGS agreed to provide the line.

University of South Carolina (USC) researchers began deriving an impedance volume from the TGS seismic data to be used in porosity calculations and in calculations of gas hydrate saturations.

In their request for continued funding for this project, USC included funds to purchase an additional, deeper, 3-D dataset from WesternGeco. A final report of findings for all phases of this task can be found in the GOM-HRC's Technical Progress Report to DOE, 42877R24, and repeated in Phase 3, Task 2 of this report.

### **TASK 3: Seismic Data Processing at the Gas Hydrate Sea-floor Observatory: MC118.**

(Subcontractor: The University of Texas at Austin Bureau of Geology; Bob Hardage, PI)

This task has been completed: software has been written, tested on data from another hydrates location, and awaits data from the MS/SFO.

#### **Abstract**

We have investigated the distinctions that occur between converted-shear (P-SV) images made with positive-offset source stations and with negative-offset source stations. We find there are differences in the images of near-seafloor geology made with these two different source-offset domains, a phenomenon that has been observed by others who process 4C OBC seismic data for deep oil and gas targets. This research finding will be helpful as we use P-SV data to build a model of the near-seafloor geology across Block MC118.

#### **Introduction**

One objective of the research work that will be done at the seafloor observatory is to deploy 4-component (4C) seismic sensors on the seafloor that can be used to monitor calendar-time variations in the P-P and P-SV reflectivities of interfaces that extend from the seafloor to the base of the hydrate stability zone. Analysis of these alterations in the seismic response will be useful for determining if and how the hydrate system beneath the observatory site varies as a function of calendar-time events such as thermal cycles in the water column and local microseisms. In our effort to ensure that we deliver optimal-quality seismic images of near-seafloor geology, we have investigated a phenomenon that is unique to 4C seismic data – P-SV images made with positive-offset source stations often differ from P-SV images made with data collected from negative-offset source stations. We find that indeed there are some differences in images made from these two offset domains.

#### **Executive Summary**

Seismic data-processing software has been developed at EGL that is structured to optimize P-P and P-SV image resolution in the immediate vicinity of 4C seafloor-based seismic sensors. This data-processing strategy can now be applied to data acquired with the actual sensor system that will be deployed across Block MC118. During this reporting period, we focused on optimizing our procedure for creating P-SV images, with particular attention focused on comparing P-SV images made with positive-offset data and with negative-offset data.



## Experimental

Experimental activity during this period concentrated on applying our seismic data-processing strategy to converted-shear (P-SV) data acquired in both the positive and negative offset directions away from the position of a seafloor sensor.

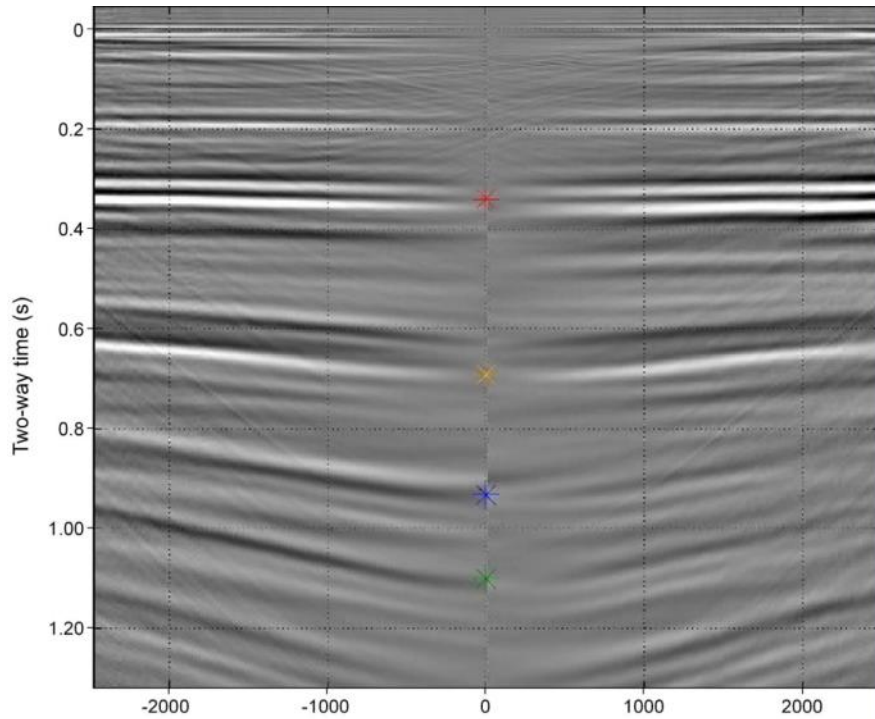
## Results and Discussion

When processing converted-shear (P-SV) data acquired as 3C seismic data in an onshore project or as 4C data acquired offshore, source stations positioned to the right of a receiver station create data that are typically referred to as positive-offset data, and source stations positioned to the left of the receiver station create data referred to as negative-offset data. The direction that is specified as “positive offset” is arbitrary; that direction can be either right or left of a receiver station, depending on the whim of the data processor.

With P-SV data, the P-to-SV conversion point is not at the midpoint between source and receiver as it is with P-P data, but is always closer to the receiver station than it is to the source station. If there is any lateral variation in seismic propagation velocities, this location of the P-to-SV conversion point means that the time-moveout of a P-SV reflection event measured between a given source station and a given receiver station is not the same as the reflection moveout when those source and receiver stations are exchanged, which is not the case when processing P-P data. The fact that the velocity field between any source and receiver station depends on whether the source is to the left or to the right of the receiver causes a data processor to have to create two versions of stacked P-SV data. One P-SV stack is made for positive-offset source stations, and a second stack is made for negative-offset source stations. In theory, the correct P-SV image is the sum of these two stacks. In practice, data processors observe that there are often phase and amplitude differences between the two stacks that result in their sum not being an optimal image. Sometimes either the positive-offset image or the negative-offset image is a better image than the summed image. All three images need to be considered. Our current research has focused on the issue of determining the differences between positive-offset and negative-offset P-SV images that may be acquired across Block MC118. We used a 4C OBC profile acquired in water depths equivalent to the water depth across Block MC118 to study this problem.

Illustrated in Figure 1 is an example of P-SV sub-seafloor reflectivity calculated at one receiver station from the common-receiver gathers of P (hydrophone) and X (inline horizontal geophone) data acquired at that station. This reflectivity was obtained by separating downgoing P-P and upgoing P-SV wavefields and then calculating the ratio “P-SV upgoing” divided by “P-P downgoing” as described by Backus and others (2006). Panels a and b of Figure 1 are the P-SV reflectivity without any moveout corrections applied to the data. We refer to this P-SV reflectivity as a “brute” estimation of reflectivity. The data in panels c and d have been adjusted for offset-dependent moveout.

(a)



(b)

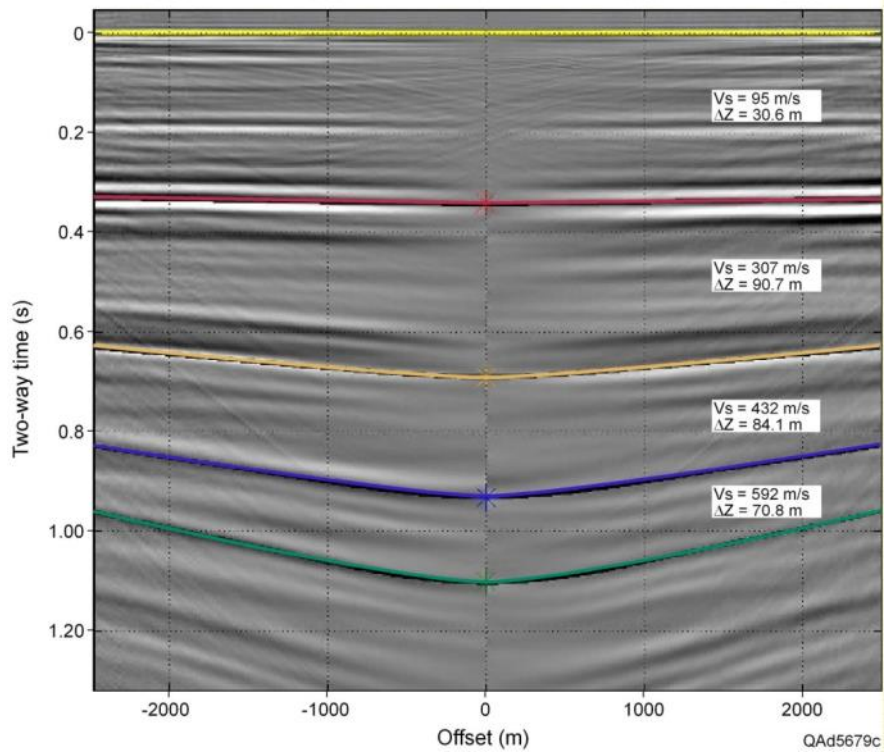


**Figure 1. P-SV reflectivity determined at one receiver station. No velocity moveout (NMO) corrections have been applied to the data in panels (a) and (b).**

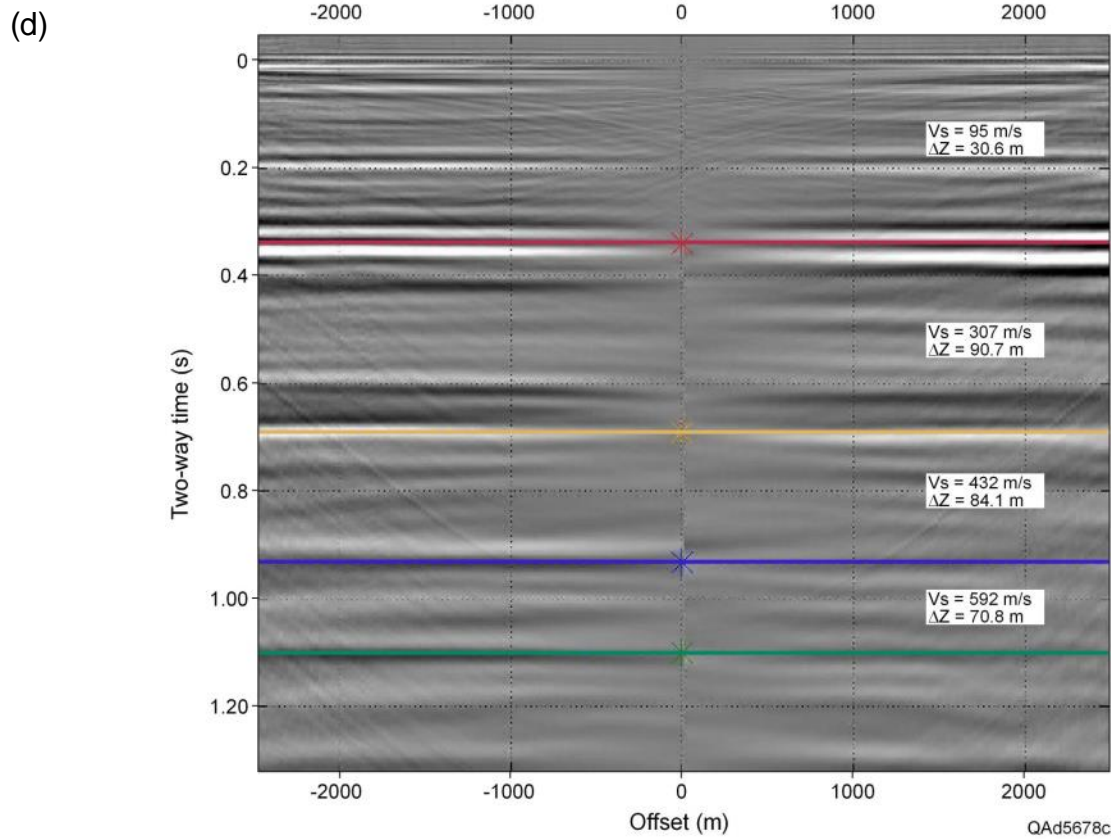
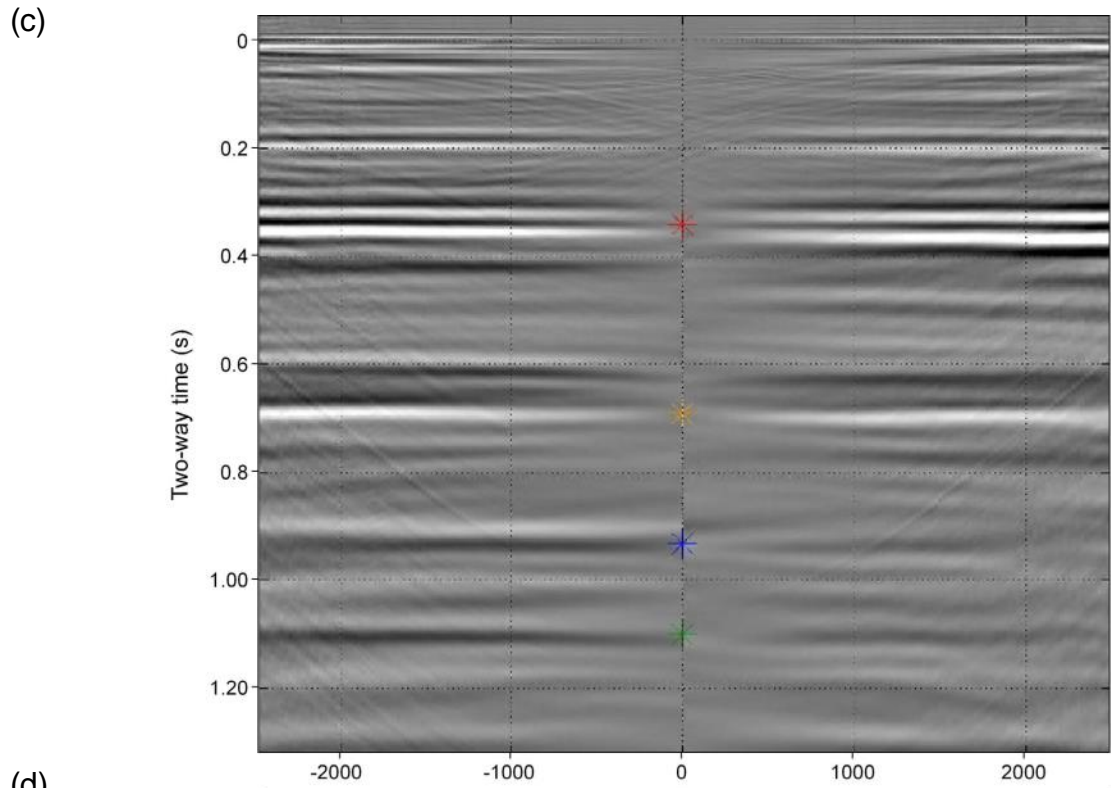


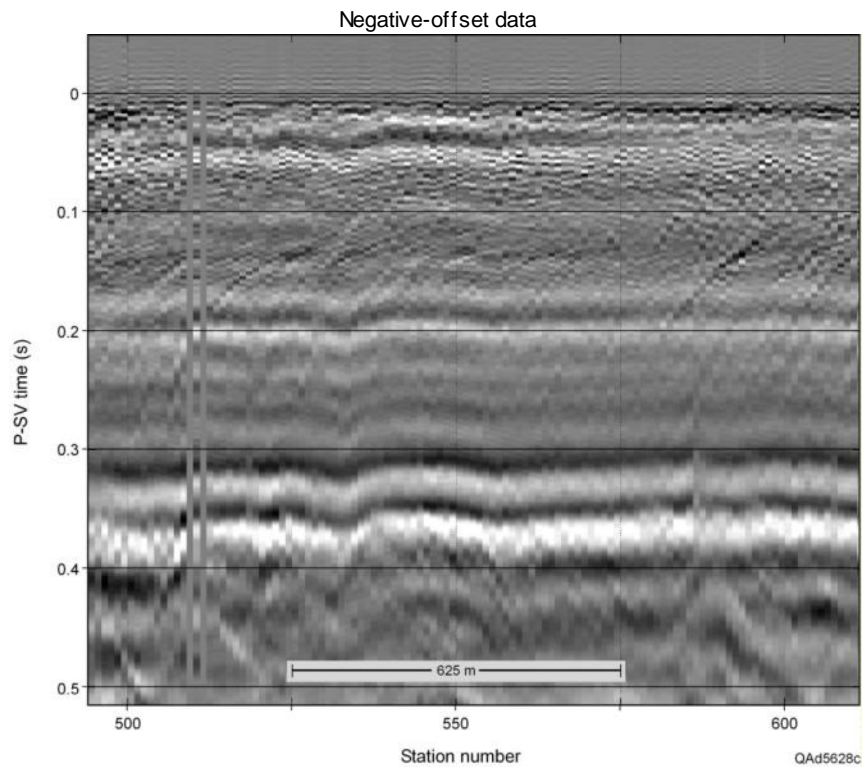
**Figure 1, cont. P-SV reflectivity determined at one receiver station. NMO corrections have been applied to the data in panels (c) and (d).**

We find that P-SV images made from data that are corrected for velocity moveout are a better description of near-seafloor geology than are images made from uncorrected data. An example of such an image comparison along Line A is provided as Figure 2. **Brute images** (panels 2a and 2b) made from uncorrected data have a large amount of diffraction-event noise, particularly evident in the first 200 ms of image time. Much of this diffraction noise is eliminated in the NMO-corrected data (panels 2c and 2d) even though the data are not migrated. Note that the positive-offset and negative-offset brute data emphasize different portions of shallow diffraction events. This behavior is best seen in the data window between 0.1 and 0.2 s. For negative-offset data, diffractions in this time window are dominated by diffraction arcs that slope down to the left (Fig. 2a). For positive-offset data, the same diffractions are dominated by events that slope down to the right (Fig. 2b). Why these differences in diffraction responses occur between positive-offset and negative-offset data will continue to be studied.

P-SV images of near-seafloor geology along the full extent of Line A are shown in Figure 3. These examples show that negative-offset data image geology across an interval located between 0.9 and 1.1 s below the seafloor better than do positive-offset data. The reason for this imaging difference between negative-offset and positive-offset data also needs further study. Any distinctions between the positive-offset and negative-offset images in the remainder of the image space are minor. There are thus three options that can be used as the P-SV near-surface image along Line A: (1) positive-offset image, (2) negative-offset image, or (3) the sum of the positive-offset and negative-offset images (Fig. 4). We use the negative-offset P-SV image (Fig. 4a) in the remainder of this discussion because this imaging option provides the best illumination of the geology across the P-SV image-time interval 0.8 to 1.2 s.



(a)



(b)

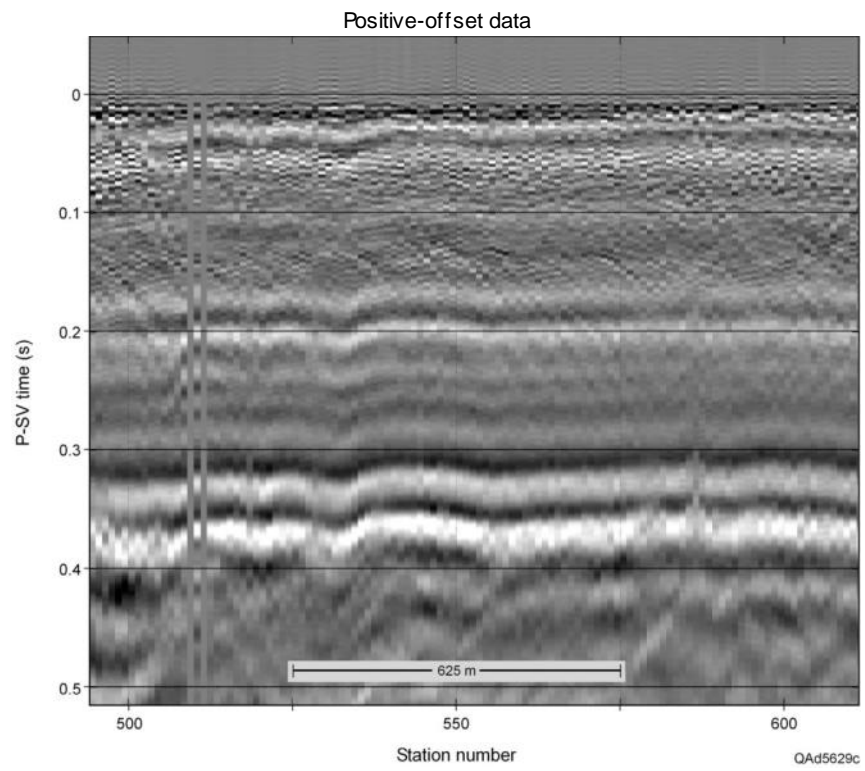
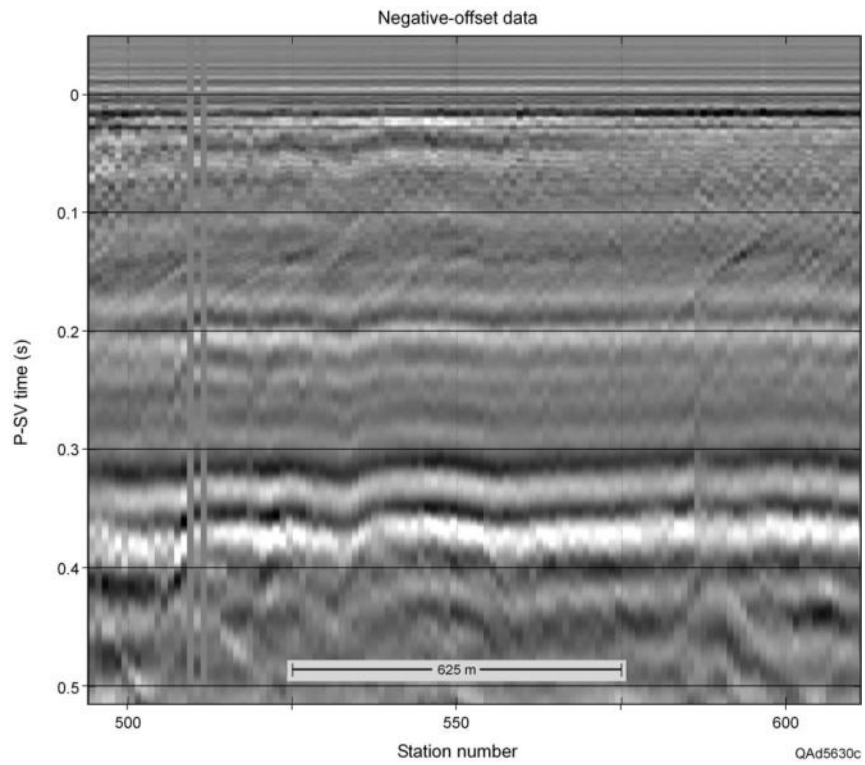


**Figure 2. (a) Brute P-SV image using uncorrected negative-offset data. (b) Brute P-SV image using uncorrected positive-offset data.**

(c)



(d)

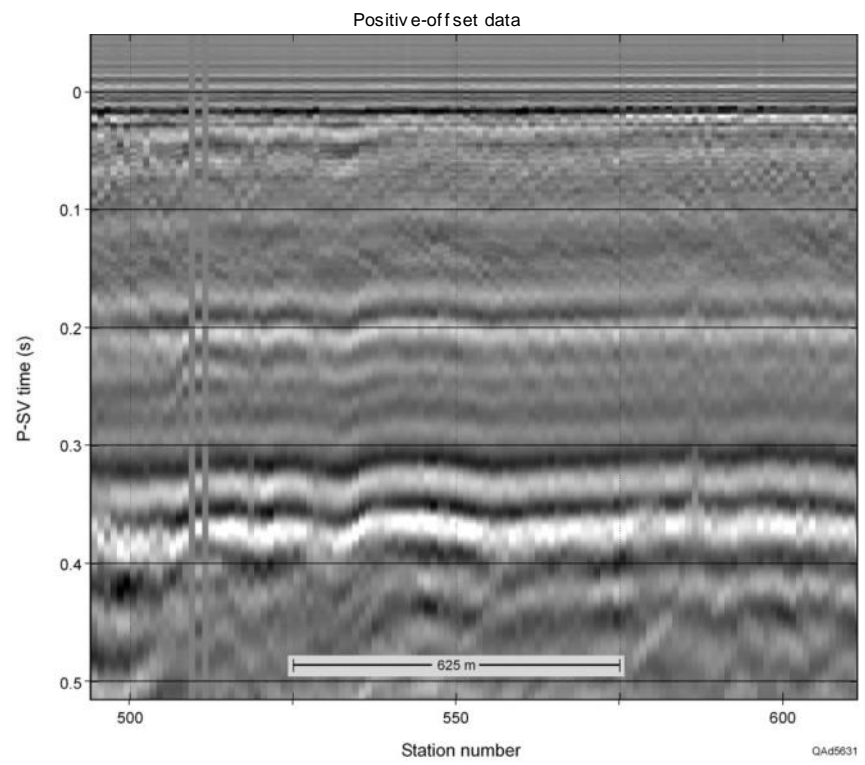


**Figure 2, cont'd. (c) P-SV image using NMO-corrected negative-offset data. (d) P-SV image using NMO-corrected positive-offset data.**

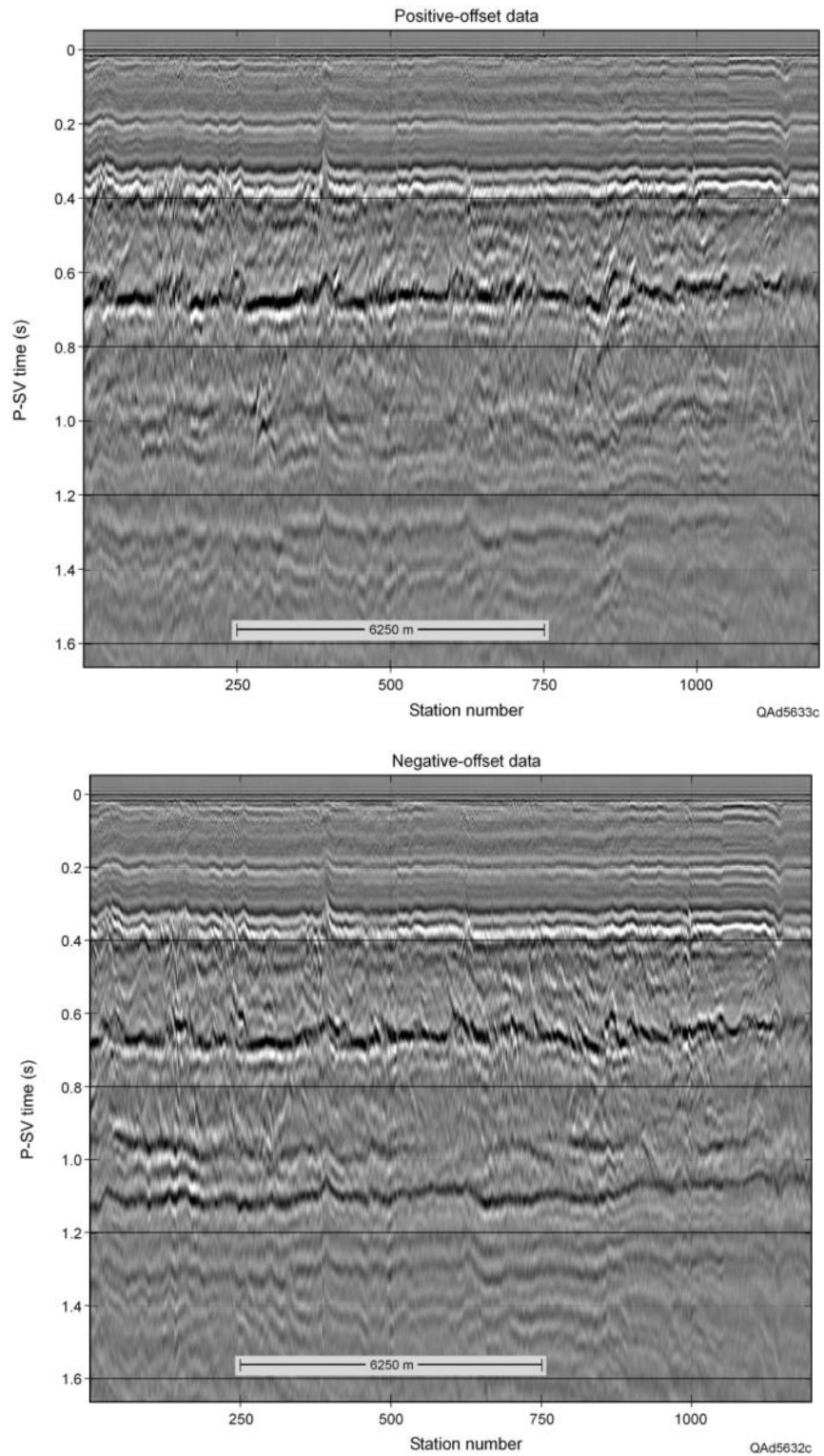


**Figure 3. (Top) P-SV image made from positive-offset data along the full extent of Line A. (Bottom) P-SV image made from negative-offset data. The negative-offset data image strata between 0.9 and 1.1 s that are not well seen with the positive-offset data.**

EGL's P-SV image is compared with the contractor's P-SV image in Figure 5. Because EGL's data-processing strategy creates a flat seafloor, the contractor image has been flattened to the seafloor for easier image comparison. This flattening was done by applying a static shift to each CDP trace that equaled water depth divided by water velocity (1468 m/s). A considerable amount of near-surface data has been muted in the contractor's data processing, with the result that Layer 1 and the top portion of Layer 2 have been eliminated. This muting causes the base of Layer 2 in the contractor image to occur more than 500 ms earlier than where it is positioned in the EGL image. The EGL image provides an improved definition of geology that extends from the seafloor to the base of the **Paleoslide** layer (Layer 2), a layer of importance in the local area of this 4C OBC profile. Below Layer 2, the distinctions between the two images are not significant. The different structural dips exhibited by the images (such as the **Glide plane** even, another local feature of importance) are probably caused by the different techniques that were used to create a flat seafloor in the two imaging strategies.

To use both P-P and P-SV attributes in an interpretation of near-seafloor geology, it is necessary to depth register the P-P and P-SV images so that depth-equivalent data windows can be defined in each image space. The P-P and P-SV images generated by EGL are shown in a depth-registered form in Figure 6 with depth-equivalent horizons marked.



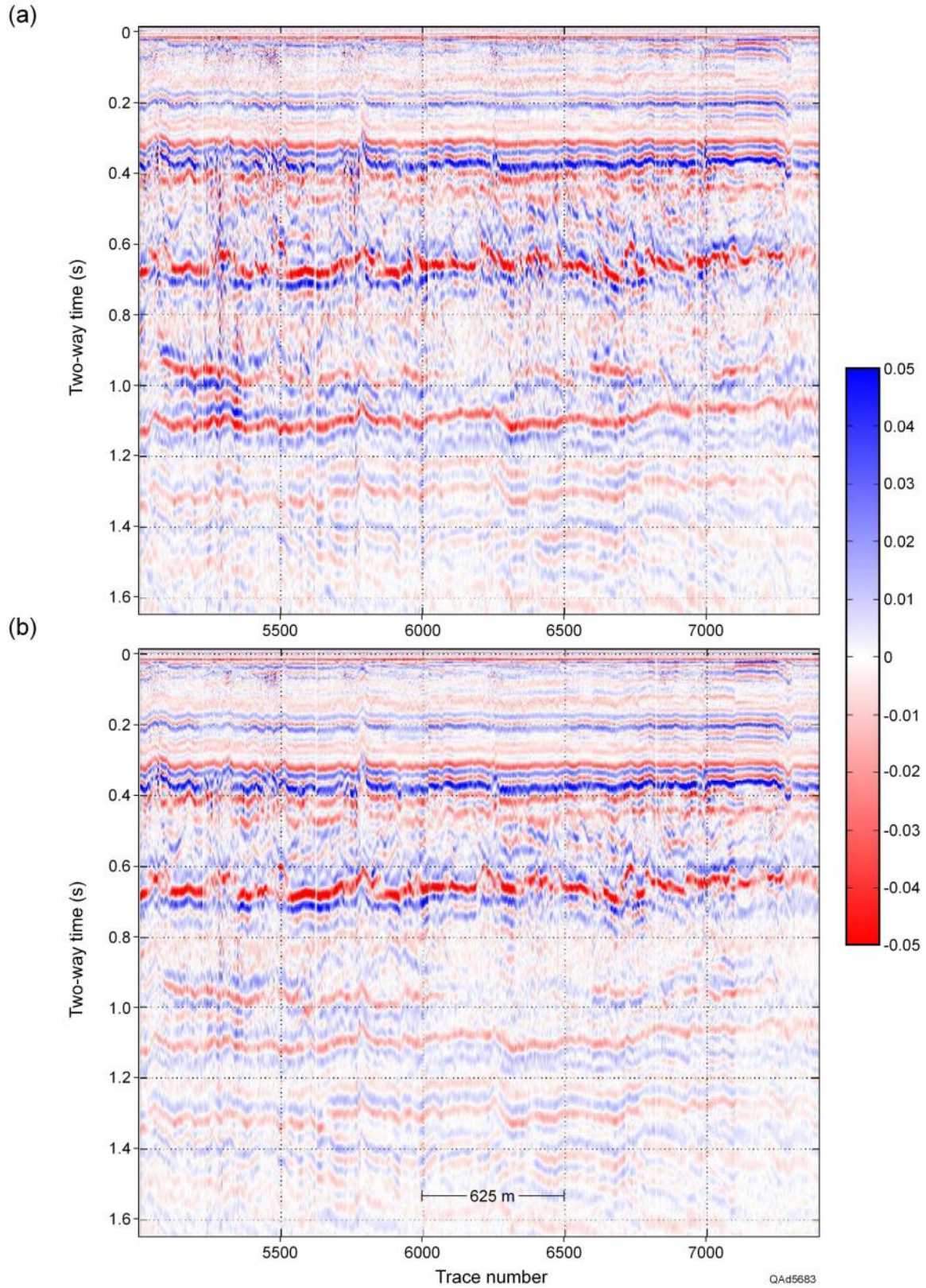


**Figure 4. (a) Negative-offset P-SV image. (b) Sum of positive-offset and negative-offset P-SV images.**



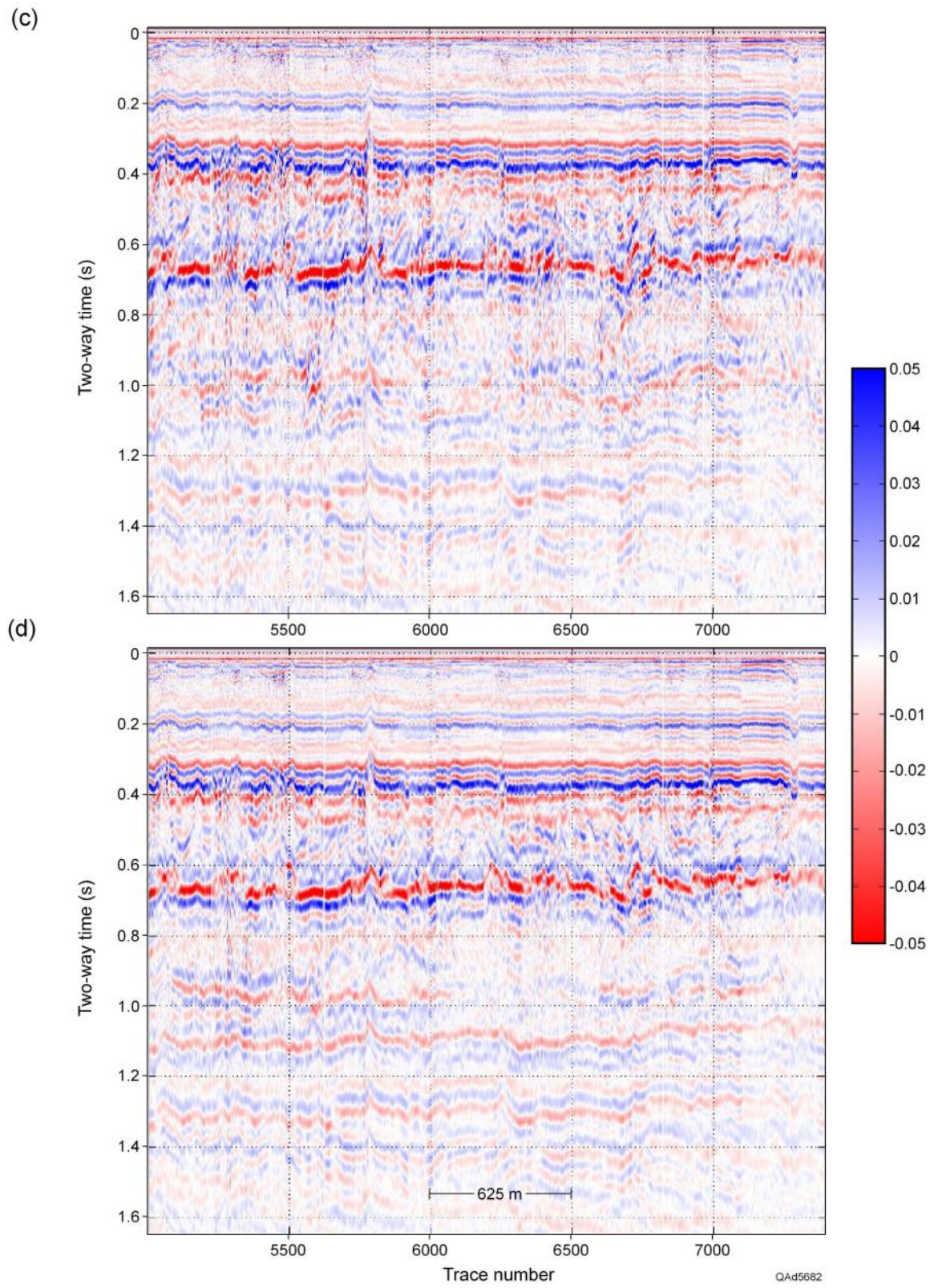


Figure 4, cont. (c) Positive-offset P-SV image. (d) Sum of positive-offset and negative-offset P-SV images.

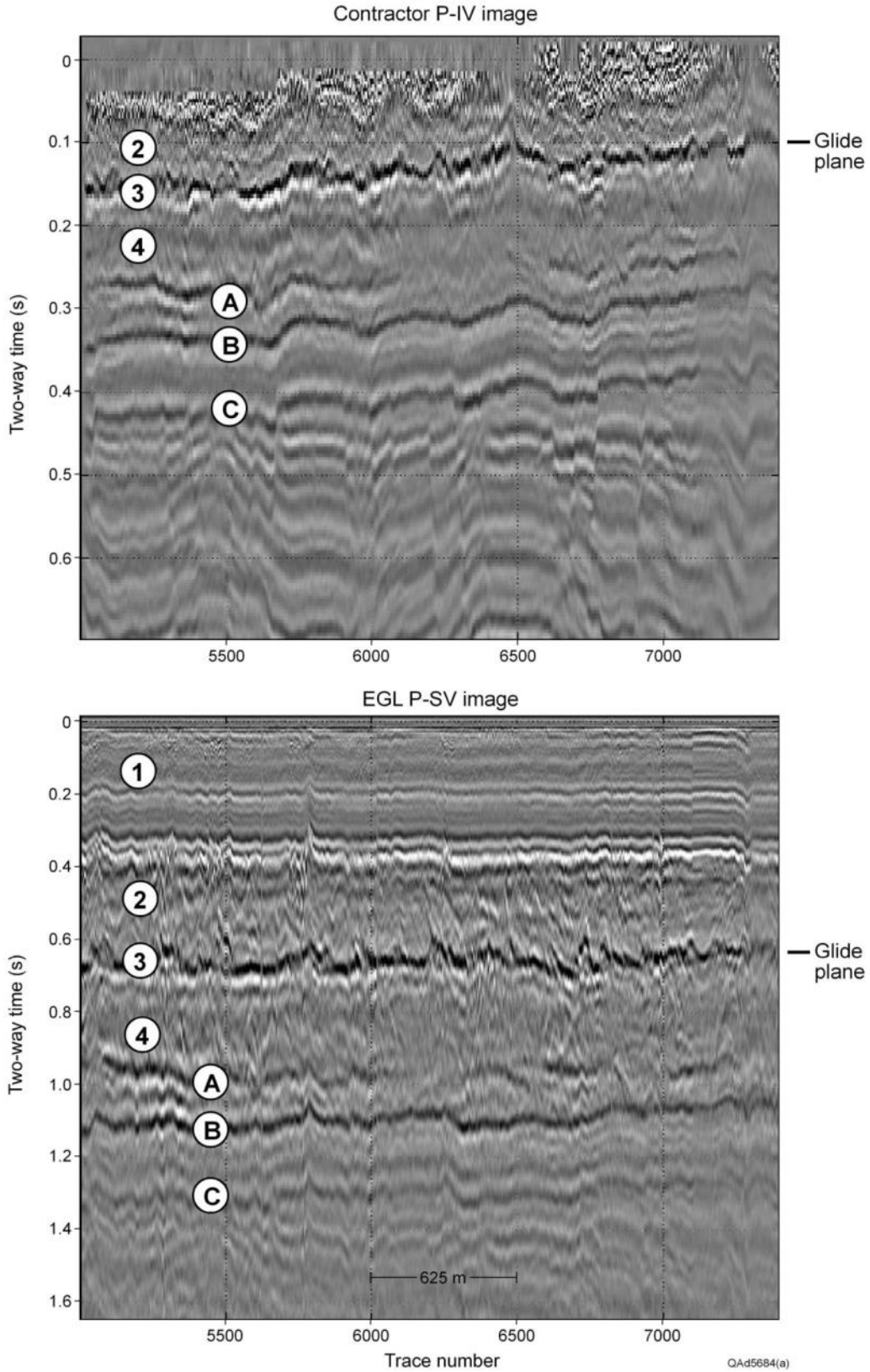
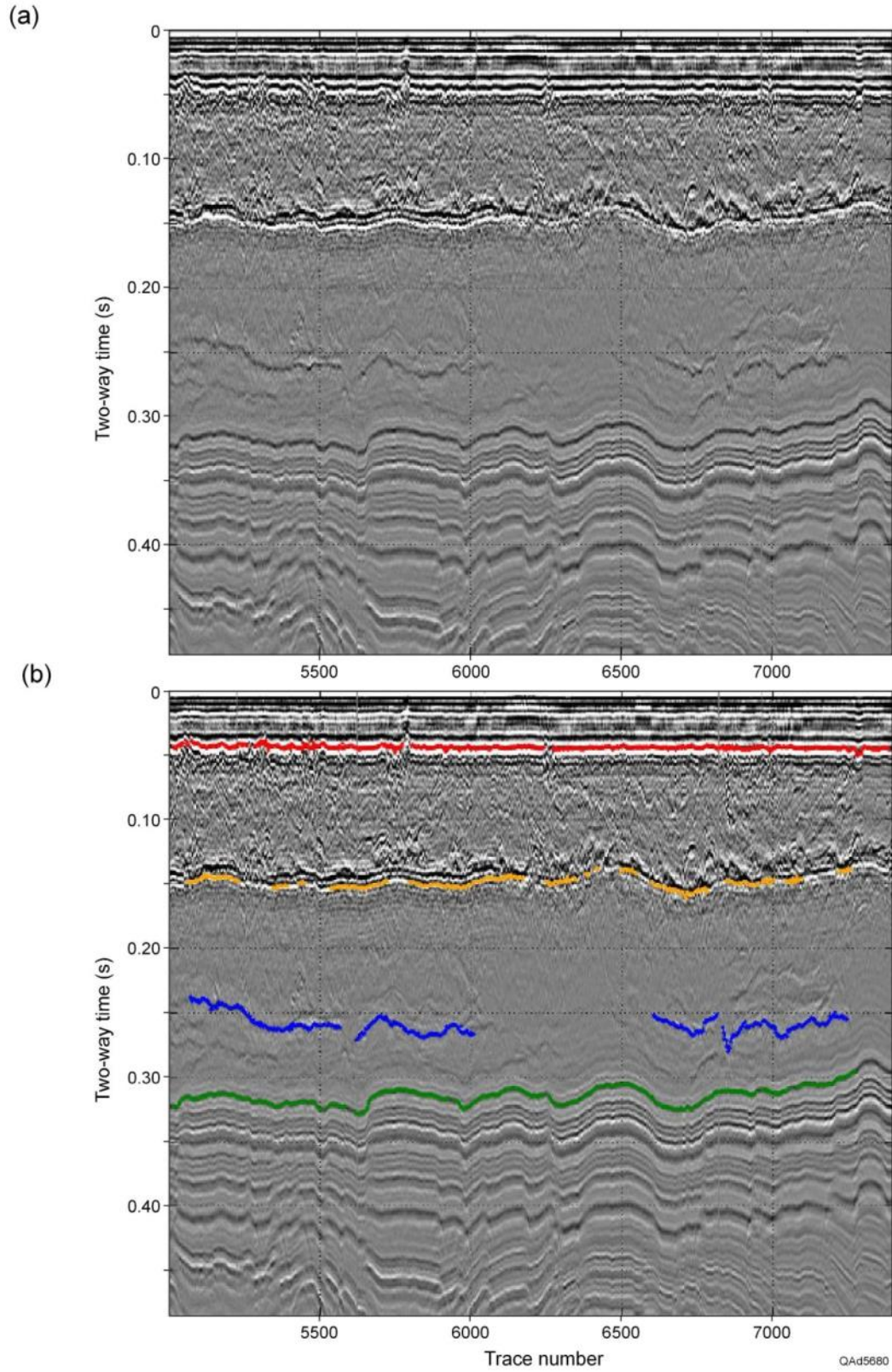


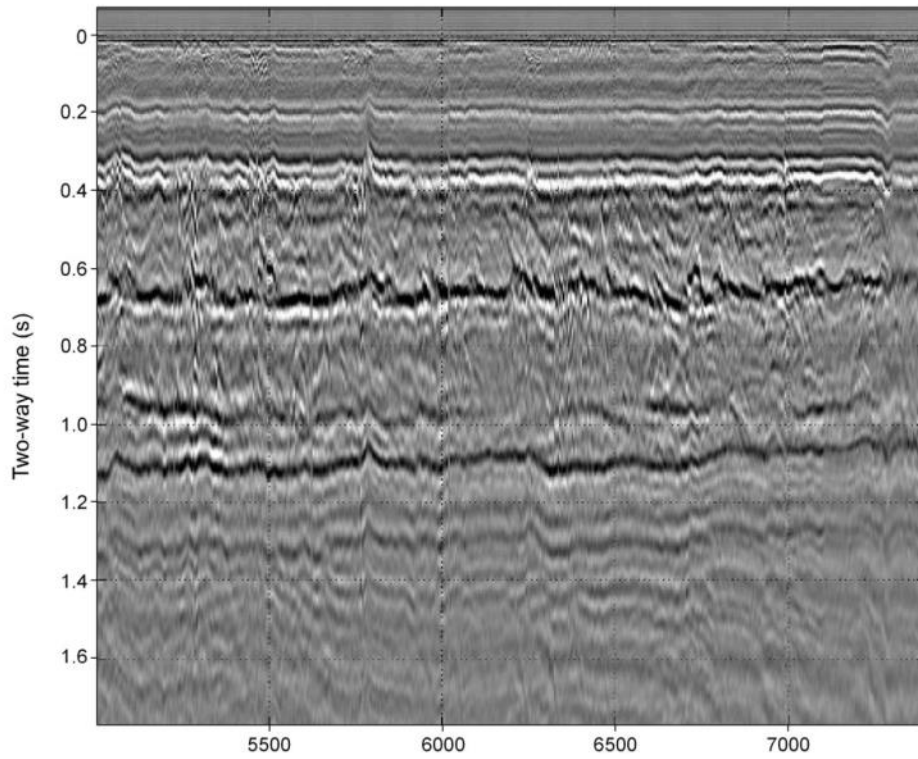
Figure 5. Comparison of contractor P-SV image with EGL's negative-offset P-SV image.





**Figure 6. Depth registration of EGL P-P and P-SV images. (a) Unmarked P-P image. (b) Interpreted P-P image.**

(c)



(d)

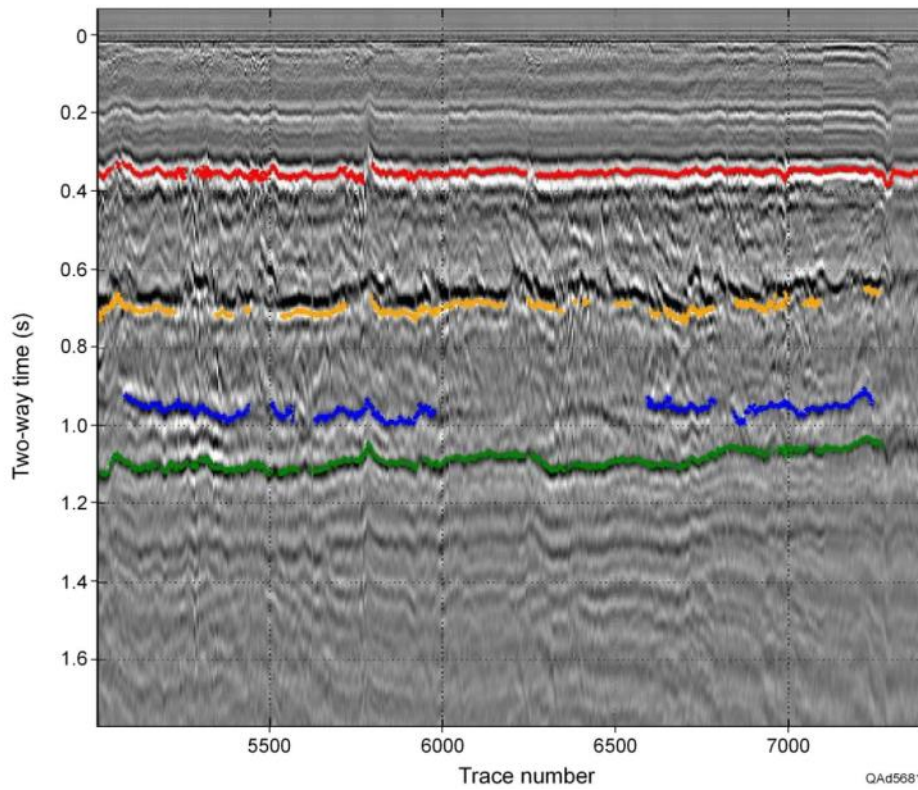


**Figure 6, cont. Depth registration of EGL P-P and P-SV images. (c) Unmarked P-SV image. (d) P-SV horizons interpreted to be depth equivalent to the P-P horizons in b.**

## Conclusions

Some features of P-SV images depend on whether the image is made with positive-offset source stations or with negative-offset source stations. For the present, there is no definitive way to decide which image is the optimal choice for studying the hydrate system across the seafloor observatory in Block MC118. Our strategy will be to make both a positive-offset P-SV image and a negative-offset image and to incorporate both images into the interpretation of the near-seafloor geology. This problem that slight differences occur in image features dependent on the direction of the energy source used to illuminate the geology is not present in P-P imaging; it is strictly a P-SV imaging issue.

## Reference

Backus, M. M., Murray, P. E., Hardage, B. A., and Graebner, R. J., 2006, High-resolution multicomponent seismic imaging of deepwater gas-hydrate systems: The Leading Edge, v. 25, p. 578-596.

## Abbreviations and Acronyms

**3-C:** three-component

**4-C:** four-component

**MC:** Mississippi Canyon

**P-P:** compressional wave mode

**P-SV:** converted shear mode

## **TASK 4: Geochemical investigations at MC 118: Pore fluid time series and gas hydrate stability.**

This task was continued into all four Phases of the MS/SFO/Hydrates project. A Final Report appears in Phase 4, task 4 and covers work from

**Phase 1, TASK 3:** Coupling of Continuous Geochemical and Sea-floor Acoustic Measurements.

**Phase 2, 3, and 4, all TASK 4:** Biogeochemical investigations at MC 118: Pore fluid time series and gas hydrate stability.

## **TASK 5: Automated Biological/Chemical Monitoring System(ABCMS) for Offshore Oceanographic Carbon Dynamic Studies.**

Development of a Marine Lander Survey Vehicle (Lander) for the next phase of gas hydrate research in the Gulf of Mexico

This task was continued into subsequent Phases of the MS/SFO/Hydrates project. A Final Report appears in Phase 4, task 5 and covers work from all phases.



## **TASK 6: Exploring the extent of microbial involvement in seafloor hydrate formation/decomposition and establishing that mechanism: Microbial techniques to extract carbon from stored hydrocarbon gases: Exploring Extent of Microbial Involvement in Seafloor Hydrate Formations/Decompositions and Establishing that Mechanism**

(Subcontractor Mississippi State University; Rudy Rogers, PI)

Phase 2 (previous Cooperative Agreement), Task #4. Geochemical investigations at MC 118. Gas hydrate stability.

Phase 3, Task #6. Utilize microbial techniques to extract carbon from stored hydrocarbon gases.

### **ABSTRACT**

In the early phase of this research, Task #4 was addressed: Establish the influence of indigenous microbes on the mechanisms and kinetics of seafloor hydrate formations and dissociations. During the project, analyses of many sediments have shown that proliferate microbial activities around MC-118 hydrates play an important part in the nucleation, accumulation, and dissociation of near-surface hydrates. The reader is referred to our refereed journal articles, technical conference presentations, and dissertation/theses derived from the work—in many cases the initial discoveries in the topic.

This current report (July 2010-December 2010) pursues the second goal (Task #6): Utilize microbial techniques to extract carbon from stored hydrocarbon gases—i.e., to assist in the production of the occluded hydrocarbon gases.

We present the intriguing finding that microbial cell wall material inhibits hydrate formation—a necessary occurrence for the bacterial cell's survival, as it prevents hydrate formation-heats from being liberated directly onto cell surfaces. We find the hydrate inhibitor to be peptidoglycan, a chemical common in microbial cell walls. Our work is the first to report hydrate inhibition by bacterial cell wall material. Data were gathered showing this peptidoglycan polymeric compound, which is water-insoluble, to be increasingly effective as an inhibitor by increasing its surface area through cell lysing.

A smaller, water-soluble, molecular component of the peptidoglycan polymer was tested and shown to retain hydrate-inhibiting properties. In tests comparing with a methanol standard, this water-soluble, glycan strand performed better in delaying gas hydrate formation (i.e., longer induction times) than similar amounts of methanol.

### **INTRODUCTION**

#### *Background of Hydrate Inhibitors*

The inaugural natural-gas pipeline from Texas to Chicago was constructed in 1931 (Zigenhain, 1931). During its first winter of gas transport, the 24-inch diameter line immediately became clogged with an ice-like material while operating at about 600 psi and 40 °F (Hammerschmidt, 1934). For roughly 50 years thereafter the main thrust, if not practically the only thrust, of gas hydrate research was directed toward preventing gas hydrates from forming in pressurized hydrocarbon lines. Methanol and glycol were

found to inhibit hydrates by shifting the thermodynamic properties of formation. Consequently, methanol injection became a standard for hydrate prevention in subsea production lines in the oilfield. For example, by 1996 some \$500 million of methanol was being injected per year (Lederhos et al., 1996). As offshore wells are drilled in increasingly deeper waters, the need for hydrate inhibition becomes more pressing, requiring methanol to the extent of 10-50% of the water content in production streams (Kelland et al., 2006; Xiao et al., 2009).

In addition to the thermodynamic inhibitors of methanol or ethylene glycol, synthetic inhibitors have been developed in recent years—namely, kinetic inhibitors and anti-agglomerates. Instead of altering the thermodynamic conditions of hydrate formation in the solution, the synthetic inhibitors increase the time for hydrates to form or cause the hydrate crystals to form along polymeric molecules at specific sites and thus delay catastrophic hydrate agglomeration for a period beyond pipeline residence time. Some of these synthetic inhibitors are effective and have been commercially used sparingly. The synthetic inhibitors are expensive.

Besides thermodynamic, kinetic, and anti-agglomerate inhibitors, other approaches have been made to the hydrate inhibition problem. Anti-freezing proteins in flounder and arctic fish, perennial rye grass, and insects have been evaluated with some success as hydrate inhibitors (Barrett, 2001; Chao et al., 1997; Gilbert et al., 2005; Gordienko et al., 2010; Gordon et al., 1962; Ramsey, 1964; Tyshenko et al., 1997; Zhang et al., 2004).

The deciding factor in using any inhibitor is cost. Therefore, methanol injection remains the primary means of inhibiting gas-hydrate formation in offshore oil and gas production, although cheaper and environmentally-friendly alternatives are still sought.

#### *Potential Role of Inhibitors in Producing Gas from Hydrates*

Future gas-hydrate research must develop a viable production technique. Seemingly insurmountable problems were overcome in developing other production methods for non-conventional natural gas (coalbed methane, shale gas, tight formations). Based on these experiences, there should be optimism that the complex problems to produce hydrate gas can be surmounted. For example, depressurization is the current favored approach (Konno et al., 2010; Mordis and Reagan, 2007; Rutqvist et al., 2009), but depressurization alone has serious limitations such as subsidence/formation-instability, incomplete production of gas from the hydrates, and ice or hydrate reforming near the wellbore. The latter fault may be a universal fault to be overcome with any hydrate-production technique.

A suitable inhibitor could possibly fit into hydrate production, either as a stand-alone process to decompose hydrates or as a process complement to prevent hydrates from reforming near the wellbore. Regardless, an inhibitor will be necessary in transporting produced gas to onshore.

Therefore, an 'ideal' hydrate inhibitor might be envisioned that has the following

properties: (1) As effective as methanol, although not necessarily via the same mechanism, (2) Low cost in large quantities, and (3) Environmentally compatible, i.e., naturally occurring in the environment and biodegradable.

## RESULTS AND DISCUSSION

The chemical structures of four Kinetic Inhibitors that other researchers have synthesized, tested and made commercially available (Ohtake, 2005) are presented in Figure 1. Most Kinetic Inhibitors are polymer-based (Xiao, 2009) and, in general, perform by two mechanisms: slowing crystal nucleation by lengthening induction time and/or retarding formation rate after critical cluster size is reached.

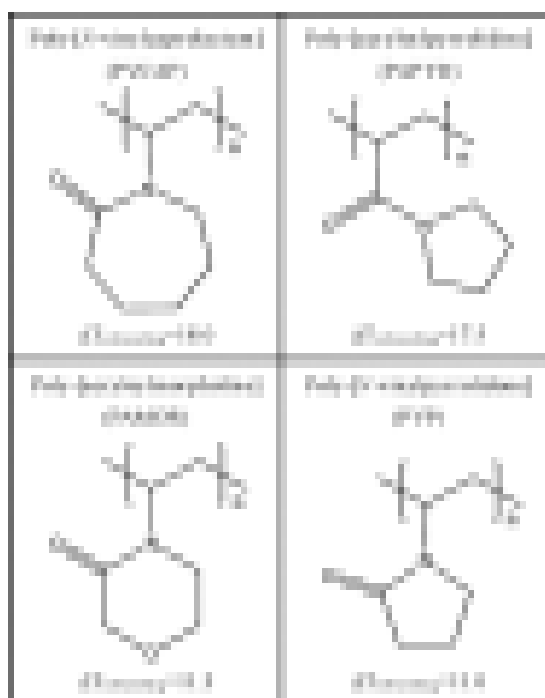


**Fig. 1. Commercial kinetic inhibitors (Ohtake, 2005).**

The functional groups of the Kinetic Inhibitors shown in Figure 1 are a lactam ring and an amide group (-N-C=O) attached to the carbon backbone. The 5-member lactam ring is thought to cover by adsorption the pentagonal face of the hydrate crystal when the amide becomes associated with the hydrate crystal. The 7-member lactam ring is thought to cover by adsorption the hydrate-crystal's hexagonal face (Lederhos, 1996).

Compare these structures with the peptidoglycan polymer structure in bacterial cell walls. See Figure 2.

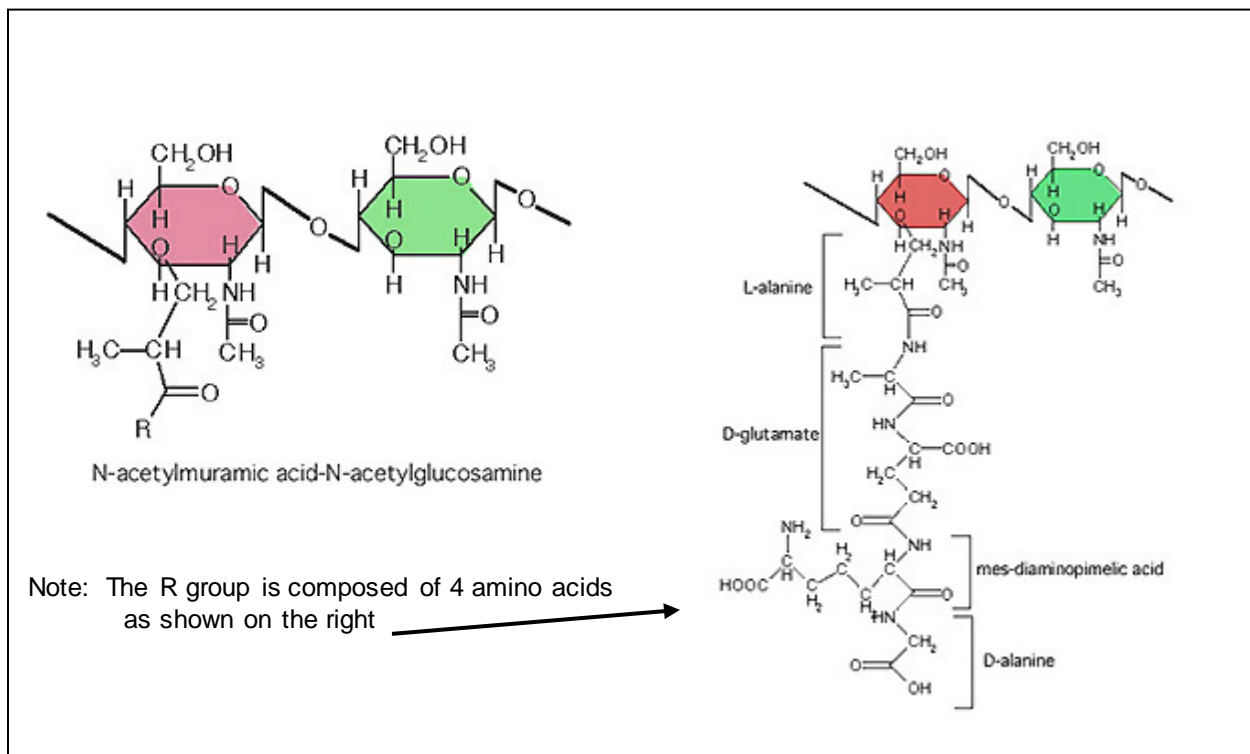


**Fig. 2. Structure of peptidoglycan (Beveridge and Murray, 1980; Vollmer et al., 2008).**

During the work on this project in a prior report period, the water-insoluble polymers comprising the cell walls from a culture of indigenous MC-118 bacteria inhibited hydrate formation in the laboratory. When we fragmented the cells by lysing to give a much greater surface area of those same particles, hydrates were inhibited to an even greater extent.

The polymer as presented in Figure 2 is water insoluble. For some important applications to hydrate inhibition, the inhibitor should be water soluble—as is methanol. Therefore, during the current report period, tests were run to evaluate the efficacy of just the N-acetylglucosamine segment of the structure shown in Figure 2; the N-acetylglucosamine by itself is water-soluble.

In Figure 3 is shown our laboratory results on hydrate induction time.

Note: The following nomenclature applies to Figure 3:

NAGA =	N-acetylglucosamine
MeOH =	Methanol
NB =	Nutrient broth

The experimental procedure involved using liquid nutrient broth, ordinarily used

in culturing of cells, as the base liquid component in all tests. The reference test was fresh nutrient broth with no additive. A constant volume of the broth was placed in a stainless-steel test-cell, pressurized with a 90/6/4 methane/ethane/propane gas to a constant initial pressure of about 500 psi, and cooled with a 0.5 °C chilling bath; induction time was the time after passing the hydrate equilibrium curve to hydrate precipitation. The indicated weights of methanol or NAGA were added individually to nutrient broth from the same batch and the test repeated for each addition.

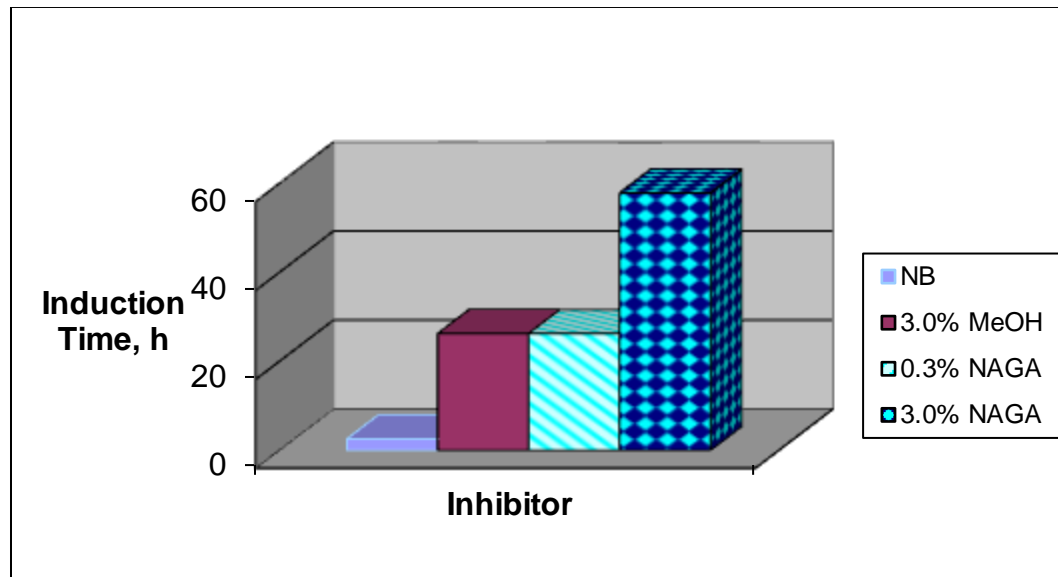


**Fig. 3.** Gas-hydrate inhibition by N-acetylglucosamine.

Note that longer induction times mean greater hydrate inhibition.

In Figure 3 it is seen that 0.3% NAGA retarded hydrate formation to the same extent as the order-of-magnitude larger concentration of methanol; 3% NAGA had 2 to 3 times lengthier induction times for hydrates to form compared to a like concentration of methanol.

## CONCLUSION

Not only is hydrate inhibition of a new compound demonstrated, but the primary importance is that compound occurs naturally in the environment and could be readily produced *en masse* at low cost.



## PUBLICATIONS

An article is in preparation pertaining to the work, and a provisional patent is under advisement.

## REFERENCES

Barrett, J., 2001. Thermal hysteresis proteins. *The International Journal of Biochemistry & Cell Biology* 33, 105-117.

Beveridge, T.J., and Murray, R.G.E., 1980. Sites of metal deposition in the cell wall of *Bacillus subtilis*. *Journal of Bacteriology* 141 (2), 876-887.

Chao, H.M., Houston, M.E., Hodges, R.S., Kay, C.M., Sykes, B.D., Loewen, M.C., Davies, P.L., Sonnichsen, F.D., 1997. A diminished role for hydrogen bonds in antifreeze protein binding to ice. *Biochemistry* 36, 14652-14660.

Gilbert, J.Z., Davies, P.L., Laybourn-Parry, J., 2005. A hyperactive,  $\text{Ca}^{2+}$ -dependent antifreeze protein in an Antarctic bacterium. *FEMS Microbiology Letters* 245, 67-72.

Gordienko, R., Ohno, H., Singh, V.K., Jia, Z., Ripmeester, J.A., Walker, V.K., 2010. Towards a green hydrate inhibitor: Imaging antifreeze proteins on clathrates, *PLoS One*, 5 (2), [www.plosone.org](http://www.plosone.org).

Gordon, M.S., Ambdur, B.H., Scholander, P.F., 1962. Freezing resistance in some northern fishes. *Biology Bulletin* 122, 52-62.

Hammerschmidt, E.G., 1934. Formation of gas hydrates in natural gas transmission lines. *Industrial & Engineering Chemistry* 26, 851-855.

Kelland, M.A., Svartaas, T.M., Ovstus, J., Tomita, T., Chosa, J., 2006. Studies on some Zwitterionic surfactant gas hydrate anti-agglomerants. *Chemical Engineering Science* 61, 4048-4049.

Konno, Y., Masuda, Y., Hariguchi, Y., Kurihara, M., Ouchi, H., 2010. Key factors for depressurization-induced gas production from oceanic methane hydrates. *Energy & Fuels* 24, 1736-1744.

Lederhos, J.P., Long, J.P., Sum, A., Christiansen, R.L., and Sloan, E.D., Jr., 1996. Effective kinetic inhibitors for natural gas hydrates. *Chemical Engineering Science* 51 (8), 1221-1229.

Moridis, G.J., Reagan, M.T., 2007. Gas production from oceanic Class 2 hydrate accumulations. *Proceedings of Offshore Technology Conference 2007*, #18866.

Ohtake, M., Yamamoto, Y., Kawamura, T., Wakisaka, A., de Souza, W.F., de Freitas, M.V., 2005. Clustering structure of aqueous solution of kinetic inhibitor of gas hydrates.

Journal of Physical Chemistry B., 109, 16879-16885.

Ramsey, J.A., 1964. The rectal complex of the mealworm *Tenebrio molitor*, L. (Coleoptera, Tenebrionidae). *Philosophical Transactions of the Royal Society of London B* 248, 279-314.

Rutqvist, J., Moridis, G.J., Grover, T., Collett, T., 2009. Geomechanical response of permafrost-associated hydrate deposits to depressurization-induced gas production. *Journal of Petroleum Science and Engineering* 67, 1-12.

Tyshenko, M.G., Doucet, D., Davies, P.L., and Walker, V.K., 1997. The antifreeze potential of the spruce budworm thermal hysteresis protein. *Nature Biotechnology* 15, 887-890.

Vollmer, W., Blanot, D., de Pedro, M.A., 2008. Peptidoglycan structure and architecture. *FEMS Microbiology Reviews* 32 (2), 149-167.

Xiao, C., and Adidharma, H., Dual, 2009. Dual function inhibitors for methane hydrate. *Chemical Engineering Science* 64, 1522-1527.

Zhang, D.Zo., Liu, B., Feng, D.R., He, Y.M., Wang, S.Q., Wang, H.H. and Wang, J.F., 2004. Significance of conservative asparagines residues in the thermal hysteresis activity of carrot antifreeze protein. *Biochemical Journal* 377, 589-595.

Ziegenhain, W.T., 1931. Every precaution taken to eliminate clogging of new Chicago gas line. *Oil & Gas Journal* 30 (19), 34.

### **TASK 7: Scoping study using Spatio-Temporal Measurement of Seep Emissions by Multibeam Sonar at MC118.**

This subcontract was continued into Phases 3 and 4 of the MS/SFO/Hydrates Project. A Final Report can be found under Phase 4, Task 6.

### **TASK 8: Validate high-frequency scatter on SDR data by acquisition of targeted cores and velocity profiles at MC118 Hydrate Mound.**

(Subcontractor Specialty Devices, Inc., Wiley, Texas; Paul Higley, PI)

Development of a Shallow Sediment Velocity Probe (SSVP) for use in the Gas Hydrates Research Consortium Sea Floor Observatory Program at MC118.

#### **Introduction**

A need for improved knowledge of sediment characteristics as part of the studies of the Gas Hydrates at the MC118 site prompted a desire to measure the velocity of these sediments. The successful installation of the Pore Fluid Array and Temperature Array with sensors installed to depths below the bottom of nearly 10 meters at MC118 opened

the possibility of installing acoustic sensors on a similar probe as a method of measuring sediment velocity.

## **Background**

The concept includes developing a series of acoustic sensors that can be attached to this type of a probe, survive the installation trauma and operate at sufficient depths to allow this concept to work. This also requires developing a data acquisition package that can survive these conditions and is capable of driving and communicating with acoustic sensors to achieve a measurement accuracy sufficient to meet the needs of the studies at MC118. SDI has offered to include this development as part of an ongoing electronics package development aimed to provide rapid acoustic shallow water sediment measurement capability.

The sediment probe being designed by SDI is being adapted to also serve as an attachment to an MMRI sediment coring device. The MMRI sediment coring device is intended to collect core samples of gas Hydrates or Hydrate bearing sediments in the Woolsey Mound portion of MC118. Inclusion of the sediment probe on this coring device presents the opportunity to collect a vertically graduated sample of the speed of sound, temperature and shear strength of Hydrate bearing sediments simultaneously with the collection of a core sample of this material. This application of the SDI sediment probe, as married to the MMRI sediment coring device, will be the 1<sup>st</sup> use of the sediment probe. This use is scheduled for the July 2014 MMRI cruise to MC118.

## **Activities during this period**

The development and construction of the sediment probe has been completed during this period.

The probe was designed to be capable of serving as an addition to the MMRI gravity core through addition of an electronics package on the top of the weight of the gravity core and a sensor string enclosed in a tube to be attached along the side of the core tube. The gravity core is being fitted with a USBL positioning system and a battery pack for the sediment probe. An acoustic sound source and an accelerometer have been included in the sediment probe electronics housing. The sound source is used for the speed of sound measurements and the accelerometer is dual purpose. It detects bottom contact and measures the deceleration rate. The bottom contact serves to trigger a time series of temperature measurements and a time delayed series of speed of sound measurements. The deceleration rate is used to determine the shear strength of the material through which the probe penetrates.

The sediment probe electronics and internal battery also enable the sediment probe to operate as a stand alone device if mounted on a weighted steel probe without a core barrel.

The software and hardware for this probe were completed and a series of lab tests were used to verify its operation prior to the planned deployment cruise. The battery pack for this sensor has been included in the electronics housing eliminating the need for an

external battery pack. The external battery pack was originally planned for the stand-alone sediment probe where multiple insertions and retrievals were planned before recovering the system to the boat. However, the internal pack has sufficient capacity to allow use as a stand alone device. The possibility of adding the external battery was retained should longer term stand-alone use be desired.

### **Design Overview and Progress**

The sediment probe attachment to the MMRI gravity core consists of a 10 meter long pipe with imbedded hydrophones and an electronics package attached to the top of the gravity core weight. The sediment probe electronics package is positioned with the acoustic source transducer installed on the end plate of the electronics package. This provides a line of sight for the acoustic source to the sensors in the receiving array in the seafloor adjacent to the core barrel. The sediment probe electronics package includes the controller/data logger, a sensor interface and A/D converter an accelerometer sensor, the battery power supply and the acoustic source.



***Electronics and housing for the Shallow Sediment Velocity Probe, SSVP.***

The operational plan for use with the gravity core includes, lowering the sediment probe/coring device to a depth of 30 to 50 meters above the sea floor, using the USBL system to navigate the sensor to the desire location, free falling the sediment probe/gravity core into the sea floor, detecting the bottom insertion with the accelerometer sensor, leaving the probe in place for a suitable time to measure sediment velocity distribution and

temperature profile along the probe length and having the ship winch pull the probe free of the sea floor and recovered to the deck for data and core sample recovery.

### **Schedule**

The sediment probe development and construction of the electronics and software has been completed.

### **TASK 9: Recipient shall model carbonate/hydrate mound in Mississippi Canyon 118 using modified version of (THROBS).**

(This task was continued in Phases 3 and 4. A Final Report appears as Phase 4, Task 3: Modeling a carbonate/hydrate mound in Mississippi Canyon 118 using modified version of THROBS).

### **TASK 10. Administrative oversight of the Monitoring Station/Sea-floor Observatory Project.**

Administration of the Consortium is the responsibility of the University of Mississippi and includes formal Project Proposals to federal funding agencies, Technical Progress Reports, Final Project Reports, informal monthly updates, reports of Consortium meetings, cruise reports, participation in national meetings, organizing meetings between researchers, organizing and participating in program reviews, organizing and participating in research activities, including research cruises. This responsibility was completed for FY08 with the completion and acceptance of the year-end report to DOE, 42877R12. Further administrative duties and responsibilities are addressed in Phase 4.



## **PHASE 3 Tasks for FY 2009:**

### **TASK 1: Project Management Plan (complete)**

### **TASK 2: Geological and Geophysical Baseline Characterization of Gas Hydrates at MC118, Gulf of Mexico**

**Temporal evolution of the gas hydrate system at Woolsey Mound via time-lapse seismic monitoring.**

(Subcontractor: University of South Carolina; Camelia Knapp, James H. Knapp, PIs; Collaborators: Antonello Simonetti, Darrell Terry)

#### **Introduction**

Cold seeps, also known as cold *vents*, are important pathways for methane and heavier hydrocarbons to leak naturally from the lithosphere into the hydrosphere and, potentially, to the atmosphere (Leifer and Boles, 2005). Consequently, cold vents contribute to ocean acidification, global warming, and provide also a long-term life-sustaining role for unique chemosynthetic communities (Bangs et al., 2011). Hence, understanding the dynamics of gas hydrates systems associated with natural hydrocarbon seepage areas and their impact on climate and ocean bio-geochemistry is crucial.

Cold seeps, when active, are extremely dynamic environments where salinity, hydrocarbon availability, temperature, pressure, and complex interactions with the biosphere can change rapidly through time (hours, days, years). Hence, the stability of a gas hydrate system would be primarily a function of whether the cold seep is active or not. In other words, as long as hydrocarbons and saltier fluids are provided into the hydrate stability zone (HSZ) from the deep sources, gas hydrates could be considered critically stable. On the other hand, when the cold seep is quiescent and there are minor external forces perturbing the equilibrium (i.e. no hydrocarbons migrating upwards) gas hydrates could be considered more stable through time.

Short-time scale changes (hours, months, years) on gas hydrate formation, accumulation and dissociation, are induced by those processes which can rapidly perturb the hydrate stability field (HSF), such as hydrocarbon fluids transiting along the fault, fault slippage (earthquakes?), seasonal variations in sea-bottom currents and/or temperature, and so on.

Long-term scale changes (thousands to hundred thousands of years) in gas hydrate formation, accumulation, and dissociation, can result from larger phenomena that produce variations within the stability field, such as glacio-eustatic variations in sea level, salt-tectonic activity versus quiescence, and so forth.

Repeating seismic surveys through time (4D seismic monitoring) in cold seep environments provides a better understanding of the time scale at which gas hydrates

form, accumulate, dissociate and through which hydrocarbons enter the system in seawater. Riedel (2007) has demonstrated that temporal changes in sub-surface anomalies over a time-span of 5 years, interpreted as seafloor hydrocarbon venting episodes from underlying gas hydrates, were clearly detectable using 4D seismic imaging at *Bullseye Vent* (offshore Vancouver Island). Similarly, Bangs et al. (2011) showed a scenario for the South Hydrate Ridge (offshore Oregon) where temporal changes in hydrocarbon anomalies within a time interval of 8 years were noticed through time-lapse seismic monitoring.

We adopted the 4D seismic monitoring approach at *Woolsey Mound*, a fault-controlled cold seep located in 900m water depth in the Northern Gulf of Mexico (Mississippi Canyon Block 118, MC118), with the aim to evaluate the short-term (3 years) and subsequently long-term mechanisms affecting gas hydrates formation, accumulation and dissociation through time.

### **1.1. Time-lapse seismic monitoring**

4-Dz seismic imaging, or time-lapse seismic monitoring, mainly consists of conducting repeated 3-D seismic surveys over the same area through time, with the aim to detect temporal changes in sub-surface anomalies induced by variations in pore fluid saturations. 4-D seismic imaging is now routinely exploited in the oil and gas industry to monitor production effects within hydrocarbon reservoirs (Watts et al., 1996; Lumley, 2001; Tura et al., 2005; Fomel and Jin, 2009), as well as in supervising CO<sub>2</sub> sequestrations (Chadwick et al., 2005; Lumley, 2010).

The most important feature of time-lapse seismic monitoring data is the ability to compare seismic images as a function of elapsed time. However, small artifacts in amplitude, phase and time of imaged seismic events can obscure real signatures of sub-surface temporal changes. Hence, careful attention to data processing issues is needed to ensure that images obtained at one time are validly comparable to subsequent images (Lumley, 1995b). The intent of 4-D processing is to attenuate the 4-D “noise” caused by changes in acquisition parameters or environmental conditions, and to emphasize the 4-D signature of the reservoir caused by changes in fluid, pressure and stress. A standard seismic processing technique in 4-D time-lapse monitoring is known as cross-equalization (Eastwood et al., 1998; Harris and Henry, 1998; Naess, 2006; Gan et al., 2004; Riedel, 2007). Essentially, the cross-equalization process allows the user to perform a time-lapse seismic monitoring by removing differences in:

- Sample rate;
- Survey geometry;
- Time and phase;
- Amplitude (gain);
- Frequency.

Although the post-processed datasets will have the same sample rate and survey geometry throughout the entire volume, time, phase and amplitude of certain seismic events may vary in zones where changes in the subsurface are expected to occur

through time (i.e. depleted hydrocarbon reservoirs). The main purpose of the 4-D seismic cross-equalization then, is to reduce differences in areas with no expected changes and to optimize differences in areas where changes have occurred (Riedel, 2007).

While this approach may be straightforward in conventional 4-D seismic monitoring, it appears to be more challenging when adopted in areas on Earth where hydrocarbon reservoirs are depleted uncontrollably, such as marine cold seep environments, which are often associated with gas hydrate systems. Particularly, at Woolsey Mound thermogenic hydrocarbons are naturally leaked into the water column through faults and they appear to be temporarily plugged in fractures by transitory gas hydrate accumulation in the shallow sub- surface. Unlike the case of controlled hydrocarbon production, in cold seeps settings the subsurface locations where temporal changes in hydrocarbon anomalies take place are unknown. However, they can be inferred directly where seafloor venting sites are active. Also, they can be estimated almost directly from seafloor features such as pockmarks and craters, which are commonly interpreted as results of episodic hydrocarbon escape into the water column (Hovland and Judd, 1988; Løseth et al., 2001). Finally, locations where hydrocarbon fluxes are more vigorous than others can be indirectly inferred by looking at the degree of biodiversity among the chemosynthetic biological communities present at the seafloor.

The time-lapse seismic analysis has been carried out essentially using the Hampson Russell CGGVeritas software. Two sets of 3-D standard seismic data were analyzed for the time- lapse seismic monitoring of Woolsey Mound:

- TGS-Nopec data, acquired in 1999-2000 (henceforth referred as 2000 data);
- Western Geco data, acquired in 2002-2003 (henceforth referred as 2003 data).

Although 2000 and 2003 data belong to the same typology of standard 3D data, namely they were acquired and processed with standard and similar parameters, in order to minimize their remaining differences related to acquisition and processing and optimize the real differences between the two some of the standard cross-equalization steps were applied. Before starting the 4D seismic processing, the oldest dataset was set as reference (2000) and the newer as monitor (2003). Then, the cross-equalization consisted of:

- re-sampling 2003 data (according to 2000 data sample rate);
- 3D geometry re-binning of the 2003 data (according to 2000 data geometry);
- static correction of the 2003 data through a cross correlation time-shift with the 2000 data;
- amplitude-balancing of the 2003 data through a gain cross-normalization with the 2000 data.

Once the two datasets were processed, as the 4-D seismic monitoring aims to detect changes in seismic amplitude anomalies through time, a new 3-D seismic volume subtracting the amplitudes of the 2003 data from the 2000 data has been created. The

resulting dataset, from now on referred to as Difference Volume, shows the subsurface spatial/temporal amplitude differences between the 2000 and 2003 data. The seismic section in Figure 1 is taken from the Difference Volume (the location is shown in Figure 1). The profile displays a portion of the shallow subsurface of MC118 where gas hydrates could be stable according to previously computed thermodynamic models (Lapham et al., 2008). It is clear how the shallow subsurface of Woolsey Mound, an active cold seep, presents higher magnitudes in changes compared to areas away from the mound (Quiescent Area) where significant changes are not expected within a relatively short time frame basing on the monotonous nature of the subsurface. We interpret the lower amplitude differences within the Quiescent Area to be the result of remnant acquisition/processing discrepancies between the 2000 and the 2003 data (greenish tones). On the other hand, we speculate that the higher differences in seismic amplitude observed below Woolsey Mound, or higher changes in acoustic impedance, are the result of variations in pore fluid contents induced by actively migrating hydrocarbons transiting through the master faults (Macelloni et al., *submitted*) and within the gas hydrates system (red-to-yellow and white tones). If our interpretations are realistic, they substantiate the idea that within a short time-frame (three years) the HSF at Woolsey Mound is critical and it is threatened by upward-migrating fluids and gases, thus confirming the highly dynamic behavior of the mound. In order to have a better understanding of how the temporal differences in amplitude are spatially distributed in the gas hydrate system at Woolsey Mound, we selected again the two areas outlined in Figure 1. Then, a series of closely-spaced RMS amplitude and RMS envelope time slices was extrapolated from the Difference Volume, starting from the seafloor down to ~0.2 sec TWT bsf, hence within the HSF.

The results, shown in Figure 2 and Figure 3 reveal again no significant changes through time in the subsurface of the Quiescent Area, while Woolsey Mound features substantial amplitude differences through time. Here, the most prominent temporal changes in acoustic impedance appear to be correlated, spatially, with either seafloor craters (shallower anomalies) and/or, most importantly, with the subsurface trend of the master faults (deeper anomalies). Assuming that such changes in acoustic impedance are the result of variations in pore fluid contents induced by actively migrating hydrocarbons, this observation would be valid proof that the master faults are the primary pathways for rising thermogenic hydrocarbons. Also, this would confirm that short term changes can be induced by transit of hydrocarbon fluids and gases along the fault (deeper anomalies) and perhaps seasonal variations in sea-bottom currents temperature (shallower anomalies). However, complex bio-geochemical interactions within the biosphere may play an important role in the changes observed at the seafloor. Figure 4a shows two coinciding profiles extrapolated from the 2000 and 2003 data that highlight different intensities of the same bright spot anomaly (free gas?) at the base of what we confirmed to be a concentration of gas hydrates in fractures near the blue fault (JPC-1 core – Simonetti et al., 2011). The cartoon in Figure 4b depicts a possible scenario to explain how gas hydrates form temporarily along the fault, thus sealing migrating thermogenic hydrocarbons at the base of the HSF where free gas and fluids continue to accumulate through time. As the pressure promotes increasing thermogenic hydrocarbons migration through time, hydraulic fracturing promotes gas

hydrates dissociation through fractures and venting into the water column. This dynamic equilibrium within the gas hydrate system is maintained through time as long as thermogenic hydrocarbons are supplied.

### Acknowledgments

We thank TGS-Nopec Geophysical Company, Western-Geco, SMT Kingdom, Landmark Graphics Corp., and CGG Veritas Hampson-Russell for providing data and software for this project.

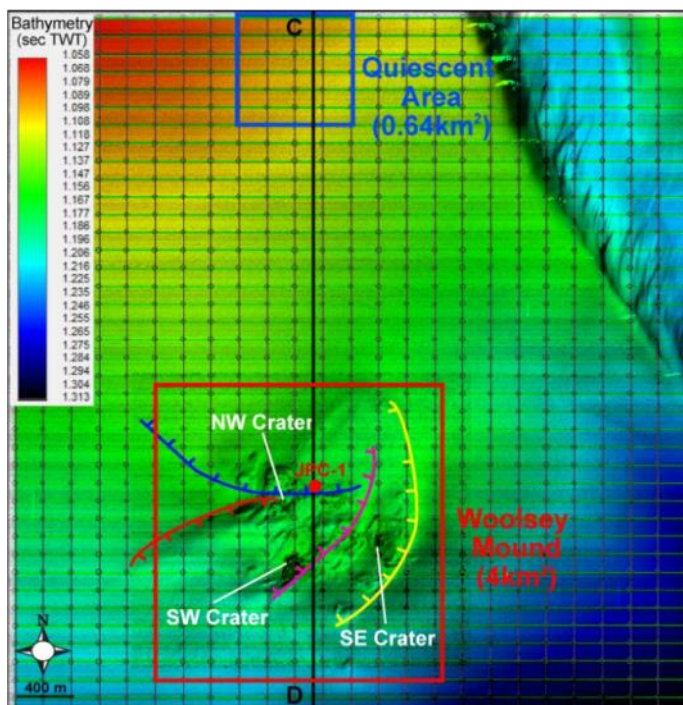
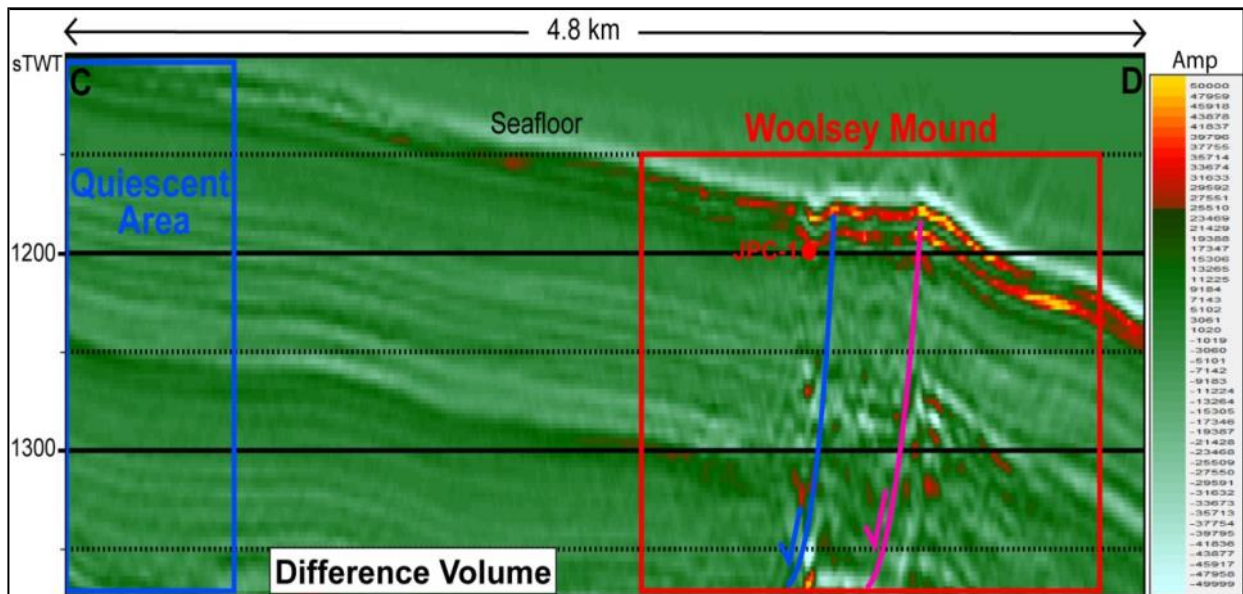


*Figure 1. (above) Seismic transect extrapolated from the Difference Volume. The profile shows the spatial and temporal differences in amplitude, or in acoustic impedance contrasts, between the 2000 data and the 2003 data. The Woolsey Mound area, outlined in red, shows more prominent amplitude differences compared to the Quiescent Area, outlined in blue. We speculate that the higher differences in seismic amplitude observed below Woolsey Mound are the result of variations in pore fluid contents induced by the active migration of hydrocarbons through the main faults and within the gas hydrates system; (left) MC118 bathymetry showing the location of the seismic transect above, the two areas analyzed, the master faults intersecting the seafloor and the three associated craters.*



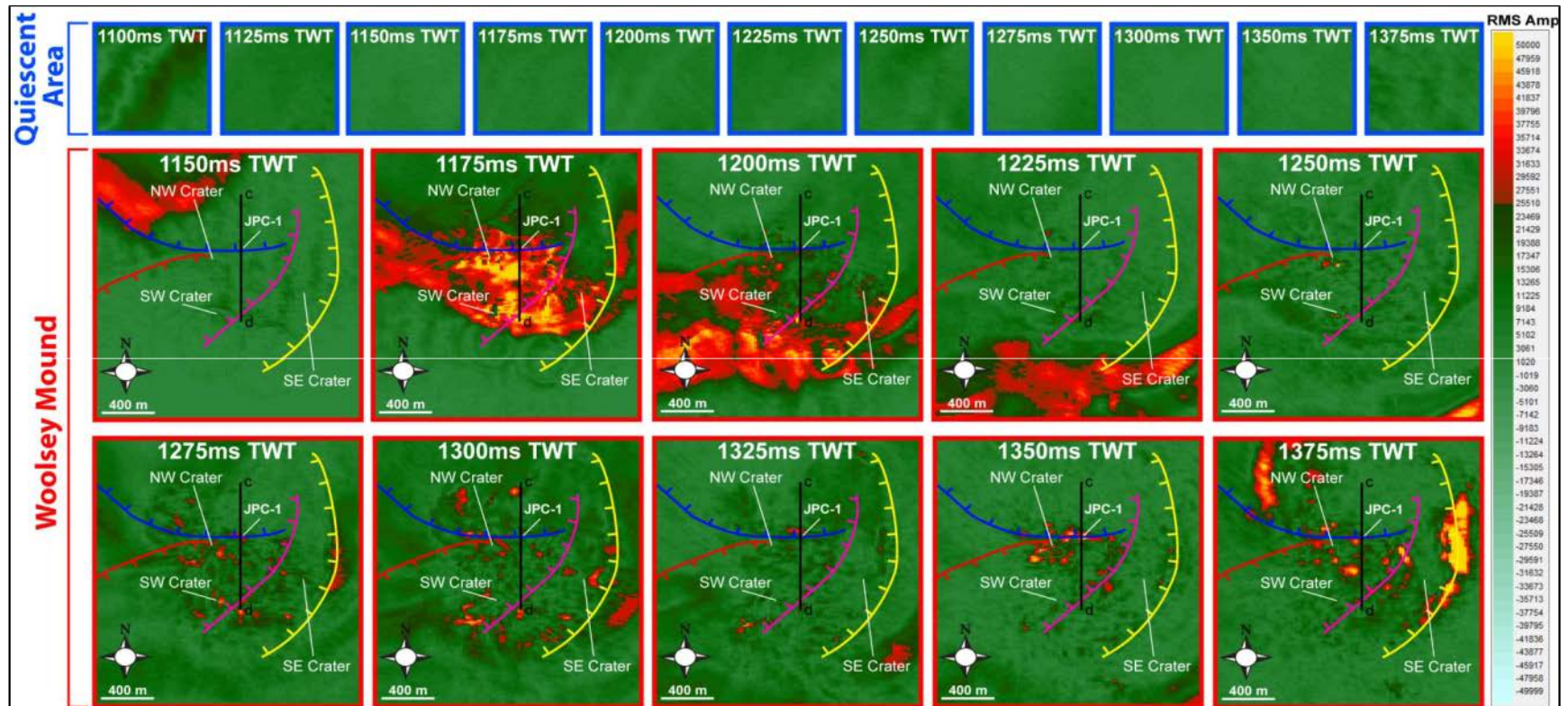


**Figure 2. RMS amplitude time slices extrapolated from the Difference Volume in the Quiescent Area and Woolsey Mound (see Fig.1 for references). The time slices were taken every 25 milliseconds with a 10 millisecond centered window. Note in Woolsey Mound the remarkable presence of (short-term) temporal changes in seismic anomalies compared to the Quiescent Area, and their spatial correlation with the trend of the main faults and seafloor craters. See text for details.**

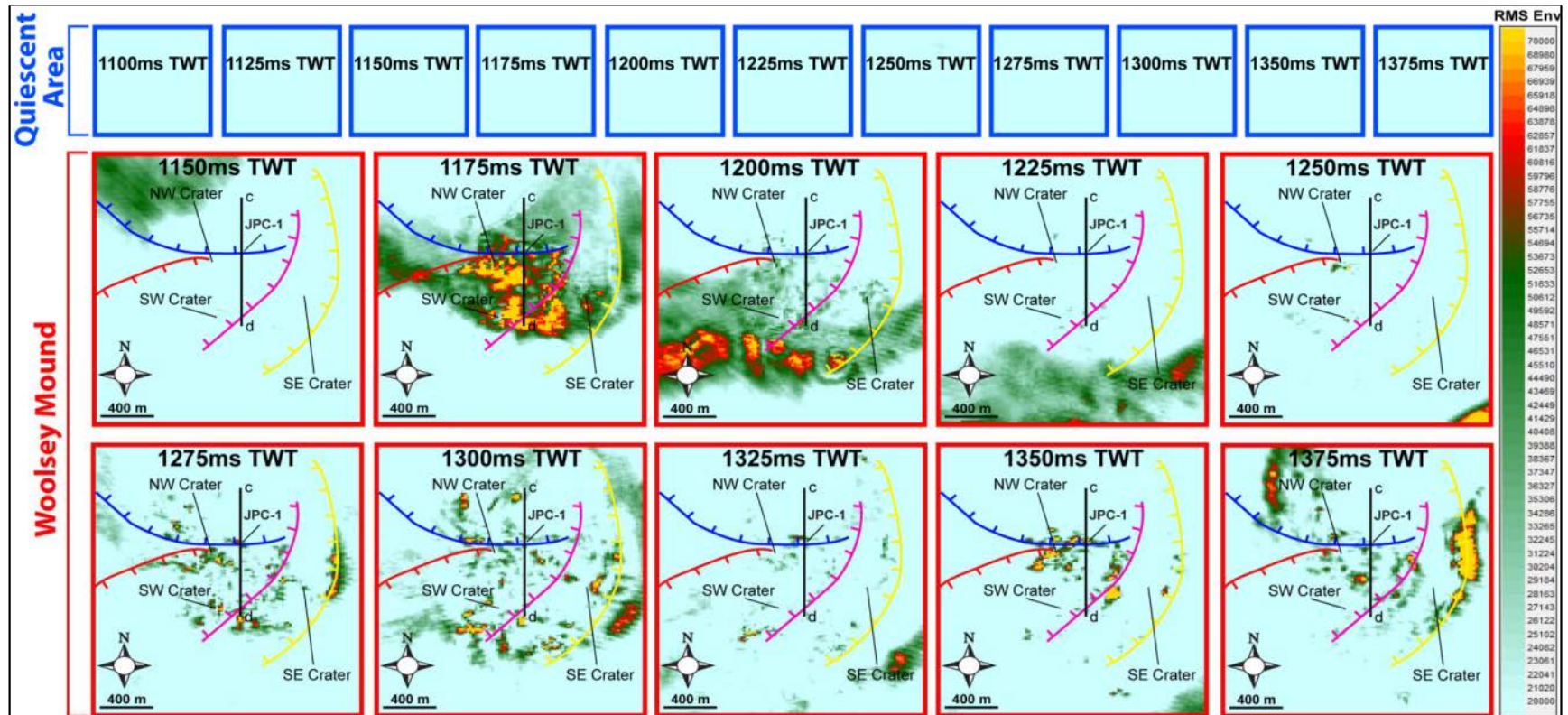
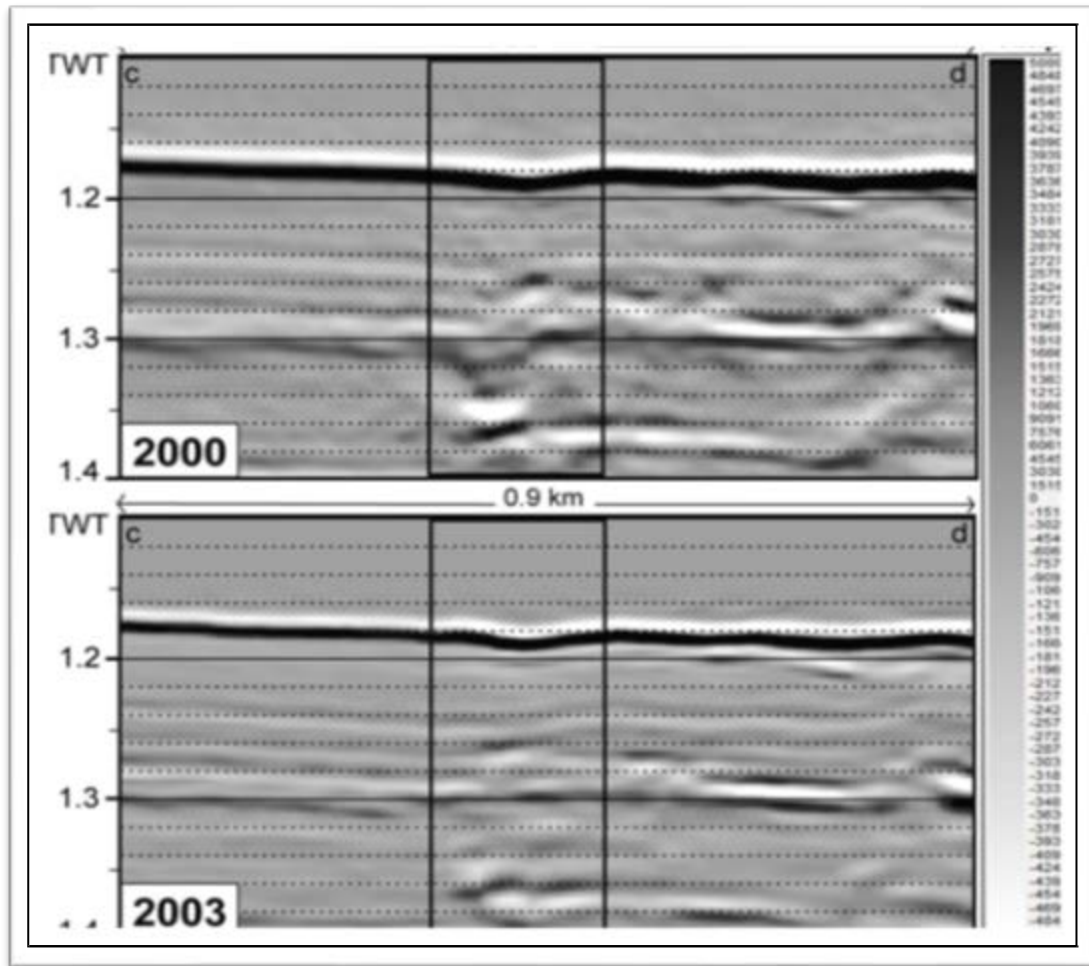
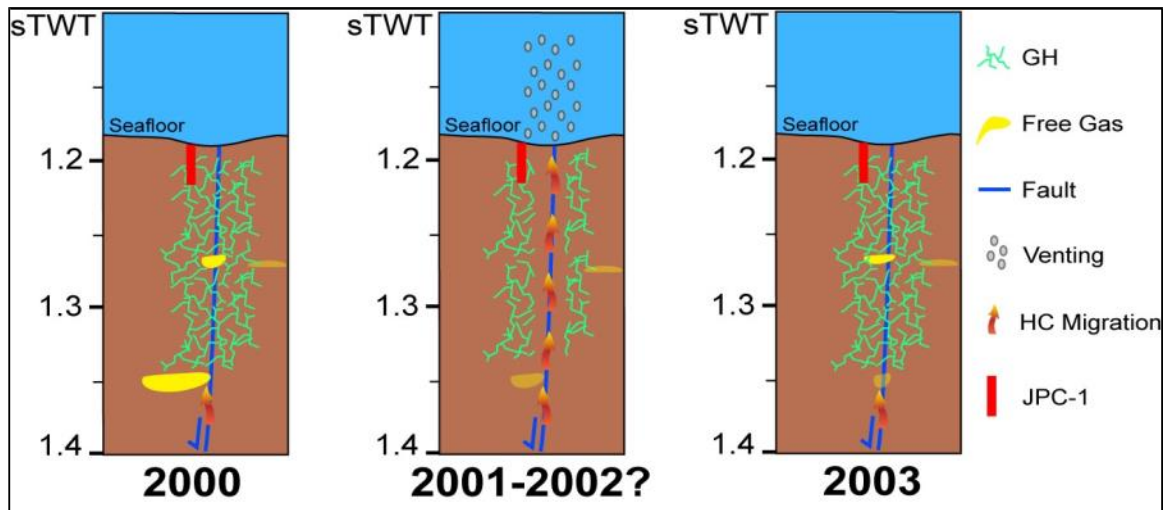


Figure 3. RMS Envelope time slices extrapolated with the same criterion of the RMS amplitude time slices in figure 2. Note in Woolsey Mound the remarkable presence of (short-term) temporal changes in seismic anomalies compared to the Quiescent Area, and their spatial correlation with the trend of the main faults and seafloor craters. See text for details. Since during the processing sequence we did not apply a phase-shift correction and since the seismic attribute Envelope (or instantaneous amplitude) is independent from the phase, the RMS Envelope time slices can be considered more realistic than the RMS Amplitude in figure 2. However, amplitude and envelope yielded comparable results.



a



b

Figure 4 a) Two coinciding profiles from the 2000 and 2003 data and b) a possible scenario to explain how gas hydrates form temporarily along the fault, accumulate and dissociate through time. See text for further details.



## Discussion

Cold seeps constitute the major source of hydrocarbons in seawater worldwide (National Academy of Science, 2002). In cold seep environments, methane (CH<sub>4</sub>) is naturally leaked from the lithosphere into the hydrosphere, and ultimately to the atmosphere (Leifer and Boles, 2005). Such methane vents sustain rare ecosystems at the seafloor and may contribute to ocean acidification and global warming (Bangs et al., 2011). Therefore, understanding the dynamics involved in marine hydrocarbon seeps is crucial to quantifying their potential impact on ocean biogeochemistry and climate.

As cold seeps rely upon hydrocarbon gas availability, they are often associated with gas hydrate systems, particularly in deep water settings where temperature and pressure are optimal for gas hydrate to form and accumulate in sediments. In such circumstances, transitory formation of gas hydrates would modulate the continuous release of hydrocarbons in the oceans.

We present data from Woolsey Mound, a hydrate/carbonate mound associated with a fault-controlled cold seep in the continental slope of the Northern Gulf of Mexico. Here, thermogenic gas hydrate accumulations along active faults, nucleating from the underlying salt dome and intermittent seafloor hydrocarbon vents, coexist. The aim of our study is to understand the nature and, most importantly, the short-term mechanisms governing gas hydrate accumulation, destabilization and subsequent methane venting into the water column.

## Results

New results from quantitative time-lapse seismic monitoring (or 4-D seismic imaging) conducted using two sets of 3-D standard seismic data acquired three years apart, suggest that the upward migration of deep-sourced hydrocarbons and brines along the faults may be the primary short-term control in the destabilization of gas hydrates (Simonetti et al., *in preparation*). Such a hypothesis would be plausible considering that the fault network not only provides the main migration pathways for rising thermogenic hydrocarbons (Macelloni et al., 2012) but also constitutes the reservoir for gas hydrates (Simonetti et al., *in review*). The main results of our 4-D analyses can be summarized as follows:

- The subsurface of Woolsey Mound shows significant changes in amplitude anomalies (or acoustic impedance) within a three-year time scale;
- These temporal anomalies are spatially associated with the major faults that intersect the seafloor;
- Since the major faults constitute the migration pathways for deep-sourced hydrocarbons, we suggest that changes in acoustic response, through time, are the result of actively migrating thermogenic hydrocarbons within the gas hydrate system;
- As the major faults constitute also the gas hydrate reservoirs, we speculate that gas hydrates may be repeatedly destabilized by transiting thermogenic hydrocarbons within the system in a very short time scale (3 years);
- Gas hydrates may be considered critically stable in active cold seep systems like Woolsey Mound, their stability through time depending primarily on the vigor of the hydrocarbon flux through the gas hydrate system.

The above results will be submitted to the Geophysical Research Letters AGU Journal. A manuscript has been accepted by the Journal of Marine and Petroleum Geology.

## REFERENCES

- Bangs, N. L. B., Hornbach, M. J., Berndt, C., **2011**, *The mechanics of intermittent methane venting at South Hydrate Ridge inferred from 4D seismic surveying*, Earth and Planetary Science Letters 310, p. 105–112.
- Chadwick, R. A., Arts, R., Eiken, O., **2005**, *4D seismic imaging of a CO<sub>2</sub> plume at Sleipner, Noerth Sea*. In: DORE, A. G. & VINING, B. A. (eds) *Petroleum Geology: North-West Europe and Global Perspectives - Proceedings of the 6th Petroleum Geology Conference, 1385–1399*. Petroleum Geology Conferences Ltd. Published by the Geological Society, London.
- Eastwood, J. E., D. Johnston, X. Huang, K. Craft, and Workman, R., **1998**, *Processing for robust time-lapse seismic analysis: Gulf of Mexico example, Lena Field*, 68<sup>th</sup> Ann. Internat. Mtg., Soc. Expl. Geophys., Expanded Abstracts, p. 20–23.
- Formel, S., Jin, L., **2009**, *Time-lapse image registration using the local similarity attribute*, Geophysics, vol. 74, no. 2, p. A7–A11.
- Gan, L., F. Yao, Y. Hu, Y. Liu, and Du, W., **2004**, *Applying 4D seismic to monitoring water drive reservoir*, SEG Expanded Abstracts 23, 2553 (2004).
- Harris, P. E., and Henry, B., **1998**, *Time lapse processing: A North Sea case study*, 68<sup>th</sup> Ann. Internat. Mtg., Soc. Expl. Geophys., Expanded Abstracts, p. 1–4.
- Hovland, M., Judd, A.G., **1988**, *Seabed Pockmarks and Seepages. Impact on Geology, Biology and the Marine Environment*. Graham and Trotman, Ltd., London, 293p.
- Lapham, L.L., **2008**, *Towards the development of a biogeochemical model to describe venting activity at MC 118*: Proceedings of the Gulf of Mexico Hydrates Research Consortium, Semiannual Meeting, Oxford MS, Feb. 26–27, 2008.
- Leifer, I., Boles, J., **2005**, *Measurement of marine hydrocarbon seep flow through fractured rock and unconsolidated sediment*. Marine and Petroleum Geology, v. 22, p.551–568.
- Løseth, H., Wensaas, L., Arntsen, B., Hanken, N., Basire, C., Graue, K., **2001**, *1000 M Long Gas Blow-Out Pipes*. Extended abstract. EAGE, Amsterdam.
- Lumley, D. E., **1995b**, *4-D seismic monitoring of an active steamflood*, 65<sup>th</sup> Ann. Internat. Mtg., Soc. Expl. Geophys., Expanded Abstracts, p. 203–206.
- Lumley, D. E., **2001**, *Time-lapse seismic reservoir monitoring*. Geophysics, 66 - 1, 50–53.
- Lumley, D. E., **2010**, *4D seismic monitoring of CO<sub>2</sub> sequestration*, The Leading Edge February 2010, v. 29 no. 2, p. 150-155.
- Macelloni L., Simonetti, A., Knapp, J.H., Knapp, C.C., and Lutken, C.B., 2012, Multiple-resolution seismic imaging of a shallow hydrocarbon plumbing system: Woolsey Mound, MC118, Northern Gulf of Mexico. *Marine and Petroleum Geology*. v. 38, p. 128-142.
- Naess, O. E., **2006**, *Repeatability and 4D seismic acquisition*, SEG Expanded Abstracts 25, 3300 (2006). National Academies of Sciences, 2002, *Oil in the sea*.
- Riedel, M., **2007**, *4D seismic time-lapse monitoring of an active cold vent, northern Cascadia margin*, Mar Geophys Res, v. 28, p. 355–371.
- Simonetti, A., Knapp, J.H., Knapp, C.C., Macelloni, L., Lutken, C.B., **2011**, *Defining the hydrocarbon plumbing system and the possible accumulation model for marine gas hydrates in a salt tectonic driven cold seep: examples from Woolsey Mound, MC118, northern Gulf of Mexico*. Proceedings of the 7th International Conference on Gas Hydrates (ICGH 2011), Edinburgh, Scotland, United Kingdom, July 17-21.
- Simonetti A., Knapp, J.H., Sleeper, K., Lutken, C.B., Macelloni, L., and Knapp, C.C., (in press), *Spatial Distribution of Gas Hydrates from High-Resolution Seismic and Core Data, Woolsey Mound, Northern Gulf of Mexico*. *Marine and Petroleum Geology*.
- Simonetti A., Riedel, M., Knapp, J.H., Knapp, C.C., and Lutken, C.B., (in prep), *4-D Seismic imaging of a thermogenic gas hydrate system in the Northern Gulf of Mexico (Woolsey Mound, MC118)*. *Geophysical Research Letters*.
- Tura, A, Barker, T., Cattermole, P., Collins, C., Davis, J., Hatcell, P., Koster, K., Schutjens, P., Wills, P., **2005**, *Monitoring primary depletion reservoirs using amplitudes and time shifts from high-repeat seismic surveys*, Shell International Exploration and Production, Houston, USA. The Leading Edge, December 2005.
- Watts, G. F. T., Jizba, D., Gawith, D. E., Gutteridge, P., **1996**, *Reservoir Monitoring of the Magnus Field Through 4D Time-Lapse Seismic Analysis*, Petroleum Geoscience 2, no. 4, p. 361–372.



### **TASK 3: Near seafloor geology at MC118 using converted shear-waves from 4C seafloor sensor data. (Processing Ocean Bottom Seismometer Data Collected On The Cruise Gom1-11-Mc118 Aboard The M/V *Bunny Bordelon*)**

Due to the death of Dr. McGee and the departure of Dr. Macelloni, the MMRI/CMRET did not have a resident geophysicist available to complete this project. We, therefore, entered into negotiations with long-time collaborator, Vaughn Goebel of Lookout Geophysical Company (LGC) to complete this task. He is familiar with the project and has remained in close communication with Dr. Macelloni, so that the transfer of information has been as clean and efficient as possible. He first evaluated the data for consistency and then presented an estimate of time required to finish the job. Goebel and Macelloni have collaborated to produce an in-depth report of the experiment and present the prospects for using OBS data in the future.

#### **Introduction**

The primary goal of this study is to process seismic recordings to isolate both P-wave and converted S-wave data over the Woolsey Mound. Of special interest are spatial changes in the ratio of P-wave to S-wave interval velocity, which may indicate changes in methane hydrate concentration across the study area. We explore two methods of processing the data to this end.

This report shows the results of processing Ocean Bottom Seismometer (OBS) data collected over Woolsey Mound, MC 118, during the spring of 2011. The OBS units are from Woods Hole Oceanographic Institution (WHOI). The data channels are for one hydrophone and three orthogonal gimbal mounted geophones at each of fifteen OBS stations. The OBS stations are at an average depth of 885 meters, deployed along a N-S line over Woolsey Mound.

Surface source lines run both N-S and E-W over the OBS stations. All three E-W lines and one N-S line use the GI Gun source. For comparison, the second N-S line repeats the first N-S line using the Water Gun source.

Each OBS station records continuously to create "Receiver Gathers" that span the days of deployment. The initial processing task is to recover just those time segments of the receiver data that correspond to source firing times, and organizing that subset of data into SegY formatted files. This processing creates a SegY file for each OBS station that contains all five source lines, with four channels (one hydrophone and three geophones) for each source firing on each source line.

Processing these SegY files then shows that a combination of hydrophone (pressure sensor) and geophone (velocity sensor) responses may be manipulated to separate P-wave and converted S-wave arrivals at each OBS station. In addition, comparison of the GI Gun source to the Water Gun source may influence the choice of sources for future surveys.

#### **Acquisition Review**

The following figures show the OBS locations and Source locations over Woolsey Mound.

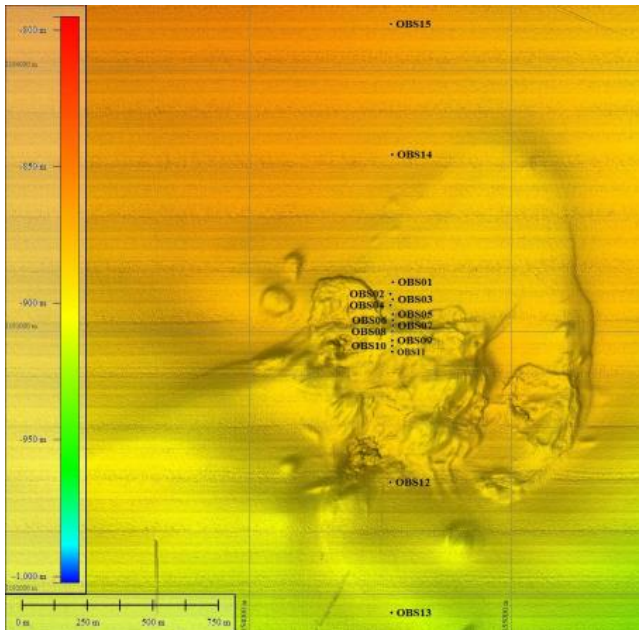


**Figure 1. OBS locations.**

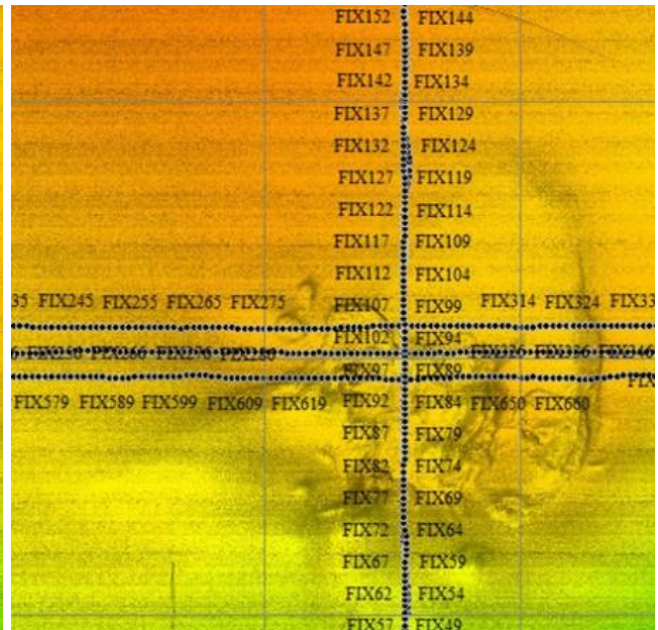


**Figure 2. Source lines.**

**OBS recording parameters:**

Nominal horizontal interval (OBS 1-11): 25 meters  
 Nominal horizontal interval (OBS 12-15): 500 meters

**Data format:**

Mini-SEED

Digitizing interval: .005 seconds  
 Maximum frequency (anti-alias limit): 100 hz  
 Hydrophone: HighTech HTI-90-U  
 Geophones (orthogonal gimbal mount): 4.5 hz Geospace GS-11D

**Surface source parameters:**

Nominal horizontal interval : 25 meters  
 Nominal ship speed: 2.5 knots ( 1.29 meters/second )  
 Nominal manual firing interval: 19.4 seconds  
 GI Gun chamber size: 90 cubic inches  
 GI Gun firing pressure: 2000 psi  
 Water Gun chamber size: 80 cubic inches  
 Water Gun firing pressure: 2000 psi

See "Lutken Cruise Report GOM01-11.docx" for the full details of the data acquisition.

## Processing – SEED to SegY

Our processing starts with data converted from Mini-SEED (OBS internal format) to SegY format. WHOI provided the conversion, creating SegY files with data traces in 30 second segments, starting with event 1 on Line 1 at 4:58 on April 7, 2011, and ending with event 882 on Line 5 at 11:57 the same day (about 7 hours of ship time, and 4.75 hours of relevant data).

Each event is labeled as a Field File ID (FFID) in SegY, 1 to 882. We use “Shot”, “Event”, and “FFID” interchangeably. Each FFID has four channels ordered as Vertical geophone (V), first Horizontal geophone (L1), second Horizontal geophone (L2), and Hydrophone (P).

Timing chatter due to manual firing is apparent in the data, shown below in Figure 3.

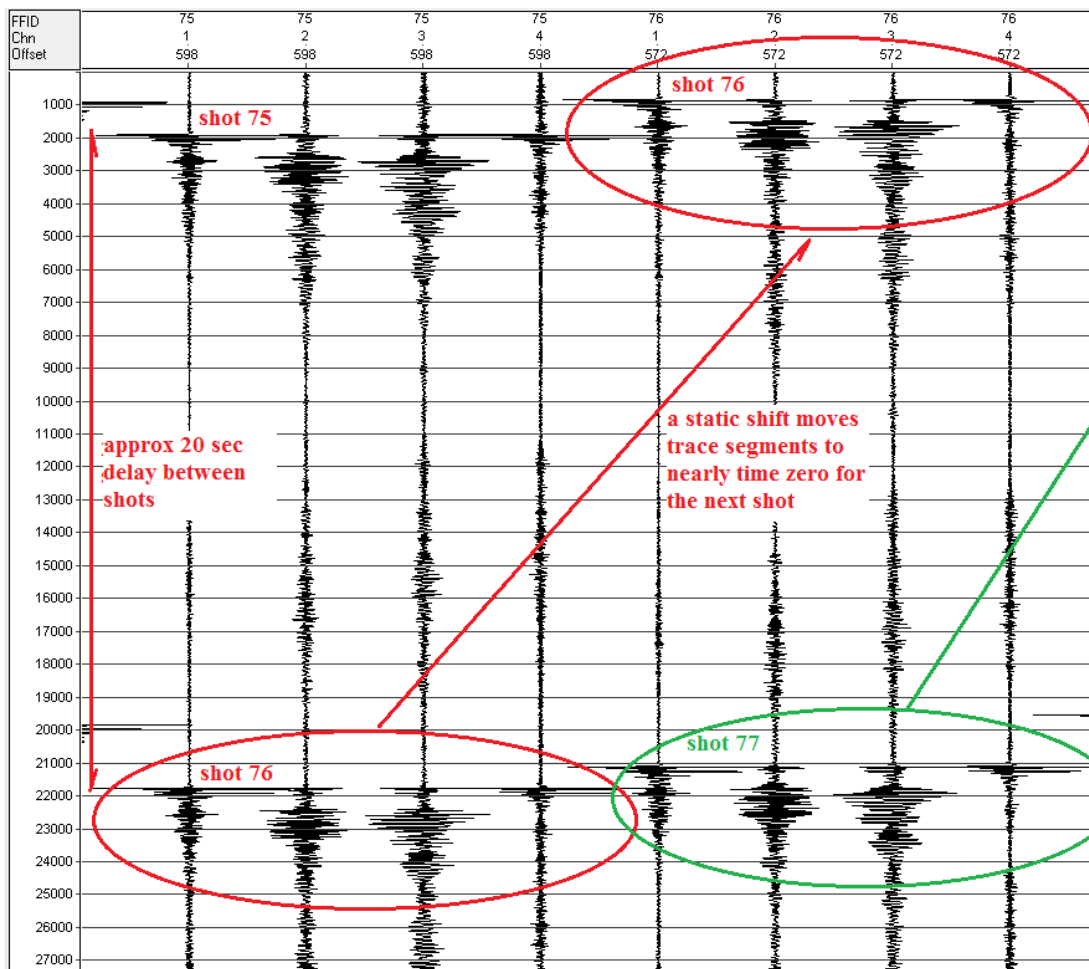


Figure 3. Example of OBS data.

Consider Figure 3. This example for OBS 5 shows extraction of trace segments from continuous recording, where the start of each set of four channels is near the firing time of each shot. The traces are 30 seconds long and contain the start of the next firing with about a 20 second delay. For example, shot 75 starts at about 2000 msec and also contains shot 76 at about 22000 msec. The next set of four channels for shot 76 starts at about 1000

msec and also contains the start of shot 77 with about a 20000 msec delay. We step through all shots in this manner.

A way to remove the timing chatter from the data is to align the direct arrival of each shot to a constant time, such as 50 msec. This is called “Reduced Time” and is used in all of the following processing examples.

### Processing – Problems and Work Delays

Several problems slowed progress in processing this OBS data. Manual source timing took considerable effort to resolve the timing for initial conversions from SEED to SegY. After conversion to SegY, review of the data showed apparent problems with some of the OBS units which took time to investigate and understand. Personnel changes were another factor. Continuation of this study required coding additional software for OBS processing, and that took additional time for completion.

Problems with OBS data were mostly with horizontal geophone channels, and that raised concerns since recording converted S-waves usually relies on the horizontal channels. Figures 4-7 show the data channels for Line 1, OBS 1 through 11. For still unknown reasons, L2 (Figure 6) shows amplitude dropouts on five of the eleven OBS units, at stations 4, 6, 7, 8, and 9. Figures 4-7 show near-trace gathers in “reduced time” with fixed gain and a low-cut display filter to remove DC offset.

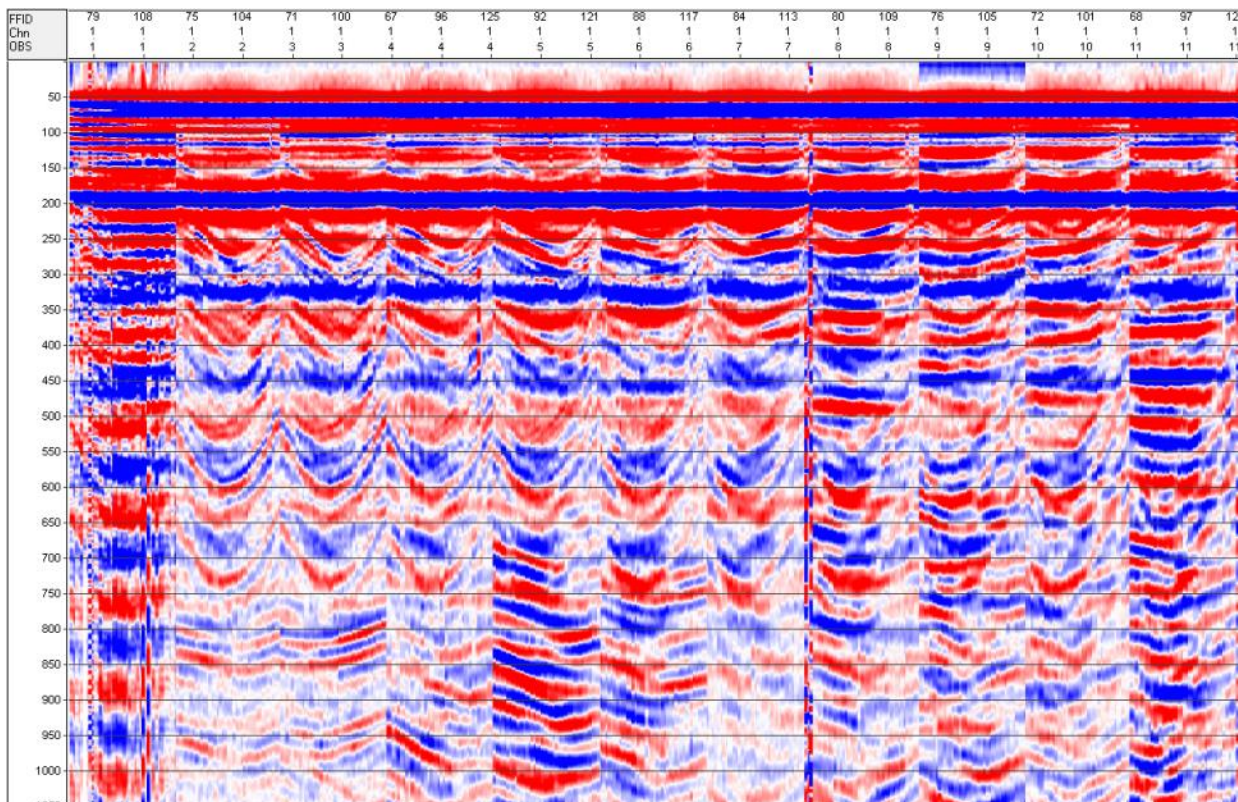
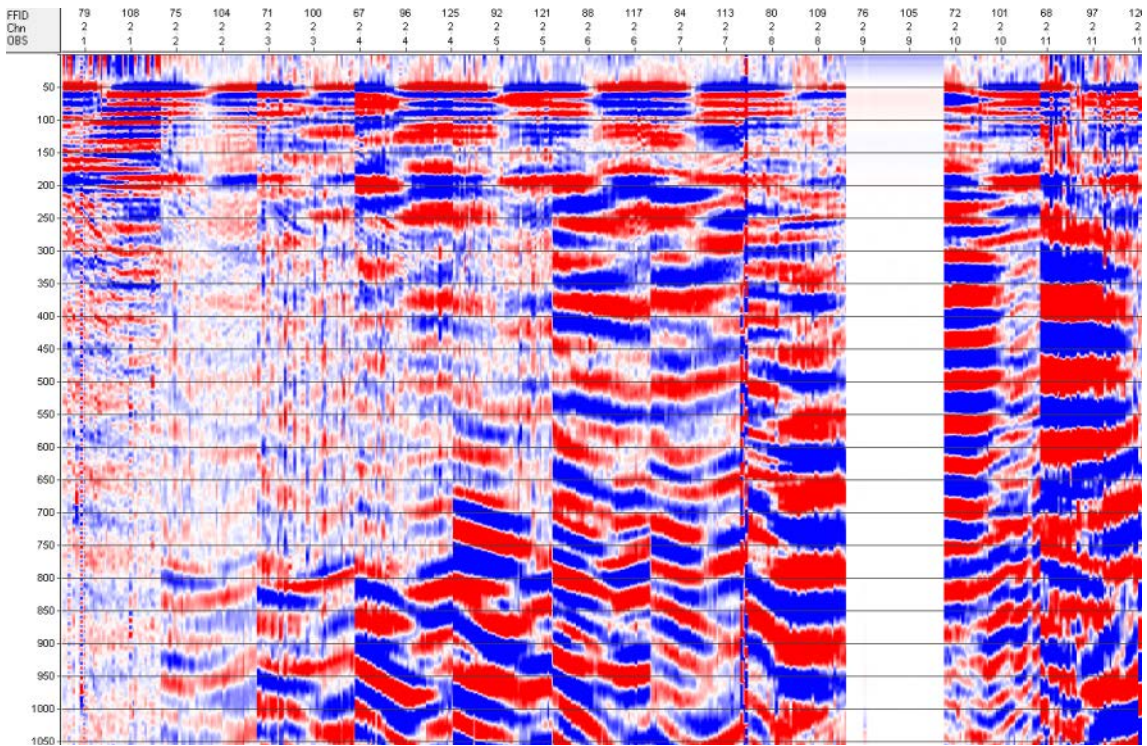
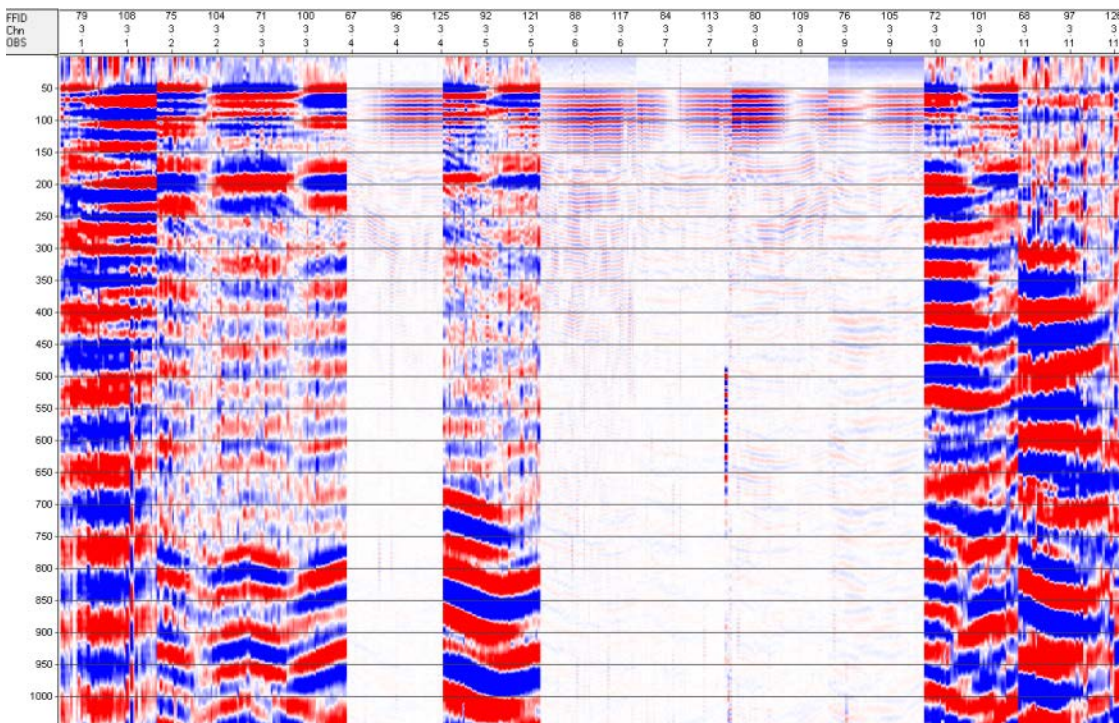


Figure 4. Line 1 Vertical geophone.





**Figure 5. Line 1, Horizontal L1 geophone.**



**Figure 6. Line 1, Horizontal L2 geophone.**



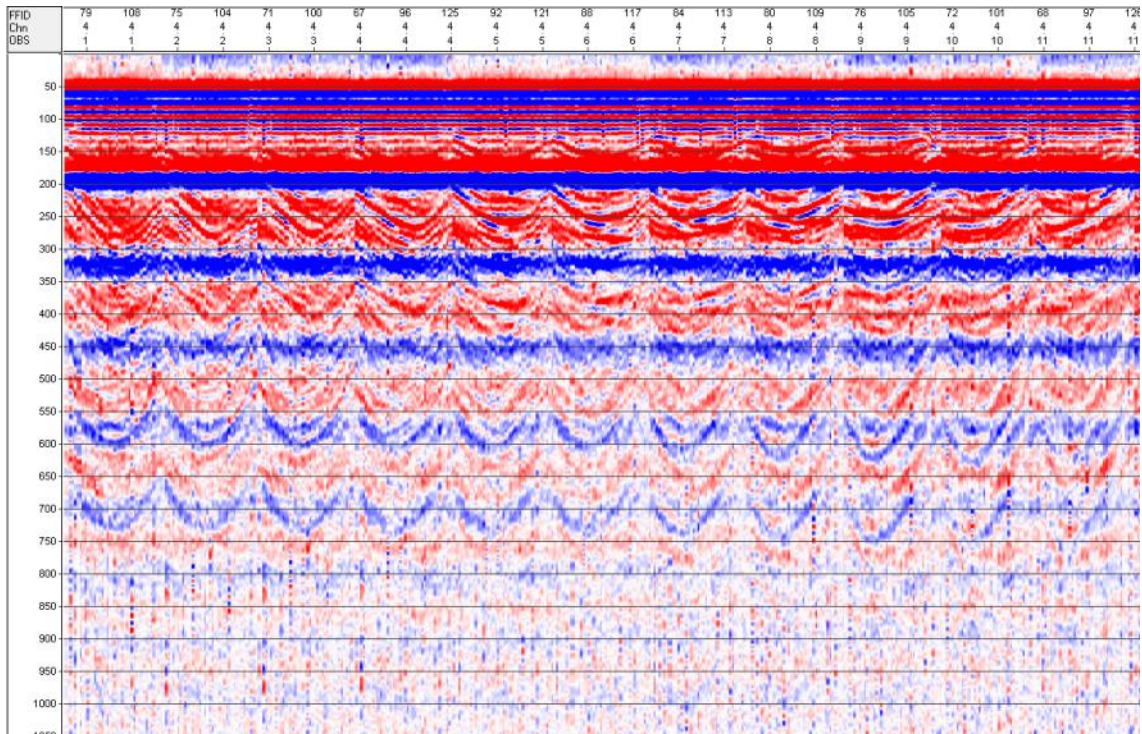


**Figure 7. Line 1, Hydrophone.**

We questioned the conversion to SegY and went back to the original OBS files in SEED format. Test code for reformatting these files to SegY confirmed the conversion to SegY, and ruled out a conversion problem.

John Collins with WOHl also reviewed the data and agreed that some OBS units were not functioning properly.

Processing continued for the six OBS stations (1, 2, 3, 5, 10, and 11) having data on all four channels. Reluctance to abandon five OBS stations was a factor that delayed processing.

## Processing - Software

Software for processing this OBS data was compiled by Lookout Geophysical and follows closely the methods presented by Bob Hardage, at the University of Texas.

For the full details of the Hardage method, see DOE Final Report, from The Bureau of Economic Geology, The University of Texas, April 30, 2009.

We followed these data processing steps:

- 1) Correct the starting times to the ocean-bottom direct arrival, called "reduced time".
- 2) Rotate the horizontal traces L1 and L2 to point in the in-line and cross-line direction.
- 3) Calibrate to equalize hydrophone and geophone response.
- 4) Separate Up-going and Down-going waves and estimate SV.
- 5) Create Reflectivity as the Up-going divided by Down-going.
- 6) Optional - Enhance Reflectivity for higher frequency.
- 7) Optional - Create Amplitude Envelopes for picking.
- 8) Optional - Convert any of the SGY output files of interest to Lookout format for additional DataTrend processing and analysis.

The processing Menu (Figure 8) shows each of these steps in order listed above.

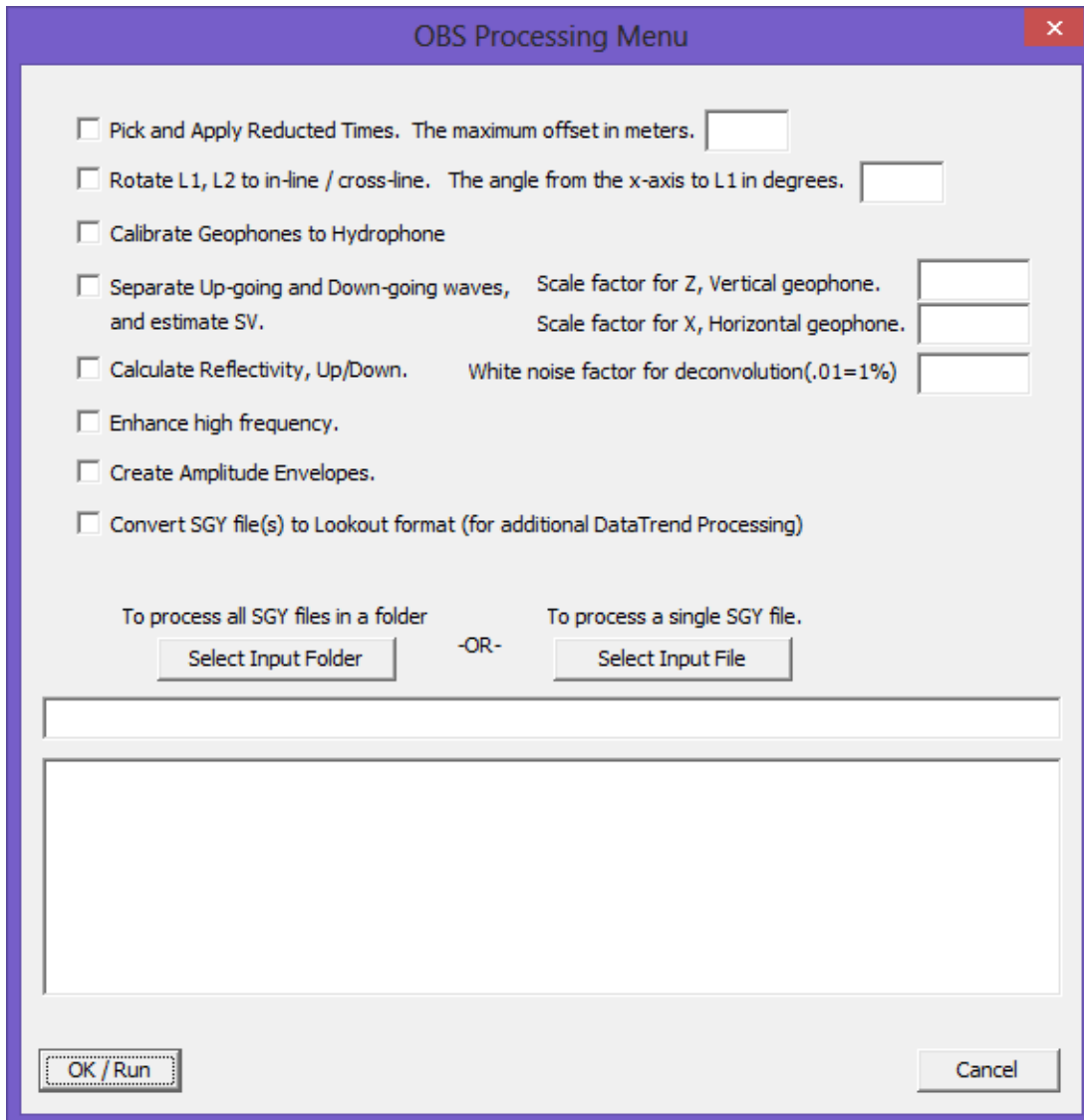


Figure 8. The processing Menu.

## Processing - Data Examples.

The following shows examples of each of the processing steps listed above. All data files are in SegY format and may be viewed with the free SegY viewer “SeiSee” from DMNG, see “<http://www.dmng.ru/seisview>”, or any other available SegY viewer.

### Step 1 - Pick and correct the starting times to the ocean-bottom direct arrival, called “reduced time”.



Pick and Apply Reduced Times. The maximum offset in meters. 1750

After experimenting with ranges of offsets, about 1750 meters looked reasonable as the maximum offset for this data. This example is for OBS 5.

The output of Step 1 (Figure 9) for the hydrophone trace shows the first arrivals at the ocean-bottom. This is the “reduced time” correction which puts the first break at about 50 msec.

The output file has “Picks” and the offset value appended to the input name.



OBS05-Picks\_1750.sgy 7/22/2013 9:07 PM SGY File 66,191 KB

Check the output file by viewing it. This display shows the output shot range (FFID) of Line 1, for hydrophone channel 4 (Chn), with offsets (Offset) above the data traces. All values are from the trace headers.

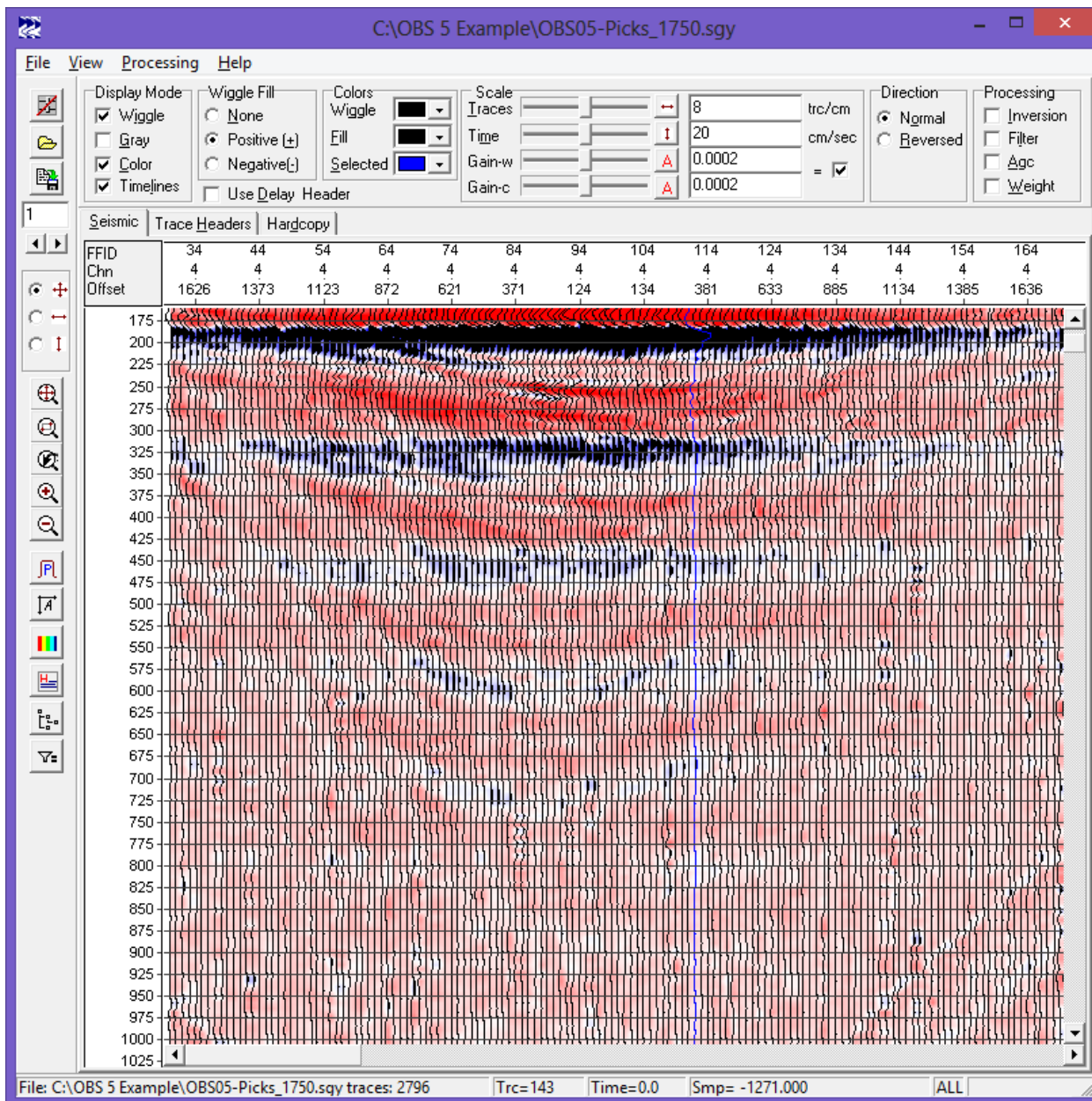


Figure 9. Line 1 hydrophone traces after direct arrival timing correction to 50 msec.



**Step 2 - Rotate the horizontal traces L1 and L2 to point in the in-line and cross-line direction.**

Select the output file from Step 1 as the input to Step 2.



Check the box for rotation of L1 and L2, and set the degrees for orientation of L1. Degrees are clockwise from the x-axis to L1. It is assumed that L2 is at an additional 90 degrees from L1. The angle for L1 is a guess, and will be refined. The angle for L1 is random and will be different for each OBS station.



This process gives two output files, one of the SEGY data after rotation, and one in CSV format with the sample values of L1 and L2 for the first breaks for each FFID of the input data and also for the rotated output data. Use Excel (or equivalent) to graph the first breaks of the CSV data to estimate the angle from the x-axis, see Figure 10.

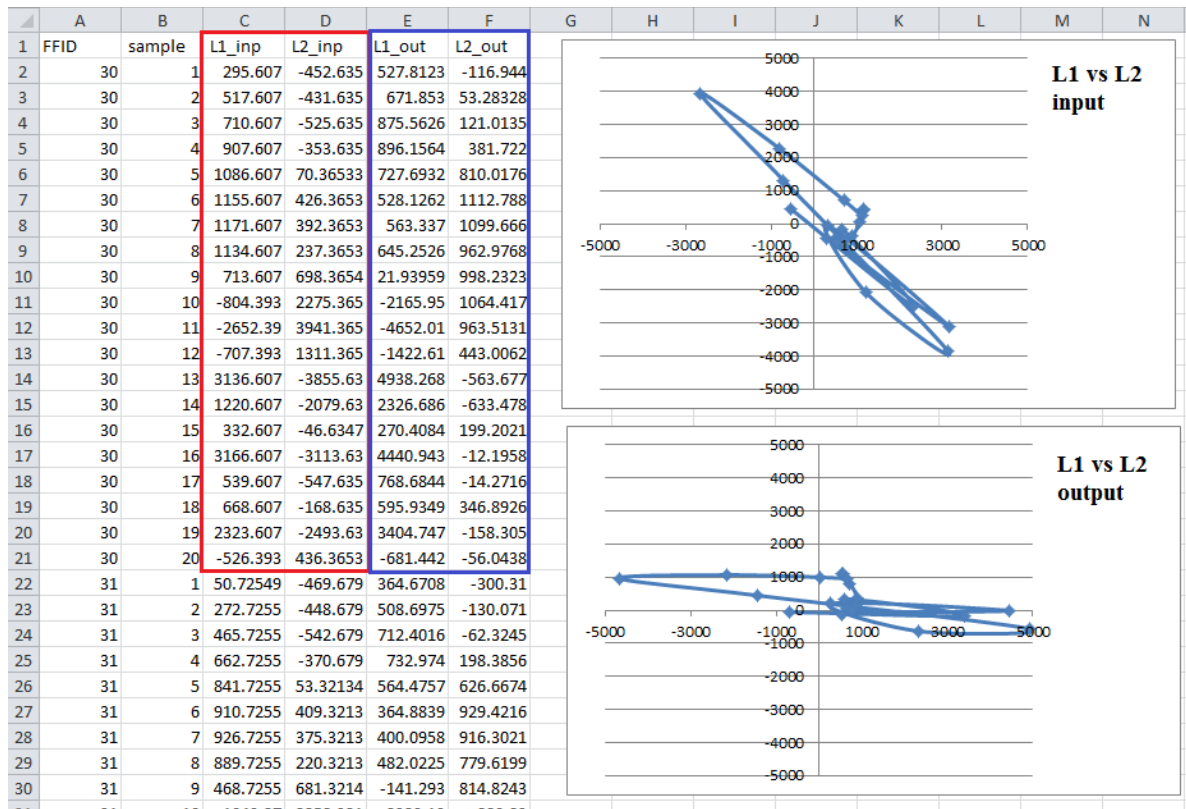


**Figure 10. The first scatter plot (or hodogram) shows the input data in the red box, and the second scatter plot shows the output data in the blue box.**

Experiment with the orientation angle to align the horizontal data to the x-axis. In this example, you might add a little more rotation. A rerun with 145 degree rotation (Figure 11) shows the new alignment. Check a number of FFIDs to make the final choice for rotation angle.

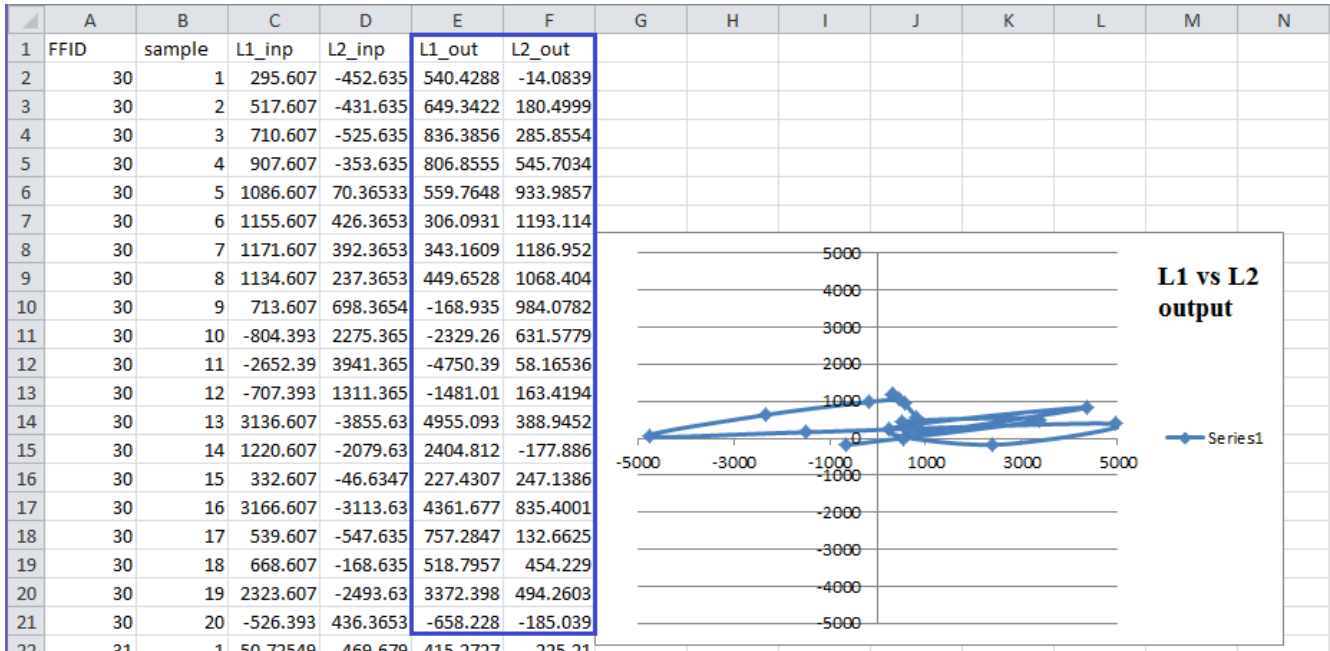


Figure 11. The same input data as Figure 10, rotated 145 degrees.

Another way to check the success of orientation to the x-axis (or X inline) is by inspection of the output data. Channel 2 or L1 of the input becomes channel 2 or X in-line on the output. Channel 3 or L2 of the input becomes channel 3 or Y cross-line on the output. Hardage shows that Y is of no use and can be ignored. Compare input (Figure 12) and output (Figure 13) data to see if most of the output amplitude is on channel 2 or X, and channel 3 or Y is nearly null.

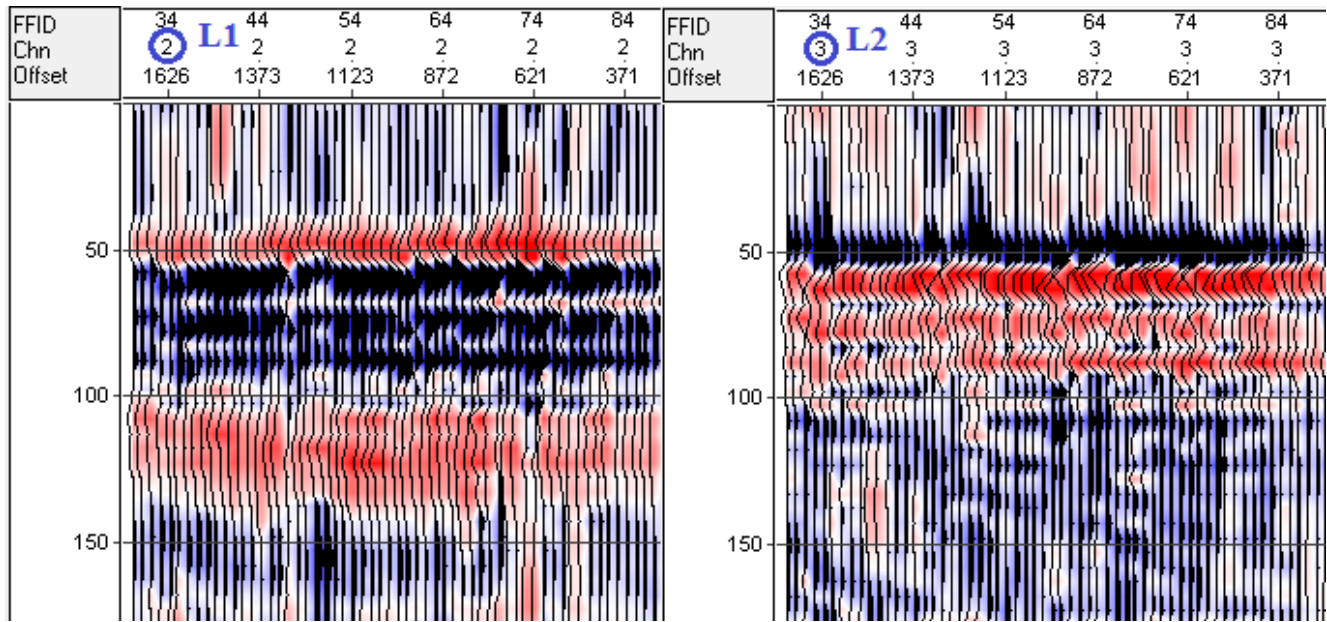


Figure 12. OBS 5, Line 1, L1 and L2 before rotation.

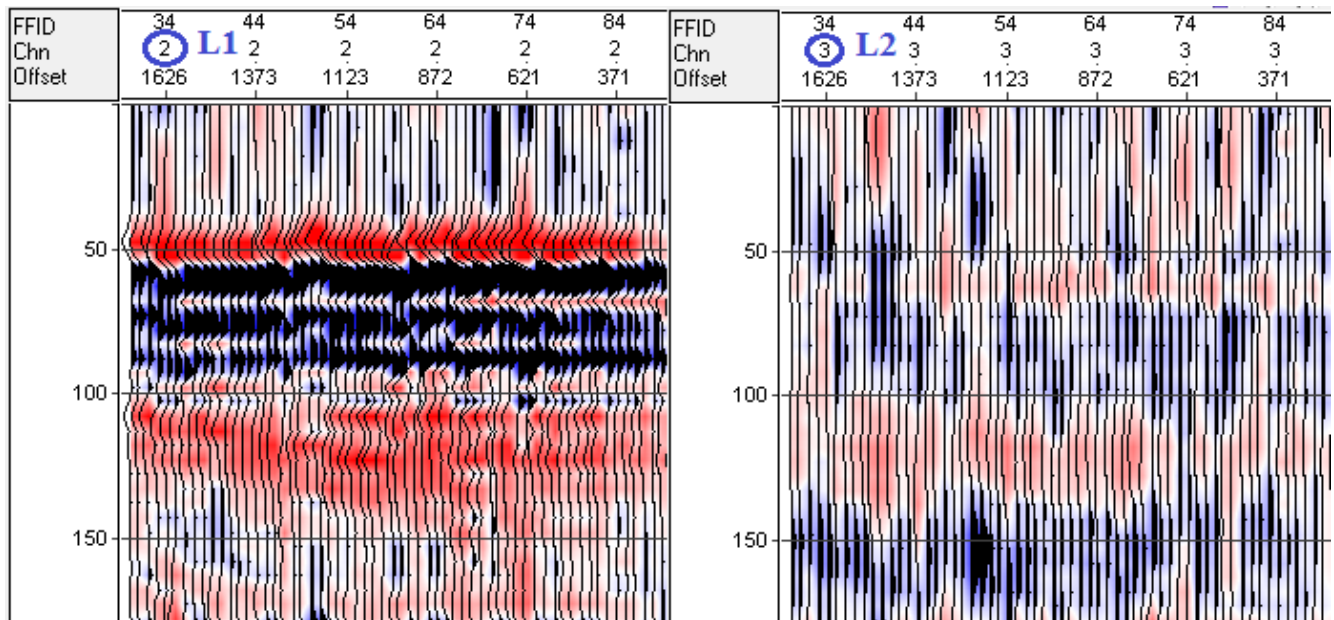


Figure 13. OBS 5, Line 1, L1 and L2 after 135 degree rotation.



### Step 3 - Calibrate to equalize hydrophone and geophone differences.

The hydrophone (High Tech 90-U) has a higher frequency output than the 3C geophones (GeoSpace 4.5 Hz). The calibration operates only on the geophone outputs to compensate the frequency response, amplitude factors follow in Step 4. See Figures 14 and 15.

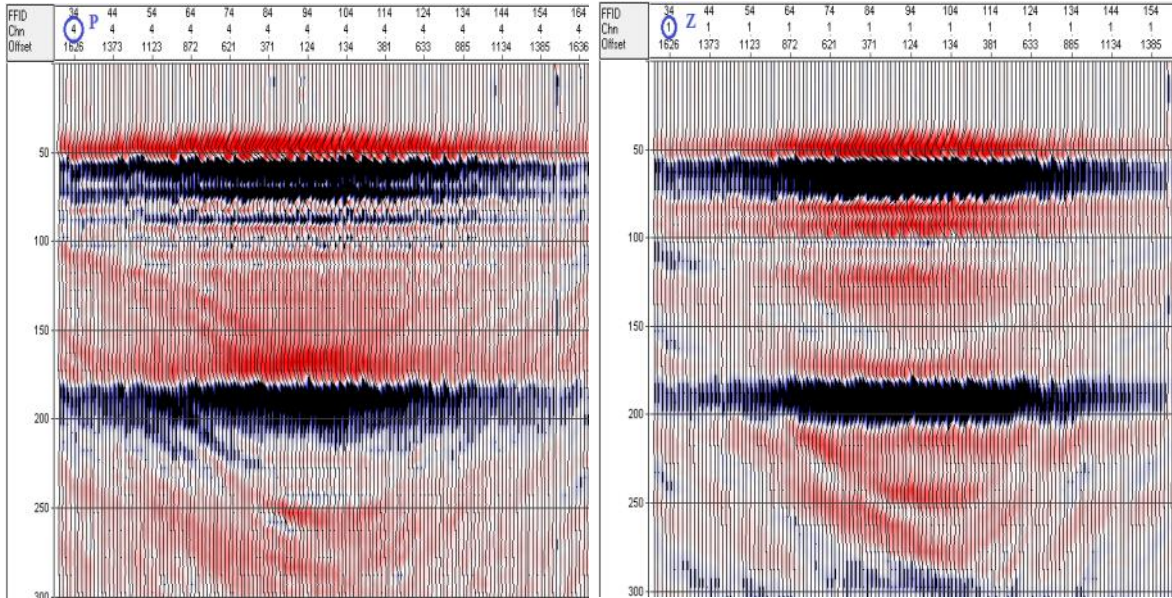


Figure 14. P and Z before calibration.

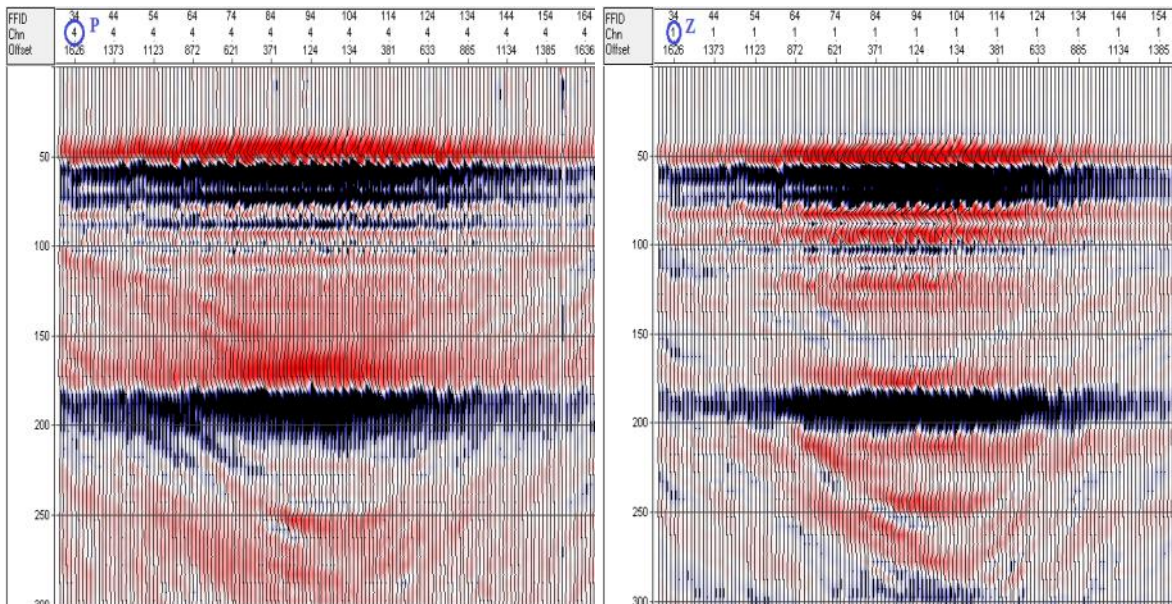


Figure 15. P and Z after calibration.

#### Step 4 - Separate Up-going and Down-going waves and estimate SV.

For the vertical (1D) case,  $P = D + U$  and  $Z = D - U$ . Summing  $P$  and  $Z$  tends to cancel  $U$ , subtracting tends to cancel  $D$ . Add an offset and  $Z$  scales by the cosine of the angle (derived from offset and water depth in the trace headers.) The sine of the angle scales the  $P$  component of  $X$ , where we assume that  $SV$  can be estimated by subtraction of  $P$  from  $X$ . The menu gives two scale factors applied to  $Z$  and  $X$  in the process, call the scaled traces  $\alpha Z$  and  $\beta X$ . Then the equations are:

Output:

Channel 1	$D = P + \alpha Z / \cos(\phi)$	
Channel 2	$U_{sv} = \beta X - P \sin(\phi)$	Up-going SV-waves
Channel 3	discard or spare	
Channel 4	$U_p = P - \alpha Z / \cos(\phi)$	Up-going P-waves

<input checked="" type="checkbox"/> Separate Up-going and Down-going waves, and estimate SV.	Scale factor for Z, Vertical geophone.	<input type="text"/>
	Scale factor for X, Horizontal geophone.	<input type="text"/>

Think of the scale factors  $\alpha$  and  $\beta$  as additional calibration, which are not necessarily identical.

Remember that the spring constant for the vertical geophone  $Z$  is not the same as the horizontal geophone  $X$  (rotation of  $L1$  and  $L2$ ). The vertical geophone opposes gravity, the horizontal does not. The geophone outputs may be matched when new, but over time may drift. Ocean-bottom coupling and gimbals leveling are other factors. The scale factors may change a little for each OBS station.

Start with  $\alpha = \beta = 1.0$  and view the output. Judge success as down-going  $D$  having only the source bubble (flat ringing) with no reflections (up-going smiles) before the ocean-bottom to surface multiple (also a smile). At short offsets, the multiple is at about 1200 msec on the reduced time display for this water depth. Since the multiple is down-going, it should be strong on  $D$  and weak on  $U$ . It is important to create a good  $D$  channel on this step, since the next step uses  $D$  (chn 1) to remove the source bubble from  $U_{sv}$  (chn 2) and from  $U_p$  (chn 4). If the output  $D$  contains some reflections, then test changes to  $\alpha$  and search for a value giving minimal reflection smiles on the output  $D$ . See Figures 16 and 17.



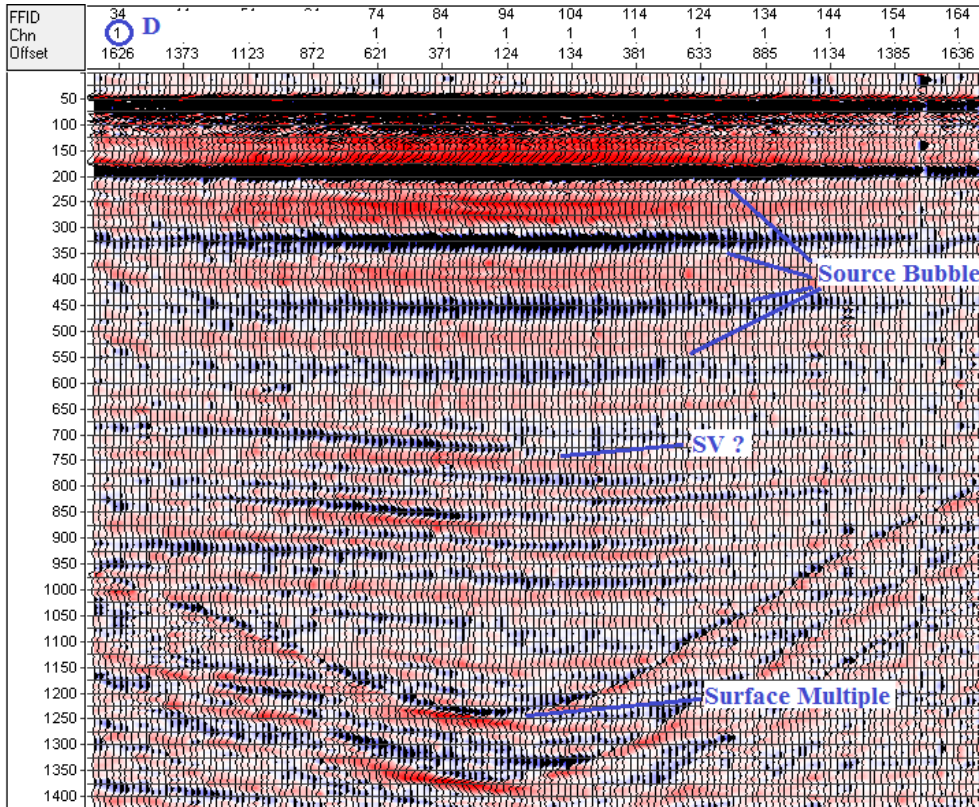


Figure 16. The output for D with  $\alpha = 1.0$ . The possibility of SV recorded on Z is a topic for the future.

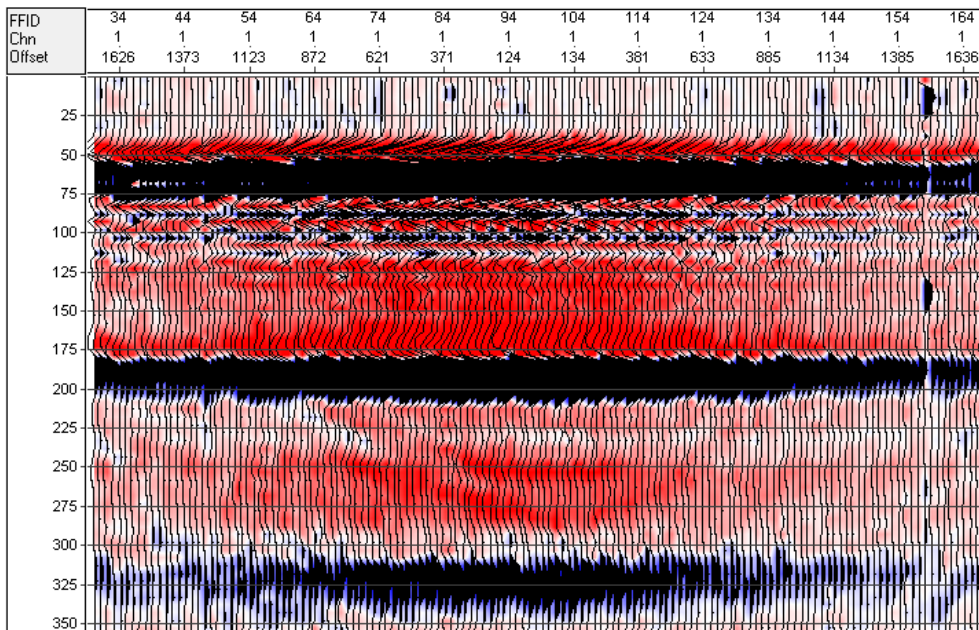
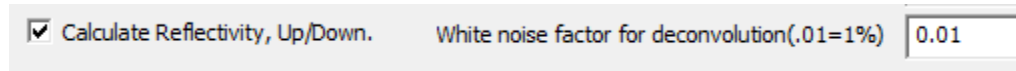


Figure 17. The bubble area shows very faint hints of smiles. If acceptable, go to the next step.

### Step 5 - Create Reflectivity as the Up-going divided by Down-going.

Think of the simple model of up-going waves as the reflection coefficient “stickogram” convolved with the source waveform,  $U_p = R_p * D$  for P-waves and  $U_{sv} = R_{sv} * D$  for S-waves, where  $*$  is for convolution. To get back to reflection coefficients, deconvolve the source waveform. In the frequency domain, deconvolution is by division, and Reflectivity is calculated as  $R_p = U_p/D$  for P-waves and  $R_{sv} = U_{sv}/D$  for S-waves. The only parameter to select is white noise to make the deconvolution division stable.



A noise factor of .01 ( 1% ) is common. Test a range, such as .1, .01, and .001. See Figure 18.

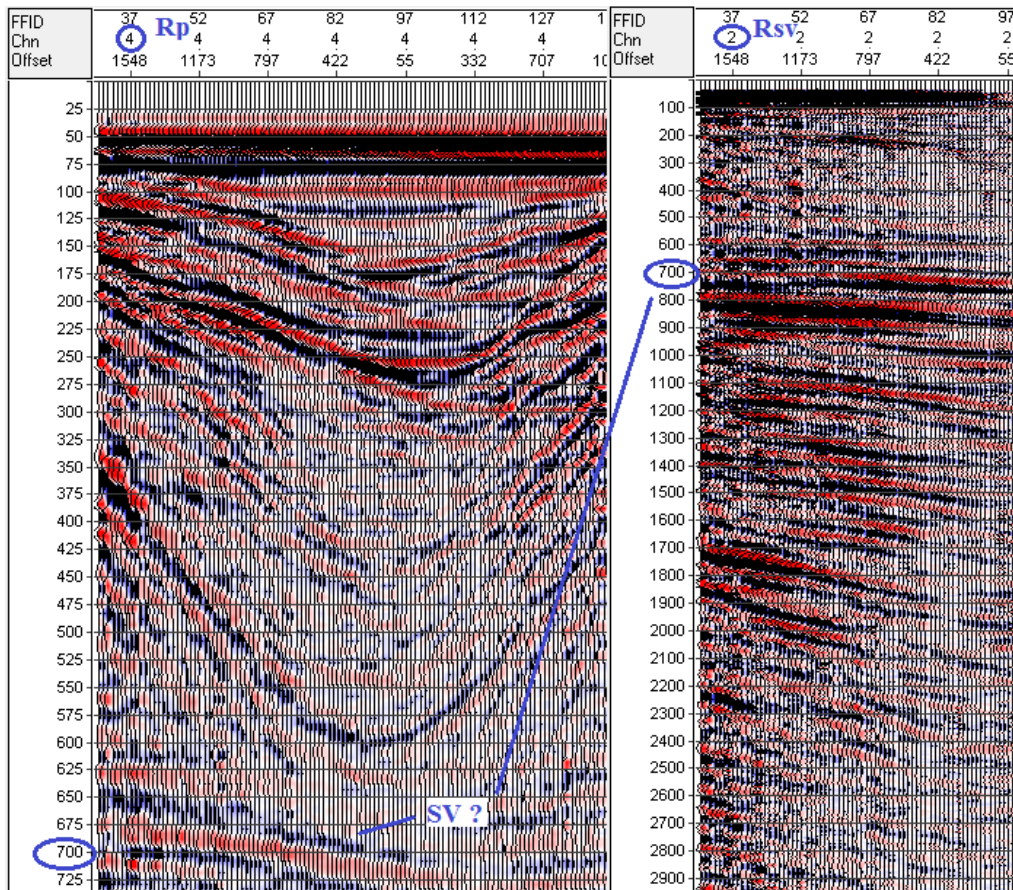


**Figure 18.** The output with 1% white noise, which may contain some SV “leaking” into the P output ? The Rsv display has a 4:1 vertical scale change compared to Rp. Only the left side of Rsv is shown.



## Step 6 - Optional - Enhance Reflectivity for higher frequency.

Following Hardage, a derivative enhances higher frequency. To avoid the 90 degree phase shift of the derivative, we use a zero phase approximation. The process may be repeated (Figure 19) for higher order derivatives, and all are zero phase. There are no parameters to select.

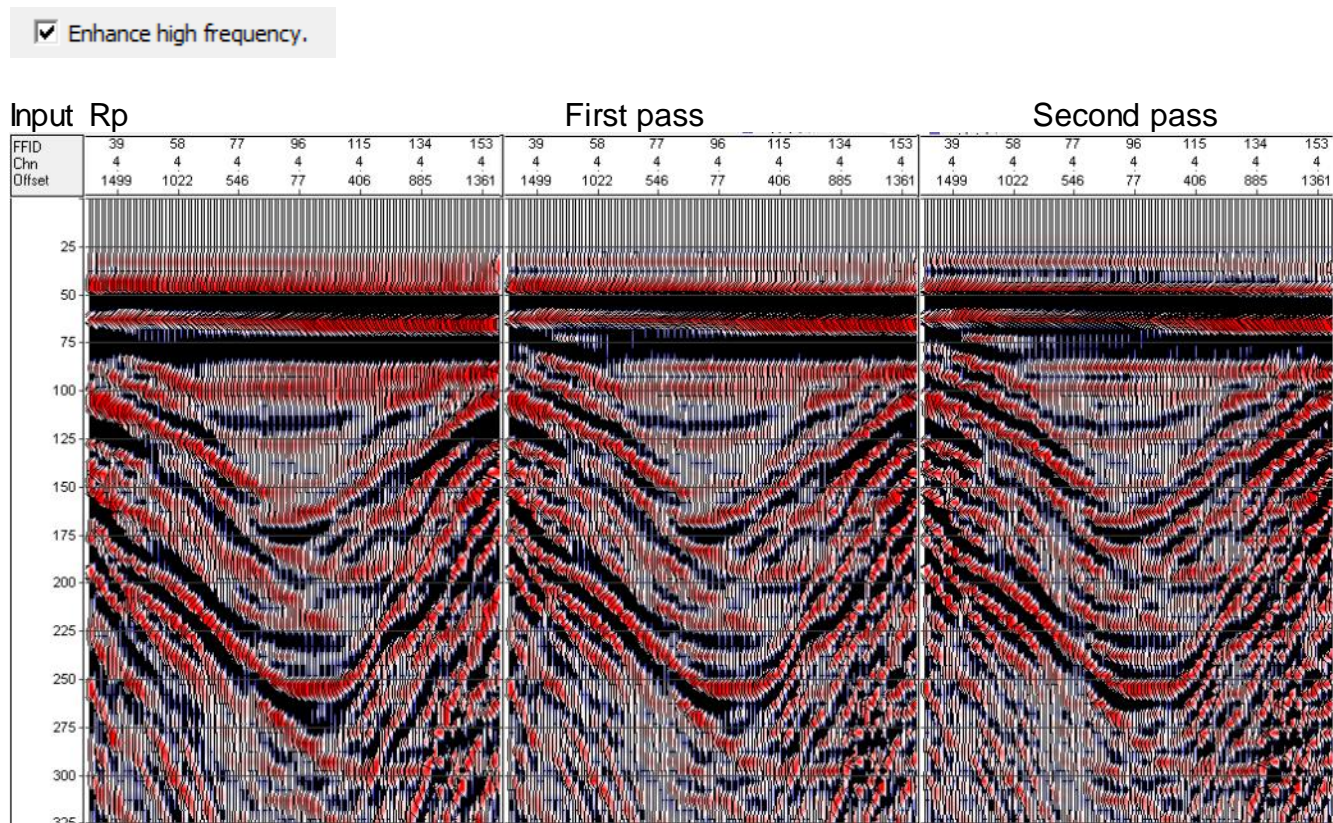
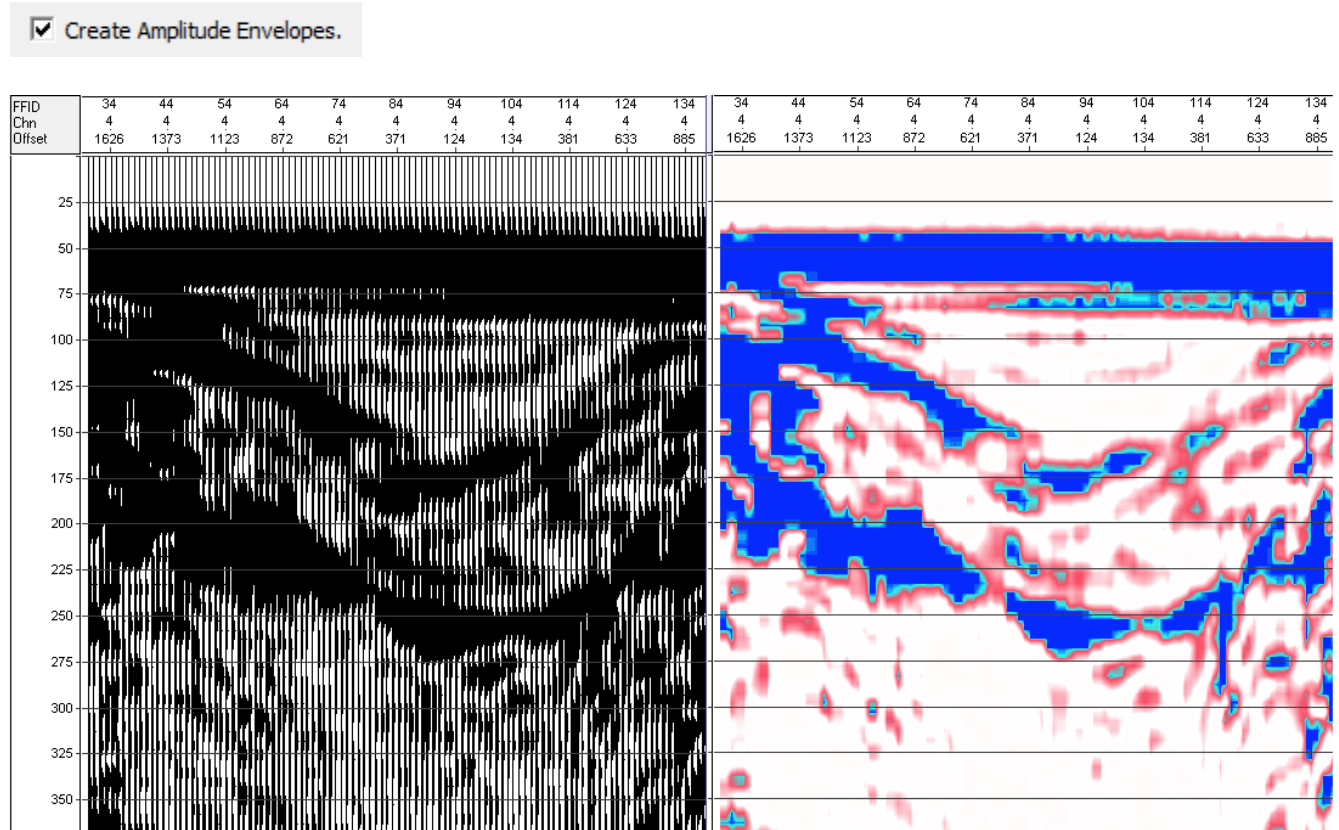


Figure 19. An example of derivatives to enhance high frequency.


**Step 7 - Optional - Create Amplitude Envelopes for picking.**

Envelopes may take the bias of phase out of event picking. If desired, run this option to create Hilbert Transform Envelopes, see Figure 20.



**Figure 20. The envelope of first derivative approximation of Rp in wiggle and in color versions.**

**Note:** The name of each output file from each step contains all of the processing information of each step that created it, in the order applied. In this case, the output name after steps 1 through 7 results from appending the following to the input file "OBS05.sgy":

 OBS05-Picks\_1750-Point\_135-Calib-UpDn\_1.000\_1.000-Reflect\_0.0100-EHiF-Env.sgy

Step 1 – Pick “reduced time” with a 1750 meter offset limit.	-Picks_1750
Step 2 – Point or rotate L1 to in-line from 135 degrees.	-Point_135
Step 3 – Calibration.	-Calib
Step 4 – Up-going Down-going separation with $\alpha = \beta = 1.000$ .	- UpDn_1.000_1.000
Step 5 – Reflectivity with white noise = 0.0100.	-Reflect_0.0100
Step 6 – Enhance High Frequency.	-EHiF
Step 7 – Envelopes.	-Env



**Step 8 - Optional - Convert any of the SGY output files of interest to Lookout format for additional DataTrend processing and analysis.**

Convert SGY file(s) to Lookout format (for additional DataTrend Processing)

This conversion passes all SEGY headers relevant to OBS processing to the output Lookout headers. See Figure 21.

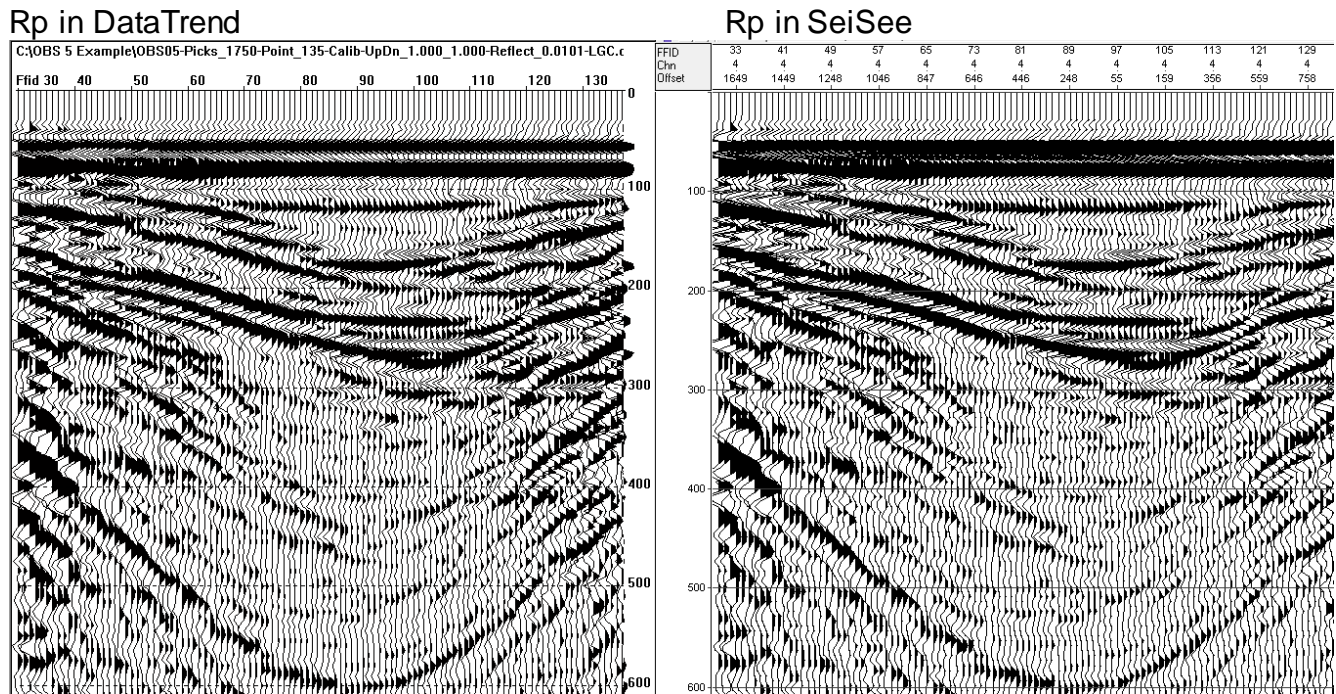


Figure 21. The same data viewed with DataTrend and SeiSee software.

For additional information about this processing software, view “OBS Processing Documentation v1.0.pdf”

**Discussion**

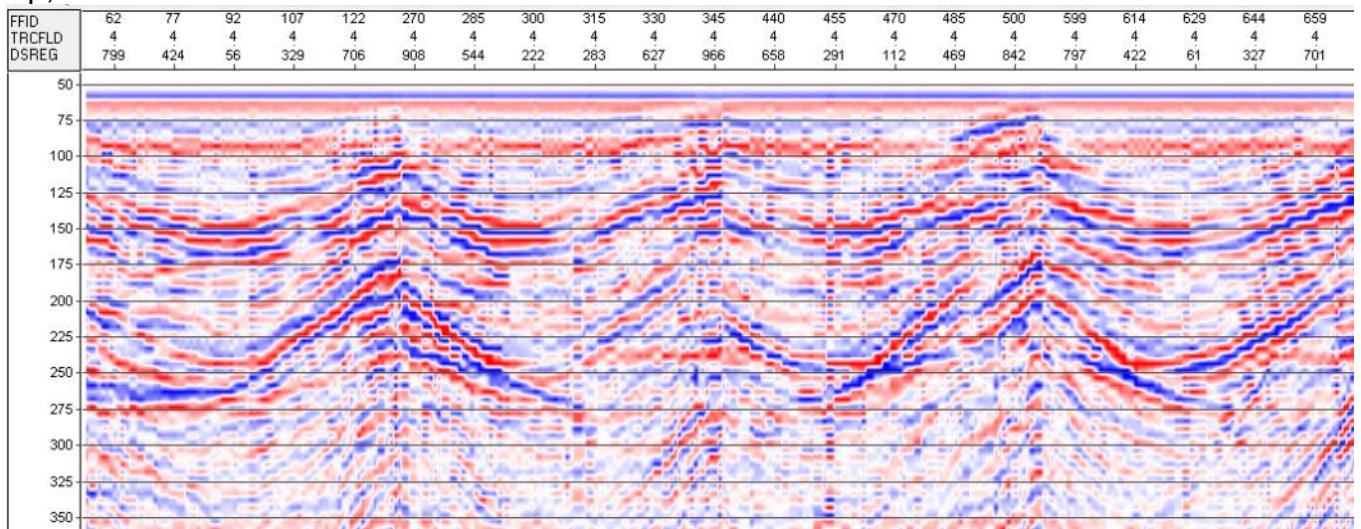
After creating Hilbert Transform Envelopes for both P and S outputs, we attempt to find the same events on both and then calculate  $V_p$  to  $V_s$  ratios. The ratios are for time intervals between layer reflections, and assumes that the same layers are identified on both P and S outputs. The coverage is sparse, and contains spatial gaps, making it difficult to present. An example of a spreadsheet summary follows (Figure 22).

OBS 2												
Line	1	1	1	2	2	2	3	3	3	4	4	4
	Rp msec	Rs msec	Vp/Vs	Rp msec	Rs msec	Vp/Vs	Rp msec	Rs msec	Vp/Vs	Rp msec	Rs msec	Vp/Vs
bottom	50	50		50	50		50	50		50	50	
dt	135	800	5.9	135	800	5.9	135	800	5.9	135	800	5.9
A pick	185	850		185	850		185	850		185	850	
dt	100	475	4.8	95	475	5.0	90	475	5.3	80	475	5.9
B pick	285	1325		280	1325		275	1325		265	1325	
OBS 3												
Line	1	1	1	2	2	2	3	3	3	4	4	4
	Rp msec	Rs msec	Vp/Vs	Rp msec	Rs msec	Vp/Vs	Rp msec	Rs msec	Vp/Vs	Rp msec	Rs msec	Vp/Vs
bottom	50	50		50	50		50	50		50	50	
dt	125	800	6.4	120	800	6.7	130	800	6.2	135	850	6.3
A pick	175	850		170	850		180	850		185	900	
dt	110	400	3.6	120	450	3.8	100	450	4.5	75	500	6.7
B pick	285	1250		290	1300		280	1300		260	1400	
OBS 5												
Line	1	1	1	2	2	2	3	3	3	4	4	4
	Rp msec	Rs msec	Vp/Vs	Rp msec	Rs msec	Vp/Vs	Rp msec	Rs msec	Vp/Vs	Rp msec	Rs msec	Vp/Vs
bottom	50	50		50	50		50	50		50	50	
dt	130	750	5.8	125	750	6.0	130	750	5.8	135	750	5.6
A pick	180	800		175	800		180	800		185	800	
dt	80	400	5.0	85	450	5.3	85	500	5.9	75	500	6.7
B pick	260	1200		260	1250		265	1300		260	1300	
OBS 10												
Line	1	1	1	2	2	2	3	3	3	4	4	4
	Rp msec	Rs msec	Vp/Vs	Rp msec	Rs msec	Vp/Vs	Rp msec	Rs msec	Vp/Vs	Rp msec	Rs msec	Vp/Vs
bottom	50	50		50	50		50	50		50	50	
dt	105	700	6.7	110	500	4.5	105	500	4.8	105	500	4.8
A pick	155	750		160	550		155	550		155	550	
dt	105	300	2.9	100	250	2.5	100	250	2.5	95	250	2.6
B pick	260	1050		260	800		255	800		250	800	
OBS 11												
Line	1	1	1	2	2	2	3	3	3	4	4	4
	Rp msec	Rs msec	Vp/Vs	Rp msec	Rs msec	Vp/Vs	Rp msec	Rs msec	Vp/Vs	Rp msec	Rs msec	Vp/Vs
bottom	50	50		50	50		50	50		50	50	
dt	105	400	3.8	105	400	3.8	105	400	3.8	110	400	3.6
A pick	155	450		155	450		155	450		160	450	
dt	115	400	3.5	95	450	4.7	95	450	4.7	90	450	5.0
B pick	270	850		250	900		250	900		250	900	
OBS 12												
Line	1	1	1	2	2	2	3	3	3	4	4	4
	Rp msec	Rs msec	Vp/Vs	Rp msec	Rs msec	Vp/Vs	Rp msec	Rs msec	Vp/Vs	Rp msec	Rs msec	Vp/Vs
bottom	50	50		50	50		50	50		50	50	
dt	105	750	7.1	90	750	8.3	90	750	8.3	90	750	8.3
A pick	155	800		140	800		140	800		140	800	
dt	115	300	2.6	105	350	3.3	105	400	3.8	110	350	3.2
B pick	270	1100		245	1150		245	1200		250	1150	

Figure 22. A spreadsheet analysis of Vp/Vs for OBS 2, 3, 5, 10, 11, & 12 for Lines 1 through 4.

The data for OBS 10 is typical, showing two reflection picks from envelopes. The conventional color wiggles show data display for the same data, see Figures 23 a and b.

Rp, OBS 10.



Rp, OBS 10.

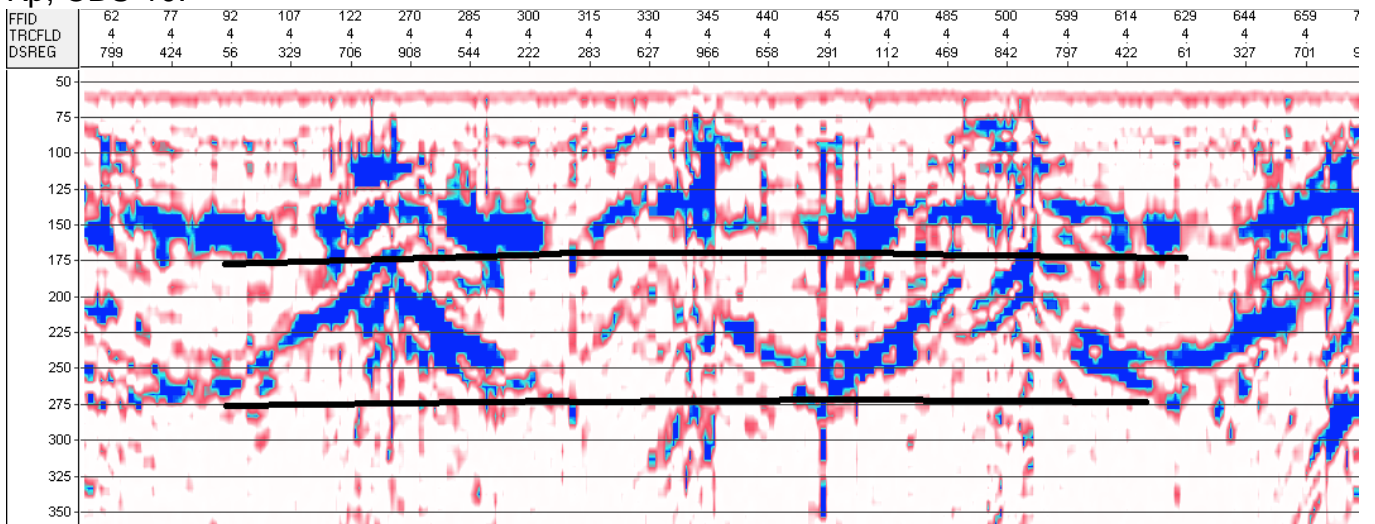
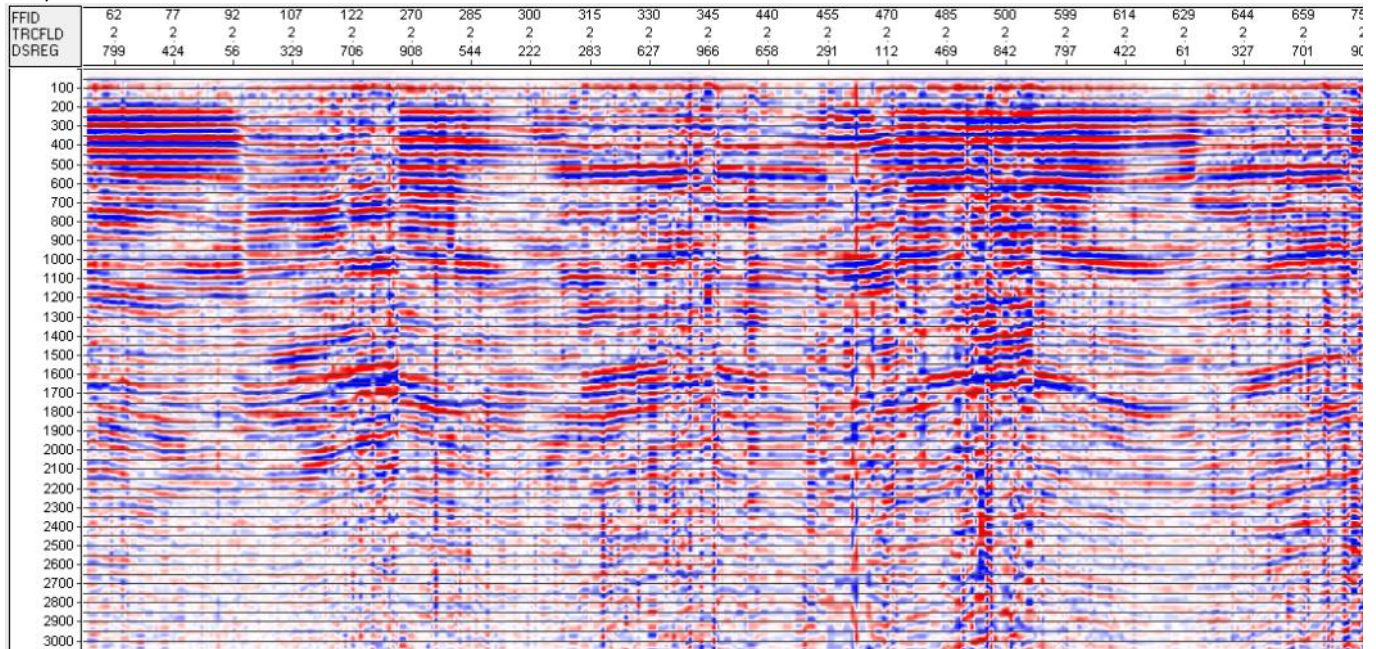


Figure 23a. An example of picking P envelopes for OBS 10, with color wiggles above.



Rs, OBS 10.



Rs, OBS10.

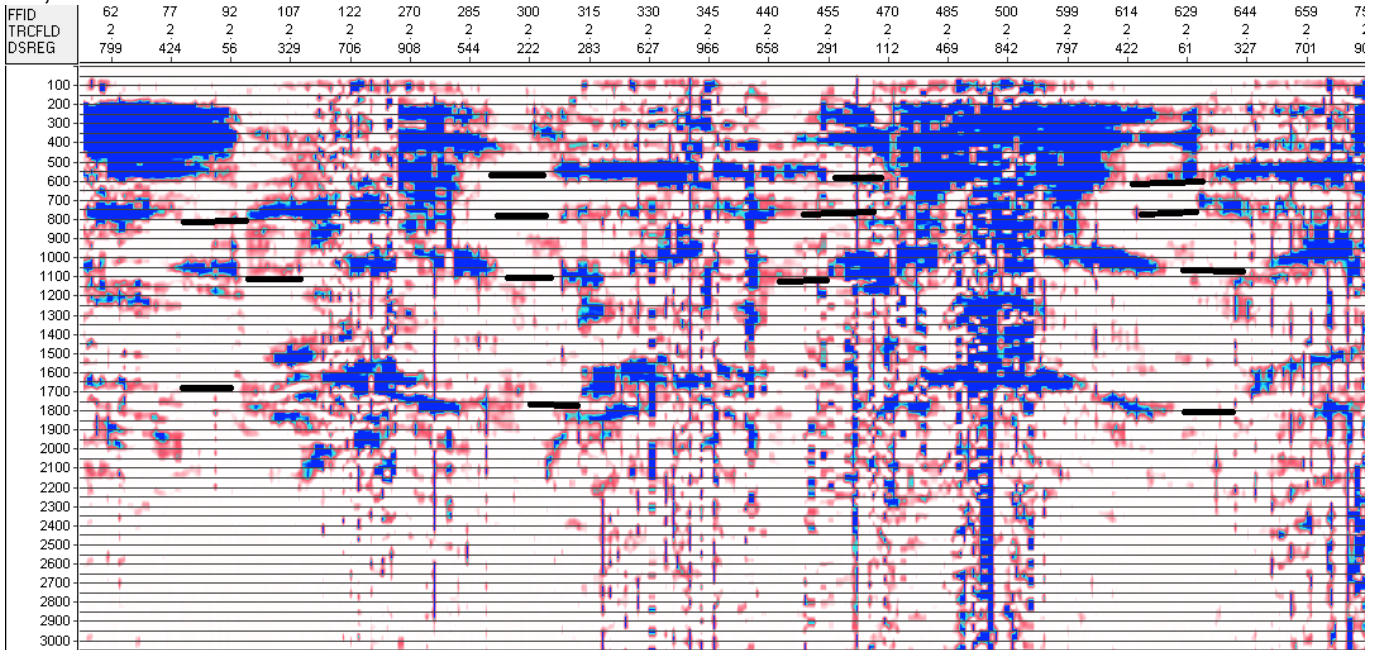
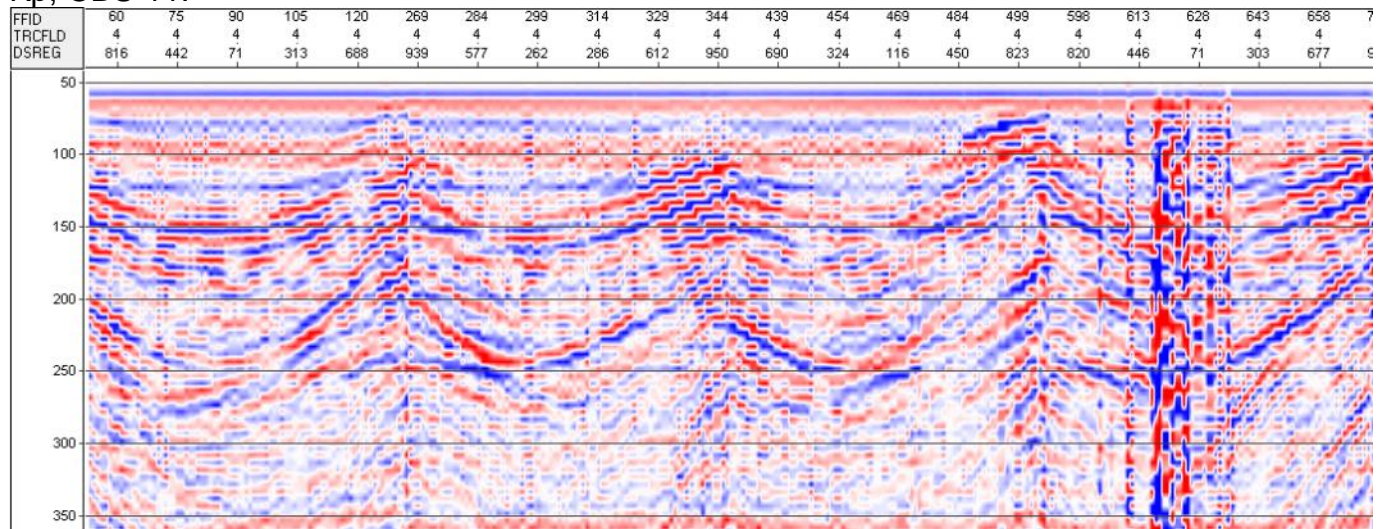


Figure 23b. An example of picking S envelopes for OBS 10, with color wiggles above.

The same displays for OBS 11 show that the S sections ring at this station and are difficult to pick, see Figures 24 a, b.

Rp, OBS 11.



Rp, OBS 11.

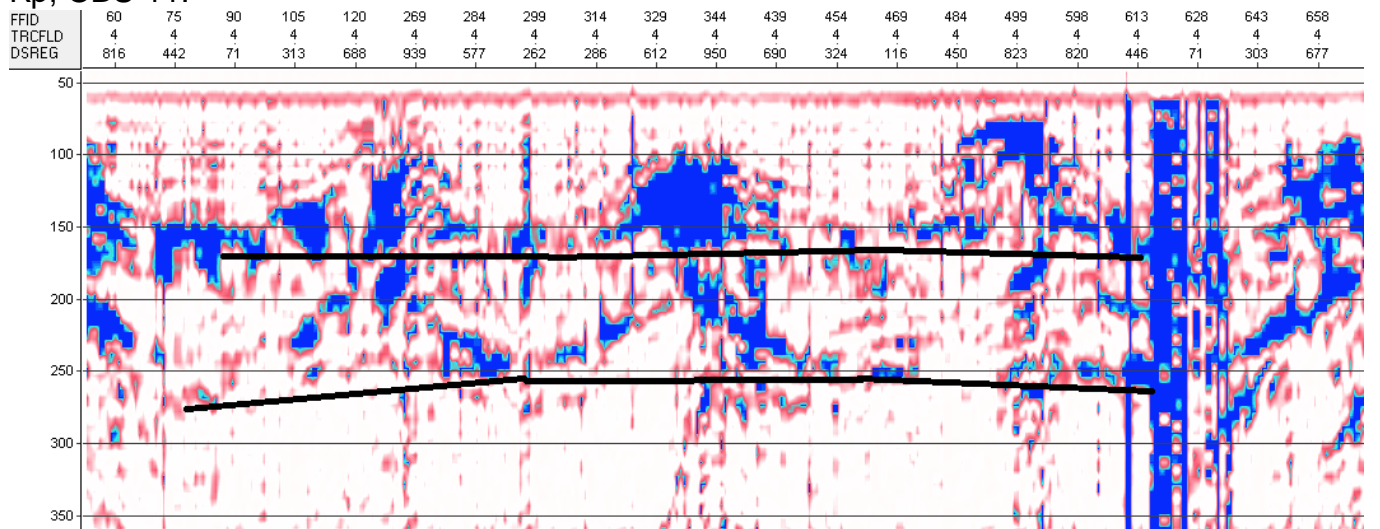
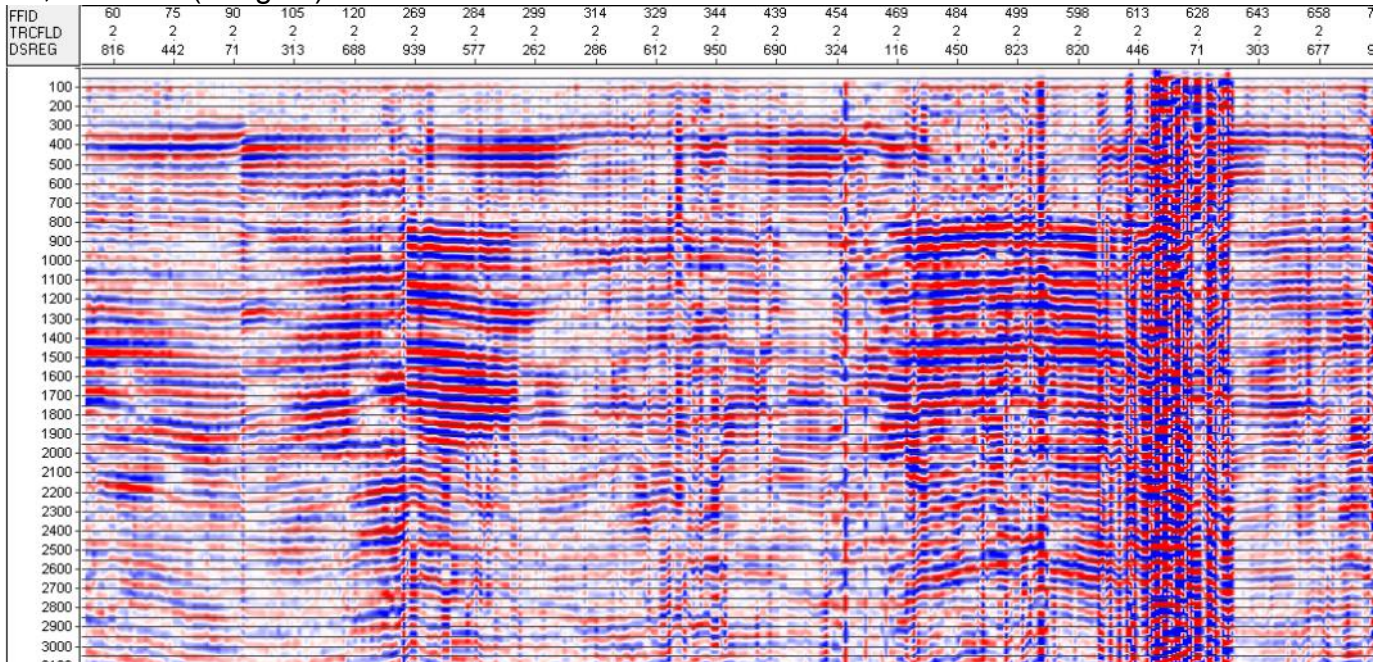


Figure 24a. An example of picking P envelopes for OBS 11, with color wiggles above.



Rs, OBS 11. (.5x gain)



Rs, OBS11

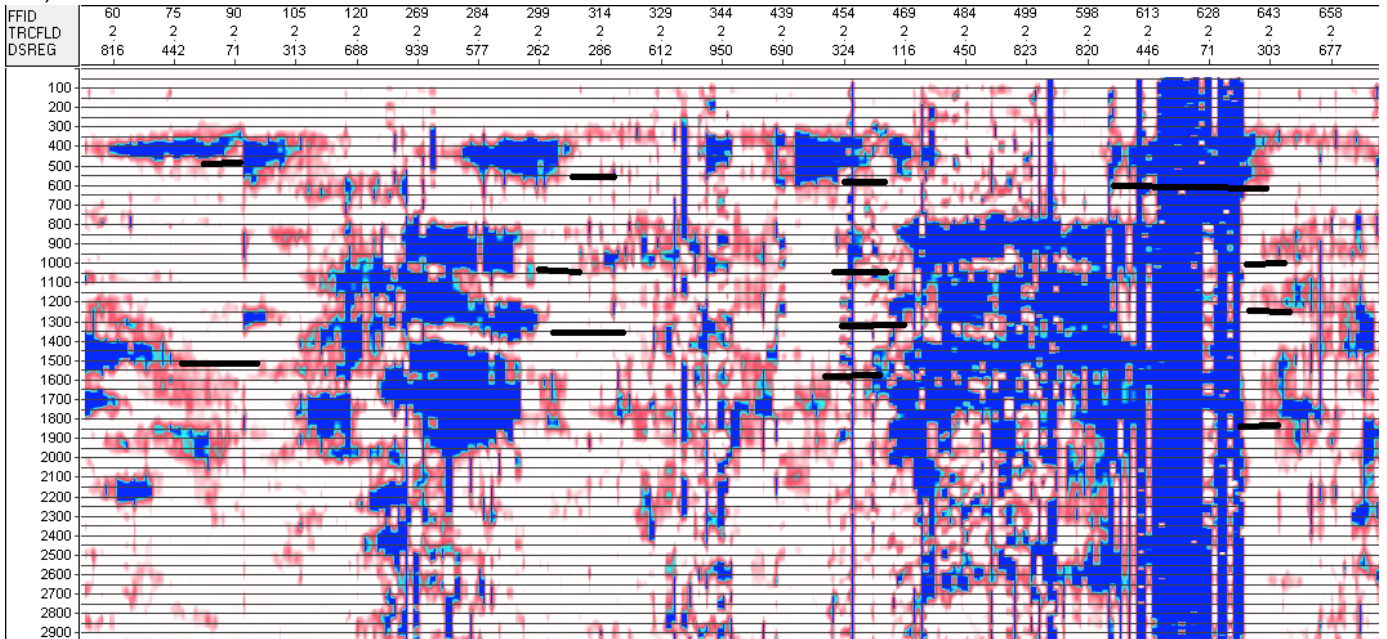


Figure 24b. An example of picking S envelopes for OBS 11, with color wiggles above.

One difficulty is that time adjustments of a few samples alters Vp/Vs. For example, look at the original picks for OBS 11 and compare those Vp/Vs values to those calculated after small changes to the picked times. In this example, Lines 1 and 2 have Rs changes of 25 msec (5 samples) and Lines 3 and 4 have Rp changes of 5 msec (1 sample). These revised pick times give Vp/Vs changes in the range of .1 to .6 (around 3% to 10%) for this example, see Figure 25.

OBS 11												
Line	1	1	1	2	2	2	3	3	3	4	4	4
	Rp msec	Rs msec	Vp/Vs	Rp msec	Rs msec	Vp/Vs	Rp msec	Rs msec	Vp/Vs	Rp msec	Rs msec	Vp/Vs
bottom	50	50		50	50		50	50		50	50	
dt	105	400	3.8	105	400	3.8	105	400	3.8	110	400	3.6
A pick	155	450		155	450		155	450		160	450	
dt	115	400	3.5	95	450	4.7	95	450	4.7	90	450	5.0
B pick	270	850		250	900		250	900		250	900	
OBS 11 repicked												
Line	1	1	1	2	2	2	3	3	3	4	4	4
	Rp msec	Rs msec	Vp/Vs	Rp msec	Rs msec	Vp/Vs	Rp msec	Rs msec	Vp/Vs	Rp msec	Rs msec	Vp/Vs
bottom	50	50		50	50		50	50		50	50	
dt	105	375	3.6	105	425	4.0	100	400	4.0	115	400	3.5
A pick	155	425		155	475		150	450		165	450	
dt	115	450	3.9	95	400	4.2	105	450	4.3	80	450	5.6
B pick	270	875		250	875		255	900		245	900	
		Rs changed 5 samples			Rs changed 5 samples			Rp changed 1 sample			Rp changed 1 sample	

**Figure 25. Variations in Vp/Vs caused by small adjustments to pick times for Rp and Rs. The original picks and Vp/Vs are at the top, and revised picks and resulting Vp/Vs are at the bottom.**



## An Alternate Approach

An important assumption for the processing method presented above is that SV-waves are isolated to the horizontal geophone channels. Inspection of the data after conversion to SegY and correction to reduced time (processing Step 1) and with no other manipulation, shows evidence of horizontal “events” on the vertical geophone.

This example uses Line 5. The bubble for Line 5, shot with the water gun, is much shorter than the GI gun and that makes the “raw” data more usable without separation of Up-Down waves. Look at about 800 msec on OBS 2 and 3. There is no event at 800 msec on P, the hydrophone. Both L1 and L2 have events (no horizontal rotation here) at 800 msec, but those events are cleaner on Z. On Z the smiles at 600 msec are big and look like P-wave velocity. At 800 msec the smile is small – closer to flat for S-waves (Figure 26.)

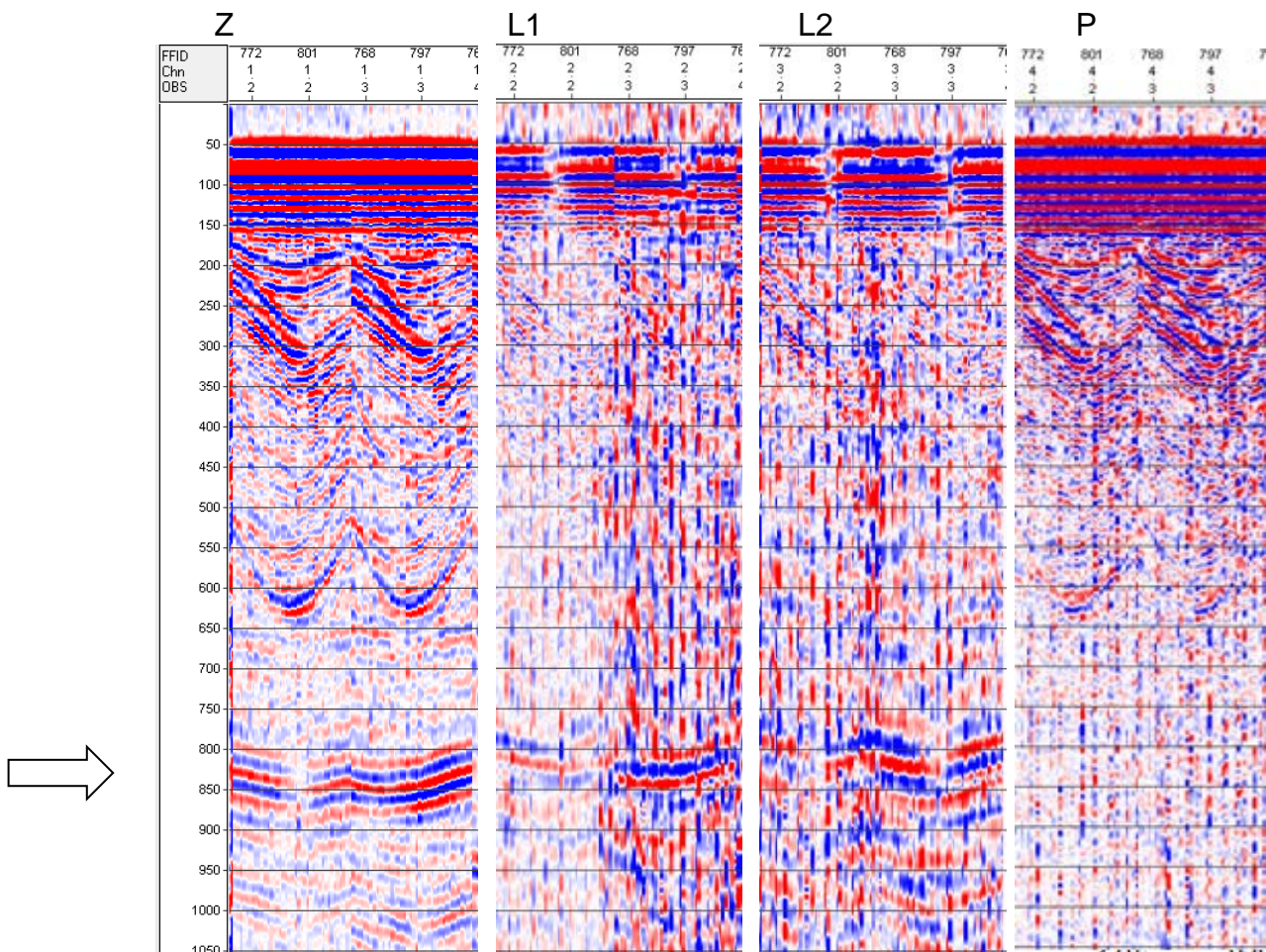


Figure 26. Line 5, OBS 2 and 3 at near offsets shows SV signal on the Z component.

The presence of SV on the vertical component puzzles us. Could this be electrical crossfeed, or a mechanical problem such as with gimbal leveling? In any case, it shows that the data does not fit the previous processing assumptions.

Since we have a vertical geophone signal for all OBS stations, we will try to use the vertical component to show SV. The alternative approach that follows comes from shallow land surveys using a sledge hammer to generate S-waves, Figure 27.



**Figure 27.** Using horizontal hits to generate S-waves.

Left and right hits have reversed S polarity, and any P motion (such as plank rebound) has the same polarity. The sum of left + right hits tends to enhance P-waves and cancel S-waves, taking the difference tends to enhance S-waves and cancel P-waves. It seems to us that the OBS geometry is similar, Figure 28.

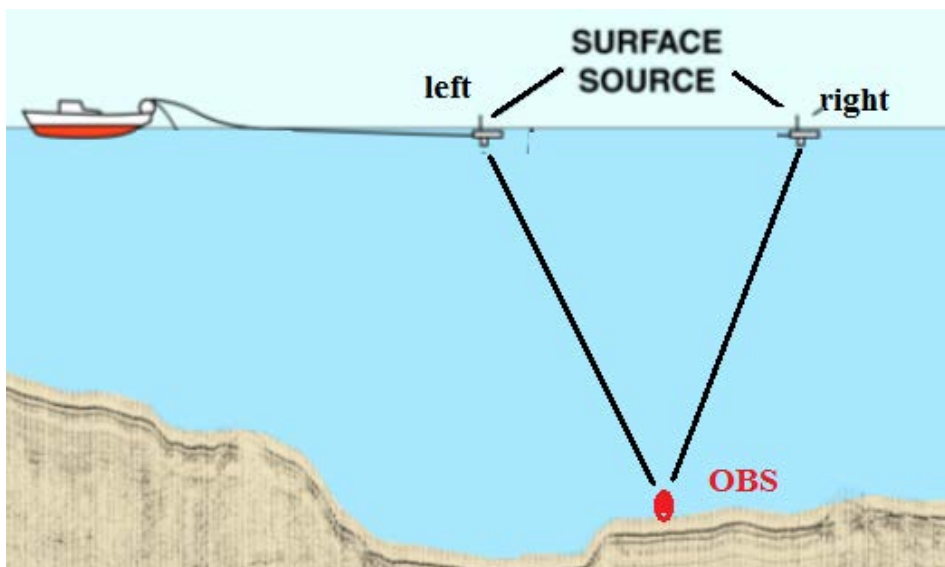


**Figure 28.** OBS geometry showing the source positions to the left and right of the OBS position.



The processing sequence for this geometry is to pair shots with about the same offset left and right of the OBS. For the pair, think of  $Z_{\text{left}} = Z + SV$  and  $Z_{\text{right}} = Z - SV$ . The sum of the pair ( $Z + SV + Z - SV$ ) leaves  $Z^*$ , and the difference of the pair ( $Z + SV - Z + SV$ ) leaves  $SV^*$ . A new assumption is that offsets are short enough that the left and right source positions have about the same  $Z$  and  $SV$  components. Steep dip or rough bottom topography are other complications. We know that Woolsey Mound is not flat (or it would not be called a mound), but this approach is still worth a try.

OBS 5 is very close to the resistivity anomaly and JPC 1. The following tests  $Z^*$  and  $SV^*$  at OBS 5 to see how it compares to previous results using L1 and L2 for  $SV$ .

The original  $Z$  traces show areas where polarity seems to change from left to right of the source on  $Z$ , these arrivals are thought to be  $SV$ -waves, Figure 29. Look close to zero offset from the OBS (center of the smile for  $Z$ ), then both  $P$  and  $S$  reflections are close to the OBS location. Note that  $Z^*$  and  $SV^*$  look like just the left side of  $Z$  with offset decreasing left to right. The  $SV$  panel dims to the right at nearly zero offset, and  $Z^*$  is bright at nearly zero offset - as expected. The source bubble goes away on  $SV$ , it cancels out.

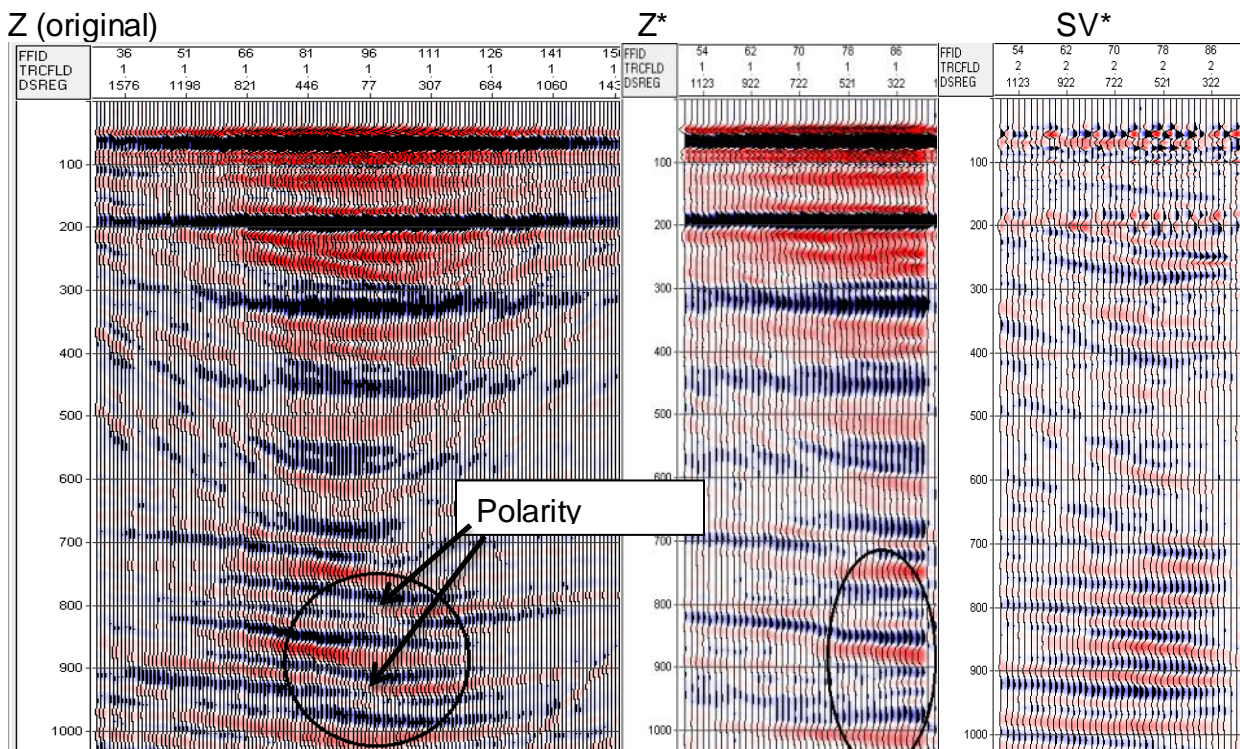
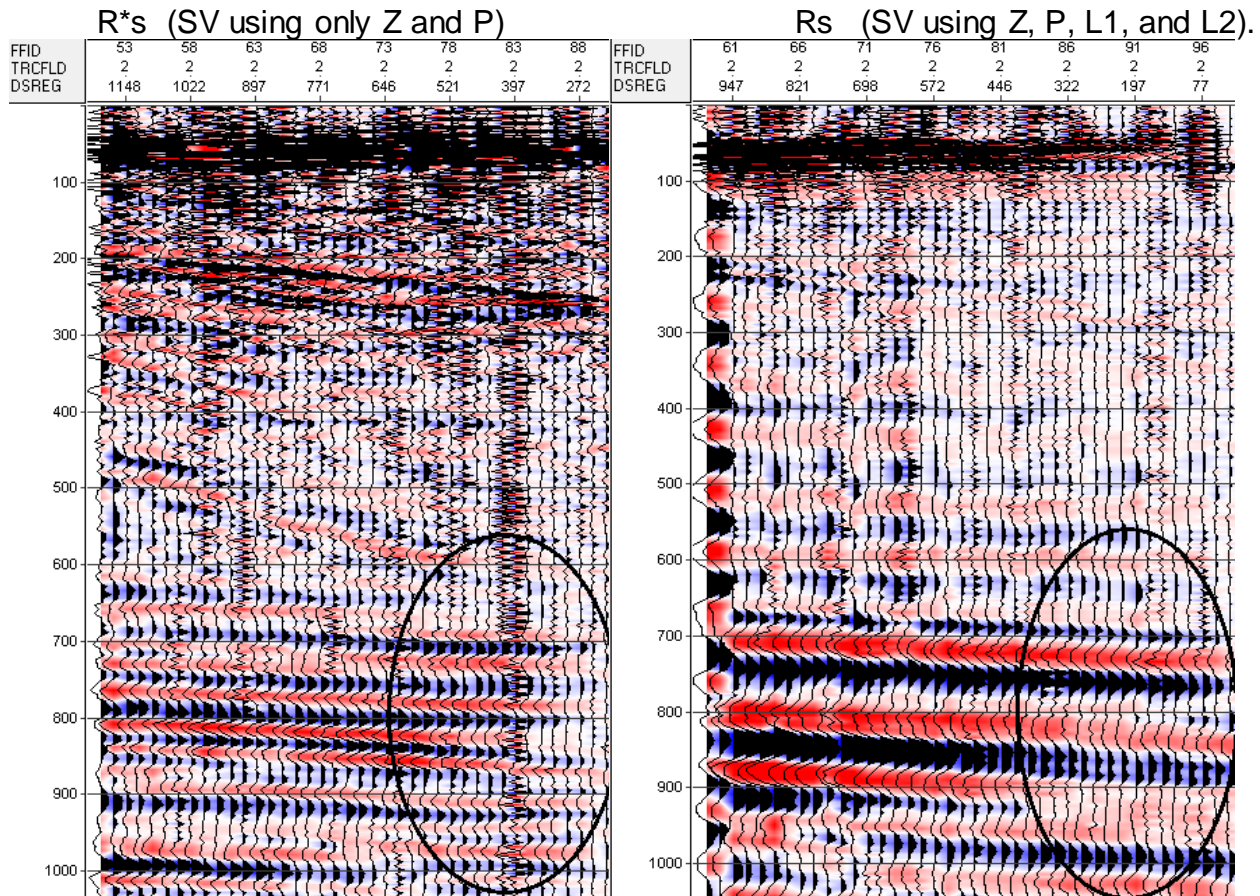


Figure 29. OBS 5, the original  $Z$ ,  $Z^* = \text{sum of trace pairs}$ , and  $SV^* = \text{difference of trace pairs}$ .

Now we use  $Z^*$  and P for separation of Up and Down going waves and for deconvolution to find reflectivity ( $R^*p$  and  $R^*s$ ). The output for  $R^*s$  (Figure 30) may have a polarity reversal in the processing, but it seems like a reasonable estimate of  $R_s$ .  $R^*s$  appears a little higher in frequency than  $R_s$ , and both have some shallow noise which is probably due to setting a low white noise factor in deconvolution.



**Figure 30.** A comparison of processing for SV with Z and P to processing with all four channels.

Going back to the raw reduced time data for Line 5, we gather the near offsets for OBS 1 through 11 for both Z and P, see Figures 31 and 32. In comparing Z and P, we see lower frequency and flatter (slower velocity) events on Z that are missing on P. We interpret these events as SV-waves on Z. From left to right on Figure 31, SV moves up, from around 850 msec at OBS 2 to as shallow as 350 msec at OBS 8 through OBS 11.

Unfortunately these observations and alternate processing ideas came late in the project and we ran out of time for a more complete investigation.



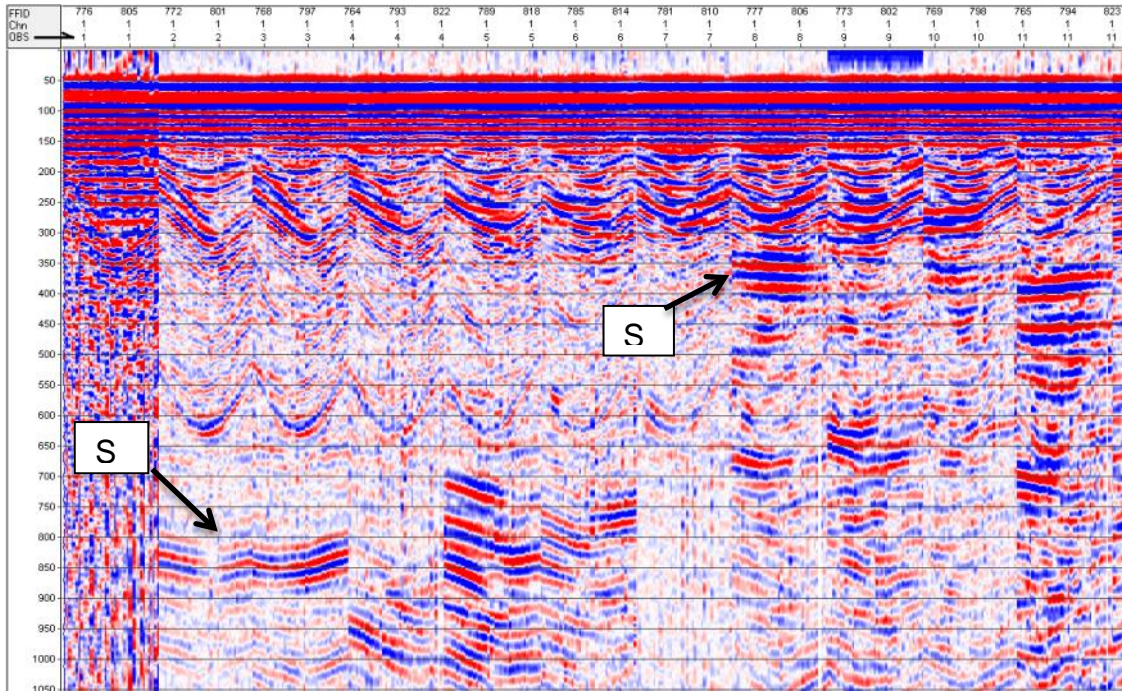


**Figure 31.** Line 5, gather of near offsets for OBS 1 through 11, raw vertical geophone, with a low cut display filter to remove DC.

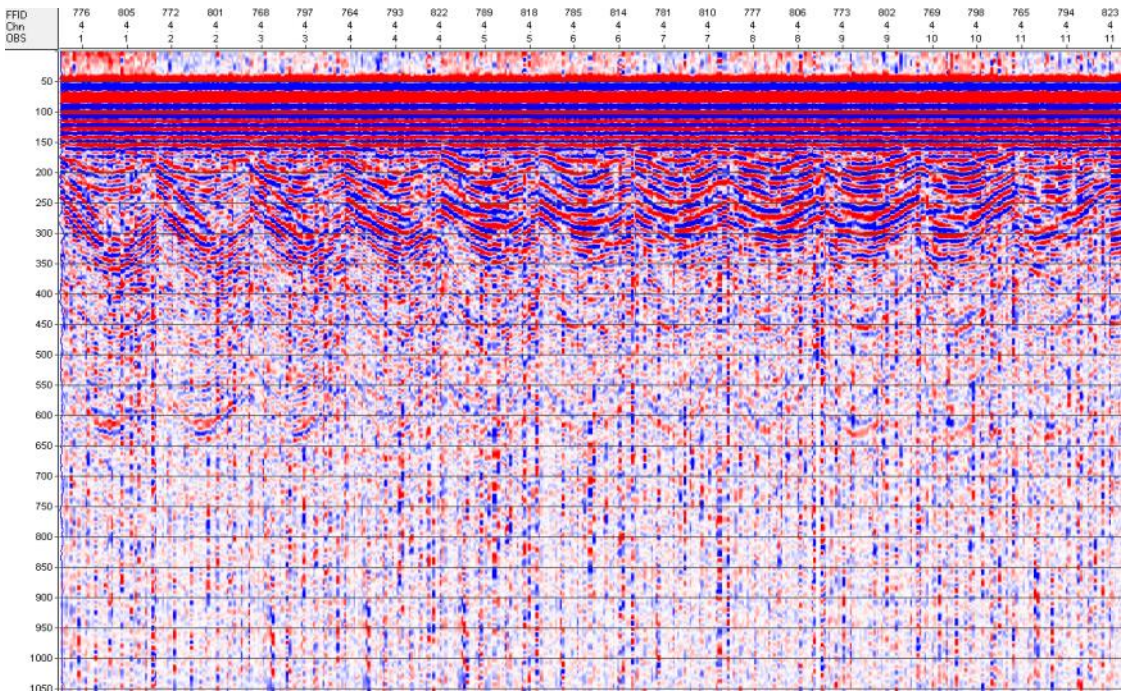
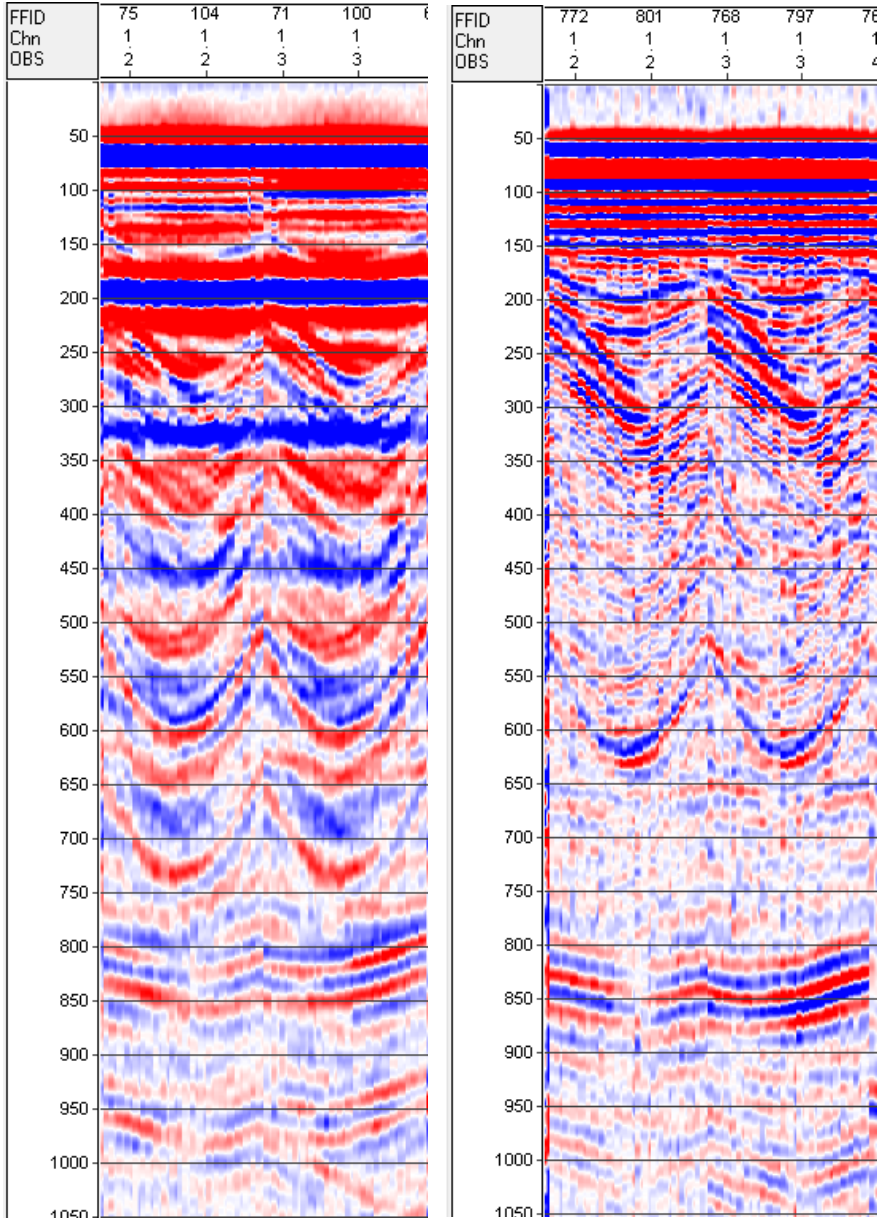


**Figure 32.** Line 5, gather of near offsets for OBS 1 through 11, raw hydrophone, with a low cut display filter to remove DC.

## Source Comparison – GI Gun vs. Water Gun

Lines 1-4 used a GI Gun source, and Line 5 used a Water Gun source. Line 1 duplicates Line 5. The frequency difference and large bubble for the GI Gun makes the two lines difficult to compare, see Figure 33.

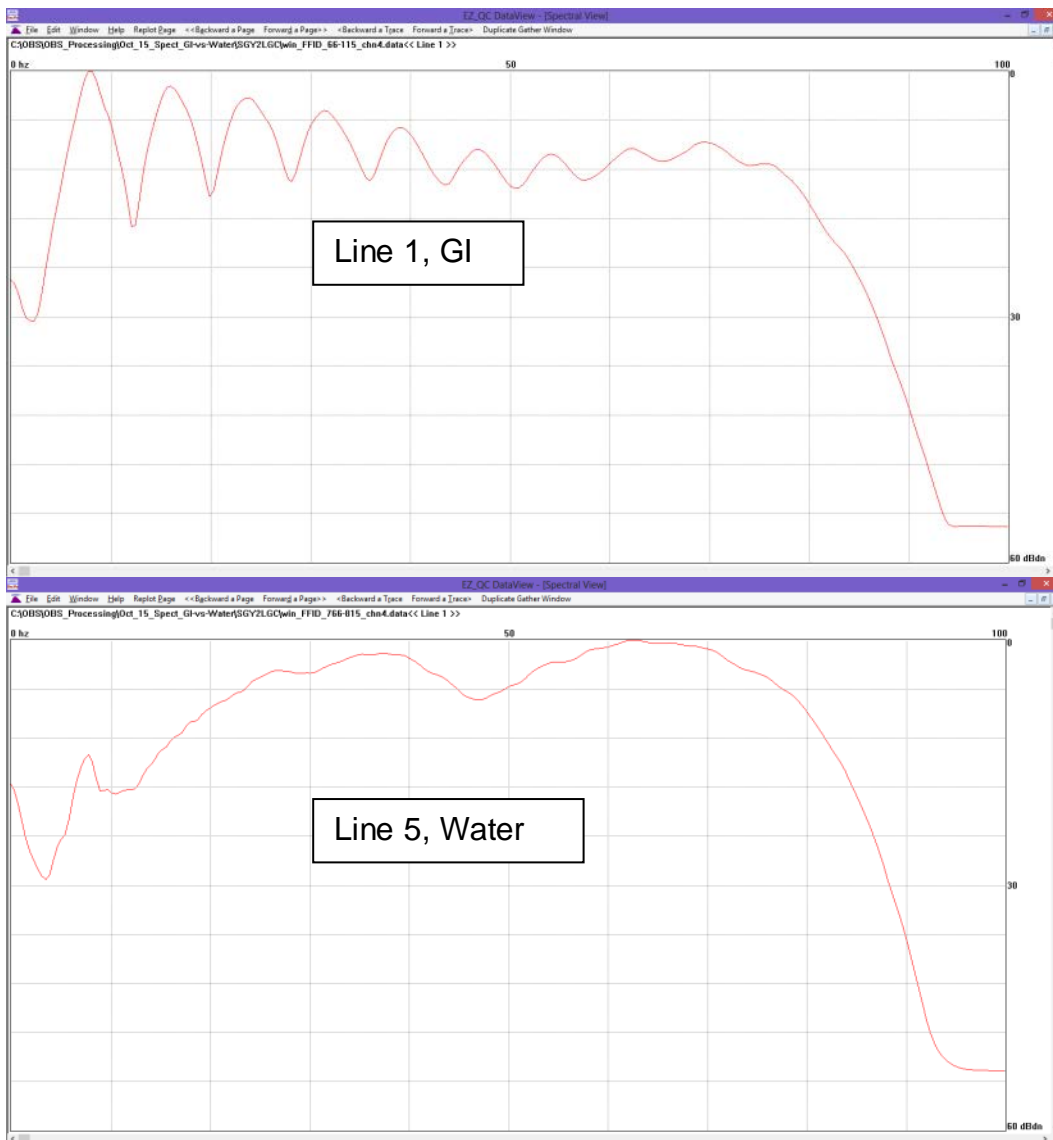
Z Line 1 – GI Gun – OBS 2,3      Z Line 5 – Water Gun - OBS 2,3



**Figure 33. Comparison of GI Gun to Water Gun shows that the Water Gun has less bubble and appears to be a little higher in frequency content.**

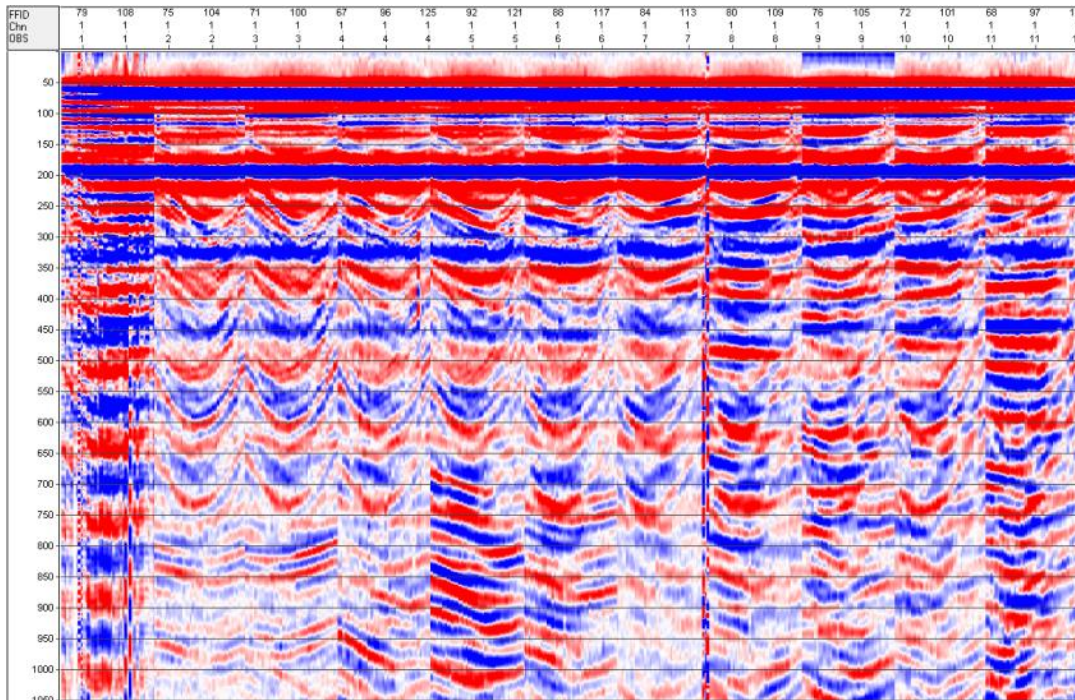


Figure 34 shows the hydrophone frequency analysis comparison at OBS 3 for the near offsets of Line 1 and Line 5. The display is the average of the data window from 0 to 2000 msec for each line.



**Figure 34. Spectral comparison of GI Gun and Water Gun.**

Gathers for OBS 1-11 on Line 1, Figures 35, 36 compare to Figures 31, 32 for Line 5.



**Figure 35. Line 1, gather of near offsets for OBS 1-11, raw vertical geophone, with low cut filter.**

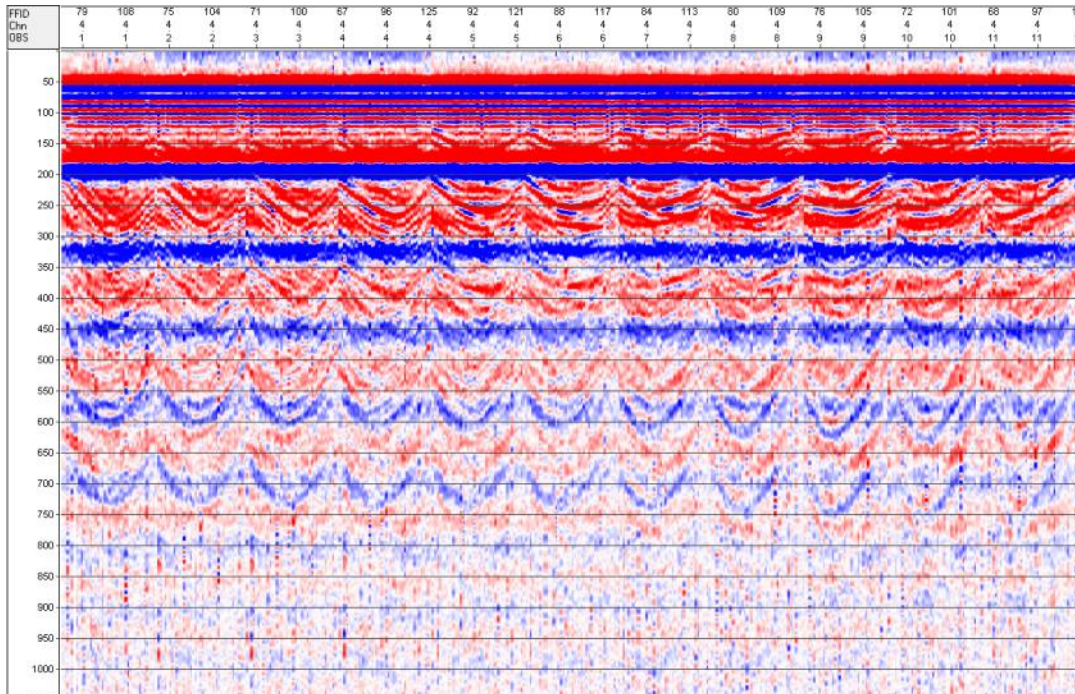


**Figure 36. Line 1, gather of near offsets for OBS 1-11, raw hydrophone, with low cut filter.**



## OBS Comparison to SSSR

SSDR Line 28 S-N, recorded in 2006, is very close to OBS Lines 1 and 5. To compare to OBS data, we converted this SSDR line to "reduced time", shown with and without display AGC, Figure 37. Figure 38 shows the line location over the OBS stations.

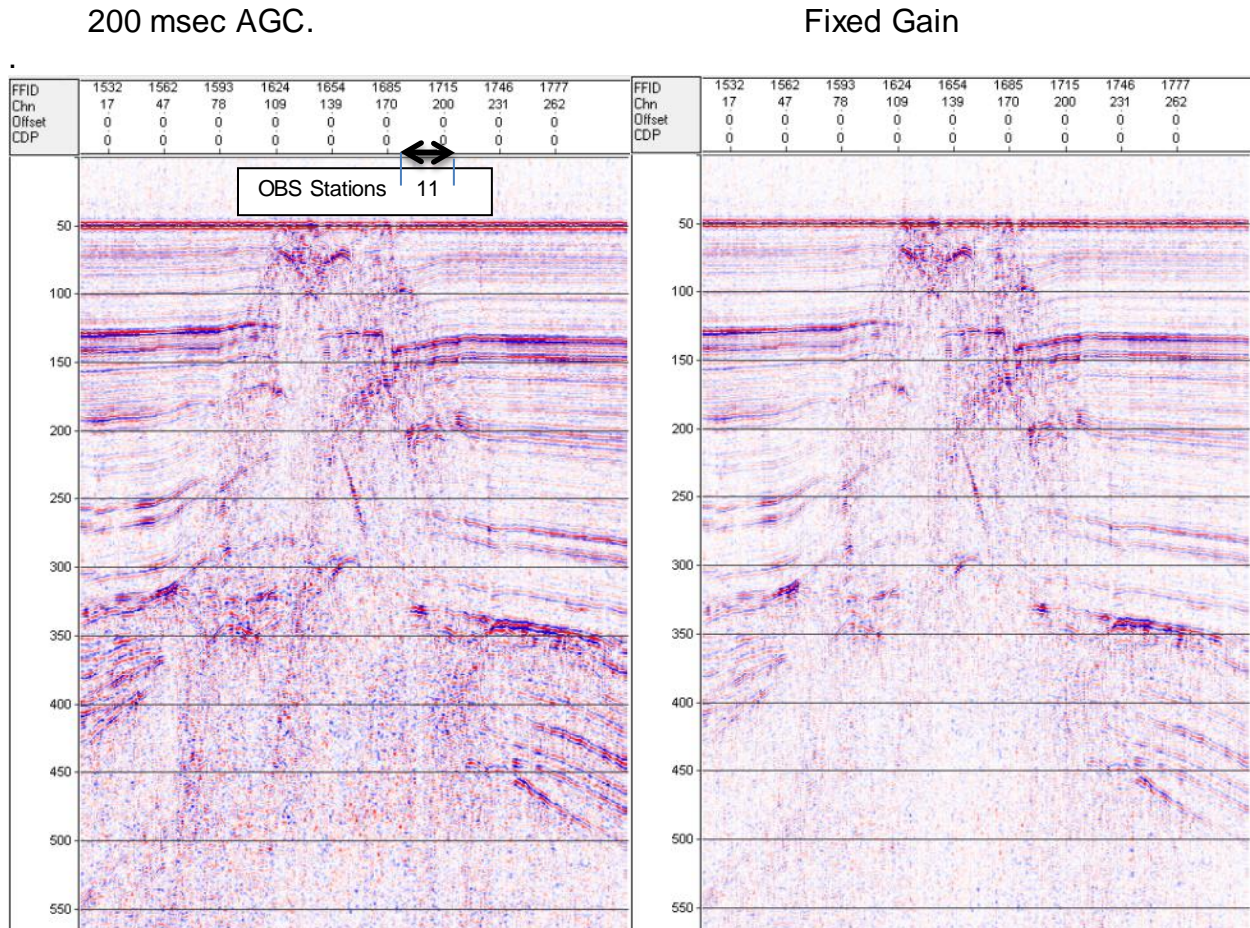


**Figure 37. SSDR Line 28 S-N with the approximate range of the OBS locations.**

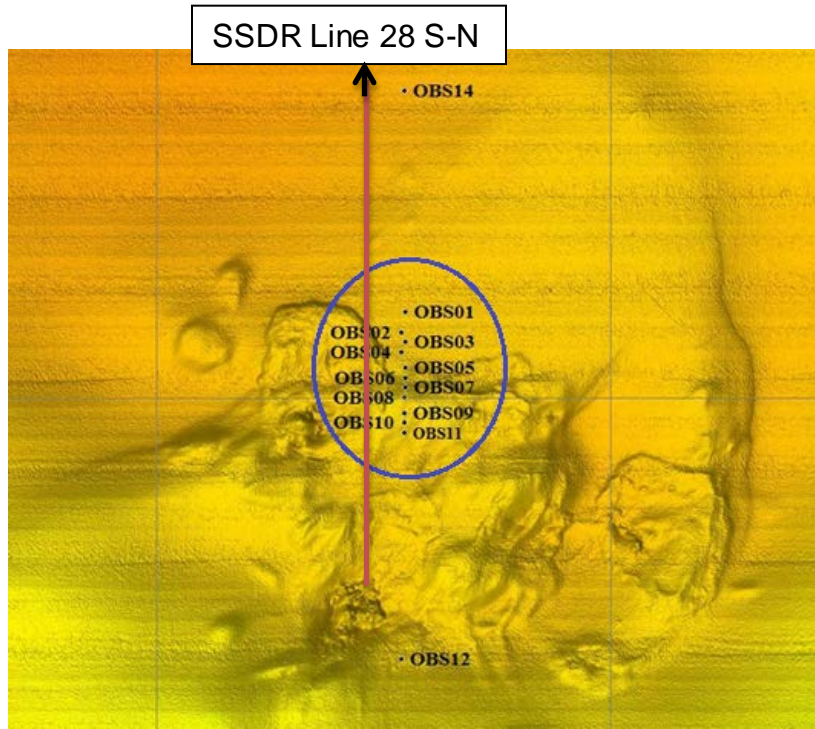


Figure 38. Map view of the approximate location of SSSR Line 28 S-N.

The near offset hydrophone channel gather for OBS 11-1 is compared to a zoom on SSSR Line 28 S-N showing the trace range corresponding to the locations of OBS 11-1, Figure 39. The frequency of the OBS data is limited to 100 hz (5 msec per sample). The SSSR line is higher frequency, high-cut filtered to 300 hz for display. There are similar trends in the reflectors.

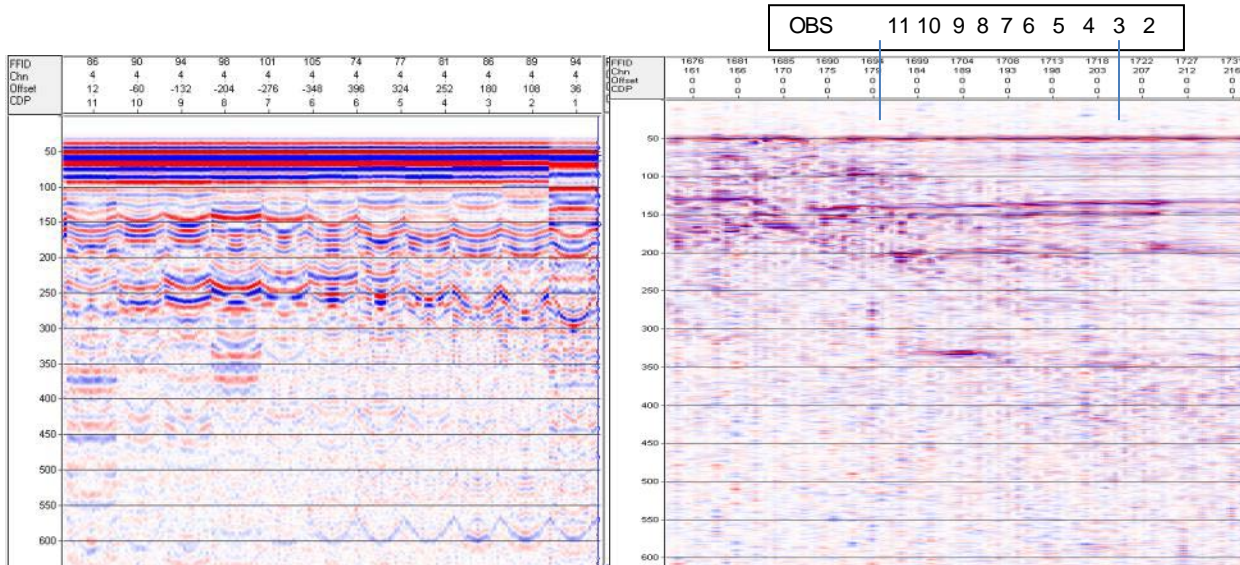


Figure 39. OBS 11-1 and SSSR Line 28 S-N.



## **Conclusions and Summary**

Processing this OBS data presented challenges. Source timing and conversion to SegY format were the first steps, and some of the OBS channels were not usable. Processing software with options to parallel the Hardage method was compiled. Processing this OBS data then produced similar results. Separation of Up-going and Down-going waves and Deconvolution to estimate Reflectivity were key, and these outputs look reasonable.

Estimation of  $V_p/V_s$  between pairs of reflection events showed spatial variability. Correlation of  $V_p/V_s$  to methane hydrate occurrence and/or concentration in the study area remains an unanswered question.

We found evidence of S-waves recorded on the vertical geophone channel, which violates an assumption that S-waves are primarily on the horizontal geophone channels. We proposed an alternate method of processing and showed that the alternate method produced results similar to the Hardage method for an example OBS station.

In comparing the GI Gun to the Water Gun source, the Water Gun has a shorter bubble and appears to have advantages. One advantage is easier quality control, with less need for processing to remove the source bubble. Another advantage is potentially better resolution with higher frequency data, although this data does not allow for a frequency comparison above 100 hz.

Comparison of OBS data to previous SSSR data was not conclusive, primarily due to different bandwidths inherent in each type of recording.

For future OBS recording we recommend several changes. One is faster digitizing for higher potential bandwidth and resolution. Another is doing external system tests, such as with a shake table, to verify recording fidelity. The level of electrical crossfeed should also be measured.

## **TASK 4: Geochemical investigations at MC 118: Pore fluid time series and gas hydrate stability.**

The Final Report for this task, supported in all four Phases, is found in Phase 4, Task 4.

## **TASK 5: Automated Biological/Chemical Monitoring System (ABCMS) for Offshore Oceanographic Carbon Dynamic Studies.**

Development of a Marine Lander Survey Vehicle (Lander) for the next phase of gas hydrate research in the Gulf of Mexico

This task was continued into subsequent Phases of the MS/SFO/Hydrates project. A Final Report appears in Phase 4, task 5 and covers work from all phases.

## **TASK 6: Scoping study using Spatio-Temporal Measurement of Seep Emissions by Multibeam Sonar at MC118.**

The Final Report for this task, supported in all four Phases, is found in Phase 4, Task 6.

**TASK 7: Modeling a carbonate/hydrate mound in Mississippi Canyon 118 using modified version of (THROBS).**

**This task was supported in Phases 2, 3 and 4. A Final Report appears in Phase 4, Task 3.**

**Task 8: Administrative oversight of the Monitoring Station/Sea-floor Observatory Project.**

Administration of the Consortium is the responsibility of the University of Mississippi and includes formal Project Proposals to federal funding agencies, Technical Progress Reports, Final Project Reports, informal monthly updates, reports of Consortium meetings, cruise reports, participation in national meetings, organizing meetings between researchers, organizing and participating in program reviews, organizing and participating in research activities, including research cruises. This responsibility was completed for FY09 with the completion and acceptance of the year-end report to DOE, 42877R18. This responsibility continues through the life of the project and a compilation of administrative duties and responsibilities is presented in Phase 4, Task 7.

**Task 9. Project Summary Updates:**

These appear as Task 8 in Phase 4.

## **PHASE 4 Tasks FOR FY2010**

### **TASK 1: Program Management Plan (complete)**

### **Task 2: Integration of Multiple Methods of Geological and Geophysical investigations to advance Shallow Subsurface Characterization at MC118, site of the Gulf of Mexico Hydrates Research Consortium's Seafloor Observatory**

(Subcontractor: The University of Mississippi; Leonardo Macelloni, Carol Lutken, Marco D'Emidio, Pls)

#### **Introduction**

The focus of this task has been to collect, assemble, integrate, and interpret multiple geo-datasets that had been collected during previous phases of the project, identify gaps and to attempt to collect and integrate new data to fill those gaps. In so doing, we hoped to present a more comprehensive picture of MC118, characterizing the hydrocarbon system at the site of the Seafloor Observatory being installed by the Gulf of Mexico Hydrates Research Consortium at MC118.

Progress has been made in data acquisition as well as in integration of datasets. However, completion of the six subtasks is unequal with some experiencing much more progress than others. In addition, Subtask 2.4 in particular remains incomplete due to the slippage of the schedule to complete the speed of sound probe. Since this equipment development is funded (and extended) under a BOEM Cooperative Agreement, it will be completed. An addendum to this report will be sent when the probe work – coordinated with additional gravity coring – is complete. Summaries of each of the subtasks follow:

#### **Subtask 2.1. Recipient shall contract heat-flow data collection surveys across the hydrate mound area at MC118.**

Heat-flow from the Observatory site had long been a goal of the HRC-GOM and was the primary goal of this Task. TDI Brooks was contacted and later contracted to do a 15-point study focused on areas within the Research Reserve that geologists and geophysicists believed would exhibit anomalous heat-flow. Heat-flow expert Trevor Lewis, familiar with the heat-flow patterns of the Gulf, was contracted to do the interpretation and was involved in the selection of targets. Lewis selected targets that he believed would exhibit "normal" heat-flow or background.

This study was completed and reported upon in the technical progress report, 42877R24 (also included here as Appendix C). The purpose of the study was to determine the thermal properties impacting the Observatory site and thus provide information regarding the general extent of hydrate stability as well as specifics regarding the role(s) of major faults in functioning as conduits for fluids migrating from depth to the seafloor, and which faults are open conduits and which are not.

A summary paper has been written and submitted for publication to the Journal of Geophysical Research. This paper addresses the distribution of heat-flow in the carbonate

complex at Woolsey Mound. The heat-flow values and hydrate compositions obtained from samples collected during a 2002 submersible dive and from core samples collected during the January, 2011 Jumbo Piston Coring cruise were used in the compositional simulator developed by SAIC (Phase 4, Task 3, this section) to model the hydrate stability zone.

**Subtask 2.2. Recipient shall contract to have giant piston cores collected from areas of interest at the Observatory site.**

The rationale behind collecting Jumbo Piston Cores for this project was 3-fold: 1. We felt we needed some subsurface data beyond our 7-10m gravity cores to 2. Ground-truth the very high resolution chirp data we had and 3. To reach the depths (~18m) where we were seeing a high frequency anomaly in our shallow-source/deep-receiver (SSDR) data that we thought might be hydrates and therefore the seismic signature for hydrates.

Five Jumbo Piston Cores (JPCs) were collected in January, 2011. Hydrate was recovered in one, from an area that *did* include the high-frequency anomaly in the SSDR data and which also exhibited a marked resistivity anomaly in a 2009 Direct Current Resistivity survey. This subtask was completed and a report of activities (42877R22) made during a previous reporting period. It appears here as Appendix A.

**Subtask 2.3. Recipient shall process and interpret the polarity-preserving chirp data collected with the AUV-borne system, to define the shallow geometry of the fluids/gas pipe system and integrate these results with the geological (core analyses) and geophysical data.**

CMRET and UVTC have established a processing protocol for the polarity-preserving chirp data from MC118.

Subbottom profiles have been converted and processed for stratigraphic interpretation/analysis. Using a converter developed in-house, the files logged by the subbottom profiler (SBP) in GeoAcoustics condensed format (.gcf) are merged with vehicle log files and exported in a variant of the SEG-Y (.sgy) geophysical data format. This allows additional processing to be carried out using standard seismic tools, thereby allowing for analysis of sediment elastic properties and, eventually, the creation of pseudo-3D volumes. The 3D representations can be combined with vehicle-derived bathymetry and backscatter measurements to derive a greater understanding of the seafloor structure. This process will allow selection of the most promising sites for the future instrument deployments and surveys. A time-lapse analysis will be made comparing the 2005 and 2012 datasets.

The polarity-preserving chirp system performed four successful data acquisitions in May 2013 and two successful acquisitions in September 2013 (including one high resolution grid) all while the chirp system ran simultaneously with the AUVs multibeam system. With the new in-house data converter, developed by UVTC and STRC, we are able to process and import the seg-y data into Kingdom for interpretation. The data acquired in the high resolution grid will be processed to create a pseudo-3D image of the sub seafloor, because the 40m line-spacing used allows us a good 3D interpolation of the profiles. Some results are illustrated below.



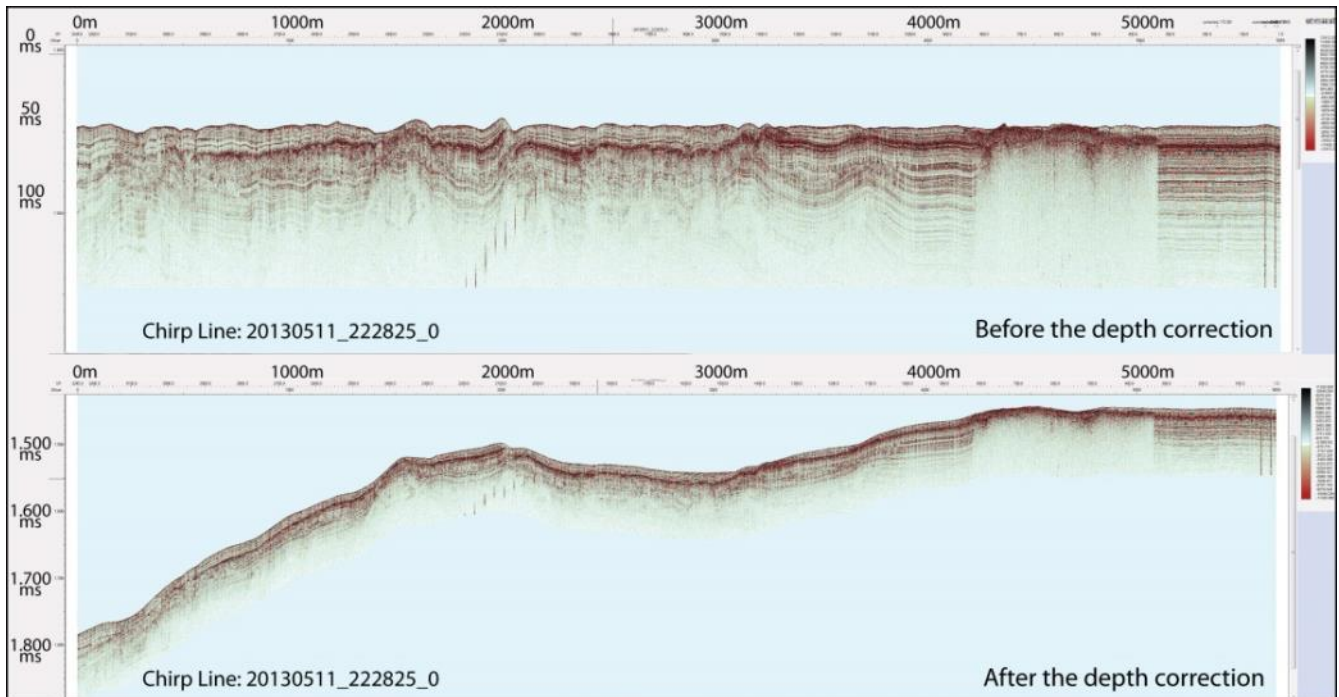


**Figure 1. Polarity-preserving chirp depth correction.**

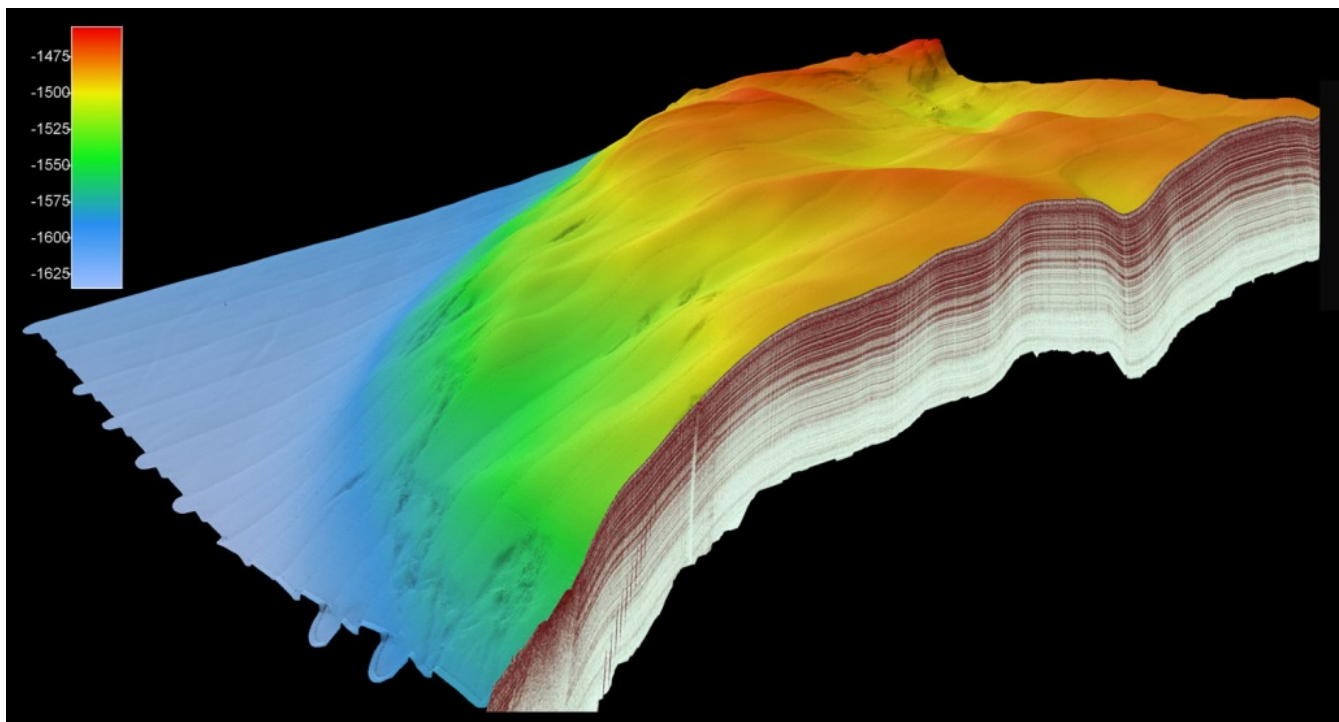


**Figure 2. 3D image of Multibeam and Chirp (multibeam data processing Alessandra Conti).**

**Subtask 2.4** The recipient shall perform sedimentological, lithological, paleontological and geophysical analyses of the newly recovered cores (Phase 4, subtask 2.2) and shall integrate the results with previous core studies. The University of Southern Mississippi core-logging team opened, photographed and described the cores from the JPC

cruise during the summer of 2011. Electric log analyses were performed at Stennis Space Center's office of NAVOCEANO.

A summary of the lithostratigraphy appeared in the previous Technical Progress Report (42877R24) and is included here as Appendix B. The biostratigraphic/time analysis is anticipated in the near future.

**Subtask 2.5 Recipient shall collect solid outcropping gas hydrates and/or authigenic carbonate/hydrates samples at the MC118 Observatory site using the existing pressure-chamber sampler in conjunction with the STRC ROV.**

The purpose of this task is to ground-truth some of the indications for hydrate that we see in seismo-acoustic data and to collect chemical data in addition to the SeaLink and JPC hydrate chemical compositions. The hydrate community actually has very little compositional data for solid hydrate and much of what we know is based upon this very limited dataset. Clearly modeling hydrate occurrence and persistence can be improved with more examples of hydrate composition.

Construction of the small pressure vessels is complete and they have been fitted to the SSD Remotely Operated Vehicle (ROV). The SSD has been in very high demand over the last 18 months mostly in post-oil spill environmental recovery work and in servicing seafloor equipment. The CMRET/STRC team will attempt to complete this task at the earliest opportunity which will likely be during a ship wrecks cruise in which we are scheduled to participate in March, 2014.

**Subtask 2.6. The recipient shall refurbish 4C nodes, donated by CGG Veritas for deployment and use in shear experiments as defined in Phase 2 task 3, and Phase 3 task 3.**

This subtask was rewritten and rebudgeted from 3 years of DOE awards to the CMRET. It now reads:

**Phase 3, Task 3: Near seafloor geology at MC118 using converted shear-waves from 4C seafloor sensor data** (Subcontractor: John Collins, Woods Hole Oceanographic Institution)

This task is complete. The data were delivered to CMRET in both SEED and SEG Y formats. After inspecting the data, CMRET copied and delivered a set to UT-Austin (Hardage) for 4-C analyses and to enable them to fulfill the FY08 subcontract. In addition a copy of the data was delivered to UCSD (Gerstoft) for analysis of ambient noise in the data. A journal article resulted from the analyses of ambient noise by Carriere and Gerstoft. A full report of cruise activities is available at the MMRI website:

<http://mmri.olemiss.edu/Home/Publications/Cruise.aspx>

As noted earlier, UT's responsibilities were transferred to the University of Mississippi. UM continues to work with UT and UCSD to complete the analyses of the Ocean Bottom Seismometer (OBS) data. UM contracted with Lookout Geophysical Co. to complete the data analyses interpretation of the data for this task. A Final Report of this activity can be found under Phase 3, Task 3, this section of this report.

### **Publications deriving, at least in part, from work described in this task:**

- Lutken, Carol, Ken Sleeper, Greg Easson, Leonardo Macelloni, Gene Smith, 2012, *The GOM GAS HYDRATES SEAFLOOR OBSERVATORY: Producing Science for National and Global Management Decisions*, AGU Science Policy Conference 2012, Washington, DC, April 29-May 2.
- \*Lutken, Carol B., Marco D'Emidio, Leonardo Macelloni, Michela Ingrassia, Martina Pierdomenico, Vernon Asper, Arne Diercks, Max U. Woolsey, Roy Jarnagin, 2013, *Challenges in imaging the deep seabed: examples from Gulf of Mexico cold seeps*, Transactions of the GCAGS, New Orleans, 2013
- \*Macelloni, Leonardo, Antonello Simonetti, James H Knapp, Camelia C Knapp, Carol B Lutken. *Multiple resolution seismic imaging of a shallow hydrocarbon plumbing system, Woolsey Mound, Northern Gulf of Mexico Gulf of Mexico*. Marine and Petroleum Geology.
- Macelloni, L., M. D'Emidio, A. Simonetti, J. Dunbar, C.B. Lutken, 2012, *Geophysical evidence of shallow hydrates formation and accumulation at Woolsey Mound (Mississippi Canyon Block 118)*, Ocean Sciences Annual Meeting, Salt Lake City, February 19-24.
- \*Macelloni, Leonardo, Charlotte Brunner, Simona Caruso, Carol Lutken, Marco D'Emidio, Laura Lapham, 2012, *Spatial distribution of seafloor biogeological and geochemical processes as proxies of fluid flux regime and evolution of a carbonate/hydrates mound, northern Gulf of Mexico*, Deep Sea Research, Part 1, in press, Manuscript Number: DSR1-D-12-00118R1.
- Pizzi, Marco, Leonardo Macelloni, Lutken Carol B., Marco D'Emidio, 2012, *Temporal Evolution of MC118 Woolsey Mound seep activity: constraints from analysis of small-scale salt-induced sediment deformation*, GRC "Natural Gas Hydrates System", Ventura, CA, March 18-23, 2012.
- Simonetti, Antonello, James H. Knapp, Camelia C. Knapp, Carol B. Lutken, 2012, *4d seismic imaging of a thermogenic gas hydrate system in the northern Gulf of Mexico (Woolsey Mound, MC118)*, The Gordon Research Conference on Natural Gas Hydrate Systems, Ventura, California, March 18<sup>th</sup>-23<sup>rd</sup>
- Wilson, R.M., L.L. Lapham, C. Martens, J.P. Chanton, H. Mendlovitz, K. Sleeper, M. Reidel, 2012, *Time-series methane monitoring in gassy sediments and the benthic boundary layer*, Ocean Sciences Annual Meeting, Salt Lake City, February 19-24.
- Wilson, R.M., L.L. Lapham, B. Anderson, N. Garapati, and J. Chanton (2012) Laboratory experiments probe hydrate dissolution rates. The Gordon Research Conference on Natural Gas Hydrate Systems, Ventura, California. March 18<sup>th</sup>-23<sup>rd</sup>

#### **In Press:**

- Carrière, Olivier and Peter Gerstoft, in press, *Deepwater subseafloor imaging using active seismic interferometry*, Geophysics.
- Simonetti, Antonello, James H. Knapp, Kenneth Sleeper, Carol B. Lutken, Leonardo Macelloni, Camelia C. Knapp, *Spatial Distribution of Gas Hydrates from High-Resolution Seismic and Core Data, Woolsey Mound, Gulf of Mexico*, submitted to Marine and Petroleum Geology.
- Wilson, Rachel, Leonardo Macelloni, Antonello Simonetti, Jeffrey Chanton, Jim Knapp, Laura Lapham, Carol Lutken, Ken Sleeper, Charlotte Brunner, Chris Martens, Marco D'Emidio, *Integrating geochemical profiles with seismic surveys to identify subsurface methane sources and migration pathways*

#### **Submitted:**

- Macelloni, L, Lutken, C. B., Garg, S., Simonetti, A., D'Emidio, M., Wilson, R., Sleeper, K., Lapham, L., Lewis, T., Pizzi, M., Knapp, J., Knapp, C., Brooks, J. and McGee T.M., *Geothermal regime and hydrate stability zone of woolsey mound (northern Gulf of Mexico): a transient, thermogenic, fault-controlled hydrate system*; submitted to Geophysics.

## **TASK 3: Modeling a carbonate/hydrate mound in Mississippi Canyon 118 using modified version of (THROBS).**

(Subcontractor: SAIC (Scientific Applications International Corporation); Sabodh Garg, PI)

### **Introduction**

The hydrate mound in Mississippi Canyon Block 118 (MC 118), as described by McGee *et al.* (2008), contains mostly Structure II thermogenic hydrates formed by gases upflowing along a nearly vertical fault system extending from a salt diapir that underlies several

hundred meters beneath the hydrate mound. The surface of the hydrate mound is characterized by several crater clusters; these crater clusters have been grouped into three major complexes based on topographic relief and gas venting (*McGee et al.*, 2008). At present, the SE complex exhibits no venting activity; the NW complex has moderate activity, and the SW complex shows moderate to high venting activity. The venting activity has most likely changed over time. In addition to variable venting activity over time, the following observations are relevant to the modeling of hydrates at this site:

1. Salinities as high as 5 times that of sea-water have been recorded around the vents in the NW complex. High salinity and gas venting suggests the presence of 3-phase conditions (gas + hydrate + liquid).
2. Chemical composition of vent gas is different from that of the hydrate. It has been suggested that the difference is due to molecular fractionation (*Saason*, 2006). Treatment of this requires a “compositional” simulator.
3. Presence of multiple BSRs. It is possible that this is due to the existence of gas hydrates that are stable to greater depths (higher temperatures?) than that encountered above the “shallowest” BSR. Clearly, a compositional simulator is needed for modeling this phenomenon.
4. Acoustic wipeout zones, observed in seismic profiles, have been interpreted to indicate the possible presence of free gas (“chimney” flow) and/or other inhomogeneities (e.g. carbonate/hydrate blocks in the sediments). Modeling of chimney flow and/or other inhomogeneities can only be done by a multi-dimensional hydrate simulator.

Prior to the start of Year 1 (2008-2009) of SAIC effort, our hydrate simulator (THROBS) was restricted to one-dimension and Structure I methane hydrate. It was recognized that THROBS will have to be generalized in several respects in order to treat the phenomena of interest. Required changes include:

1. Incorporation of the stability curve and other hydrate properties (heat of melting, hydration number, and thermomechanical properties) for structure II hydrates.
2. Replacement of methane gas equation-of-state (EOS) and gas solubility relationship by an EOS and solubility curve that reflects the gas composition.
3. Development of a multi-dimensional version of THROBS.

Given the fiscal constraints, SAIC undertook a limited research effort during the first year (2008-2009). Specifically, we incorporated structure II hydrate stability curve and relevant properties (item 1 above) into THROBS simulator. The gas mixture forming the hydrate was represented as a single gas. The modified THROBS simulator was used to model (1) the hydrate distribution above the shallowest BSR, (2) presence of high salinity fluids within the hydrate stability zone, and (3) gas venting at the sea-floor. The work performed during Year 1 is described in a report by Garg and Pritchett (S. K. Garg and J. W. Pritchett, Modeling Studies of Hydrate Mound, Mississippi Canyon 118, Gulf of Mexico, Report submitted to the University of Mississippi, September 2009).

As previously mentioned, a “compositional” (i.e. multi-gas) simulator is needed to account for the various gas components present in MC 118 hydrates; such a treatment for the gas



composition is necessary for modeling phenomena such as molecular fractionation and multiple BSRs. During Year 2 (2009-2010), we initiated the development of a multi-component (methane, ethane, and propane) simulator. Because of funding limitations, this effort had to be spread over a couple of years. The work was divided into two parts, i.e. (1) development of a computationally efficient multi-component equation-of-state (i.e. PVT behavior of 3-gas components, water, and salt; phases will include hydrate and precipitated salt as solid phases, water with dissolved gases and salt as a liquid phase, and a gas phase), and (2) modification of the simulator to accommodate the new equation –of-state.

In preparation for the extension of the approach to treat multidimensional problems, SAIC completed the adoption of the existing (single gas) THROBS equation-of-state for use in the multidimensional STAR simulator. Test calculations have verified that, with the new STAR/HYDCH4 constitutive description, the two codes (THROBS and STAR) produce identical results when used to solve 1-D problems. Since the MC 118 site analysis will eventually require a multidimensional treatment, this is a necessary step in the development. With the existing THROBS constitutive description incorporated into STAR, it is now possible to carry out preliminary multidimensional studies and we are in a better position to proceed toward the final goal of a multidimensional, multi-component modeling capability. A description of STAR/HYDCH4 was provided in a previous letter report (J.W. Pritchett and S. K. Garg, Modeling Studies of Hydrate Mound, Mississippi Canyon 118, Gulf of Mexico, Informal report for the period January 1, 2010 to June 30, 2010, July 2010).

The work during Year 3 (2010-2011) mainly consisted of developing a multi-component equation-of-state (i.e. PVT behavior of 3-gas components, water, and salt; phases will include hydrate and precipitated salt as solid phases, water with dissolved gases and salt as a liquid phase, and a gas phase) for incorporation into STAR and/or THROBS simulators. The progress made till the end of December 2011 was described in a previous letter report (J.W. Pritchett and S. K. Garg, Modeling Studies of Hydrate Mound, Mississippi Canyon 118, Gulf of Mexico, Informal report for the period July 1, 2011 to December 31, 2011, January 2012), and in a paper by Garg and Pritchett (2011).

## **Work performed during the report period**

### **Contract Matters**

SAIC subcontract for Year 3 with the University of Mississippi was finalized towards the end of September 2010. A no-cost extension till the end of June 2012 was granted in the fall of 2011. An additional no-cost extension till the end of June 2013 was approved in the fall of 2012. This report constitutes the Final Report for the SAIC subcontract with the University of Mississippi.

### **Technical Progress**

During 2011, work was continued on debugging and testing the new equation-of-state package (HYDGAS). As reported in the January 2012 letter report, the contract funds were nearly exhausted (around 97% of the total) by the end of 2011. Since the remaining amount was insufficient to complete this HYDGAS package, a decision was made in January 2012 to suspend this effort pending the availability of additional support. Effort is continuing on identifying additional resources that may become available for this work. If we are successful in obtaining additional support, we will complete the HYDGAS package, and perform

preliminary calculations to characterize the effect of a gaseous mixture on hydrate formation at the Hydrate Mound.

In June 2012, SAIC was informed by the University of Mississippi that recently very accurate heat flow data were collected at 15 sites in and around MC118. We have used the completed HYDGAS correlations to compute the base of the hydrate stability zone (for 100% methane gas, and a mixture of methane, ethane and propane) at these 15 sites. This work is included in a multi-author paper recently submitted to a peer-reviewed journal (Macelloni et al., 2013).

## References

- Garg, S.K., Pritchett, J.W., Katoh, A., Baba, K., Fuji, T. (2008), A mathematical model for the formation and dissociation of methane hydrates in the marine environment, *Journal of Geophysical Research*, Vol. 113, B01201, doi:10.1029/2006JB004768.
- Garg, S.K., Pritchett, J.W. (2011), Modeling Studies of Hydrate Mound, Mississippi Canyon Block 118, Gulf of Mexico, Proceedings of the 7<sup>th</sup> International Conference on Gas Hydrates (ICGH 2011), Edinburgh, Scotland, United Kingdom, July 17-21, 15 pp.
- Macelloni, L., Lutken, C. B., Garg, S., Simonetti, A., D'Emidio, M., Wilson, R.M., Sleeper, K., Lapham, L., Lewis, T., Pizzi, M., Knapp, J., Knapp, C., Brooks, J., and McGee, T. submitted, Geophysics, Heat-flow regimes and the hydrate stability zone of Woolsey Mound (Northern Gulf of Mexico): a transient, thermogenic, fault-controlled hydrate system, in review.
- McGee, T., Woolsey, J.R., Lapham, L., Kleinberg, R., Macelloni, L., Battista, B., Knapp, C., Caruso, S., Goebel, V., Chapman, R., Gerstoft, P. (2008), Structure of a Carbonate/Hydrate Mound in the Northern Gulf of Mexico, Proceedings of the 6th International Conference on Gas Hydrates (ICGH 2008), Vancouver, British Columbia, Canada, July 6-10, 10 pp.

## **TASK 4: Coupling of Continuous Geochemical and Sea-floor Acoustic Measurements and Biogeochemical investigations at MC 118: Pore fluid time series and gas hydrate stability**

**Phase 1, TASK 3:** Coupling of Continuous Geochemical and Sea-floor Acoustic Measurements (Subcontractor: Florida State University, FSU)

And Phase 2:

**Phases 2, 3, 4, TASK 4:** Biogeochemical investigations at MC 118: Pore fluid time series and gas hydrate stability (Subcontractor: Florida State University, FSU)

### **Final Report Fiscal years 2006-2012**

Laura Lapham, FSU (currently at UMD)

Rachel Wilson, FSU

Jeff Chanton, FSU

### **1. Publications:**

- Lapham, LL, JP Chanton, CS Martens, PD Higley, HW Jannasch, and JP Woolsey (2008) Measuring temporal variability in pore-fluid chemistry to assess gas hydrate stability: development of a continuous pore-fluid array. *Environmental Science and Technology* **42**: 7368-7373
- Lapham, LL, JP Chanton, CS Martens, K Sleeper, and JR Woolsey (2008b) Microbial activity in surficial sediments overlying acoustic wipeout zones at a Gulf of Mexico cold seep. *Geochemistry Geophysics Geosystems* **9**(6): 1-17
- Lapham, LL, JP Chanton, R Chapman, and CS Martens (2010) Methane under-saturated fluids in deep-sea sediments: implications for gas hydrate stability and rates of dissolution. *Earth and Planetary Science Letters* **298**(3-4):275-285
- Lapham, LL, RM Wilson, and JP Chanton (2012) Pressurized laboratory experiments show no stable carbon isotope fractionation of methane during gas hydrate dissolution and dissociation. *Rapid Comm Mass Spec* **26**: 32-36
- Lapham L. L., Wilson R. M., MacDonald I. R., and Chanton J. P. (submitted 2013) Gas hydrate dissolution rates quantified with laboratory and seafloor experiments. *Geochimica et Cosmochimica Acta* in review.

### **2. Manuscripts in Preparation:**

- Wilson, Rachel, Laura Lapham, Michael Riedel, and Jeff Chanton. Time-series in situ methane concentrations from sediment porewaters overlying a hydrate outcrop  
*Wilson, Rachel, Leonardo Macelloni, Laura Lapham, Antonello Simonetti, Jim Knapp, Camelia Knapp, Carol Lutken, Ken Sleeper, Charlotte Brunner, Marco D'Emidio, and Jeff Chanton. Integrating geochemical profiles with seismic surveys to identify subsurface methane sources and migration pathways*
- Lapham, L., R. Wilson, J. P. Chanton, C. Paull, and M. Riedel, Temporal variability of in situ methane concentrations in gas hydrate bearing sediments near Bullseye Vent, In preparation for *Global Biogeochem. Cycles*.

### **3. Presentations**

- Wilson, RM, LL Lapham, B Anderson, N Garapati, and J Chanton (2012) Laboratory experiments probe hydrate dissolution rates. The Gordon Research Conference on Natural Gas Hydrate Systems, Ventura, California. March 18<sup>th</sup>-23<sup>rd</sup>
- Lapham, LL, RM Wilson, M Riedel, and J Chanton (2012) Measuring in-situ methane concentrations over time near Bullseye vent, Vancouver Island. The Gordon Research Conference on Natural Gas Hydrate Systems, Ventura, California. March 18<sup>th</sup>-23<sup>rd</sup>
- Wilson, RM, LL Lapham, M Riedel, and J Chanton (2011) Measuring in situ dissolved methane concentrations in gas hydrate-rich systems to understand hydrate stability. The 7<sup>th</sup> International Conference on Gas Hydrates (ICGH7) 2011 Meeting in Edinburgh, Scotland. July 17<sup>th</sup>-21<sup>st</sup>
- Wilson, RM, LL Lapham, M Riedel, and J Chanton (2010) Measuring in situ Dissolved Methane Concentrations in Gas Hydrate-Rich Systems, Part 2: Investigating Mechanisms Controlling Hydrate Dissolution. American Geophysical Union 2010 Fall Meeting in San Francisco, CA. December 12<sup>th</sup>-18<sup>th</sup>
- Lapham, LL, RM Wilson, M Riedel, and J Chanton (2010) Measuring in situ Dissolved Methane Concentrations in Gas Hydrate-Rich Systems. Part 1: Investigating the correlation between tectonics and methane release from sediments. American

Geophysical Union 2010 Fall Meeting in San Francisco, CA. December 12<sup>th</sup>-18<sup>th</sup>  
Lapham, LL, RM Wilson, RT Short, RJ Bell, and JP Chanton (2010) Mechanisms influencing hydrate dissolution rates in under-saturated systems. Goldschmidt 2010, in Knoxville, TN. June 13<sup>th</sup>-18<sup>th</sup>  
Wilson, RM, LL Lapham, RT Short, RJ Bell, and JP Chanton (2010) Using continuous mass spectrometry to monitor dissolution of artificial methane and mixed-gas hydrates. Gordon Research Conference on Gas-Hydrates, in Waterville, ME. June 6<sup>th</sup>-11<sup>th</sup>

#### **4. Cruise Participation**

*April 2008:* Lapham, Wilson and former FSU graduate student J Nelson participated in the coring cruise led by chief scientist Carol Lutken aboard the RV Pelican  
*July 2009:* Lapham and Chanton participated in the DOE funded HYFLUX cruise led by chief scientist Ian MacDonald aboard the RV Brooks McCall.  
*August 2009:* Lapham participated in the cruise to Cascadia Margin to test deploy mini-PFAs  
*March 2010:* Wilson and J Nelson to MC-118 to retrieve and replace PFA sampler box.  
*April 2010:* Wilson to Victoria, BC, Canada to receive the mini-PFA.  
*June 2010:* Chanton to MC 118 to retrieve and replace sampler box.  
*September 2010:* Wilson aboard the RV Pelican to deploy ROVARD, CSA, and peepers  
*September 2010:* Chanton to MC 118 to retrieve and replace PFA sampler box.  
*January 2011:* Wilson and FSU graduate student S. Hodgkins participated in the Jumbo Piston Coring cruise led by chief scientist Carol Lutken aboard the RV Brooks McCall.  
*June 2011:* Wilson and FSU graduate student Brian DeSanti participated in the RV pelican cruise led by chief scientist Carol Lutken to retrieve the ROVARD, CSA, and peepers.

**FY2006**

***TASK 3: Coupling of Continuous Geochemical and Sea-floor Acoustic Measurements (Subcontractor: Florida State University, FSU)***

*The principal goal of this task shall be the continuation of activities for coupling of continuous sampling of pore-fluid chemistry with sea-floor acoustic and accelerometer measurements and to ground-truth acoustic anomalies identified with geophysics. This shall be accomplished by correlating the seismic and thermal data (as measured by the down-hole and water-column geophysical/acoustic arrays) with the geochemical data (as measured by the downhole arrays of pore-fluid samplers). This correlation shall be used to infer gas hydrate decomposition or formation. Geochemical parameters to be monitored shall include (but not be limited to) methane and other light dissolved hydrocarbon gas concentrations and perturbations in salinity. The goal of this effort is to assess and document the stability of hydrates by characterizing their origin, fate, and genesis on the sea-floor.*

#### ***Subtask 3.1: Continuous and Directed Sampling Using Pressurized Equipment***

*This task shall include construction of equipment that will replace the osmo-pump and sampling head Pore-Fluid Array (PFA) packages previously constructed under separate funding (Figure 1). One of the previously constructed PFA packages was deployed via the CMRET's Sea-floor Probe in the shallow subbottom of the sea-floor at MC118 in 2005 and the other will be deployed following assessment of the samples collected using the first probe. Activity under this task shall be carried out to construct and deploy replacement osmo-pumps and sampling head PFA packages that will replace the original packages build under previous funding. This replacement and deployment shall provide for continuous collection of pore-fluids from 8 depths over a 10m interval during a 3-year period at two separate sites in different environments in close proximity to the carbonate mound at MC118. The second deployment site shall be in close proximity to the water-column and proposed borehole geophysical array MS/SFO components. Samples to be collected with the PFA as well as samples collected from cores recovered from*



the sea-floor in MC118 during the deployment cruise shall be analyzed for light hydrocarbon composition and concentration, isotopic composition, and chlorinity. With the additional equipment, pressurized time series gas and salinity samples shall be retrieved at 6-12 month intervals and analyzed at Florida State University. In May, 2005, the initial 10m probe with OsmoSamplers was deployed in MC118 as part of the MS/SFO. Effort under this task shall include activities necessary for:

**Subtask 3.1a:** construction of two additional OsmoSampler packages that shall be exchanged with the existing packages to allow for continuous sampling of pore-fluids at the site of the MS/SFO



**Figure 1.** A fully constructed OsmoSampler package. The copper coil stores sample until package retrieval. This size copper coil is sufficient to hold ~10 months of samples. Four coils and osmopumps per package allow up to four sediment depths to be monitored simultaneously.

Replacement OsmoSamplers have been completed and are awaiting deployment at MC-118 once the two deployed packages have been retrieved.

**Subtask 3.1b:** retrieval of the existing osmo-sampling packages from the seafloor at MC118 and their replacement with the newly constructed units.

Due to difficulties encountered with the SSD, deployed packages have yet to be recovered from the seafloor.

**Subtask 3.1c:** recovery, sample collection and redeployment of “peeper” sensors for collecting in situ samples on the sea-floor and maintaining them at sea floor pressure.

Six peepers were deployed at MC-118 during September 2006. One peeper, deployed at Mandyville, was located about 50cm from an outcropping hydrate formation and 50cm from a bacterial mat. The peeper was inserted into the sediment until it made contact with buried hydrate so that the sampler would measure the gradient from the hydrate surface. We hypothesized that methane concentrations would be highest near the hydrate and decrease with distance. Contrary to our prediction, when we analyzed methane concentrations in the peeper, we found that methane concentrations nearest the hydrate surface were 100 $\mu$ M and increased to 325 $\mu$ M at 10cm from the hydrate surface as portrayed in Figure 2. This suggests there may be a methane sink, such as microbial oxidation, occurring near the hydrate surface.

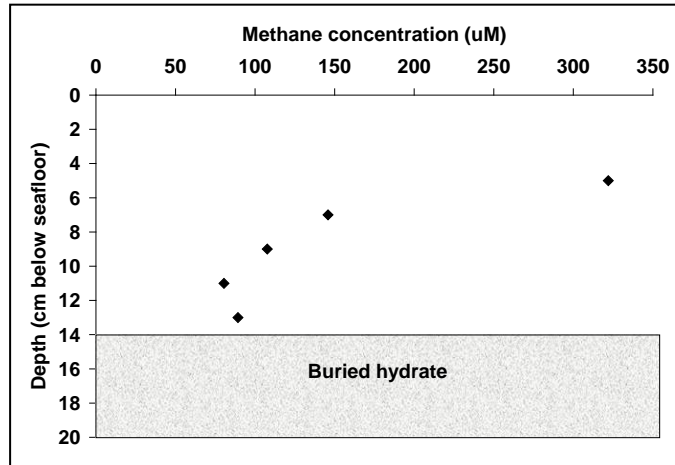


**Figure 2.** Methane concentrations with depth relative to the Mandyville buried hydrate, sampled using the peeper sensor.

**Subtask 3.1d:** conducting chemical analyses on the samples recovered with the equipment described in 3.1a - c. Chemical Analysis results for the first PFA retrieved from the MC-118 site are presented in Figure 3.

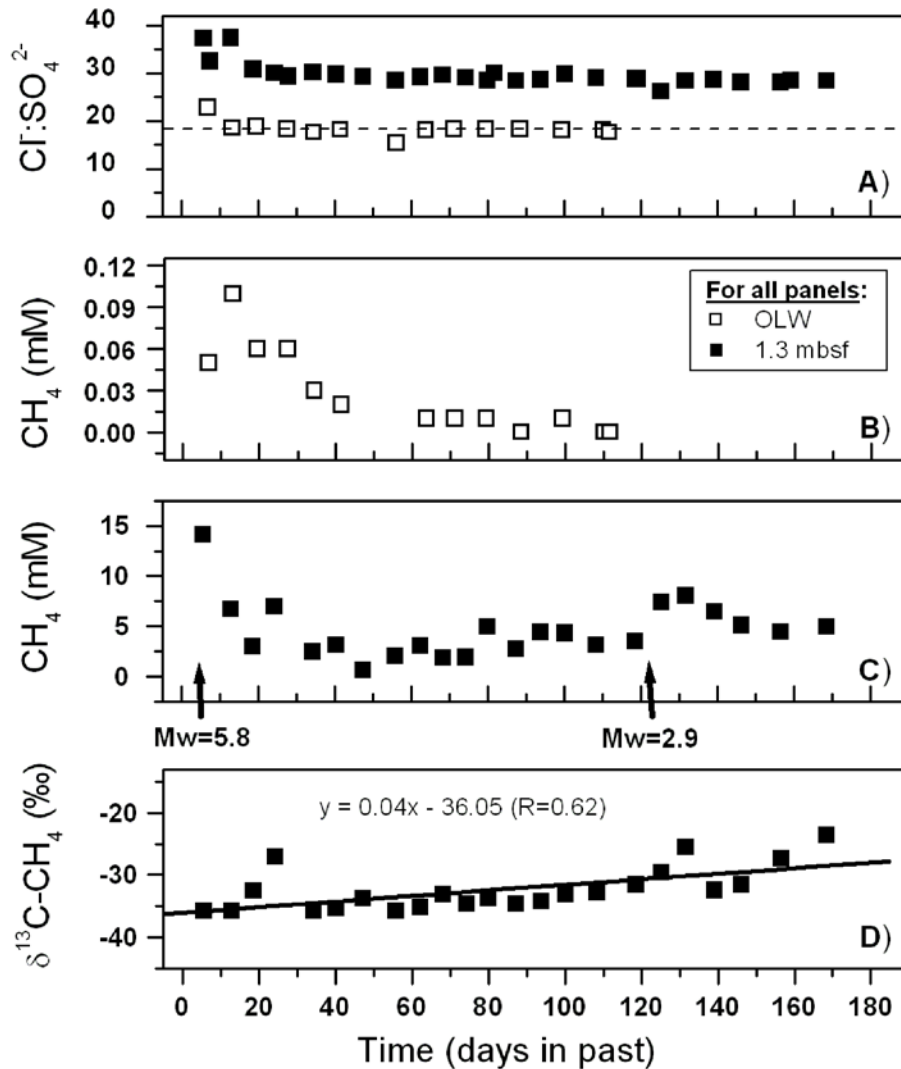


**Figure 3. Temporal record of geochemical parameters measured via the pore fluid array OsmoSampler package deployed at MC-118. Figure adapted from Lapham et al. 2008.**

The methane spikes at 10 days and 120 days were correlated with nearby earthquakes confirming our hypothesis that seismic events influence geochemical parameters.

Results from this study have been published in:

Lapham, LL, JP Chanton, CS Martens, PD Higley, HW Jannasch, and JP Woolsey (2008) Measuring temporal variability in pore-fluid chemistry to assess gas hydrate stability: development of a continuous pore-fluid array. *Environmental Science and Technology* **42**: 7368-7373.

**Subtask 3.2: Feature Investigation at MC-118. The Recipient shall conduct activities necessary to investigate and document features of interest in the area of MC-118 identified by geophysical data. The recipient shall**

conduct coring investigations to establish vent activity by geochemical determinations, specifically, hydrocarbon concentrations, isotope ratios, and chlorinity.

Ten gravity cores were collected at MC-118 during the May 2005 cruise from sites identified in the chirp profiles to be of geophysical interest. Areas with acoustic wipe-out zones were specifically targeted during this study. Cores were subsampled every 0.5m. In nine of the cores, methane concentrations were low and sulfate concentrations were not different from seawater (28mM) throughout. We found no evidence of seep activity. In the final core, Core 9, sulfate was below detection by 50cmbsf. Methane concentrations in the core increased with depth to a maximum of 3.5mM at 75cmbsf (Figure 4). Because the cores likely degassed during ascent, these methane concentrations represent minimum values, actual in situ values were likely much higher. Methane carbon isotopes became heavier with depth to -49.7‰, which indicates a thermogenic source of the methane. The decrease in sulfate with depth is consistent with microbial reduction coupled to methane oxidation. Thus we characterized this site as a microbial ‘hot spot’.

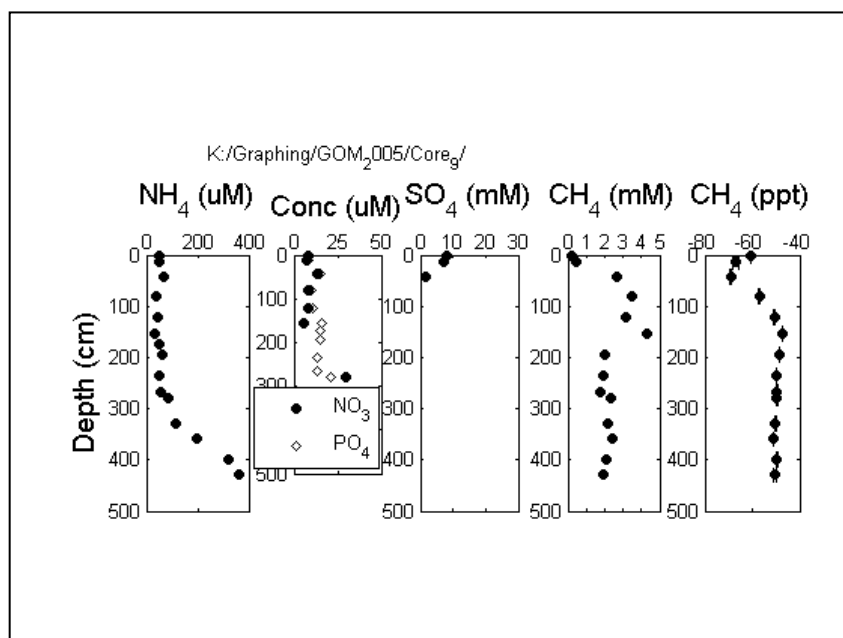


Figure 4. Geochemical profiles for core 9: The microbial ‘hot spot’.

**Subtask 3.3: Development of a Vent Genesis Model.** Recipient shall develop a vent genesis model by defining Flux Regimes based on Geochemistry. The model shall address the issue of variation of geochemistry with geophysical features and shall attempt to establish a link between geophysics and specific stages in vent gas evolution.

As of 2006, we were still accumulating the necessary data to develop the Vent Genesis Model. We had made substantial strides however, in identifying a microbial ‘hot spot’. Within half a meter of sediment depth, the sulfate was completely consumed at this site, taken cumulatively with the heavy methane isotopes, this core gave indications that thermogenic methane supplied from a deep reservoir was influence subsurface geochemistry and fueling microbial activity at the site.



**Subtask 3.4:** *Investigation of Controls of Gas Hydrate Dissolution.* The recipient shall perform work necessary to investigate the control of gas hydrate dissolution at MC-118 through the use of high resolution pressurized pore-water samples. The Recipient shall attempt, through this work, to define and document geochemical constraints on gas hydrate dissolution.

Overall thirty gravity cores were collected during the May and October 2005 cruise at MC-118 from areas determined to be of seismic interest based on Chirp profiles. Fifteen of these cores were from within acoustic wipe-out zones. Cores collected outside of the wipe-out zones exhibited low methane and DIC concentrations and high sulfate concentrations. The geochemical profiles generated from cores collected within the wipe-out zones varied substantially among sites but could be grouped into three general categories. High sulfate concentrations at depth coinciding with low concentrations of thermogenic methane, that nevertheless exhibited an advective profile with methane isotopes decoupled from DIC isotope values were characterized as a low microbial activity site. This core is thought to be representative of an early stage vent. At this site, we infer that methane supply has not been present long enough for the establishment of an active chemosynthetic community. Cores that exhibited high methane concentrations and sulfate depletion with depth signified a more robust microbial community, hence an active vent that had been established for some time. These areas were characterized as a 'middle stage' vent. Late stage vents were characterized by low methane concentrations and high sulfate concentrations, but with carbonate isotopes significantly different from DIC values (see Figure 5). Since carbonate precipitation is a non-fractionating event, this indicates that the carbonates precipitated sometime in the past when the DIC isotopes were different than their current values. Cumulatively, these data are consistent with past methane oxidation with concomitant DIC production and the resulting precipitation of carbonates which has since ceased at the site.

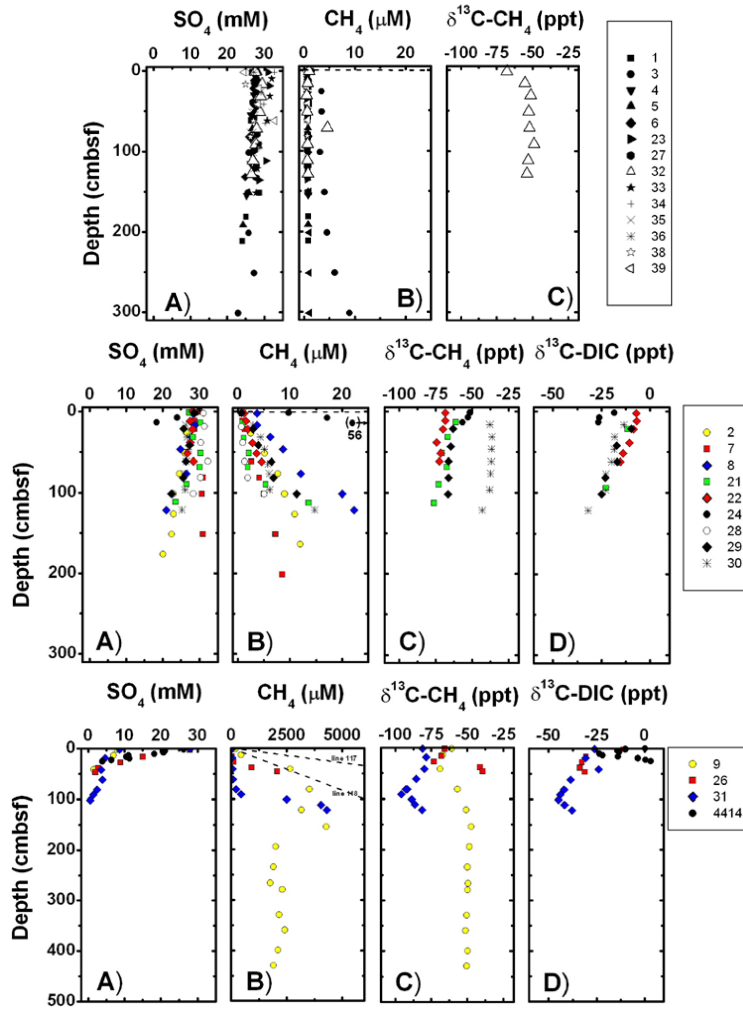


**Figure 5. Geochemical profiles from 30 cores collected at MC-118. The top panel presents results from the low activity cores designated as ‘early’ stage vent. The middle panel presents results from the ‘middle’ stage vent site. The bottom panel presents results from the ‘late’ stage vent site. Figures from Lapham et al. (2008b).**

Results reported in:

Lapham, LL, JP Chanton, CS Martens, K Sleeper, and JR Woolsey (2008b) Microbial activity in surficial sediments overlying acoustic wipeout zones at a Gulf of Mexico cold seep. *Geochemistry Geophysics Geosystems* **9**(6): 1-17

**Final Products:** Two replacement OsmoSampler packages, in situ pore-fluid samples, chemical analyses of in situ pore-fluid samples for light hydrocarbon composition and concentration, isotopic composition, and chlorinity, chemical analyses of pore-fluid samples from cores for light hydrocarbon composition and concentration, isotopic composition, and chlorinity, a gas genesis model that links geochemistry to geophysics, and an analysis of geochemical constraints on formation and dissolution of gas hydrates.

**FY2008**

**TASK 3: Coupling of Continuous Geochemical and Sea-floor Acoustic Measurements (Subcontractor: Florida State University, FSU)**

The principal goal of this task shall be the continuation of activities for coupling of continuous sampling of pore-fluid chemistry with sea-floor acoustic and accelerometer measurements and to ground-truth acoustic anomalies identified with geophysics. This shall be accomplished by correlating the seismic and thermal data (as measured by the down-hole and water-column geophysical/acoustic arrays) with the geochemical data (as measured by the downhole arrays of pore-fluid samplers). This correlation shall be used to infer gas hydrate decomposition or formation. Geochemical parameters to be monitored shall include (but not be limited to) methane and other light dissolved hydrocarbon gas concentrations and perturbations in salinity. This goal of this effort shall be to assess and document the stability of hydrates by characterizing their origin, fate, and genesis on the sea-floor.

**Subtask 3.1: Continuous and Directed Sampling Using Pressurized Equipment**

This task shall include construction of equipment that will replace the osmo-pump and sampling head Pore-Fluid Array (PFA) packages previously constructed under separate funding. One of the previously constructed PFA packages was deployed via the CMRET's Sea-floor Probe in the shallow subbottom of the sea-floor at MC118 in 2005 and the other will be deployed following assessment of the samples collected using the first probe. Activity under this task shall be carried out to construct and deploy replacement osmo-pumps and sampling head PFA packages that will replace the original packages build under previous funding. This replacement and deployment shall provide for continuous collection of pore-fluids from 8 depths over a 10m interval during a 3-year period at two separate sites in different environments in close proximity to the carbonate mound at MC118. The second deployment site shall be in close proximity to the water-column and proposed borehole geophysical array MS/SFO components. Samples to be collected with the PFA as well as samples collected from cores recovered from the sea-floor in MC118 during the deployment cruise shall be analyzed for light hydrocarbon composition and concentration, isotopic composition, and chlorinity. With the additional equipment, pressurized time series gas and salinity samples shall be retrieved at 6-12 month intervals and analyzed at Florida State University. In May, 2005, the initial 10m probe with OsmoSamplers was deployed in MC118 as part of the MS/SFO. Effort under this task shall include activities necessary for:

**Subtask 3.1a:** construction of two additional OsmoSampler packages that shall be exchanged with the existing packages to allow for continuous sampling of pore-fluids at the site of the MS/SFO

An OsmoSampler package was deployed at MC-118 during the April 2008 cruise. The package was placed on the western rim of the northwest vent complex (Figure 6).

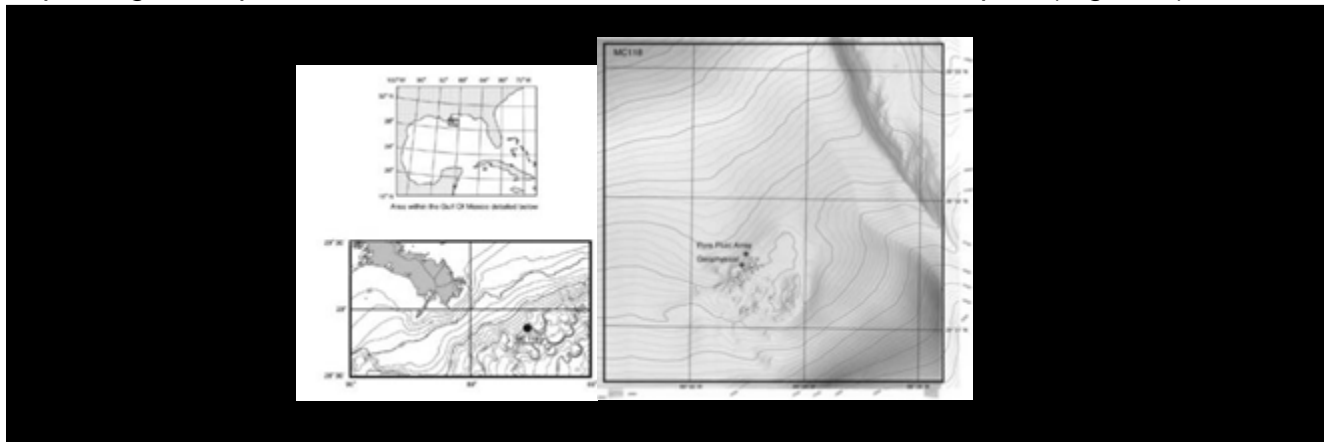


**Figure 6. Site map showing deployment placements for the OsmoSampler packages.**

During this same cruise a gravity core was collected prior to package deployment. Hydrates were found upon inspection of the core confirming that this placement will allow us to address questions of hydrate stability. The deployed Osmosampler package is of a new design. Specifically, the valve that allows the samples to be isolated during retrieval has now been encased in an oilbox (Figure 7). This protects the metal valve components from exposure to seawater, and is intended to inhibit corrosion during deployment.

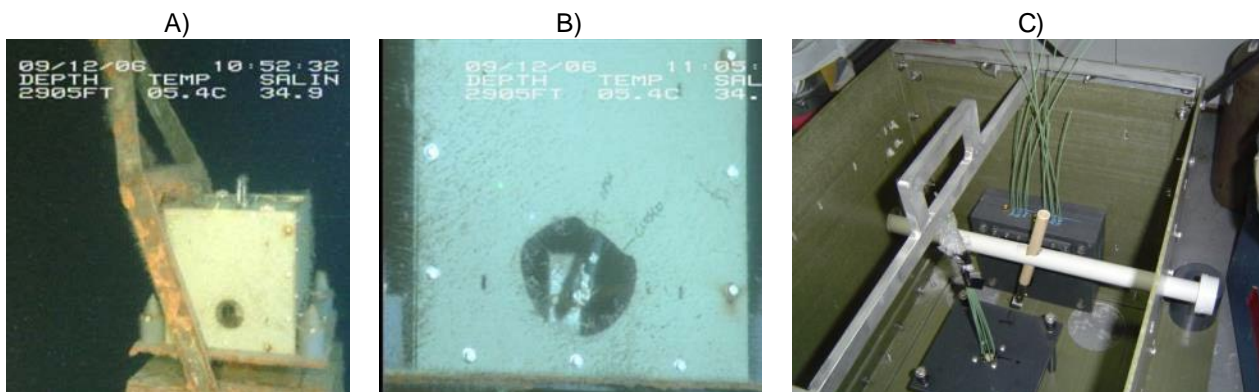


**Figure 7.** A) The OsmoSampler package shown on the seafloor with minimal biofouling and all parts intact. B) Close up of the original valve exposed to seawater. C) Modified sampler box with valve enclosed in oil box (gray box with green tubes emanating from it) and manual lever arm (white PVC tube) for ease of closing on the seafloor.

**Subtask 3.1b:** retrieval of the existing osmo-sampling packages from the seafloor at MC118 and their replacement with the newly constructed units.

Samplers were not collected during the June 2008 cruise due to problems with the SSD.

**Subtask 3.1c:** recovery, sample collection and redeployment of “peeper” sensors for collecting in situ samples on the sea-floor and maintaining them at sea floor pressure.

Samplers were not collected during the June 2008 cruise due to problems with the SSD.

**Subtask 3.1d:** conducting chemical analyses on the samples recovered with the equipment described in 3.1a - c.

Samplers deployed, but no samples were recovered.

**Subtask 3.2:** Feature Investigation at MC-118. The Recipient shall conduct activities necessary to investigate and document features of interest in the area of MC-118 identified by geophysical data. The recipient shall conduct coring investigations to establish vent activity by geochemical determinations, specifically, hydrocarbon concentrations, isotope ratios, and chlorinity.



Gravity cores were collected across the mound during the April 2008 cruise, adding to the total gravity core inventory for this site (Figure 8). No chloride anomalies indicative of hydrate formation or dissociation were observed in any of the cores (see Figures 9 and 10). Steep sulfate and methane gradients were observed in a core targeting an acoustic anomaly off of the main MC-118 mound suggesting additional routes of fluid and gas flow. Interestingly, we noted wide variation in the depth of sulfate penetration across sites suggesting that there are large differences in microbial sulfate reduction rates across the mound complex. This may be due to variability in substrate (i.e. methane) availability, indicating that there may be several hydrocarbon conduits off the main mound.

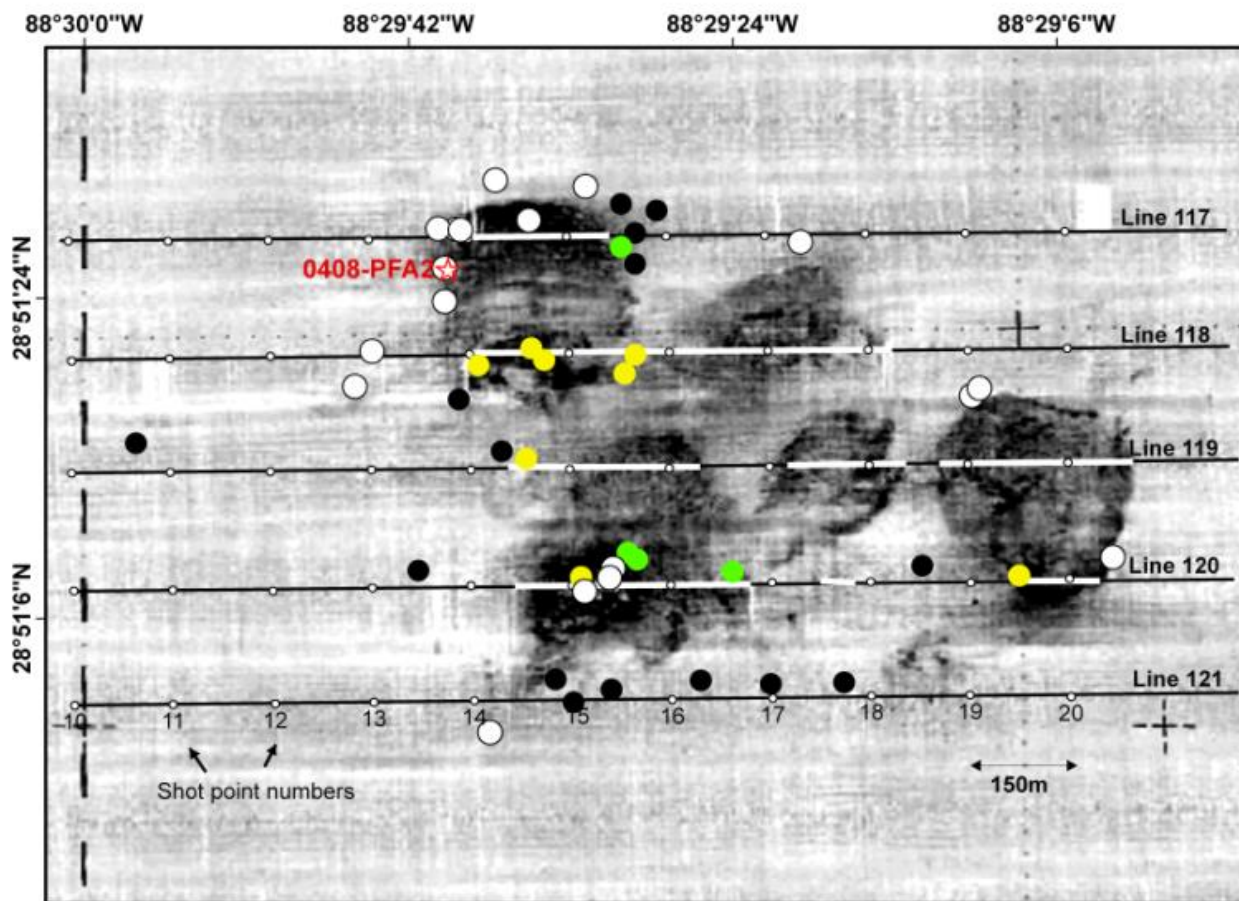


**Figure 8. Acoustic backscatter map of the sampling site showing the location of all cores collected to date. White circles represent locations of cores collected during the April 2008 cruise. Black circles represent low activity 'early' stage vent location cores as defined above. The green circles represent locations of cores collected from the 'middle' stage vent area. The yellow circles represent the locations of cores collected from 'late' stage vents locations.**

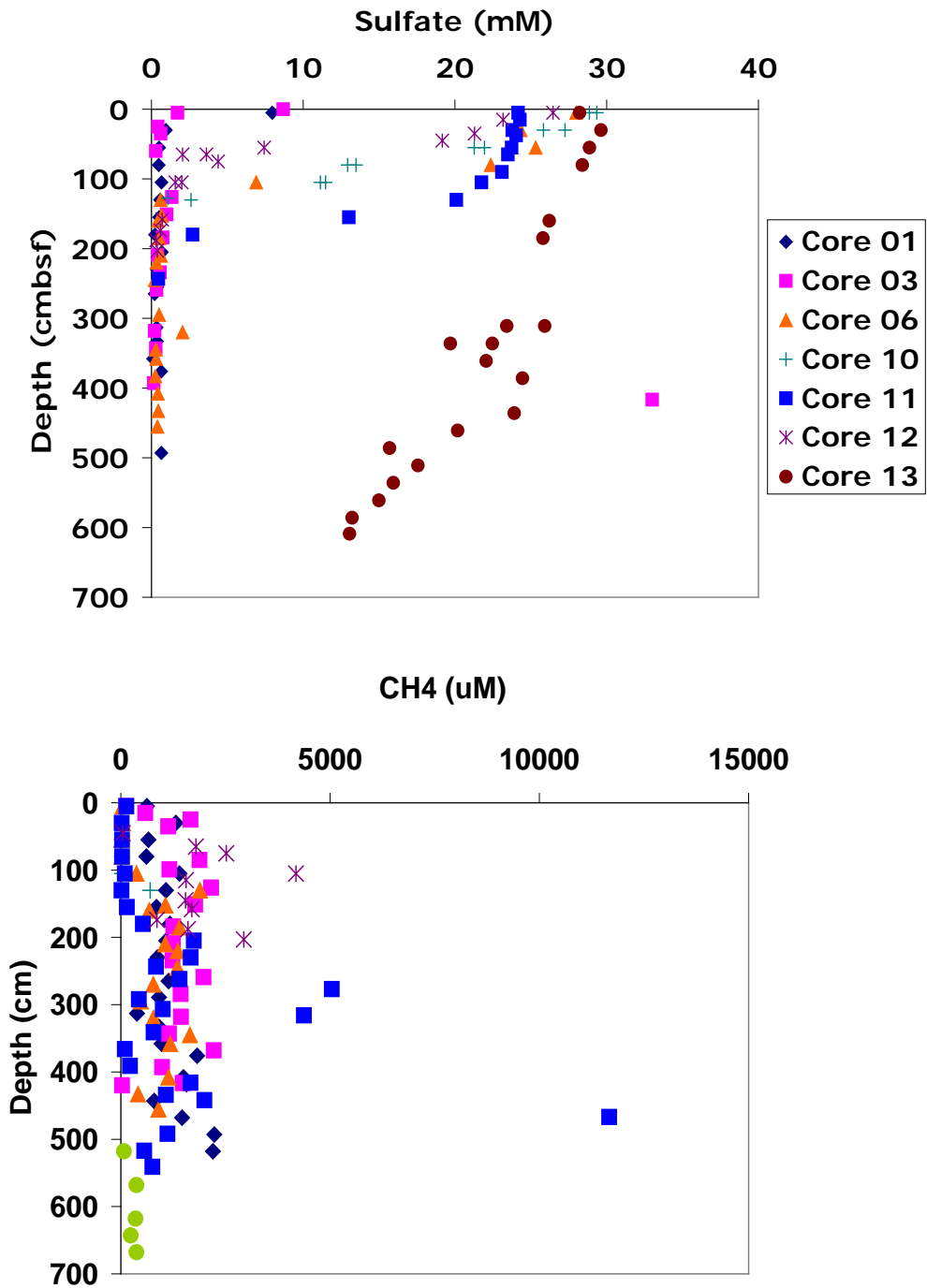


**Figure 9. Sulfate and methane concentrations in the cores collected during the April 2008 cruise. These data present the first results of sulfate depletion observed off of the main mound. This core was collected off of the main mound but in an area with acoustic backscatter. The high methane concentrations and sulfate depletion in this core are consistent with our findings in other acoustic wipe-out zones and suggest additional conduits of fluid flow off of the main mound complex.**

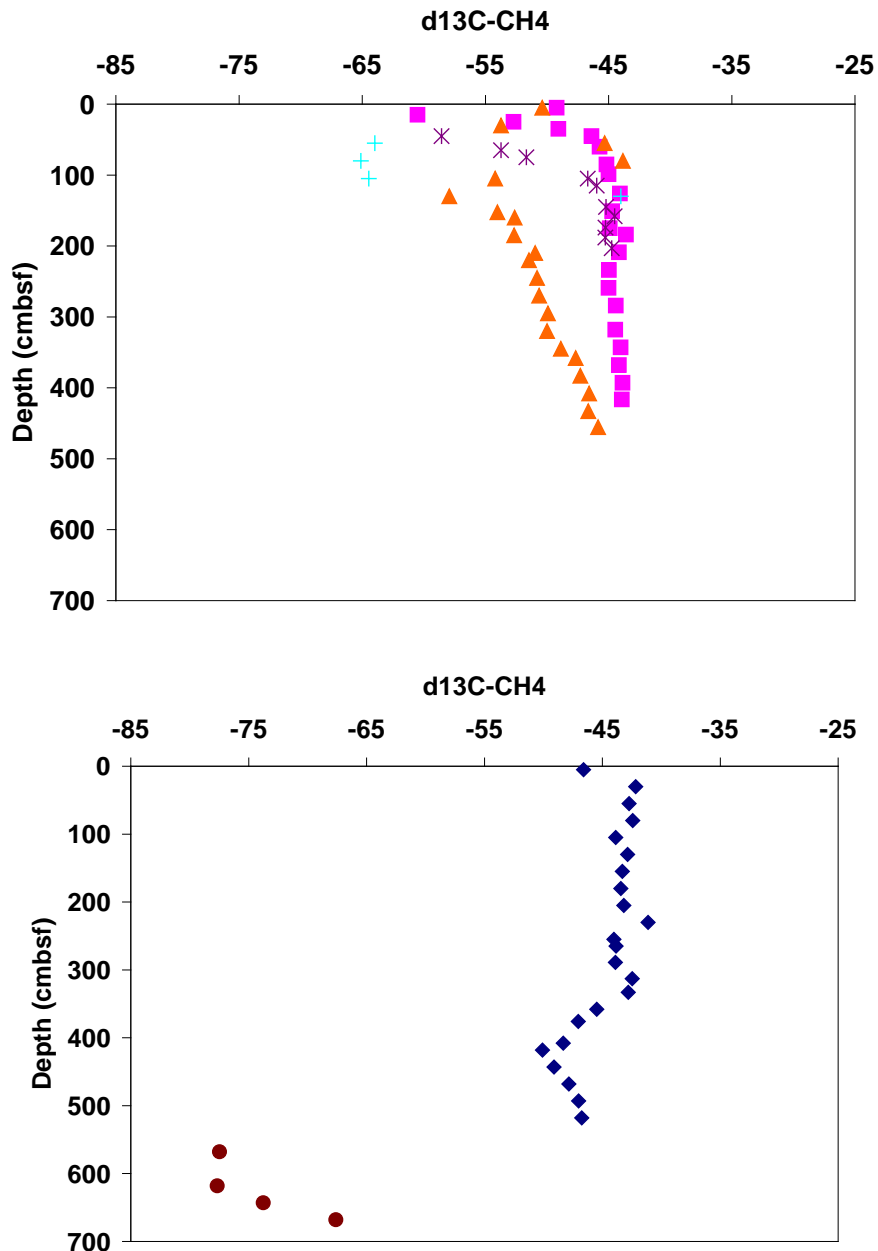


**Figure 10. Methane isotope profiles for cores collected during the 2008 cruise. The left panel presents results of ‘traditional’ shaped profiles, while the anomalous cores are presented in the right panel. The cores presented in the left panel are consistent with expectations from sites where there is anaerobic oxidation of methane. Where sulfate was depleted and methane began to increase, isotope values became more enriched in  $^{13}\text{C}$  to a value of  $-45\text{‰}$ , indicating a narrow zone of methanogenesis. These cores also exhibited a tailing of around  $-45\text{‰}$ , indicating a thermogenic source gas from deep below. In the cores presented in the right panel, isotope values are relatively consistent with depth up to the SMTZ, after which isotope values become heavier. Hydrate flakes were found in core 14 (red symbols).**

**Subtask 3.3: Development of a Vent Genesis Model.** Recipient shall develop a vent genesis model by defining Flux Regimes based on Geochemistry. The model shall address the issue of variation of geochemistry with geophysical features and shall attempt to establish a link between geophysics and specific stages in vent gas evolution.

Overall the geochemical gradients observed in all cores collected to date can be grouped into one of the three previously defined categories of ‘low’, ‘moderate’, and ‘high’ microbial activity sites. These sites in turn are associated with either background (no vent) levels, high flux vents where lots of methane is being supplied and microbial activity is highest, moderate flux vents which have a more established chemosynthetic community and methane flow may be reduced by carbonate and/or hydrate ‘plugging’, and low flux seeps where past microbial activity has led to substantial flow reduction via the precipitation of authigenic carbonates (see Figure 11).

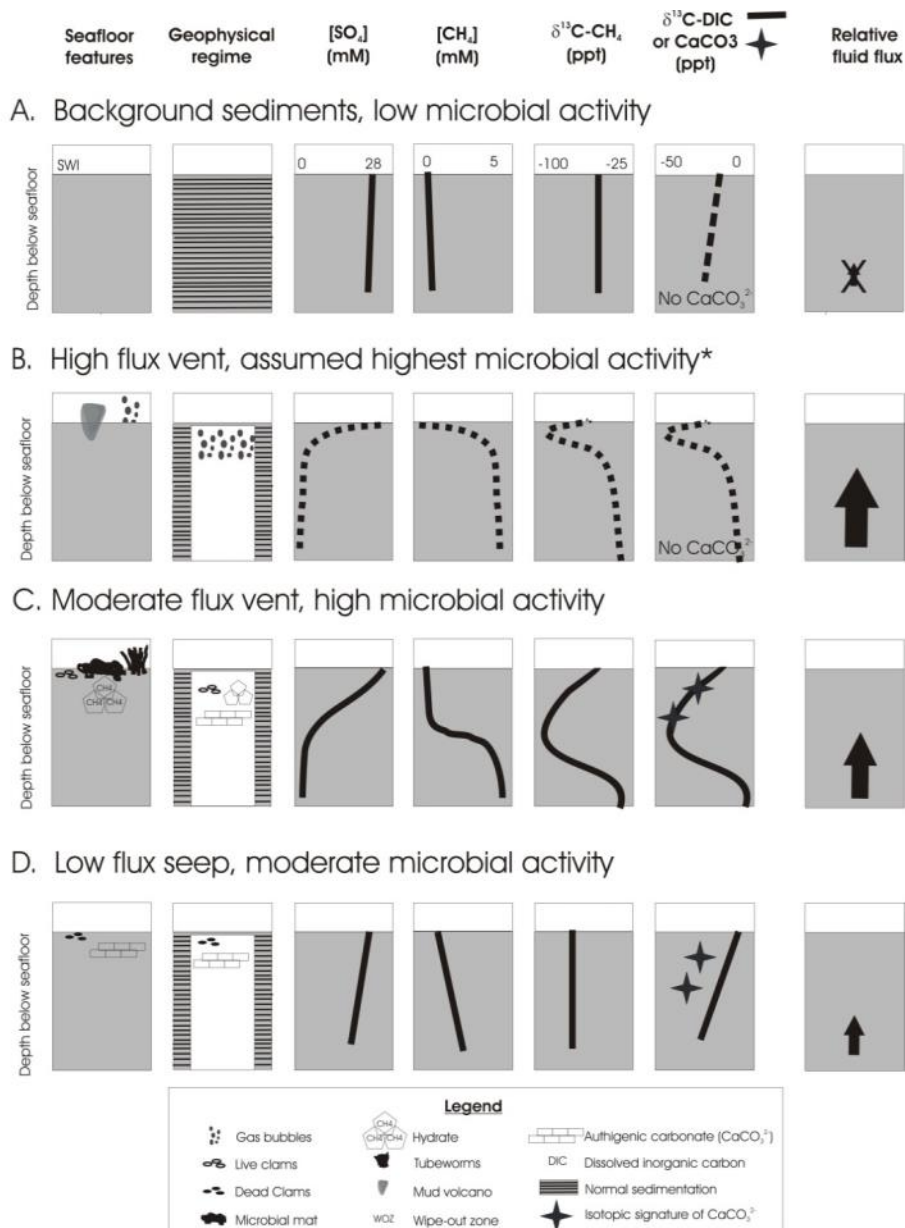


**Figure 11. Generalized geochemical profiles and related physical features for each of the vent stage categories identified.**



The distribution of these sites is patchy across the mound complex. We hypothesize that the patchiness is spatially related to the underlying fault system radiating from the rising salt dome. We continue to work with Jim and Camelia Knapp to create an integrated model of fault driven geochemistry.

**Subtask 3.4:** *Investigation of Gas Hydrate Dissolution Control. The recipient shall perform work necessary to investigate the control of gas hydrate dissolution at MC-118 through the use of high resolution pressurized pore-water samples. The Recipient shall attempt, through this work, to define and document geochemical constraints on gas hydrate dissolution.*

Further analysis of the recovered PFA samples revealed the presence of ethane, propane, butane, and pentane in addition to methane. Further, we find temporal variability in the relative proportions of hydrocarbons present. Data such as these can provide important insights that may allow us to detect specific hydrate formation and decomposition events.

**Final Products:** *Two replacement OsmoSampler packages, in situ pore-fluid samples, chemical analyses of in situ pore-fluid samples for light hydrocarbon composition and concentration, isotopic composition, and chlorinity, chemical analyses of pore-fluid samples from cores for light hydrocarbon composition and concentration, isotopic composition, and chlorinity, a gas genesis model that links geochemistry to geophysics, and an analysis of geochemical constraints on formation and dissolution of gas hydrates.*

**FY09**

**TASK 3:** *Coupling of Continuous Geochemical and Sea-floor Acoustic Measurements*

*The principal goal of this task shall be the continuation of activities for coupling of continuous sampling of pore-fluid chemistry with sea-floor acoustic and accelerometer measurements and to ground-truth acoustic anomalies identified with geophysics. This shall be accomplished by correlating the seismic and thermal data (as measured by the down-hole and water-column geophysical/acoustic arrays) with the geochemical data (as measured by the downhole arrays of pore-fluid samplers). This correlation shall be used to infer gas hydrate decomposition or formation. Geochemical parameters to be monitored shall include (but not be limited to) methane and other light dissolved hydrocarbon gas concentrations and perturbations in salinity. This goal of this effort shall be to assess and document the stability of hydrates by characterizing their origin, fate, and genesis on the sea-floor.*

**Subtask 3.1: Continuous and Directed Sampling Using Pressurized Equipment**

*This task shall include construction of equipment that will replace the osmo-pump and sampling head Pore-Fluid Array (PFA) packages previously constructed under separate funding. One of the previously constructed PFA packages was deployed via the CMRET's Sea-floor Probe in the shallow subbottom of the sea-floor at MC118 in 2005 and the other will be deployed following assessment of the samples collected using the first probe. Activity under this task shall be carried out to construct and deploy replacement osmo-pumps and sampling head PFA packages that will replace the original packages build under previous funding. This replacement and deployment shall provide for continuous collection of pore-fluids from 8 depths over a 10m interval during a 3-year period at two separate sites in different environments in close proximity to the carbonate mound at MC118. The second deployment site shall be in close proximity to the water-column and proposed borehole geophysical array MS/SFO components. Samples to be collected with the PFA as well as samples collected from cores recovered from the sea-floor in MC118 during the deployment cruise shall be analyzed for light hydrocarbon composition and concentration, isotopic composition, and chlorinity. With the additional equipment, pressurized time series gas and salinity samples shall be retrieved at 6-12 month intervals and analyzed at Florida State*

University. In May, 2005, the initial 10m probe with OsmoSamplers was deployed in MC118 as part of the MS/SFO. Effort under this task shall include activities necessary for:

**Subtask 3.1a:** construction of two additional OsmoSampler packages that shall be exchanged with the existing packages to allow for continuous sampling of pore-fluids at the site of the MS/SFO

The package on the first probe has been replaced and the data analyzed. The second probe has been emplaced.

**Subtask 3.1b:** retrieval of the existing osmo-sampling packages from the seafloor at MC118 and their replacement with the newly constructed units.

The first package has been replaced (using the JSL SeaLink) and the samples analyzed. The second has not. We are still striving to recover this package with the SSD.

**Subtask 3.1c:** recovery, sample collection and redeployment of “peeper” sensors for collecting in situ samples on the sea-floor and maintaining them at sea floor pressure.

The peepers have been recovered and replacements constructed. Three peepers were deployed at the Rudyville site, Figure 12, where shell hash and outcropping hydrate was visible on the seafloor.

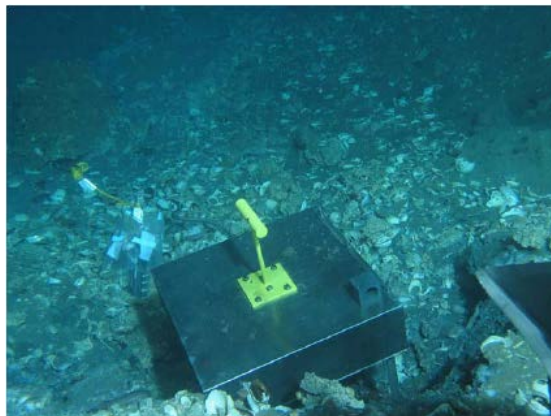


**Figure 12.** Site of peeper deployments at Rudyville, MC118.

The goal was to obtain a horizontal gradient of methane concentrations from the hydrate surface which could then be used to determine hydrate dissolution rates. During deployment, the peepers encountered a hard surface assumed to be a buried portion of the adjacent hydrate outcrop. Only one peeper was ultimately recovered from the site as two were lost from the SSD carrying basket during retrieval.

**Subtask 3.1d:** conducting chemical analyses on the samples recovered with the equipment described in 3.1a - c.

Because only one peeper was recovered (see results in Figure 13), we were unable to measure a concentration gradient. Upon analysis, methane concentrations in the bottommost portion (flush with the hydrate surface) of the peeper that was recovered were 400 $\mu$ M. This is much lower than predicted methane saturation (67mM) which is what we expect for water in equilibrium with hydrate. Isotope values for the methane were -42‰ consistent with a thermogenic methane source. DIC  $\delta^{13}\text{C}$  values were also obtained and were consistent with products of anaerobic oxidation of methane.

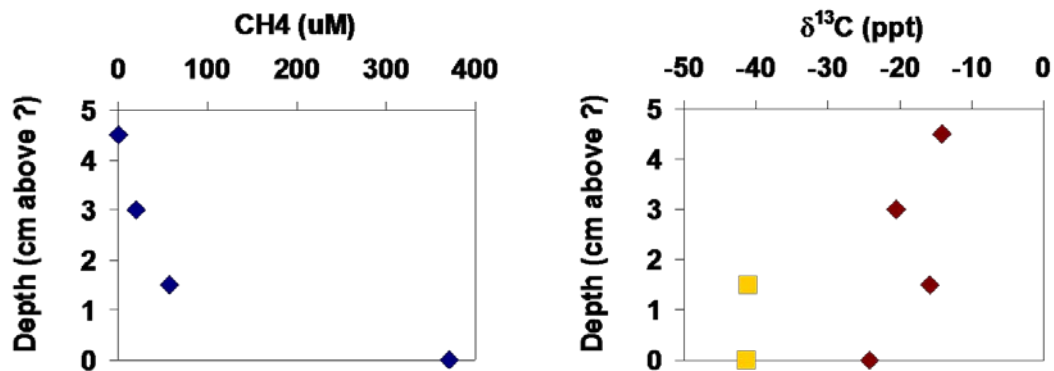


Figure 13. Results of the pore fluid analysis from the peeper sampler deployed at the Rudyville site.

**Subtask 3.2:** Feature Investigation at MC-118. The Recipient shall conduct activities necessary to investigate and document features of interest in the area of MC-118 identified by geophysical data. The recipient shall conduct coring investigations to establish vent activity by geochemical determinations, specifically, hydrocarbon concentrations, isotope ratios, and chlorinity.

Five cores were collected during the HYFLUX cruise ( Figures 14 and 15) from areas deemed to be of interest both from a geophysical and geochemical perspective.

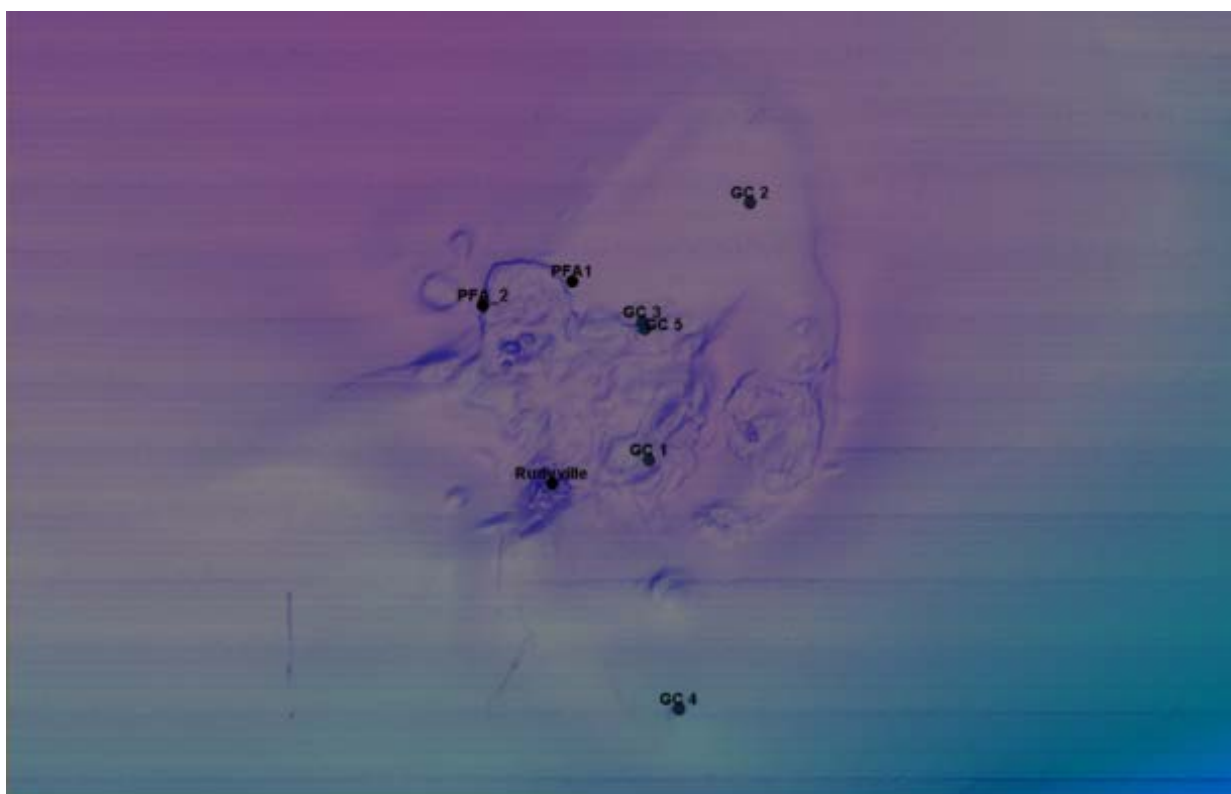
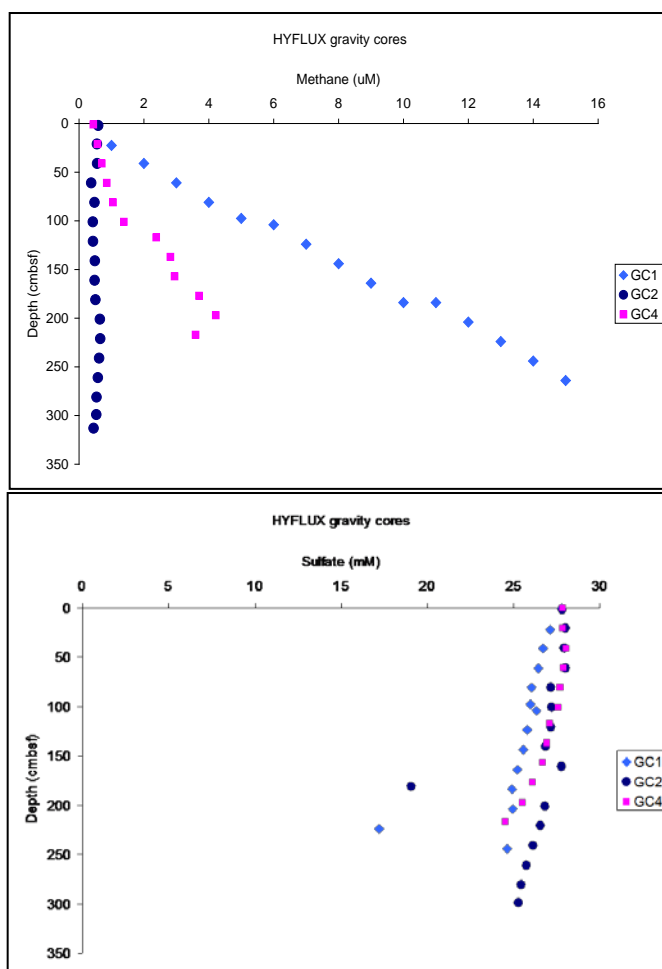


Figure 14. Core target locations relative to the PFA positions and Rudyville where the peeper instruments were deployed.

One core, GC1, was collected from a novel area off the mound associated with a deep acoustic anomaly and enriched water column methane identified during a 2009 AUV mass spectrometer survey (R. Camilli). Methane was the dominant hydrocarbon, ethane made up less than 10% of the remainder, and no propane was found in this core. Methane concentrations in the core reached a maximum of 14 $\mu$ M in the deepest portion of the core. Despite the strong smell of sulfide upon opening the core, sulfate concentrations decreased only about 3mM from the sediment water interface to depth, suggesting low microbial activity at this site. Curiously, DIC  $\delta^{13}\text{C}$  values decreased linearly with depth, which typically indicates organic matter oxidation. The mechanism by which this oxidation occurs is still under investigation. GC2 was collected along the yellow fault in an area assumed to be relatively quiescent and representative of the area background. Consistent with this assumption, we found low methane concentrations, high sulfate concentrations, and DIC  $\delta^{13}\text{C}$  values similar to typical deep sea sediments in other sites. GC4 was collected to investigate an apparently blind fault identified in the industry seismic data. Methane concentrations increased with depth up to 4 $\mu$ M. Sulfate concentrations indicated low microbial activity, but decreasing DIC  $\delta^{13}\text{C}$  values with depth suggests organic matter oxidation. Perhaps via the same unknown mechanism that is occurring at GC1.



**Figure 15. Methane and sulfate concentration results from gravity cores GC1, GC2, and GC4 collected during the HYFlux cruise.**



GC3 and GC5 were both attempts to collect sediments from the area identified from the industry data as the 'blue fault'. Neither core was able to penetrate the hard grounds in the area. No sediments were recovered only shell fragments. The presence of shell fragments suggests this area is either an active or fossil vent feature.

Results from this coring effort have been published in:

Lapham, LL, JP Chanton, R Chapman, and CS Martens (2010) Methane under-saturated fluids in deep-sea sediments: implications for gas hydrate stability and rates of dissolution. *Earth and Planetary Science Letters* **298**(3-4):275-285

**Subtask 3.3:** *Development of a Vent Genesis Model. Recipient shall develop a vent genesis model by defining Flux Regimes based on Geochemistry. The model shall address the issue of variation of geochemistry with geophysical features and shall attempt to establish a link between geophysics and specific stages in vent gas evolution.*

A model has been developed and is subject to refinement as new data become available.

**Subtask 3.4:** *Investigation of Gas Hydrate Dissolution Control. The recipient shall perform work necessary to investigate the control of gas hydrate dissolution at MC-118 through the use of high resolution pressurized pore-water samples. The Recipient shall attempt, through this work, to define and document geochemical constraints on gas hydrate dissolution.*

This task is ongoing.

**Final Products:** *Two replacement OsmoSampler packages, in situ pore-fluid samples, chemical analyses of in situ pore-fluid samples for light hydrocarbon composition and concentration, isotopic composition, and chlorinity, chemical analyses of pore-fluid samples from cores for light hydrocarbon composition and concentration, isotopic composition, and chlorinity, a gas genesis model that links geochemistry to geophysics, and an analysis of geochemical constraints on formation and dissolution of gas hydrates.*

#### **FY2010**

**TASK 4:** *Geochemical investigations at MC 118: Pore-fluid time series and gas hydrate stability*

**Subtask 4.1.** *Recipient shall continue monitoring the two Pore-Fluid Arrays (PFA) devices already installed at MC-118 and add a third PFA. Activity shall seek to address the hypothesis that geophysical temporal variability and geophysical "events" will result in geochemical variability. This shall be done by monitoring geochemical variability with PFAs, over time, which can be used to associate the effect and extent of geophysical events.*

**Subtask 4.1a.** *Recipient shall continue geochemical monitoring via the two PFA devices installed at MC-118, measuring concentrations of Chloride (Cl), sulfate ( $SO_4^{2-}$ ), methane ( $CH_4$ ) and stable carbon isotope ratios of methane ( $\delta^{13}C-CH_4$ ).*

Attempts to recover the installed PFAs continue to be unsuccessful.

**Subtask 4.1b.** *Recipient shall participate in cruises to recover, sample and redeploy Pore-Fluid collecting devices.*

### Cruise Participation:

**March 2010:** Wilson and J Nelson to MC-118 to retrieve and replace PFA sampler box.

**April 2010:** Wilson to Victoria, BC, Canada to receive the mini-PFA.

**June 2010:** Chanton to MC 118 to retrieve and replace sampler box.

**September 2010:** Wilson aboard the RV Pelican to deploy ROVAR, CSA, and peepers

**September 2010:** Chanton to MC 118 to retrieve and replace PFA sampler box.

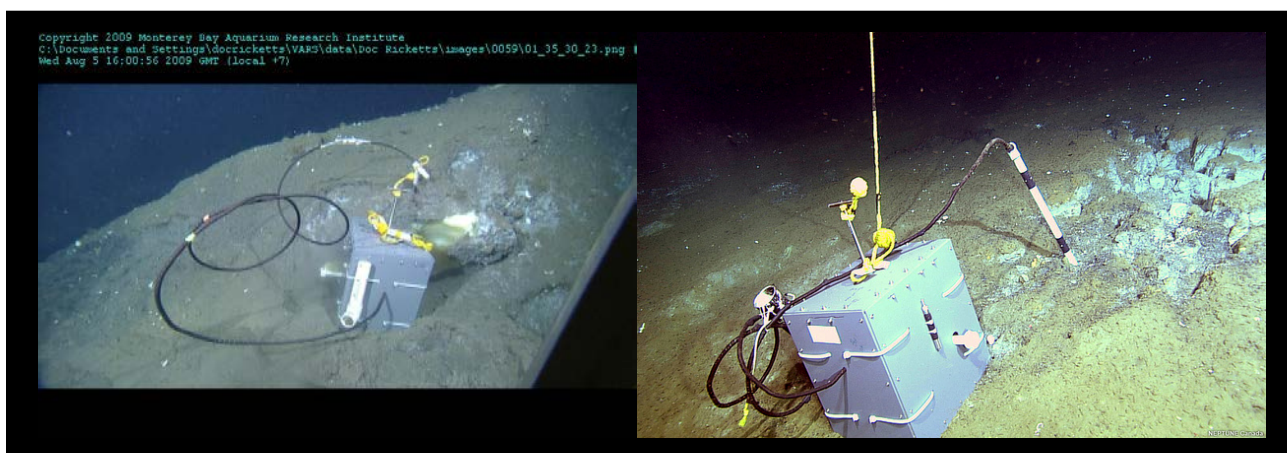
**Subtask 4.1c.** Recipient shall modify, construct and deploy one additional PFA at a site to be determined following Consortium discussion.

Two instruments were collected from the Cascadia hydrate site verifying the utility of the new streamlined design and ease of retrieval. This newly designed system may be deployed at MC-118 with similar success in retrieval of the unit package.

**Subtask 4.2.** Recipient shall recover and deploy additional smaller devices (osmo-landers and deep sea peepers) to measure methane concentrations in the pore-fluids in sediments surrounding the hydrates associated with faults at the MC118 observatory site. The recipient shall address the hypothesis that the faults at MC-118 represent a chrono-sequence of seep evolution, from the hypothesized older NE fault to the middle fault to the north-western fault and that both fluid flux rate and fluid composition vary across these systems.

**Subtask 4.2a.** Recipient shall deploy two or three osmosamplers to measure methane concentrations in the sediments surrounding the hydrates associated with faults.

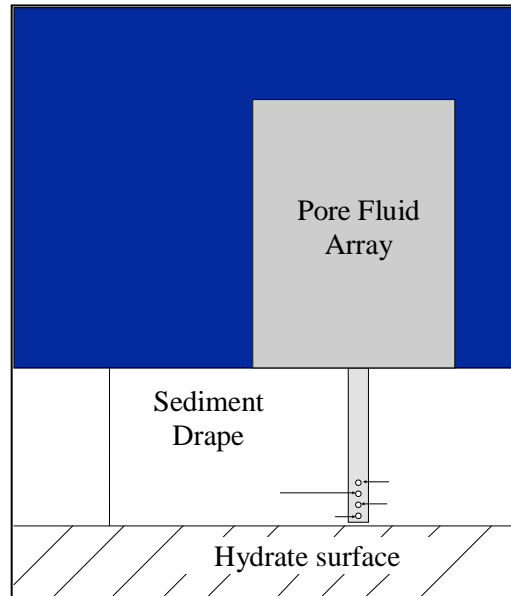
The newly designed 'mini'-PFAs are similar in function to the PFAs deployed at MC-118. The overall footprint of the sampler package is smaller and the probe tip is shorter allowing more precise placement and fine resolution sampling of shallow sediments. The samplers store up to ten months of water sample at in-situ pressure and provide a temporal resolution of ~4days. Two packages were deployed off of Vancouver Island in August 2009 and collected in May 2010 (Figure 16).



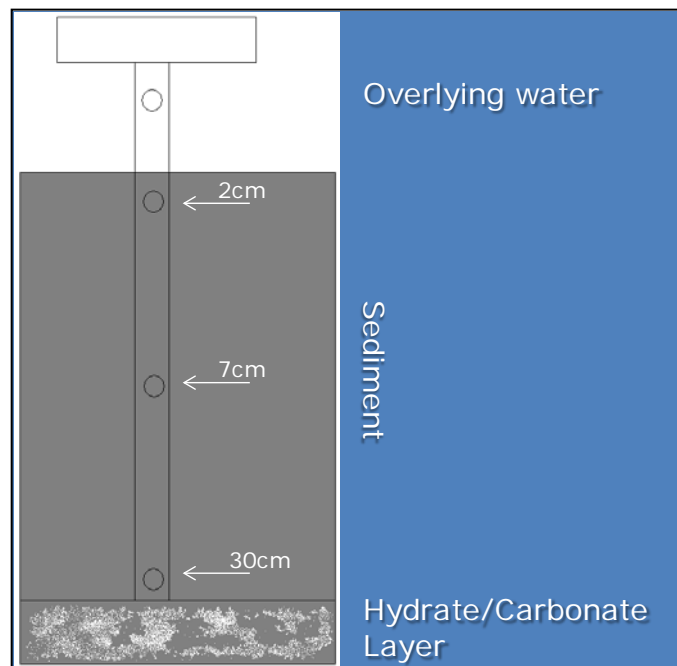
**Figure 16.** OsmoSampler packages deployed at the Barkley Canyon Hydrate site (photo courtesy of MBARI) and the Bubbly Gulch vent site (photo courtesy of NEPTUNE Canada).

The first package was deployed at an actively venting methane seep site. Although there was no outcropping hydrate, there was a buried hydrate/carbonate layer at about 30cm below seafloor.

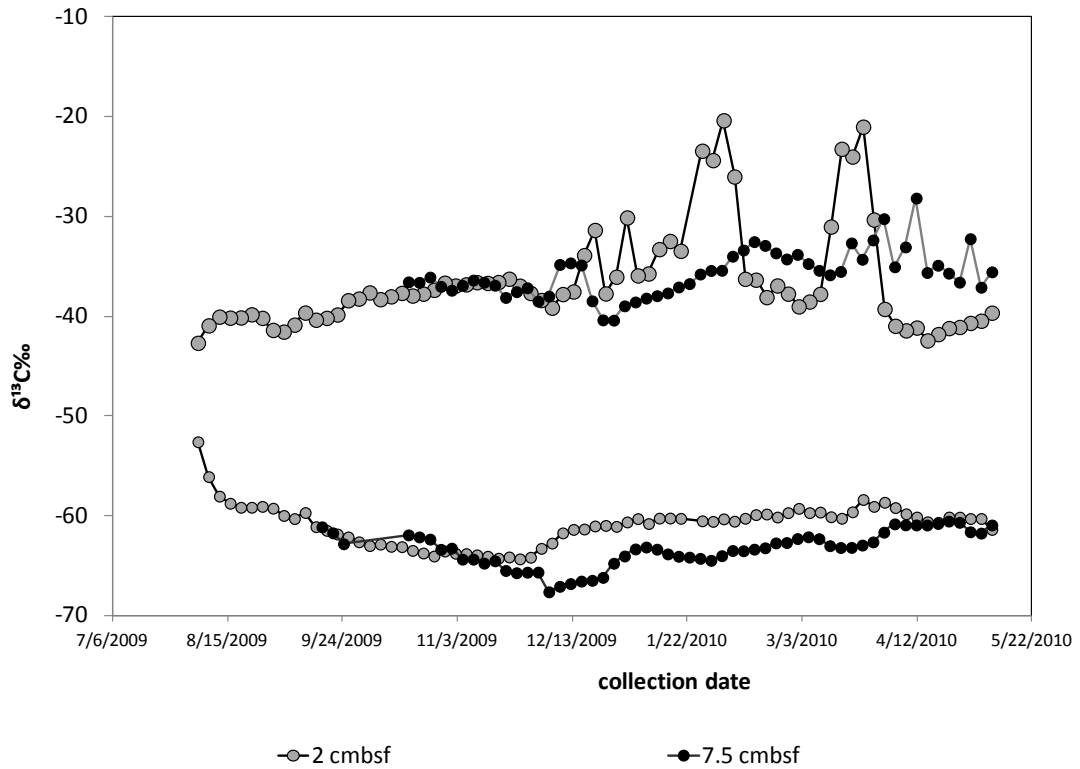
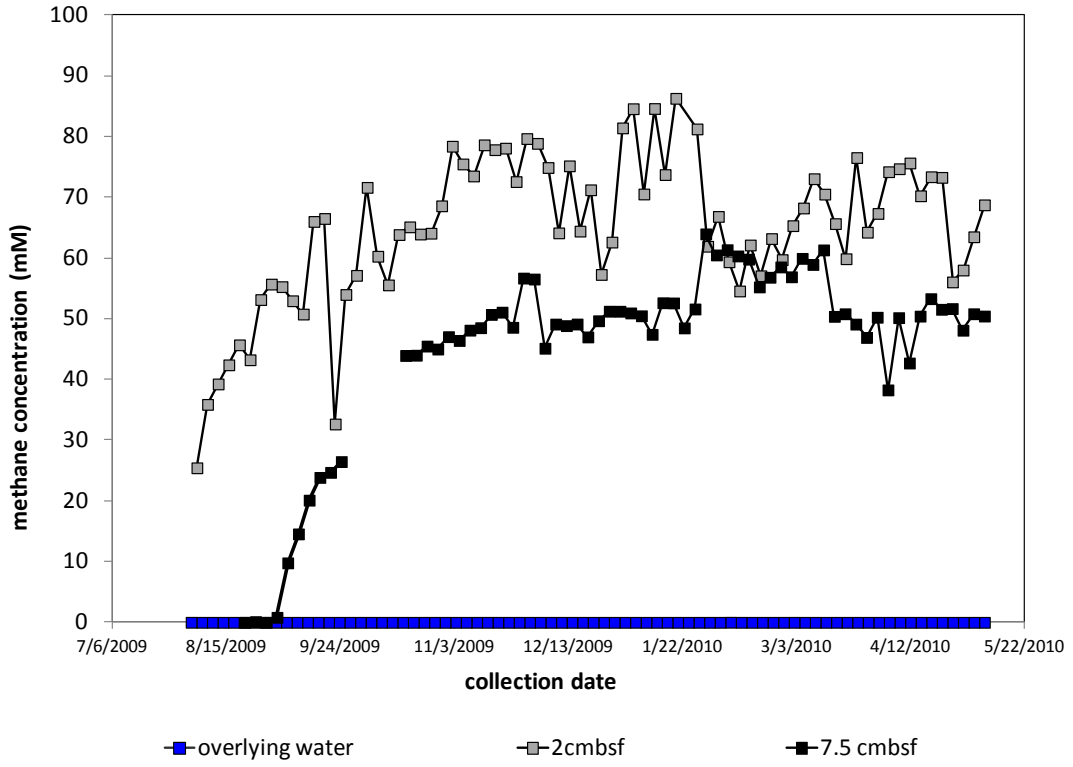
The probe tip was placed to collect samples in a gradient from just above the seafloor in the overlying water to this hydrate/carbonate layer (Figure 17 and 18). Although four pumps were deployed, the deepest pump failed; thus we only have data from the three shallower sediment depths and do not have values closest to that buried hydrate/carbonate layer. Results of the chemical analysis are given in Figure 19.



**Figure 17. Schematic of OsmoSampler placement atop the hydrate outcrop. Sampling ports are positioned at 1cm intervals away from the hydrate surface.**



**Figure 18. Schematic of sampling location showing the placement of the probe tip in the sediment relative to the hydrate/carbonate layer and the sampling port positions.**





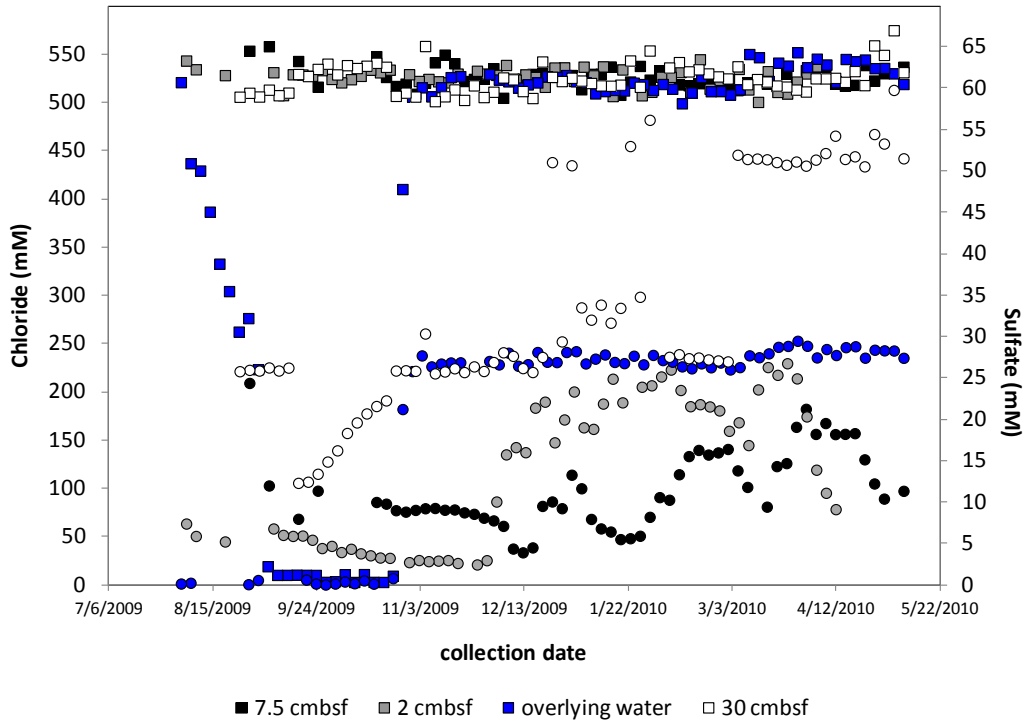
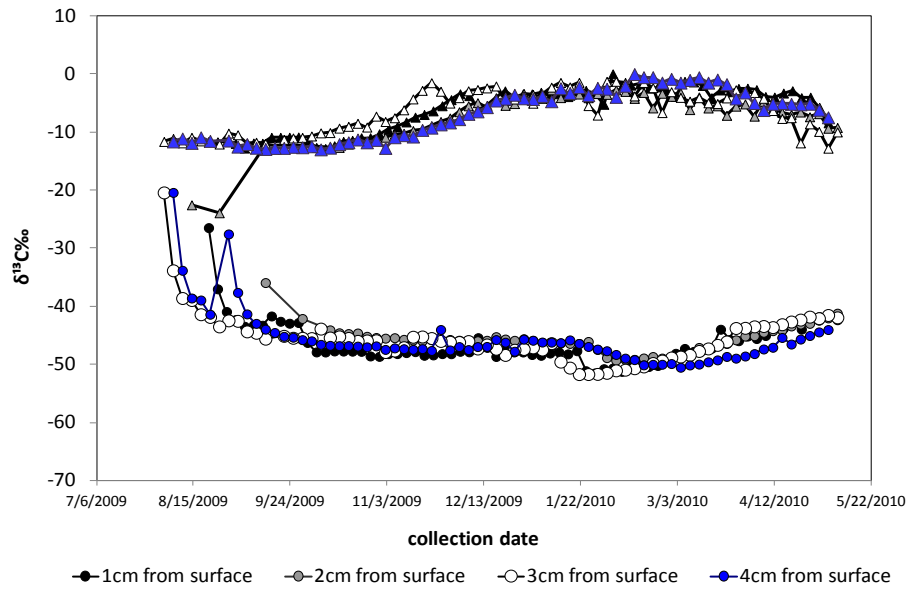
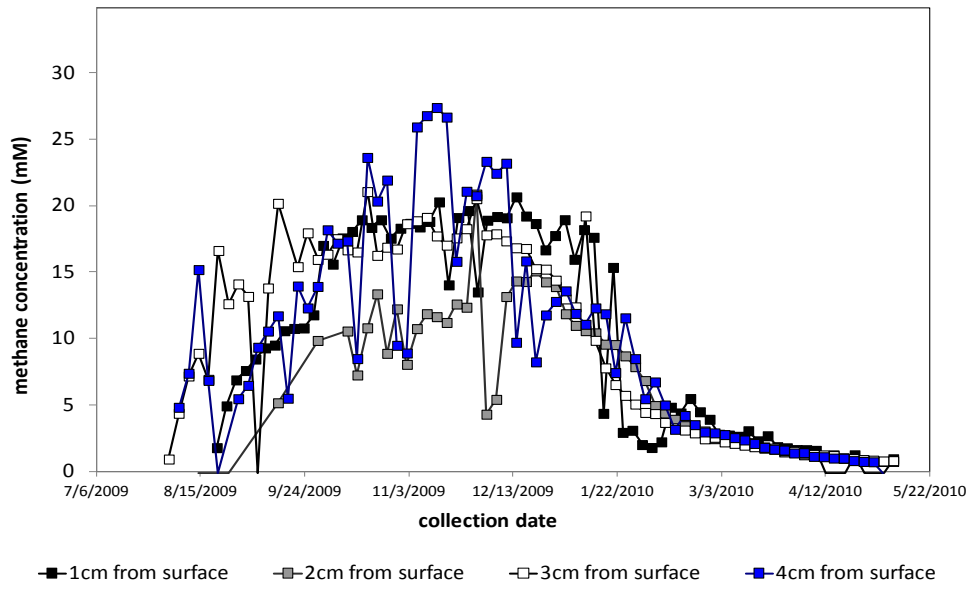


**Figure 19. Chemical analyses at three depths of the first PFA's probe tip.**

Methane concentrations were the highest we've ever sampled and slightly exceeded theoretical saturation at this site. Thus, we are confident that this sampler design allows us to measure in situ methane concentrations without sample loss from degassing. To our knowledge these were the first in situ measurements of saturated methane concentrations collected from depth. Both the DIC  $\delta^{13}\text{C}$  and sulfate profiles have similar deviations towards seawater values over the course of the time series. This suggests to us that seawater is being actively advected downwards at certain times, perhaps in balance with the upward advection of methane.

The second package was deployed atop a hydrate outcrop and the probe tip was placed in the overlying sediment drape until it was flush with the hydrate surface. Samples were collected at 1cm intervals in a gradient away from the hydrate surface.

Chemical analysis results for the mini-PFA deployed at Barkley Canyon are shown in Figure 20.



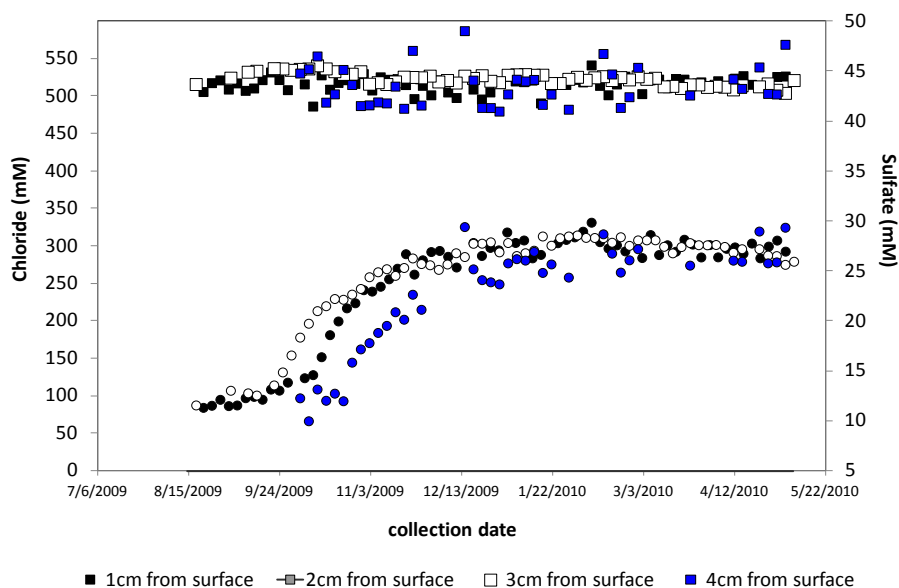


**Figure 20. Chemical analysis results for the mini-PFA deployed at Barkley Canyon.**

Methane concentrations in these samples are much higher than we've measured next to hydrate surface before, but are still below predicted saturation suggesting that the hydrate is not in equilibrium with the surrounding water. The isotopes of the methane are -40‰ to -50‰ consistent with thermogenic contributions to the hydrate. There is a distinct trend over time in methane concentrations: lower at the beginning and end of the deployment and higher concentrations during the middle. Although sulfate concentrations do vary over the timescale of sampling, the trend is not consistent with oxidation of the methane. The increase in methane concentration does not seem to be the result of hydrate dissociation because no chloride anomalies were detected over the sampling period. We suspect that local changes in current direction and/or velocity may result in a flushing of the sediments surrounding this hydrate outcrop. This influx of bottom water would essentially flush the excess methane out during the spring and summer months and resupply fresh sulfate.

**Subtask 4.2b.** Recipient shall deploy eight deep sea peepers to measure methane concentrations in the sediments surrounding the hydrates associated with faults.

Peepers were deployed attached to the University of North Carolina-Chapel Hill Chimney Sampler Array. Upon retrieval, it was noted that peeper bags and some of the membranes had been destroyed either during deployment or during retrieval of the ROVARD device. Samples from these peepers were likely contaminated by overlying seawater and concentrations were lost due to sample degas upon ascent and are therefore not reported.

**Subtask 4.3.** Recipient shall collect core samples from areas of high geophysical interest to address the hypothesis that geophysical anomalies that are observed spatially reflect geochemical anomalies. Efforts shall focus on the determination of how these anomalies are expressed. Activity shall include, but not be limited to, obtaining pore water samples from areas surrounding the differing faults and contrasting fluid evolution at those faults.

**Subtask 4.3a.** Recipient shall retrieve cores from areas of interest, as determined from seismic records, and their interpretation, particularly concentrating on faults recently identified under Phase 2 Task 2 and Phase 3 Task 2 to define geophysical anomalies. Ten 3m gravity cores shall be obtained.

The gravity coring cruise scheduled for 2010 was canceled due to problems with the speed of sound probe. Jumbo Piston Cores were collected aboard the Brooks McCall from the MC-118 mound site.

**Subtask 4.3b.** Recipient shall analyze core samples collected for geochemical constituents, including but not limited to,  $Cl$ ,  $SO_4$ ,  $CH_4$  and  $\delta^{13}C$  following the methods described in Lapham et al, 2008.

Five cores were collected from areas identified to be of interest based on acoustic anomalies in the seismic data. Piston assisted gravity cores (JPC; TDI Brooks International) were used to collect up to 20m long cores which were sampled at approximately 1m intervals. Two of the cores had additional samples taken at about 30cm and 60cm depth below seafloor.

JPC-03 was chosen as an off-fault background location in an area northwest of the blue fault. Profiles were linear from the sediment-water interface to depth suggesting the area is at advection-controlled equilibrium. The sulfate-methane transition depth occurred at about 12m deep, suggesting low microbial activity. Methane was the dominant hydrocarbon present, with an average  $\delta^{13}C = -94\text{‰}$ . Cumulatively this suggests the methane present originated from a microbial (rather than deep thermogenic) source (Figure 21).

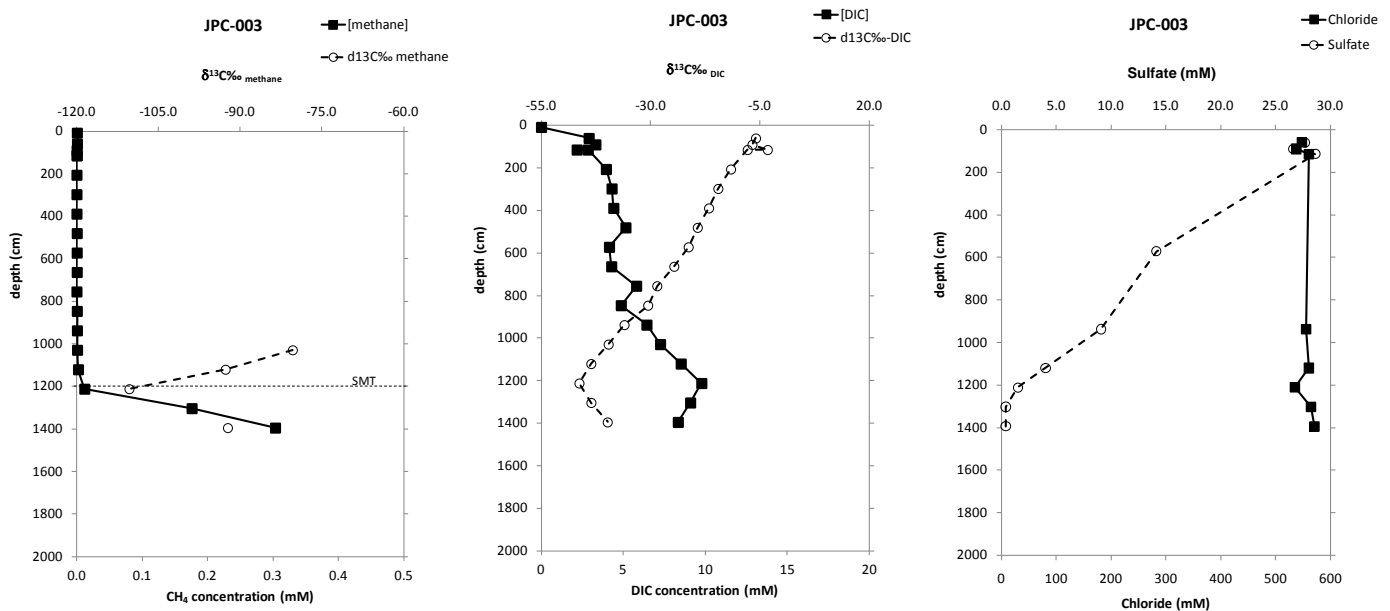


**Figure 21. Geochemical data for core JPC-003. The far left panel presents the methane concentration and isotope profiles with depth in the sediment. The middle panel presents the DIC concentration and isotope profiles. The far right panel presents the chloride and sulfate profiles with depth. This site was chosen as a 'background' off-fault site.**

JPC-01 was collected from a site near the blue fault associated with high acoustic backscatter. The seafloor has an extensive bacterial mat community and earlier coring efforts identified this as a site of high microbial methane oxidation. The cumulative geochemical and seismic evidence suggests that the blue fault acts as major conduit for thermogenic methane –rich fluids to reach the seafloor. Upon retrieval, gas expansion resulted in the loss of several meters from the top of this core (JPC-01). Thus all depths are estimates based on core liner section number Figure 22).

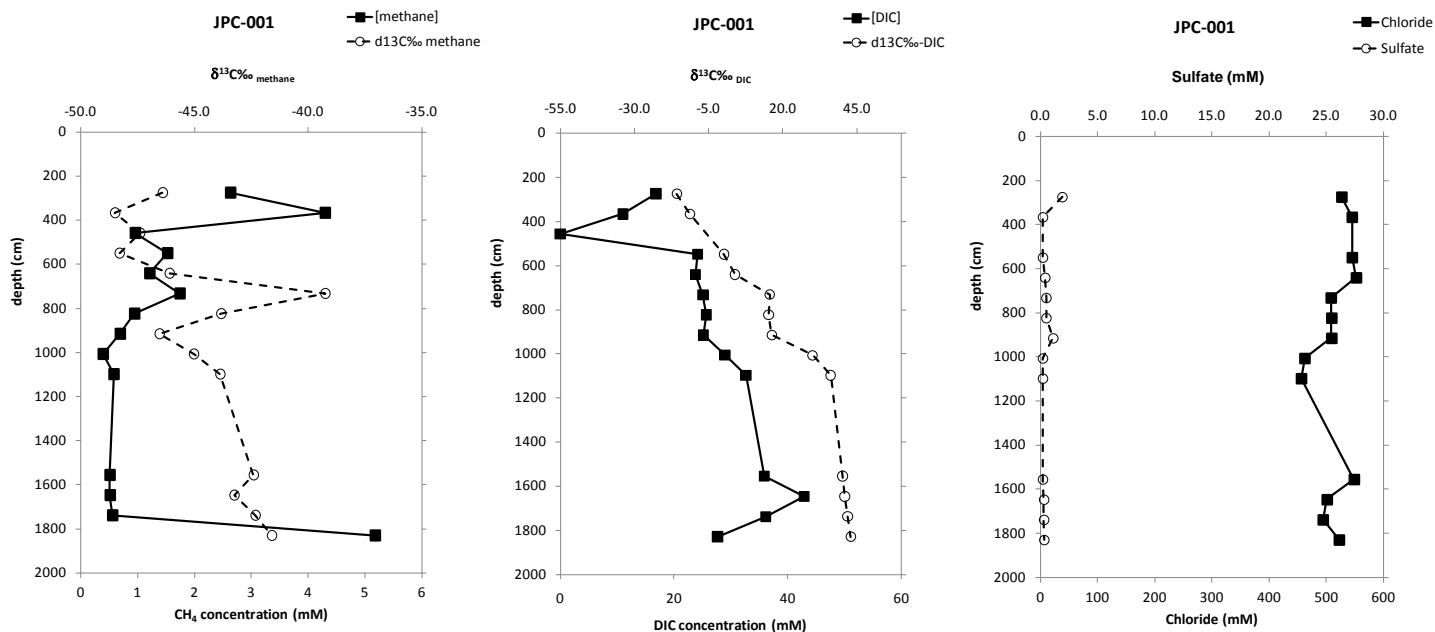


**Figure 22. Geochemical data for core JPC-01. The far left panel presents the methane concentration and isotope profiles with depth in the sediment. The middle panel presents the DIC concentration and isotope profiles. The far right panel presents the chloride and sulfate profiles with depth. Hydrate was collected from the bottom two sections of this core. Approximately the top three meters of sediment were lost due to expulsive degassing during recovery.**

In general, methane concentrations increased with depth, reaching nearly 3.5mM in the deepest section of the core. Because these cores visibly degassed on retrieval the reported concentrations are likely minimum values. Sulfate concentrations were below 5mM in the topmost sample we were able to collect (~3msbf) suggesting high rates of sulfate reduction probably in response to the enhanced availability of hydrocarbons supplied via the fault. Hydrates were recovered from JPC-01. Small pieces of the hydrate were placed into serum vials and capped. To collect the evolving gas, a needle and syringe was placed through the septum and the gas was allowed to passively fill the syringe. The syringe was purged twice and then filled a final time and preserved for hydrocarbon and isotope analysis. Methane was the dominant gas (79%) followed by ethane (11%), propane (9%), and butane (1%). The  $\delta^{13}\text{C}_{\text{methane}}$  was  $-40.4\text{‰} \pm 0.7$  (n=9). Cumulatively, the relatively high proportion of ethane and propane, as well as the heavy methane carbon isotopes confirm that the source for the hydrate is thermogenic.



JPC-02 was collected from the southwest region of the mound complex, near the purple fault in a seismically quiet area. Sulfate was detectable up to 11m, the resulting flux estimate ( $-185 \text{ mmol m}^{-2} \text{ y}^{-1}$ ) is similar to that for JPC-03, thus fluid supply from depth is slight to non-existent Figure 23).

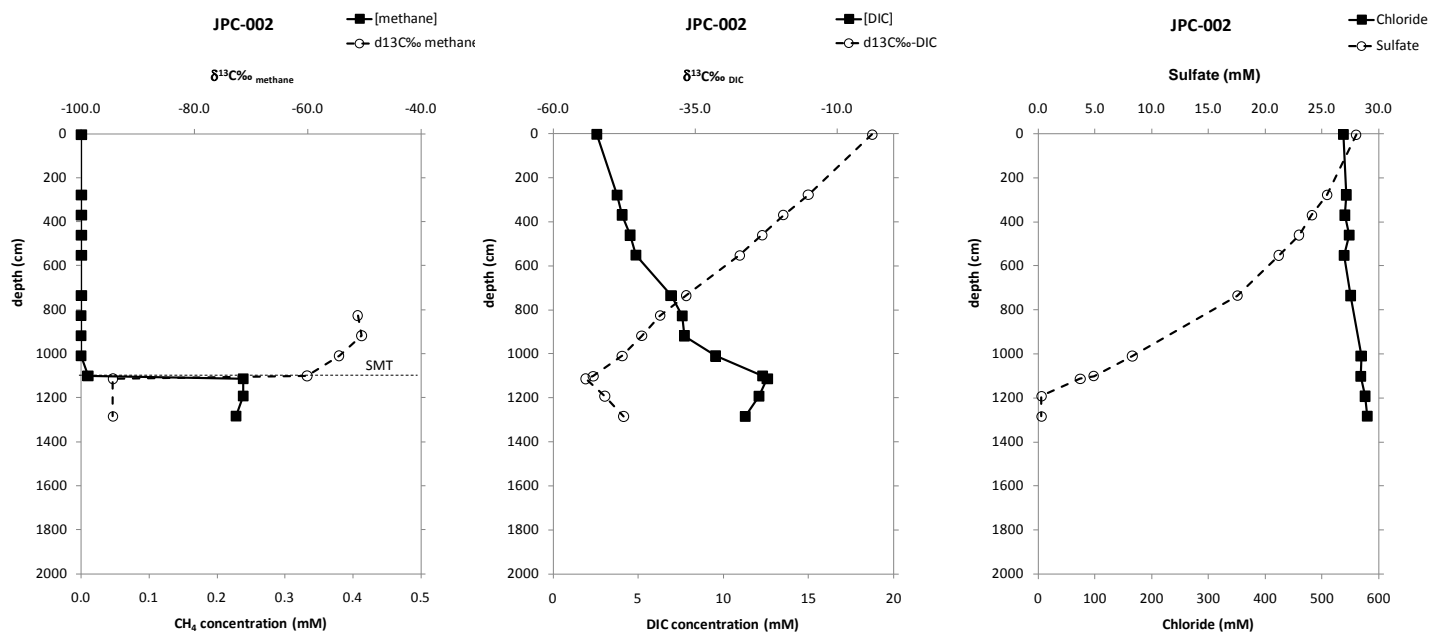


**Figure 23. Geochemical data for core JPC-002. The far left panel presents the methane concentration and isotope profiles with depth in the sediment. The middle panel presents the DIC concentration and isotope profiles. The far right panel presents the chloride and sulfate profiles with depth. SMT denotes the approximate depth of the sulfate-methane transition zone.**

JPC-06 was chosen in an area near the purple fault where acoustic blanking suggested the presence of free gas. The blanking was constrained below the 10m depth but extended below to the shallow gas reservoir identified in the industry data. The presence of early stage chemosynthetic organisms at the site suggests that some hydrocarbons are making it to the surface to fuel production of the community, but the conduit for fluid flow is as yet unidentified.

Sulfate concentrations trend generally downward with depth, although most geochemical profiles appear non-linear suggesting that conditions at the site are not at steady-state. Non-linear profiles sometimes imply bioturbation; however, bioturbation to 4m or more at this site seems unlikely. Similar profiles have been observed at other sites (i.e. Coffin et al. 2008; Pohlman et al. 2008), where chloride concentrations were used as a conservative tracer to infer biogeochemical removal of sulfate (i.e. via organoclastic sulfate reduction). However, while chloride concentrations do trend slightly positive with depth, the values are not very different from expected seawater values, so a similar technique would not apply at this site. Another explanation is that the geochemical profiles are not at steady-state because a new fault has opened up and is supplying methane to the shallow sediments. If the supply opened recently enough the profiles would not have had time to establish linear steady state profiles and would take on the appearance we see at this site (see Figure 24).

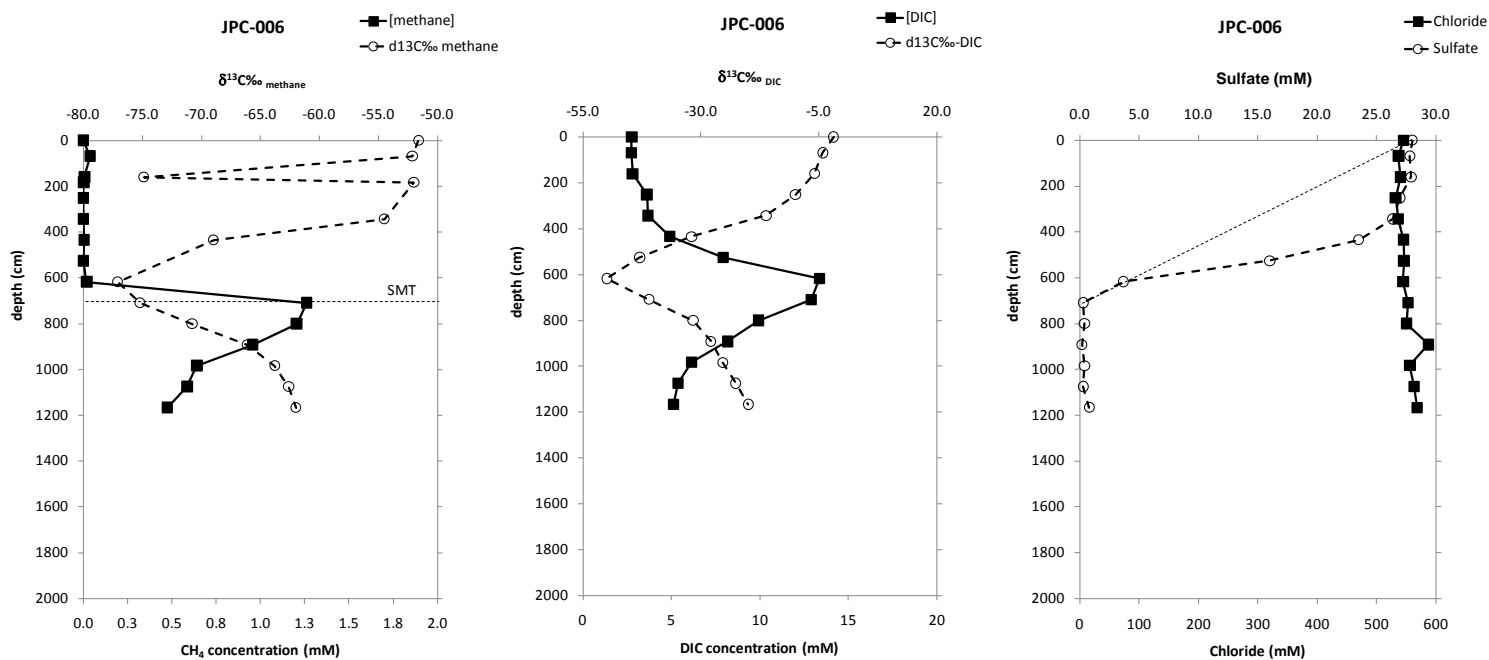


**Figure 24. Geochemical data for core JPC-006. The far left panel presents the methane concentration and isotope profiles with depth in the sediment. The middle panel presents the DIC concentration and isotope profiles. The far right panel presents the chloride and sulfate profiles with depth. Note the non-linear DIC and sulfate profiles. The dashed line in the sulfate profile indicates the expected steady-state diffusion profile. SMT denotes the approximate depth of the sulfate-methane transition zone. Strong acoustic backscatter was evident, but the feature did not appear to reach the seafloor.**

JPC-07 was collected from the northeast section of the mound in a pockmark formed by the intersection of the yellow fault with the seafloor. A pockmark is diagnostic evidence of expulsive fluid flow (Macelloni et al., 2011), thus, with this core we were attempting to define the influence of such events on the surrounding sediment geochemistry. Methane and sulfate profiles in this core were similar to the background site (JPC-03) and linear, suggesting steady-state conditions (see Figure 25). So while there may be intermittent fluid supply via the yellow fault, the hydrocarbons appear to be constrained within the fault and not affecting the surrounding sediment geochemistry.

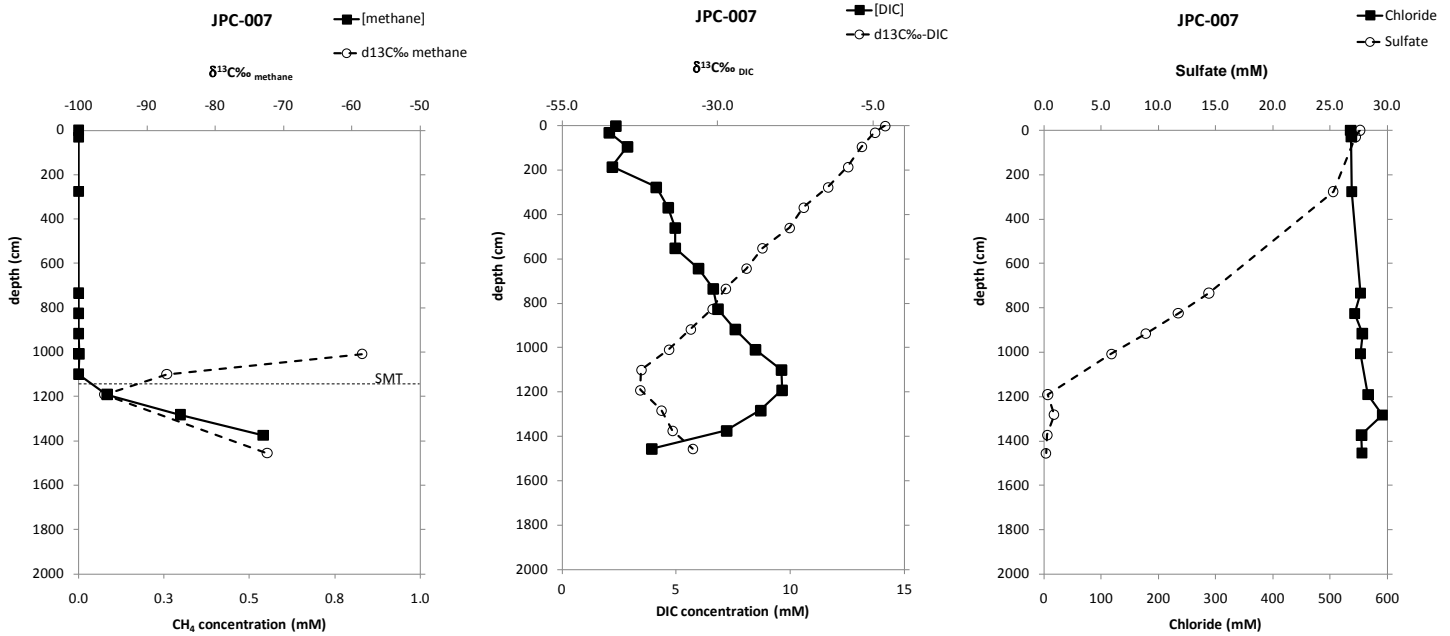


**Figure 25. Geochemical data for core JPC-007. The far left panel presents the methane concentration and isotope profiles with depth in the sediment. The middle panel presents the DIC concentration and isotope profiles. The far right panel presents the chloride and sulfate profiles with depth. SMT denotes the approximate depth of the sulfate-methane transition zone.**

In conclusion, we saw a range of microbial activities and evidence of both biogenic and thermogenic methane sources across the mound complex. In general, areas that had faults but little acoustic backscatter showed little influence of thermogenic methane suggesting that transported hydrocarbons are constrained with the fault itself and not affecting surrounding sediment geochemistry. On the other hand, areas near faults with high acoustic backscatter do show evidence of thermogenic sources contributing to the methane pool and generally have higher methane fluxes and microbial activity rates (as inferred from sulfate reduction rates).

A manuscript reporting these results is being prepared for submission:

*Wilson, Rachel, Leonardo Macelloni, Laura Lapham, Antonello Simonetti, Jim Knapp, Camelia Knapp, Carol Lutken, Ken Sleeper, Charlotte Brunner, Marco D'Emidio, and Jeff Chanton*  
*Integrating geochemical profiles with seismic surveys to identify subsurface methane sources and migration pathways*

**Subtask 4.4. Recipient shall conduct laboratory analyses in an attempt to define hydrate stability to address the hypothesis that while within the appropriate temperature and pressure field, hydrate deposits are “meta-stable” when exposed to in situ pore water CH<sub>4</sub> concentrations well below saturation. Experiments shall investigate the observed phenomenon in which hydrates dissolve at rates significantly below those predicted by thermodynamic equilibrium (Lapham et al. in review). The recipient shall continue laboratory hydrate pressure chamber experiments to define hydrate stability and shall attempt to define whether meta-stability is caused by features of hydrate crystal structure or due to external coatings that form on the hydrate surface.**

Studies of natural hydrate dissolution rates, based on field measurements of hydrate loss, report rates of around  $30\text{cm y}^{-1}$  (MacDonald et al. 2005; Lapham et al. 2010). Studies investigating the dissolution of artificial hydrates report rates  $>100\text{ cm y}^{-1}$  (Hester et al. 2004; Bigalke et al. 2009; Rehder et al. 2009). Our objective is to investigate possible controls on hydrate dissolution to reconcile the discrepancies between field observations and experimental results in an effort to gain a deeper understanding of hydrate stability. We hypothesized that hydrate gas composition would alter the dissolution rate. Specifically we hypothesized that the addition of ethane and propane, and the resulting formation of sII hydrate would show increased resistance to dissolution when compared to a pure methane (sI) hydrate. Two pure methane hydrate experiments were conducted with the resulting dissolution rate =  $30\text{ cm y}^{-1}$ . Three mixed gas hydrate experiments were then conducted. The average resulting dissolution rate for these experiments was  $27\text{ cm y}^{-1}$ . Although slightly lower, the results were not statistically different, suggesting that, while hydrate structure does impart stability against lower pressures and higher temperature, it does not contribute to hydrate stability against dissolution (see Figure 26).

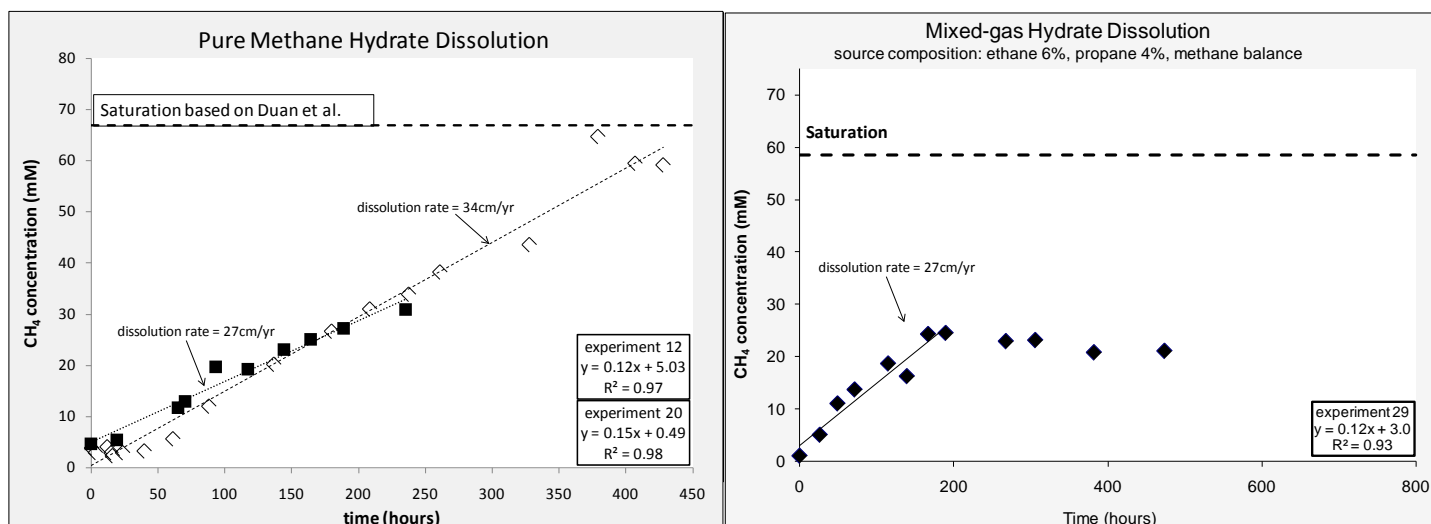


**Figure 26. Dissolution experiments comparing a pure methane (sI) hydrate with a mixed gas (sII) source hydrate.**

A manuscript reporting these results is being prepared for submission:

Lapham, Laura L., Rachel M. Wilson, Brian J. Anderson, Nagasree Garapati, Ian R. MacDonald, Jeff P. Chanton. Gas hydrate dissolution rates quantified with laboratory and seafloor experiments

Stable carbon isotope ratios are often used to make inferences about gas provenance and microbial activity within sediments. However, fractionation during hydrate dissolution could alter conclusions based on isotopic analysis. Although, most assume that there is no isotope fractionation upon dissociation, no previous study has shown this to be true for hydrate dissolution. Our experimental conditions for measuring hydrate dissolution rates also allowed us to test the assumptions about isotopic fractionation during hydrate dissolution (Figure 27).

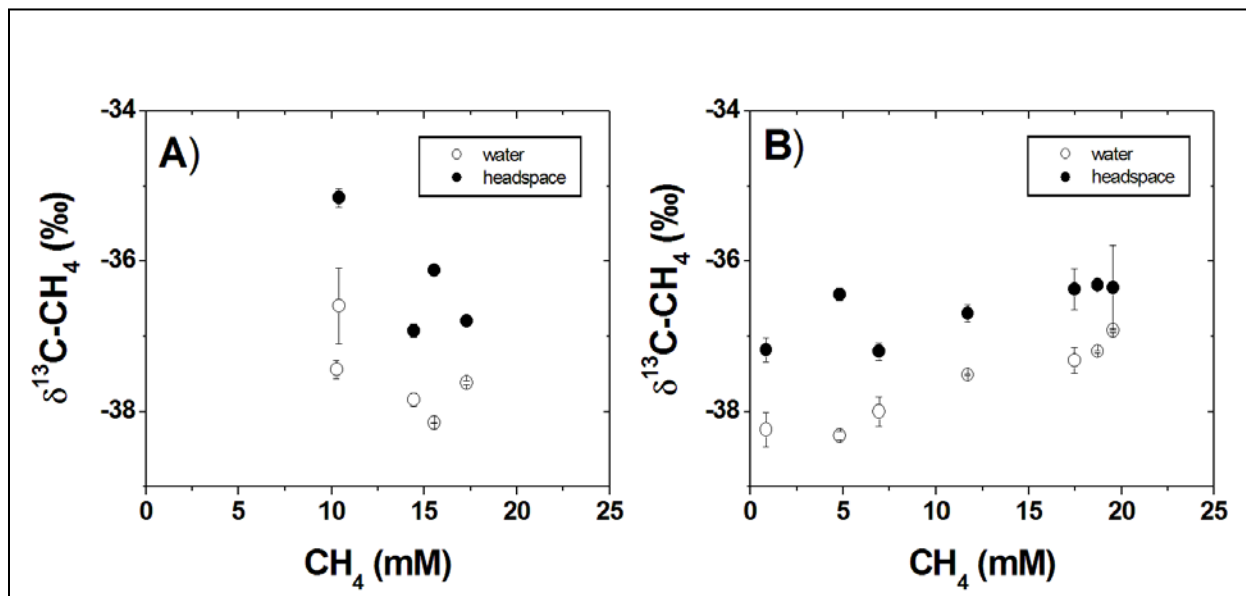


**Figure 27.** Results of two replicated experiments showing the  $\delta^{13}\text{C}$  versus methane concentration as the hydrate dissolved into the surrounding water. There was no significant trend over time, demonstrating that there is no fractionation of methane isotopes during hydrate dissolution. (This figure is adapted from Lapham et al. 2012).

The results of this study are reported in:

Lapham, LL, RM Wilson, and JP Chanton (2012) Pressurized laboratory experiments show no stable carbon isotope fractionation of methane during gas hydrate dissolution and dissociation. *Rapid Comm Mass Spec* **26**: 32-36

**Final Products:** Two replacement OsmoSampler packages, in situ pore-fluid samples, chemical analyses of in situ pore-fluid samples for light hydrocarbon composition and concentration, isotopic composition, and chlorinity, chemical analyses of pore-fluid samples from cores for light hydrocarbon composition and concentration, isotopic composition, and chlorinity, a gas genesis model that links geochemistry to geophysics, and an analysis of geochemical constraints on formation and dissolution of gas hydrates.

- Two replacement OsmoSampler packages have been built, but not deployed due to difficulties encountered in recovering the first two packages
- Two additional newly designed mini-PFA packages have been built and tested at Cascadia Margin hydrate and seep sites confirming their suitability for use at MC-118
- Pore fluids from the first OsmoSampler packaged recovered from MC-118 as well as the two mini-PFA packages recovered from the Cascadia test site have been analyzed for methane concentrations and isotopes, DIC concentrations and isotopes, light hydrocarbon fractions, sulfate concentrations and chloride concentrations



- A total of 44 cores have been collected from across the MC-118 mound and have been analyzed for methane concentrations and isotopes, DIC concentrations and isotopes, light hydrocarbon fractions, sulfate concentrations and chloride concentrations, as well as a subset that have also been analyzed for nitrate and ammonia concentrations. Cumulatively these data have been used in the development of the Gas Genesis Model
- A Gas Genesis Model linking variability in microbial activity and seafloor biotic communities to subsurface faults and seismic anomalies via geochemical profiles has been developed and is continuously being updated as new data are collected.
- Measurements of methane and other hydrocarbons in concert with geochemical gradients suggest that saturated methane conditions are not obligatory for natural hydrate occurrence. However, experimentally, we have shown that artificial hydrates will continue to dissolve until the surrounding water reaches saturation. Further investigation is needed to determine whether natural conditions are contributing to the stability of hydrate outcrops as observed at MC-118.

### **TASK 5: Automated Biological/Chemical Monitoring System(ABCMS) for Offshore Oceanographic Carbon Dynamic Studies.**

Development of a Marine Lander Survey Vehicle (Lander) for the next phase of gas hydrate research in the Gulf of Mexico

This task extended from Phase 2 through Phase 4 of the MS/SFO/Hydrates project. This Final Report covers work and accomplishments from all phases.

(Subcontractors: *The University of Georgia; Scott Noakes, John Noakes, Chuanlun Zhang, Pls; Collaborator: Lewis Fortner SRI International; Tim Short, PI; Collaborator: Ryan Bell*)

The University of Georgia (UGA) and SRI International (SRI) research team has developed a unique survey instrument capable of surveying the methane rich seafloor and collecting biomass and suspended sediment samples on demand.

#### **Introduction**

Since the establishment of the Gulf of Mexico Hydrates Research Consortium in 1999, tremendous progress has been made in monitoring the activities of gas hydrates on the Gulf seafloor. Substantial achievements include the design and deployment of the Pore-Fluid Array (PFA) and the prototype thermistors Geophysical Line Array (GLA) at the selected hydrate site MC 118. Positive indications for hydrate were observed in cores from the area corresponding to the northwestern periphery of the mound as determined by AUV Multibeam, sidescan, and chirp data. To date, the MMRI has improved technology and experience in underwater supplies of power and light, video capability, LLD sensing capability, and positioning capability. These capabilities are maintained by a well- trained, well-equipped staff at MMRI who can perform instrument deployment during field cruises on a routine basis.

Previous surveys have been confined to a limited area of the hydrate mound at site MC 118. Recently, a new technology has been developed by the University of Georgia--SRI International team funded by University of Mississippi grant 09-09-025, which integrated a high throughput deep water filtration system (DWFS) for microbiological sampling and a membrane introduction mass spectrometer (MIMS) for chemical analysis (Fig. 1). The package was also equipped with a CTD sensor and altimeter. This integrated capability allowed for a rapid survey of large areas in the water column for detecting methane and measuring a variety of other chemical and physical components such as temperature, dissolved CO<sub>2</sub> and nitrogen above a hydrate mound. The DWFS can be activated any time for biomass and surficial sediment collection associated with methane gas.

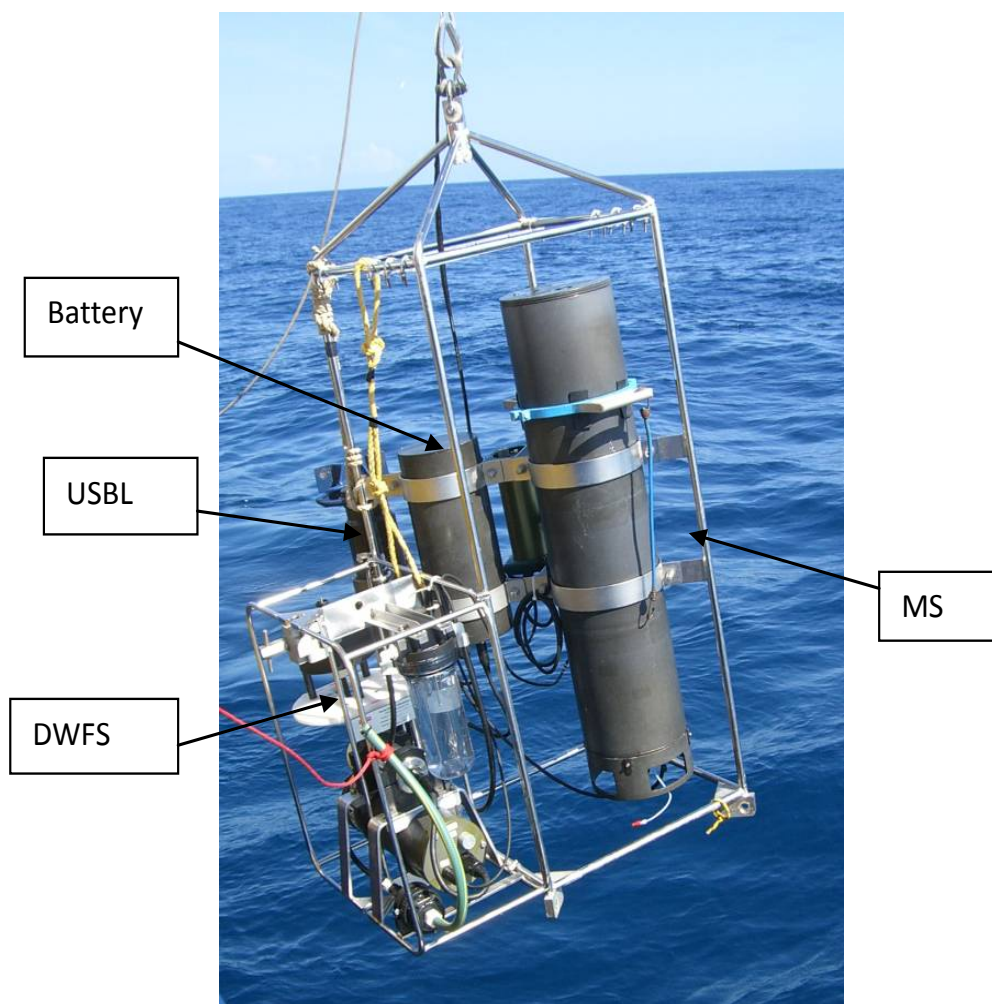


**Fig. 1. The DWFS-MIMS system being deployed from the R/V Pelican**

In February 2009, the system was successfully deployed three times to depths greater than 860 m. The DWFS was activated with 100% success by shipboard commands while monitoring data from the MIMS and peripheral instruments (e.g., CTD, altimeter, and USBL) as the instrument package drifted above the sea floor over the northwestern crater complex at MC118. A first of its kind experiment was accomplished in which the instrument package was lowered to deliberately perturb the sediment. The MIMS detected a strong methane

signal upon impact with the seafloor and the DWFS immediately collected a filter sample containing biomass and sediment particles (Fig. 2). The success of this field trial opened the door for a new approach to sea floor sediment hydrate surveying.

The DWFS and MIMS combination was the forerunner of a new Automated Biological/Chemical Monitoring System (ABCMS) which is capable of collecting multiple filter samples at operator-programmed seawater volume, and at depths exceeding 1000 meters. The filtered samples can be used to study the microbial community thriving in the water column and in the sediment pore water that is released due to the impact of the instrumentation with the seafloor. The filtered samples can also be used to study the surficial sediment associated with the methane seeps. The multi-filter capability allows the ABCMS to be deployed for an extended duration and have the ability to collect up to 30 filter samples from selected locations. With the extended deployment and multi-filter capability, the MC118 site can be surveyed for potential methane “hot spots”.

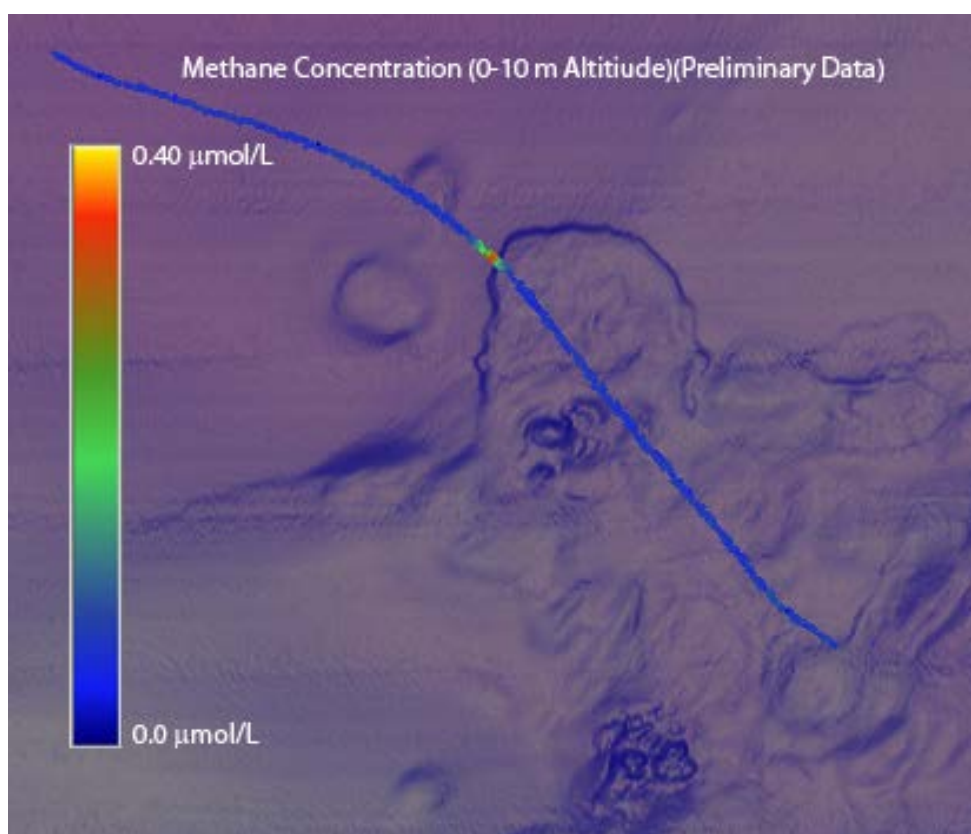
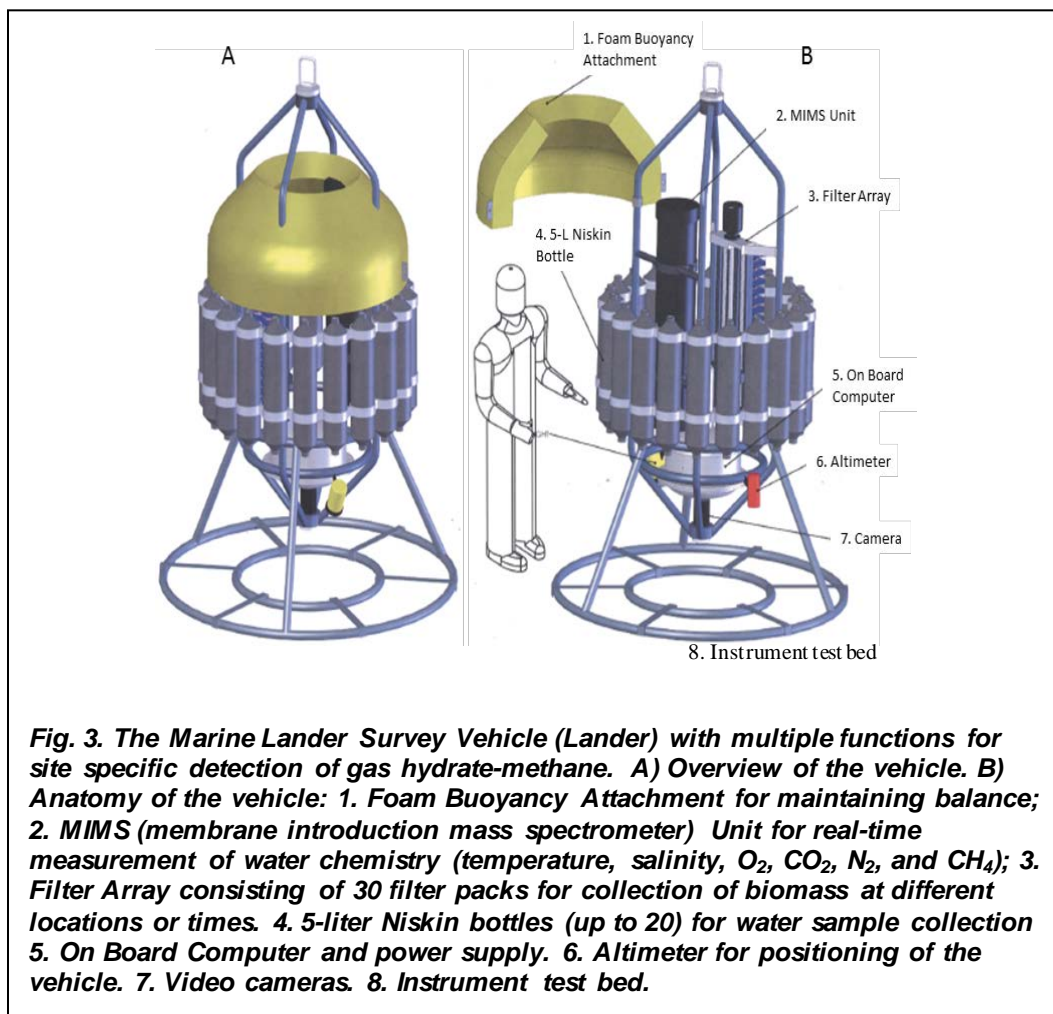


**Fig. 2. Preliminary data showing methane concentration determined by the MIMS over the MC 118 northwestern crater complex.**

Due to the light weight of the existing DWFS-MIMS test package, it can only be deployed from the R/V Pelican hydroline cable located mid-ship, which limits the system to a drifting survey capability. However, the ABCMS is configured for stern deployment similar to the MMRi SSD Remotely Operated Vehicle (ROV). This will allow the ABCMS to be deployed off the stern and will also allow greater mobility during deployment. The ABCMS also utilizes the same fiber optic cable as the SSD. To further enhance the methane survey capability, an advanced system was designed. The original conceptual design consists of a

programmable; site specific Marine Lander Survey Vehicle (Lander), capable of video, positioning, and photography while performing real time measurements of water chemistry (Fig. 3). The Lander significantly increases the efficiency of locating methane “hot spots” for gas hydrate detection and provides an instrument test bed for introducing new sensing capabilities for studying chemical, physical, and microbiological dynamics at targeted seafloor locations. Furthermore, the vehicle is capable of landing where a methane anomaly is detected and can perform physical and chemical measurements while collecting samples for biological and sediment analysis.



## Marine Lander Survey Vehicle

The University of Georgia entered into a contract with the University of Mississippi/DOE to design and construct the new marine lander. In addition, a contract was established between the University of Georgia (UGA) and SRI International (SRI) to support SRI efforts to integrate in situ mass spectrometry with microbe sampling for gas hydrates research. General schematics were drawn for the Lander components which include the underwater mass spectrometer and multi filtration system. The Lander and surface vessel were linked by the same fiber optic cable as used for the SSD ROV. The electronics interfacing the fiber optic cable and Lander instrumentation were installed and tested in a pressure housing. SRI utilized an existing MIMS during the initial Lander design and development while the new MIMS was constructed.

Individual filter assemblies or packs were constructed (Figure 4) to be utilized in the Lander in groups of 30. Over 60 filter packs were constructed to allow two complete filter groups to be deployed (one at a time) prior to disassembly, cleaning and reloading. The filter packs were pre-filled with distilled water to prevent contamination from surrounding water during deployment. Once deployed and upon pump activation, the distilled water was displaced with seawater at the desired depth and location. Upon activation, the pump will continue to move seawater through the filter until the desired volume is reached or the filter has been clogged. After collecting a sample, the pump injector was moved from one filter pack to another so that multiple filters can be collected. The filter packs were designed with pressure relief valves to aid in equalizing the internal pressure that could potentially build as a result of deep water sampling.



*Figure 4. Filter assembly mounted on distilled water pumping station.*



The Lander frame was constructed of stainless steel and was configured to house the filter rack (containing up to 30 individual filter packs); membrane introduction mass spectrometer (MIMS) and lithium battery pack; and Lander battery packs (Figure 5). The Lander was also equipped with a color video camera that can send live video through the fiber optic interface to the surface vessel. The camera (with LED light ring) is positioned downward to view the seafloor and the additional lighting is angled to avoid backscatter from suspended solids. The camera and lights can be turned on/off as needed to avoid unnecessary drain on the Lander's batteries. The MIMS was mounted with multiple hinge clamps that can readily fasten the MIMS housing and battery pack in position. The MIMS interfaced with the Lander's electronics package where the RS-232 communication is converted to the fiber optic cable mounted on the RV Pelican.

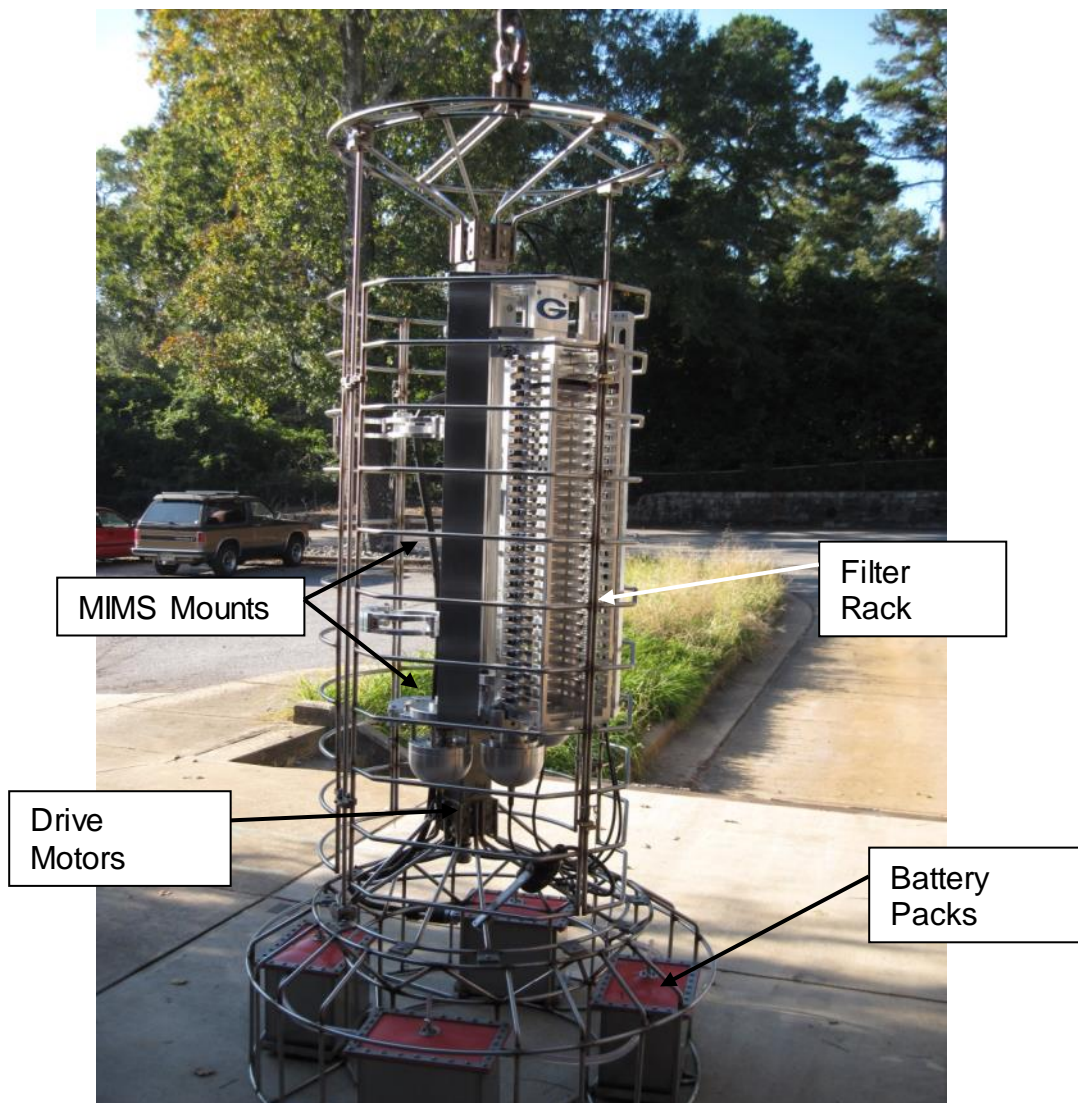


**Figure 5. Lander assembly.**

In January 2011, the Lander was transported to the Southwest Research Institute (SWRI) in San Antonio, Texas for a simulated deployment. The Lander was equipped with the filter rack, video, MIMS, conductivity/temperature/depth sensor (CTD), and altimeter (Figure 6). Prior to placing the Lander into the pressure chamber, communications were established between the Lander communication package and the MIMS. The Lander was placed into the 48" pressure chamber, chamber lid installed and filled with water (Figure 7). Once sealed in the chamber, the simulated deployment was initiated by slowly raising the pressure in the chamber. The chamber was pressurized to simulate a deployment to 1000m. Communication with the Lander was maintained throughout the simulated deployment. The MIMS, CTD and altimeter successfully sent a data stream through the Lander pressure housing to the bench top computer. Commands to the MIMS were successfully received with corresponding responses returned to the bench top computer. The video camera and lights continued to work successfully and could be turned on and off during the test deployment.

During the simulated deployment, one set back was experienced. At approximately 300m (simulated) depth, a bulkhead connection on one of the Lander drive motor housings controlling part of the filtration system leaked causing the motor to burn out. It was later determined that the connector was defective and replaced. The housing and new connector was later tested in Athens at the UGA shop to a simulated 1000m depth without failure.

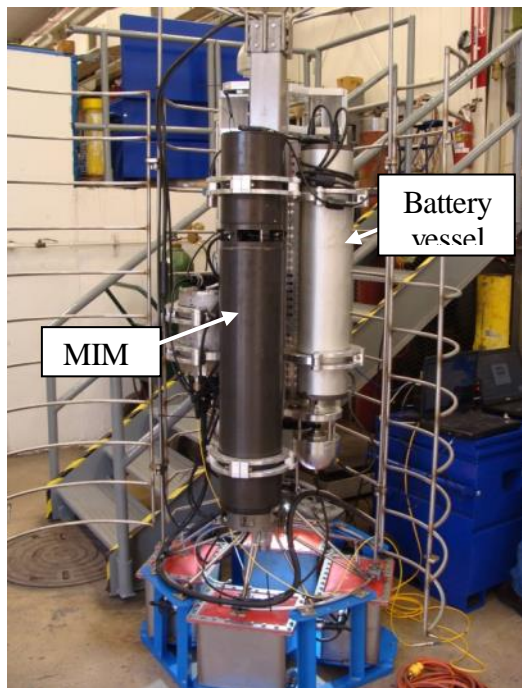


**Figure 6. MIMS and battery pack loaded into the Lander.**



**Figure 7. Loading the Lander into the SWRI pressure chamber.**



The General Oceanics Model 1018 Rosette was incorporated into the Lander design. It was originally thought that the rosette would be fully integrated into the Lander. However, after a study of the existing Lander configuration, it was determined that it would be cost prohibitive to continue on this track. Instead, the rosette was installed as an add-on accessory to the Lander (Figure 8). With this design, the rosette can be readily installed or removed as needed dependent on the mission goals. This also keeps the rosette available as a standalone instrument if needed.

The new Lander operational software was written and lab tested (Figure 9). The software allowed the operator to view the filters available for collection and which filter is ready for sampling. It also allowed the operator to input site coordinates and field notes. The rosette was integrated into the software and allowed the operator to fire bottle samples on demand. The software indicates which bottle sample is ready for collection and which bottles have already been collected. System drive motors and pumping information are also monitored giving insight to potential problems during deployment. In addition to the sampling controls, the software allows the operator to turn the onboard camera and lights on and off. The majority of the screen is dedicated to the live-feed video streaming from the onboard camera.



**Figure 8. Rosette installation.**

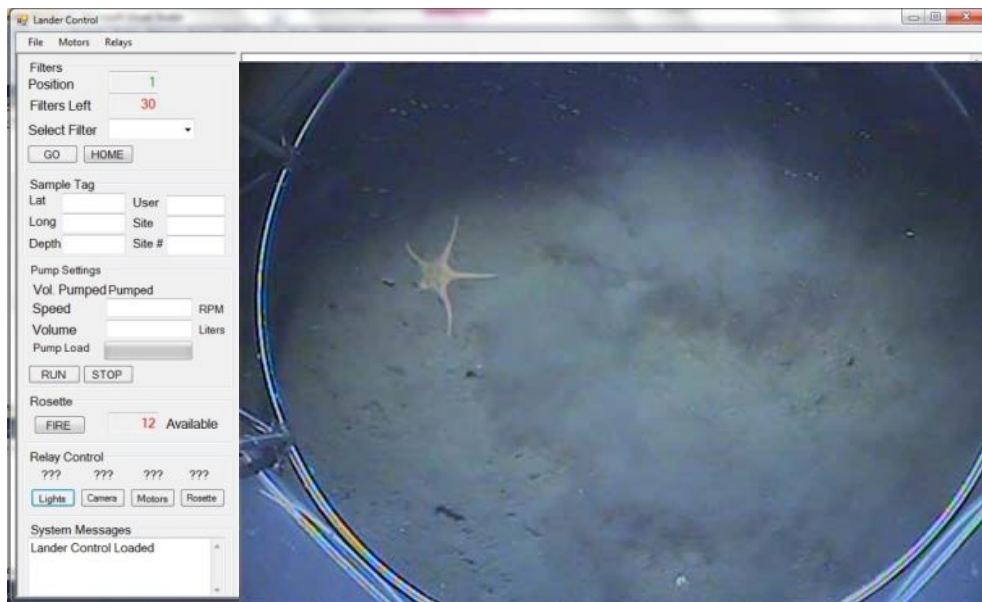


**Figure 9. Lander operational software (test video stream from previous deployment).**

## Membrane Introduction Mass Spectrometer

The conceptual design for a new smaller and lower power MIMS instrument was established in late 2010 and all of the major internal components (e.g., mass analyzer, high vacuum pump, roughing pump, and water sampling pump) were identified as part of the design process. An InficonE3000 200 atomic mass unit (amu) sensor served as the mass analyzer. This analyzer has a more rugged construction than the CPM200 sensor used in previous SRI underwater MIMS systems. It also has two filaments in the ion source that are designed for high water vapor environments. The two filaments provide redundancy in case one filament fails during deployment. The high vacuum pump for the new system is a Pfeiffer HiPace10 turbo pump, which is smaller and required lower power than the Varian pumps used in prior instruments, and also allows for the use of a smaller lower power KNF diaphragm pump as the backing pump. Figure 10 is an engineering model of the new MIMS underwater system components and pressure housing (without electrical wiring). Figure 11 is a photograph of the major components of the new MIMS system (without the membrane inlet probe, power distribution board and microcontroller board) and Figure 12 is a photograph of the new pressure housing (rated and tested to 2000 m depth). The new system will not have an embedded computer. Instead all data will be stored on a removable storage device and all operations will be controlled by the microcontroller.

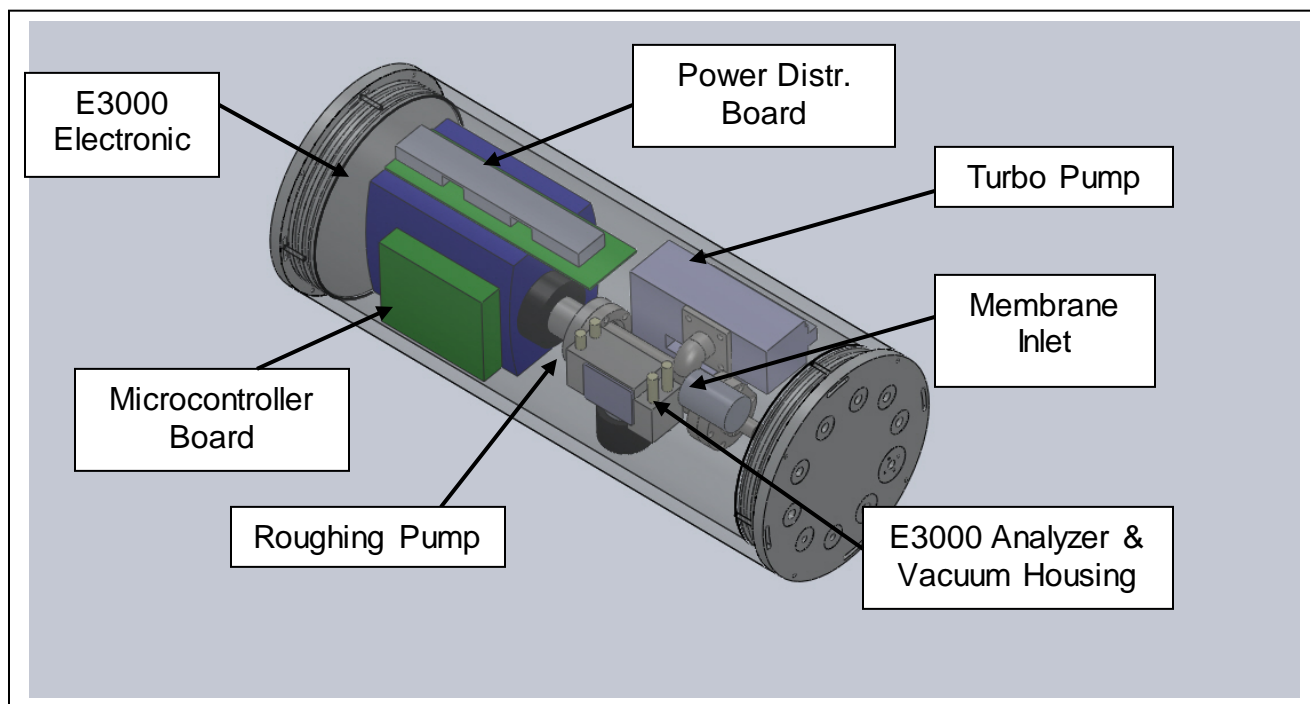


*Figure 10. 3-D solid model of the new MIMS system. Major components are labeled.*

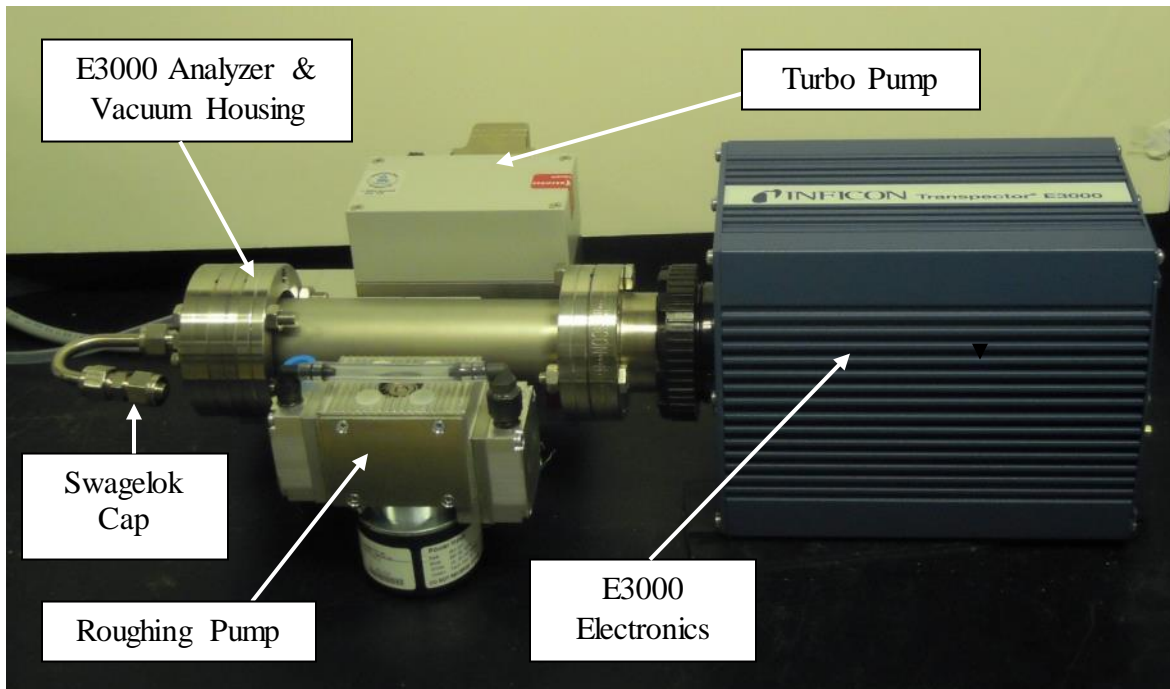


**Figure 11. Major components of new SRI MIMS system. The membrane inlet module will replace the Swagelok cap noted in the figure. The roughing pump is not connected to the turbo pump at this time. The power distribution and microcontroller boards are currently under development and are not shown (as well as the internal wiring). All components will be mechanically supported on the feed through end cap.**

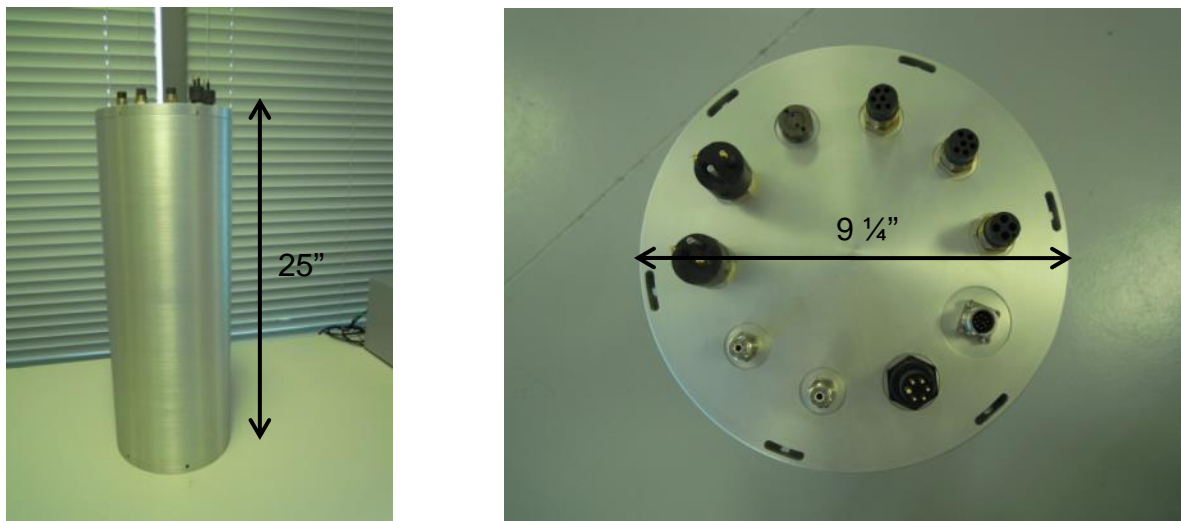


**Figure 12. New SRI MIMS pressure housing. At left, Side view; At right, Top view showing all electrical and fluidic connections are on one end cap. The overall length of the housing is 25 in. and the outer diameter is 9 1/4 in.**



In order to minimize or eliminate condensation of water vapor on the cooler cold finger, the operational environment for the cooler must be evacuated or back-filled with a dry inert gas, such as argon. The pressure housing was fitted with a custom end cap for mounting the cooler and provided electrical connectors to power the chiller, and vacuum connections between the membrane inlet probe and the vacuum housing of the mass spectrometer (Figure 13).

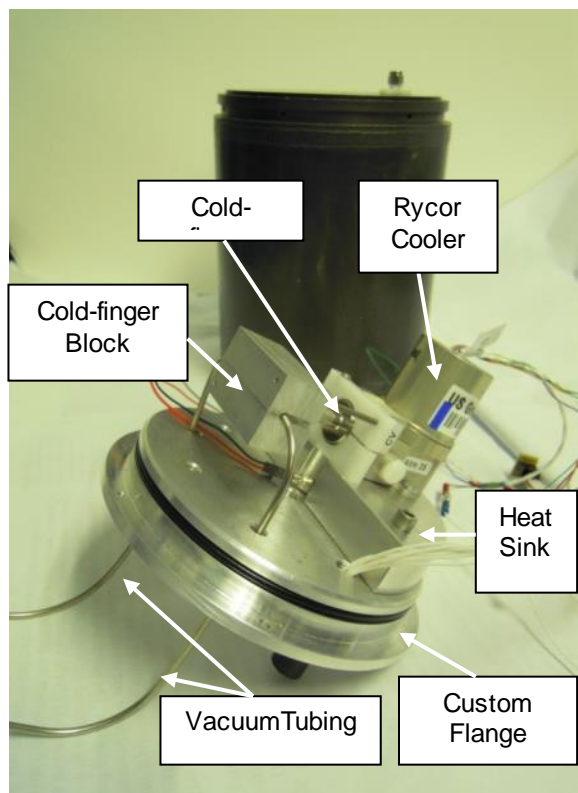
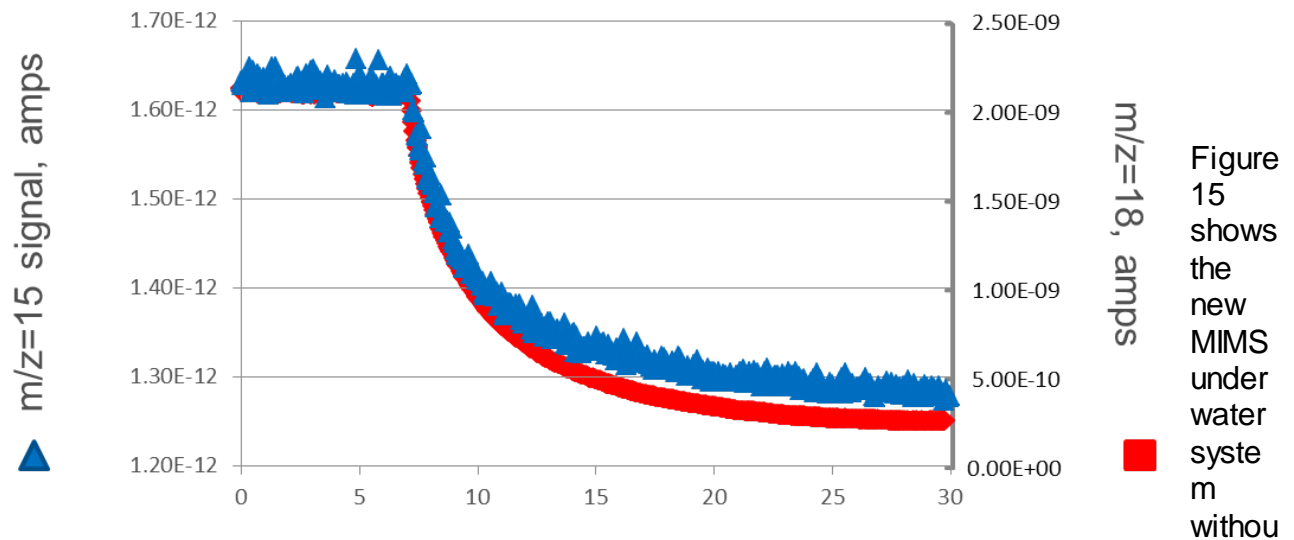
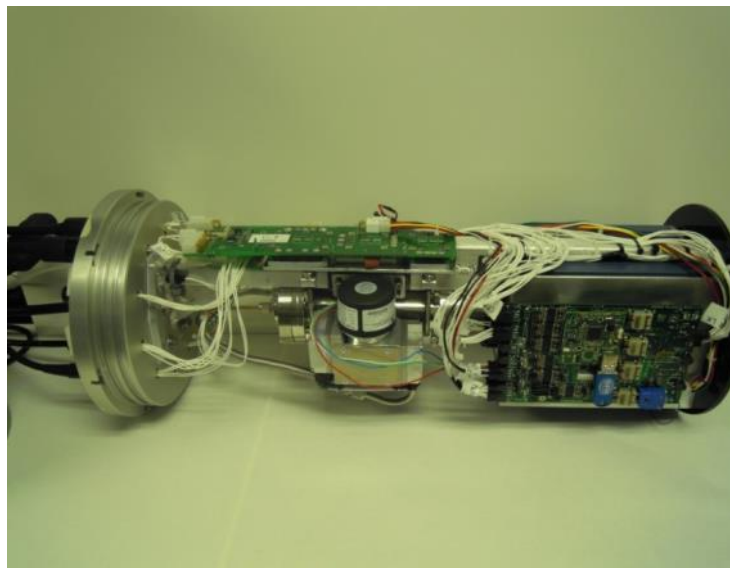


**Figure 13. SRI cold-trap system for improving methane detection limits. Water vapor in the vacuum tubing will be trapped in the cold-finger block section at approximately -90 deg. C. Major components are labeled.**

Experiments with a laboratory MIMS system similar to the underwater MIMS instrument have shown that the chiller significantly reduces the magnitude and standard deviation of the mass spectrometer background signal at  $m/z$  15, the diagnostic ion for methane (Figure 14). The background intensity (signal level in absence of methane) has contributions from the low abundance nitrogen isotope  $^{15}\text{N}$  (derived from fragmentation of  $\text{N}_2$  during ionization, and from the “tail” of the highly abundant  $^{16}\text{O}$  isotope (derived from fragmentation of  $\text{H}_2\text{O}$  and  $\text{O}_2$  in the ion source). The chiller freezes out water vapor ( $\text{H}_2\text{O}$ ) in the vacuum line between the membrane interface and the ion source, thereby reducing the  $^{16}\text{O}$  contribution considerably. The current chiller set up could be integrated with the underwater MIMS at some point in the future for field use.



t the pressure housing. System functional tests proved successful paving the way for a full field test. The new MIMS system was designed for deployment to a depth of 2000 m. Initial tests have demonstrated a power consumption of 50 Watts (24 VDC), without running the sample pump and membrane probe heaters. These components will add up to 20 Watts additional power consumption, depending on the set point of the membrane probe heater system and the initial temperature of water being analyzed. The instrument has a length of 64 cm (without considering connectors) and a diameter of 24 cm. Its weight in air is approximately 25 kg and has close to neutral buoyancy in water.



Time (min)

**Figure 15. New MIMS system with components mounted on pressure housing end cap.**

As part of the final construction of the MIMS, SRI conducted a number of system tests. These tests included both bench testing and field tests. Prior to deployment, the MIMS was bench tested with gas standards to determine the system functionality and performance (Figure 16). During one of the field methane detection tests, SRI deployed the MIMS at MC118 in June 2010 to investigate potential changes in dissolved gas and volatile organic concentrations in the water column that may be due to the Deepwater Horizon spill. Data from three vertical profiling casts were collected, and in each case the data indicate elevated concentrations of methane (over previous profiling casts performed before the spill in approximately the same area) at approximately 600 m and 800 m depths. Figure 17 shows raw UMS data (shown as a time series of intensity of  $m/z$  15, diagnostic of methane) for the one of the profiling casts at a site within MC118.

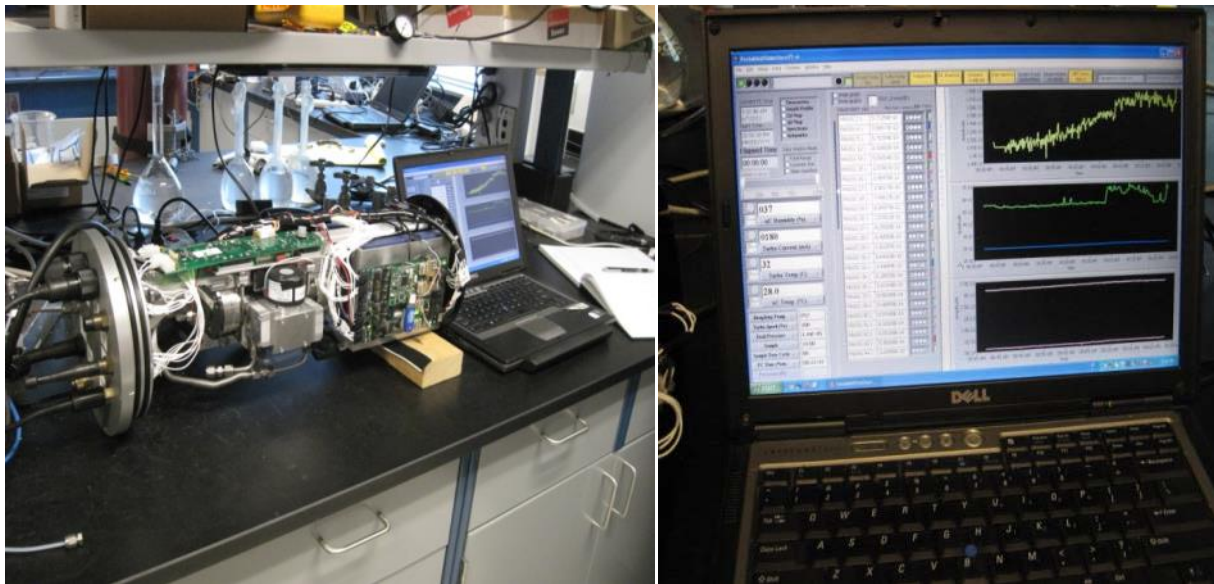


**Figure 16. MIMS calibration and system test prior to deployment.**

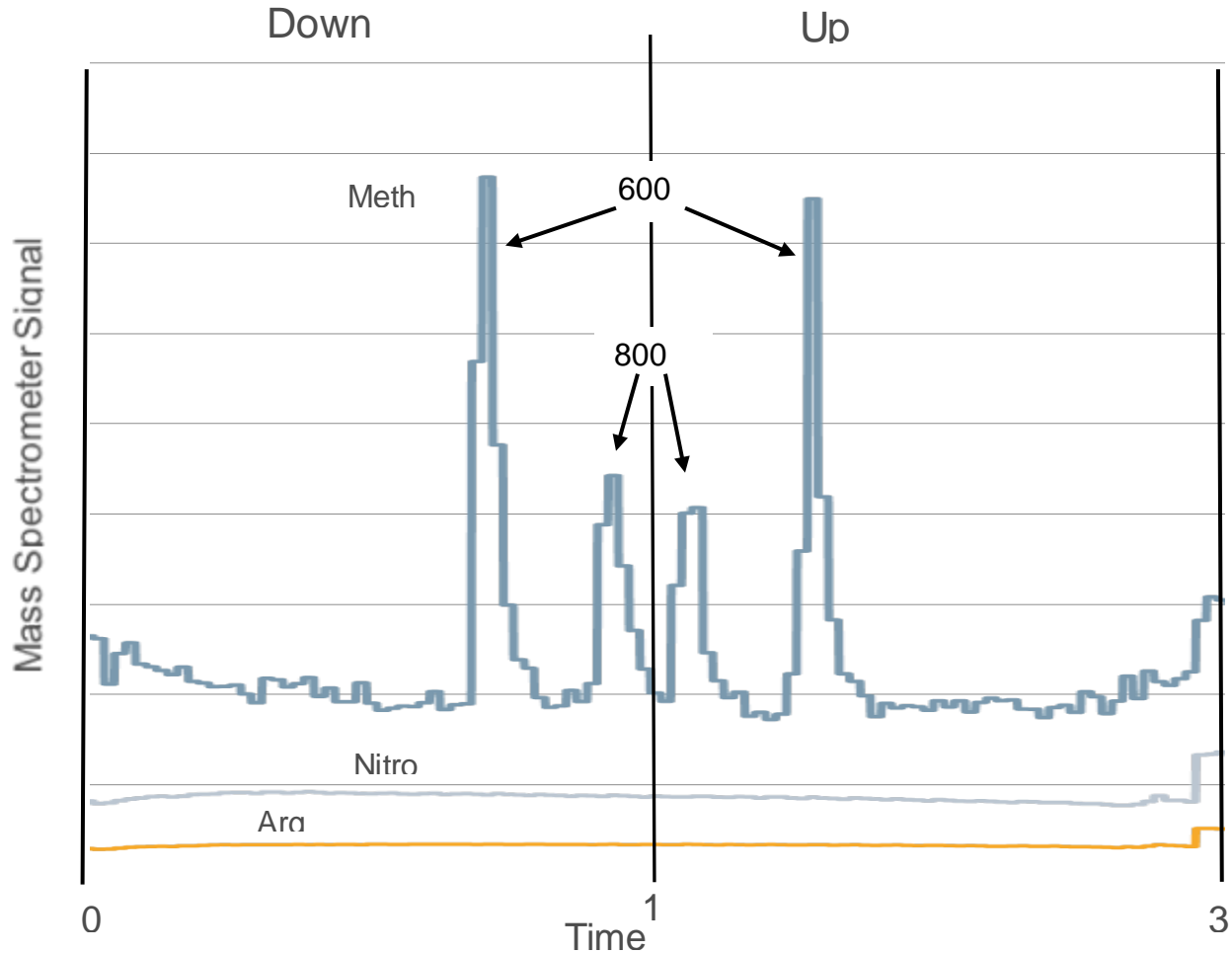


*Figure 17 Time series MIMS data for  $m/z$  15 (diagnostic for methane) for a vertical profiling cast at MC118. Also shown are concurrent data for nitrogen and argon. The time period for the down cast and up cast are noted on the figure.*

### Field Deployment and Modifications

The Lander was scheduled for the October 2011 cruise to test the mechanical systems and fiber optic communication. The Lander had been pressure tested in February 2011, but had not been previously tested in the marine environment. The Lander was transported to Cocodrie, LA on October 12, 2011 and loaded onto the LUMCON RV Pelican the following day. The RV Pelican departed the LUMCON facility around 9:00 pm October 13 and headed for the MC118 research area.

After several projects were deployed, the Lander was staged on the stern for pre-deployment preparations. The membrane introduction mass spectrometer (MIMS), installed inside the Lander frame was experiencing problems with a vacuum leak, so could not stream data during the deployment. Even though the MIMS could not be in full operational mode, it was decided to mount it on the Lander to test communication during deployment.

After the fiber optic cable splice was completed linking the Lander to shipboard computers, it was ready for deployment. The Lander was launched from the Pelican's stern at midnight, October 15 ready for testing (Figure 18). Floats were attached to the fiber optic cable to keep it buoyant during times when the Lander touched down on the seafloor (Figure 18).



**Figure 18. Lander deployment (left) and floats attached to fiber optic cable (right).**

Test filter samples were collected near the surface to ensure that the system was functioning after deployment. Since this was the first saltwater deployment for the Lander, care was taken to check the system for potential structural leaks which might cause system failure. Computer commands were sent to the Lander and four filters were collected. The pump was run for 15 minutes per filter which pumped an estimated 4 liters of water. The Lander was then lowered to 200 m and 400 m depth with four more filters per depth collected. The same procedure of 15 minutes pumping was conducted at both depths. The Lander was then lowered to 600 m depth. At this point, the pump did not appear to respond to surface commands giving concerns of a potential leakage. The Lander was returned to the surface and back on deck by 5:00 am. After removal of the pump housing, no water had been detected, but the pump's magnetic drive had been moved slightly by the housing flexing while under pressure. The drive was repositioned and the pump housing replaced. All systems were tested on deck and proved functional.

The Lander was redeployed by 6:00 am and lowered back to 600 m. The pump was tested and proved to be working properly. The Lander was then lowered to 800 meters with the pump still functioning properly. At this time, it was decided to lower the Lander to the seafloor to test filter collection while running video and lights. All communications with the Lander proved successful with the video, light, and pump responding as requested. Even though the MIMS was not producing water sample analysis, communication with the MIMS was successful throughout the deployment. During deployment, various pump speeds were tested which led to a successful maximum increase of water flow to one half liter per minute.



While deployed directly above the seafloor, the Lander visited 3 sites at MC118 (28° 51.4089'N/88° 29.5088'W; 28° 51.4214'N/88° 29.5894'W; and 28° 51.1877'N/88° 29.2056'W). The seafloor was viewed at each station with limited video saved on the computer hard drive. The longest video file saved was approximately 30 minutes and required 25 megabyte space on the hard drive. With a terabyte of storage space, considerable video can be collected with the Lander. The video gave sufficient detail that allowed the identification of shells, fish, starfish, and worms on the seafloor (Figure 19). Holes in the seafloor were noted as signs of biological activity or potential gas seepage. While the video was in operation, the filter pump was also employed effectively allowing the Lander to collect filter samples while viewing the seafloor. After approximately 9 hours of use, the Lander was back on deck by 10:00 am. Except as noted, all systems continued to function properly during the deployment.

As a result of the October 2011 deployment, several Lander functions were identified as needing attention. It was determined that the connection between the filter cartridge and the moveable cam connector was leaking allowing outside water to be pulled into the pump line. This lowered the suction to the filters keeping seawater from being pulled through the filters. A new connection was designed and constructed. The connection is now powered by hydraulic action using the filter pump as the hydraulic source. The redesign eliminated an electrical drive motor and mechanical interface and replaced it with a hydraulic system that is automatically controlled through the system software. The filter cartridge intake was also redesigned eliminating four ball valve intakes. In their place, a single centrally located reed valve was installed. This allowed for easier purging of distilled water prior to deployment and also allows free flowing input of saltwater into the filter assembly (Figure 20).



**Figure 19. Example of video collected during the Lander deployment.**

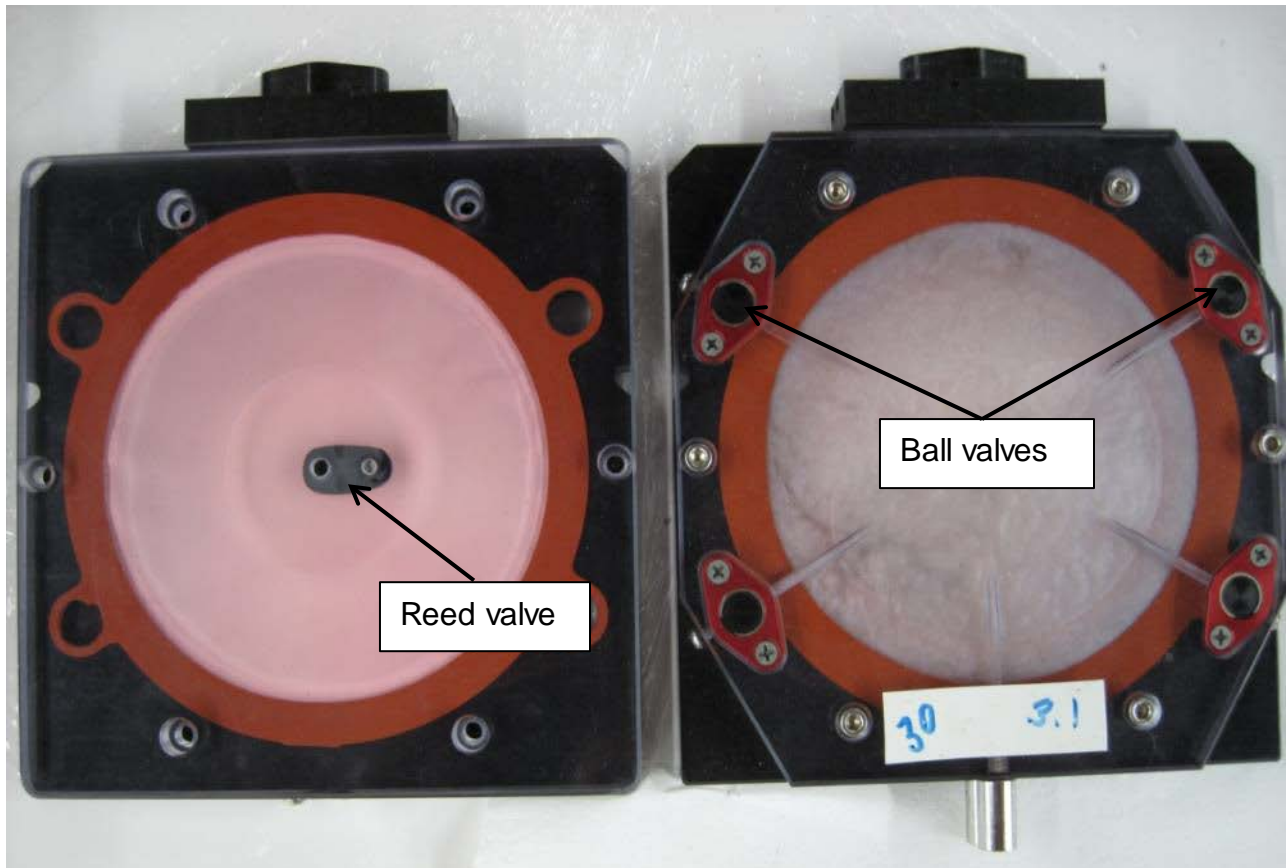


*Figure 20. Redesigned filter pack (left) and original filter pack (right).*

### **Final Deployment**

The final Lander deployment was scheduled for June 30 to July 3, 2013 on the RV Pelican. The UGA and SRI personnel arrived at the LUMCON facility in Cocodrie, LA on June 30 and loaded the Lander and MIMS onto the RV Pelican. Initial set up and testing of the Lander with the MIMS installed was completed prior to leaving the dock that evening. The Lander was deployed at MC118 by 1405 h on July 1 and lowered to 20 m for systems test. A fiber communication error occurred and the Lander was returned to the deck. The problem was a fiber jumper cable used in the electronics lab that routed the communications from one electrical component to another. After replacing a short section of fiber optical cable, communications to the Lander resumed.

The Lander was once again lowered to a depth of 20 m for communications tests. The MIMS was still experiencing a delay in communications which made it difficult to send and receive commands, but the decision was made to continue the deployment deeper. At approximately 100 m, all communications with the MIMS were lost so the Lander was returned to the deck for inspection. The MIMS battery pack had apparently failed causing the MIMS to shut down completely. The MIMS and battery pack were removed from the Lander for further inspection in the lab. The Lander was tested on deck and determined that no damage had occurred as a result of the MIMS battery failure. The Lander was again deployed at 1855 h and sent to the seafloor to start surveying. The Lander was set to hover

approximately 1.5 m above the seafloor, but due to seafloor elevation changes and sea conditions, the actual range off the seafloor varied between close contact to a couple of meters. The Lander was allowed to slowly drift over target areas while the position was tracked utilizing the USBL. During this deployment, the Lander video recorded two seafloor vents with bubbles streaming upward (Figure 21). Multiple filter samples were also collected as well as bulk water samples with the onboard rosette. The Lander continued to collect video and filter samples until it was returned to deck at 0600 h July 2. Once the Lander was on deck, the filter samples were removed from the Lander and packed into plastic vials and placed in liquid nitrogen for storage.

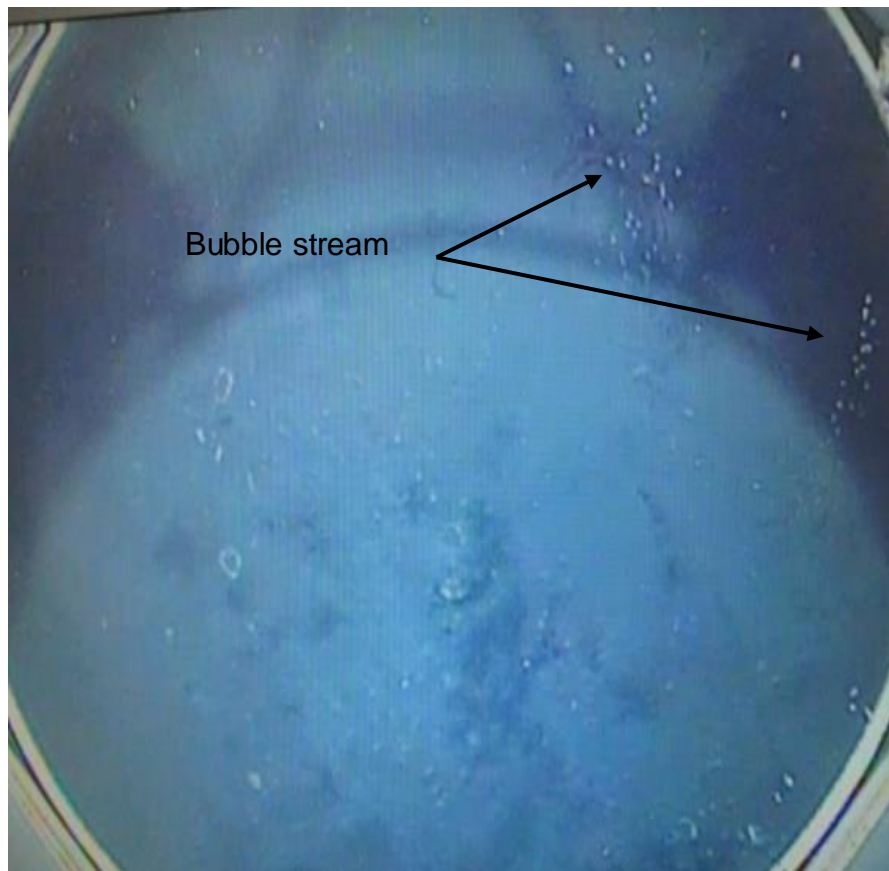


***Figure 21. Vent and bubble stream recorded during Lander deployment.***

While the Lander was deployed through the night of July 1 and into the early morning hours of July 2, the MIMS was tested first with a power supply and then with a backup battery pack. It was determined that no serious damage had occurred as a result of the battery failure and that the MIMS was readied for deployment. While another instrument was deployed on the seafloor, the MIMS was installed in the Lander and tested. All systems appeared to be working properly. The Lander was redeployed at 1300 h on July 2 and sent to the seafloor. During this deployment, the MIMS continuously streamed realtime data back to the surface and recorded two strong methane peaks (Figure 22). Mass spectrometry data, video and filter samples were collected for approximately two hours during the deployment. The Lander was returned to deck by 1500 h and prepared for transport back to Georgia.

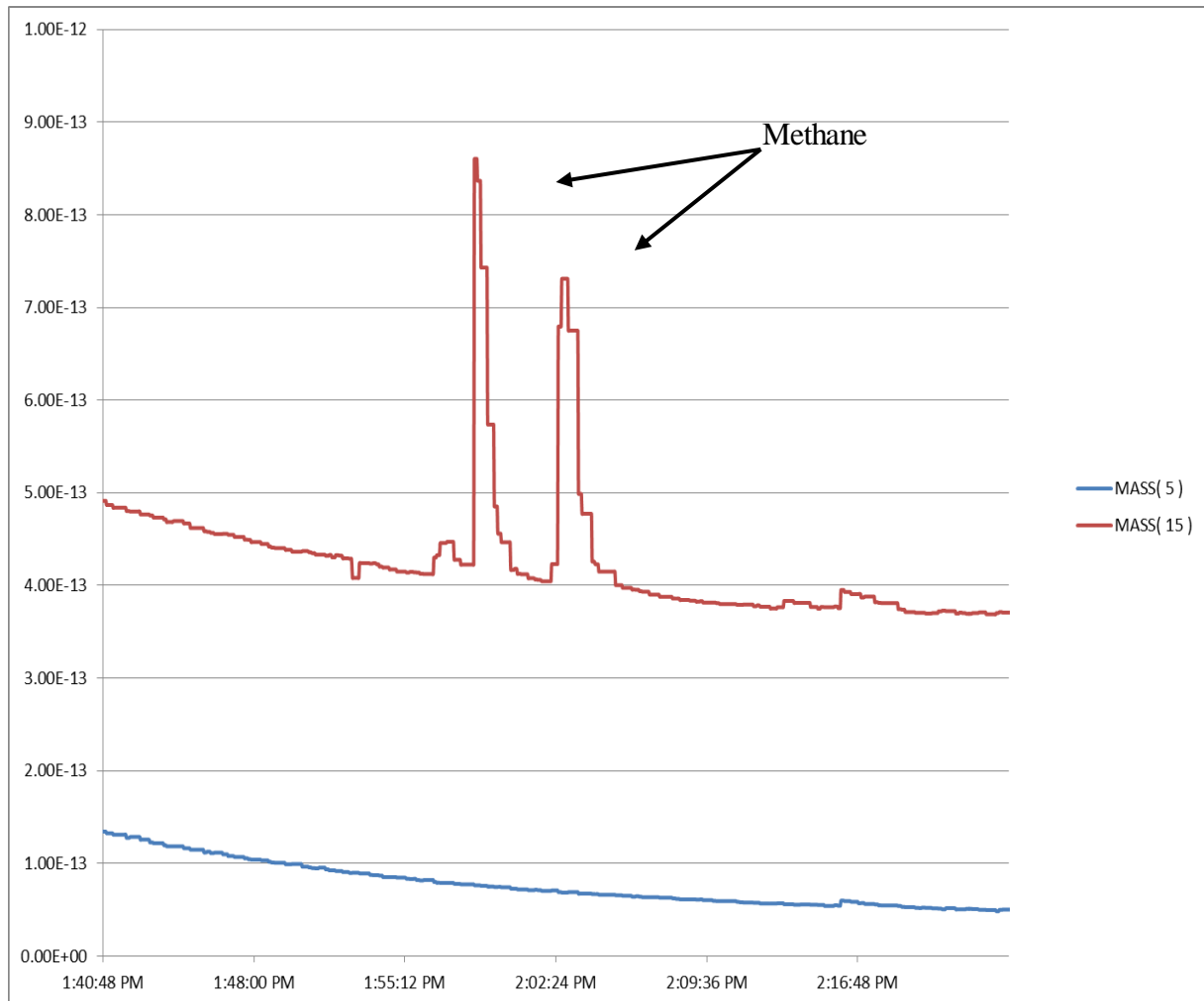


**Figure 22. Methane peaks detected by the MIMS during the final deployment.**

## DNA Isolation and Amplification on Filter Samples.

During the July 2013 cruise, 10 filter samples were collected. The sample numbers ranged from 1 to 16 with no samples collected on filters 9, 10 and 13. These filters were skipped due to the need to restart the Lander operational software. Once restarted, the software has a failsafe code to keep a filter from being used more than once. Station 0 was a deck test completed prior to launching the Lander. Table 1 lists the data related to sample collection and includes notes on the date, filter number, coordinates, depth, site identification and volume. The filters were collected while the Lander was slowly moving across sites at MC118, so the coordinates represent a general starting location.

Bulk DNA was extracted from 10 filter samples using FastDNA SPIN Kit (MP Biomedicals, USA) in accordance with the manufacturer's instructions. Bacterial 16S rRNA gene fragments were amplified using primers 27f (5'-AGA GTTGATCCTGGCTCAG-3') and 1492r (5'-GGTTACCTTGTACGACTT-3'). The conditions for amplification of archaeal 16S rRNA genes were as follows: initial denaturation at 95°C for 3 min; 30 cycles of denaturing (1 min at 94°C), annealing (1 min at 55°C), and extension (1.5 min at 72°C); and a final extension at 72°C for 10 min. The PCR products were checked with agarose gel electrophoresis to determine the presence and size. The results showed that bacteria were determined in filters MC118-5, MC118-6, MC118-8, MC118-11 and MC118-12. It is undetermined that these bacteria are related to the biogeochemistry processes. Bacterial clone libraries will be constructed from these samples to learn more from them.

**Table 1. Filter samples collected during the July 2013 cruise.**

*Note: Samples marked in bold had bacteria present*

Filter	Date	Latitude (Deg Min Sec)	Longitude (Deg Min Sec)	Depth (meter)	Site ID	Volume (liter)
0	7/1/2013				Deck test	0.07
1	7/1/2013	28 51 08.77	88 29 33.78		20m	8.56
2	7/1/2013	28 85 18.12	88 29 44.3	20	20m	4.29
<b>5</b>	<b>7/1/2013</b>	<b>28 51 6.44</b>	<b>88 29 36.82</b>		<b>SWCrater</b>	<b>10.37</b>
<b>6</b>	<b>7/1/2013</b>	<b>28 51 12.86</b>	<b>88 29</b>			<b>6.52</b>
7	7/1/2013	28 51 12.86	88 29		SWCrater	48.75
<b>8</b>	<b>7/1/2013</b>	<b>28 51 12.86</b>	<b>88 29</b>	<b>830</b>		<b>21.02</b>
9	7/1/2013				No sample	
10	7/1/2013				No sample	
<b>11</b>	<b>7/2/2013</b>	<b>28 51 39.01</b>	<b>88 29 43.72</b>	<b>881</b>		<b>20.72</b>
<b>12</b>	<b>7/2/2013</b>	<b>28 51 39.01</b>	<b>88 29 37 22</b>	<b>881</b>		<b>20.74</b>
13	7/2/2013				No sample	
14	7/2/2013	28 51 27.56	88 29 05.72	881	SE crater	48.03
15	7/2/2013					31.85
16	7/2/2013	28 51 19.32	88 29 40.67		Bravo Vent	21.23



## Conclusion

The MIMS equipped Lander has been successful with surveying the seafloor of the Gulf of Mexico. During the Lander deployment, scientists were able to identify multiple methane vents on the seafloor utilizing streaming mass spectrometer chemical data and visual observation from the onboard video. Benthic organisms and geological features can also be identified as part of a Lander survey. The Lander was also able to collect filter and bulk water samples at the same time the MIMS and video data were streaming shipboard. Real-time data are now readily available to researchers mapping unexplored seafloor. Marine scientists can now effectively explore the seafloor prior to deploying instrumentation.

## TASK 6: Quantification of Seep Emissions by Multibeam Sonar at MC118.

(Subcontractor: University of California – Santa Barbara; Ira Leifer, PI)

### Accomplishments:

1. Bubble model
2. Analysis of HYFLUX data demonstrating that methane from MC118 can reach the sea surface.
3. Demonstration of a sonar rotator in the East Siberian Arctic Sea
4. Demonstration of a sonar rotator at MC118
5. Collection of transcontinental data in support of the method

### Introduction

Atmospheric methane, CH<sub>4</sub>, is an important greenhouse gas at least 20 times more potent than carbon dioxide, CO<sub>2</sub> [Khalil and Rasmussen, 1995] whose atmospheric mixing ratio has more than doubled during the last century [Rowland, 1985]. CH<sub>4</sub> has anthropogenic (360-430 Tg yr<sup>-1</sup>; 1 Tg = 10<sup>12</sup> g) and natural sources (160-240 Tg yr<sup>-1</sup>) of biologic or geologic origin [IPCC, 2007; K. A. Kvenvolden and Bruce W. Rogers, 2005]. Ranges are large, because the quantification of CH<sub>4</sub> budget sources and sinks has numerous problems [Reeburgh, 2003].

Natural geologic sources include marine seepage associated with hydrate dissociation and leakage from deeper hydrocarbon marine and terrestrial reservoirs. Recently, [Keith A. Kvenvolden and Bruce W. Rogers, 2005] estimate that the natural geologic source to the atmosphere is 45 Tg yr<sup>-1</sup>. Global emission estimates for marine seeps (neglecting methane hydrates) are ~10-30 Tg yr<sup>-1</sup> [Kvenvolden et al., 2001] or ~13% of natural emissions. The estimate is poorly constrained because few quantitative seep emission rates have been published, e.g., Hornafius et al. [1999], despite the presence of seeps on all continental shelves [Hovland et al., 2002]. Moreover, these estimates do not include seepage emissions from submerged permafrost and hydrates in the Arctic Ocean [N. Shakhova et al., 2010], which are predicted to increase as the Arctic Ocean warms [Natalia Shakhova et al., 2013].

Complicating estimation is the well known temporal and spatial variability in emissions. The Coal Oil Point (COP) seep field is one of the best studied areas of seepage releasing order 10<sup>5</sup> m<sup>3</sup>/day methane from ~ 3 km<sup>2</sup> of seabed. Studies of the COP seep field have demonstrated emission variability on time scales from seconds to decades [Leifer and Boles, 2005a; b; Quigley et al., 1999] including documenting large transient releases [Leifer

and Boles, 2005b; Leifer et al., 2006]. Consideration of two decades of air quality data allowed Bradley et al. [2010] to identify large scale, seep field-wide changes on seasonal to decadal times, but also smaller scale changes over years. For example, one of the major mega-seeps ( $> 0^6 \text{ L dy}^{-1}$ ) in the inshore seeps, termed Coal Oil Point seep, disappeared for several years, until then three new seeps appeared in the area, named Trilogy seeps. Trilogy and the Coal Oil Point seep shared common geologic structures [Leifer et al., 2010].

Thus, the critical need that work on this study has focused on is increasing our capabilities to quantify seabed methane emissions, a problem that has two components – spatial and temporal. Although there remains a clear need for additional survey measurements, the inherent variability in these geologic systems demonstrates that annual extrapolation from a the short-term data generally collected during an expedition likely is not robust. Thus, this study focused on demonstration of an approach to provide long-term monitoring data using a benthic lander platform to support a sonar rotator and key ancillary equipment, including demonstration of using a In Situ Mass Spectrometer for dissolved seep plume component detection and characterization.

### **Bubble and bubble plume transport processes**

The contribution of these seafloor sources to atmospheric  $\text{CH}_4$  is uncertain due to the likelihood that some or all of the emitted  $\text{CH}_4$  dissolves into the ocean during transit from the seabed to the sea surface [Clark et al., 2003; Heeschen et al., 2003; Leifer and Judd, 2002]. In particular, where seeps emit single bubbles, it is highly likely that with the exception of very shallow seeps (order 10 m), all the released methane dissolves subsurface [Leifer and Patro, 2002]. The fate of  $\text{CH}_4$  escaping from below the winter mixed-layer is dissolution followed by microbial oxidation because the deep-sea time-scale for microbial  $\text{CH}_4$  oxidation is  $\sim 1$  yr [Watanabe et al., 1995], significantly shorter than the time scale to diffuse to the winter mixed-layer,  $\sim 50$  yr [G. Rehder et al., 1999]. Note, the criteria for seep/hydrate  $\text{CH}_4$  to affect atmospheric budgets is transport to the winter-mixed layer, which can be 100-200 m deep in many oceans, rather than the sea surface.  $\text{CH}_4$  in the winter-mixed layer will air-sea exchange to the atmosphere on time scales significantly faster than microbial degradation time scales.

Generally, seeps bubbles escape as bubble plumes [Leifer, 2010]. Bubble plumes have unique synergistic group properties, including enhanced aqueous concentrations relative to the surrounding water [Leifer et al., 2006], and vertical fluid motion, the upwelling flow, which transports methane enhanced water [Leifer et al., 2009]. These plume processes enhance bubble survival and vertical methane transport both for direct bubble-mediated transport, and indirectly, by transport by the upwelling flow.

The observation of Solomon et al. [2009] of a methane layer at the thermocline above Bush Hill (GC-185, 550 m) could not be explained by individual bubble transport. Although MacDonald et al. [2002] had proposed oil coatings to explain acoustic observations of methane bubbles rising from 550 m to the thermocline, this would simply support a less steep exponential decreasing methane profile. The Solomon et al. (2009) data required bubble plume processes, specifically related to the upwelling flow.

### **Hydrates and Bubbles**

The importance of hydrate skin formation to bubble methane transport is significant. Rehder et al. [1999] showed significantly enhanced bubble lifetime (slower dissolution rate) within the hydrate stability field. Specifically bubble dissolutions were well simulated where

dissolution was controlled by hydrate solubility rather than free gas solubility. Hydrate skins are critical to explaining sonar data showing natural seepage bubbles rising hundreds to order kilometer [Granin et al., 2010; Greinert et al., 2006; Sauter et al., 2006], or even to more than two kilometers [Spiess and Artemov, 2010].

Within the hydrate stability field (HSF), methane and/or other natural gas compounds smaller than pentane combine with water to produce a metastable ice where the methane is trapped in a water molecule cage, allowing 164 volumetric compression compared to the gas phase at STP [Beauchamp, 2004]. There are two natural hydrate forms, Type I hydrates (46 water molecules), which can contain methane and ethane (as well as acetylene and ethylene), and Type II hydrates (136 water molecules) which can contain large molecules like propane, butane, and benzene [Sloan and Koh, 2008]. The HSF depth depends on the temperature and pressure and hydrate type. Type II hydrates are stable to far shallower depths, greatly enhancing bubble survival.

More recent data collected under the HYFLUX study extended the GC185 findings of Solomon et al (2009) to MC118 for seepage at 890 m. Specifically, bubbles were tracked across much of the water column by ROV, and water samples from down-current of the rising bubble plumes found higher hydrocarbons in the upper water column, demonstrating that Type 2 hydrate processes were involved [Texas\_A&M, 2011], and that plume and hydrate processes can allow methane from hydrate deposits in water approaching 1 km deep can reach the atmosphere, contributing to atmospheric budgets.

### **Bubble model**

To understand better the importance of these processes to bubble survival, a numerical bubble model was improved to incorporate Type 2 hydrate effects. The model simulates deep-sea processes including hydrate skin effects based on analysis of single-bubble release data, depth-dependent solubility, compressibility, and enhanced bubble density that slows bubble rise (note compressibility increases bubble density), and is described in Rehder et al. [2009]. Because the parameterization of individual bubble gas exchange depends on the rise velocity, increased density affects the gas exchange parameterization; however, second order effects on gas exchange are not considered, primarily due to an absence of literature. A significant improvement over the model as described in Rehder et al. (2009) is the incorporation of temperature profiles in the calculation of depth-dependent solubility and diffusivity as well as water column properties affecting bubble rise and transfer, like water viscosity and density. Whereas the deep sea is approximately isothermal over rises of hundreds of meters, this clearly is inappropriate for bubbles reaching the thermocline from 900-m deep.

The model first loads physical, fluid dynamical, plume, and chemical parameters (see model flowchart, **Fig. 1**). The model first reads (a) a wide range of parameters, separated into those related to flow, those related to the simulation, including the bubble size distribution to use and temperature profile, and those related to bubble properties, such as gas composition, surfactant condition, hydrates, and depth dependent solubility. An example parameter file for a MC118 simulation is shown in **Fig. 2**. The model then initializes arrays for storing simulation results. Next, the model calculates lookup tables that are used to speed the numerical integration. Lookup tables (b) are calculated for fluid flow properties, like upwelling flow, as well as bubble parameters like rise velocity, and gas properties like solubility and water density with respect to depth.

The model then simulates a bubble (c-e) by solving the coupled differential equations until convergence or dissolution or surfacing including imposed fluid motions like the upwelling

flow as well as buoyant rise. A second-third order Runge-Kutta approach (a leap frog approach tends not to converge numerically as this equation set is stiff) with tolerances chosen based on parameters affecting bubble evolution, such as bubble size and depth [Leifer et al., 2006; Gregor Rehder et al., 2009].

Simulation output is interpolated to a smooth depth grid (f), and the mass flux (to the water column) for the bubble (or plume) at each depth is calculated. The bubble simulation including lookup table recalculation is repeated for bubbles spanning a range of size classes that is user specified, or determined from the bubble plume specified. Once all bubble size classes in the plume have been simulated (which can be a mono-disperse bubble plume), the dissolution rate of each bubble class is combined with the bubble class population to calculate fractional molar loss and retention for each gas in each size class. These values then are integrated to estimate total plume mass loss and the size distribution as a function of depth. At this point, the simulation can display and archive the results; however, the calculated concentration profile then can initialize a resimulation of the bubble plume. This resimulation cycle then is continued iteratively until convergence. The entire model is implemented in Matlab (Mathworks, MA).

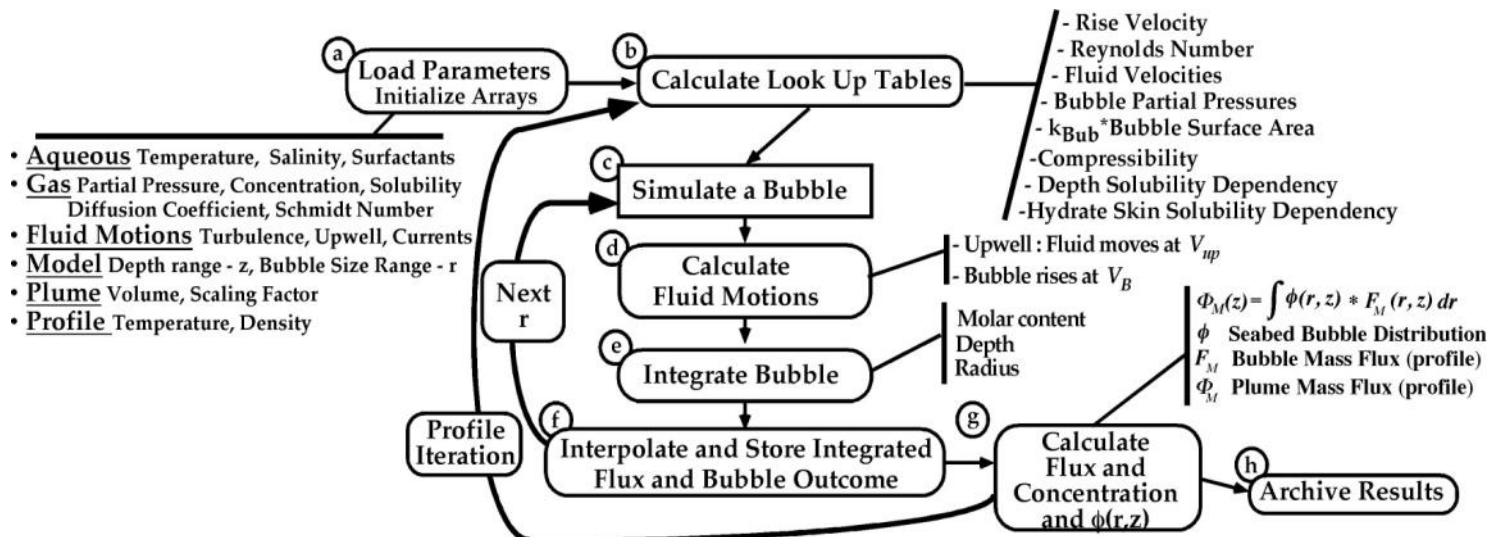


Fig. 1. Bubble model flowchart. Updated from Rehder et al. (2009).

<b>r9004 RPar9007 GPar9004 FlwPar9000</b>	<b>Model: Leifer</b>	<b>VB: Leifer&amp;Patro</b>	<b>Ver: 767</b>	
<b>Bubbles :</b> uniplume	<b>Tip Rate:</b> 30 s	<b>Turb Vel1 :</b> OFF	<b>Turb Len1 :</b> OFF	
<b>Source :</b> Submerged	<b>Atm Pres:</b> 1 atm	<b>Turb Vel2 :</b> OFF	<b>Turb Len2 :</b> OFF	
<b>Prof Scale:</b> *1	<b>Surfact :</b> 100 %	<b>Lang X-Vel:</b> OFF	<b>Lang Width:</b> OFF	
<b>Plum Scale:</b> 100 %	<b>Oiliness:</b> Off	<b>UpWell Vel:</b> 10.00 cm/s	<b>UpWell Tau:</b> 9999.0 s	
<b>Model Area:</b> 1 cm2	<b>Salinity:</b> 35 ppt	<b>Inject-Vel:</b> OFF	<b>Inject Tau:</b> OFF	
<b>Model Dep :</b> 890.0 m	<b>Temp :</b> mc118			
<b>Dens Corr :</b> On	<b>Compress:</b> On	<b>Depth Sol :</b> On	<b>Hydrate :</b> Typ1	
	<b>CH4 evasion</b>	<b>ETH evasion</b>	<b>PRO evasion</b>	
<b>Init. Conc :</b> 1.6400e-07 mol/l	4.5700e-09 mol/l	4.5700e-09 mol/l	1.2700e-09 mol/l	
<b>Part. Press:</b> 0.9324 atm	0.0412 atm	0.0412 atm	0.016 atm	
<b>Sc Number :</b> 1702.7881	2101.1029	2101.1029	2631.2376	
<b>Diff Coeff :</b> 8.70e-06 cm2/s	7.05e-06 cm2/s	7.05e-06 cm2/s	5.63e-06 cm2/s	
<b>Solubility :</b> 0.039319 atm/atm	0.02488 atm/atm	0.02488 atm/atm	0.017799 atm/atm	
<b>Henry :</b> 570.0777 atm/mol/l	900.9141 atm/mol/l	900.9141 atm/mol/l	1259.3 atm/mol/l	
<b>Satur Conc :</b> 1.64e-03 mol/l	4.57e-05 mol/l	4.57e-05 mol/l	1.27e-05 mol/l	
	<b>BUT evasion</b>	<b>PEN evasion</b>	<b>O2 invasion</b>	
<b>Init. Conc :</b> 6.1200e-10 mol/l	1.9700e-10 mol/l	1.9700e-10 mol/l	2.3750e-04 mol/l	
<b>Part. Press:</b> 0.0116 atm	0.0058 atm	0.0058 atm	1e-06 atm	
<b>Sc Number :</b> 2862.2297	3156.2088	3156.2088	1453.6694	
<b>Diff Coeff :</b> 5.18e-06 cm2/s	4.69e-06 cm2/s	4.69e-06 cm2/s	1.02e-05 cm2/s	
<b>Solubility :</b> 0.011834 atm/atm	0.0076038 atm/atm	0.0076038 atm/atm	0.034241 atm/atm	
<b>Henry :</b> 1894.1 atm/mol/l	2947.8 atm/mol/l	2947.8 atm/mol/l	654.6188 atm/mol/l	
<b>Satur Conc :</b> 6.12e-06 mol/l	1.97e-06 mol/l	1.97e-06 mol/l	1.53e-09 mol/l	
	<b>N2 invasion</b>			
<b>Init. Conc :</b> 4.7700e-04 mol/l				
<b>Part. Press:</b> 4e-06 atm				
<b>Sc Number :</b> 1640.8983				
<b>Diff Coeff :</b> 9.03e-06 cm2/s				
<b>Solubility :</b> 0.016516 atm/atm				
<b>Henry :</b> 1357.1 atm/mol/l				
<b>Satur Conc :</b> 2.95e-09 mol/l				

**Fig. 2. Sample simulation parameter including Type 1 hydrates and a 10 cm/s upwelling flow and the MC118 temperature profile.**

### MC118 bubble emissions and model predictions

Bubble size and seep depth are critical parameters for predicting the fate of seabed methane bubbles, and therefore bubble size distribution measurements are critical. Video from MC118 was analyzed and the bubble emission size distribution derived. The overall size distribution showed similarities both to size distributions reflective of vents with single bubble emissions (**Fig. 3**, at 2483  $\mu\text{m}$  equivalent spherical radius), and a broad size distribution characteristic of a bubble plume with breakup (major plume), with a power law exponent of 0.79. A secondary poorly characterized single bubble vent that produced large bubbles is with a fundamental radius of  $\sim 4900 \mu\text{m}$  was identified as well, but could be simply from poor resolution of the fall-off distribution of the major bubble plume. Bubble size distributions were calculated as in Leifer [2010]. The 2500- $\mu\text{m}$  equivalent spherical radius emission mode contributes approximately equally to two other larger emission modes. Overall, this plume had a flux of  $10.25 \text{ (cm}^3 \text{ s}^{-1}\text{)}$ .



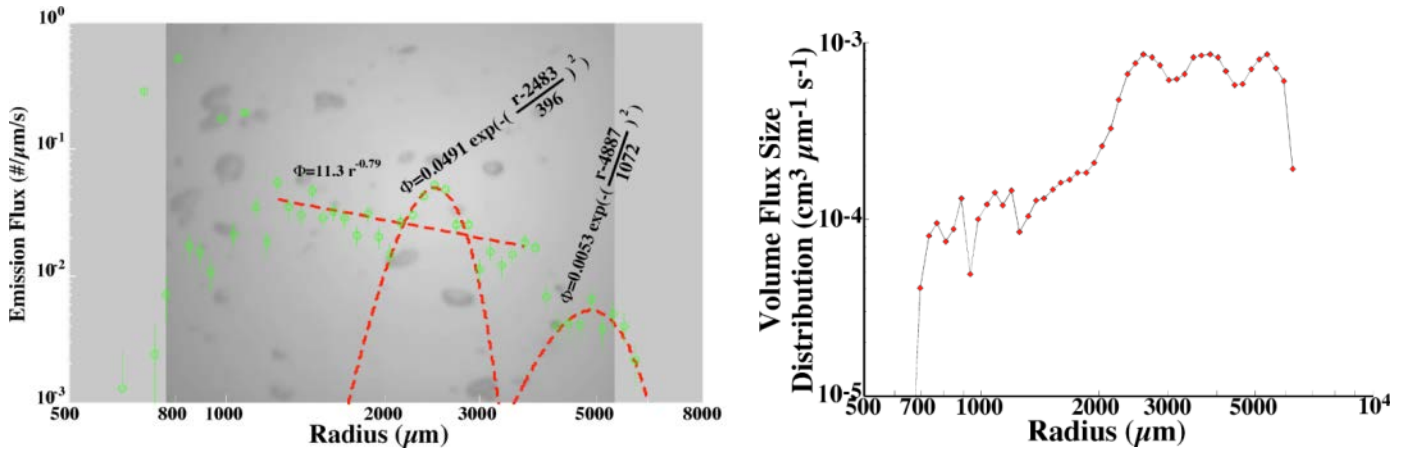


**Fig. 3. A) Bubble emission size distribution from MC118 and plume image. B) Volume emission size distribution from MC118 bubble plume.**

Type II hydrate solubility depends on composition, pressure, and temperature. Infochem simulations were conducted for four C1-C3 mixtures in ratios of 1:0:0; 0.95:0.025:0.025; 0.9:0.05:0.05; and 0.8:0.1:0.1 for methane:ethane:propane (**Fig. 4**). Calculation of hydrate solubility (Type 1 or 2) depends on the temperature profile (**Fig. 5A**).

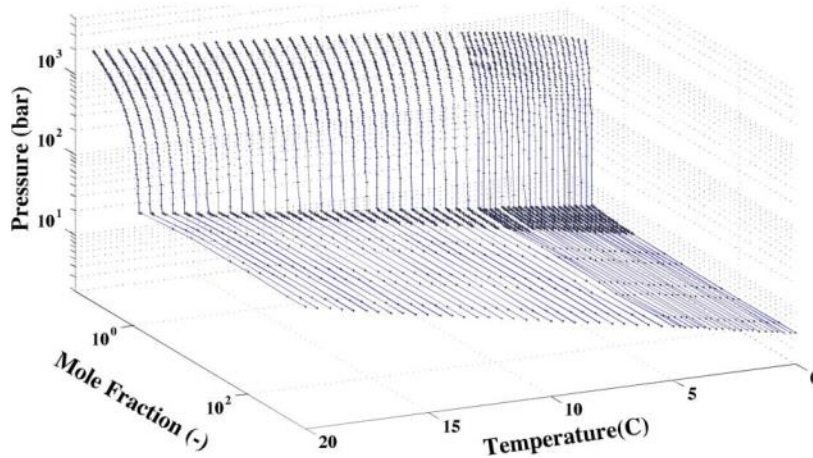


**Fig. 4. Mole fraction equilibrium with respect to mole fraction and temperature for a 80:10:10 mixture of methane, ethane, and propane.**

Type II hydrates are stable to far shallower depths (~ 250 m) than Type I hydrates (~500 m) at MC118 (**Fig. 5**). For Type II hydrates, the solubility is decreased significantly compared to Type I hydrates (**Fig. 5B**). Because hydrate solubility is for a cage, and Type II hydrates include a range of gases trapped in its cages, the solubilities of the individual gases converge to that of a single value within the hydrate stability field. In the model this is implemented as a smooth transition between the non-hydrate and hydrate solubilities (**Fig. 5C**).

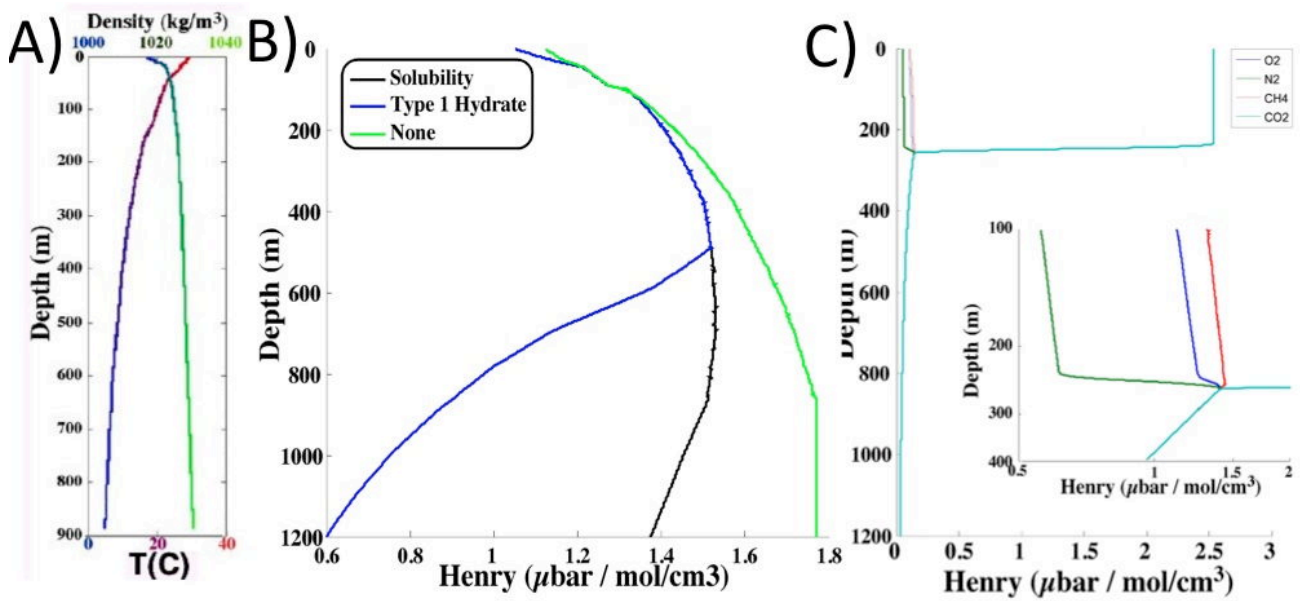


Fig. 5. A) density and temperature profile for MC118. B) Calculated methane solubility neglecting pressure effects (none), with pressure effects, and for a Type I hydrate skin. C) Type II hydrate solubility for a C<sub>1</sub>-C<sub>3</sub> alkane mixture.

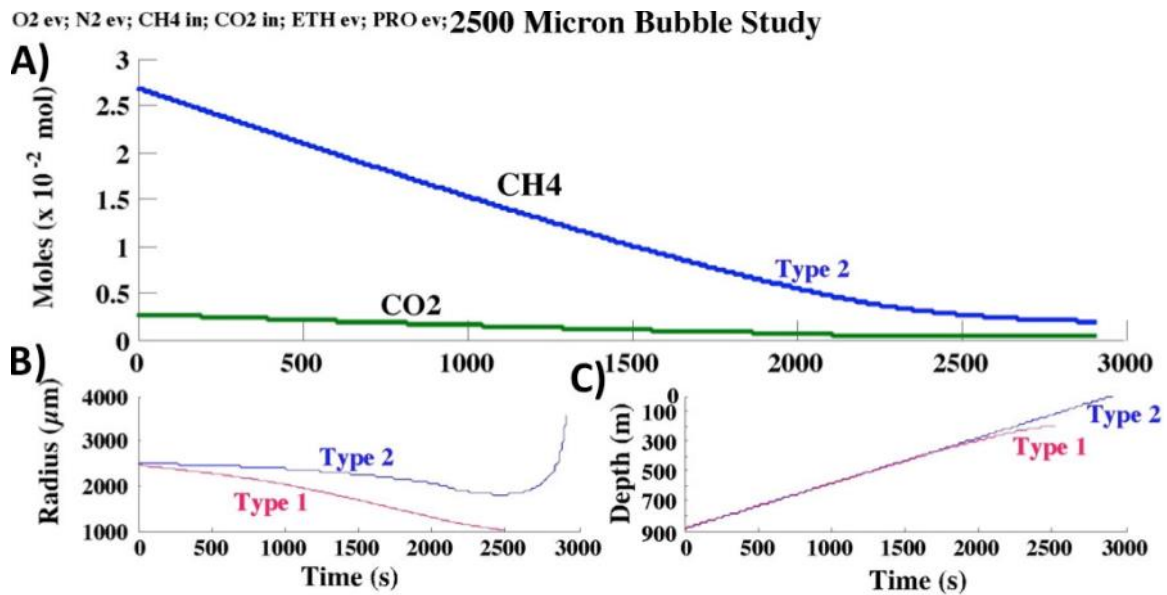
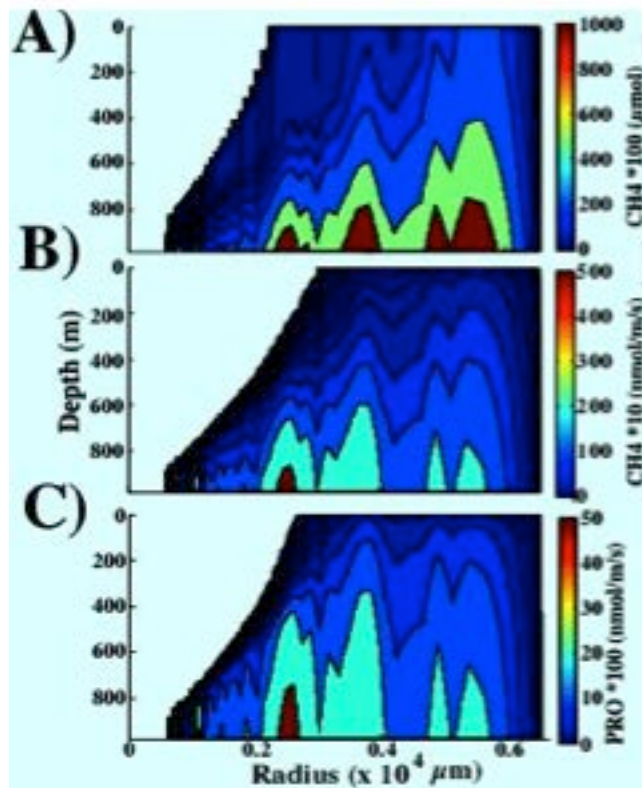


Fig. 6. Single bubble simulation for Type I and Type II hydrate skins.

A simulation of a single 2500- $\mu\text{m}$  radius bubble (Fig. 6) showed significantly enhanced bubble survival and also methane bubble content to the upper water column (Fig. 7). Thus, the model shows that hydrate processes were critical to explaining data showing methane and higher n-alkanes in the upper water column [Evan Solomon et al., 2013].



*Fig. 7. Predicted Type 2 bubble plume methane A) transport and B) dissolution and C) propane dissolution for the measured bubble size distribution (Fig 3).*

### **Sonar Benthic Lander**

Two benthic landers were constructed and deployed as part of the scope of this project. The first, featured a project aquired DeltaT (Imagenex, British Columbia, Canada) multibeam sonar and a Sidus (San Diego, California) rotator to replace a defective one built by the UCSB electronics shop. This benthic lander could support a single Deepsea battery and a CTD. The second benthic lander used a much larger aluminum frame that supported both the DeltaT, a Reson 7125 Multibeam system, powered by up to seven deep sea batteries, and capable of supporting a range of instruments including CTD, In Situ Mass Spectrometer, etc. The lander, batteries, and associated instrumentation, (~\$500,000 of equipment) were loaned to the project by Dr. Leifer's company, Bubbleology Research International. The benthic lander was constructed with commercial support for deployment in the North Sea.

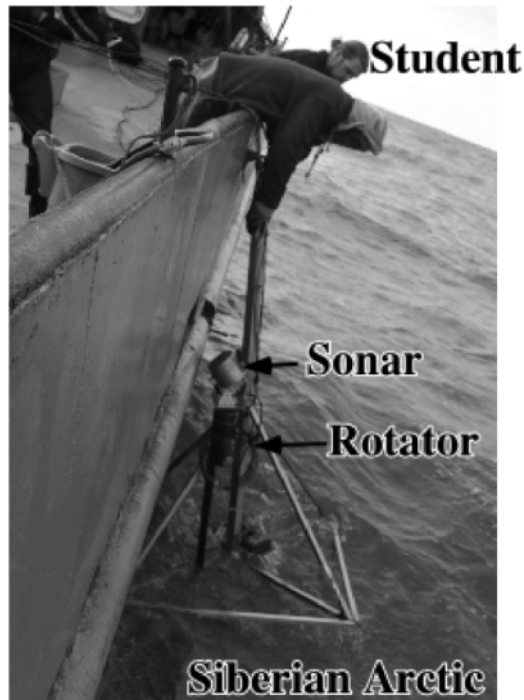


*Fig. 8. Photo of cabled, Siberian Arctic Ocean sonar rotator deployment to investigate methane bubble emissions from submerged permafrost and hydrates bubbles (depth ~20 m) in Aug. 2009.*

### **Small Benthic Lander**

Development of the scanning multibeam-sonar continued. The Imagenex multibeam operates in vertical fan mode (**Fig. 8**), scanning a complete 3D volume up to 50-m radius. A new Sidus rotator (value \$5000) was donated for the effort by the University of Alaska, Fairbanks, and can rotate as fast as  $10^{\circ} \text{ s}^{-1}$ . The scanner can be cabled to the sea surface through a 100-m or through a 300-m cable (via underwater housing). Cabled deployment allows real-time adjustment of sonar parameters (range, gain, ping rate, etc.) and scanner parameters (speed, angular limits). Sonar direction is recorded digitally in a separate housing. The lander can be deployed by dropping it over the side from an A-Frame, using the sonar to position the lander relative to the bubble stream, then leap frogging the system closer.

The sonar was deployed in the Coal Oil Point seep field at Shane Seep for in situ field calibration tests (**Fig. 9**). To better plan the benthic lander deployment, a multibeam sonar survey was conducted using a pole mount, fabricated for mounting the Imagenex multibeam sonar on a small (7 m) university Boston Whaler. The Shane Seep Area was surveyed on March 2, 2009. There were several purposes of this mission. First, it was critical to confirm that the noise problems of the earlier version of the units were solved. Previous versions suffered significant noise if the boat was motored at faster than 7 knots, which prevented collection of useful data from deeper than 20 m. Data were acquired without significant noise from depths to 50 m, although for greater range, there were noise issues.

Shane Seep is in water 22 m deep (**Fig. 10**) and is comprised of numerous vents along a WSW-ENE trend line. Also revealed by the dense multibeam survey dataset (80% overlap) were subtle structures along an east-west trend.

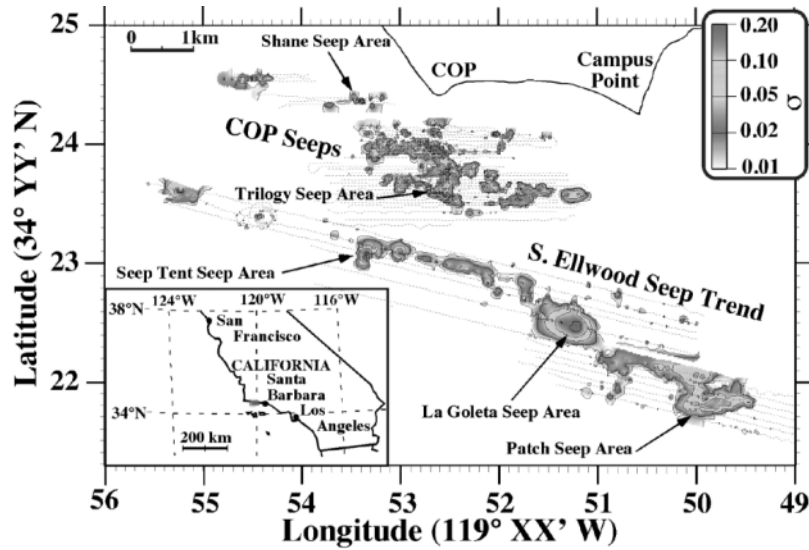


Fig. 9. Water-column, bottom-bounce normalized sonar return, the Coal Oil Point (COP) seep field, Santa Barbara Channel, California. Seep names are informal. Contours and colorbar on figure. From [Leifer et al., 2010].

□, amplitude

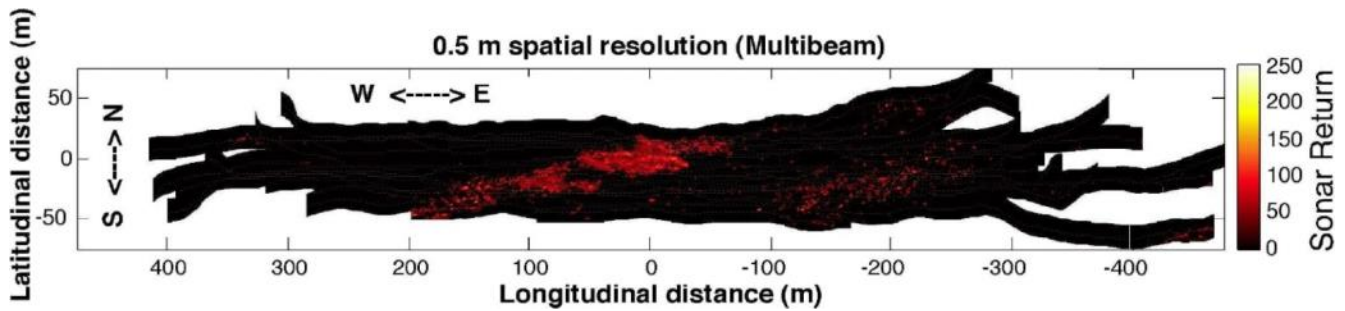
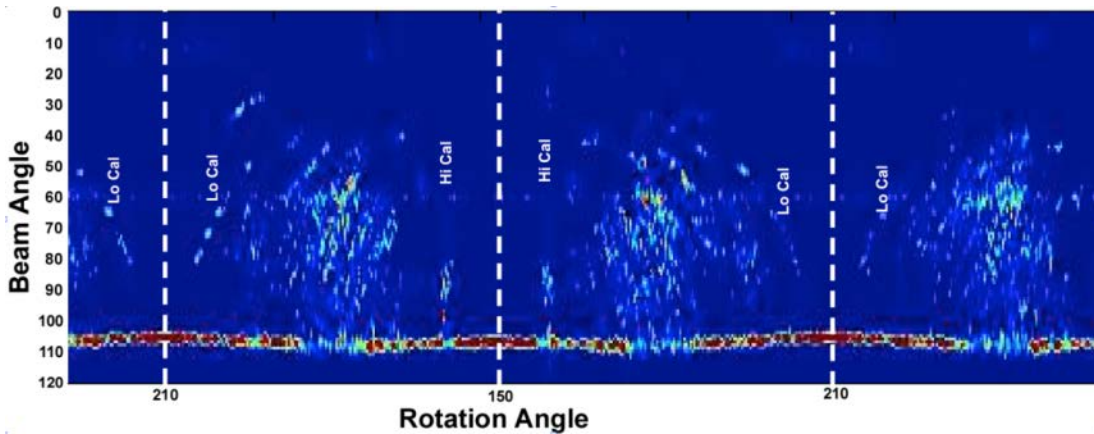


Fig. 10. Multibeam sonar return map for a 2-meter thick, bottom-following window from 20 transects (dashed line) of the Shane Seep area. Sonar survey lines had 80% overlap.

During the Shane Seep deployment, two calibration flows also were deployed that could be controlled from the boat by a rotameter manifold. The calibration flows were deployed by scuba divers at the edge of an area of active seepage at Shane Seep (Fig. 11). In different rotations, variations can be seen in the seepage strength.





**Fig. 11. Shallow water, Coal Oil Point (COP) seep field deployment showing a spherical (time) slice (more of a spherical “onion like” layer) at Shane Seep in 20m water. Full data include time slices with 50cm resolution. High and low calibration flow bubble plumes are identified in the data.**

A laboratory study was conducted in a large (5 m x 40 m x 3 m deep) tank to understand how to relate field sonar return with flow rate (**Fig. 12**). The laboratory experiment used controlled air flows and allowed the sonar to rotate past the engineered plume. The integrated sonar return in the plume was then related to the flow, showing that increased flow rate correlated with increased sonar return. However, the data also indicated complexity in that the sonar return increased with height. These laboratory air bubbles do not change size significantly from dissolution or from hydrostatic pressure change in this shallow tank. As a result, the increase in sonar return arises from changing plume geometry—expansion, implying that for dense bubble plumes, multiple scattering prevents a unique derivation of flow rate based on sonar return.

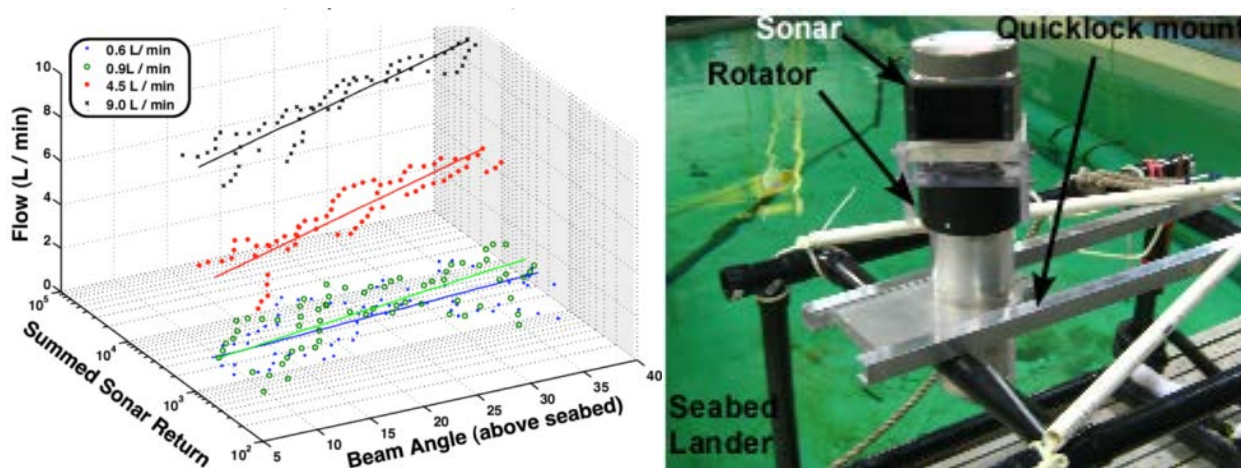


**Fig. 12. Left. In situ field sonar calibration of Coal Oil Point seep field, sonar rotator data (Fig. 11). From Natalia Shakhova et al. [2013]. Right. Image of test lander for tank calibration experiment.**

Four dimensional (time-varying) mapping of all scatterers in the scan volume can be derived from the sonar data with 20 to 50 cm spatial precision or better, depending upon range

setting (**Fig. 11**). An example rotator dataset from a deployment in the Trofimov Seep Field, East Siberian Arctic Sea (**Fig. 14**) is shown in **Fig. 13**. See **Fig. 14** for location. The 8-bit dynamic range limitation of the Delta T is compensated for by a technique developed for this project, termed *multiping*. In multiping applications, the gain of each sequential ping cycles from 0 to 20 db, greatly expanding the dynamic range. Cycling is fast, completing an intensity cycle in less than 200 ms during a 2009 East Siberian Arctic Sea deployment (**Fig. 13**). The data show bubble plumes deviating significantly from straight rise due to a complex vertical current profile including distinct surface and benthic currents.

In addition, extensive East Siberian Arctic Sea (ESAS) survey data were collected and interpreted in terms of bubble emissions (**Fig. 14**). The survey data were central to the MS Thesis of Chris Stubbs [Stubbs, 2010], while the sonar rotator data is published in a Nature Geoscience manuscript [Natalia Shakhova *et al.*, 2013] deriving a new, and significantly larger estimate of total methane emissions from the shallow East Siberian Arctic Sea arising from submerged permafrost.

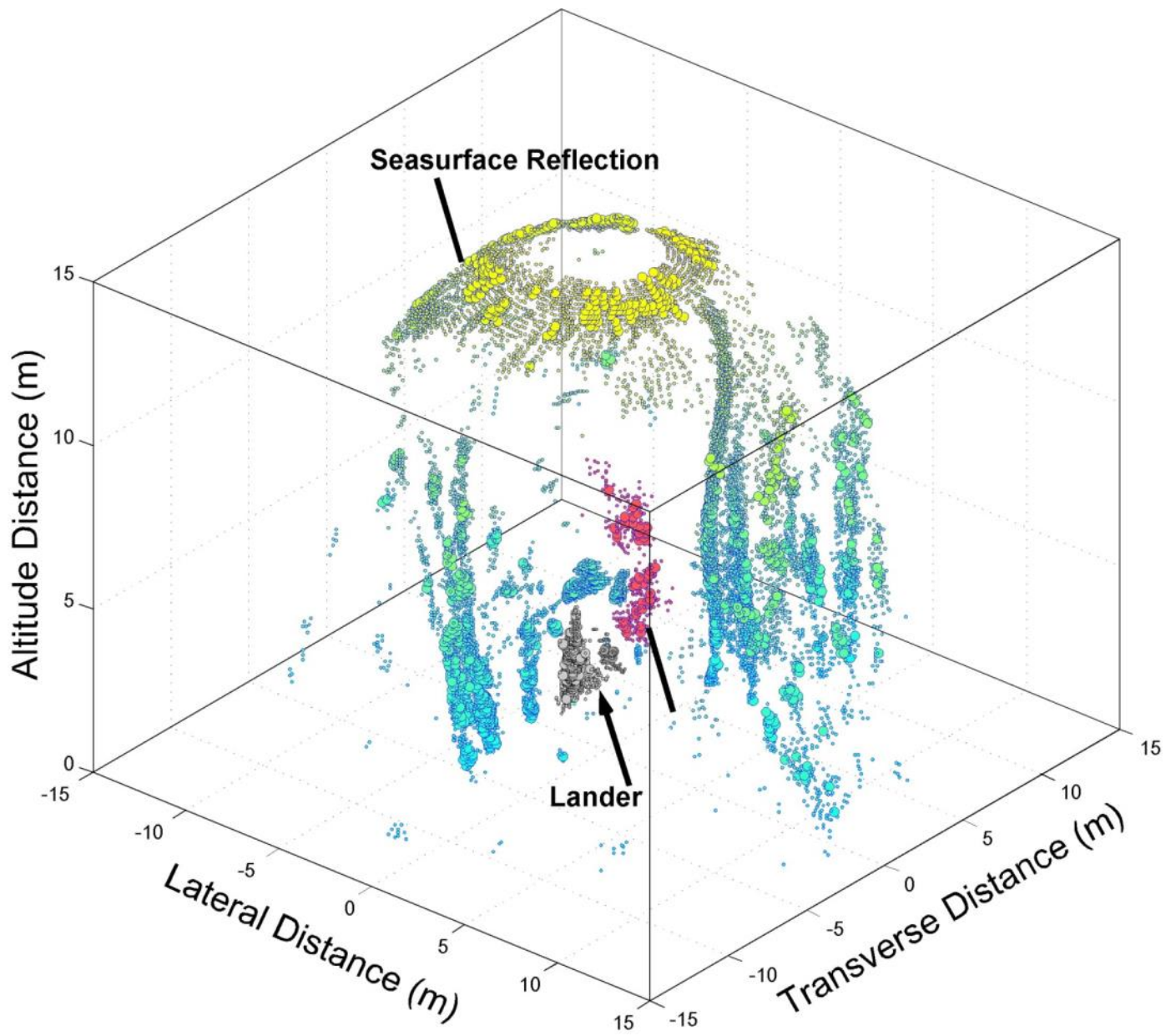


**Fig. 13. Sonar-scanner data (10-min average) from 2009 ESAS cruise, showing spatial distribution of bubbles as well as the return from the lander, cable, and sea surface. From Natalia Shakhova et al. [2013].**

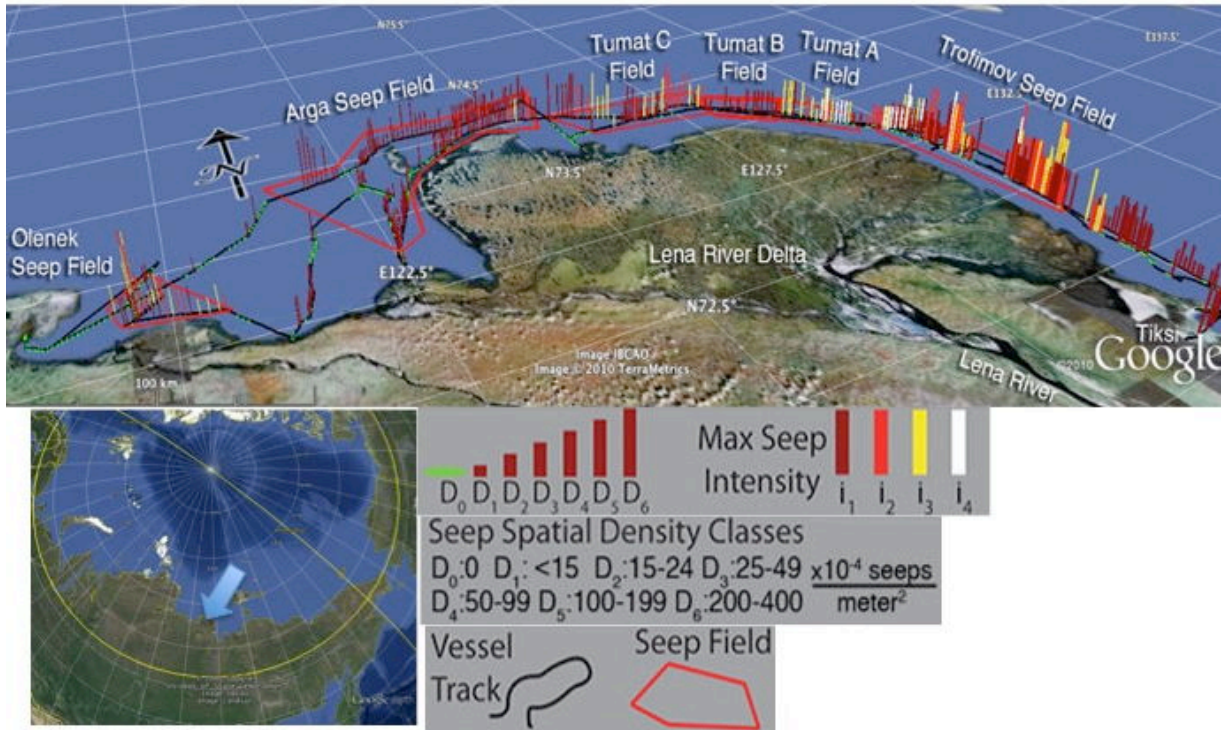


**Fig. 14.** Map of seep density and intensity in the East Siberian Arctic Sea. Each bar represents 6000 pings. Inlet shows survey location. Benthic lander (Fig. 8) was deployed in the Trofimov Seep field. From Stubbs [2010].

### Large Benthic Lander

A powerful 7125 (Reson, Goleta, CA) multibeam sonar was made available to this project from Dr. Leifer's company, Bubbleology Research International. The sonar had been obtained from a commercial contract and has a true 256 beams, as well as far higher spatial and temporal resolution and dynamic range than the Delta T. A large aluminum lander (Fig. 15) was also provided to support the 7125 as well as a more powerful rotator from ROS Systems. Also contributed were underwater batteries (Deepsea Power and Light, San Diego, CA) to support the unit's far greater power draw. The Consortium Delta T was mounted to collect continuous horizontal fan data, while the 7125 rotates in vertical fan mode. In addition, previous deployment problems arose from electrical issues for the large number of wires inside the electronics bottle. All signals and power were routed with a custom built printed circuit board by SCRIPPS, which also includes short circuit and over voltage protection. Several spare boards also were acquired. A large (12") diameter, long (36"), housing was provided to house the ICPU and all supporting electronics. The housing includes a large (8") window and monitor display to allow a ROV confirm system status including data collection, particularly useful for confirming successful autonomous deployment. The lander was deployed at MC118 in July 2013 and included a range of cameras and lights to improve visibility during deployment (Fig. 15). A detailed description of the benthic lander is provided in Appendix 1.



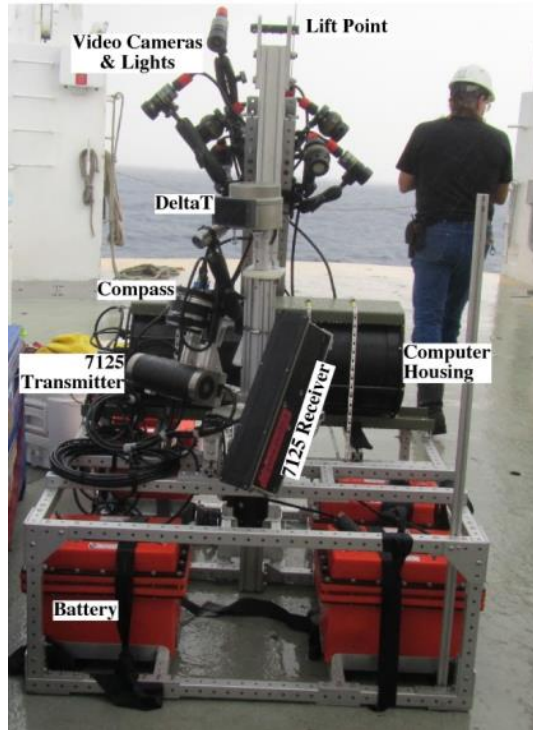


**Fig. 15. Benthic lander configured for July 2013 deployment.**

During the deployment, the MC118 bubble plumes of different strengths were imaged repeatedly (**Fig. 16**). Here, the plume is deflected – by currents - about 20 m above the lander.



**Fig. 16. Photo of portable computer onboard the RV Pelican, showing streaming sonar data of bubble plume rising from A during descent. Sonar is in vertical fan mode, 50 m range. Rotation to simulate correct orientation is approximate.**

Unfortunately, partial computer housing flooding during the deployment led to an inability to boot the computer and to download the data until servicing by Reson, in September 2013,



which provided some quick looks at part of the data; however, all the data have not yet been recovered. An example of a bubble plume by the 7125 from data that were recovered is shown in **Fig. 17**.

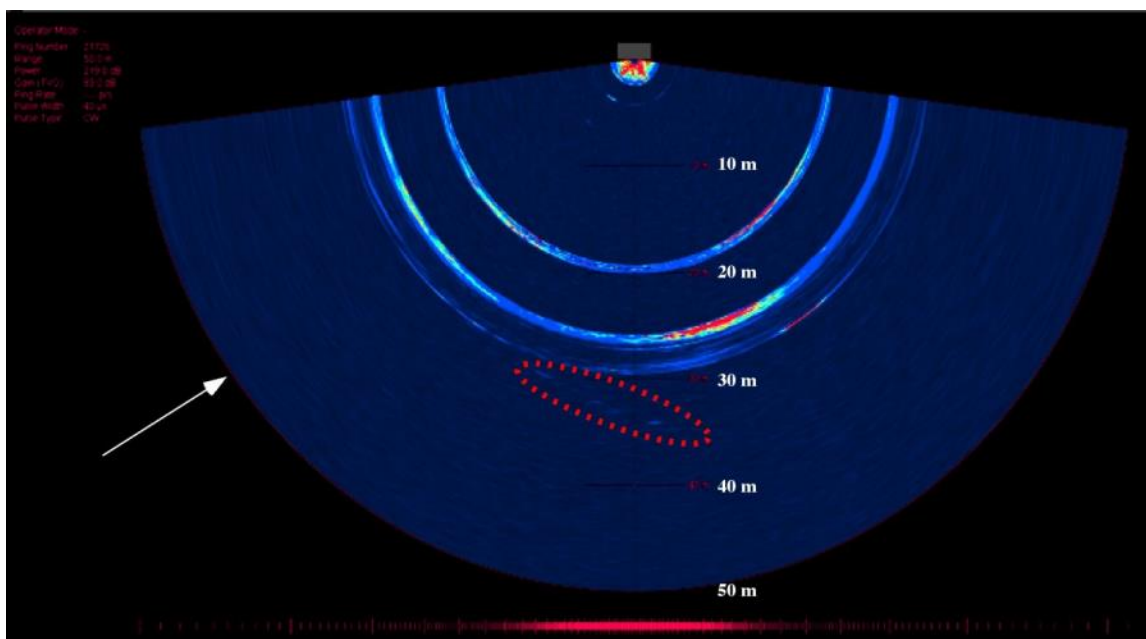


**Fig. 17.** Example sonar data showing a rising bubble plume (dotted outline) from the 7125 multibeam. Horizontal is indicated by the white arrow. Up is to the right.

### Supporting Instrumentation : In Situ Mass Spectrometer

The SRI underwater mass spectrometer (UMS) was installed in the cabin of the *CHINOOK* and power was applied to the instrument on the morning of November 12 2012 (**Fig. 18**). The UMS then ran continuously until the end of the day on November 19 2012. The SRI UMS is a membrane introduction mass spectrometry system capable of in-situ detection and quantification of dissolved gases and volatile organic compounds (VOCs). The instrument is based on a 200-amu (atomic mass unit) linear quadrupole mass analyzer (E3000 Ecotech Sensor, Inficon, Inc., Syracuse, NY). Introduction of analytes into the mass spectrometer occurs through a high-pressure polydimethyl siloxane (PDMS) membrane introduction system that has been pressure tested to a depth of 2000 meters [Pétron *et al.*, 2012]. The membrane interface used in these systems provides parts-per-billion (ppb) level detection of many VOCs and sub parts-per-million (ppm) detection limits for many dissolved light stable gases.

For these experiments, the UMS was not submersed in the water. Instead water was pumped from various depths (by either a submersed or shipboard pump) and routed to the UMS through a ¼" OD tube to which the UMS sample inlet was connected. Primary target compounds for this exercise were methane, ethane, propane, butane, pentane, benzene and toluene, although diagnostic ions for all of the major light stable gases (e.g., oxygen, nitrogen, argon, and carbon dioxide) also were monitored.



**Fig. 18.** The SRI Underwater Mass Spectrometer inside the cabin of the R/V CHINOOK.

Samples were analyzed continuously whenever the main sampling pump was operational for vertical profiling in the water column and horizontal transects. On multiple occasions at Trilogy Seep, La Goleta Seep and the Tent Seep returned significant UMS signals that are diagnostic for methane ( $m/z=15$ ), ethane ( $m/z=30$ ), propane ( $m/z=39$ ) and butane ( $m/z=58$ ) were observed (see **Figs. 19 and 20**). In a few instances, the intensity of the diagnostic ion signal for pentane ( $m/z=72$ ) was also seen to increase (**Fig. 20**), and in one instance there may have been a slight increase in the diagnostic ion signal for benzene ( $m/z=78$ ) at Trilogy Seep (data not shown here).

From approximately 4:00 pm to 4:08 pm the *CHINOOK* tried to stay in the seep. Starting at approximately 4:11 pm the *CHINOOK* crossed the seep plume numerous times at increasing distances downstream from the source. Time (x-axis) is PST and all ion intensities (y-axis) are detector current in amperes (A).

Geo-referenced zig-zag data outlined the downcurrent plume from the Seep Tent Seep (**Fig. 21**) demonstrating the power of a UMS. As the plume drifts downcurrent, it broadens due to turbulence, and decreases due to sea air gas exchange allowing basic oceanographic characteristics to be derived from UMS data.

## Vicarious Data

The Pelican cruises in 2010 and 2013 were used as an opportunity to collect large scale methane data while transporting equipment to and from port. Specifically, opportunities were taken to collect transcontinental methane data to better understand emissions from a range of sources and to validate satellite data. A total of 6600 measurements along 7020 km of roadways were made by flame ion detection, gas chromatography (GC) onboard a recreational vehicle in 2010. Findings were published in two manuscripts [Farrell *et al.*, 2013; Leifer *et al.*, 2013]. In 2013, more extensive transcontinental data were collected using a cavity ring down spectrometer (Los Gatos Research).

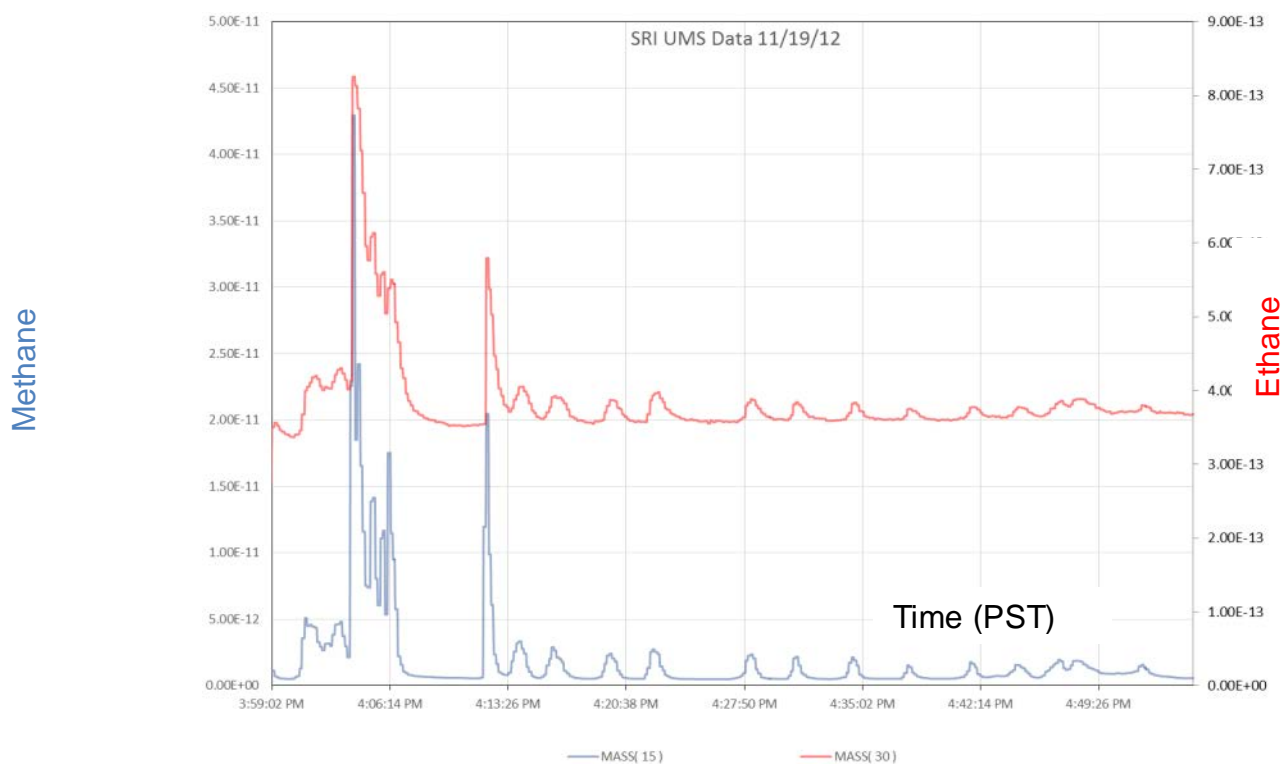


**Fig. 19. UMS time series data for methane ( $m/z$  15 – left scale) and ethane ( $m/z$  30 – right scale) at Tent Seep on 11/19/12.**

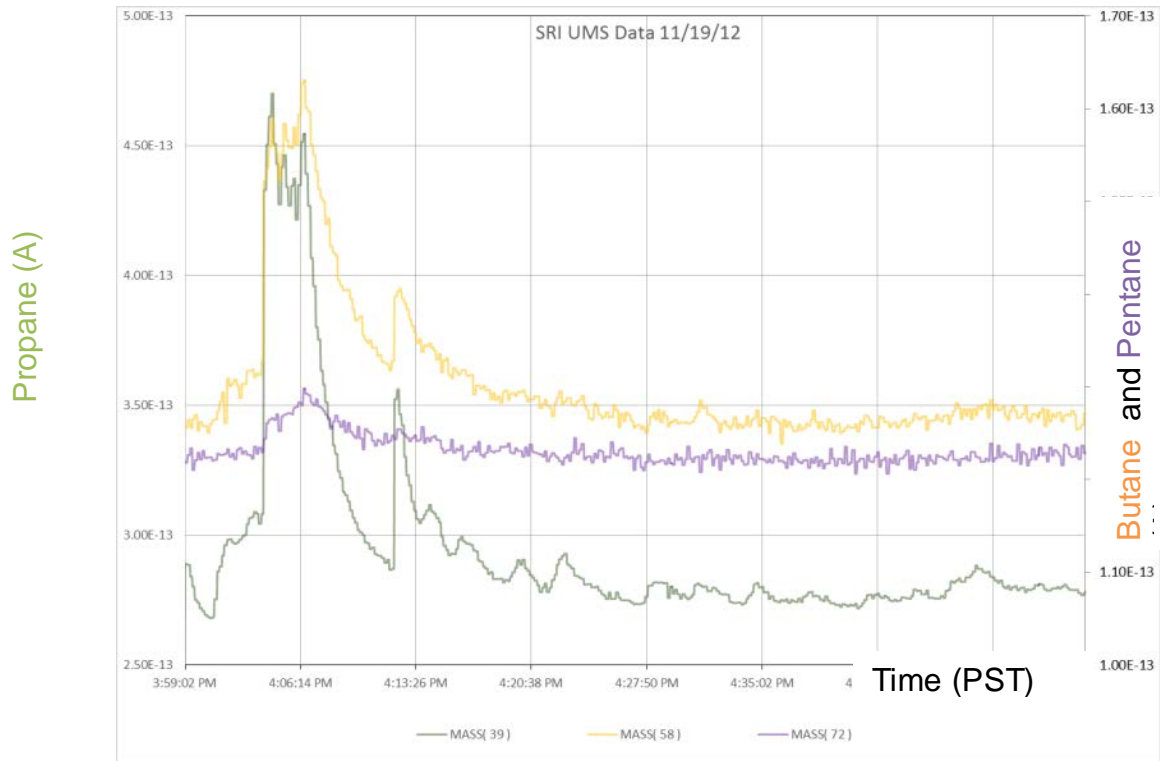


**Fig. 20.** UMS time series data for propane ( $m/z$  39 – left scale), butane ( $m/z$  58 – right scale) and pentane ( $m/z$  72 – right scale) at Tent Seep on 11/19/12. From approximately 4:00 pm to 4:08 pm the CHINOOK tried to stay in the seep. Starting at approximately 4:11 pm the CHINOOK crossed the seep plume numerous times at increasing distances downstream from the source. Time (x-axis) is PST and all ion intensities (y-axis) are detector current in amperes

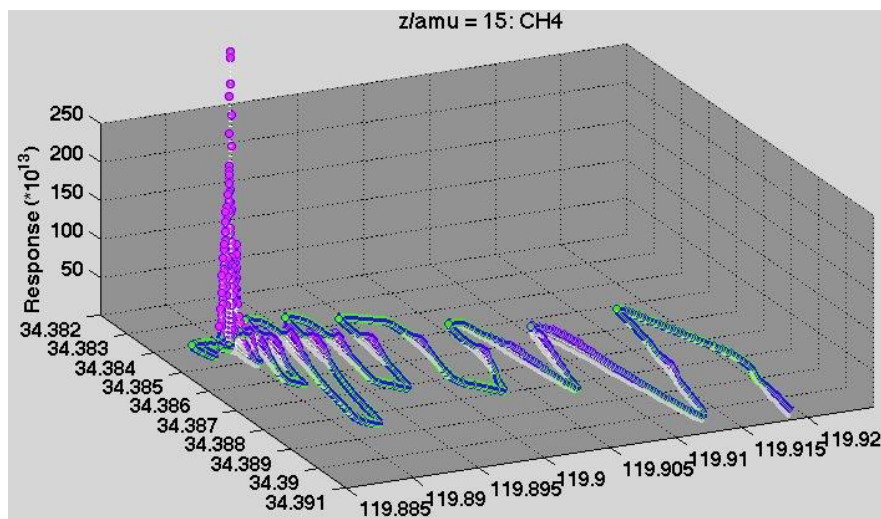


**Fig. 21.** Dissolved downcurrent, near surface methane plume from the Seep Tent Seep in Santa Barbara Channel, collected November 2012.

### 2010 Survey

Unlike studies that use vans [Herndon et al., 2005; JTIF, 2011; Shorter et al., 1996], RV-based measurements enable continuous, mobile data collection over extended areas,



including nocturnal measurements through driver rotation. Most urban areas were traversed nocturnally when vehicular CH<sub>4</sub> emissions are much lower [Shorter et al., 1996] – vehicular emissions are strongly spatially road-biased. Some daytime measurements were along heavily trafficked urban and rural interstate corridors; however, for winds not parallel to the roadway (i.e., not east/west), exhaust from preceding vehicles should affect data minimally. In some cases, sources were studied by transecting plumes, in other cases through slower, convoluted search patterns, necessarily road limited.

Air samples were collected continuously through a roof “air ram” to prevent exhaust entering the sample line while the RV was moving (Fig. 22). Air was pumped through ¼” plastic sample tubing attached 0.25 m from the air ram’s end into multiple streams that entered the 4-channel GC, which was configured to achieve the fastest possible measurement time while yielding adequate CH<sub>4</sub> peak/air valley separation. Adequate separation meant that custom (MatLab, Mathworks, MA) routines could separate the peak from the valley, despite overlap. Real-time analysis was by conventional chromatography software (PeakSimple, SRI, CA), which is challenged by peaks with baseline drift, noise, and poor separation. Daily calibration used 1-mL injections, typically ten repetitions, of a high (10 ppm) and low (1 ppm) standard.

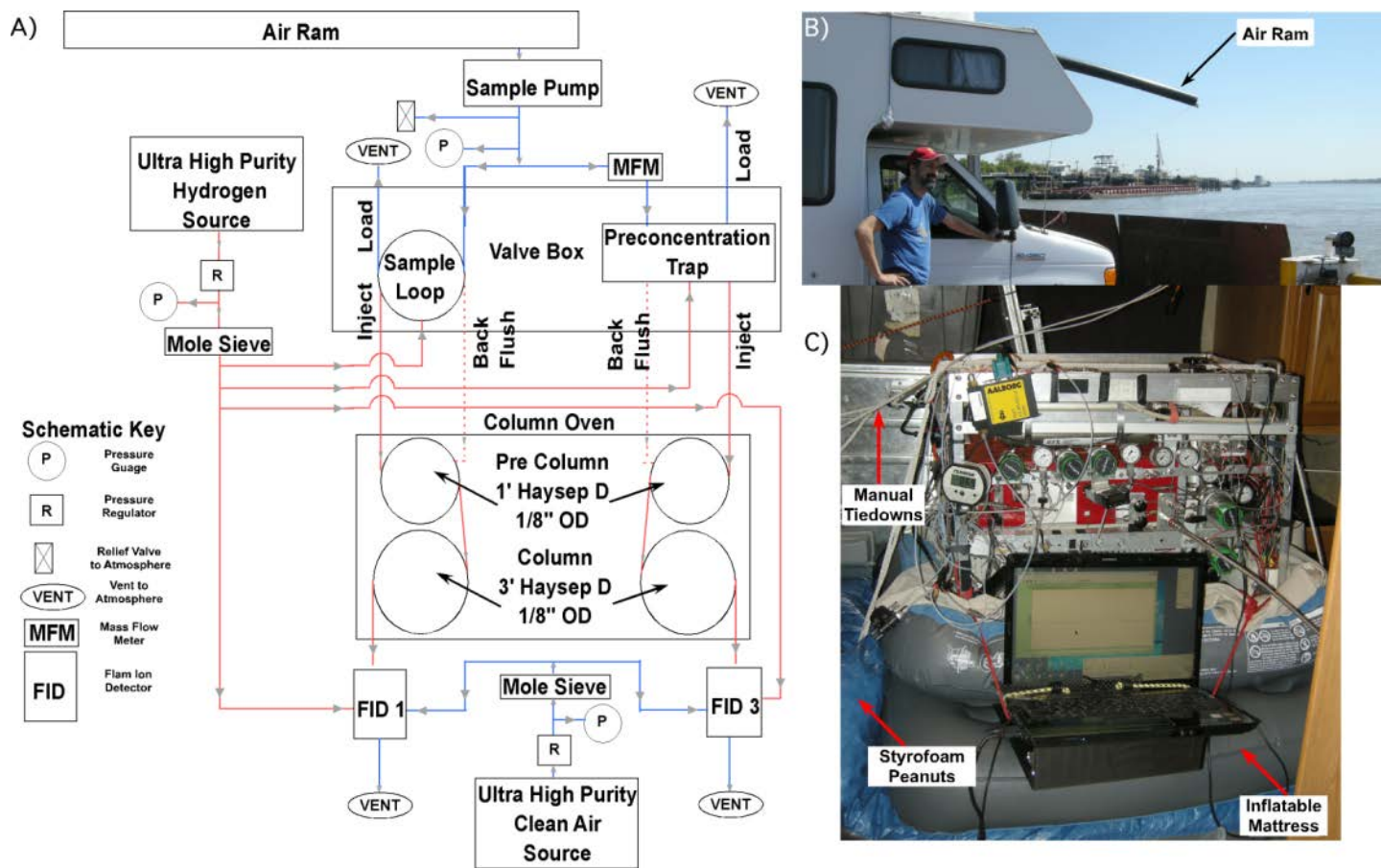
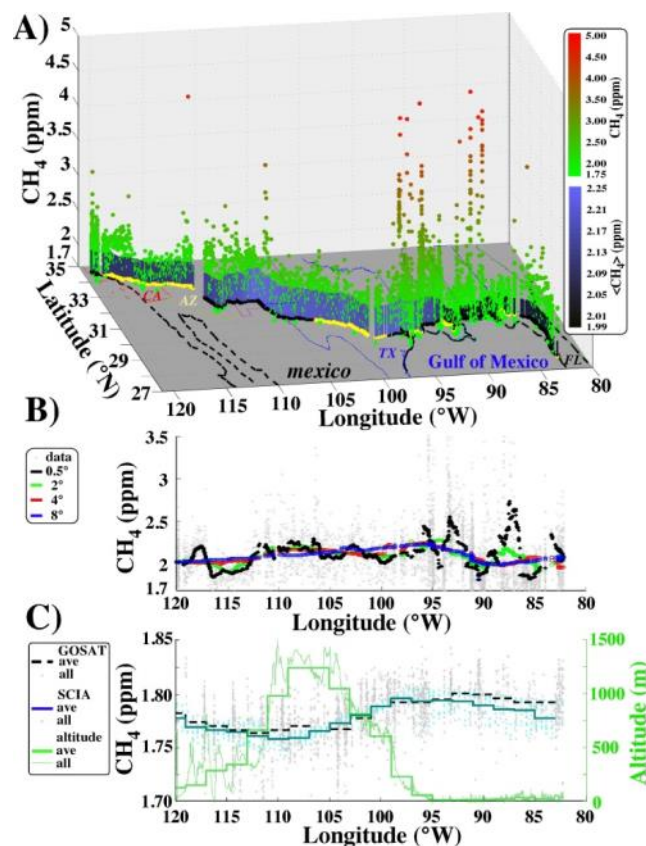


Fig. 22. A) Experimental set-up. B) Photo of recreational vehicle, RV, and “air ram”, C) Photo of RV gas chromatography setup including vibration reduction. From Farrell et al. [2013].



The survey data provides a single-route snapshot; thus, satellite data are required for larger spatial and temporal context. Surface data and SCIAMACHY  $\text{CH}_4$  anomaly trends along the survey path showed similar patterns that were not correlated with retrieval factors like altitude (**Fig. 23C**) or humidity. Seasonal SCIAMACHY  $\text{CH}_4$  data then were compared qualitatively with inventories for anthropogenic and natural sources and winds to identify large and unambiguous inventory errors even for qualitative comparison.



**Fig. 23.** A) Unfiltered transcontinental methane,  $\text{CH}_4$ , data and filtered ( $8^\circ$  spatial median) data including survey path. Day/night track is yellow/black. B) Methane,  $\text{CH}_4$ , data from 2010, versus along-path longitude and spatial averages from  $0.5$  to  $8^\circ$ .  $\text{CH}_4$  mixing ratios above  $3.5$  ppm not shown. C) Altitude, and total dry  $x\text{CH}_4$  column abundance for SCIAMACHY 2003-2005 and GOSAT values for 2009-2011 within  $2^\circ$  of survey track, and altitude, both all data and longitudinal bin-averaged. Legend on figure. State boundaries shown.

Spatial averages of the transcontinental data where each point was replaced by the average of all points within a set distance suggest  $\text{CH}_4$  anomalies generally had spatial scales of  $\sim 2$ - $4^\circ$ , larger spatial averaging (**Fig. 23B**) only shows the continental-scale trends. For example, the  $8^\circ$  trend shows a general decrease from the more urban areas of Florida into the panhandle through E. Louisiana, rapidly increases towards East Texas, then decreases nearly monotonically towards California. Although synoptic systems also impress a scale on these data, these spatial scales correspond to the spatial scale of Fossil Fuel Industrial (FFI) activity—the distance from E. Louisiana to Houston is  $\sim 500$  km or  $5^\circ$ .

Comparison between SCIAMACHY column-averaged, dry-air mole fraction of atmospheric CH<sub>4</sub> for 2003-2005 using ver. V2.0.2 of the WFM-DOA retrieval algorithm [Schneising *et al.*, 2011] and the survey surface data show similar large-scale trends for the South US (Figs. 23B and 24), with highest surface CH<sub>4</sub> in Louisiana and Eastern Texas and in the prevailing downwind direction (west-northwest). Westward, CH<sub>4</sub> decreased until the California desert. The sparser and more variable GOSAT (Greenhouse gases Observing SATellite (GOSAT) Project) data (Figs. 23B and 24B) for 2009-2011 show a similar spatial pattern, demonstrating that dominant regional sources have not changed dramatically during the years spanning these satellite datasets. These satellite instruments require numerous orbits to generate high quality maps, thus spatial patterns represent long-term averages of sources and transport.

The satellite data help provide regional context for Gulf of Mexico sources which include both FFI activities and natural seepage.

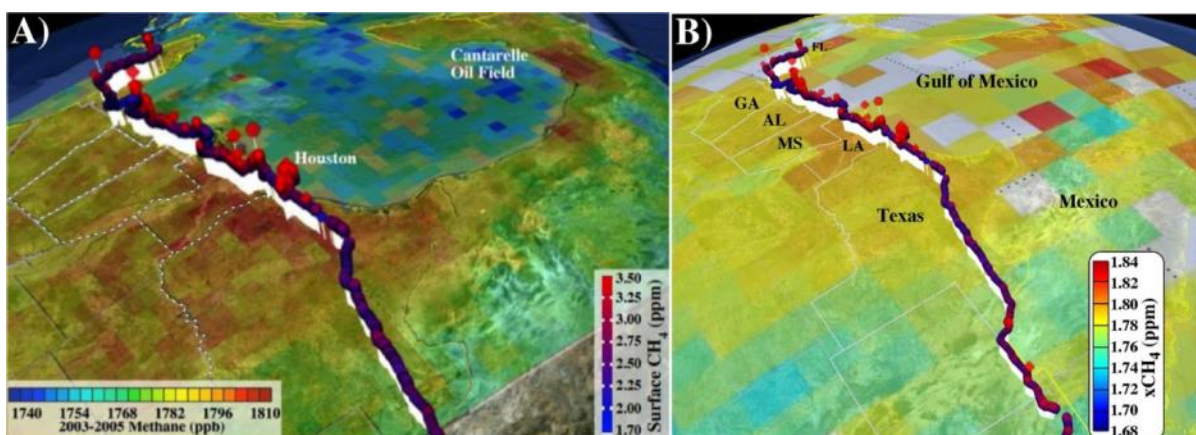


Fig. 24. Southeastward view of surface CH<sub>4</sub> survey data (e.g., Fig. 6A), A) SCIAMACHY total dry xCH<sub>4</sub> column abundances 2003-2005 (0.5°x0.5°), and B) xCH<sub>4</sub> column abundance for GOSAT for 2009-2011. Colorbar on figure.

### 2013 Survey

A number of important improvements were pioneered in the 2013 to address mobile measurement challenges highlighted in a 2010 transcontinental survey. Key was the addition of real-time data monitoring, which was applied in 2012 in S. California with a cavity ring down spectrometer [Leifer *et al.*, 2013]. However, realtime data was recognized as insufficient – realtime data visualization and integration in a mapping environment (Google Earth), including winds, have been integrated to aid adaptive survey route planning in the wind frame of reference.

A key improvement was to use a custom modified RV, named MACLab (Mobile Atmospheric Composition Laboratory) for air quality measurements. MACLab is a 12-ton, 37' diesel RV toyhauler, whose garage was converted for air chemistry analysis, including 4 gas chromatographs (SRI GC) on an independent air suspension rack, ultrapure air and hydrogen generators, 8.5 kw generator, 18-m pneumatic mast, greenhouse gas cavity ringdown spectrometer, high flow vacuum lines, meteorology station, 3D sonic anemometer,

continuous video scene recording, and internal network allowing all MACLab computers to access all instruments/video streams. The habitation module supports to a 4-person team, allowing round-the-clock data collection without regards to proximity to hotels, restaurants, and bathrooms, allowing extended mobile air quality measurement. See **Fig. 25** for an example MACLab dataset for Houston.

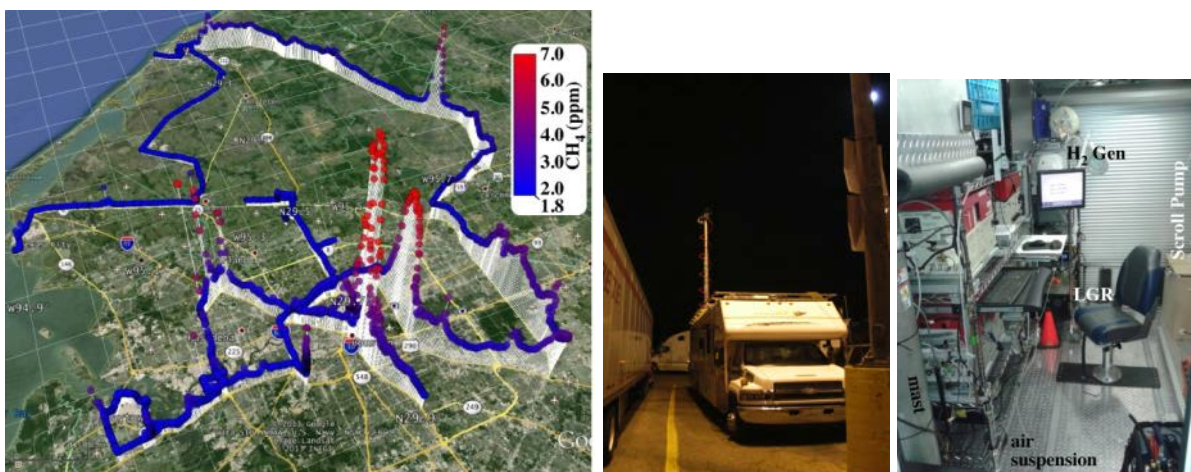


**Fig. 25.** Houston  $\text{CH}_4$ , downwind of refineries collected with MACLab (Mobile Atmospheric Composition Laboratory).

Houston GHG data show the dominant  $\text{CH}_4$  and  $\text{CO}_2$  sources related to the extensive FFI facilities and activities near I-10. The Houston survey first investigated the source and vicinity, while noting wind directions during wind-measurement pauses. Then, cross-wind transects were taken (north-south) for several downwind distances. Given plume dimensions, the transect sequence took ~7 nocturnal hours to complete. Nocturnal measurements provide effective urban mobility (traffic) and decreased (road-biased) vehicular emissions compared to daytime surveys. Estimated boundary layer height was ~75 m based on refinery vapor plume observations.

These 2013 data (**Fig 26**) will be analyzed in terms of satellite data. Also, offshore greenhouse gas data were collected between Cocodrie and MC118 as well as on site, which are being analyzed.





Fig. 26. 18000+ km CH<sub>4</sub> MACLab, 2013 data. Preliminary calibration.

## References

- Beauchamp, B. (2004), Natural gas hydrates: Myths, facts and issues, *C.R. Geoscience*, 336, 751-765.
- Bradley, E. S., I. Leifer, and D. A. Roberts (2010), Long-term monitoring of a marine geologic hydrocarbon source by a coastal air pollution station in Southern California, *Atmospheric Environments*, 44, 4973-4981.
- Clark, J. F., I. Leifer, L. Washburn, and B. P. Luyendyk (2003), Compositional changes in natural gas bubble plumes: Observations from the Coal Oil Point marine hydrocarbon seep field, *Geo-Marine Letters*, 23, 187-193 DOI 10.1007/s00367-00003-00137-y.
- Farrell, P., I. Leifer, and D. Culling (2013), Transcontinental methane measurements: Part 1. A mobile surface platform for source investigations, *Atmospheric Environment*, 74, 422-431.
- Granin, N., M. Makarov, K. Kucher, and R. Gnatovsky (2010), Gas seeps in Lake Baikal— detection, distribution, and implications for water column mixing, *Geo-Marine Letters*, 30(3), 399-409.
- Greinert, J., Y. Artemov, V. Egorov, M. De Batist, and D. McGinnis (2006), 1300-m-high rising bubbles from mud volcanoes at 2080 m in the Black Sea: Hydroacoustic characteristics and temporal variability, *Earth and Planetary Science Letters*, 244(1-2), 1-15.
- Heeschen, K. U., A. M. Tréhu, R. W. Collier, E. Suess, and G. Rehder (2003), Distribution and height of methane bubble plumes on the Cascadia Margin characterized by acoustic imaging, *Geophysical Research Letters*, doi:10.1029/2003GL016974.
- Herndon, S. C., et al. (2005), Characterization of urban pollutant emission fluxes and ambient concentration distributions using a mobile laboratory with rapid response instrumentation, *Faraday Discussions*, 130, 327-339.
- Hornafius, S. J., D. C. Quigley, and B. P. Luyendyk (1999), The world's most spectacular marine hydrocarbons seeps (Coal Oil Point, Santa Barbara Channel, California): Quantification of emissions, *Journal Geophysical Research - Oceans*, 104(C9), 20703-20711.
- Hovland, M., J. Gardner, and A. Judd (2002), The significance of pockmarks to understanding fluid flow processes and geohazards, *Geofluids*, 2, 127-136.
- IPCC (2007), Contribution of Working Group I to the Fourth Assessment Report of the Intergovernmental Panel on Climate Change Rep., 996 pp, Cambridge.

JTIF, J. I. O. S. P. a. R. T. F. (2011), Progress Report on Industry Recommendations to Improve Oil Spill Preparedness and Response *Rep.*, 33 pp.

Khalil, M. A. K., and R. A. Rasmussen (1995), The changing composition of the Earth's atmosphere, in *Composition, Chemistry, and Climate of the Atmosphere*, edited by H. B. Singh, pp. 50-87, Van Nostrand Reinhold, New York.

Kvenvolden, K. A., and B. W. Rogers (2005), Gaia's Breath - Global Methane Exhalations, *Marine and Petroleum Geology*, 22(4), 579-590.

Kvenvolden, K. A., and B. W. Rogers (2005), Gaia's breath-global methane exhalations, *Marine and Petroleum Geology*, 22(4), 579-590.

Kvenvolden, K. A., T. D. Lorenson, and W. S. Reeburgh (2001), Attention turns to naturally occurring methane seepage, *EOS (American Geophysical Union Transactions)*, 82, 457.

Leifer, I. (2010), Characteristics and scaling of bubble plumes from marine hydrocarbon seepage in the Coal Oil Point seep field, *Journal Geophysical Research*, 115, C11014.

Leifer, I., and R. K. Patro (2002), The bubble mechanism for methane transport from the shallow sea bed to the surface: A review and sensitivity study, *Continental Shelf Research*, 22(16), 2409-2428.

Leifer, I., and A. G. Judd (2002), Oceanic methane layers : A bubble deposition mechanism from marine hydrocarbon seepage, *Terra Nova*, 16, 471.

Leifer, I., and J. Boles (2005a), Turbine tent measurements of marine hydrocarbon seeps on subhourly timescales, *Journal of Geophysical Research-Oceans*, 110(C1).

Leifer, I., and J. Boles (2005b), Measurement of marine hydrocarbon seep flow through fractured rock and unconsolidated sediment, *Marine and Petroleum Geology*, 22(4), 551-568.

Leifer, I., B. P. Luyendyk, J. Boles, and J. F. Clark (2006), Natural marine seepage blowout: Contribution to atmospheric methane, *Global Biogeochemical Cycles*, 20(GB3008).

Leifer, I., H. Jeuthe, S. H. Gjørsund, and V. Johansen (2009), Engineered and natural marine seep, bubble-driven buoyancy flows, *J. Phys. Oceanography*, 39(12), 3071-3090.

Leifer, I., M. Kamerling, B. P. Luyendyk, and D. Wilson (2010), Geologic control of natural marine hydrocarbon seep emissions, Coal Oil Point seep field, California, *Geo-Marine Letters*, 30(3-4), 331-338.

Leifer, I., D. Culling, O. Schneising, P. Farrell, M. Buchwitz, H. Bovensmann, and J. P. Burrows (2013), Transcontinental methane measurements: Part 2. Mobile surface investigation of fossil fuel industrial fugitive emissions *Atmospheric Environment*, 74, 432-441.

MacDonald, I. R., I. Leifer, R. Sassen, P. Stine, R. Mitchell, and N. Guinasso (2002), Transfer of hydrocarbons from natural seeps to the water column and atmosphere, *Geofluids*, 2, 95-107.

Pétron, G., et al. (2012), Hydrocarbon emissions characterization in the Colorado Front Range: A pilot study, *J. Geophys. Res.*, 117(D4), D04304.

Quigley, D. C., J. S. Hornafius, B. P. Luyendyk, R. D. Francis, J. Clark, and L. Washburn (1999), Decrease in natural marine hydrocarbon seepage near Coal Oil Point, California, associated with offshore oil production, *Geology*, 27(11), 1047-1050.

Reeburgh, W. S. (2003), Global methane biogeochemistry, in *The Atmosphere. Treatise on Geochemistry*, edited by R. Keeling, pp. 65-69, Elsevier-Pergamon, Oxford.

Rehder, G., R. S. Keir, E. Suess, and M. Rhein (1999), Methane in the Northern Atlantic controlled by microbial oxidation and atmospheric history, *Geophysical Research Letters*, 26(5), 587-590.

Rehder, G., I. Leifer, P. G. Brewer, G. Friederich, and E. T. Peltzer (2009), Controls on



methane bubble dissolution inside and outside the hydrate stability field from open ocean field experiments and numerical modeling, *Mar. Chem.*, 114(1/2), 19-30.

Rowland, F. S. (1985), Methane and chlorocarbons in the Earth's atmosphere, *Origins of Life*, 15, 279.

Sauter, E. J., S. I. Muyakshin, J.-L. Charlou, M. Schlüter, A. Boetius, K. Jerosch, E. Damm, J.-P. Foucher, and M. Klages (2006), Methane discharge from a deep-sea submarine mud volcano into the upper water column by gas hydrate-coated methane bubbles, *Earth and Planetary Science Letters*, 243(3-4), 354-365.

Schneising, O., M. Buchwitz, M. Reuter, J. Heymann, H. Bovensmann, and J. P. Burrows (2011), Long-term analysis of carbon dioxide and methane column-averaged mole fractions retrieved from SCIAMACHY, *Atmospheric Chemistry Physics Discussion*, 11, 2863-2880.

Shakhova, N., I. Semiletov, I. Leifer, P. Rekant, A. Salyuk, and D. Kosmach (2010), Geochemical and geophysical evidence of methane release over the East Siberian Arctic Shelf, *J. Geophys. Res.*, 115, C08007.

Shakhova, N., et al. (2013), Massive methane release via ebullition and storms on the East Siberian Arctic Shelf, *Nature Geoscience*, *In Press*.

Shorter, J. H., et al. (1996), Methane emission measurements in urban areas in Eastern Germany, *Journal of Atmospheric Chemistry*, 24(2), 121-140.

Sloan, D., and C. A. Koh (2008), *Clathrate hydrates of natural gases*, Third ed., Taylor & Francis Group, Boca Raton.

Solomon, E., M. Kastner, I. R. MacDonald, and I. Leifer (2009), Considerable methane fluxes to the atmosphere from hydrocarbon seeps in the Gulf of Mexico, *Nature Geoscience*, 2, 561-565.

Solomon, E., I. Leifer, M. Kastner, J. Levine, and G. Rehder (2013), Type 2 hydrates enables deepsea methane to reach the atmosphere, *Nature Geoscience*, *In Progress*.

Spiess, V., and Y. Artemov (2010), Fine Scale sediment and water column structure at deep sea seepage sites derived from spatial seismoacoustic surveys, paper presented at 10th International Conference on Gas in Marine Sediments, Lake Baikal, Russia, 6-12 Sept 2010.

Stubbs, C. (2010), Spatial distribution of near-shore gas seepage from sub-sea permafrost in the Laptev Sea Shelf, Arctic Ocean 118 pp, University of California, Santa Barbara, Santa Barbara.

Texas\_A&M (2011), Remote sensing and sea-truth measurements of methane flux to the atmosphere (HYFLUX project) *Rep.*, 164 pp.

Watanabe, S., N. Tsurushima, M. Kusakabe, and S. Tsunogai (1995), Methane in Izena Cauldron, Okinawa Trough, *Journal of Oceanography*, 51, 239.

## **Appendix – Large Benthic Lander**

### **Lander frame**

The lander frame is designed from 1.5" extruded aluminum using the 80/20 fastening system as well as custom aluminum and stainless brackets. The lander is about 4'x4'x2' with 7 battery carriers on the base. Attachments include the rotator assembly which carries the sonar systems and the compass, the mast with a high strength alloy hitch pin, a 1" square reference post 5' long positioned on the lander corner at left of the sonar projection and sonar-side camera, and a horizontal stabilizing frame that prevents the lander from tipping onto the sonar assembly when landing on uneven terrain.

## **Installed Equipment**

Two active sonar systems were installed on the lander, a 200kHz RESON SeaBat multibeam projector and receiver and a 260kHz Imagenex model 837 "Delta T" multibeam profiling sonar. The RESON system provided visualization in a vertical plane up to 450m out while the Imagenex projected horizontally up to 50m out.

The sonar systems installed on a rotating bracket connected to a ROS heavy-duty rotator. The longer ranging RESON system was mounted with its 128° by 1° projection centered 30° up from the plane of the lander, and rotated 156° left and right to observe a total swath of 306° from 0.5 to 450m. The Imagenex sonar head, mounted on top of the rotator assembly, projected in a 120° by 3° scan parallel to the plane of the lander at a range of 50m and rotated through the same swath.

A 3-axis digital compass from Ocean Server Technologies was mounted on the RESON bracket and oriented at 30° up to match the RESON projection.

4 video cameras with floodlights were installed around the lander mast by University of Mississippi technician Matt Lowe. The HD video and illumination provided visualization of the landing sites, surrounding short-range features, lander orientation, and identification of hazards. Two 24 VDC Deep Sea batteries supported the video installation.

4 48 VDC Deep Sea sea batteries provided power to the RESON ICPU which also powered the rotator, compass, and Imagenex. 2 24 VDC Deep Sea batteries powered the cameras and lights, installed by University of Mississippi technician Matt Lowe.

The RESON Integrated Control and Processing Unit (ICPU), installed in an aluminum pressure vessel, served as ringmaster for instrument control and data routing. The RESON, Imagenex, digital compass, and rotator were all controlled through the ICPU with optional MIMS attachment not used during this survey. Communications between the ICPU and the ship were fiber-optic during this deployment with Ethernet converters at both ends.

During the deployment, sonar and rotator control was done through a pc laptop computer serving as a remote desktop for the ICPU controller. Data were saved to a 2 Tb drive inside the ICPU. University of Mississippi technicians Matt Lowe and Max Woolsey oversaw acquisition and display of on-board HD video.

Inside the pressure vessel, in addition to the RESON ICPU, a custom circuit board pipelines communication between all components and distributes power. The board also provides short circuit, overvoltage, and inversion protection in case of incorrect wiring or seawater intrusion into the pressure vessel. Diagnostic LEDs indicate power and communication. Pipelining of the communication and power on this board improves on the original design streamlining the assembly of electronics inside the vessel to add space and prevent accidental damage to connectors.

## **Pre-deployment Adjustments**

Before deployment, the rotator, and compass were oriented. The digital compass housing was oriented on board the ship using a cell phone (figure 8 isotropy correction performed) as a north reference, and compass software to indicate north. The north arrow was aligned

parallel to the direction of the RESON sonar projection. The rotator orientation center and limits were found with the rotator controller software. The center position of the rotation frame (parallel to the lander face) provided a north arrow for whole lander orientation during hops.

All equipment and the ICPU were tested on board before deployment, and the main cable fiber optic interface was finalized and verified. We thank Matt Lowe and Max Woolsey (University of Mississippi) for their help in troubleshooting this.

On the bottom, the video cameras and lighting were adjusted for brightness, focus and range. The sonar was activated and the reference pole sonar signature was noted on the RESON and Imagenex.

### **Deployment Protocol**

After initial equipment checks and adjustments of video and lighting, the lander was deployed to the bottom of the Mississippi Channel MC118 seep site. The rotator control software initiated automatic sweeps through the 306° range of motion. The RESON and Imagenex displays were observed for evidence of bubble plumes. RESON, Imagenex, and digital compass data were recorded on the data drive continuously during the deployment.

The closest returns on the sonar images could be attributed to the reference post, lander frame, and the main cable; more distant returns were attributed to seafloor returns or echoes from more distant objects. Intermediate short streaks on the RESON image were interpreted as bubble plumes crossing the swath at a slightly oblique angle, offset by currents. With the sonar stationary, a vertical bubble plume should cross the image in a straight line, but no such plumes were observed.

The lander was hopped around the site after completing viewing and recording of observed plumes, or when no detection was concluded. The lander was carefully hopped using the boat winch so lifts and landings would not disturb sediments significantly. At each new hop location, the video cameras provided situational awareness on all four sides of the lander, the view ahead (along sonar projections) was checked for target bubble plumes, and if none were visible, a standard one minute automatic sweep of was conducted between the pre-set limits.

If bubble plumes were detected during the one minute sweep, the sonars were rotated to the observed plume and adjusted so that the rising plume had maximum expression in the RESON sonar image. Data on each plume would be collected for 1 minute. For this survey of MC118, only one main plume was detected, but the procedure remained in effect. The lander observed and recorded the main plume several times during the 2 hour and 21 minute deployment.

## **Task 7: Administrative Oversight of the Monitoring Station/Sea-floor Observatory Project.**

Administration of the Consortium is the responsibility of the University of Mississippi and includes formal Project Proposals to federal funding agencies, Technical Progress Reports, Final Project Reports, informal monthly updates, organization of Consortium meetings which occurred twice annually through the greater part of the life of this award, reports/publication of Consortium meetings' proceedings, preparation for merit reviews, participation in merit reviews, cruise reports, reports of publications, participation in national meetings, organizing meetings between researchers, organizing and participating in program reviews, organizing and participating in research activities, including research cruises, publishing results as appropriate, and keeping track of Consortium publications..

### ***Final Technical Report:***

Specific Administrative tasks appear in the semiannual reports for the project for the last 12 years. Since the last semiannual report, covering activities through June 30, 2013, the major activity of the Administrative team has been to collect property reports, patent certifications, technical reports, and financial reports, including reports of cost-share provided to the DOE through the life of the subcontracts, and to accomplish the same for the University of Mississippi. This vastly time-consuming endeavor has, at last, resulted in this final technical report, the final responsibility of the University of Mississippi for this Cooperative Agreement.

### ***Research Cruises:***

As noted earlier, 30 research cruises have been designed, planned – ships reserved and leased, permission secured to conduct research (from MMS/BOEM), equipment provided for deployment, operation and recovery of instruments, - executed, concluded and reports written and circulated. Hundreds of efforts have been accomplished through these research activities and a wealth of marine instrumentation, techniques, advancement and publications have resulted. Cruise reports can be found on the MMRI website at <http://www.mmri.olemiss.edu/Home/Publications/Cruise.aspx>.

### ***Recovery of data from the Seafloor:***

The Consortium has recovered geophysical, geological, chemical and some biological data as well as a wealth of seismo-acoustic data from the MS/SFO site. We have multiple multibeam surveys that reveal changes in bathymetry/sediment accumulation over short periods of time indicating activity over four years or less. Core data reveal areas of active sediment accumulation as well as areas from which sediment appears to be removed, perhaps by active venting of gases. The ROVs have documented much of the Woolsey Mound seafloor photographically. We have gained access to photographic data from MC118 by cooperating with Jason II and Alvin cruises and contracting the Jason SeaLink. In 2013, the NIUST AUV, *Eagle Ray*, made a complete photo-survey – now being mosaicked and analyzed – of Woolsey Mound. In this way, CMRET/STRC has developed habitat maps for MC118 based on multiple video, coring, and acoustic surveys of the site. These maps can be used as baselines for habitat development/change over time as well as documentation of active seeps and plumes and where activity has ceased. Over the life of this project, we have recovered many sets of chemical data: pore-fluids from cores as well as PFAs, benthic boundary data from the CSA and BBLA deployments, water-column data from the BBLA and targeted chemical data from the ABCMS and survey chemical data from the MIMS/ABCMS. Coring efforts have returned not only sediment data but, on two occasions, hydrate that has been analyzed and used for input to the hydrate modeling program.

**Recovery of data from the HSZ:**

The MMR/CMRET has been instrumental in acquiring data from a wide range of sources. We developed the SDR system and surveyed all of Woolsey Mound using this system that targets the HSZ. We contracted C&C Technologies to run multibeam and chirp sonar of MC118 and have since repeated the surveys, making time-series analysis of the HSZ possible. We have made one such analysis (2005 and 2009) and have a 2013 survey in-hand, making another possible. Together with SDR and the TGS and WesternGeco industry seismic datasets we acquired, processed and interpreted, we have made extremely detailed maps and interpretations of the seafloor and subseafloor from Woolsey Mound. We have made repeat multibeam (bathymetry and backscatter) and chirp AUV surveys that show features not visible on less detailed (instrument mounted on the ship's hull) surveys. We have recovered cores that ground truth our shallow subsurface data and have performed chemical analyses on the pore-fluids from these cores to learn the chemistry of the hydrate birthing grounds. We have also recovered OBS data and noise data from MC118.

**Technical Support:**

In addition to ships' facilities, the MMR/CMRET shop facilities and expertise have been made available to many projects – too many to count. Our team prepares for every cruise including where instruments will reside during transit, how they will be moved and maneuvered, how they will be powered, how they will be deployed and recovered, who will operate them and when. Our navigation team leads the effort to get the ship to the desired sites, usually selected by our team of geologists and geophysicists. Aided by USBL and advanced, continuously updated positioning, our ability to locate instruments, structures, hazards, etc. on the seafloor is top-notch. Our onshore expertise has resulted in the design, creation and successful operation of two ROVs custom built to suit the needs of the Consortium research and researchers.

**Remotely operated Vehicles:**

The SSD (NOAA) and the I-SPIDER (BOEM), designed and built for this project, and including fiber-optic communications from the vessel to the water-column and seafloor, have been made available to DOE projects without reservation. DOE projects have provided much of the drive for these vehicles to perform and the projects will continue, due in part to this built-in interdependency.

**Instruments and Landers:**

The SDR seismic data system was developed especially to target the otherwise largely neglected HSZ. Deployment techniques developed especially for the MS/SFO are many. They include the Seafloor Probe deployment system (BOEM), the ROVARD (NOAA) and ABIL (BOEM) landers, USBL innovations (BOEM), the PFA (DOE) and variations, the hydrates collector (DOE), the CSA (NOAA), the BBLA (NOAA), the ABCMS Lander (DOE), the reduced-size (for lander and AUV travel) mass spectrometer (DOE), the HLAs (DOE), the speed of sound measurement capability (DOE), novel multibeam plume monitoring (3D) (DOE).

**Processing Innovations:**

The need for custom processing has led to the development of many innovative data-processing/treatment techniques that include SDR processing techniques, applying Empirical Mode Decomposition (BOEM) to a variety of seismic data, multiple-resolution processing (DOE; BOEM; NOAA), the development of a multigas hydrate modeling program to identify the HSZ (DOE), new software to image shallow sediments via 4C data (DOE), processing of chirp data with the polarity preserved (NOAA) and using them to image the



HSZ (DOE), the use of noise to investigate the HSZ (DOE, BOEM).

***Graduate Students:***

The Consortium has hosted many visiting scholars and provided opportunities for many graduate students from a host of universities. These student scholars have produced a very large percentage of the products for this award. Two – Laura Lapham and Rachel Wilson – have received DOE fellowships as a result of their work with the Consortium. They have impressive lists of publications and have begun their own scientific careers. Brad Battista is now a geophysical consultant with a part ownership in a consulting firm. Several are employed by geophysical companies and some by oil companies. Michela Ingrassia, Alessandra Conti and Martina Pierdomenico, graduated from the Department of Marine Sciences, University of Rome with highest honors for the work they did while at the University of Mississippi, working with Consortium geoscientists at the University of Mississippi at the Pennsylvania State University and at the NOAA Northeast Fisheries Science Center, New Jersey. Francesca Marra, Marine Geoscientist from the University of Rome, La Sapienza, continues her work, begun with the Consortium and will graduate in early 2014 after having helped complete some MS/SFO projects that remained incomplete: the mathematical/statistical analyses of the geochemical data recovered during three deployments of the Benthic Boundary Layer Array (BBLA) at MC118. Alessandra will return to UM to continue the processing and interpretation of new AUV multibeam data, correcting for noise, navigation errors and extracting bathymetry and backscatter from which images and morphological, biological and geological analyses are being made.

***Incomplete tasks:***

Although some of the tasks have not been completed, all have been attempted and effort expended above and beyond the allotted time and resources. Several remain on the task-list for future cruises and incorporation into future special reports to the agency, deployment of the HLAs being first and foremost but also including a biostratigraphic report on the MC118 site and at least an attempt to apply the UT processing techniques designed with the MS/SFO in mind.

***Publications:***

The list of publications and presentations accompanies this report. It is growing ever-greater, and includes award-winning articles and posters, invited presentations and contributions as well as many, many peer-reviewed articles and proceedings contributions to scientific literature and scholarly meetings, national and international. The duplicate WesternGeco dataset acquired by CMRET has been evaluated and has already led to the discovery of multiple characteristics not previously identified in any dataset from MC118. Beginning data analyses have contributed to the Consortium effort and some of these are represented in presentations and publications.

## **Task 8. Project Summary Updates:**

Periodic website updates are the responsibility of the CMRET together with DOE.

Publications are added to the Consortium list as they appear or as notification is received and a list of recent publications accompanies this report.

The Consortium website continues to be expanded and updated though there is much information still awaiting posting. Unfortunately, reductions in personnel as well as funding have necessitated shifting personnel from this important task to other more pressing duties.

It is a goal of the CMRET to get many of the older reports, logs and other data posted. Geological and geophysical pages for the website include core locations and descriptions, cruise reports, meeting presentations, online geophysical data collected by the CMRET, reports of meetings and many maps derived from Consortium effort.

This report – although lacking in some areas - is the project summary for the MS/SFO and hydrates project since the selection of the site for the Observatory.

## **CONCLUSIONS**

This report covers the accomplishments of the Cooperative Agreement, #DE-FC26-06NT42877, between the Department of Energy and the Center for Marine Resources and Environmental Technology, University of Mississippi. The efforts of the Hydrates Research Consortium are reviewed: scientific approaches and innovations, experimental design, testing and execution, data evaluation and analyses, laboratory, shop and cruise efforts, innovations in design and redesign of instruments, systems, and procedures, reporting via presentations at national and international meetings as well as at local and regional venues, and publication of results including cross-discipline publications between Consortium members cooperating on projects serving the overall effort.

Industry data have been analyzed and integrated with high-resolution data validating a capability to merge multiple datasets to predict hydrate in the shallow subsurface with greater accuracy than any known single method can provide. Innovative data processing techniques and approaches are being employed to evaluate seismic datasets, both standard and Consortium-developed, and an improved image of the subsurface structure of the carbonate-hydrate mound at MC118 is emerging. HLA configuration and deployment challenges continue and we continue to develop new deployment and recovery approaches and techniques to overcome them. A preliminary hydrate 3-gas model has been used with actual MC118 data to predict the range of hydrate stability at our observatory site. Manuscripts have been submitted and resubmitted and, in some cases, accepted and published in peer-reviewed journals. Every effort has been made to maximize Consortium members' access to and benefit from the cruises scheduled throughout the life of this award. New funding sources continue to be sought. Additional efforts to monitor developments resulting from the vast amounts of hydrocarbons spilled into the seawater at MC252 are ongoing, with Consortium researchers are making significant findings/contributions to unraveling that developing predicament. Funding through DOE will continue through an award to conduct simultaneous resistivity and oceanographic studies.

## ACRONYMS AND ABBREVIATIONS

1-D	one-dimensional
3-C	3-component
3-D	3-dimensional
4-C	four component
ABCMS	Automated Biological Chemical Monitoring System
ABIL	Autonomous Benthic Instrument Lander
A/D	analog to digital
AGU	American Geophysical Union
AUV	autonomous underwater vehicle
AVO	amplitude vs. offset
BBLA	Benthic Boundary Layer Array
BEG	Bureau of Economic Geology (University of Texas)
BLA	Borehole Line Array
BOEM	Bureau of Ocean Energy Management
BSR	bottom-simulating reflector
C&C	Chance and Chance
CFs	cross-corellated functions
CGGVeritas	Compagnie Générale de Géophysique (CGG) and Veritas
CH <sub>4</sub>	methane
CMRET	Center for Marine Resources and Environmental Technology
CMSHYD	stand-alone computer program; Sloan's statistical thermodynamic approach
CSA	Chimney Sampler Array
CSEM	Controlled-source Electro-Magnetic
CTD	Conductivity, Temperature, Depth
DATS	data acquisition and telemetry system
DCR	direct current resistivity
DF	double frequency
DIC	dissolved inorganic carbon
DOC	Department of Commerce
DOE	Department of Energy
DOI	Department of the Interior
DRS	Data Recovery System
DWFS	deep water filter system
ECOGIG	ECosystem impacts of Oil and Gas Inputs to the Gulf
EGL	Exploration Geophysics Laboratory
EMD	Empirical Mode Decomposition
EOS	equation-of-state
FFID	field file identification
FSU	Florida State University
FY	Fiscal Year
GI	gas-injection (energy source)
GOM	Gulf of Mexico
GOM-HRC	Gulf of Mexico-Hydrates Research Consortium
GRI	Gulf Recovery Initiative
HF	heat flow
HLA	horizontal line array

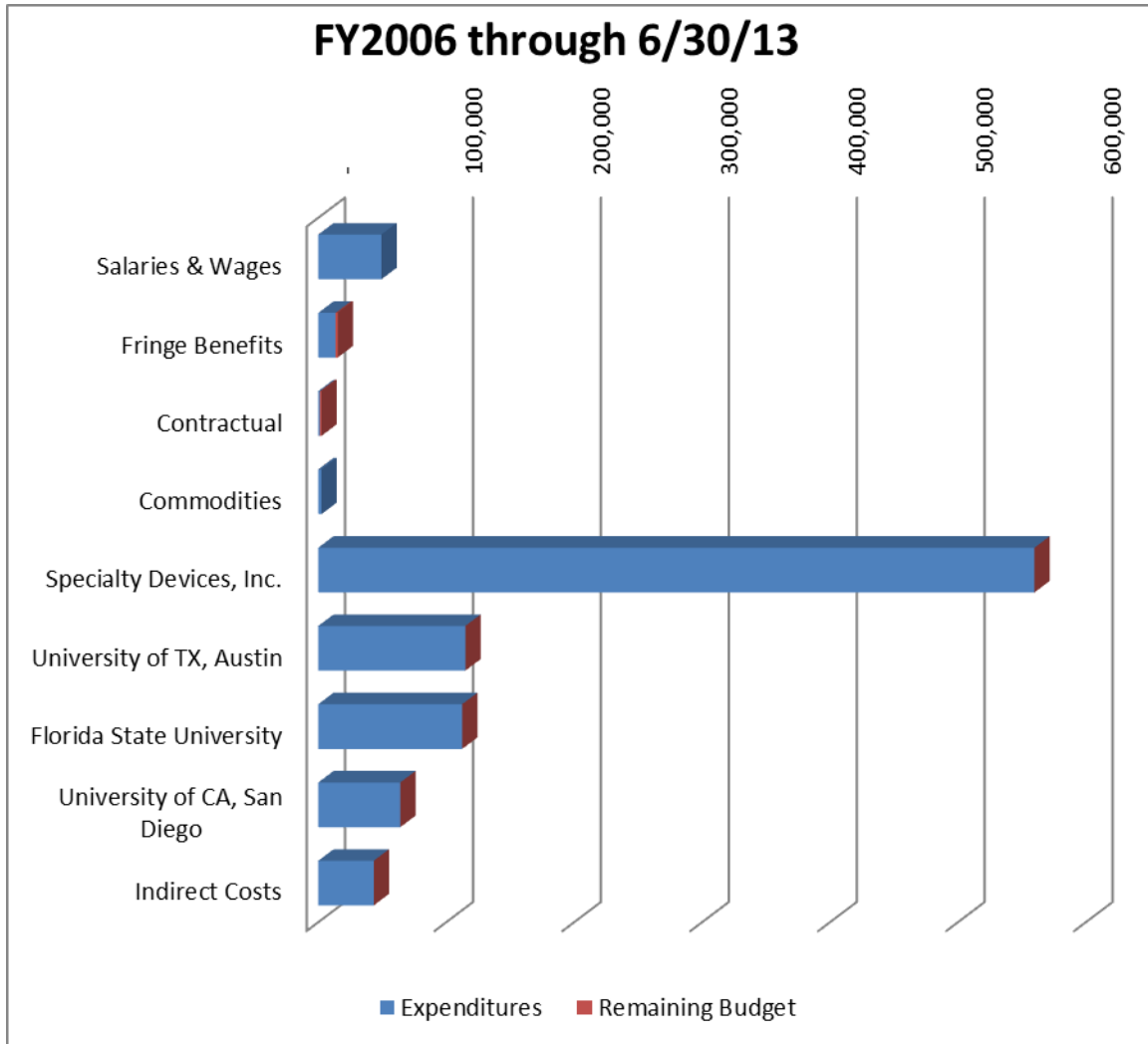
HRC	Hydrates Research Consortium
HSF	Hydrate Stability Field
HSZ	Hydrate Stability Zone
HYDGAS	new hydrate equation-of-state
IDP	Integrated Data Power Unit/Interconnection and Data Recovery device
IODP	Integrated Ocean Drilling Program
IR	Infrared
ISE	International Submarine Engineering
I-SPIDER	Integrated Scientific Platform for Instrument Deployment and Emergency Recovery
JPC	Jumbo Piston Core/Coring
JSL	Johnson SeaLink
LARS	launch and recovery system
LGC	Lookout Geophysical Company
LUMCON	Louisiana Universities Marine CONsortium
MC	Mississippi Canyon
METS	methane sensor
MIMS	membrane introduction mass spectrometer
MMRI	Mississippi Mineral Resources Institute
MMS	Minerals Management Service
MS/SFO	monitoring station/sea-floor observatory
MSU	Mississippi State University
M/V	merchant vessel
NAVOCEANO	U.S. Naval Oceanographic Office
NETL	National Energy Technology Laboratory
NIUST	National Institute for Undersea Science and Technology
NMO	no velocity moveout
NOAA	National Oceanographic and Atmospheric Administration
NRDA	Natural Resource Damage Assessment
NRL	Navy Research Laboratory
NURP	National Undersea Research Program
OBS	ocean bottom seismometer
OER	Ocean Exploration and Research
OLA	Oceanographic Line Array
<i>P-wave</i>	compressional wave/pressure wave
PFA (=PCA)	pore-fluid array
PI	primary investigator
P-P	P-wave mode (P wave down and P wave up)
PPChirp	polarity-preserving chirp subbottom profiling system
P-SV	converted-shear mode (P-wave to SV-shear wave conversion)
PVT	pressure-volume-temperature
RMS	root mean squared
ROV	remotely operated vehicle
ROVARD	ROV Assisted Recovery Device
R/V	Research Vessel
SAIC	Science Applications International Corporation
SDI	Specialty Devices, Inc.
SEED	computer script used in seismology

SEG-Y	computer format used by many varieties of commercial data processing software
SFO	Sea Floor Observatory
SFP	Sea Floor Probe
SRI	SRI, International
SSD	Station Service Device
SS/DR	Surface-Source Deep Receiver
SSVP	shallow sediment velocity probe
STAR	SAIC's multidimensional simulator
STAR-HYDCH4	Constitutive descriptor
STRC	Seabed Technology Research Center
<i>S-wave</i>	shear wave
SWRI	SouthWest Research Institute
TA	thermistor array
TGS-NOPEC	geophysical data (2-D, 3-D) acquisition company
THROBS	SAIC's hydrate simulator
TWT	two-way travel time
UCSB	University of California, Santa Barbara
UCSD	University of California, San Diego
UGA	University of Georgia
UM	University of Mississippi
UMD	University of Maryland
USBL	ultra-short baseline navigation system
USC	University of South Carolina
USGS	United States Geological Survey
USM	University of Southern Mississippi
UT	University of Texas
UVTC	Underwater Vehicle Technology Center
VDC	volts of direct current
VLA	vertical line array
WesternGeco	Western Geophysical Company
WHOI	Woods Hole Oceanographic Institution

## **COST STATUS**

As can be seen in the figures and tables that follow, \$21 remain in Phase 1 (FY06) funds while all other Phases are spent out. All cost-share obligations have been met. The speed of sound probe is due to go to sea in July on a BOEM-funded cruise and that will complete testing for that instrument. The HLAs will go in on a cruise or cruises of opportunity and a report to DOE will follow that activity.

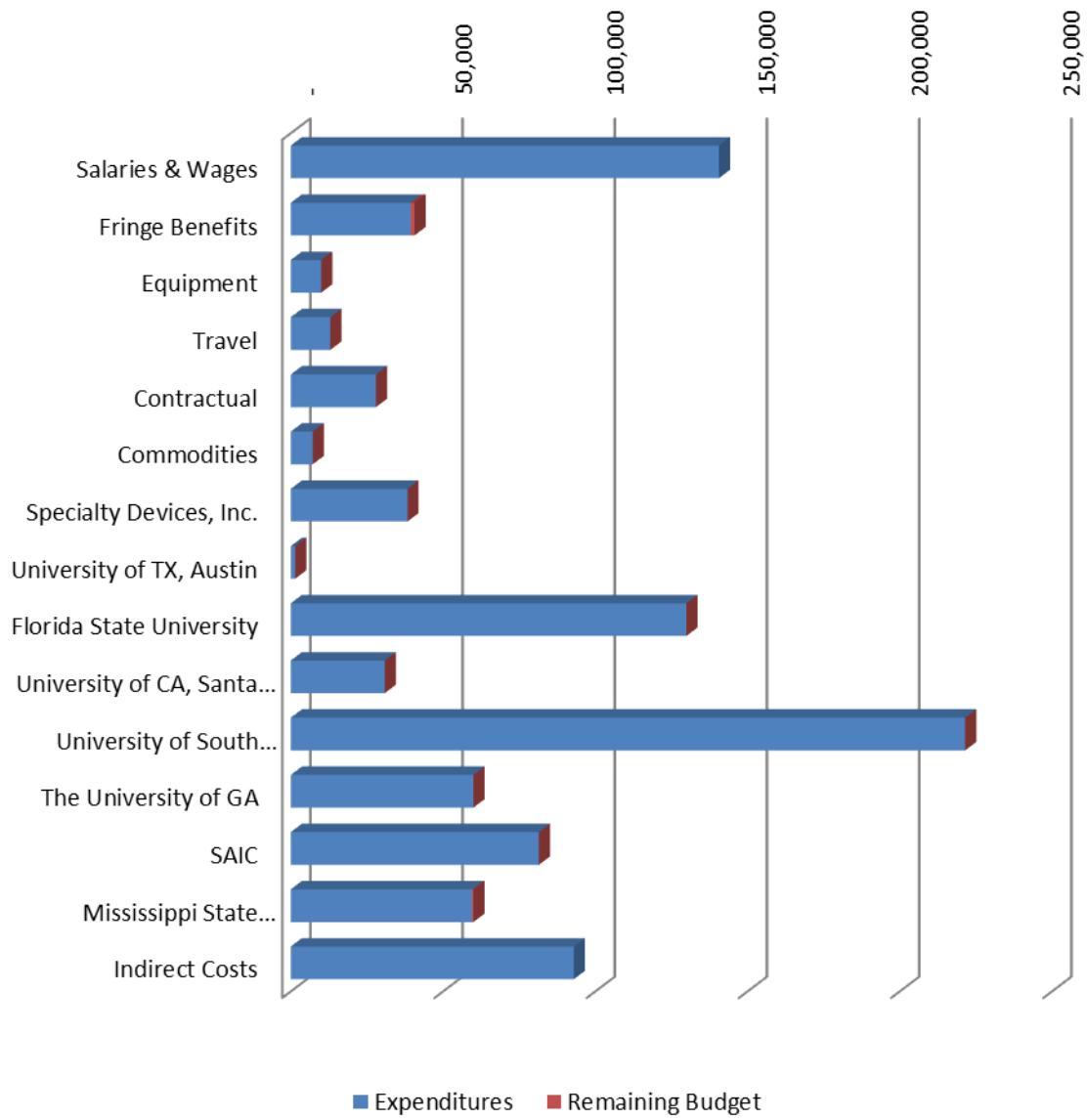




**Mississippi Mineral Resources Institute**  
**DOE DE-FC26-06NT42877**  
**Funding Status as of 7/31/13**

<b>FY2006</b>	<b>Expenditures</b>	<b>Remaining Budget</b>
<b>Salaries &amp; Wages</b>	49,309	(229)
<b>Fringe Benefits</b>	13,471	1,646
<b>Contractual</b>	1,355	1,145
<b>Commodities</b>	2,562	(2,562)
<b>Specialty Devices, Inc.</b>	559,912	-
<b>University of TX, Austin</b>	114,979	21
<b>Florida State University</b>	112,520	-
<b>University of CA, San Diego</b>	64,113	-
<b>Indirect Costs</b>	43,342	-
<b>Total</b>	<b>961,563</b>	<b>21</b>

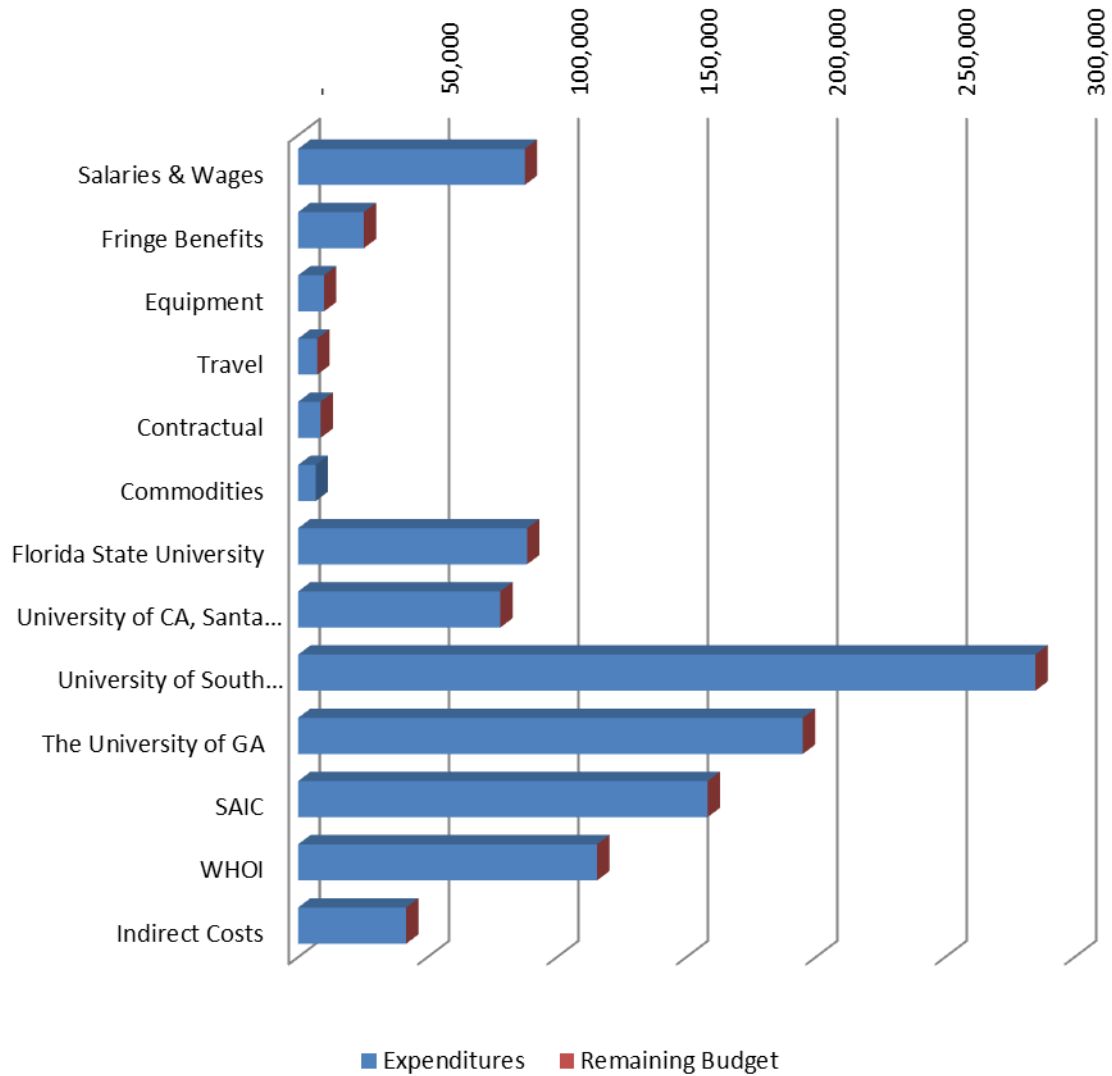
## FY2008 through 6/30/13



**Mississippi Mineral Resources Institute**  
**DOE DE-FC26-06NT42877**  
**Funding Status as of 7/31/13**

<b>FY2008</b>	<b>Expenditures</b>	<b>Remaining Budget</b>
Salaries & Wages	140,624	(713)
Fringe Benefits	39,369	1,251
Equipment	10,000	-
Travel	13,000	-
Contractual	28,000	-
Commodities	7,215	-
Specialty Devices, Inc.	38,336	-
University of TX, Austin	1,445	-
Florida State University	129,972	-
University of CA, Santa Barbara	30,881	-
University of South Carolina	221,516	-
The University of GA	60,000	-
SAIC	81,527	-
Mississippi State University	59,539	463
Indirect Costs	92,976	(1,001)
<b>Total</b>	<b>954,400</b>	<b>-</b>

## FY2009 through 6/30/13

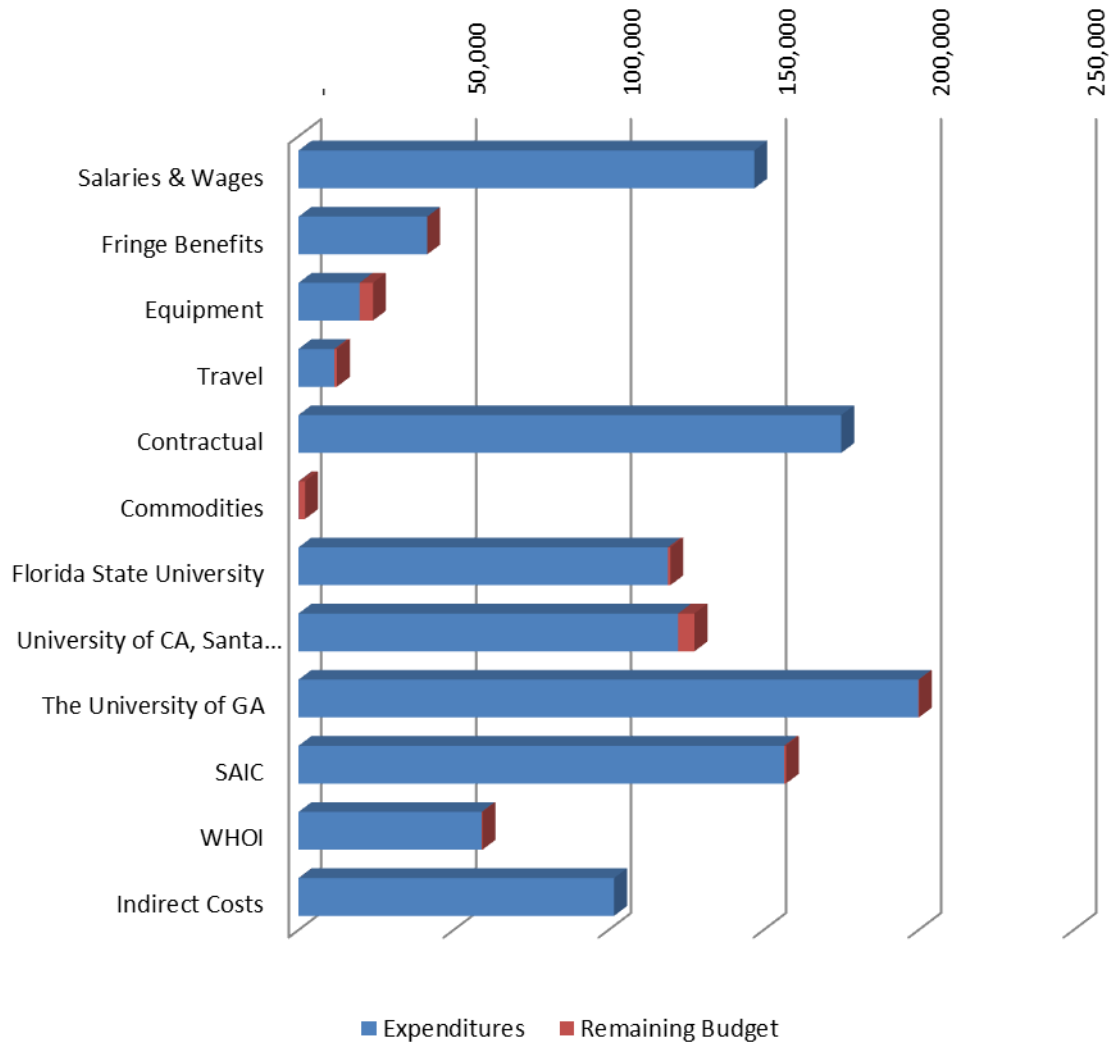


**Mississippi Mineral Resources Institute**  
**DOE DE-FC26-06NT42877**  
**Funding Status as of 7/31/13**

<b>FY2009</b>	<b>Expenditures</b>	<b>Remaining Budget</b>
Salaries & Wages	87,602	-
Fringe Benefits	25,405	-
Equipment	10,000	-
Travel	7,400	-
Contractual	8,717	2
Commodities	6,769	(2)
Florida State University	88,508	-
University of CA, Santa Barbara	78,118	-
University of South Carolina	284,899	-
The University of GA	195,029	-
SAIC	158,252	-
WHOI	115,550	-
Indirect Costs	41,775	-
<b>Total</b>	<b>1,108,024</b>	<b>-</b>



## FY2010 through 6/30/13



**Mississippi Mineral Resources Institute**  
**DOE DE-FC26-06NT42877**  
**Funding Status as of 7/31/13**

<b>FY2010</b>	<b>Expenditures</b>	<b>Remaining Budget</b>
<b>Salaries &amp; Wages</b>	147,047	(3,896)
<b>Fringe Benefits</b>	41,514	-
<b>Equipment</b>	19,694	4,306
<b>Travel</b>	11,549	851
<b>Contractual</b>	175,098	(5,598)
<b>Commodities</b>	82	2,026
<b>Florida State University</b>	119,127	854
<b>University of CA, Santa Barbara</b>	122,446	5,297
<b>The University of GA</b>	199,963	158
<b>SAIC</b>	156,605	654
<b>WHOI</b>	59,062	266
<b>Indirect Costs</b>	101,813	(4,918)
<b>Total</b>	1,154,000	-

## MILESTONE STATUS

Milestones identified in the Project Management Plan are discussed below and related to their status.

**Milestone 1: Complete the baseline characterization of the subsurface at the Observatory site, MC118 for presentation to the panelists at the DOE Merit Review. Complete Seismic Analysis of data from MC118 including defining features that relate to the occurrence of gas hydrates.**

Baseline character of the Observatory site at MC118, as revealed in several seismic data sets is complete. Three different resolution datasets have been evaluated and integrated. Jumbo piston cores, heat-flow data, and polarity-preserving chirp data have been recovered and are being integrated and evaluated. We have yet to complete the hydrate vessels for collection from the SSD and we have yet to complete the biostratigraphic analysis of the cores, but we definitely have a much clearer view of the surface and subsurface at MC118 than we did in 2010 when this proposal was tendered. We have, at last, recovered a photo survey of the western craters of the Woolsey Mound in order to complete our surface structures and benthic faunal analyses. We have also acquired a high resolution multibeam and polarity-preserving chirp survey of Woolsey Mound and vicinity and are working on the processing possibilities and interpretation. Chemical surveying has added valuable information to the site baseline characterization and a student is completing the analysis of the data from the BBLA.

**Milestone 2: Recover instruments from the seafloor and analyze data for baseline geochemistry and microbiology for the model (Task 9).**

All landers have been recovered. CMRET began analyses of the BBLA data in the summer of 2012 and now has a Visiting Scholar dedicated to the completion of this task.

**Milestone 3: Deploy horizontal line arrays, connect them to the data recovery system and collect test data from the data-logger. All components of the deployment have been tested successfully.** Deployment strategy has been redesigned to include a lander for delivery of the arrays, one-at-a-time to the seafloor. This will likely not occur until 2013. DOE will receive an addendum report when this milestone is achieved.

**Milestone 4: Complete installation of all Observatory components and collect geophysical data for input into model (Task 9).** Due to deployment logistics, this milestone will necessarily follow the deployment of the horizontal arrays. However, time-series geochemical data from the BBLA and CSA are now being processed and evaluated. Heat-flow, pore-fluid and JPC have been made available to modeling efforts. The heat-flow study was conducted in part to fulfil this goal and has done so. Data have been plugged into the SAIC model and vertical extent of the HSZ calculated. A paper detailing the approach and results has been submitted for publication to the Journal of Geophysical Research.

**Milestone 5: Complete additional surveys – SSSR, Mass spectrometer (STRC-funded), multibeam (NIUST-funded) to provide important updated baseline seismic data prior to the commencement of true monitoring.** The multibeam and mass spectrometer surveys are complete. We have received a complementary update in the multibeam from the Navy C&C along with very high resolution side-scan sonar data from MC118. The hydrophone array – necessary for the SSSR survey with the AUV-borne receiver - in Phase 2 of development by NOAA has been tabled for the moment, until the NOAA-NIUST budget is reinstated.

**Milestone 6: Complete 4C survey and analyze data for new software:** This dataset has been collected. When the original subcontractor was forced to abandon the project, CMRET took the lead. Eventually LGC was contracted to do the analyses, working with the CMRET.

This task is complete and the final report is part of this DOE report, Phase 3, Task 3.

**Milestone 7: Establish a “final” model of the observatory site, from which changes can be determined and monitoring established.** The initial phases of the modeling effort are complete. Real data are now being incorporated into the final model. Unfortunately, funds are exhausted so this project remains incomplete though SAIC researchers are seeking additional funds to enable them to complete it. If funds sufficient to complete the model are not secured, the approximation of the base of hydrate stability, determined in this reporting period, can surely serve until additional funds are found. This model was used to produce the base for the JGR submission.

**New Milestones – and status - from FY10 Program Management Plan**

**Milestone 5: Collect and evaluate giant piston cores from the MC118 Sea Floor Observatory. This Phase 4 milestone is tied to Task 2 and is estimated to be complete in July, 2013.** This task is essentially complete. The cores have been collected, logged and described and a report of their lithostratigraphy completed (APPENDIX B, and previous report, 42877R24). We still hope to get a complete biostratigraphic analysis that will help refine the history of this complex hydrate site.

**Milestone 6: Collect heat-flow data from MC118. This Phase 4 milestone is tied to tasks 2 and 3 and is estimated to be complete by March, 2012.** This task is complete. A complete report appears as Appendix C, this report.

**Milestone 7: Collect and evaluate additional gravity cores to complete sedimentation model, support geochemical and geophysical (structural) characterization of MC118. This Phase 4 milestone is tied to Tasks 2, 3 and 4 and is estimated to be complete by July, 2013.** This task has slid as two cruises had to be cancelled in light of certification issues with the vessel and failure of our equipment. We have rescheduled to coordinate coring with speed of sound probe testing. This cruise is now anticipated to occur in July, 2014, after which an addendum report will be made to DOE.

**Milestone 8: Integrate geophysical datasets with geochemical and biological data. This Phase 4 milestone is tied to tasks 2 and 3 and is partly complete but ongoing.** This task is in progress and results thus far have contributed significantly to numerous evaluations of MC118, most significantly the selection of sites for both the JPC and heat-flow cruises as well as our gravity coring cruise. An updated habitat map, tentatively tied to the shallow high resolution seismic and acoustic data was presented at the 2011 International AAPG in Milan and was awarded a “top ten” poster status for the entire meeting. We intend to continue this novel approach to seep evaluation into the foreseeable future.

**Milestone 9: Purchase and learn to operate an Infrared camera for the purpose of distinguishing hydrates in unopened cores. This Phase 4 milestone is tied to task 2 and is estimated to be complete by April, 2011.** This task is complete. The camera was used on the JPC cruise. Initial results were very promising and significant work has been done to improve the carriage and scale display. The goal is to use it on our coring cruise to identify which cores and sections are likeliest to contain hydrates and/or exhibit gas expansion.

**Milestone 10: Collect and analyze hydrate and “slime”(= protective ? biofilm) at hydrate outcrops in an effort to explain the existence and persistence of hydrate in seawater undersaturated for methane. This Phase 4 milestone is tied to tasks 2 and 4 and is estimated to be complete by September, 2013.** Pressure chambers have been designed and built with this goal in mind but not installed on a vehicle, either the SSD or the SRC. Installation will follow a March ECOGIG cruise that will require the SSD.

**Milestone 11: Recover additional pore-fluid time-series via additional instrument (PFAs, osmolander, peepers) deployments and recoveries. This Phase 4 milestone is tied to task 4 and is estimated to be complete by October, 2012.** We have deployed several systems of pore-fluid collection. Peepers were collected via the ROVARD. Analyses counterindicate this collection technique as the collection bags leaked. However, series of pore-fluids have been collected via cores and a variety of instruments. Although we will continue to try to retrieve the osmoboxes that remain, this task is complete. The technology won a spot as an ECOGIG PI for Dr. Lapham.

**Milestone 12: Deploy the ABCMS lander in upgraded configuration including video, lights reduced-size mass spectrometer, and altimeter. This Phase 4 milestone is tied to task 5 and is estimated to be complete by April, 2013.** This milestone was achieved in October, 2011, with the exception of the mass spectrometer functions. These were proven on the very successful July 2013 cruise when the MIMS identified seeps at the seafloor (see Phase 4, Task 5, final report).

## ACCOMPLISHMENTS

Following is a list of remarkable “firsts” that have been accomplished through this Cooperative Agreement:

- *MC118 has been designated by BOEM as a Research Reserve, the only such reserve in the Gulf of Mexico;*
- *The GOM-HRC’s Seafloor Observatory is the only such facility in the Gulf;*
- *Consortium researchers developed the SSSR especially to target the HSZ. They now have an entire pseudo-3D dataset from Woolsey Mound that has been vital to the success of much of the subsequent work at the MS/SFO;*
- *Consortium researchers have developed innovative processing techniques/strategies to suit different types of data and targets, culminating in the multiple-resolution approach to data-processing;*
- *Consortium researchers have successfully merged multiple resolution datasets to reveal a continuous 12sec seismic record with great detail in the shallow section and great depth but less detail from the industry data;*
- *Woolsey Mound resides atop a salt structure and contains “master faults” that connect the deep subsurface – hydrocarbon source – with the seafloor that control the migration of fluids, heat flow, seeps and other shallow features;*
- *The subsurface of Woolsey Mound shows significant changes in amplitude anomalies (or acoustic impedance) within a three-year time scale;*
- *These temporal anomalies are spatially associated with the major faults that intersect the seafloor;*
- *Since the major faults constitute the migration pathways for deep-sourced hydrocarbons, we suggest that changes in acoustic response, through time, are the result of actively migrating thermogenic hydrocarbons within the gas hydrate system;*
- *As the major faults constitute also the gas hydrate reservoirs, we speculate that gas hydrates may be repeatedly destabilized by transiting thermogenic hydrocarbons within the system in a very short time scale (3 years);*
- *Gas hydrates may be considered critically stable in active cold seep systems like Woolsey Mound, their stability through time depending primarily on the vigor of*



- the hydrocarbon flux through the gas hydrate system;*
- *Researchers have established a connection between the microbial communities and hydrate formation and, through experimental analyses of MC118 microbial consortia, that microbial cell wall material inhibits hydrate formation;*
  - *Consortium Researchers have now conducted the first Mola Mola photosurvey with proper navigation, enabling them to produce georeferenced seafloor photo-mosaics;*
  - *Consortium Researchers were successful in retrieving data from the observatory via optic modem, the first instance of real data being retrieved, optically, from the seafloor;*
  - *Consortium Researchers have been successful in verifying both resistivity and shallow-source-deep-receiver findings that indicated the possibility of hydrate in the shallow subsurface;*
  - *Consortium Researchers have verified the presence of “new” water-column methane plumes at depth via mass spectroscopy - ~600m and ~800m – following the Deep Water Horizon oil spill;*
  - *Consortium Researchers have succeeded in predicting areas of hydrated sediments and proven these speculations by coring target locations;*
  - *Consortium Researchers have acquired over 30 hours of resistivity data using the SSD as the transport for the 1100m DCR towed cable (the first time such a survey has ever been attempted with an ROV);*
  - *Consortium researchers have imaged the shallow subsurface using OBS data and vertical seismic profiling;*
  - *Consortium researchers have made initial images of the subsurface using noise as an energy source;*
  - *Consortium researchers have perfected USBL locating by attaching a transponder to every vehicle, lander, instrument, coring device, etc. that is deployed. Exceptional navigation enables us to return with ease to these locations months and years later;*
  - *Consortium Researchers have designed and executed complete multibeam and polarity-preserving chirp surveys via AUV – including a high-resolution survey conducted at 15m above seafloor – that returned data of unparalleled detail: 25cm horizontal, 10cm vertical resolution;*
  - *Consortium researchers have constructed a custom ROV to service the observatory. The SSD has dived to 1,600+m and recovered samples, landers and instruments, recovered imagery that verified lander and instrument locations and orientations moved instruments, etc. all while video-recording activities;*
  - *Consortium researchers have developed processing strategies for multibeam and polarity-preserving chirp data from MC118;*
  - *The UM has established a long-term relationship with the University of Rome, and has hosted 12 extremely capable students particularly expert in processing and interpreting multibeam data. These students are responsible for much of the seminal work with the seafloor data at MC118;*
  - *Consortium members have produced many journal papers, meetings transactions and made countless presentations at meetings around the world and have received several awards for their outstanding work;*
  - *Consortium members have collected a wealth of geochemical data and sediment samples from the water-column, the near-seabed and shallow seabed – BBLA and CSA and ROVARD;*

- *Consortium geochemists have defined areas of high, moderate and low microbial activity at Woolsey Mound through time, thereby unraveling a major component of the evolution of the site.*

## **PROBLEMS/DELAYS**

The majority of delays in the program derived from challenges presented by weather, working at 900m water depth and/or shortage of funds and personnel. Cruises have had to be cancelled due to weather, operator/participant illness and/or death, systems (electronics, cables, vehicle components, etc.) failures, inability to get replacement parts in a timely fashion, etc. The SDI/CMRET team continues to work diligently to overcome these challenges by increasing redundancy of systems and parts and increasing pre-cruise testing. The electronics of the SSD have been completely overhauled as parts are replaced but these are time-consuming enterprises. In addition, we have been forced to take on additional marine research work, particularly lander work, in order to keep our capabilities moving forward. We acknowledge that additional difficulties in the future are part of working in extremely challenging environments.

A major difficulty for the CMRET is loss of personnel. Director and project founder, J. R. Woolsey died tragically in July, 2008 and Tom McGee, our Senior Scientist/Geophysicist and charter member of the Consortium died unexpectedly in February, 2012. Due to lack of funding into the future, Leonardo Macelloni, our lead on many aspects of Consortium overall scientific effort, resigned to accept a position with Western Geco, effective in July, 2012. Two of our shop team have retired and another took a job involving no time at sea. Fortunately, our shop has been cooperating with the NIUST shop as both groups are short-handed and we benefit from complementary expertise, and a very dedicated core has banded together to be sure the spirit of this award was never violated and that the project would come to a successful conclusion.

## **PRODUCTS**

Important products of this project are many. Some of the more remarkable include:

1. Complete seismic data, analyses and interpretation from the SFO;
2. Acquisition, processing and analyses of multiple datasets via AUV (multibeam and chirp);
3. Multiple sets of cores, sediment analyses, pore-fluids analyses, mineralogical analyses, biological analyses;
4. Heat-flow and JPC data from Woolsey Mound;
5. Completion and successful use of the SSD and I-SPIDER ROVs;
6. Successful transitioning of systems to fiber-optic via 4000m Rochester Cable;
7. Multiple landers and instruments: PFA, CSA, BBLA, ABIL, ROVARD, ABCMS, HLA's, SSVP, ;
8. Innovative custom, data-processing and data analyses;
9. Superior navigation and locating capabilities;
10. Training and experience resulting in capable geoscientists;
11. Publications in peer-reviewed – and other - Journals;
12. Capabilities shared with other researchers and institutions.

## **PUBLICATIONS BY CONSORTIUM MEMBERS DERIVING IN FULL OR IN PART FROM DOE FUNDING (2006-2013):**

### **2006**

Backus, M. M., Murray, Paul, Hardage, B. A., and Graebner, R. J., 2006: High-resolution multicomponent seismic imaging of deepwater gas-hydrate systems. *The Leading Edge*, v. 25, no. 5, p. 578– 598.

Bradley Battista, A. Addison, Camelia Knapp, T. McGee, Application of the Empirical Mode Decomposition to Seismic Reflection and Ground Penetrating Radar Data, AGU Fall Meeting, Dec. 2006.

Camilli, R., C. Martens, J. Whelan, O. Pizarro, N. Farr, J. Goudreau, H. Mendlovitz, V. Ferrini, 2006, "Coordinated mapping and characterization of ocean floor methane sources with manned submersibles, AUVs and modular observatory arrays." In EOS: Trans. Amer. Geophysical Union Fall Meeting Supplement, 2006, Abstract.

Curtis, Andrew, Gerstoft, Peter, Sato, Haruo, Snieder, Roel, Wapenaar, Kees, 2006, *Seismic interferometry—turning noise into signal*, THE LEADING EDGE SEPTEMBER 2006, p. 1082-1092.

Dobbs, G. T., B. Balu, C. Young, A. Sinha, D. W. Hess, B. Mizaikoff, 2006: Plasma-assisted Deposition of Fluorocarbon Films for Molecular Recognition Layers in Mid-Infrared Attenuated Total Reflection Chemical Sensors. FACSS, Orlando/FL, September 24-28.

\*Dobbs, G., and B. Mizaikoff, 2006: Shining New Light at Old Principles: Localization of Evanescent Field Interactions at IR-ATR Sensing Interfaces. *Appl. Spectrosc.*, v.60, pp.573-583.

Dobbs, G. and B. Mizaikoff, 2006: In-situ monitoring of gas hydrate formation/dissociation with mid-IR fiber-optic evanescent field spectroscopy. Europt(r)ode VIII, Tuebingen, Germany, April 2-5.

Dobbs, G., Y. Raichlin, A. Katzir, B. Mizaikoff, 2006: Mid-Infrared Fiberoptic Evanescent Field Spectroscopy on the Nucleation of Gas Hydrates. Eastern Analytical Symposium, Somerset, NJ, November 13-16.

Hardage, B. A., DeAngelo, Michael, Sava, Diana, and Remington, Randy, 2006: Technology can avoid the fizzles. AAPG Explorer, Geophysical Corner, March, p. 28–29.

Hardage, B. A., and Murray, Paul, 2006: High resolution P-P imaging of deepwater near-seafloor geology. AAPG Explorer, v. 27, no. 7, p. 30.

Hardage, B. A., and Murray, P. E., 2006: Detailed imaging of deepwater hydrate geology with horizontal arrays of seafloor sensors. Offshore Technology Conference, paper 17929, 3 p.

Hardage, B. A., and Murray, P. E., 2006: P-SV data most impressive image. AAPG Explorer, Geophysical Corner, v. 27, no. 8, p. 30.

Hardage, B. A., Murray, Paul, Sava, Diana, Backus, M. M., Remington, R. L., Graebner, R. J., and Roberts, H. H., 2006: Evaluation of deepwater gas-hydrate systems. *The Leading Edge*, v. 25, no. 5, p. 572– 577.

Hardage, B. A., Remington, R. L., and Roberts, H. H., 2006: Gas hydrate—a source of shallow water flow? *The Leading Edge*, v. 25, no. 5, p. 634– 636.

Hardage, B. A., and Roberts, H. H., 2006: Gas hydrate in the Gulf of Mexico: what and where is the seismic target? *The Leading Edge*, v. 25, no. 5, p. 566– 571.

Lapham, L.L., Chanton, J.P., Martens, C.S., Higley, P.D., Jannasch, H.W., Woolsey, J.R., 2006: Pore Fluid Array Construction and Deployment at Mississippi Canyon 118, Gulf of Mexico. Offshore Technology Conference, Houston, TX, #18170.

\*Lloyd, K.G., L. Lapham, and A. Teske. 2006. An anaerobic methane-oxidizing community of ANME-1 archaea in hypersaline Gulf of Mexico sediments. *Applied and Environmental Microbiology*. Volume 72, p. 7218-7230.

Lutken, C.B., Brunner, C.A., Lapham, L., Chanton, J., Rogers, R., Sassen, R., Dearman, J., Lynch, L., Kuykendall, J., Lowrie, A., 2006: Analyses of Core Samples from Mississippi Canyon 118. Offshore Technology Conference, Houston, TX, #18208.

Lutken, C., T. McGee, A. Lowrie, C. Brunner, R. Rogers, L. Macelloni, A. Bosman, K. Sleeper, J. Dearman, R. Woolsey, L. Lynch, 2006: Comparison Of Two Candidate Sites For Gas Hydrates Sea Floor Monitoring. Vicksburg, MS, Mississippi Academy of Sciences' Annual Meeting, February 21-22.

\*Lutken, Carol, Tom McGee, Allen Lowrie, Charlotte Brunner, Rudy Rogers, Leonardo Macelloni, Alessandro Bosman, Ken Sleeper, Jennifer Dearman, J. Robert Woolsey, Leo Lynch, 2006: Comparison of Two Gas Hydrates Sites for Sea Floor Monitoring, Transactions of the 56th Annual Meeting of the GCAGS, Lafayette, LA.

Lutken, C., T. McGee, and R. Woolsey, 2006: Gulf of Mexico Gas Hydrates Monitoring Station and Sea-floor Observatory: A Status Report. The American Association of Petroleum Geologists Annual Meeting, Houston, TX, April 9-12.

Martin, Kevin, M.S. theses, 2006, Geological Oceanography, University of Southern Mississippi, *Development of a technique to quantify the volume of bubbles released from hydrocarbon seeps, using an inductive conductivity cell.*

McGee, Thomas M., 2006: A sea-floor observatory to monitor gas hydrates in the Gulf of Mexico. The Leading Edge, May, p. 644-647.

McGee, Thomas M., 2006: A sea-floor observatory to monitor a cold seep in the Gulf of Mexico. US-EU Baltic Workshop, Klaipeda, Lithuania, 23-25 May.

McGee, Tom, and Hardage, B. A., 2006: Hydrate system to be monitored: AAPG Explorer, Geophysical Corner, May, p. 24.

McGee, T., C. Lutken, R. Sassen, C. Brunner, R. Rogers, L. Macelloni, A. Bosman, K. Sleeper, J. Dearman, J.R. Woolsey, L. Lynch, 2006: Preliminary results at a hydrate/carbonate mound in the northern Gulf of Mexico. Fifth International Methane Hydrates Workshop, Edinburgh, U.K., 9-12 October.

McGee, Tom, and Leonardo Macelloni, 2006: Overview of observatory development and the site selection process. OTC Paper No. 18204, Houston, 3 May.

McGee, T., L. Macelloni and V. Goebel, 2006: Seismo-acoustic imagery of a carbonate/hydrate mound in the Gulf of Mexico. AGU Fall Meeting, San Francisco, CA, 11-15 December.

McGee, T., L. Macelloni, A. Bosman, C. Lutken, C. Brunner, R. Rogers, J. Dearman, K. Sleeper, and J. Woolsey, 2006, Hydrocarbon gas hydrates in sediments of the Gulf of Mexico, Burlington House, Piccadilly, U.K., Geological Society of London, January.

Mizaikoff, B., 2006: Mid-Infrared Chemical Sensors based on Quantum Cascade Lasers: The Next Generation. International Symposium on Spectral Sensing Research, Bar Harbor, ME, May 29-June 2.

Mizaikoff, B., 2006: Environmental Analysis with Optical Sensors - Quo Vadis? Invited Presentation, Europt(r)ode VIII, Tuebingen/Germany, April 2-5.

Mizaikoff, B., 2006: Next-Generation Mid-Infrared Sensors in Harsh Environments. Invited Presentation, ACS Fall Meeting, San Francisco/CA, September 10-14.

Mizaikoff, B., 2006: A New Frontier: Mid-Infrared Chemical Sensors Based on Single-Mode Waveguides. Invited Presentation, SPIE Optics East, Boston, MA, October 1-4.

Murray, P.E., C. Zala and M. Dunham-Wilkie, 2006: Storage and Distribution of Digital Data from the Gulf of Mexico Seafloor Observatory. Proceedings of the Houston, TX, Offshore Technology Conference (OTC 17962), May 1-4.

Pi Y., Li S., Pearson A., Noakes J., Culp R., and Zhang C. L. Effects of gas hydrates on archaeal community structure and carbon cycle in the Gulf of Mexico. American Geophysical Union Annual Meeting. December 10-16, 2006. San Francisco.

Pizarro, Oscar, Norm Farr, Richard Camilli, Jean Whelan, Chris Martens, Joanne Goudreau, Howard Mendlovitz and Luis Camilli, 2006, In-situ Optical Characterization of Methane Seeps and Bubble Plumes, AGU Annual Meeting.

Roberts, H. H., Hardage, B. A., Shedd, W. W., and Hunt, J., Jr., 2006: Seafloor reflectivity--an important seismic property for interpreting fluid/gas expulsion geology and the presence of gas hydrate. The Leading Edge, v. 25, no. 5, p. 620– 628.

Rogers, R.E., Sassen, R., Dearman, J.S., and Zhang, G., 2006: Factors Prompting Seafloor Experiments to Investigate Microbial/Hydrate Relationships. Paper No. 2006-TK-01, The Sixteenth (2006) International Offshore and Polar Engineering Conference & Exhibition, San Francisco, May 28- June 2.

Sassen, R., H. Roberts, W. Jung, C. Lutken, D. DeFreitas, S. Sweet, and N. Guinasso, Jr., 2006: The Mississippi Canyon 118 gas hydrate site: a complex natural system. Proceedings, 38th Offshore Technology Conference, paper 18132.

Sava, Diana, and Hardage, B. A., 2006: Rock physics characterization of hydrate-bearing deepwater sediments. The Leading Edge, v. 25, no. 5, p. 616– 619.

Sleeper, K., Lowrie, A., Bosman, A., Macelloni, L., Swann, C.T., 2006: Bathymetric Mapping and High-Resolution Seismic Profiling by AUV in MC118. Offshore Technology Conference, Houston, TX, #18133.

Wang F., Wang S., Jiang L., Ye G., Xiao X., Noakes J., Zhang C. L., 2006, Community structure and population dynamics of bacteria and Archaea at hydrocarbon seeps/gas hydrates in the Gulf of Mexico. American Geophysical Union Annual Meeting. December 10-16, San Francisco.

Zhang C. L., J. Noakes. 2006. Sea-floor Observatory in the Gulf of Mexico: Tracing the Carbon Flow in Gas-Hydrate Environments. OTC publication. Paper number: OTC 17804-pp.

Zhang C.L. and Noakes J. 2006, Hydrates As An Energy Source: Lipid Biomarkers And Carbon-Isotope Signatures For Tracing The Carbon-and-Energy Flow In The Gulf of Mexico Gas-Hydrate Systems. Ocean Technology Conference, May 2006. Houston, TX.

Zhang C. L., Yan T., Ye Q., Pancost R. D., and Noakes J. Lipid Biomarkers, Isotope Signatures, and Genomics of Gas Hydrates and Hydrocarbon Seeps in the Gulf of Mexico. Environmental Systems Microbiology Symposium. March 29-31, 2006. GaTech, Atlanta.

## 2007

\*Battista, Bradley, Camelia Knapp, Tom McGee and Vaughn Goebel, 2007: Application of the Empirical Mode Decomposition and Hilbert-Huang Transform to seismic reflection data. Geophysics, 72(2), pp. H29-H37.

Battista, Bradley, A. Addison, Camelia Knapp, T. McGee, Application of the Empirical Mode Decomposition to Seismic Reflection and Ground Penetrating Radar Data, AGU Fall Meeting, Dec. 2007

Camilli, R., and A. Duryea. "Characterizing marine hydrocarbons with in-situ mass spectrometry" *in proceedings of IEEE OCEANS Vancouver 2007.*



Caruso, Simona, M.S. theses, 2007, *Definition of Mississippi Canyon Block 118 Seafloor bio-geological processes, combining acoustic, video, and geological data*. University of Rome, La Sapienza.

Chanton, J. P., L. L. Lapham, C. S. Martens, P. D. Higley, and J. R. Woolsey. 2007. Gulf of Mexico Hydrate Research Consortium Geochemistry Overview. Geochemistry Department of Energy-National Energy Technology Laboratory Merit Review Board Meeting. Oral presentation. Golden, Colorado. September 17-21.

Dearman, J.L., 2007, *Gas hydrate formation in Gulf of Mexico sediments*. Ph.D. Dissertation, Mississippi State University.

Dobbs, Gary T, 2007, PhD dissertation, 2007, *Analysis of chemical signals from complex oceanic gas hydrate ecosystems with infrared spectroscopy*, Georgia Tech.

\*Dobbs, Gary T., Balamurali Balu, Christina Young, Christine Kranz, Dennis W. Hess, and Boris Mizaikoff, 2007, *Mid-Infrared Chemical Sensors Utilizing Plasma-Deposited Fluorocarbon Membranes*, Anal. Chem., 79(24), 9566-9571.

Dobbs, Gary T., An Nguyen, Yulia Luzinova, Yosef Raichlin, Christine Kranz, Abraham Katzir, Roger Sassen, and Boris Mizaikoff, 2007, *Infrared Spectroscopy for Exploring Complex Oceanic Gas Hydrate Ecosystems*, FACSS, 10-07, Memphis, TN.

Geresi, Erika, 2007: Ph.D. dissertation: Vertical line array performance in gas hydrate bearing sediment in the northern Gulf of Mexico. University of Victoria, B.C.

Gerstoft, P, LA Brooks, S Fried, B Kuperman, K Sabra, 2007, *Ocean acoustic interferometry using noise and active sources*, invited paper presented by Peter Gerstoft at the American Geophysical Union Meeting, San Francisco, CA.

Hardage, B. A., 2007: Gas hydrate and LNG tankers. AAPG Explorer, v. 28, no. 5, Geophysical Corner, p. 36.

Hardage, B. A., Sava, Diana, DeAngelo, Michael, and Remington, R. L., 2007: Which seismic wave mode is best? AAPG Explorer, v. 28, no. 4, Geophysical Corner, p. 32.

Higley, Paul, 2007: New Concepts in Robotic Operated Vehicle (ROV) Design. Mid-South Area Science and Engineering Conference, Oxford, MS, MAESC 10071.

\*Kelleher, B.P., Simpson, A.J., Rogers, R.E., Dearman, J., Kingery, W.L., 2007: Effects of natural organic matter from sediments on the growth of marine gas hydrates. Marine Chemistry, 103: 237- 249.

Lapham, L., 2007, *In situ* measurements of methane cycling in cold seep sediments containing gas hydrates and brines. Ph.D. Thesis, University of North Carolina.

Lapham, Laura, Jeff Chanton, Chris Martens, Ken Sleeper, and J. R. Woolsey, 2007, *Methane and biogeochemical gradients within acoustic wipe-out zones at a Gulf of Mexico cold seep*, presented by Lapham at the American Geophysical Union Meeting, San Francisco, CA.

Lapham, L. L., J. P. Chanton, C. S. Martens, K. Sleeper and J. R. Woolsey. 2007. Spatial variability in microbial activity associated with acoustic wipe-out zones in the northern Gulf of Mexico. Abstract. American Geophysical Union, Acapulco, Mexico, May 22-25.

Lapham, L.L, J. Chanton, C.S. Martens, K Sleeper and J.R. Woolsey. 2007. Methane and biogeochemical gradients within acoustic wipe-out zones at a Gulf of Mexico cold seep. American Geophysical Union. Oral presentation. Acapulco, Mexico, May 22-25.

Lapham, L., J. Chanton, C. Martens, P. Higley, H. Jannasch, J. Woolsey, and K. Sleeper, 2007, Biogeochemical sensors: design and applications of the Pore Fluid Array for the Mississippi Canyon 118 Gas Hydrate Seafloor Observatory, Oxford, MS, Mid-South Area Engineering and Sciences Conference, University of Mississippi, May 17-18, 10075.

Lapham, L. L., J. P. Chanton, C. S. Martens, P. D. Higley, H. W. Jannasch, and J. R. Woolsey. 2007. Monitoring long-term gas hydrate stability using a Pore-Fluid Array (PFA). Hydrate observatory meeting. Poster presentation. Joint Oceanographic Institutions Gas Hydrate Observatories Workshop on July 18-20 in Portland, Oregon.

Lutken, C. B. and J. R. Woolsey, 2007: A Sea Floor Observatory for Real-Time Investigation of Gas Hydrates. Mid-South Area Science and Engineering Conference, Oxford, MS, MAESC 10070.

Lutken, C.B., 2007, *Gulf of Mexico Gas Hydrates Research Consortium and Sea-floor Observatory*, Report to the Department of Energy's Methane Hydrate Merit Review, Golden, Colorado September 20.

Lutken, C.B., 2007, *Gulf of Mexico Gas Hydrates Research Consortium and Sea-floor Observatory* Report to the Department of Energy's Methane Hydrate Advisory Committee, Golden, CO, April 24 – 25.

Macelloni, L., 2007: AUV Multibeam Sonar: Survey, Mapping Application and Relevant Data Processing. Mid-South Area Science and Engineering Conference, Oxford, MS, MAESC 10078.

Macelloni, L., S. Caruso, T. M. McGee, C. B. Lutken, A. Bosman, K. Sleeper and J.R. Woolsey Jr., 2007: Mississippi Canyon Block 118 Hydrates Mound: a complex hydrates structure in the Northern Gulf of Mexico. Oral Presentation, Sesto Forum Italiano di Scienze della Terra - Geoitalia 2007, Rimini, September, 12-14.

Martens, Christopher, Howard Mendlovitz, Rich Camilli, Norman Farr, J. Robert Woolsey, Kenneth Sleeper, 2007: Design and application of the Chimney Sampler and Benthic Boundary Layer Arrays for the Mississippi Canyon 118, Gas hydrate seafloor observatory. Mid-South Area Science and Engineering Conference, Oxford, MS, MAESC10074.

McGee, Thomas, 2007: Implementation of Shallow-Source/Deep-Receiver Technology to Obtain High Seismic Resolution of Sub-bottom Sediment in Deep Water. Mid-South Area Science and Engineering Conference, Oxford, MS, MAESC10062.

McGee, Thomas, 2007: Geophysical Sensors: Design and Applications of the Acoustic Water-column Line Array and Seismic Sea-floor Line Arrays for the Gulf of Mexico Sea-floor Observatory. Mid-South Area Science and Engineering Conference, Oxford, MS, MAESC10063.

McGee, T.M., 2007: Using ambient noise for subsurface imaging. Underwater noise workshop, International Association of Oil and Gas Producers, Burlington, Massachusetts, 4-5 June.

McGee, Tom, Peter Gerstoft, and Ross Chapman, 2007: Using ambient noise to image the interior of a carbonate/hydrate mound. Gas-Hydrate Observatories Workshop, Portland, Oregon, 18-20 July.

McGee, T., C. Lutken, R. Rogers, C. Brunner, P. Verdugo and J. R. Woolsey, 2007: Why and how hydrates fill fractures in soft sediments. Gas-Hydrate Observatories Workshop, Portland, Oregon, 18-20 July.

McGee, T. M., L. Macelloni, Vaughn Goebel, 2007, Seismo-acoustic imagery of a carbonate/hydrate mound in the Gulf of Mexico. In McKay, M. and J. Nides (eds) 2007, *Proceedings: Twenty-third Gulf of Mexico information transfer meeting*, January 2007. U.S. Dept. of the Interior, Minerals Management Service, Gulf of Mexico OCS Region, New Orleans, La. OCS Study MMS 2007-066. 612 pp.

Mizaikoff, B., 2007: Good Vibrations - Infrared Spectroscopy and Sensing in Extreme Environments. Invited Presentation, ANAKON 2007, Jena, Germany, March 27-30.

Mizaikoff, B. and C. Kranz, 2007: From Infrared Chemical Sensors to Multifunctional Scanning Probes - Research at the Applied Sensors Laboratory, Friedrich Schiller Universität Jena, Jena, Germany, March 29.

Morley, Michael G. M.S. Theses Ocean Sci, 2007, *Acoustic Inversion Methods Using Ship Noise*, University of Victoria, B.C.

\*Rogers, R., Zhang, G., Dearman, J., and Woods, C., 2007: Investigation into surfactant/gas-hydrate relationship. in Gas Hydrates and Clathrates, special volume of the Journal of Petroleum Science & Engineering, 56, 1-3.

Sassen, R., S. T. Sweet, A. V. Milkov, D. A. DeFreitas, G. G. Salata, and E. C. McDade, 2007, Geology and Geochemistry of Gas Hydrates, Central Gulf of Mexico Continental Slope, Corpus Christi Geological Society Bulletin, January.

Woolsey, J. R., L. Macelloni, T. M. McGee, C. B. Lutken, K. Sleeper and P. Higley, 2007: A Deep Sea Floor Observing System For Real-Time Observation In The Northern Gulf Of Mexico. Poster, Sesto Forum Italiano di Scienze della Terra - Geoitalia 2007, Rimini September, 12-14.

\*Zhang, G., Rogers, R.E., French, W.T., and Lao, W., 2007: Investigation of microbial influences on seafloor gas-hydrate formations. Marine Chemistry, 103 (2007) 359- 369.

## 2008

Battista, Bradley M., 2008, *Advanced Nonlinear Signal Processing Tools for use with High-Resolution Seismic Reflection and Ground-Penetrating Radar Data*, PhD Thesis, University of South Carolina.

Bowles, M.W., and S.B. Joye (2008) Nitrate reduction pathways in sediments from a Gulf of Mexico cold seep. Denitrification RCN Meeting, Cambridge Maryland, May.

Bowles, M.W., V.A. Samarkin, and S.B. Joye. (2008) Activity, diversity and relative abundance of sulfate reducing bacteria in oil-rich sediments from a lower continental slope Gulf of Mexico cold seep. ASLO-AGU-ERF-TOS Ocean Sciences, Orlando Florida, March.

Brooks, Laura, PhD thesis: Ocean acoustic interferometry, 2008.

\*Garg, Sabodh K., John W. Pritchett, Arata Katoh, Kei Baba, and Tetsuya Fujii, 2008, *A mathematical model for the formation and dissociation of methane hydrates in the marine environment*, JOURNAL OF GEOPHYSICAL RESEARCH, VOL. 113, B01201, doi:10.1029/2006JB004768.

Haacke, R., M. Riedel, J. Pohlman, K. Rose, L. Lapham, T. Hamilton, R. Enkin, G.D. Spence, and R.D. Hyndman. *Investigations on the role of gas hydrate in wide-spread slope failures at frontal ridges of the accretionary wedge of the northern Cascadia margin*. American Geophysical Union meeting, Dec 2008.

Ingram, Wesley, Meyers, S., Brunner, C., and Martens, C., 2008, *Centennial-millennial scale stability of a large gas hydrate field in the northern Gulf of Mexico*, The Geological Society of America, Southeastern Section, 57th Annual Meeting, 10 -11 April, Abstracts and Program, v. 40, no. 4, p. 278.

Ingram, W.C., Meyers, S.M., Brunner, C., and Martens, C., *Centennial-Millennial scale stability of a large Gas Hydrate field in the Northern Gulf of Mexico*, Abstract. Presented at the Society of Exploration Geophysics Meeting on Unconventional Resources, Vancouver, British Columbia, Canada, Sept. 2008.

\*Lapham, L., J. Chanton, C. Martens, K. Sleeper and J. Robert Woolsey, 2008, *Microbial activity in surficial sediments overlying acoustic wipeout zones at a Gulf of Mexico cold seep*, *Geochemistry, Geophysics, Geosystems*, Volume 9, No. 6, June 4.

Lapham, L. L., J. P. Chanton, Martens, C. S., Mendlovitz, H. P., Higley, P. D., Lutken, C. B., and Woolsey, J. R. (2008). *Unique tools sample sediment pore water near seafloor hydrate mounds in the Gulf of Mexico*. *Fire in the Ice, Methane Hydrate Newsletter*. Winter: 20pg.

\*Lapham, L.L., J .P. Chanton, C.S. Martens, P. D. Higley, H. W. Jannasch and J.R. Woolsey (2008). *Measuring temporal variability in pore-fluid chemistry to assess gas hydrate stability: Development of a continuous pore-fluid array*, Environmental Science and Technology, 42, 7368-7373.

\*Lapham, L.L., M.J. Alperin, J.P. Chanton, and C.S. Martens (2008). *Upward advection rates and methane fluxes, oxidation, and sources at two Gulf of Mexico brine seeps*. Marine Chemistry, 112, 65-71. <http://dx.doi.org/10.1016/j.marchem.2008.06.001>

Lapham, L.L., J .P. Chanton, C.S. Martens, P. D. Higley, H. W. Jannasch and J.R. Woolsey, 2008, *Temporal variability in pore-fluid chemistry at a Gulf of Mexico gas hydrate site*. American Geophysical Union meeting, Dec 2008.

Lloyd. K.G., MacGregor, B.J., and A. Teske, 2008, Quantification of archaeal RNA and DNA in marine sediments with qPCR and qRT-PCR. Cairns, Australia, 12<sup>th</sup> Meeting of the International Society for Microbial Ecology (ISME), August 11-15.

Lutken, C., 2008: In Memorium: J. Robert Woolsey, Jr., Fire in the Ice Newsletter, Fall, p. 22-24.

Macelloni, Leonardo, Bradley M. Battista, Thomas M. McGee and Vaughn Goebel, 2008, *A Band-Modulated Hilbert-Huang Transform For Seismic Attribute Analysis In Shallow, Hydrate-Bearing Sediments*, IEEE/OES Chile-US Workshop on Ocean Observation Systems, Working Group on Observation and Assessment of Gas Hydrates in the Coastal Ocean, Viña Del Mar , Chile, 4-7 Nov., 2008.

\*McGee, T., L. Macelloni, A. Bosman , C. Lutken, C. Brunner, R. Rogers, J. Dearman, K. Sleeper and J. R. Woolsey, 2008, Hydrocarbon gas hydrates in sediments of the Mississippi Canyon area, northern Gulf of Mexico. In Special Publication of the Geological Society of London, Sediment-hosted gas hydrates: New insights on natural and synthetic systems, D. Long (ed.)

\*McGee, T, J. R. Woolsey, L. Macelloni, B. Battista, S. Caruso, L. Lapham, V. Goebel and J. Carroll, 2008, *Progress toward a sea-floor observatory at a carbonate/hydrate mound in the northern Gulf of Mexico*, US/EU Baltic 2008 International Symposium Tallin, Estonia May 27-29

McGee, T., and R. Rogers, 2008: Biogeophysics in the context of natural gas hydrates: northern Gulf of Mexico. AGU Chapman Conference on Biogeophysics, Portland, Maine, 13-16 October.

McGee, T., J. R. Woolsey, L. Lapham, R. Kleinberg, L. Macelloni, B. Battista, C. Knapp, S. Caruso, V. Goebel, R. Chapman, P. Gerstoft, 2008, *Structure Of A Carbonate/Hydrate Mound In The Northern Gulf Of Mexico*. Proceedings of the 6<sup>th</sup> International Conference on Gas Hydrates (IGCH 2008), Vancouver, British Columbia, Canada.

McGee, T., J. R. Woolsey, L. Lapham, R. Kleinberg, L. Macelloni, B. Battista, C. Knapp, S. Caruso, V. Goebel, R. Chapman and P. Gerstoft, 2008: Structure of a carbonate/hydrate mound in the northern Gulf of Mexico and possible hydrate distribution within it. Proceedings of IEEE/OES Chile-US Workshop on Ocean Observing Systems, Valparaiso, Chile, 3-6 November.

McGee, T., V. Goebel, A. Bosman and L. Macelloni, 2008: Recent techniques for acquiring and processing ultra-high-resolution images of the sea floor and shallow sub-bottom in deep water. Proceedings of IEEE/OES Chile-US Workshop on Ocean Observing Systems, Valparaiso, Chile, 3-6 November.

Radich, J., R. Rogers, W. French, and G. Zhang, 2008, Microbial and sediment effects on kinetics of gas hydrate formation," Philadelphia, PA, American Chemical Society National Meeting & Exposition, August.

Rawn, Claudia J., Roger Sassen, Shannon M. Ulrich, Tommy J. Phelps, Bryan C. Chakoumakos, E. Andrew Payzant, 2008, *Low temperature x-ray diffraction studies of natural gas hydrate samples from the Gulf of Mexico*, Proceedings of the 6th International Conference on Gas Hydrates (ICGH 2008), Vancouver, British Columbia, CANADA, July 6-10.

Rogers, R., G. Zhang, J. Dearman, and W. Wilson, 2008, Laboratory Tests of Hydrate Formation in Porous Media Influenced by Bioproducts, Orlando, FL, Annual Ocean Sciences Meeting, March 30-April 3.

Rogers, R.E., J. L. Dearman, G. Zhang, W.W. Wilson, C.B. Lutken, 2008, Gulf of Mexico Sediment Evaluations for Microbial-Mineral-Hydrate Associations, AAPG Annual Meeting San Antonio, April 20-24.

Rogers, R., G. Zhang, J. Radich, and S. Xiong, 2008, Role of microbe-mineral interactions in seafloor gas hydrate accumulations, Oxford, MS, 38<sup>th</sup> Annual Underwater Mining Institute, November.

Teske, A, 2008, Deep subsurface archaea – Diversity and Detection. Institute for the Chemistry and Biology of the Oceans, Oldenburg University, Germany. March 5.

\*Traer, James, Peter Gerstoft, Peter D Bromirski, WS Hodgkiss, and Laura A Brooks (2008), Shallow-water seismo-acoustic noise generation by Tropical Storms Ernesto and Florence, J Acoust. Soc. Am EL, 124, EL170-EL176, DOI:10.1121/1.2968296.

Zhang, G., R. Rogers, and T. French, 2008, Laboratory Tests to Determine Role of Bioproducts in Seafloor Gas Hydrate Accumulations, San Antonio, TX, AAPG Annual Convention and Exhibition, April 20- 23.

## 2009

\*Addison, A. D., B. M. Battista, and C. C. Knapp, 2009, Improved Hydrogeophysical Parameter Estimation from Empirical Mode Decomposition Processed Ground Penetrating Radar Data, *Journal of Environmental and Engineering Geophysics* vol. 14, no. 4, pp. 171-178.

\*Battista, B. M., A. D. Addison, and C. C. Knapp, 2009, Empirical Mode Decomposition Operator for Deep-sea GPR Data, *Journal of Environmental and Engineering Geophysics*, vol. 14, no. 4, pp.163-169.

Bell, Ryan J., PhD dissertation, 2009, *Development and deployment of an underwater mass spectrometer for quantitative measurements of dissolved gases*, University of South Florida.

Bell, R. J., S. K. Toler, R. T. Short, R. H. Byrne, In Situ Mass Spectrometry for Chemical Measurements in the Water Column and on the Sea Floor (poster), OceanObs '09 meeting in Venice, Italy (2009).

Biddle, J.F., S.M. Huse, M.L. Sogin, K.G. Lloyd, A. Ramette, A. Boetius, and A. Teske, 2009, Microbial Census of Marine Microbes at Methane Seeps: Initial results. Marine Biological Laboratory, Woods Hole, MA, ICOMM User workshop, April 6-9.

Bowles, M.W., and S.B. Joye (2009) A geochemical and microbiological analysis of nitrate reduction at a hydrothermal vent and a cold seep. 19th Annual V. M. Goldschmidt Conference, Davos, Switzerland, June.

\*Brooks, Laura A, Peter Gerstoft (2009), Green's function approximation from cross-correlations of 20–100 Hz noise during a tropical storm, *Journal of Acoust. Soc. Am* 125, 723-734 (PDF).

\* Brooks, Laura A, Peter Gerstoft (2009), Green's function approximation from cross-correlation of active sources in the ocean, *J Acoust. Soc. Am.*, 126, 46-55.([PDF](#))

Camilli, R., L. Macelloni, V. Asper, M. Woolsey, J. Williams, A. Diercks, C.B. Lutken, K. Sleeper, 2009, Discovery and characterization of cold seeps using a mass spectrometer operating aboard an autonomous underwater vehicle, AGU fall meeting, San Francisco, CA, December, 17, 2009.

\*Dearman, J.L., Wilson, W.W., Rogers, R.E., and Zhang. G., 2009. "Gas-Hydrate Promotion by Smectite-Bioproduct Interactions," *Marine Chemistry*, 115, Issues 1-2, 21-30.

\*Geresi, Erika, Ross Chapman, Tom McGee and Bob Woolsey, 2009, *Monitoring seafloor instability caused by the presence of gas hydrate using ocean acoustical and geophysical techniques in the northern Gulf of Mexico*. in Collett, T., A. Johnson, C. Knapp and R. Boswell, eds., *Natural Gas Hydrates: Energy Resource and Associated Geologic Hazards*, The American Association of Petroleum Geologists Hedberg Special Publication.



\*Hardage, B., H. Roberts, P. Murray, R. Remington, D. Sava, W. Shedd, J. Hunt Jr., 2009, *Multicomponent seismic technology assessment of fluid-gas expulsion geology and gas hydrate systems: Gulf of Mexico*. in Collett, T., A. Johnson, C. Knapp and R. Boswell, eds., *Natural Gas Hydrates: Energy Resource and Associated Geologic Hazards*, The American Association of Petroleum Geologists Hedberg Special Publication.

Lapham, L.L., C.S. Martens, and J.P. Chanton. *Controls on gas hydrate stability in methane-depleted sediments: Laboratory and field measurements*, American Geophysical Union (AGU) fall meeting, San Francisco, CA, December, 17, 2009.

Lloyd, K.G., 2009, *Microbially driven methane and sulfur cycling in a Gulf of Mexico methane seep and the White Oak River estuary*, Ph.D. thesis, University of North Carolina.

Lloyd, K.G., 2009, *Spatial structure and activity of shallow microbial communities in a Gulf of Mexico methane seep*. Goldschmidt Conference, Davos, Switzerland, June 21-26.

McGee, T. 2009, *Geologic structures associated with the carbonate/hydrate mound in Mississippi Canyon Block 118, Gulf of Mexico*, AGU fall meeting, San Francisco, CA, December, 17, 2009.

\*McGee, Thomas, Carol Lutken, Rudy Rogers, Charlotte Brunner, Jennifer Dearman, F. Leo Lynch and J. Robert Woolsey, 2009, *Can fractures in soft sediments host significant quantities of gas hydrates?* in Collett, T., A. Johnson, C. Knapp and R. Boswell, eds., *Natural Gas Hydrates: Energy Resource and Associated Geologic Hazards*, The American Association of Petroleum Geologists Hedberg Special Publication Memoir 89.

McGee, T.; J. R. Woolsey, L. Lapham, R. Kleinberg, L. Macelloni, B. L Battista, C. Knapp, S. Caruso, V. Goebel, R. Chapman, P. Gerstoft, 2009, *A Multidisciplinary Sea-Floor Observatory in the Northern Gulf of Mexico*. Proceedings of the Virtual Institute of Scientific Users of Deep-Sea Observatories, Tromsø, Norway, June 11-12

\*McGee, T., L. Macelloni, C. Lutken, A. Bosman, C. Brunner, R. Rogers, J. Dearman, K. Sleeper and J. R. Woolsey (2009): Hydrocarbon gas hydrates in sediments of the Mississippi Canyon Area, northern Gulf of Mexico. In *Sediment Hosted Gas Hydrates: New Insights on Natural and Synthetic Systems*, GeoSocLondon Spec Pub 319.

McGee, T.,<sup>1</sup> C. Lutken<sup>1</sup>, L. Macelloni<sup>1</sup>, J. R. Woolsey<sup>1</sup>, L. Lapham<sup>2</sup>, R. Kleinberg<sup>3</sup>, B. Battista<sup>4</sup>, C. Knapp<sup>4</sup>, S. Caruso<sup>5</sup>, V. Goebel<sup>6</sup>, R. Chapman<sup>7</sup>, P. Gerstoft<sup>8</sup>, 2009, *A multidisciplinary sea-floor observatory in the northern Gulf of Mexico*, Oceans 2009 in Biloxi, MS.

\*Morley, M.G., Dosso, S.E. and Chapman, N.R., 2009, *Array element localization using ship noise*, J. Acoust. Soc. Am. Volume 125, Issue 3, pp. 1403-1409.

Radich, J.G., 2009, *Laboratory and theoretical investigations of direct and indirect microbial influences on seafloor gas hydrates*. M.S. Thesis, Mississippi State University.

\*Radich, J., R.E. Rogers, W.T. French, and G. Zhang, 2009, *Biochemical reaction and diffusion in seafloor gas hydrate capillaries: Implications for gas hydrate stability*, *Chemical Engineering Science* 64, p4278-4285.

\*Sassen, R., H. Roberts, W. Jung, B. Phaneuf, A. Milkov, C. Lutken, D. DeFreitas, S. Sweet, and N. Guinasso, 2009, *Geologic and geochemical setting of the Mississippi Canyon 118 gas hydrate site, Gulf of Mexico: significance to hydrate volume*. in Collett, T., A. Johnson, C. Knapp and R. Boswell, eds., *Natural Gas Hydrates: Energy Resource and Associated Geologic Hazards*, The American Association of Petroleum Geologists Hedberg Special Publication.

Short, R. T., R. J. Bell, A. Chaudhary, S. K. Toler, F. H.; W. van Amerom, *In Situ Mass Spectrometry for Marine Applications: Present and Future* (oral), 57th American Society of Mass Spectrometry Conference on

Mass Spectrometry and Allied Topics, in Philadelphia, PA (2009).

Simonetti, Antonello, M.S. theses, 2009 - *Multiple resolution seismic data integration as a tool for the shallow hydrocarbon plumbing system definition. Examples from the Mississippi Canyon Block 118 carbonate-hydrate mound (Gulf of Mexico)*. University of Rome, La Sapienza.

\*Teske, A. 2009, Sulfate-reducing and methanogenic hydrocarbon-oxidizing microbial communities in the marine environment. Chapter 104. In K. Timmis (ed.), *Handbook of Hydrocarbon Microbiology*, Springer.

Toler, S. K., R. J. Bell, R. T. Short, Underwater Mass Spectrometry: Developments and Deployments (poster), 7th Harsh-Environment Mass Spectrometry Workshop, in Santa Barbara, CA (2009).

Weitemeyer, K. A., Constable, S., 2009: Preliminary results from the Gulf of Mexico gas hydrate CSEM experiment. *Eos, Transactions, American Geophysical Union, Fall Meet. Suppl.*, Abstract GP33A-0735, San Francisco, California.

Xiong, Shangmin, 2009, *Microbially induced and disrupted memory phenomena during gas-hydrate occurrences in seafloor sediments*, M.S. Thesis, Mississippi State University.

#### **2010:**

Bell, R. J., S. K. Toler, R. T. Short, In Situ Chemical Analyses by Underwater Mass Spectrometry (oral), Goldschmidt Conference on Earth, Energy and the Environment in Knoxville, TN (2010).

\*Bowles, M.W., and S.B. Joye, 2010. High rates of denitrification and nitrate consumption in cold seep sediments. *The ISME Journal*, doi:10.1038/ismej.2010.134.

\*Bowles, M.W., V. A. Samarkin, K. L. M. Bowles, and S.B. Joye, 2010. Weak coupling between sulfate reduction and the anaerobic oxidation of methane in methane-rich seafloor sediments in *ex situ* incubations. *Geochimica et Cosmochimica Acta*, doi:10.1016/j.gca.2010.09.043.

Bowles, M.W., V.A. Samarkin, and S.B. Joye. Pressure regulation of microbial methane cycling in deep-sea sediments. Goldschmidt 2010 Conference, Knoxville, TN, June.

\*Camilli, R.; Bowen, A.; Farr, N., 2010, "Bright Blue: Advanced Technologies for Marine Environmental Monitoring and Offshore Energy" Oceans 2010. pp 1-7.

Chapman, Ross, Mike Morley, Erika Geresi, Tom McGee, Paul Higley, *Characterizing the gas hydrate stability zone using a vertical hydrophone array*, The Leading Edge, October 2010, p. 800-804.

Constable S, and Weitemeyer, K., 2009: Applying marine EM methods to gas hydrate mapping, MARELEC Meeting, Stockholm, Sweden - July 7-9 2009

Diercks, A.R., V.L. Asper, R. Highsmith, M. Woolsey, S. Lohrenz, K. McLetchie, A. Gossett, M. Lowe, D. Joung, L. McKay, S. Joye, and A. Teske, 2010. The NIUST Deepwater Horizon Oil Spill Response Cruise. OCEANS 10 MTS/IEE Conference, Seattle.

\*Ingram, W.C., Meyers, S.R., Brunner, C.A., and Martins, C.S., 2010, Evaluation of Late Pleistocene-Holocene sedimentation surrounding an active seafloor gas hydrate and cold seep field on the Northern Gulf of Mexico Slope, *Marine Geology*, v. 278, no. 104, p. 43-53.

Innman, A., Easson, G., Asper, V. L., and Diercks, A. -R., 2010, *The Effectiveness of Using MODIS Products to Map Sea Surface Oil*, OCEANS 2010 MTS/IEEE Seattle, Sept. 20-23, 2010.

Innman, A., Macelloni, L., Easson, G., and Woolsey, M., 2010, *Incorporating Seafloor Data into GIS*, IEEE OES South American International Symposium, Buenos Aires, Argentina, April 12-16, 2010.

Joye, S.B., A. Diercks, A. Teske, and D. Valentine, 2010. Open ocean impacts of the BP Oil Well Blowout. American Geophysical Union, Fall Meeting, Union

Knapp, James H., Camelia C. Knapp, Leonardo Macelloni, Antonello Simonetti, Carol Lutken, 2010, *Subsurface Structure and Stratigraphy of a Transient, Fault-Controlled Thermogenic Hydrate System at MC-118, Gulf of Mexico* AAPG 2010 Annual Convention Oral Presentation, Abstracts Volume, p.134.

Knapp, Camelia C., James H., Knapp, Adrian Addison, Leonardo Macelloni, Michael Waddell, 2010, *Geophysical Baseline Characterization of Subsurface Gas Hydrates at MC-118, Gulf of Mexico*, AAPG 2010 Annual Convention Poster Presentation, Abstracts Volume, p.134.

\* Lapham, Laura L., Jeffrey P. Chanton, Ross Chapman, Christopher S. Martens, 2010, *Methane under-saturated fluids in deep-sea sediments: Implications for gas hydrate stability and rates of dissolution*, Earth and Planetary Science Letters (2010), 298 275-285. doi:[10.1016/j.epsl.2010.07.016](https://doi.org/10.1016/j.epsl.2010.07.016)

Lapham, LL, RM Wilson, RT Short, RJ Bell, and JP Chanton (2010) Mechanisms influencing hydrate dissolution rates in under-saturated systems. Goldschmidt 2010, in Knoxville, TN. June 13<sup>th</sup>-18<sup>th</sup>

Lapham, L. R. Wilson, C. Paull, J. Chanton and M. Riedel. Measuring *in situ* dissolved methane concentrations in gas hydrate-rich systems Part 1: Investigating the correlation between tectonics and methane release from sediments. , presented at 2010 Fall Meeting, AGU, San Francisco, Calif., 13-17 Dec.

\*Lloyd, K. G., D. Albert, J. F. Biddle, J. Chanton, O. Pizarro, and A. Teske. 2010. Spatial structure and activity of sedimentary microbial communities underlying a *Beggiatoa* spp. mat in a Gulf of Mexico hydrocarbon seep. *PLoS One*, 5(1): e8738.

\*Lloyd, K. G., B. J. MacGregor, and A. Teske. 2010. Quantitative PCR methods for RNA and DNA in marine sediments: Maximizing yield while overcoming inhibition. *FEMS Microbiology Ecology*. 72: 143-151.

Lutken, Carol B., Leonardo Macelloni, Laura Lapham, Simona Caruso, Mariangela Lodi, Richard Camilli, Vernon Asper, Arne Diercks, Camelia Knapp, Jim Knapp, 2010, *Monitoring Seafloor Morpho-Geological Evolution of the MC118 Hydrate/Carbonate Mound via Multiple AUV Missions*, AAPG 2010 Annual Convention Poster Presentation, Abstracts Volume, p.155.

\*Macelloni, L., S. Caruso, L. Lapham, C. Lutken, C. Brunner, and A. Lowrie, 2010, *Spatial distribution of seafloor biogeological and geochemical processes as proxy to evaluate fluid-flux regime and time evolution of a complex carbonate/hydrates mound, northern Gulf of Mexico*: Gulf Coast Association of Geological Societies Transactions, v. 60, p. 461-480.

\*McGee, Thomas, 2010: Single-channel seismic profiling and the analysis of multiple events. LAP LAMBERT Academic Publishing GmbH & Co., Saarbrücken, Germany.

McGee, T., 2010, *Geologic Features Associated with a Carbonate/Hydrate Mound in the Northern Gulf of Mexico: Results of Preliminary Studies*, IEEE Oceanic Engineering Society, US-Argentina International Symposium, Buenos Aires, Argentina, 12-14 April 2010

McGee, T. (2010): Geologic characteristics in the vicinity of the Deepwater Horizon oil spill. In *Proceedings of the US/EU Baltic International Symposium*, keynote presentation to the IEEE/ Oceanic Engineering Society, Riga, Latvia, 24-27 August 2010.

Short R. T., R. J. Bell, S. K. Toler, F. H. W. van Amerom, *Recent Developments and In Situ Measurements of Underwater Mass Spectrometers* (poster), 58<sup>th</sup> ASMS Conference on Mass Spectrometry and Allied Topics in Salt Lake City, UT (2010).

Short, R. T., R. J. Bell, A. M. Cardenas, A. Chaudhary, S. K. Toler, F. H. W. van Amerom, Miniature Ion Trap Mass Spectrometers and Applications for In Situ Analysis of Seawater (invited oral), Annual meeting of the Center for Analytical Instrumentation Development at Purdue University in West Lafayette, (2010).

Short, R. T., R. J. Bell and S. K Toler, 2010, *In situ characterization of distributions of dissolved gases, volatile organics, and light hydrocarbons using underwater membrane introduction mass spectrometry*, American Chemical Society meeting in Boston, MA, oral presentation, August 24.

Simonetti, Antonello, Leonardo Macelloni, James H. Knapp, Camelia C. Knapp, Carol B. Lutken, 2010, Multiple resolution seismic data integration as a tool for the shallow hydrocarbon plumbing system definition. Examples from Mississippi Canyon Block 118 carbonate-hydrate mound (Gulf of Mexico), Gordon Research Conference on Natural Gas Hydrates, Colby College, Waterville, Maine, June.

Sleeper, K., Bell, R., Short, T., Chanton, J., Wilson, R. D'Emidio, M., Macelloni, L. (2010), The Detection of Elevated Methane Concentration Indicate The Presence of Deep-Water Plumes Northwest of the DWH Site, Abstract OS21G-05 presented at 2010 Fall Meeting, AGU, San Francisco, Calif., 13-17 Dec.

Terry, D. A.; Knapp, C. C.; Knapp, J. H.; 2010. Comparison of Effective-Medium Models for Marine Gas Hydrate Templates. Poster Presentation at the 2010 American Geophysical Union Fall Meeting, 13-17 December 2010 (Poster OS53A-1361).

\*Teske, A. 2010. *Sulfate-reducing and methanogenic hydrocarbon-oxidizing microbial communities in the marine environment*. Part 21: Microbial Communities based on hydrocarbons, oils and fats: Natural habitats. Pp. 2203-2223. Handbook of Hydrocarbon Microbiology, Edited by Kenneth Timmis. Springer, DOI 10.1007/978-3-540-77587-4\_160.

Wade, T.L., Sweet S.T., Sericano, J.L., Guinasso, N.L. Jr., Lohrenz, S.E., Shiller, A.M., S.B. Joye, Dierks, A.R., Asper, V.L. and Highsmith, R.C. . 2010 Documentation of Sub-Surface Oil Plume by Analyses of Toxic PAH in Water Samples from the Deep Water Horizon Oil Spill. SETAC 31th Annual Meeting, November 7-11, 2010, Portland OR.

\*Weitemeyer, K., and S. Constable, 2010: Mapping shallow seafloor structure with marine CSEM, examples from the Gulf of Mexico gas hydrate experiment. *First Break*. **6** (28), 97-102.

\*Weitemeyer, K., G. Gao , S. Constable, and D. Alumbaugh, 2010. The practical application of 2D inversion to marine controlled source electromagnetic data. *Geophysics*, 75(6), doi:10.1190/1.3506004

Weitemeyer, K., and S. Constable, 2010: Preliminary results from the Gulf of Mexico gas hydrate CSEM experiment. Fire in the Ice Spring 2010. Methane Hydrate Newsletter US Department of Energy Office of Fossil Energy National Energy Technology Laboratory. p 13-17. [http://www.netl.doe.gov/technologies/oil-gas/publications/Hydrates/Newsletter/MHNews\\_2010\\_03.pdf](http://www.netl.doe.gov/technologies/oil-gas/publications/Hydrates/Newsletter/MHNews_2010_03.pdf)

Weitemeyer, K. and S. Constable, 2010: Mapping gas hydrates and shallow sedimentary structure in the Gulf of Mexico using marine controlled source electromagnetics, 20th International Workshop on EM Induction in The Earth, Giza, Egypt - Sept 18-24 2010.

Wilson, RM, LL Lapham, RT Short, RJ Bell, and JP Chanton (2010) Using continuous mass spectrometry to monitor dissolution of artificial methane and mixed-gas hydrates. Gordon Research Conference on Gas-Hydrates, in Waterville, ME. June 6<sup>th</sup>-11<sup>th</sup>

Wilson, R M., L. L. Lapham, M. Riedel, and J. P. Chanton. Measuring In situ Dissolved Methane Concentrations in Gas Hydrate-Rich Systems. Part 2: Investigating Mechanisms Controlling Hydrate Dissolution. presented at 2010 Fall Meeting, AGU, San Francisco, Calif., 13-17 Dec.

Wood, W. T.; Knapp, C. A.; Knapp, J. H.; 2010. Constraints on Methane and Methane Hydrate Distribution at a Gulf of Mexico Seep Using Waveform Inversion of Seismic Data. Oral Presentation at the 2010 American Geophysical Union Fall Meeting, 13-17 December 2010 (Paper OS44A-04).

Yao, H , P Gouedard, P Gerstoft, J McGuire, J A Collins, R van der Hilst, Analysis of fundamental and higher mode surface waves from noise correlation near Eastern Pacific Rise, AGU fall meeting 2010.

\*Zhang, Jian, Peter Gerstoft, and Peter D. Bromirski (2010), Pelagic and coastal sources of P-wave microseisms: Generation under tropical cyclones, *Geophys. Res. Lett.*, 37, L15301, doi:10.1029/2010GL044288.

\*Zhang, Jian, Peter Gerstoft, Peter M. Shearer (2010), Resolving P-wave travel-time anomalies using seismic array observations of oceanic storms, *Earth and Planetary Science Letters*, 292, 419-427, doi:10.1016/j.epsl.2010.02.014.

Zhang, J., P. Gerstoft, P. M. Shearer, P. D. Bromirski, H. Yao, 2010, Imaging Earth Structure and Microseism Sources Using Seismic Array Observations of Oceanic Storms, AGU fall meeting, 2010.

## 2011

Bowles, Marshall W, PhD 2011, Carbon, nitrogen, and sulfur cycling interactions in organic carbon rich extreme environments, Marine Sciences, University of Georgia

Brunner, C.A., Ingram, W., Meyers, S., and Lutken, C., 2011, Sedimentation at the Woolsey gas-vent complex in the northern Gulf of Mexico, *Journal of the Mississippi Academy of Sciences*, v. 56, No. 1, p. 69.

Carrière, Olivier; Peter Gerstoft (2011) *Monitoring gas hydrate with noise*, Abs OS12-06, American Geophysical Union Fall Meeting, San Fran. CA, 5-8 Dec.

Falcini, Federico; Chunyan Li; Marco D'Emidio; Carol Lutken; Leonardo Macelloni; Alessandro Salusti; Douglas J. Jerolmack (2011) *Hydrographic and suspended sediment measurements of the Mississippi River plume during the historic 2011 flood: a coupled satellite analysis and boat survey approach to determine an efficiency factor for sediment trapping in the nearshore zone*, Abs EP44A-07, American Geophysical Union Fall Meeting, San Fran. CA, 12-16 Dec.

Farr, Norman, Kenneth Sleeper, Richard Camilli, Clifford Pontbriand, Jonathan Ware (2011) *New developments in optic modems and chemical sensors in deep marine environments*, Abstract OS13D-1558, American Geophysical Union Fall Meeting, San Fran. CA, 12-16 Dec.

Garg, Sabodh K. and John W. Pritchett, 2011, *Modeling studies of hydrate mound, Mississippi Canyon Block 118, Gulf of Mexico*, Proceedings of the 7th International Conference on Gas Hydrates (ICGH 2011), Edinburgh, Scotland, United Kingdom, July 17-21, 2011.

Ingrassia, Michela, M.S. theses in Ocean Science, 2011, High Resolution benthic habitat mapping of Woolsey Mound (Mississippi Canyon Block 118, Northern Gulf of Mexico). University of Rome, *La Sapienza*.

Leifer, I., Rehder, G.J., Solomon, E.A., Kastner, M., Asper, V.L., Joye, S.B., 2011, Methane rising from the deep: Hydrates, bubbles, oil spills, and global warming. AGU Fall Meeting 2011.

Lutken, Carol B., Leonardo Macelloni, Ken Sleeper, Marco D'Emidio, Tom McGee, Antonello Simonetti, James H. Knapp, Camelia C. Knapp, Simona Caruso, Jeff Chanton, Laura Lapham, Mariangela Lodi, Michela Ingrassia, Paul Higley, Charlotte Brunner, Rich Camilli, Brad Battista, Tim Short, Ryan Bell, Peer Fietzek, 2011, *New discoveries at Woolsey Mound, MC118, northern Gulf of Mexico*, Proceedings of the 7th International Conference on Gas Hydrates (ICGH 2011), Edinburgh, Scotland, United Kingdom, July 17-21, 2011.

Lutken, Carol B., Antonello Simonetti, Michela Ingrassia, Leonardo Macelloni, James H. Knapp, Charles Fisher, Simona Caruso, Marco D'Emidio, 2011, *Biogeophysical Classification of Seafloor Seeps at a Carbonate-Hydrate Mound, Northern Gulf of Mexico*, AAPG International Conference and Exhibition, Milan, Italy, October 23-27, 2011.

Lutken, Carol; Marco D'Emidio; Federico Falcini; Benjamin P. Horton; Douglas J. Jerolmack; Nicole S. Khan; Chunyan Li; Leonardo Macelloni; Karen L. McKee (2011) *Connecting the historic 2011 Mississippi River flood to marsh sedimentation on the Delta*, Abs B24D-08, American Geophysical Union Fall Meeting, San Fran. CA, 12-16 Dec



\*Luzinova, Y, G. T. Dobbs, L. Lapham, J. Chanton, B. Mizaikoff. Detection of cold seep derived authigenic carbonates with infrared spectroscopy. *Marine Chemistry*, vol.125(1-4), p.8-18.

\*Macelloni, Leonardo, Bradley M Battista, Camelia C Knapp, 2011. *Optimal Filtering High-Resolution Seismic Reflection Data Using a Weighted-Mode Empirical Mode Decomposition Operator*. *Journal of Applied Geophysics*, 75 (2011) 603-614.

Martens, Christopher, Howard Mendlovitz, Brian White, Daniel Hoer, Kenneth Sleeper, Jeffrey Chanton, Rachel Wilson, Laura Lapham (2011) *Continuous In Situ Measurements of Near Bottom Chemistry and Sediment-Water Fluxes with the Chimney Sampler Array*, Abstract OS31B-08, American Geophysical Union Fall Meeting, San Fran. CA, 12-16 Dec.

\*McGee, Thomas, 2011: Probabilistic concepts in signal analysis. LAP LAMBERT Academic Publishing GmbH & Co., Saarbrücken, Germany.

Pierdomenico, Martina, M.S. theses in Ocean Science, 2011, Mesoscale Benthic habitat mapping of Hudson Canyon Head. University of Rome, *La Sapienza*.

Rogers, R.E., Radich, J.G., and Xiong, S., "The Multiple Roles of Microbes in the Formation, Dissociation and Stability of Seafloor Gas Hydrates," Paper presented by Rogers at 7<sup>th</sup> International Conference on Gas Hydrates, Edinburgh, Scotland, July 17-21, 2011.

Simonetti, Antonello, James H. Knapp, Camelia C. Knapp, Leonardo Macelloni, Carol B. Lutken, 2011, Defining the hydrocarbon leakage zone and the possible accumulation model for marine gas hydrates in a salt tectonic driven cold seep: examples from Woolsey Mound, MC118, northern Gulf of Mexico, Proceedings of the 7th International Conference on Gas Hydrates (ICGH 2011), Edinburgh, Scotland, United Kingdom, July 17-21, 2011.

R. T. Short, R. J. Bell, P. G. Wenner, S. K. Toler and L. Langebrake, 2011, "In situ characterization of subsurface chemical distributions using underwater mass spectrometry," Invited oral presentation at the Sustainable Remediation Forum (SURF) 16 Meeting Tampa, FL, 3 February 2011.

R. T. Short, R. J. Bell, S. K. Toler and P. G. Wenner, 2011, "In situ characterization of subsurface chemical distributions using underwater mass spectrometry" Invited oral presentation at the Marine Technology Society TechSurge Workshop, Sarasota, FL, 13 April 2011.

R. T. Short, R. J. Bell, A. Chaudhary, S. K. Toler and F. H. W. van Amerom,, 2011, "In situ characterization of distributions of dissolved chemicals using underwater mass spectrometry," Invited oral presentation at the SPIE Defense, Security, and Sensing Conference, Orlando, FL, 27 April 2011.

R. T. Short, R. J. Bell and S. K. Toler, 2011, "Characterization of subsurface distributions of dissolved gases near the Deepwater Horizon site using in situ membrane introduction mass spectrometry," Poster presentation at the 59<sup>th</sup> ASMS on Mass Spectrometry and Allied Topics, 5-9 June 2011.

R. T. Short, S. K. Toler, R. J. Bell and R. H. Byrne, 2011, "Underwater membrane introduction mass spectrometers: Recent developments and deployments" Oral presentation at the 8<sup>th</sup> Harsh-Environment Mass Spectrometry (HEMS) Workshop, St. Petersburg Beach, FL, 19-22 September 2011.

Sleeper, Kenneth, Rachel Wilson, Jeffery Chanton, Laura Lapham, Norman Farr, Richard Camilli, Christopher Martens, Clifford Pontbriand (2011), *Geochemical Arrays at Woolsey Mound Seafloor Observatory*, Abstract OS13C-1545, American Geophysical Union Fall Meeting, San Fran. CA, 12-16 Dec.

Solomon, E.A., Kastner, M, Leifer, I., MacDonald, I., Chanton, J., Robertson, G., 2011. Sea-Air hydrocarbon fluxes associated with a 900-m seafloor gas hydrate deposit in the Gulf of Mexico, Proceedings of the 7th International Conference on Gas Hydrates (ICGH 2011), Edinburgh, Scotland, United Kingdom, July 17-21, 2011.

Terry, Darrell A.; Camelia C. Knapp; James H. Knapp (2011) *Effective-medium models for marine gas hydrates, Mallik revisited*, Abs OS13C-1540, American Geophysical Union Fall Meeting, San Fran. CA, 12-16 Dec.

Traer, James A., PhD thesis: Geophysical Inversion with Adaptive Array Processing of Ambient Noise, 2011,

Wilson, RM, LL Lapham, M Riedel, and JP Chanton, 2011, Measuring in situ dissolved methane concentrations in gas-hydrate rich systems to understand hydrate stability and dissolution rates, Proceedings of the 7th International Conference on Gas Hydrates (ICGH 2011), Edinburgh, Scotland, United Kingdom, July 17-21, 2011.

## 2012

Camilli, R., N. Farr, C. Pontbriand, J. Kapit, J. Ware, O. Pizarro, J. Whelan, 2012, Long-term benthic boundary layer monitoring at the Mississippi Canyon Block 118 hydrates observatory, Ocean Sciences Annual Meeting, Salt Lake City, February 19-24.

\*Carrière, Olivier and Peter Gerstoft, 2012, *Deepwater subseafloor imaging using active seismic interferometry*, Geophysics 78, Q15-Q24. [.dx.doi.org/10.1190/geo2012-0241.1](https://doi.org/10.1190/geo2012-0241.1)

Carrière, O. and P. Gerstoft. Cross-correlation processing for deepwater subseafloor imaging with an OBS array. In GRC conference on Natural Gas Hydrate Systems. Gordon Research Conference, Mar. 2012.

D'Emidio, M., M. Ingrassia, C.B. Lutken, L. Macelloni, A. Simonetti, L.L. Lapham, R.M. Wilson, P. Hsing, and C. Fisher, 2012, *Biogeophysical Classification of Seafloor Seeps at a Carbonate-Hydrate Mound, Northern Gulf of Mexico*, Ocean Sciences Annual Meeting, Salt Lake City, February 19-24.

D'Emidio, Marco, Michela Ingrassia, Lutken Carol B., Leonardo Macelloni, Antonello Simonetti, Marco Pizzi, Laura Lapham, Rachel Wilson, Pen-Yuan Hsing, Charles Fisher, 2012, *Biogeophysical Classification of Seafloor Seeps at a Carbonate-Hydrate Mound, Northern Gulf of Mexico*, GRC "Natural Gas Hydrates System", Ventura, CA, March 18-23, 2012.

Dunbar, J.A., 2012, Extrusion model for the distribution of hydrate at Woolsey Mound, Mississippi Canyon, Block 118, Gulf of Mexico, Ocean Sciences Annual Meeting, Salt Lake City, February 19-24.

Easson, Greg, Carol Lutken, Ken Sleeper, Leonardo Macelloni, and Marco D'Emidio, 2012, *Gas Hydrates Observatory at Mississippi Canyon 118*, Ocean Sciences Annual Meeting, Salt Lake City, February 19-24.

Kapit, J., R. Camilli, N. Farr, J. Ware, C. Pontbriand, B. Hammer, S. Backus, 2012, *Improving the sustainability of long-term uncabled hydrate observatories: Technologies for efficient data retrieval and renewable power*, Ocean Sciences Annual Meeting, Salt Lake City, February 19-24.

\*Lapham, L., R. M. Wilson and J. P. Chanton, 2012, *Pressurized laboratory experiments show no stable carbon isotope fractionation of methane during gas hydrate dissolution and dissociation*. Rapid Communications in Mass Spectrometry. 26, 32-36, DOI: 10.1002/rcm.5290

Lapham, LL, RM Wilson, M Riedel, and J Chanton (2012) *Measuring in-situ methane concentrations over time near Bullseye vent, Vancouver Island*. The Gordon Research Conference on Natural Gas Hydrate Systems, Ventura, California. March 18<sup>th</sup>-23<sup>rd</sup>

\*Lewis, Michael and Peter Gerstoft, 2012, *Shear wave anisotropy from cross-correlation of seismic noise in the Parkfield pilot hole*, Geophys. Res. Int 188, 626-630, doi: 10.1111/j.1365-246X.2011.05285.x

Lutken, Carol, Ken Sleeper, Greg Easson, Leonardo Macelloni, Gene Smith, 2012, *The GOM GAS*

*HYDRATES SEAFLOOR OBSERVATORY: Producing Science for National and Global Management Decisions*, AGU Science Policy Conference 2012, Washington, DC, April 29-May 2.

\*Macelloni L., Simonetti, A., Knapp, J.H., Knapp, C.C., and Lutken, C.B., 2012. *Multiple-Resolution Seismic Imaging of a Shallow Hydrocarbon Plumbing System, Woolsey Mound, Northern Gulf of Mexico*. *Marine and Petroleum Geology* 38: 128-142.

Macelloni, L., M. D'Emidio, A. Simonetti, J. Dunbar, C.B. Lutken, 2012, *Geophysical evidence of shallow hydrates formation and accumulation at Woolsey Mound (Mississippi Canyon Block 118)*, Ocean Sciences Annual Meeting, Salt Lake City, February 19-24.

Pizzi, Marco, Leonardo Macelloni, Lutken Carol B., Marco D'Emidio, 2012, *Temporal Evolution of MC118 Woolsey Mound seep activity: constraints from analysis of small-scale salt-induced sediment deformation*, GRC "Natural Gas Hydrates System", Ventura, CA, March 18-23, 2012.

Simonetti, Antonello, James H. Knapp, Camelia C. Knapp, Carol B. Lutken, 2012, *4d seismic imaging of a thermogenic gas hydrate system in the northern Gulf of Mexico (Woolsey Mound, MC118)*, The Gordon Research Conference on Natural Gas Hydrate Systems, Ventura, California, March 18<sup>th</sup>-23<sup>rd</sup>

Simonetti, Antonello, James H. Knapp, Michael Riedel, Camelia C. Knapp, 2012, *Short and long-term dynamics of a thermogenic gas hydrate system in a cold seep area in the Gulf of Mexico deep waters (Woolsey Mound, MC118)*, 15th Annual AAPG-SEG Student Expo in Houston, Texas, USA, 17-18 September 2012.

Wilson, R.M., L.L. Lapham, C. Martens, J.P. Chanton, H. Mendlovitz, K. Sleeper, M. Reidel, 2012, *Time-series methane monitoring in gassy sediments and the benthic boundary layer*, Ocean Sciences Annual Meeting, Salt Lake City, February 19-24.

Wilson, RM, LL Lapham, B Anderson, N Garapati, and J Chanton (2012) Laboratory experiments probe hydrate dissolution rates. The Gordon Research Conference on Natural Gas Hydrate Systems, Ventura, California. March 18<sup>th</sup>-23<sup>rd</sup>

## **2013**

Lowe, P. M., M. Woolsey, R. Jarnagin, C. B. Lutken, B. Noakes, L. Overstreet, S. Tidwell, Development of I-SPIDER: a towed platform for video survey and instrument placement, Proc. OCEANS Conf. 2013.

\*Lutken, Carol B., Marco D'Emidio, Leonardo Macelloni, Michela Ingrassia, Martina Pierdomenico, Vernon Asper, Arne Diercks, Max U. Woolsey, Roy Jarnagin, 2013, *Challenges in imaging the deep seabed: examples from Gulf of Mexico cold seeps*, Transactions of the GCAGS, New Orleans, 2013.

\*Macelloni, Leonardo, Charlotte Brunner, Simona Caruso, Carol Lutken, Marco D'Emidio, Laura Lapham, 2013, *Spatial distribution of seafloor biogeological and geochemical processes as proxies of fluid flux regime and evolution of a carbonate/hydrates mound, northern Gulf of Mexico*, Deep Sea Research, Part 1, Manuscript Number: DSR1-D-12-00118R1.

\*Simonetti, Antonello, James H. Knapp, Kenneth Sleeper, Carol B. Lutken, Leonardo Macelloni, Camelia C. Knapp, 2013, *Spatial Distribution of Gas Hydrates from High-Resolution Seismic and Core Data, Woolsey Mound, Northern Gulf of Mexico*, *Marine and Petroleum Geology* 44 (2013) 21-33.

\*Simonetti A., 2013, *Spatial and Temporal Characterization of a Cold Seep-Hydrate System (Woolsey Mound, Deep-Water Gulf of Mexico)*, PhD Dissertation, University of South Carolina, Columbia, South Carolina, USA, 14 November 2013, 100p.

Woolsey, M., R. Jarnagin, K. Sleeper, L. Macelloni, M. D'Emidio, A.-R. Diercks, V. L. Asper, Integration of a Polarity-Preserving Chirp Subbottom Profiler into the NIUST AUV Eagle Ray, Proc. OCEANS Conf. 2013.

In Press:

\*Wilson, Rachel, Leonardo Macelloni, Antonello Simonetti, Jeffrey Chanton, Jim Knapp, Laura Lapham, Carol Lutken, Ken Sleeper, Charlotte Brunner, Chris Martens, Marco D'Emidio, 2013, in press, Integrating geochemical profiles with seismic surveys to identify subsurface methane sources and migration pathways, G-Cubed, (DOI: 10.1002/2013GC004888).

*Submitted:*

\*Macelloni, L, Lutken, C. B., Garg, S., Simonetti, A., D'Emidio, M., Wilson, R., Sleeper, K., Lapham, L., Lewis, T., Pizzi, M., Knapp, J., Knapp, C., Brooks, J. and McGee T.M., Geothermal regime and hydrates stability zone dynamic of Woolsey Mound a transient, thermogenic, fault-controlled hydrates system (northern Gulf of Mexico), submitted JGR solid earth.

Simonetti A., Knapp, J.H., and Robinson, N., 2013. *Tectonic Controls on the Long-Term Fluxes of Methane from Cold Seep-Hydrate Systems*. Earth and Planetary Science Letters (*in review*).

**Appendix A.** Jumbo Piston Coring Cruise aboard the TDI Brook, R/V *Brooks McCall*  
GULF OF MEXICO HYDRATES RESEARCH CONSORTIUM  
SUMMARY OF ACTIVITIES FOR JANUARY, 2011

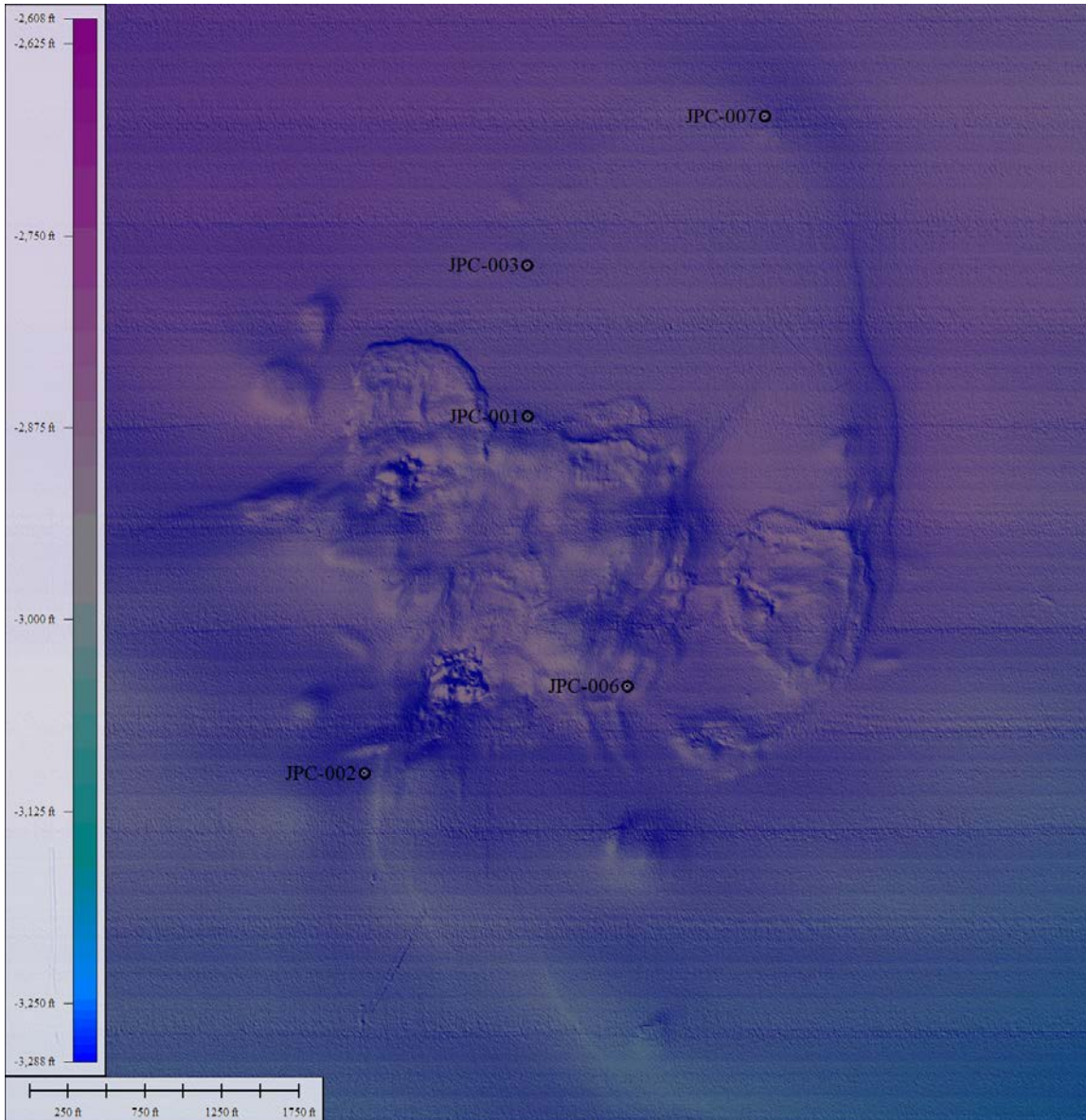
A research cruise to Mississippi Canyon 118 (MC118), site of the Hydrates Research Consortium's Seafloor Observatory, was executed aboard the R/V Brooks McCall with the Mississippi Mineral Resources Institute (University of Mississippi), University of South Carolina and Florida State University participants aboard.

The research objective was the collection of 5 Jumbo Piston cores to support the further geological, geophysical and geochemical characterization of the shallow seafloor at Woolsey Mound, the primary bathymetric/morphological feature on the seafloor at MC118. Although work at the site has been ongoing since early 2005, important gaps remain in our understanding of the complex geomorphological and geochemical forces driving the tectonics, seep development and resultant chemosynthetic communities at the site. No deep cores (>10m) had yet been recovered. Several months of discussion by 12-14 Consortium members preceded final selection of the core sites. In general, sites were targeted because they showed promise of providing tie-in to geophysical datasets, could reveal the geologic section to greater depths that has been possible with MMR's 10m capability, might provide information regarding geophysical/seismic anomalies (high frequency scatter, blanking, hot spots, pockmarks), provide information regarding faulting noted in seismic data, confirm presence of resistivity anomalies found in a survey conducted in June, 2009.

Five cores were recovered from the area of the mound and its periphery. Cores were sectioned, tops photographed and sampled for geochemical parameters, closed, and scanned for temperature anomalies using infrared imagery. A subset of these sections was tested for shear strength using minivane techniques. Top sections were windowed and sampled for sulfate and methane. In one case a core section was opened and examined for hydrate occurrence based on the IR readings. This section was found to contain hydrates in a variety of occurrences: massive chunks, blades, nodules and disseminated grains/granules. Some of the hydrate was collected for chemical analyses. The cores will be transported to the Navy Research Laboratory at Stennis Research Facility where they will be analyzed with a Geotek logger for resistivity, compressional strength, density, and magnetic susceptibility. They will then be opened, examined visually, photographed, logged and subsampled for additional geochemical analyses and bio- and lithostratigraphy. The FSU participants will analyze chemical samples collected onboard prior to the opening of the cores. These results will be used to determine sites for extensive coring in April to extend the range of geologic and geophysical characterization of Woolsey Mound and to aid in determining sites from which to recover heat-flow data later in 2011.

Visiting Scholar, Michela Ingrassia, completed the physical component of her project for the Consortium. Michela moved to Pennsylvania State University to begin the biological component of her investigations of the benthic fauna at MC118. She will be working with Chuck Fisher.





**Locations of the 5 Jumbo Piston Cores recovered from Woolsey Mound, January, 2011.**

**JPC-001** Justification: growth section along the “Blue Fault”, ground-truth on SSDR data; about 100 m west from high resistivity anomaly A.

**JPC-002** Justification: south-west of the SW Crater Complex, in a compressed stratigraphic section, close to the “Pink Fault”.

**JPC-003** Justification: calibration JPC-001, penetrate complete marker unit (age constraint for blue fault movement).

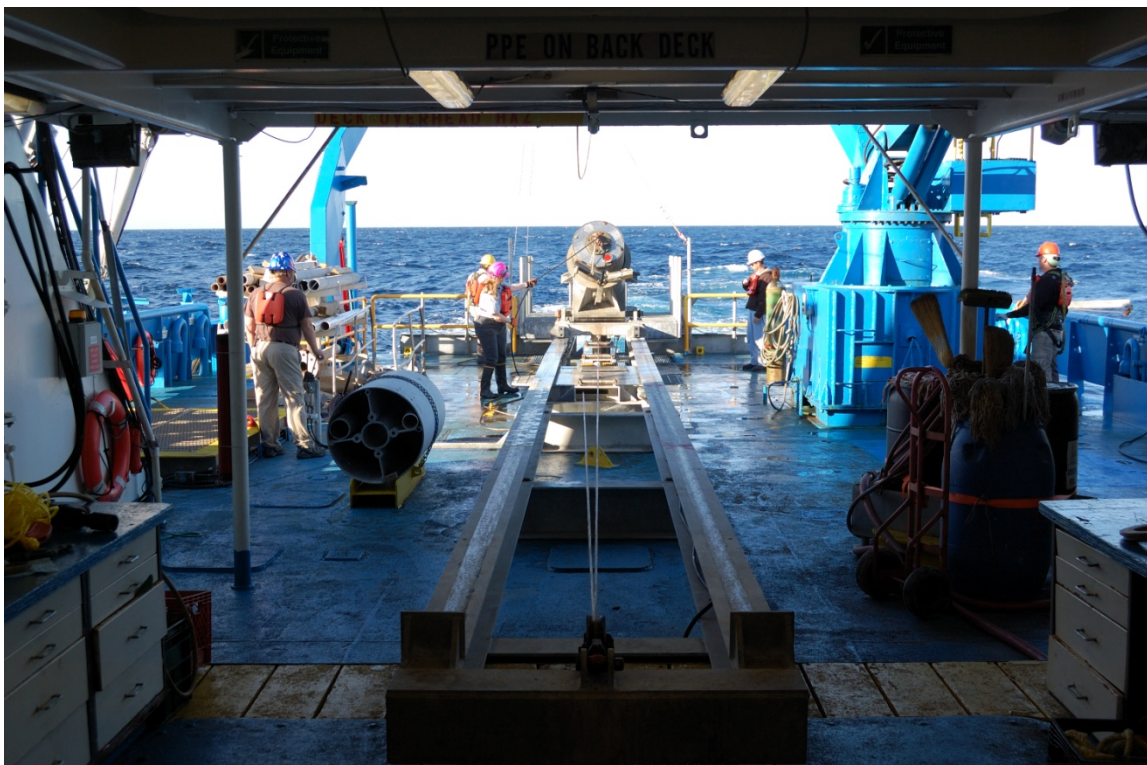
**JPC-006** Justification: between SW and SE Crater Complexes, close to the Pink Fault, acoustic blanking on CHIRP data.

**JPC-007** Justification: in the northern portion of the parabola, NE of Woolsey Mound, exhibits high-frequency scatter in SSDR data, it is in a pock mark and the surface expression of the “Yellow Fault”.





**Recovery of the Jumbo Piston Corer to the deck.**



**Launch and recovery tracks for JPC. Maximum possible recovery is 64 feet though normally about 50 ft recovery can be expected.**





**Sampled top of a section of JPC-006 shows high organic content and gas expansion.**



**Note gas expansion, typical of JPC-006.**





**Chunks of hydrate 6 feet from the base of JPC-001.**



**A disk of hydrates ~.8 in thick covered the entire cross-sectional area of JPC-001, 5.5 ft from the bottom of the core section.**





**Highly disturbed base of JPC-001.**





**Bottom 3 ft section of JPC-001 contained hydrate nodules, blades, grains and granules.**

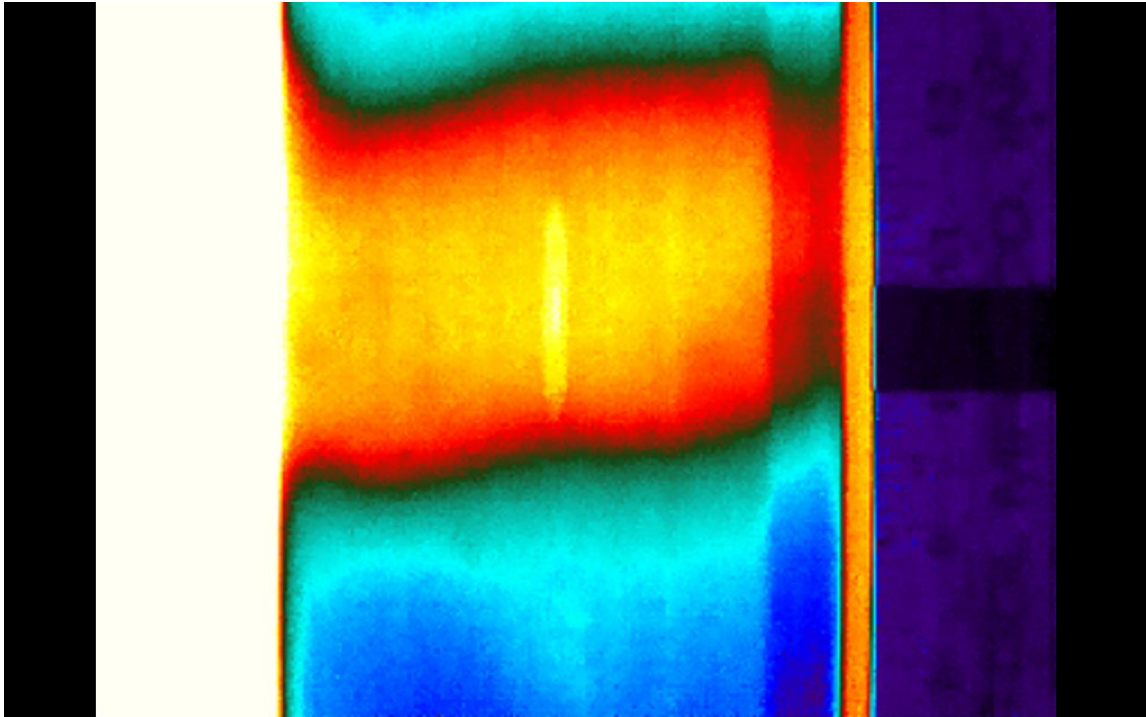


**Extremely fine-grained material hosts hydrates at JPC-001 core-site.**

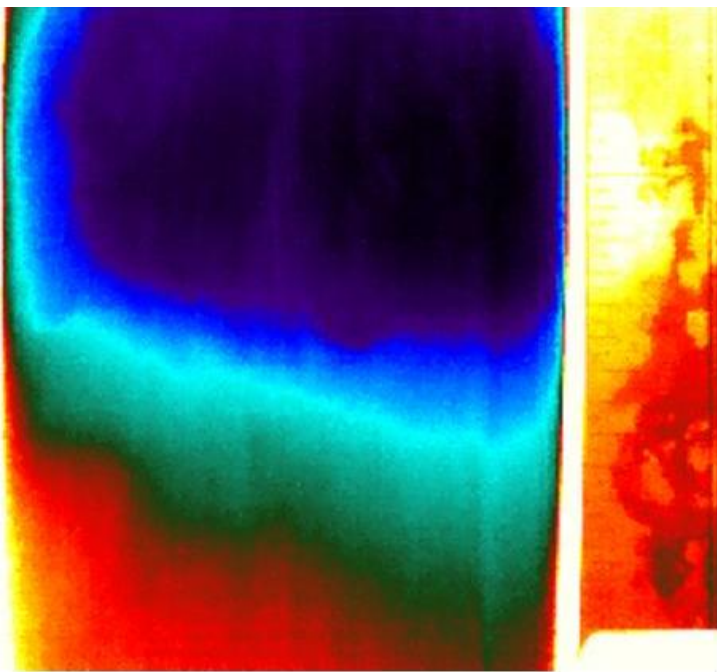




**After 2 hours on deck, hydrate can still be observed in the bottom sections of JPC-001.**

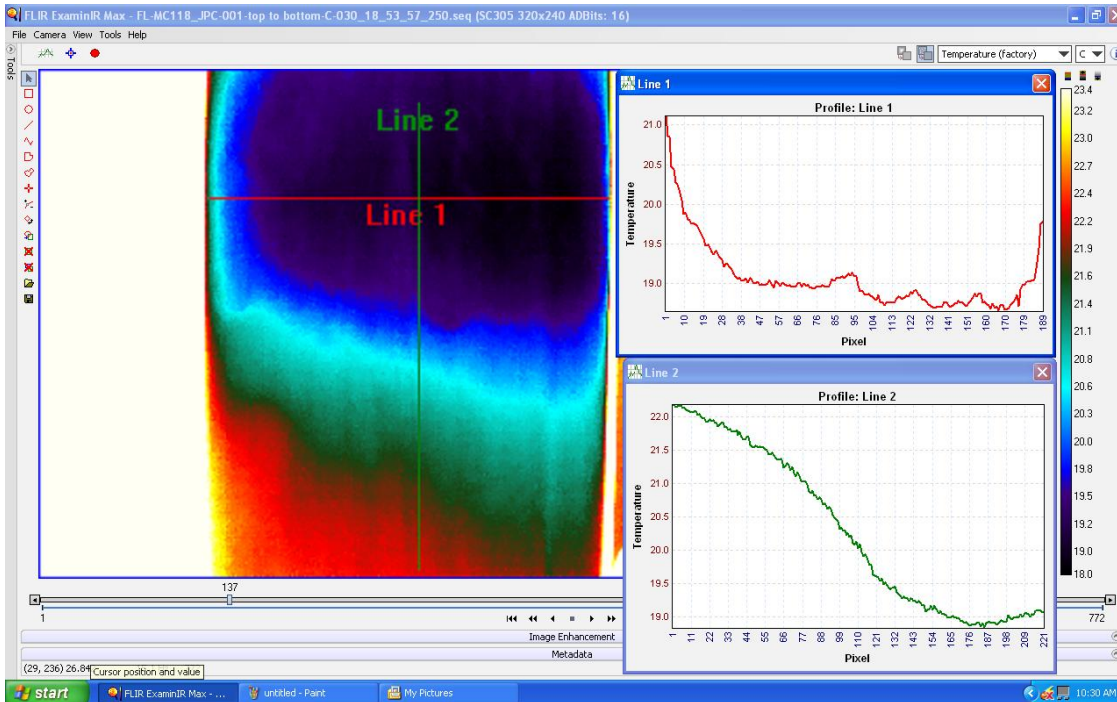


A void appears as a “warm spot” on the IR imagery.

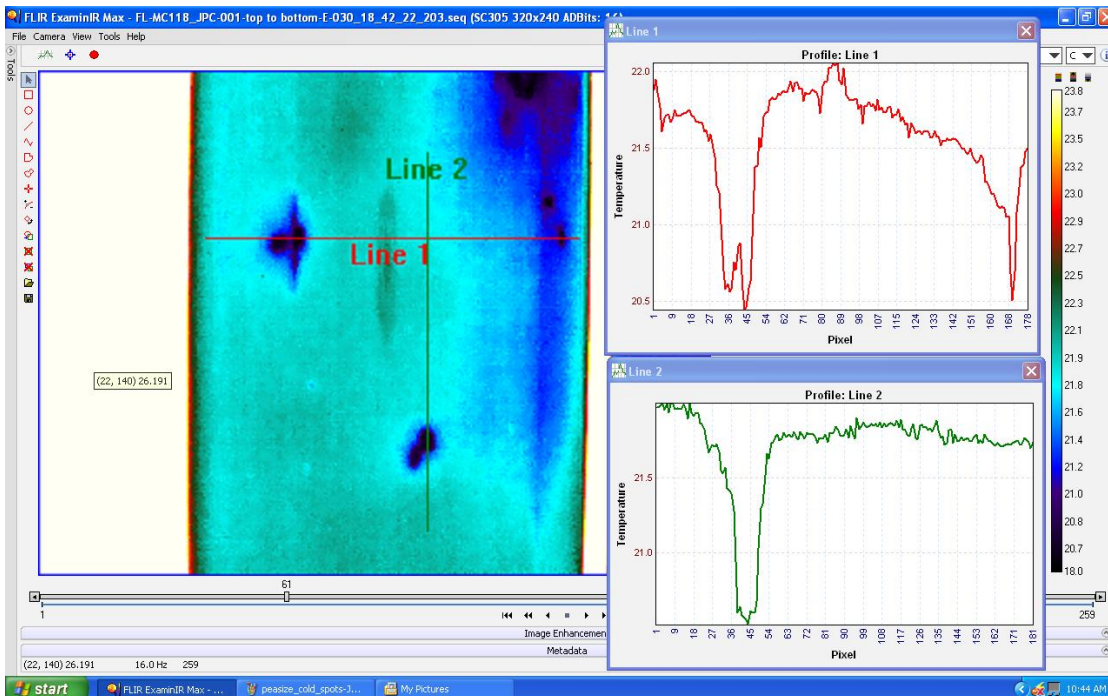


A “cold spot” appears as blue.





A screen-capture shows a 4"x6" section of core believed to contain hydrate (blue). The color-coded sections - green = longitudinal, red = transverse – show temperatures along/across the core.



A screen-capture shows small cold spots, possibly hydrate nodules, and the temperature variations they produce.

## APPENDIX B:

### Report on the Lithostratigraphy of the Jumbo Piston Cores taken from MC118 in January 2011. C. Brunner, Department of Marine Science, University of Southern Mississippi

February 23, 2012

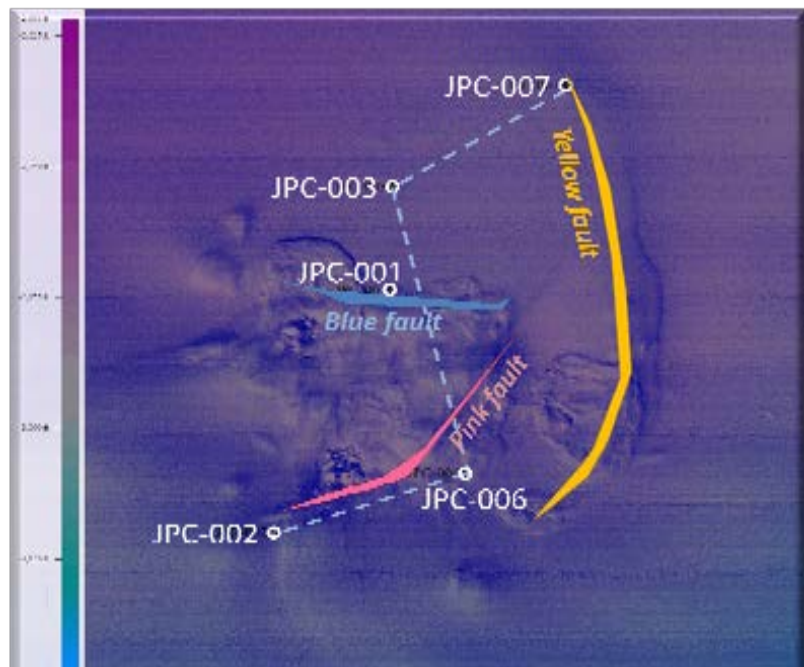
In January of 2011, five jumbo piston cores were taken from MC118 (see cruise report for details). The cores were located in proximity to the three major faults that radiate up from the salt dome 600 m below the sea floor at the Woolsey Mound. One of the cores, JPC 001, was charged with methane hydrate and self-extruded during core recovery. The remaining cores were suitable for lithostratigraphic assessment.

The cores were analyzed on the NRL GEOTEK core logger in April of 2011 with corrections made in July. Cores JPC 003, -5 and -6 were opened, photographed and described in late July, and Cores JPC 001 and -2 were opened, photographed and described in late August.

The lithostratigraphy of the deeper parts of the cores was assessed by Jennifer Brizzolara and added to lithostratigraphic units identified in past years by Lutken, Sleeper and Brunner from conventional gravity cores.

The topmost unit, Unit 1, is a homogeneous mud with abundant planktonic foraminifers lending a distinctly sandy component to the texture. The texture appears completely mixed by bioturbation. It is underlain by Unit 2, which is a dark mud without appreciable sand and with distinct light colored mottles from large, burrowing macrofauna. The contact between Units 1 and 2 is gradational. A distinctive reddish layer lies at or near the base of Unit 2.

Figure 1. Location of JPC cores relative to the major faults at the Woolsey Mound





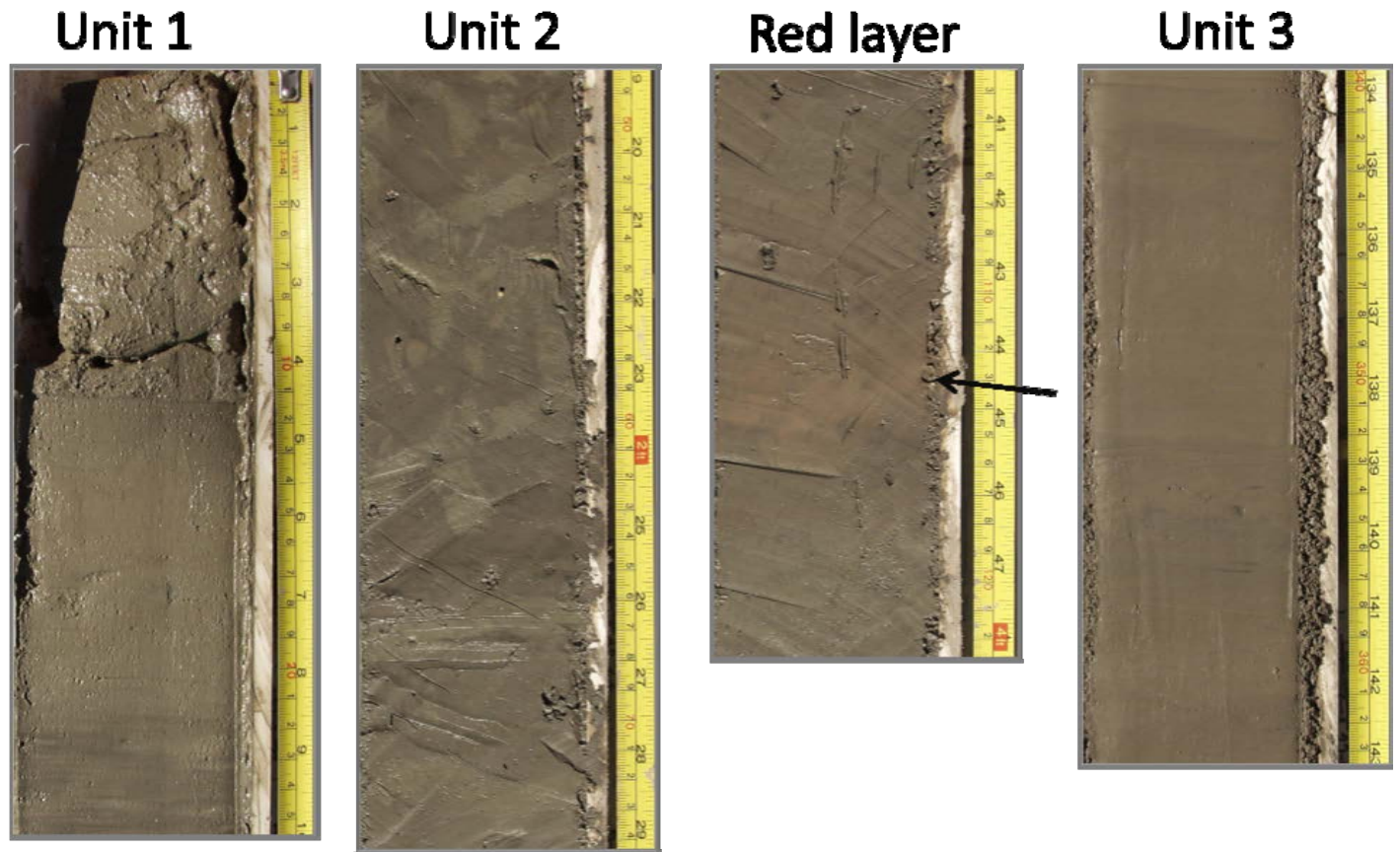


Figure 2. Lithostratigraphic Units 1-3 and the reddish layer.

The lower four units consist of stratal layers with slightly different appearances. Unit 3 is comprised on centimeter-thick stratal layers with gradational boundaries. It should be noted that stratal layers sometimes appear above the red layer. Unit 4 consists of distinctly light and dark stratal layers often with distinct contacts and with abundance silt laminae interspersed throughout the unit. Unit 5 consists of gradational stratal layers with abundant silt laminae. Unit 6 consists of indisinct stratal layers few silt laminae and is generally similar to Unit 3.

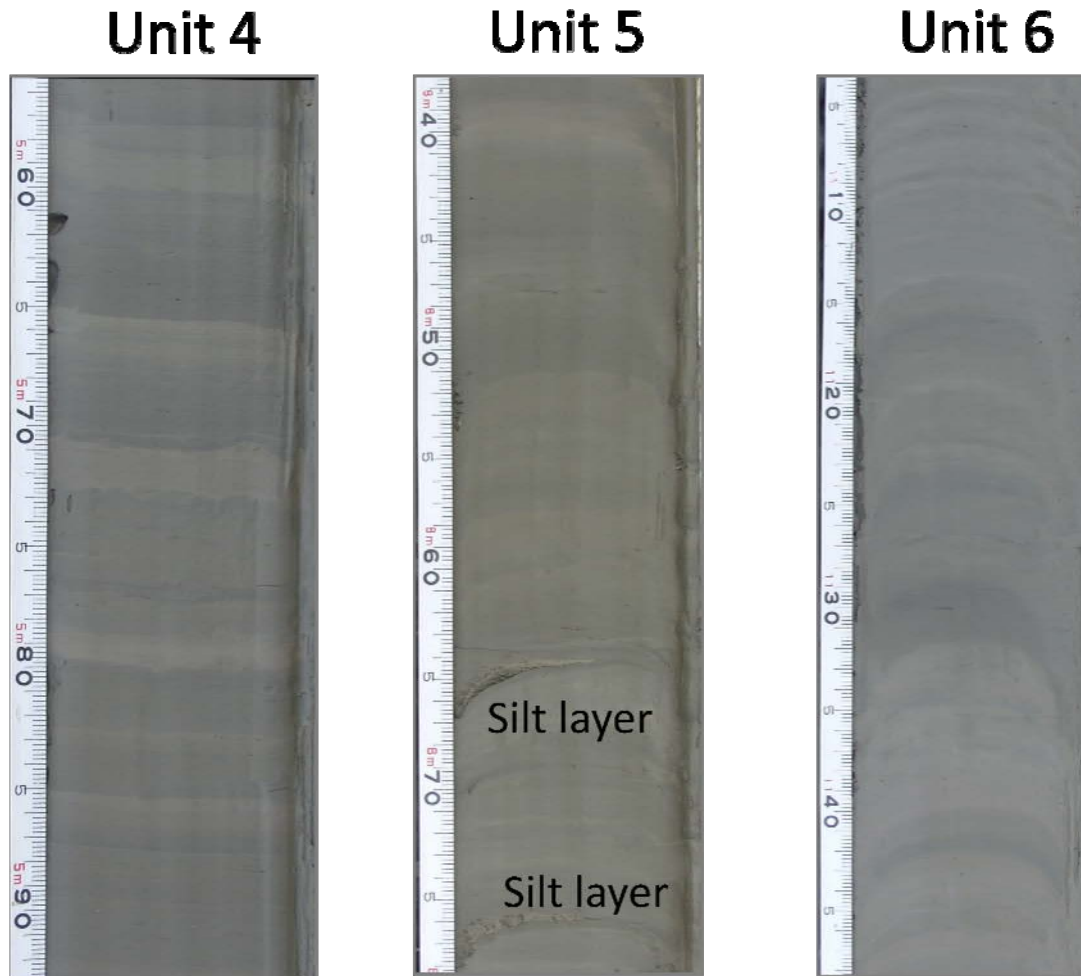


Figure 3. Lithostratigraphic Units 4-6.

The lithostratigraphic section is interpreted to be a succession from the Wisconsin low stand of sea level to the present-day high stand. The stratal layers formed when deposition rates exceeded bioturbation mixing rates. The stratal layers are enriched in fine silt from the Mississippi Fan or other river/fan systems that overbanked into MC118. As sea level rose, sedimentation rates slowed, riverine sources diminished as estuaries and bayhead deltas captured more of their sediment, and bioturbation rates began to exceed deposition rates. Mottles were preserved (Unit 2), and ultimately bioturbation rates far exceeded deposition rates so sediments were mixed into the homogeneous appearance of Unit 1. The red layer warrants special mention. This clay-rich, reddish layer near the base of Unit 2 can be correlated across much of the northern Gulf of Mexico and is likely related to deposition processes associated with Meltwater Event 1A during the last deglaciation. Another reddish layer occurs below it in Unit 3 (337-344 cm) in core JPC-7, and is presumably formed by similar processes. Finally, the section at the top of JPC-6 is unusual and does not look like Units 1 or 2. This section remains under study.

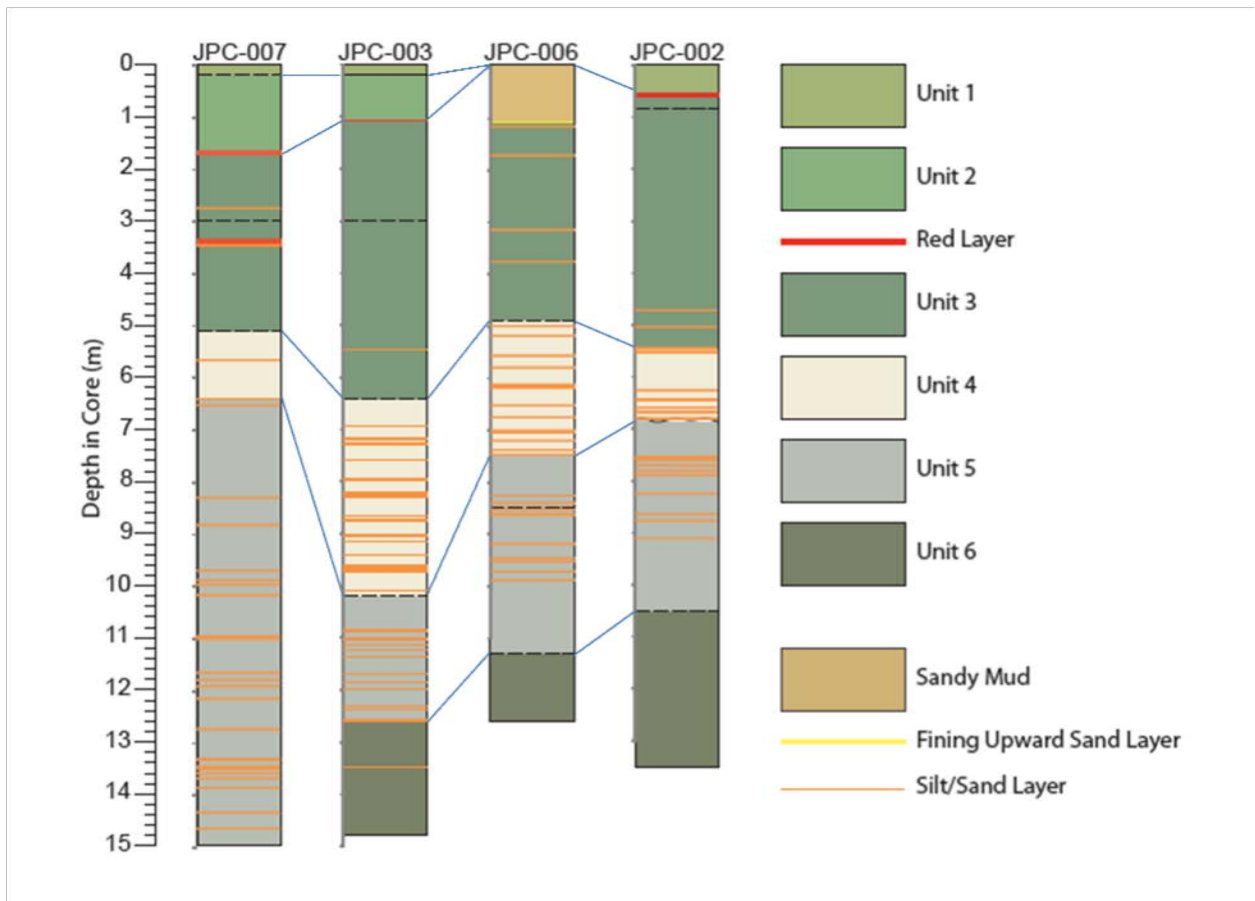


Figure 4. Correlation of lithostratigraphic units.

**Figure 5. Depth of bases of lithostratigraphic units (cm).**

Core	Base of	Base of	Red layer	Base of	Base of	Base of
JCP-	56	61	61	542	682	1053
JPC-	23	131	132	652	1010	1262
JPC-	?	?	?	490	749	1135
JPC-7	27	175	177	512	640	Below base

The density of the four cores ranges between 1.3 and 1.8 g/cm<sup>3</sup> with JPC-2 and -6 being firmer at the top than cores JPC-7 and -3. The four cores show other interesting differences. The trend in density in JPC-2 generally increases with depth, but the other cores differ. JPC-6 increases to a maximum density, then decreases slightly, whereas JPC 7 and -3 increase but with several intervals of constant density in the middle and lower sections. On a finer scale, all of the cores, especially in the units bearing stratal layers, have a lot of variability that might result from compositional changes between colored layers. Further, the density shows longer cycles that are about 1.25 m in length. The cause for these large cycles remains under study. Deviation from increasing density could be caused by underconsolidation processes and by interaction with methane hydrates at depth.

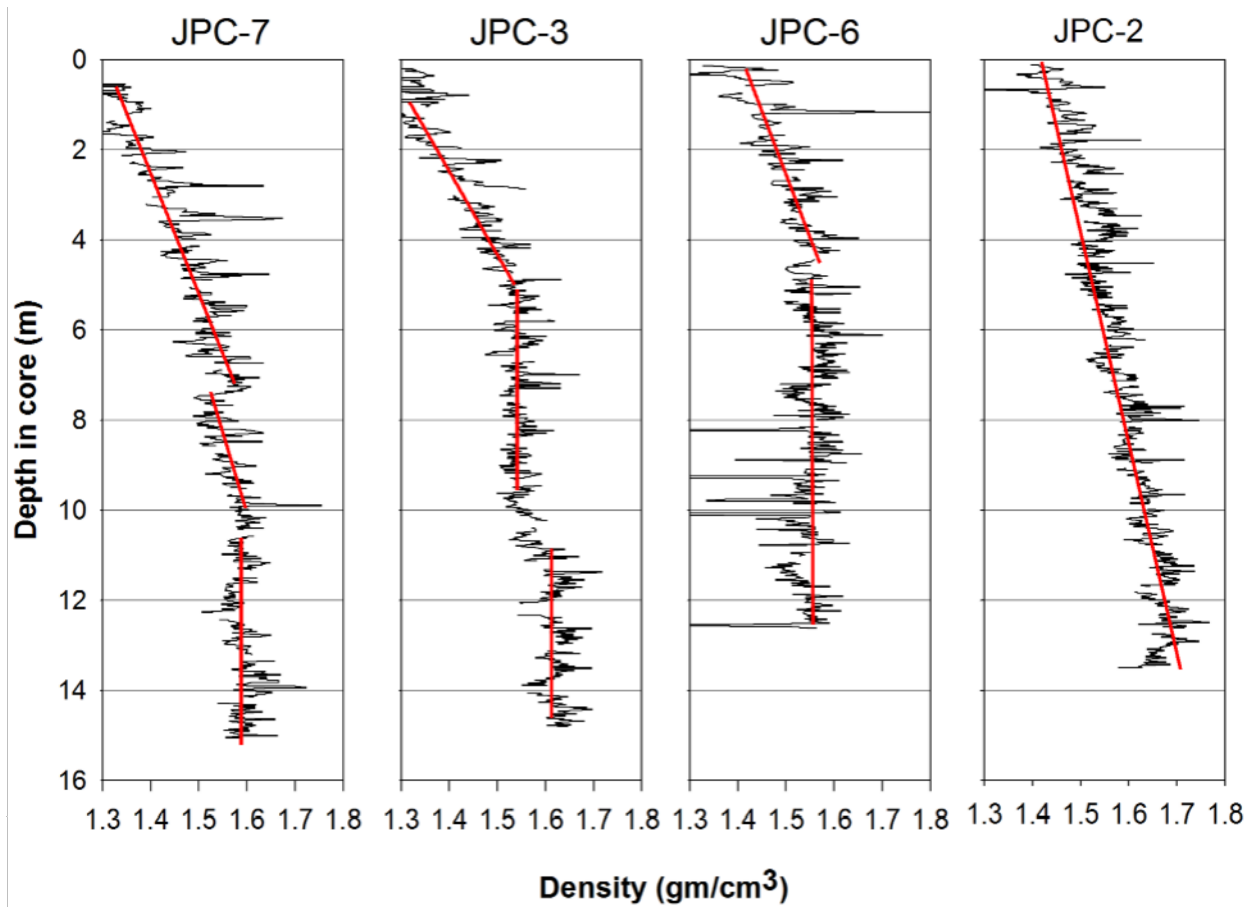
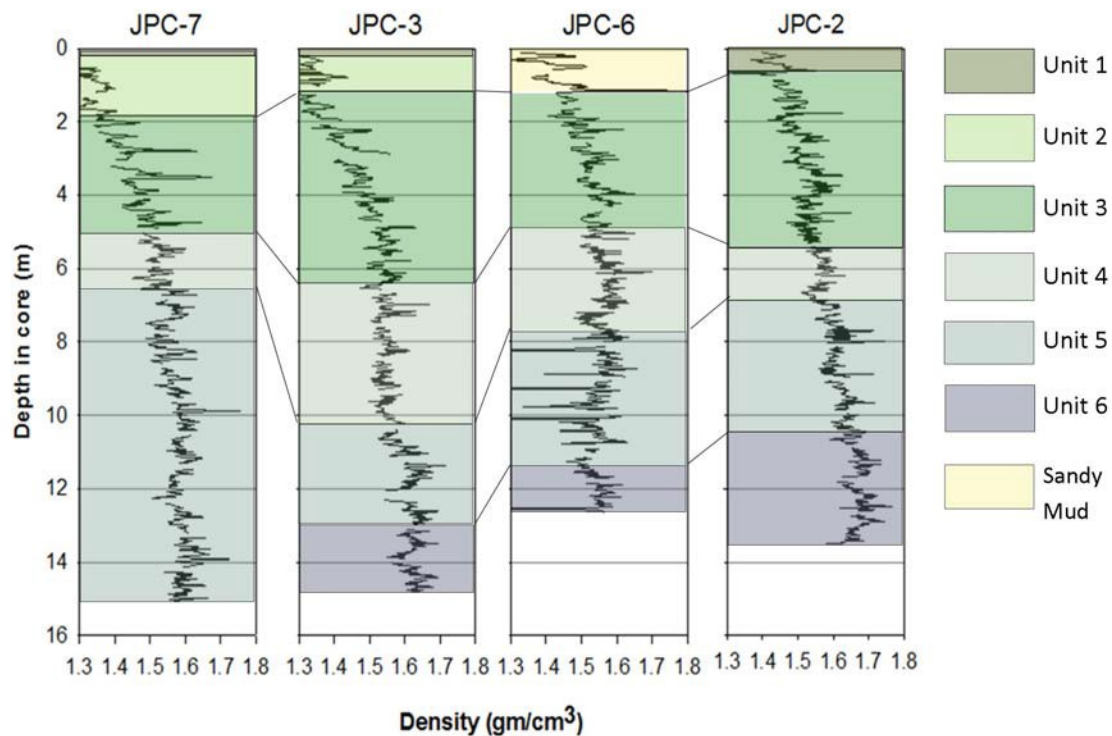


Figure 6. Density of the JPC cores measured by gamma-ray attenuation.





**Figure 7. Lithostratigraphic units overlay the density curves.**

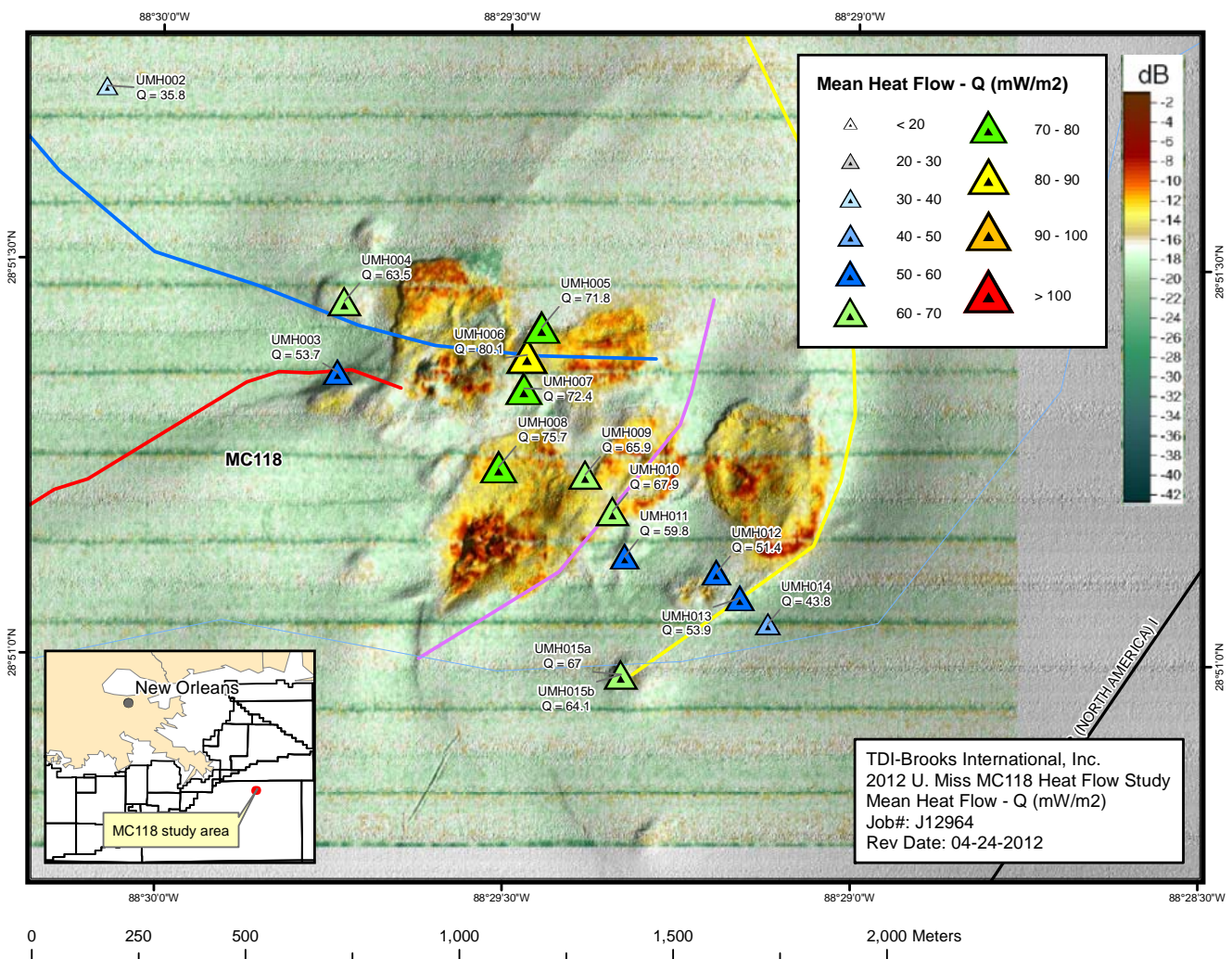
The densities within units are similar across the four cores. Densities are lowest in Unit 1, about 1.3 g/cc, but these sections are too short to define a pattern. Unit 2 ranges from 1.3 to 1.5 g/cc but with distinct variability. In Unit 3, density increases monotonically on average from 1.3 to 1.55 with considerable variability and with distinct cycles of a bit more than 1 m. In Unit 4, density remains relatively constant, around an average of 1.6 g/cc, though it is variable and has cycles longer than 1 m in length. Units 5 and 6 are variable across the cores, perhaps due to the influence from faults and methane from below.

In general, the lithostratigraphy and densities of the stratal units are similar to that of cores taken from the middle Mississippi Fan during Leg 96 of the Deep Sea Drilling Project.



# University of Mississippi Heat Flow Interpretive Report

Technical Report Number: 12-2832



April 2012

## TABLE OF CONTENTS

<b>SUMMARY</b> .....	1
<b>GENERAL</b> .....	2
<b>Geologic Context of Heat Flow Measurements</b> .....	2
<b>Description of the Heat Flow Probe</b> .....	3
<b>Operation of the Heat Flow Probe</b> .....	6
<b>Processing Data from the Probe</b> .....	7
<b>THIS PROGRAM</b> .....	12
<b>Bottom Water Temperatures</b> .....	12
<b>Thermal Conductivity of the Sediments</b> .....	21
<b>Heat Flow</b> .....	25
<b>REFERENCES</b> .....	33
<b>APPENDIX 1 - GRAPHICAL SUMMARY DISPLAYS OF THE DATA FOR EACH STATION</b>	
<b>APPENDIX 2 - DESCRIPTION OF THE DIGITAL HEAT FLOW DATA FILES</b>	
<b>APPENDIX 3 - DETAILED ANALYSIS OF THE HEAT FLOW AT EACH STATION</b>	
<b>APPENDIX 4 - BULLARD PLOTS OF DATA IN MS EXCEL</b>	

## TABLES

Table 1. Heat probe components.....	3
Table 2. Order of stations and equipment used.....	16
Table 3. Average measured values for each station (WGS84). ....	21
Table 4: Calculated heat flows, using different sensor calibrations .....	26

## FIGURES

Figure 1. TDI-Brooks heat flow probe schematic.....	4
Figure 2. TDI-Brooks heat flow probe photo.....	5
Figure 3. Annotated example of a sensor output plot.....	8
Figure 4. Example of Bullard Plots, comparing two sites.....	10
Figure 5. Bullard Plot comparing replicate ( <i>pogo</i> ) sites.....	11
Figure 6. Water column temperatures measured above three sites in the main basin. ....	13
Figure 7. Temperatures from the hold at every heat flow site.....	14
Figure 8: Calibration temperatures wrt T1 values, in order of measurement. ....	15
Figure 9: Example of calibration temperatures wrt T1 values, from another project.....	17
Figure 10: A detailed plot of the sensors on screen,.....	19
Figure 11: The calibration temperatures from 6 sites, used to calculate the heat flows designated with an “x”. ....	20
Figure 12: Measured thermal conductivities, as a function of sediment depth. ....	22
Figure 13: Maximum sensor temperature rises produced by the heat pulses. ....	23
Figure 14: Measured thermal conductivities as a function of depth at the pogo site, UMH015. ....	25
Figure 15. A histogram of the heat flow values at each site.....	29
Figure 16: Heat flows measured in the mounds area.....	30
Figure 17: Heat flows measured in the mounds area detail.....	31
Figure 18: Heat flows measured on sections crossing three crestal fault traces.....	32

## SUMMARY

Heat flow data were measured in the gas hydrate mounds area in MC118, Gulf of Mexico. Over the period 29-30 March, 2012, TDI-Brooks International collected geothermal data at 15 sites aboard the RV GEOEXPLORER. After completion of each station, the data were transmitted from the ship, via satellite and e-mail, to Dr. Trevor Lewis of Sidney Geophysical Consultants Ltd. for analysis and interpretation. This report includes a description of the probe and its operation, as well as a description of the analysis methods and the measured heat flow values from this cruise.

The water depth at the 13 sites in the mounds area ranged from 888 to 914 m, with a bottom water temperature of approximately 5.5 C. The water column above these sites was not isothermal, and holding the probe at a fixed depth above many stations was difficult, and therefore did not produce constant sensor temperatures, for intercalibration purposes. Comparison of these temperatures showed that at 6 of the stations with water depths between 877 and 897 m, the temperature differences were fairly constant. The averages of these values were used for intercalibrations of the thermistors, as well as the values above a single site, UMH010. The heat flows were later corrected for the average measured temperature gradient in the water column.

Over the mounds area, the average values of measured thermal conductivity varied from 0.954 W/m K to 1.066 W/m K, the average being  $1.001 \pm 0.032$  W/m K. Sporadic higher values of thermal conductivity, up to 1.43 W/m K, were probably caused by small, quasi-horizontal fluid flows. There were only 11 values above 1.1 W/m K, out of total of 176 measurements.

At UMH015 the probe was lowered into the sediments twice. The difference between the averages of the repeated thermal conductivity measurements was 0.2 %, and the two heat flow values differed by 3.8 %, not a lot considering the local complexity of the sediments.

Heat flows from 13 sites in the mounds area vary between 43.8 and 80.1 mW/m<sup>2</sup>, the average being  $63.5 \pm 10.6$  mW/m<sup>2</sup>. The two heat flows measured outside of the mounds on this cruise were 27.7 (UMH001) and 35.8 (UMH002) mW/m<sup>2</sup>. Heat flow measured in Mississippi Canyon to the southwest (Blocks 798 – 891) was 25 mW/m<sup>2</sup> or less, and to the south, in block 518, it was 37 mW/m<sup>2</sup>. The heat flow within the mounds area is higher, compared to the surrounding region. Three sets of three measurements (UMH005-007, UMH009-UMH011 and UMH012-UMH014) across three different fault traces reveal a higher heat flow above the fault trace, compared to the heat flow on either side of it, consistent with fluids rising up the faults.



## GENERAL

### GEOLOGIC CONTEXT OF HEAT FLOW MEASUREMENTS

Seabed heat flow measurements serve two important purposes in oil exploration. The first is to identify areas of anomalous heat flow that may indicate localized fluid flow within the sediments. The second is to provide the upper boundary condition for thermal models that can predict temperature, burial, fluid generation and fluid transport histories within a basin. The upper boundary condition for such models is the measured heat flow at the top of the sediments, *i.e.*, the seafloor. Such models are used to indicate, on a regional scale, where and when the creation of oil is possible, and to where it might have migrated. The generation and preservation of oil within basins is highly temperature dependent. Also, for the purpose of field development subsequent to a discovery, the measured temperatures determine how stable gas hydrates are in shallow sediments, which sometimes determines the stability of the ocean floor in deep waters.

The average, “equilibrium” heat flow in a region is generally considered to include heat flowing upward into the bottom of the basin, in addition to heat generated by the radioactive decay of long-lived, naturally occurring isotopes and any other exothermic chemical reactions within the sedimentary column itself. Anomalous heat flow values imply the presence of a surficial disturbance or an additional heat source or heat sink that may indicate fluid flow. When combined with stratigraphy and structure defined by seismic data, anomalous heat flow values may identify upward (or downward) fluid migration. Surface geochemical information, in conjunction with seismic and heat flow data, often determines whether the flowing fluid is petroleum related.

It is important to consider the effects of fluid flow when modeling basin temperatures because often the advective component of heat flow is quite significant to the models. Hydrologic pressures can drive formation waters from one side of a basin to the other, mostly horizontally, over thousands of kilometers. Fluids tend to flow along formations due to differing permeabilities, in adjoining formations of differing lithologies. Any vertical component of a fluid flow carries heat toward or away from the surface, causing the vertical heat flow to vary with geographic location. If fluids are flowing systematically across a basin, a vertical component of fluid flow is expected at the basin edge with higher elevation recharge and at the edge where there is pinching out of beds at lower elevations. At outcrops of more permeable, compacted formations, fluid may flow into or out of the formation.

On both local and regional scales, fluid flow along faults across formations can modify the conductive thermal regime, as can topographic highs. Fluid flows, when accompanied by gases at pressures above local hydrostatic, can percolate across formation boundaries and yield local geographic anomalies that can point directly to hydrocarbon generation at depth.

Other heat flow variations are produced by differing amounts of stretching during basin formation and by varying sedimentation rates. Also, the enhanced thermal conductivity

of salt structures refracts heat, and any enhanced radioactive heat generation, especially in black shales, (Keen and Lewis, 1982) produces additional heat that must be considered when formulating heat flow interpretations.

### DESCRIPTION OF THE HEAT FLOW PROBE

**TDI-Brooks International Inc.** performs heat flow surveys using "Lister-type" probes, which, in addition to measuring the sediment/pore fluid temperatures, also measure the thermal conductivity *in situ* (Lister, 1979). With this method, a heavy probe assembly is lowered from a ship and penetrates the upper few meters of seabed sediments, where it comes to rest. It then measures the temperature of the sediments at several points in the sediment column using a string of sensors in a tube. The probe also has a wire-heater to generate a heat pulse inside the sensor tube. The heat decay over time from this heat pulse allows the measurement of the thermal conductivity of the surrounding sediments. Determination of the temperature gradient and the sediment conductivity allows the calculation of the heat flow through these sediments.

The current TDI-Brooks marine heat flow probes are the latest version of a series of probes developed under the direction of Dr. Earl Davis and colleagues at the **Pacific Geoscience Centre (PGC)** of The Geological Survey of Canada. The probe electronics were designed and produced by Richard Brancker Research Ltd. of Ottawa, Canada.

The basic construction of the probe and examples of its data are described by Davis *et al.* (1997). The heat probe consists of three parts:

**Table 1. Heat probe components.**

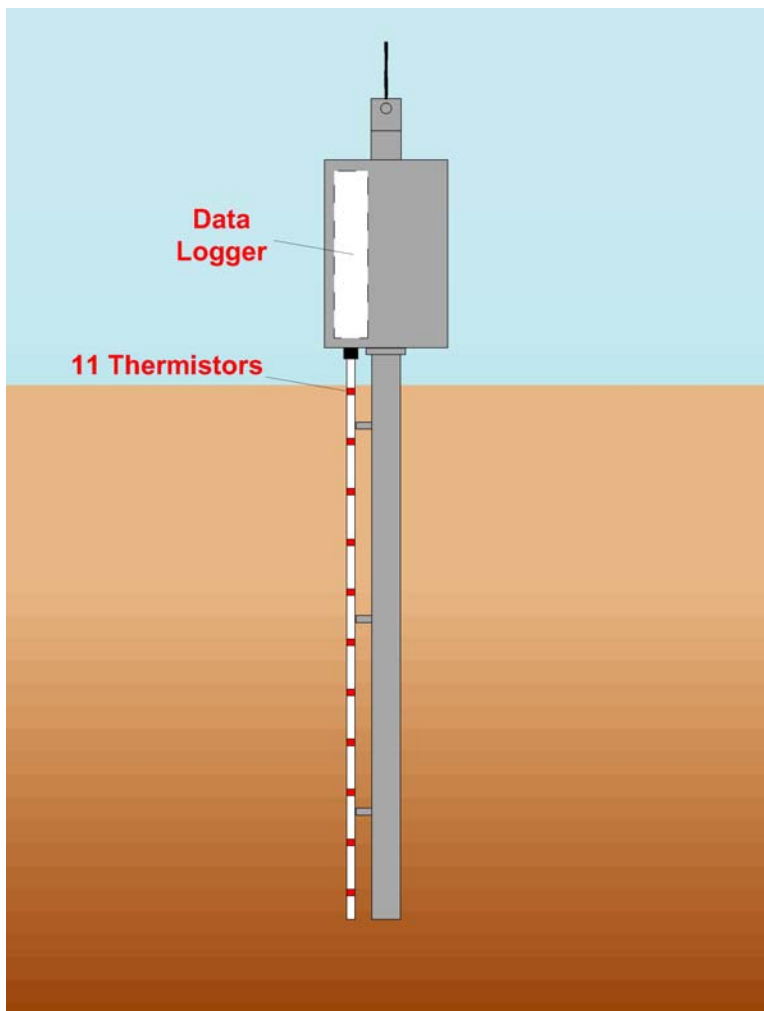
<b>Part</b>	<b>Description</b>
<b>Instrumentation</b>	1-cm diameter <i>sensor string tube</i> with temperature sensors
	computerized electronic data logger
	heat pulse system, batteries, and ports for cable connection
<b>Mechanical components</b>	weight stand
	cylindrical pressure case for the electronics
	6-cm diameter solid steel bar termed a <i>strength member</i> , which extends continuously from the wire termination at the top to the sensor tube support fin at the bottom of the probe
<b>Software</b>	modules for communication, operation of the probe, data analysis and graphics display.

The probe uses sixteen sensors for the measurement of temperature, pressure, and tilt angle. Each of these is described in detail in **Appendix 2** at the end of this report. Eleven sensors are glass-bead thermistors contained inside the sensor string tube, a high-strength 10-mm diameter stainless steel tube supported in tension 10 cm away from the strength member. These thermistors measure temperature at 30-cm (or 50-cm for a 5.5 m probe) vertical intervals when the probe is inserted into the sediment. This arrangement is shown schematically in **Figure 1**.

Sensor 12 measures the water temperature above the sediment surface when the probe is inserted into the sediment. Sensor 13 measures the internal temperature of the probe electronics. Sensor 14 is the reference (constant) resistor, used to determine the stability of the system. Sensor 15 measures the tilt of the probe over a range of 0° to 41° from vertical, with a resolution of approximately 0.1°.

Sensor 16 measures the water pressure (converted to water depth) using a quartz crystal sensor as the probe travels down and back up through the water column and at the sediment surface when the probe has been inserted into the sediment. This pressure transducer is absolute, and is calibrated for fresh water and absolute pressure, and thus requires a conversion factor to convert the data to depth in meters below sea level. It is precise enough to discern a change of a few centimeters water depth, even at 3,000 m water depth. Consequently, virtually any settling of the probe with time in the sediment

(which is disruptive to the temperature measurements) can be detected in the pressure record when the data are processed upon probe retrieval.



Because the readings from all of the sensors are logged at a set time interval (usually 10 seconds) from the time of probe deployment until the time of deck retrieval, each of the sensors reflects the corresponding conditions it is designed to measure throughout the trip down and back up. These data are used to confirm calibrations, to examine the water temperature structure with depth, for proper deployment and function, and for quality control.

**Figure 1. TDI-Brooks heat flow probe schematic.**

**Figure 2** is a photograph of an assembled heat flow probe, resting in its cradle under the A-frame used for deployment. The out-rigged sensor string tube can be seen above and parallel to the solid steel strength member that penetrates the sediment.



**Figure 2. TDI-Brooks heat flow probe photo.**

The length of the probe and the distance the probe ultimately penetrates into the seabed is dependent on the "stiffness" of the sediments under investigation. A probe length of 5.5 meters is used for deep ocean work. The driving weight for insertion into the sediment is provided by the weight of the strength member and the 500 kg weight stand, constructed of galvanized steel and lead fill. This weight stand also houses and protects the instrument pressure cases. Access to all external connectors on the instrument cases is possible without removing the cylinders from the weight stand (for battery charging and communication).

The one-ton instrument is suspended from a 5/8-inch diameter oceanographic Plasma rope. A universal swivel termination at the top of the heat flow probe prevents fouling of the rope around the weight stand and resulting damage to the sensor string. Once the probe penetrates into the seabed, the winchman and helmsman must work together for at least 25 minutes of station-holding to minimize the possibility of tugging on the main line during sediment measurements.

## OPERATION OF THE HEAT FLOW PROBE

When the probe is on-deck in its cradle, a laptop computer can be remotely connected using an RS232 serial cable to the probe electronics (through water-tight connectors in the pressure-tight housing) in order to program and control settings, to start and stop data acquisition, and to upload data from the probe between deployments. The probe's internal batteries can be charged when needed (about every twenty sites) while the vessel is underway between sites. Once the vessel is positioned over a site and probe data acquisition has been initiated, the probe is deployed. Special care is taken to keep the thermistor string tube oriented outboard as the probe is lowered over the side, in order to avoid any contact of this more fragile part of the probe with a rolling vessel. Proper orientation of the vessel with respect to the sea is also important to minimize deployment difficulties.

Seabed depth must be known within several meters for proper and safe deployment of the probe. At most sites the probe is lowered through the water at a rate of 45-60 m/min to within 50 m of the bottom and held there for at least 3 minutes to equilibrate in the isothermal bottom waters. This isothermal environment allows for the continued intercalibration of the thermistors. The probe is then lowered into the sediment where the strength member and thermistor string tube penetrate and remain stationary for at least 20 minutes. While the probe is left stationary, care must be taken by teamwork on the helmsman and winchman to pay out just enough main line to avoid jerking or tugging the probe with a rolling or drifting vessel. Too much main line slack can result in rope wrap around the probe upon pullout. Too little main line slack can result in wiggling the probe in the sediment, spoiling the temperature readings. The probe can be raised after pullout at 60 to 80 m/min.

The friction from insertion into the sediment typically heats the thermistor string tube and its immediately surrounding sediments. As a result, the temperature logged from each thermistor that penetrates cohesive sediment quickly jumps and peaks. The subsequent temperature decay curve of each thermistor is logged for a pre-set *stationary time* (typically 10 minutes) from the time the probe comes to rest (according to the accelerometer) in the sediment. The accelerometer monitors any vertical movement at this point, and this stationary time is extended until the probe has stayed motionless for that pre-set time. Stationary resting of the probe is important to ensure that the probe has not moved to due cable tugging from vessel movement or gradual subsidence into the sediment. This first set of temperature data ultimately yields the temperature gradient in the sediment spanned by the set of inserted thermistors. This is done by mathematically projecting the stationary-time temperature decay curves to infinite time. To accurately extrapolate these curves, well-behaved decay curves from a stationary probe are essential.

After the probe has rested in the sediment for the pre-set stationary time, a heat pulse of known energy is automatically triggered to the heater wire inside the thermistor string tube assembly. Power to the heater wire inside the tube is applied for a pre-set time (typically 10 seconds). The total power-time product delivered to the probe heater wire



during a heat pulse is measured, and is repeatable and stable. At least fifty properly regulated heat pulses per battery charge are available.

The pulse distinctly and dramatically heats the thermistor string tube and its immediately surrounding sediments. As a result, the temperature logged from each thermistor in the tube radically jumps and peaks. The subsequent temperature decay curve of each thermistor is logged for another pre-set time (typically another 10 minutes) from the time of the heat pulse. This second set of temperature data ultimately yields the thermal conductivity in the sediment spanned by the set of inserted thermistors. This is done by mathematically examining the rate of decay of the second set of temperature decay curves, which are superimposed on top of the initial frictional decay curves.

Once a heat pulse has been triggered, further heat pulses are inhibited until the pressure sensor has experienced a pre-set water depth change (typically 10 meters). This design feature allows multiple insertions (called *pogo* measurements) at a site, for the purpose of measurement replication without probe retrieval to the deck. Pogo measurements are achieved simply by raising the probe past the pulse-inhibit depth-change threshold and then re-inserting it. Because all of the sensors are logging data from the time the probe is activated on deck until the time it is de-activated back on deck, the only event needing such control is the heat pulse.

Once back upon deck, the data from all of the sensors for the site are downloaded from the probe's data logger to a laptop computer and immediately evaluated to assess the probe's penetration and performance at the site. The display is adjusted so that the fine detail in the sediment temperatures can be viewed to ascertain that the quality of the data. Such a display is shown as **Figure 3** and described in the next section.

### PROCESSING DATA FROM THE PROBE

A computer program is used to display the data visually on the computer monitor, pick the penetration times, and create the data input files for data processing. **Figure 3** is an annotated representation of this screen output. The temperature range is approximately equal to one degree. **Appendix 1** in the heat flow report includes non-annotated plots of the corresponding display for each penetration of this study.

The resolution of the temperatures from the thermistors in the sensor tube is greatly amplified in this graphical display so that details of the sediment temperatures can be seen. At this site the probe was lowered to within 50 m of the bottom, held there for at least 3 minutes, then lowered into the bottom where it remained about 25 minutes, with the heat pulse occurring at 10 minutes from probe stability after insertion. The temperature peaks that occur upon penetration, heat pulse, and pullout are easily seen.

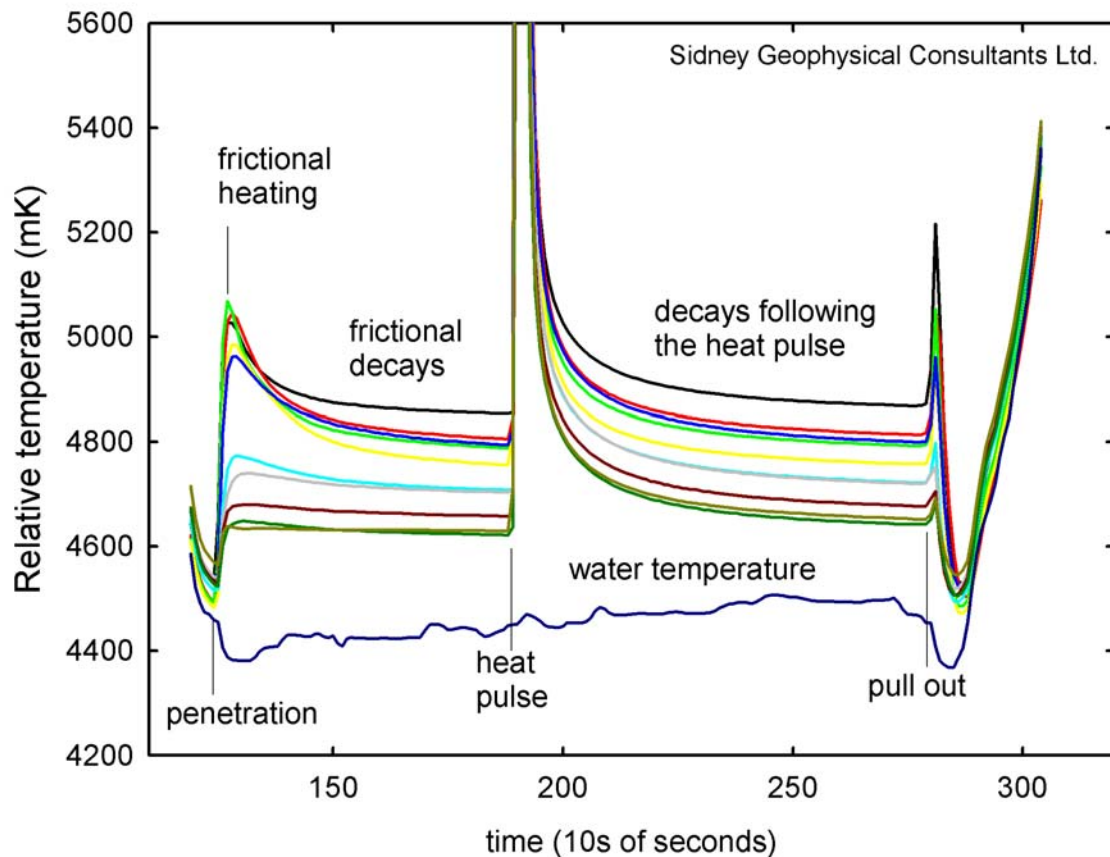


**Figure 3. Annotated example of a sensor output plot.**

The 11 thermistors in the sediment show the temperatures as measured 50 cm apart, with sensor 1 being the deepest. These sensor temperatures appear as a cluster of lines with the same value (water temperature), until they divide into separate values when the probe enters the sediment. They respond very sharply to the heat pulse, and may be heated by frictional heating on probe penetration and pullout.

For at least three minutes before penetrating the sediment, the probe being held approximately 50 m above the bottom is easily seen. This equilibration time is important to ensure proper intercalibrations of the thermistors in isothermal surroundings. When the heat flow probe is deployed for measurements in water not deep enough for isothermal bottom waters, the equilibration data for the deepest site(s) are used.

In order to measure vertical heat flow, a correction factor is applied for all sites with a tilt value greater than  $5^\circ$ . The tilt correction is the inverse of the cosine of the tilt angle. For sites with measured tilt less than  $5^\circ$  (which produces a correction factor of less than 1.004, or an increase in the heat flow of up to 0.4%), the correction is ignored. During normal operations, tilt is almost always less than  $5^\circ$ .

Once data are selected according to the penetration time and the heat pulse, data reduction is performed using a computer program named HFRED. This method was developed and described by Villinger and Davis (1987b), following the method first suggested by Lister (1979). One potential shortcoming of this method is that the thermal conductivity is measured in the horizontal radial direction from the probe, whereas the value in the vertical direction is required. Anisotropy in the thermal conductivity of shale (including unconsolidated shale) can cause a considerable difference between the horizontal and vertical values. Fortunately, anisotropy doesn't affect local measurement of thermal conductivity in most near-surface sediments.

The sediment thermal conductivity is mainly controlled by the *water content* of the sediment, since the thermal conductivity of water, 0.6 W/m-K (watts per meter-Kelvin), is much less than that of the rock matrix, which might typically be 2.3 W/m-K. As an example, the thermal conductivities of sediment from The Gulf of Mexico deep-water sites typically range from 0.85 to 1.1 W/m-K. This is consistent with a variation in porosity from approximately 75 to 55% (for an assumed rock matrix thermal conductivity of 2.3 W/m-K). A thermal conductivity of approximately 1.6 W/m-K is consistent with a porosity of 25%. The thermal conductivity measurements from the heat flow probe are accurate to 1% of value, so such measured variations are real.

At any point in the sediment column, the conductive heat flow is the product of the temperature gradient and thermal conductivity. Heat flow (Q), measured in mW/m<sup>2</sup>, (milliwatts per square meter) is determined by combining the site thermal conductivity (k) measured in W/m-K, with the geothermal gradient (G) measured in mK/m as determined from the thermistors, according to the following relationship:

$$Q = kG$$

The actual heat flow for a tested site is determined by constructing a graph called a ***Bullard Plot***. This plot of sediment temperature (T), reported in mK, versus the thermal resistance (R), reported in m<sup>2</sup>K/W, is graphed for each site. Thermal resistance is the integral of the inverse of thermal conductivity over the appropriate depth interval. Each plotted trend illustrates the relative temperature as a function of the thermal resistance, integrated from the top sensor downward through the sediment. ***The reciprocal of the slope of the resulting best-fit line is the heat flow*** (thermal resistance is plotted as the vertical Y parameter because it tracks depth; while heat flow is  $\Delta T/\Delta R$ ). Under the ideal conditions of a constant vertical heat flow in a conductive regime, this would be a straight line.

**Figure 4** displays examples of Bullard Plots for two sites (plotted on the same axes for comparison of heat flow values). The slope of the best-fit line through each of the valid data points on the Bullard plot is used to determine the most representative heat flow value for each site. In **Figure 4**, the upper-most two points for Site ABC002 have been ignored in fitting the best-fit line through the data. This is because the upper-most measurements deviate from the general trend, likely due to perturbations of bottom water temperature or some other influence on the near-surface temperature gradient. In fact,

changes in bottom water temperature can cause severe problems with interpretation of data in shallow waters. We have on occasion detected the evidence of bottom water temperature changes at sites deeper than 2,000 m. For this reason, we do not recommend attempting heat flow measures at water depths less than about 600 m.

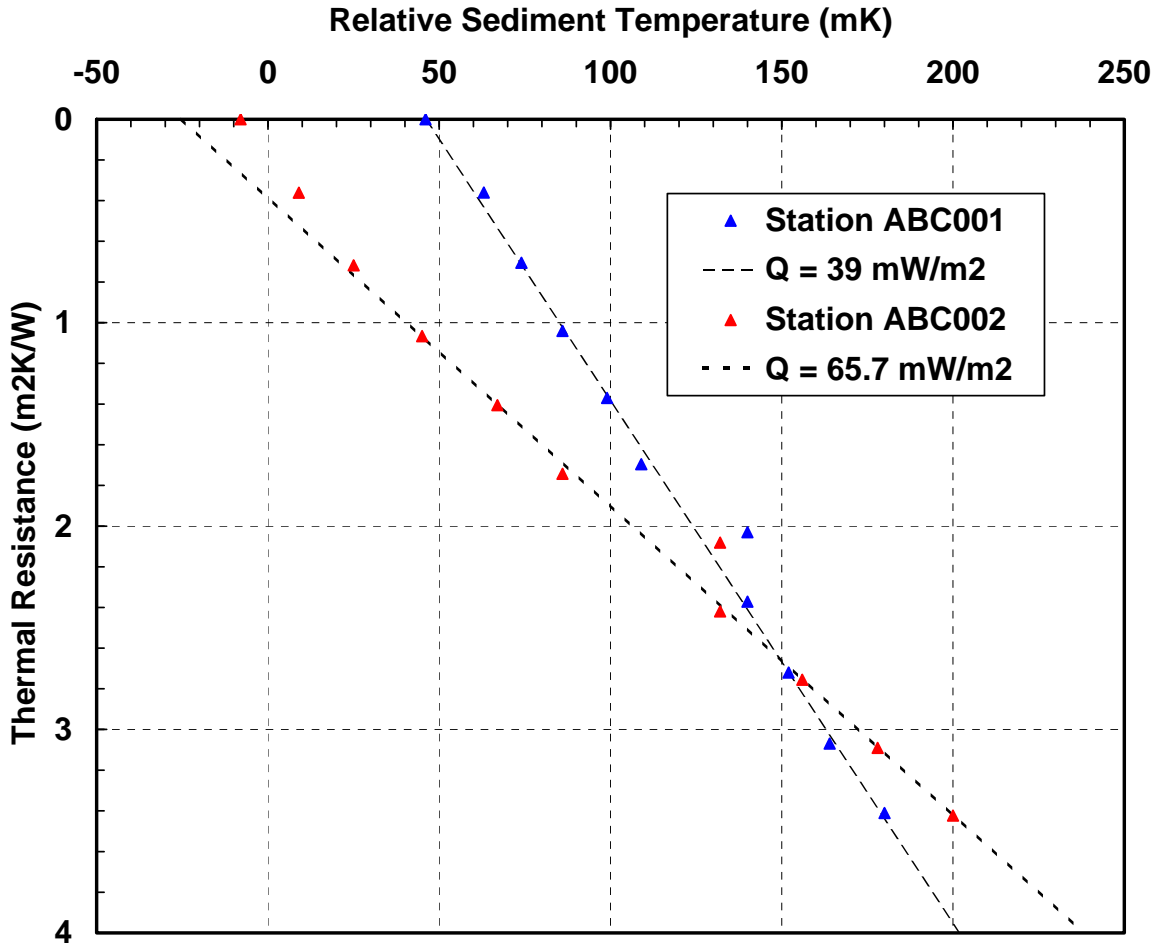


Figure 4. Example of Bullard Plots, comparing two sites.

Referring to **Figure 4**, note that the slope of the line for Site ABC001 is greater than the slope for Site ABC002. This difference illustrates typical variability in heat flow for a given region. The heat flow value of  $39 \text{ mW/m}^2$  is typical, perhaps, of a background value, and the heat flow value of  $65.7 \text{ mW/m}^2$  is considered a high value for the region, perhaps due to unusual fluid flow within the vicinity.

In order to test reproducibility, two penetrations are typically performed at one or more sites (referred to as *pogo* sites). Replicate sites are plotted on the same Bullard Plot in order to verify the resulting heat flow for a site. **Figure 5** is an example of such a comparison, taken from an earlier program. This figure illustrates the typical repeatability of results for a particular site. Note that the *slopes* of the two lines dictate the measured heat flow and the *offset* between the two lines is of no consequence.

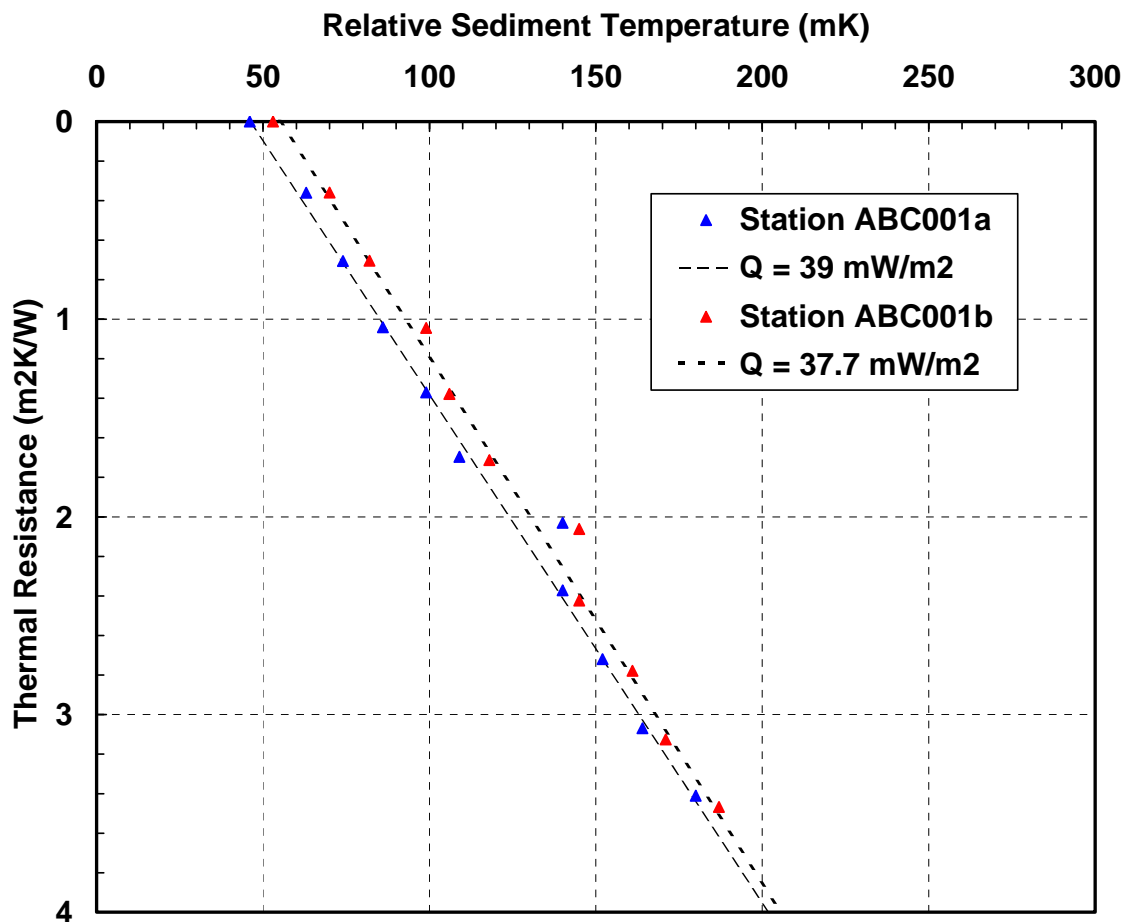


Figure 5. Bullard Plot comparing replicate (*pogo*) sites.



## THIS PROGRAM

### BOTTOM WATER TEMPERATURES

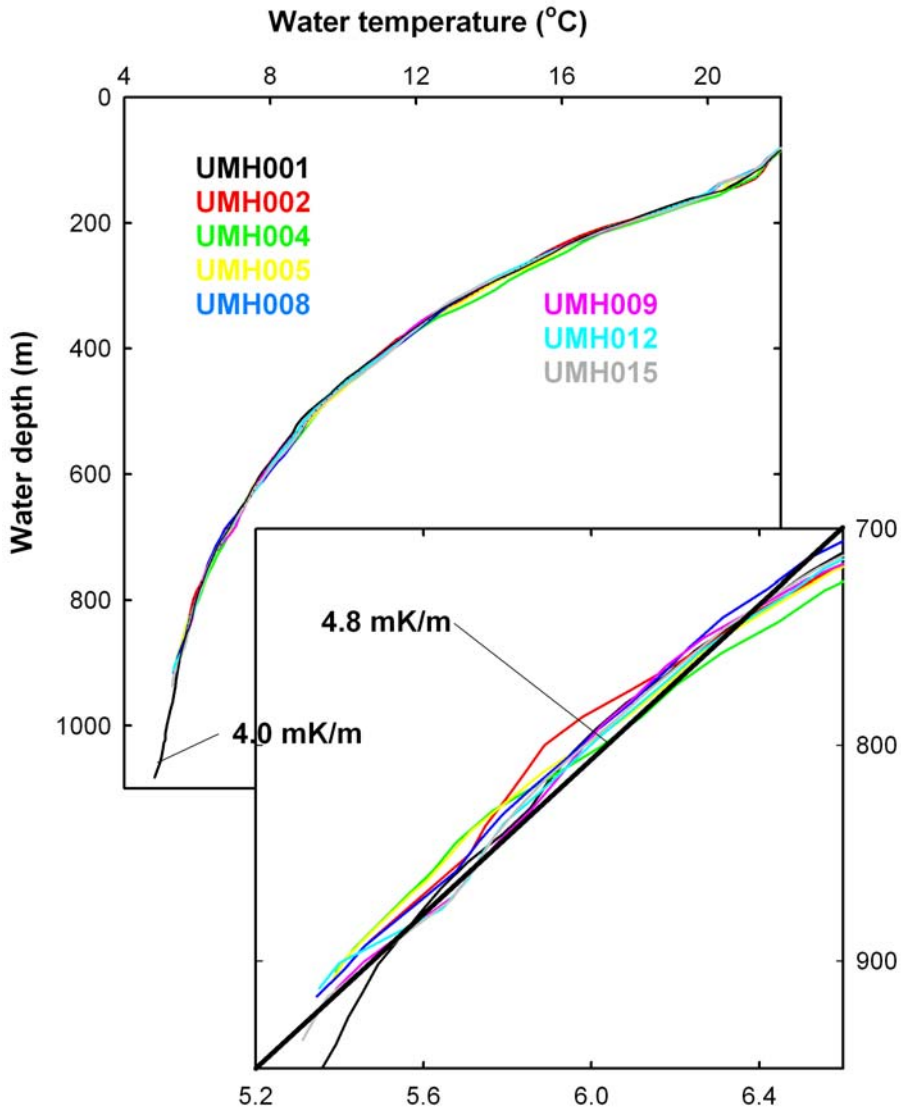
The bottom water temperature (BWT) controls the boundary condition for conduction of heat upward through the sediments. Understanding changes to it is extremely important. If it cools down by a small amount suddenly, then this sends a temperature anomaly propagating downward into the sediments. Over time, relatively cool water must replace water already in the water column, or it would keep heating from the small heat input of the sediments and the much higher surface temperatures. Sometimes such changes in the BWT are responsible for large temperature variations in the 5-m interval of sediments we measure, particularly at shallow water sites. Normally in the deep ocean the BWT is fairly stable over time, and varies only slightly with depth, but in shallow waters, BWTs are not generally as stable, so larger transients are expected in the sediments. To determine the heat flow in the presence of such transients is extremely difficult (*e.g.*, Lewis *et al.*, 1991). The changes in BWT are not generally the same in magnitude or timing from year to year. This will be discussed later.

There are numerous water temperature data from the Gulf of Mexico. Unfortunately none of them were measured at the seafloor of the mounds area in the weeks and months before the measurements were made.

Screen plots of the outputs from all of the sensors recorded while the probe was activated were examined immediately following the retrieval of the data, after the probe was turned off. **Appendix 1** contains copies of all of these plots. The original hexadecimal formatted files \*.raw are converted to \*.dat files, and then they are plotted on screen by the software PRO40. From these plots, the \*.pen files are created, by choosing visually the time periods for determining the hold temperatures, and the time periods to be used to fit temperatures to decay curves. The program HFRED fits the decays, in order to determine the undisturbed sediment temperatures and the thermal conductivities of the sediments, near to each sensor.

Plots of water column temperature versus water depth for the six times that the probe descended through the water column to the sea floor are shown in **Figure 6**. Note that the depths used are uncorrected at this stage. Sensor T1 was used for these measurements, as the probe descended. The water temperature sensor did not function during the entire cruise. The variation between the six different profiles can be seen, and the largest difference at any depth was 123. mK. Also shown are average temperature gradients in the water column at UMH001 (3.97 mK/m) and the approximate average value above the mounds area where the holds would be made, 4.8 mK/m. The latter is used to calculate a correction to the heat flow, by subtracting it from the measured gradient obtained with calibration temperatures measured in the water column, which are assumed to be all at the same temperature. This correction is applied at the end, subtracting the product of the gradient (4.8 mK/m) times the average thermal conductivity from the values measured over the appropriate depth interval.

When comparing temperatures measured while the probe is descending and ascending, it is important to note that the response times of the sensors, inside the sensor tube, produce an apparent hysteresis effect. This is caused by the delay of the thermistors sensing the outside water temperature through the sensor tube wall. During the hold, the sensor tube has time to cool and to reach the equilibrium temperature. But while descending, for example, the measured temperature is some convolved average of the water temperature during the last 50 seconds while it was cooling to the water column temperatures it was passing through.



This is over a depth interval of approximately 50 m, dependent on the winch speed. So the plotted measured temperature at a particular depth is warmer than that measured during ascent. The water sensor has a faster response time, unless it is covered with mud on the ascent, if it were working. The speeds of descent and ascent may be different, and the sensors are not calibrated for absolute temperature.

**Figure 6. Water column temperatures measured above three sites in the main basin.**

**Figure 7** shows the hold temperatures from all of the sites plotted onto the water column temperature profiles from **Figure 6**. These temperatures are plotted at the uncorrected depth also. The hold temperatures are colder, due to the time constant for the sensors inside the sensor tube (see above).

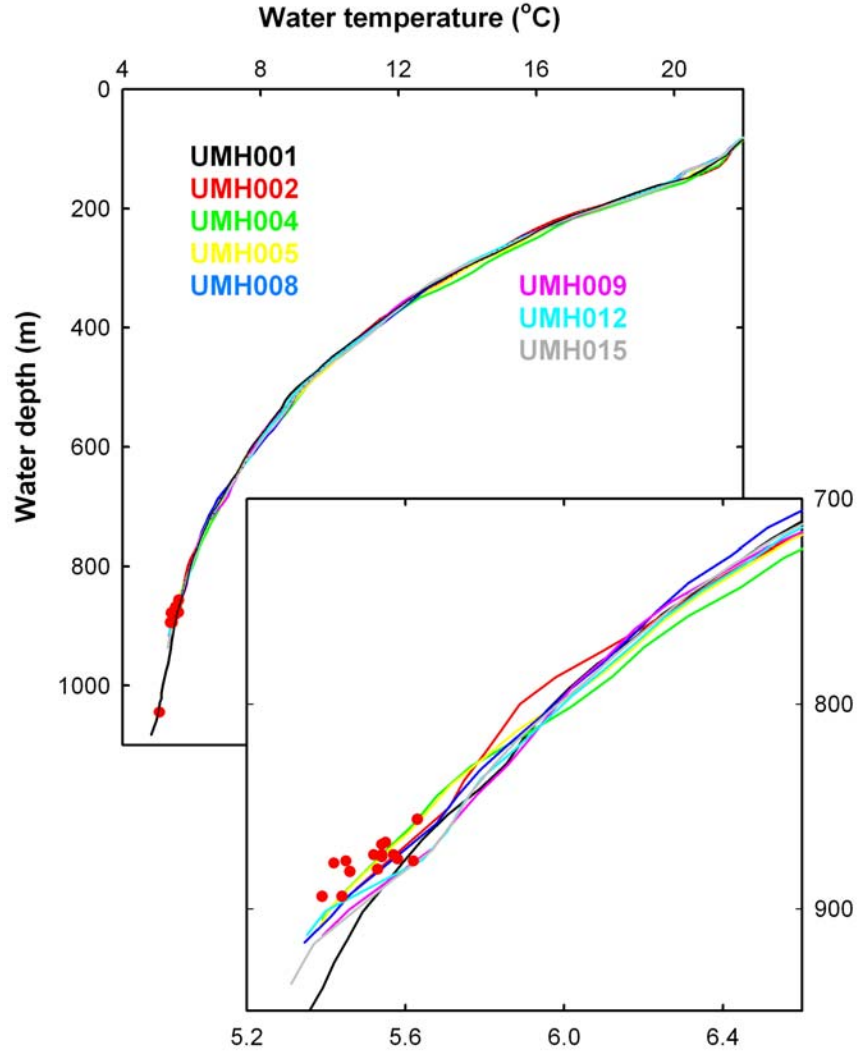


**Figure 7. Temperatures from the hold at every heat flow site.**

As noted previously, the absolute calibration of the temperature sensors is to  $\pm 0.1$  °C; their accurate, relative calibrations are normally obtained by measurements in isothermal water above each station, during a “hold”. One of our conclusions from observations in many areas is that there can be more variation in the water column temperatures than indicated by the measurements as the probe is lowered or raised through the water column. This effect is due to the time constant for the sensors inside the sensor tube to sense the water temperature. Also, the water temperature variations can be due to fine structure in the water column, and/or due to fluids and gas rising in the water column.

As a check on the stability of the temperature measurement system and on the sensor string, the measured calibration temperatures for each sensor, with respect to that of sensor T1, are plotted, (**Figure 8**) in the order in which they were measured (**Table 2**). The same sensor string was used for the entire cruise. The equipment used is recorded in **Table 1**. These plots may be used on most cruises to detect an occasional site where the

reference temperatures are incorrect due to a temperature gradient in the water, or movement of the probe, or a temperature disturbance above the site. They also can show any gradual deterioration (small salt water leak) in the sensor string and associated connectors and wires. From data obtained on previous cruises, we know the expected variation in the absence of any of these problems is usually a couple of mK. An example of the expected stability from another cruise is shown in **Figure 9**. Note that the total range of temperature in **Figure 8** is larger than in **Figure 9**.

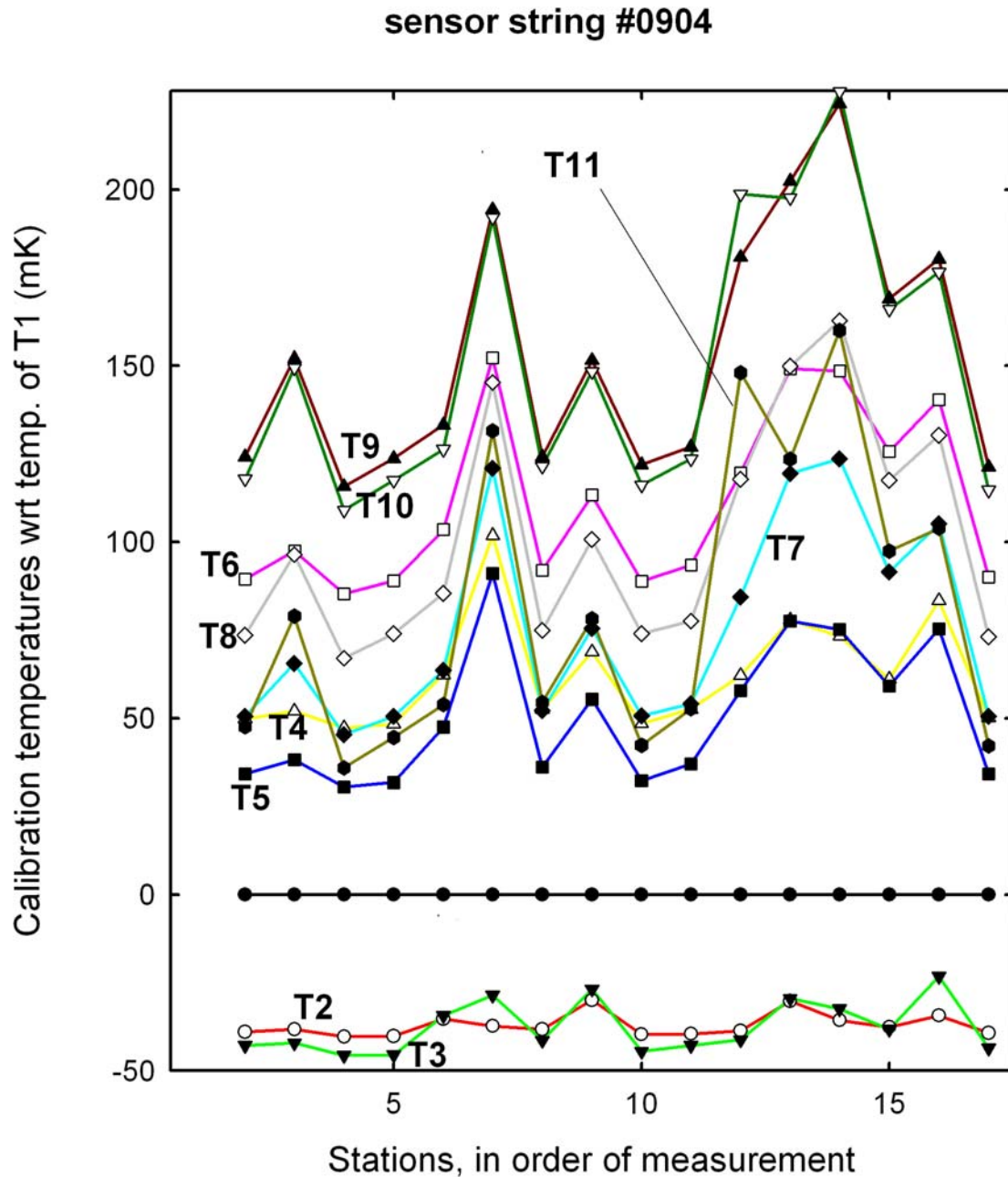


**Figure 8: Calibration temperatures wrt T1 values, in order of measurement.**

**Table 2. Order of stations and equipment used.**

<b>Date</b>	<b>Time</b>	<b>Station</b>	<b>Depth (m)</b>
29 Mar	1338	UMH001	1,092
29 Mar	1751	UMH002	904
30 Mar	0625	UMH004	917
30 Mar	0736	UMH003	918
30 Mar	0925	UMH005	923
30 Mar	1011	UMH006	928
30 Mar	1105	UMH007	924
30 Mar	1235	UMH009	924
30 Mar	1327	UMH010	926
30 Mar	1412	UMH011	924
30 Mar	1530	UMH012	925
30 Mar	1620	UMH013	931
30 Mar	1706	UMH014	932
30 Mar	1832	UMJ015a	941
	1904	UMH015b	944
30 Mar	2042	UMH008	921

Electronics # 9202

Sensor string # 0904

Pressure sensor #78973.



### sensor string #0902

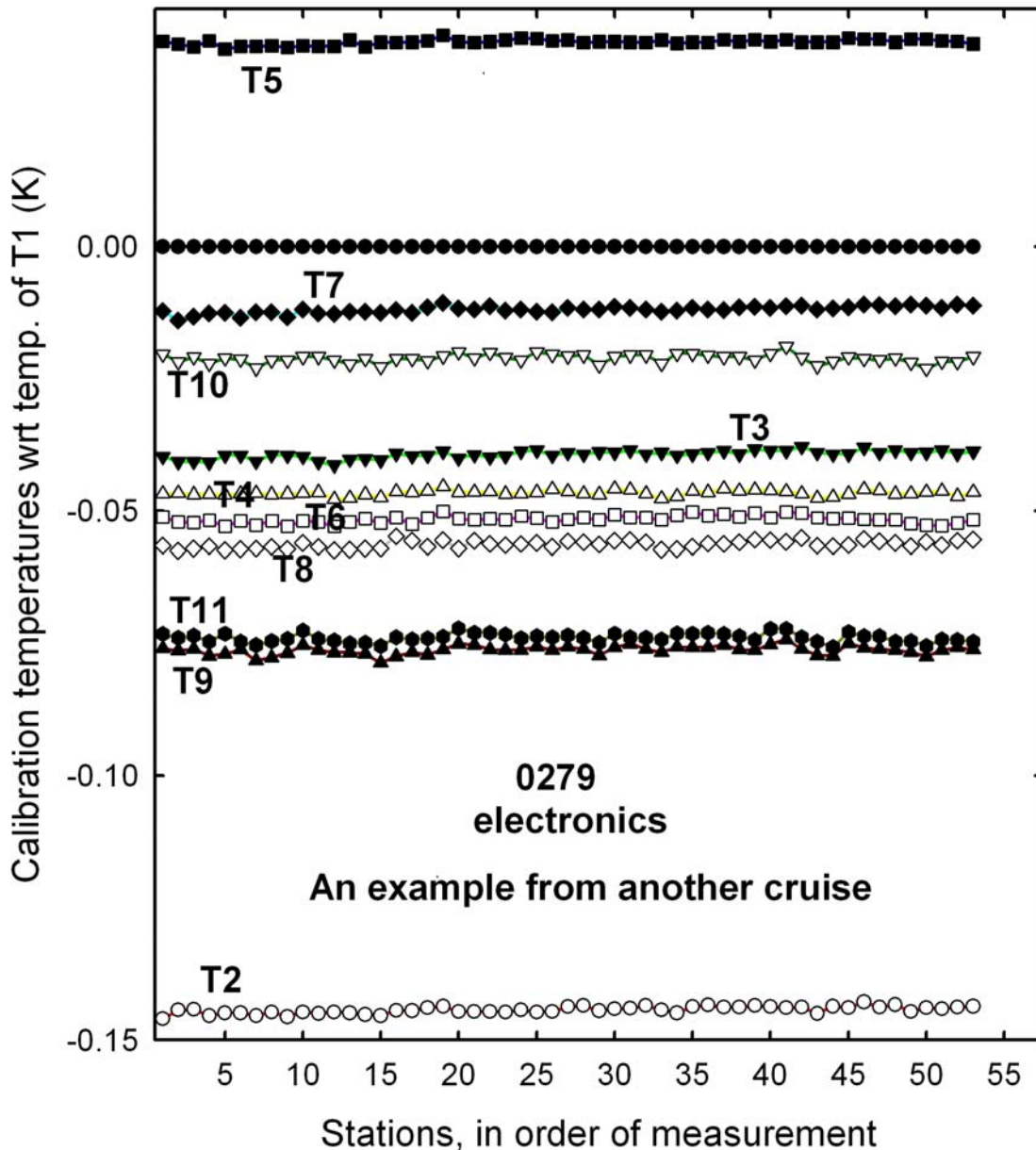


**Figure 9: Example of calibration temperatures wrt T1 values, from another project.**

The calibration temperatures obtained during the holds on this cruise vary much more than at any of the many other sites I am familiar with, consisting of thousands of such measurements. Initially the data were thought to show that these variations were not due to changes in depth nor probe inclination during the hold (e.g., see **Appendix 1**, UMH003ex, UMH008ex, etc.). They are not due to any electronic malfunction: the stability channel is very stable and the changes are slow enough to be coming through sensing of the outside water column temperature. At UMH001 the sensors were a little noisy, maybe due to condensation on the electronics. This improved for all of the other sites, and may have been due to time needed for the desiccant to absorb the water vapor.

The initial, preliminary heat flow calculations were made using the sensor calibrations based on the temperatures from the hold immediately before each station. These values are identified by a “p”, as in UMH001p, when the values are presented or discussed. The associated files are defined by the simple number of the station (e.g., UMH001.pen, or UMH015a where there were two stations at the site). As will be discussed, these values were not always useful as the water column temperatures sometimes varied in time. Two other sets of calibration temperatures were used, and values and files for these are marked with an addition of “x” or “y” to the station designation. The corresponding file names would be marked for .pen, .out, .res, .r, and .jnb files (e.g., UMH001x.pen or UMH015ax.pen, and UMH001y.pen or UMH015ay.pen). All of the corresponding results are derived from the altered, original .pen files, in which the only changes are new calibration temperatures have been substituted for the original ones (line 6 of the .pen file).

During the two days when these data acquired two reasons for the poor calibration temperatures were considered. Part of the variation in calibration temperatures might be due to the larger temperature gradients in the shallower water column. Part of it might be due to releases of fluid and/or gas from the mounds. During later data analysis screen plots of the data were used to show that the probe was not stationary during some of the holds, but changing its depth, probably due to maneuvering of the ship. **Figure 10** is a plot just like the other screen plots in **Appendix 1**, except the resolution of the depth and temperature are greatly increased – the time axis from left to right, is still the same. (Please refer to UMH009 in **Appendix 1**). The two station designations indicate the decay curves from the frictional heating and the heat pulse. The time of the hold preceding each of these stations, 3-4 minutes, is indicated by a horizontal bar at the bottom of the figure.

The depth is indicated by the olive green line, and the full height of the graph is equivalent to 10 m for the depth range, and 200 mK for the temperature range. (The other green line, the internal temperature of the electronics package, is on a different scale.) During the hold before UMH010 the depth is closer to a constant value than during the hold before UMH009. (The calibration from the hold before UMH010 is the one used for the analysis of all sites – see below.) The temperatures shown during the hold before UMH010 (the 11 varying lines of which 9 are black) approach a constant, equilibrium value much better than do the ones during the hold before UMH009.

Consequently the movement of the probe during the hold in shallow water with a large vertical temperature gradient is thought to be the main reason for the many poor calibration temperatures. Regardless of the reason, the calibration temperatures from the holds were not reliable for many sites: calibrations had to be obtained in a different manner than usual. Two approaches were tried.

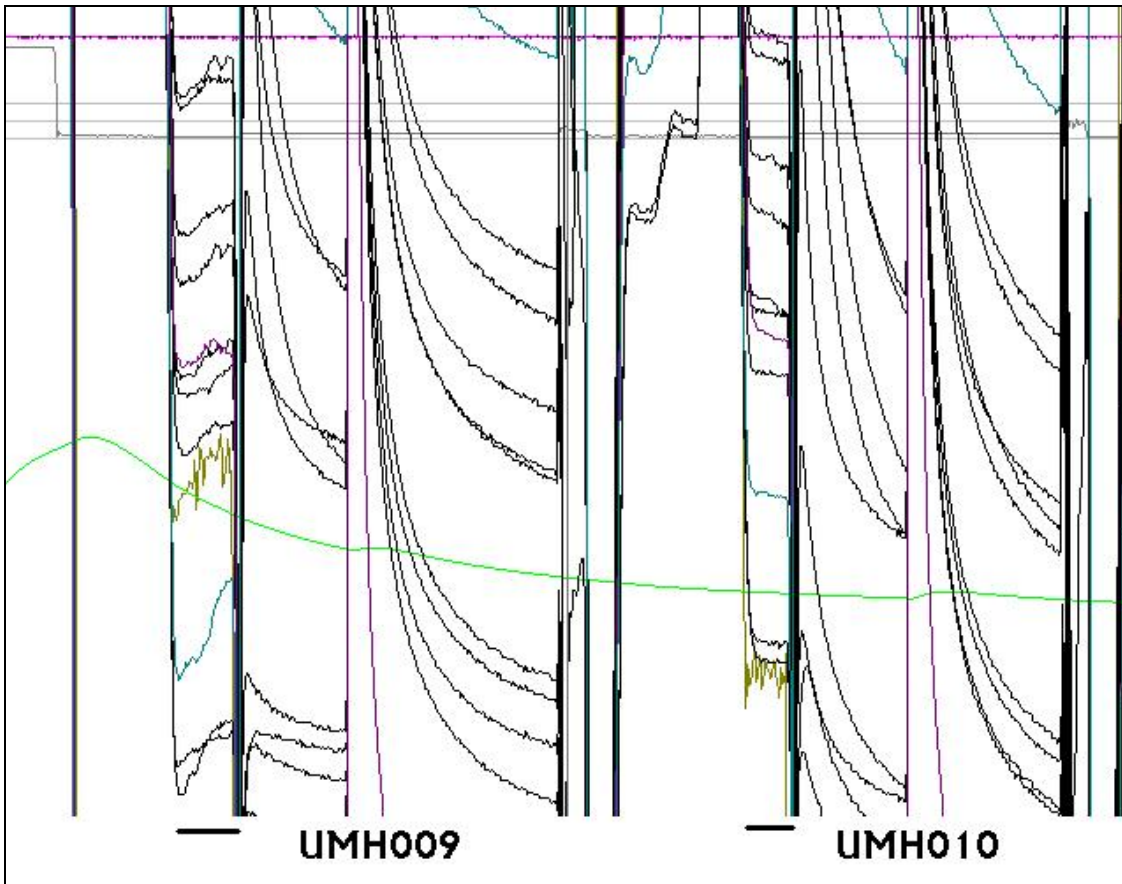


**Figure 10: A detailed plot of the sensors on screen,**

For the first approach (x added to file names and results), the calibration temperatures from **Figure 8** which were in best agreement (plotted as 3, 4, 7, 9, 10 and 16 in **Figure 8**) and which are listed and shown in **Figure 11**, were averaged to give a calibration temperature for each sensor. It is important to note that they were scattered throughout the entire cruise, indicating that there was no change within the sensor tube during the cruise. UMH001 (plotted as 2 in **Figure 8**) was not used for this since it was from a different location in deeper water.

sensor string #0904

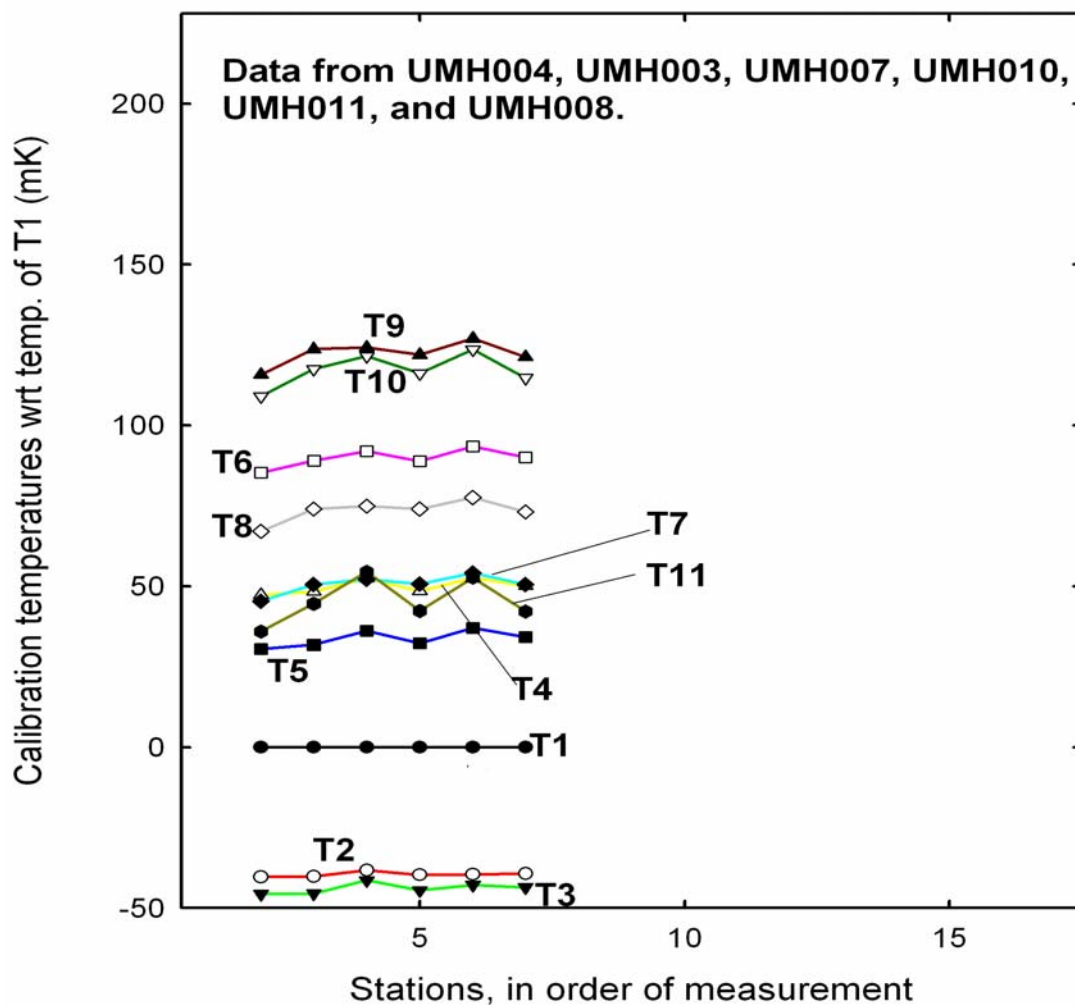


Figure 11: The calibration temperatures from 6 sites, used to calculate the heat flows designated with an “x”.

For the second approach (y added to file names and results), the calibration temperatures from a single hold, above UMH010, were used. These temperatures might be more constant than ones from most other sites on **Figure 8**. This approach has been used for other data sets before: the calibration temperatures from a single, deeper site were used for nearby sites if they were in shallower water. However, fluid and gas flows in the water column were not suspected at any of the former sites. The resulting heat flows from the original calibrations and from these two methods are discussed below, under heat flows.

In 2000, at a heat flow site in the mounds area of MC Block 798, the probe was inadvertently stopped just above the seafloor at one site, and recorded the temperatures of a brine pool. At 8 of the 15 sites on this cruise the probe was pulled up out of the sediments only 5 m, then stopped for 3 minutes, then pulled up another 4 m and stopped

for a further 3 minutes, looking for such pools. The depth and the tilt were amplified on screen plots, in order to see if any temperature anomalies were present, and if they were due to the tip of the probe being pulled through the top of the sediments. At every site during the first hold with sensor T1 approximately at the former depth of T11, some of the lowest sensors recorded increased temperatures. However, these temperatures often varied during the hold, and these variations seemed to be related in time to unexpected variations in the tilt, indicating that the bottom of the probe was being dragged through the sediment, producing frictional heating. There were no unexpected variations in the tilt nor the temperature during any of the second holds.

### THERMAL CONDUCTIVITY OF THE SEDIMENTS

These conductivity measurements are accurate to 1% of their value, so measured variations are significant. Average measured values for each station are given in **Table 3**, and individual measured values are contained in **Appendix 3**, in the digital .out files. Values are plotted for every station in **Figure 12**, as a function of the depth below T11, the sensor closest to the seafloor. This type of measurement assumes a conductive regime; in the mounds there might be fluids moving, which would move the heat more quickly. This will be discussed below.

**Table 3. Average measured values for each station (WGS84).**

Station	Lat	Lon	Depth (m)	BWT (°C)	Q (mW/m <sup>2</sup> )	Tilt (°)	No. of sensors	k (W/m K)
UMH001	28.810273	-88.517913	1,062	5.07	27.7	2.1	7 of 11	0.894
UMH002	28.861978	-88.501296	877	5.63	35.8	1.1	8 of 11	0.944
UMH003	28.856000	-88.495696	888	5.55	53.7	1.4	8 of 11	0.954
UMH004	28.857498	-88.495548	889	5.54	63.5	2	8 of 11	0.996
UMH005	28.857000	-88.490815	895	5.54	71.8	3.3	8 of 11	0.965
UMH006	28.856406	-88.491156	898	5.42	80.1	2.9	5 of 11	1.039
UMH007	28.855700	-88.491218	894	5.54	72.4	1.5	7 of 11	1.024
UMH008	28.854050	-88.491806	894	5.52	75.7	5	7 of 11	1.032
UMH009	28.853905	-88.489731	896	5.58	65.9	3.1	8 of 11	0.989
UMH010	28.853145	-88.489061	897	5.62	67.9	3.3	8 of 11	1.013
UMH011	28.852190	-88.488760	894	5.57	59.8	4.1	7 of 11	0.991
UMH012	28.851873	-88.486553	897	5.45	51.4	2.9	8 of 11	0.979
UMH013	28.851343	-88.485986	901	5.53	53.9	3	7 of 11	1
UMH014	28.850800	-88.485311	902	5.46	43.8	1.3	8 of 11	0.968
UMH015a	28.849691	-88.488811	914	5.39	67	4.9	5 of 11	1.065
UMH015b	28.849691	-88.488811	914	5.44	64.1	2.2	5 of 11	1.067



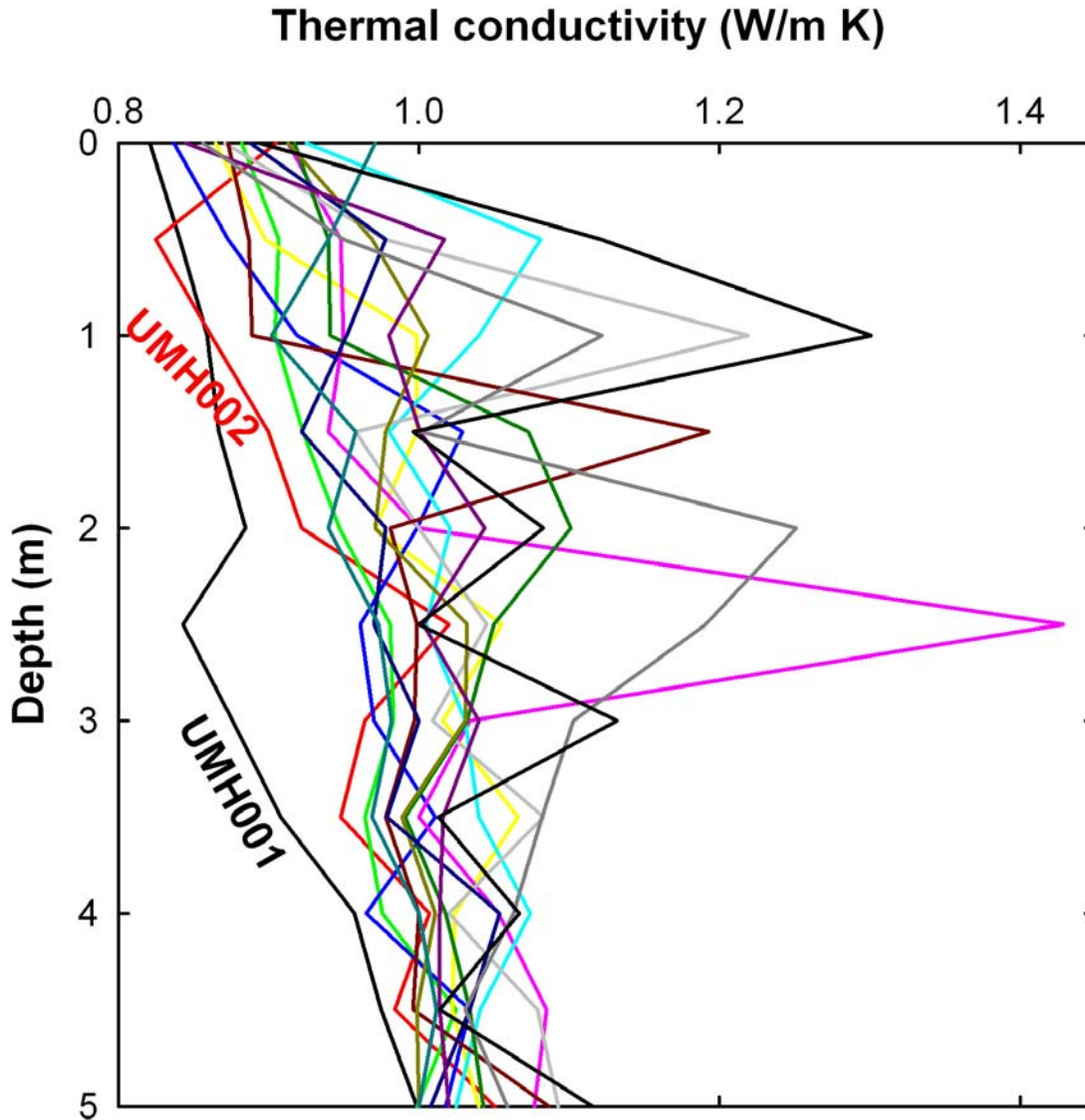


**Figure 12: Measured thermal conductivities, as a function of sediment depth.**

The heat pulse, used for determining the thermal conductivity, should always contain the same energy, from this PGC-style probe. A check was made on the value of the heat pulse, by looking at the maximum temperature rise it produced at each sensor. Since the pulse is synchronized with the logger clock, and since the same sensor tube configuration was used for every insertion of the probe, the maximum temperature rise should be constant for each sensor. **Figure 13** contains these data, in the order in which they were measured. It shows that the largest changes between pulses are less than 1% of the total temperature rises.

## Maximum temperature rise from the heat pulse.

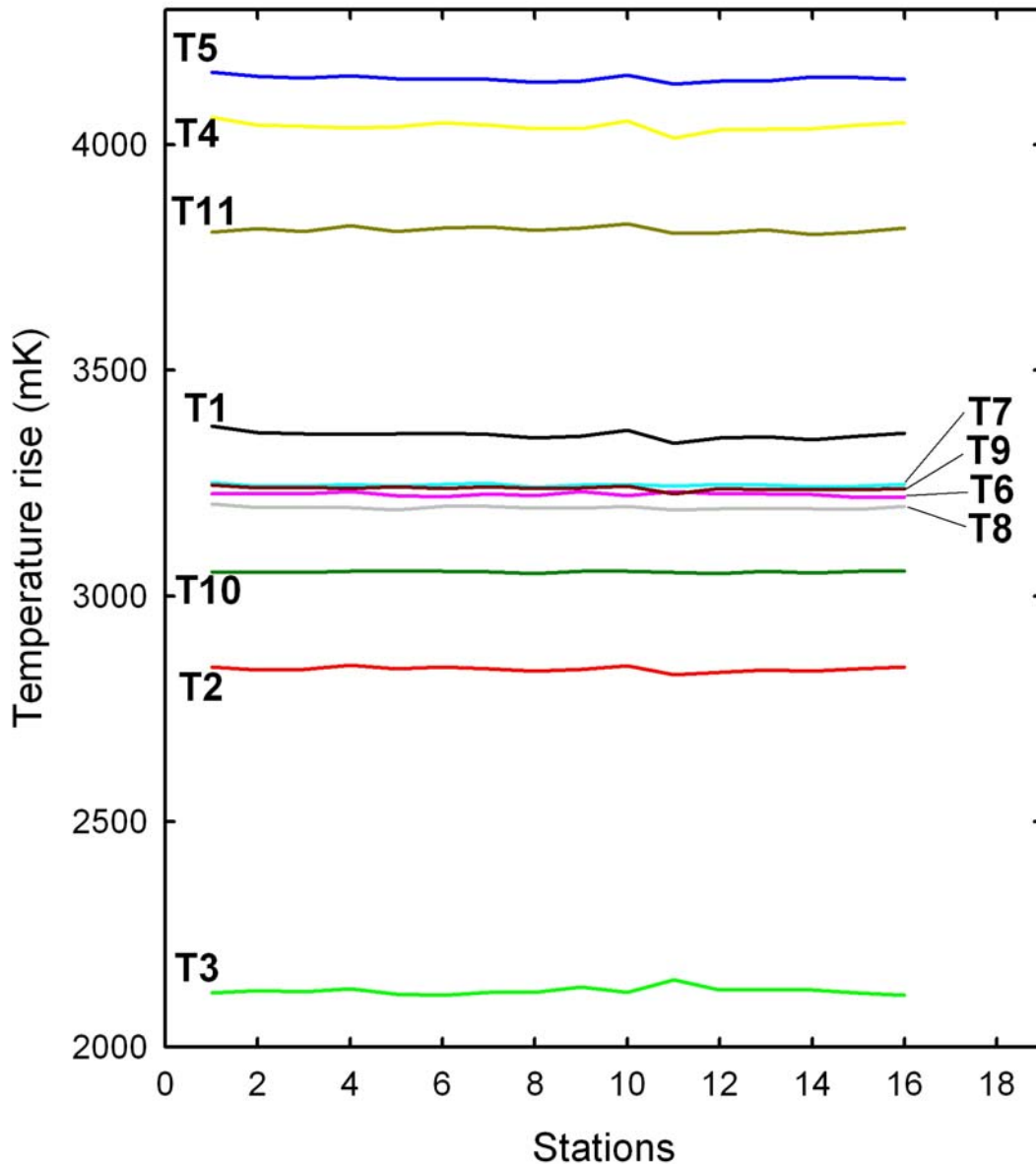


**Figure 13: Maximum sensor temperature rises produced by the heat pulses.**

Normally, the heat flow probe penetrates the sediments to its full length in a matter of seconds, a time much less than the time constants (approximately 30 seconds) for the sensors to detect temperatures in the surrounding sediments. The heating from the heat pulse and the decay of the temperature are superimposed on top of the tail of the curve from the original frictional heating. So an error in analyzing the frictional decay curve affects the thermal conductivity calculation as well.

The thermal conductivity determined at sensor T11, the closest to the seafloor, was not used for calculating any of the heat flow values. The position of this sensor can be very

close to the sea floor, it is in the sediments most disturbed by the insertion, and the value of water content is varying the most near the seafloor. Consequently, it is most often ignored.

The thermal conductivity reflects the porosity of the sediments, and increases as they are compacted. Generally the probe cannot fully penetrate sediments with a thermal conductivity much greater than 1.2 W/m K. At all of the sites on this cruise, it was able to penetrate the sediments. However, the measured thermal conductivity in the mounds area (UMH003-UMH015b) was quite high, averaging  $1.00 \pm 0.03$  W/m K, and there were 10 measurements of thermal conductivity exceeding 1.1 W/m K, and 5 measurements exceeding 1.2 W/m K.

In a normal, slow, constant sedimentation regime, the sediments are de-watering and this would be generally reflected in a slight variation of the thermal conductivity with depth near the seafloor. The uppermost sediments should contain the most water, up to 80 % porosity, and have the lowest thermal conductivity, and the conductivity would normally be between 0.7 and 0.9 W/m K. Generally, the expected variation with depth is seen in the results plotted in **Figure 12**. The value of thermal conductivity at UMH001 is more normal, averaging 0.894 W/m K. UMH001 is located away from the mounds area. UMH002, which is just outside of the mounds, has the next lowest average thermal conductivity, 0.944 W/m K. If a thermal conductivity of 2.3 W/m K is assumed for the matrix of the sediments, then the average porosity of the sediments penetrated in the mounds area is 61 %, if this were a completely conductive regime. At UMH001 the average porosity would be 70 %.

Probably most of the thermal conductivities over 1.1 W/m K are affected by quasi-horizontal fluid flows. This would reduce the thermal conductivity and therefore the conductive heat flow determined by the in situ heat pulse method. The moving fluid would transport heat away from the sensor tube. However, omitting these high values, the average measured thermal conductivity for the mounds area is still above average. This will be discussed further below.

UMH015 was a pogo site, where the heat flow probe was re-inserted into the sediments after being pulled up 60 m from the initial insertion. The two penetrations will be located within tens of m of each other. Digital files associated with the two penetrations are labeled a and b: e.g., the digital .pen files are UMH015a.pen and UMH015b.pen. The thermal conductivities are plotted as a function of depth in **Figure 14**. Although the average value for each insertion is very similar, 1.065 and 1.067 W/m K, some of the individual values are quite different at equivalent depths. This is probably an example of a quasi-horizontal fluid flow affecting three or four of the determinations and producing high values.

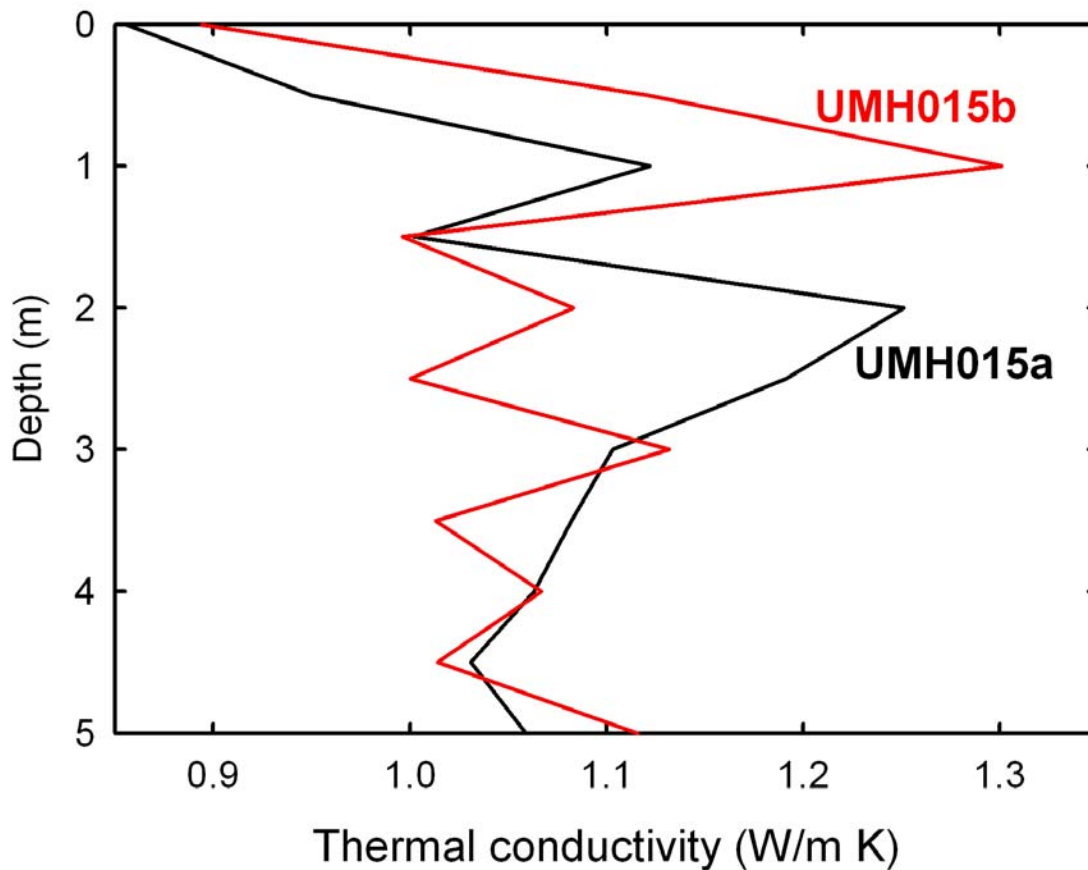


**Figure 14: Measured thermal conductivities as a function of depth at the pogo site, UMH015.**

## HEAT FLOW

**Table 3** summarizes the measured heat flow values as well as other relevant parameters for each station. Note that all results and files are identified by their site identifications (e.g., UMH001.dat). Note that these values assume a conductive regime. The water depths in **Table 3** are corrected for absolute pressure and salt water. A Bullard plot constructed using data from each station is contained in **Appendix 4**. The conductive heat flow is the reciprocal of the slope of the Bullard plot, and a constant heat flow is indicated by a linear Bullard plot.

The tilt sensor signal was recorded every 10 seconds, and is relative to vertical. The tilt correction used to obtain the vertical heat flow is the inverse of the cosine of the tilt angle. The tilt was less than  $3.3^\circ$ , for all penetrations except three. A tilt of  $3.3^\circ$  produces a correction factor of less than 1.003, or an increase in the heat flow of less than 0.3%. Results from the 3 insertions with larger tilts were corrected.

In this region, the heat flow is nearly constant in at least the bottom 2.0 m of sediments penetrated. In **Table 3** and **Table 4** the number of sensors from which data are used to calculate the heat flow is indicated, as well as the number of sensors penetrating the sediments. E.g., an entry of 5 of 11 indicates that 11 sensors were in the sediments, meaning that at least 5 m of the active sensor tube was within the sediments. The first number is the number of sensors from which data are actually used to calculate the heat flow, always the deepest sensors defining a straight line.

**Table 4: Calculated heat flows, using different sensor calibrations**

Site	Sensors	Heat Flow <sub>p</sub>		Heat Flow <sub>x</sub>		Heat Flow <sub>y</sub>	
		Value	r <sup>2</sup>	Value	r <sup>2</sup>	Value	r <sup>2</sup>
1	5 of 11	33.2	1.92	33.4	2.28	32.4	2.87
2	5 of 11	42.4	2	40.4	0.66	39.8	0.43
	8 of 11			40.5	1.4	40.5	1.4
003*	8 of 11	58.5	3.51	58.3	3.06	58.4	4.02
004*	7 of 11	67.2	3.85	68.8	4.35	68.6	3.68
5	5 of 11	85.9	4.28	78.5	2.11	77.9	2.69
	8 of 11			76.3	4.33	76.6	3.12
6	5 of 11	122	25.8	86.2	3.07	85.1	1.6
007*	7 of 11	77.9	2.5	77.2	2.56	77.4	3.18
008*	6 of 11	81.2	4.26	81.2	4.56	81	5.18
9	7 of 11	80.2	7.8	71.5	1.7	70.8	2.81
	9 of 11			71.4	1.53	71.7	2.91
010*	8 of 11	72.9	4.6	72.7	6.26	same as Q <sub>p</sub>	
011*	7 of 11	66.8	2.9	65	1.89	64.8	0.61
12	8 of 11	69.3	7.71	55.9	3.13	56.2	2.75
13	7 of 11	83.7	7.41	59	4.03	58.8	3.39
14	5 of 11	74.9	13.6	49.7	1.25	49.3	2.61
015a	5 of 11	84.1	7.2	72.9	0.33	72.4	0.67
015b	5 of 11	94.5	11.3	70.2	10.9	69.2	11.5

\* used for average intercalibration temperatures

**Table 4** contains the values of heat flow and an indication of the linearity (r<sup>2</sup>) for the three different calibrations of the sensors used, as described previously. These heat flow values are not corrected for the temperature gradient in the water, which will be nearly the same at each site. At each site, the sensors used are indicated by the value on the same line as any results. The main conclusion from these data is that the nine calibrations in **Figure 8** that appear at variance to the seven (including UMH001) that have similar calibrations, give incorrect results. The two sets of sensor calibrations used and their results identified with an x and y, give very similar heat flows at all sites. The preliminary heat flows from UMH005, UMH006, UMH009, UMH012, UMH013, UMH014, UMH015a and UMH015b, calculated using the hold temperatures measured



immediately before each station, give very different results, from 9 to 40 % higher, averaging 24 % higher. The linearity, over the same depth intervals, is also better for the x or y methods. The y method, based on a single hold calibration, is assumed the best. It was important to use also an average of calibration values, to see if there was any influence due to fluids and or gases rising in the water column at the single station hold.

Transients due to changes in the BWT “must” be recorded in the sediments. At 11 of the 15 sites there are apparent transients, consistent with an increase in the BWT in the weeks before the measurements were made, superimposed on a fairly constant vertical heat flow. This can be seen in the Bullard plots for UMH001-UMH005, UMH007, UMH009, UMH011-UMH14 (**Appendix 4**). It is also possible that such a change in BWT was imposed at the seafloor at the other 4 sites, although some other process has also affected the temperatures.

Nine of the 10 thermal conductivities above 1.10 W/m K were measured at these four sites where the heat flow was not so linear: UMH006, UMH008, UMH010 and UMH015. At UMH006, sensor T6 measured a thermal conductivity of 1.43 W/m K, the depth at which the heat flow non-linearity occurred. At UMH008, sensor T9 measured a thermal conductivity of 1.22 W/mK, where the heat flow non-linearity occurred. This non-linearity is so abrupt that it must be caused by fluid flow. There are other, similar correspondences for more than one sensor at UMH015a and UMH015b where heat flows are not constant. At UMH009, sensor T8 measured a thermal conductivity of 1.19 W/m K. The corresponding Bullard plot (**Appendix 4**, UMH009y) has a very constant heat flow up to within 1 m of the top sensor, unlike any other station.

It appears that all of the obviously high values of thermal conductivity are caused by quasi-horizontal fluid movements. Average values from the thermal conductivity measured above and below can be substituted in place of the one high value and the heat flow can be recalculated. These values (and associated files) are identified by adding a z to the name.

The heat flow at UMH006 (see the Bullard plot in **Appendix 4** for UMH006z) becomes constant up to T8, except for the temperature at T6. This is probably because the actual fluid flow is concentrated around the probe (sensor tube) where it penetrates the more permeable horizon, causing a larger temperature anomaly. But the temperatures 50 cm and 1 m above it are much more influenced by the conductive regime through the bulk of the sediments (i.e., getting the correct value of thermal conductivity at that depth). Or it might be that the insertion of the probe triggered the flow.

At UMH009, the insertion of a more likely thermal conductivity at the depth of T8, produces a transient similar to the transients seen at most of the other sites (compare the Bullard plots in **Appendix 4**). The slightly lower heat flow  $Q_z$  obtained using 8 of 11 sensors is accepted as the correct value.

At UMH015, values of thermal conductivity greater than 1.1 W/m K are measured by adjacent sensors (see **Figure 14**), suggesting either multiple fluid flows or fluid flows

over 50 cm in depth. Also the thermal conductivities from all the sensors are quite high, averaging 1.07 W/m K. Consequently this determination of heat flow assuming a conductive regime over the length of the probe is invalid. Fluid flows are the likely cause of the non-linearities shown on the Bullard plots for this site. An estimate of the conductive vertical heat flow can be obtained by using the average value of thermal conductivity for the whole area. Combining this with the measured gradients over the deepest 2 –m interval gives a heat flow of 63 mW/m<sup>2</sup> for this site, not much different from the measured values reported in **Table 4**. This is because the higher values of thermal conductivity were measured in the upper 3 m of sediments.

Fluids flowing upward through the sediments, including free gas and gas in solution, enhance the heat flow, and flowing downward diminish the heat flow at the seafloor. The fluid can be produced in the volume beneath the measurement site by compaction of the sediments or by dissociation of gas hydrate, or it can be transported quasi-horizontally into this volume along permeable beds, or beneath particularly impermeable horizons such as formed by gas hydrate. Generally the fluids escape into the ocean.

Is there a small, bulk permeability throughout the mounds area, in addition to the more prominent, discrete ones we have discussed? The conductive upward heat flow in the uppermost metre of sediments decreases at all sites, going to zero or negative at 7 of the 15 sites. An upward dispersed fluid flow would produce just the opposite effect, whereas a downward flow might produce the observed effect. If there were a bulk, upward flow throughout the entire mounds area, correcting the average thermal conductivity for it could only lower the thermal conductivity to a value such as 0.8 W/m K, lowering the overall average heat flow from 63.5 to 50.8 mW/m<sup>2</sup>. And this value would be only the conductive component and therefore a minimum value for the total vertical heat flow.

In obtaining the heat flow from the Bullard plots, data near the seafloor that did not fall on a straight line defined well by several deeper data were rejected; this is shown in **Table 2**, by the number of sensors used. The observed changes in the heat flow at the more shallow depths could be caused by varying sedimentation rates, changes in the BWT and/or fluid flows. Without local data on these processes, measured for the periods before the cruise, this problem is too complex to address properly. However, it is unlikely that sedimentation rates would be similar over the topographically complex mounds. And seismic data show that accumulations of gas vary and sedimentary layering has been disturbed, making a constant fluid flux out of the area very unlikely. Consequently, the reduction in heat flow measured in the most shallow 2 metres of sediments is probably due to a change in BWT over the entire area in the weeks before the cruise. If this happened, the expected transient in the sediments would be very similar over the entire area, as measured. This effect can be ignored by only accepting the heat flows measured in the deeper depth interval of 2 to 5m.

Any changes in the BWT over longer periods of time may have affected the heat flow at these deeper depths. Temperature data at the exact location of the heat flow measurements are required for a long time before the heat flow measurement was made. Even when such data are available, they may not define the upper boundary condition for

the conductive regime within the sediments, presumably due to complications at the interface (Lewis et al, 1991). The constancy of the heat flow over the deeper depth interval down to 5 m justifies its acceptance as representing the heat flow at deeper depths; but it does not guarantee the absence of any transient. The effect of a 14-month period sinusoidal change in BWT is nearly negligible at a depth of 5 m.

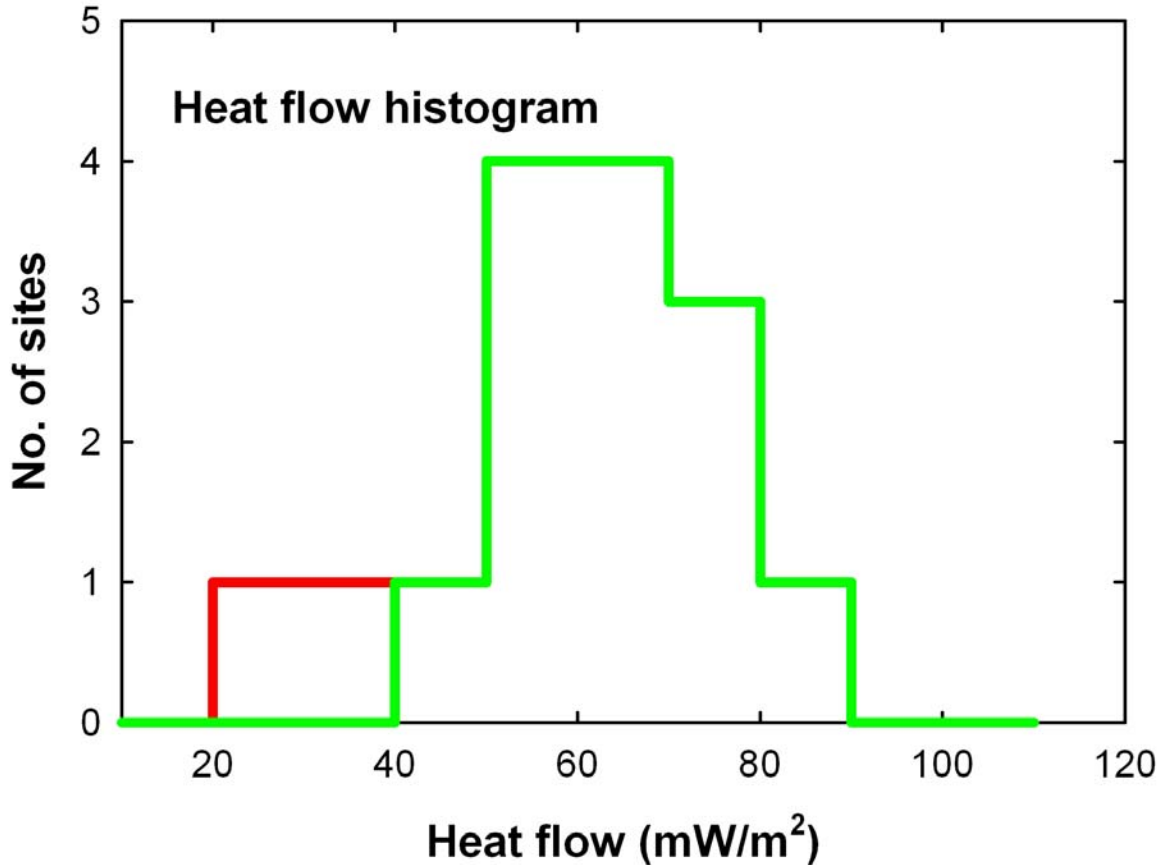


**Figure 15.** A histogram of the heat flow values at each site.

The values of heat flow measured on this cruise range from 27.7 to 80.1 mW/m<sup>2</sup>. In the mounds area they range from 43.8 to 80.1 mW/m<sup>2</sup>, averaging 63.5 mW/m<sup>2</sup>. **Figure 15** is a histogram of the heat flow values. The two lowest values in this figure were measured outside the mounds area. At the pogo site, UMH015, the two values of heat flow were 3.8 % different.

The geographical variation of the measured heat flow is shown in **Figures 16** and **17**. The average conductive heat flow measured in the mounds area is larger than in the surrounding area. The two heat flows measured outside of the mounds on this cruise were 27.7 (UMH001) and 35.8 (UMH002) mW/m<sup>2</sup>. Heat flow measured in Mississippi Canyon to the southwest (Blocks 798 – 891, TDI-BI, 2001) was 25 mW/m<sup>2</sup> or less, and to the south, in block 518 (TDI-BI, 1999), it was 37 mW/m<sup>2</sup>. This suggests a range of

heat flow in the surrounding areas of 25 – 37 mW/m<sup>2</sup>, and an anomaly in the mounds area averaging 26 – 39 mW/m<sup>2</sup>. However, more measurements of heat flow outside the mounds area are required to determine this accurately.

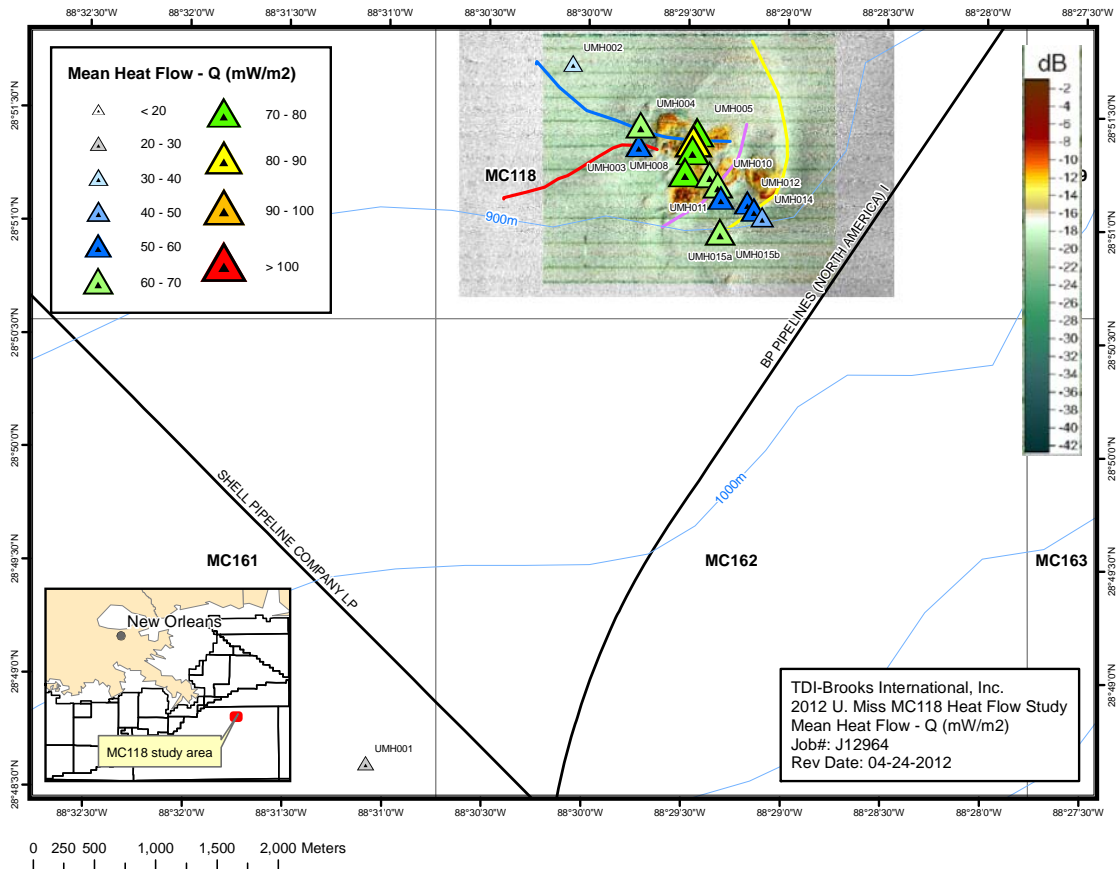
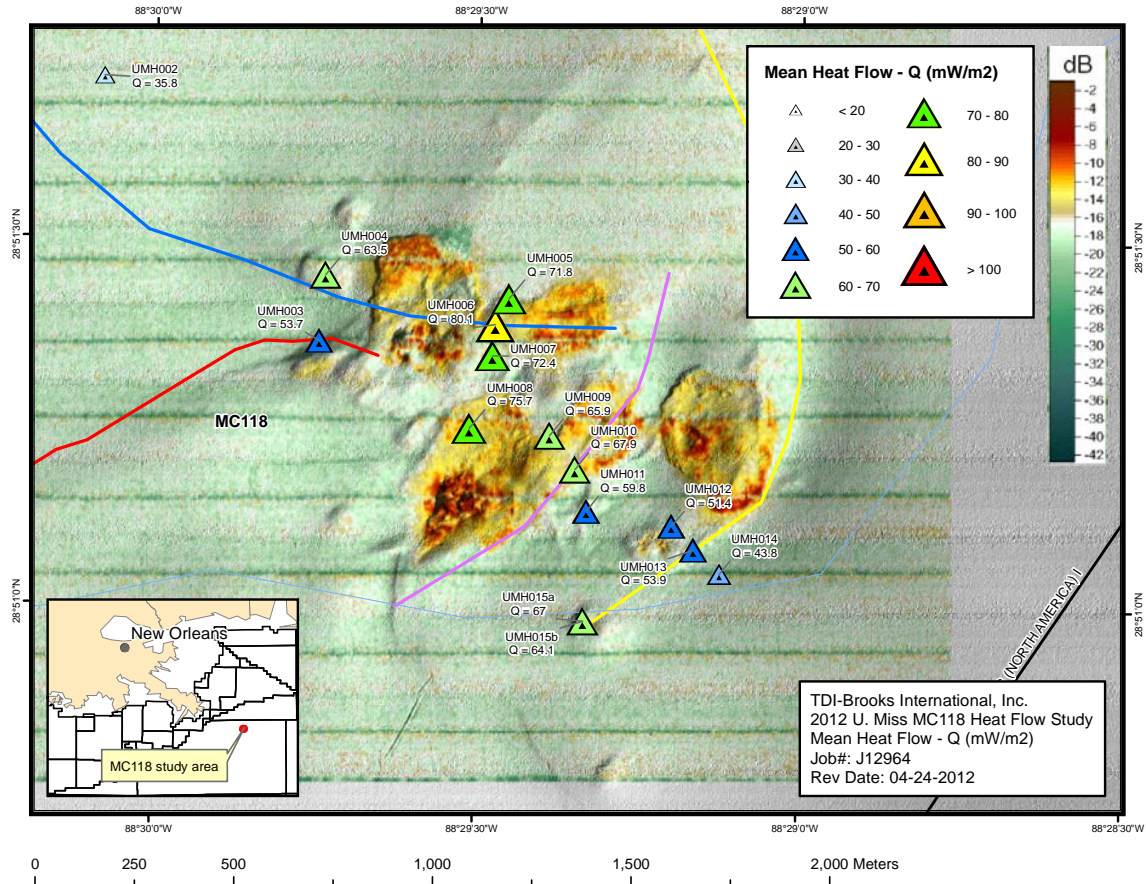


Figure 16: Heat flows measured in the mounds area.



**Figure 17: Heat flows measured in the mounds area detail.**

There are three sets of heat flows measured across traces of crestal faults. These values are plotted in **Figure 18** as sections crossing the traces of the faults. These results are consistent with fluids flowing up the faults and then spreading out into the overlying, surficial sediments as they make their way to the seafloor. Since the permeability of sediments is much more constant along the bedding, most fluid flows, other than ones with enough strength to rupture the bedding, flow along the bedding, to a fault or irregularity which causes a vertical weakness.



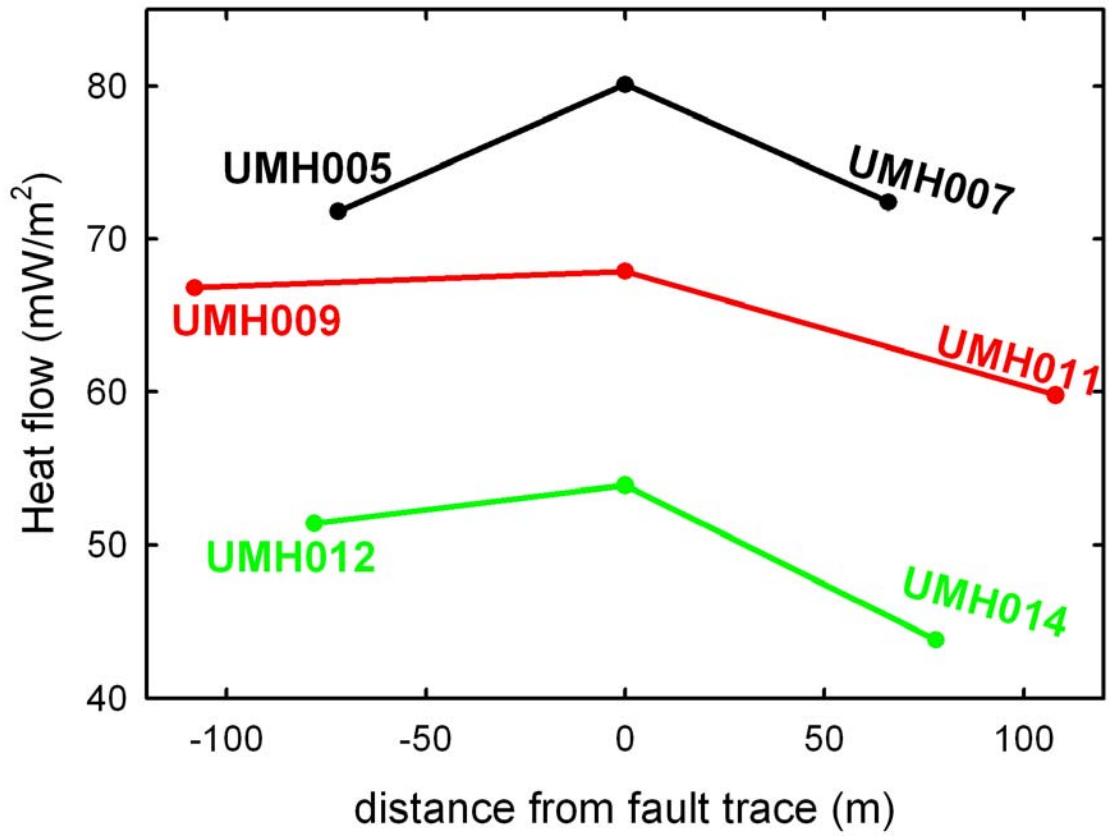


Figure 18: Heat flows measured on sections crossing three crestal fault traces.

## REFERENCES

- Bredehoeft, J.D. and I.S. Papadopoulos, Rates of vertical groundwater movement estimated from the earth's thermal profile, *Water Resources Research*, 1, 325-328, 1965.
- Davis, E.E., D.S. Chapman, H. Villinger, S. Robinson, J. Grigel, A. Rosenberger and D. Pribnow, Seafloor heat flow on the eastern flank of the Juan de Fuca ridge: Data from "Flankflux" Studies through 1995, *in Proceedings of the Ocean Drilling Program, Initial Reports*, **168**, 23-33, Davis, E.E., A.T. Fisher, J.V Firth, et al., (eds.), 1997.
- DSDP Scientific Party, Leg 47 Part 1, Initial Reports of the Deep Sea Drilling Project, Vol. 47, part 1, pp 69-70, National Science Foundation National Ocean Sediment Coring Program, 1976.
- Keen, C.E. And T.J Lewis, Radiogenic heat production in sediments from the continental margin of eastern North America: Implications for hydrocarbon generation, *American Association of Petroleum Geologists Bulletin*, **66**, 1402-1407, 1982.
- Lewis, T.J. and A.E. Beck, Analysis of heat-flow data- Detailed observations in many holes in a small area, , *Tectonophysics*, 41, 41-59, 1977.
- Lewis, T.J., W.H. Bentkowski and J.A. Wright, Thermal State of Queen Charlotte Basin, British Columbia: Warm, *in Evolution and Hydrocarbon Potential of the Queen Charlotte Basin, British Columbia*, edited by G. Woodsworth, Paper 90-10, 489-506, Geological Survey of Canada, 1991.
- Lister, C.R.B., The pulse-probe method of conductivity measurement, *Geophysical Journal of the Royal Astronomical Society*, **57**, 451-461, 1979.
- TDI-Brooks International, Mississippi Canyon Heat Flow Program, University of Mississippi, Technical Report # 01-697, 2001.
- TDI-Brooks International, Central & Eastern Gulf Consortium Heat Flow Program, Technical Report # 99-323, 1999.
- Villinger, H. and E.E. Davis, A new reduction algorithm for marine heat flow measurements, *Journal of Geophysical Research*, **92**, 12,846-12,856, 1987a.
- Villinger, H. and E.E. Davis, HFRED: A program for the reduction of marine hear flow data on a microcomputer, Geological Survey of Canada, Open File 1627, 78 pp, 1987b.

## APPENDIX 1 - GRAPHICAL SUMMARY DISPLAYS OF THE DATA FOR EACH STATION

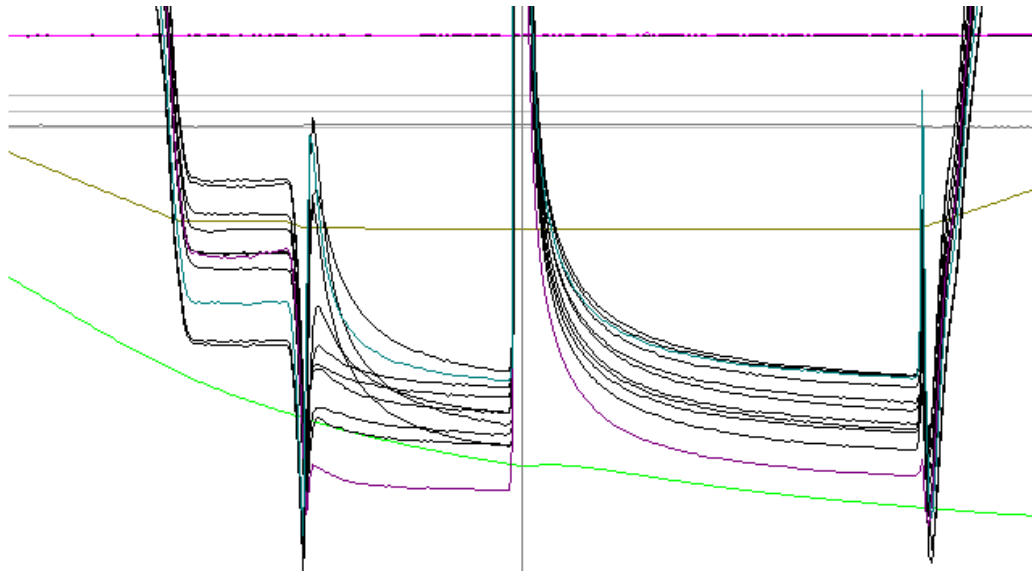
For each station, a graphical plot of the temperature was used to evaluate data within minutes after probe data acquisition and translation. Copies of the plots are reproduced in this appendix, for each station in numerical order.

The resolution of the temperatures from the thermistors in the sensor tube is greatly amplified in the graphical displays, so that details of the sediment temperatures can be seen. The display is plotted with time proceeding from left to right, and data were sensed and recorded every 1 or 2 seconds.

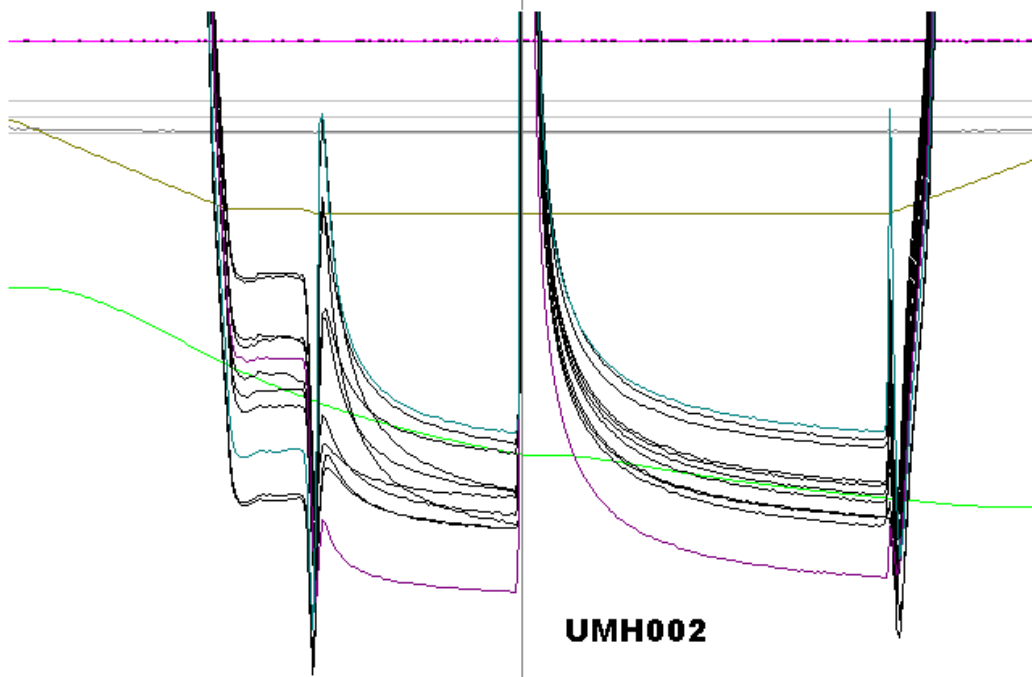
At all stations the probe was lowered to within 50 m of the bottom, held there for 3 minutes, then lowered into the bottom where it remained 20 minutes or longer, with the heat pulse occurring 10 minutes after penetration. At UMH015, after pulling out of the sediments, the probe was again held for 3 minutes above the sediments, then lowered into them for an additional 20 minutes, with a heat pulse going off after 10 minutes. This is called a pogo site, with the two different penetrations identified by an a and b added to the site identification.

The data from 11 temperature sensors are plotted on these graphs, from the **UMHnnn.dat** (etc.) files that are included in the CDROM of this report (where nnn represents a station number such as 001):

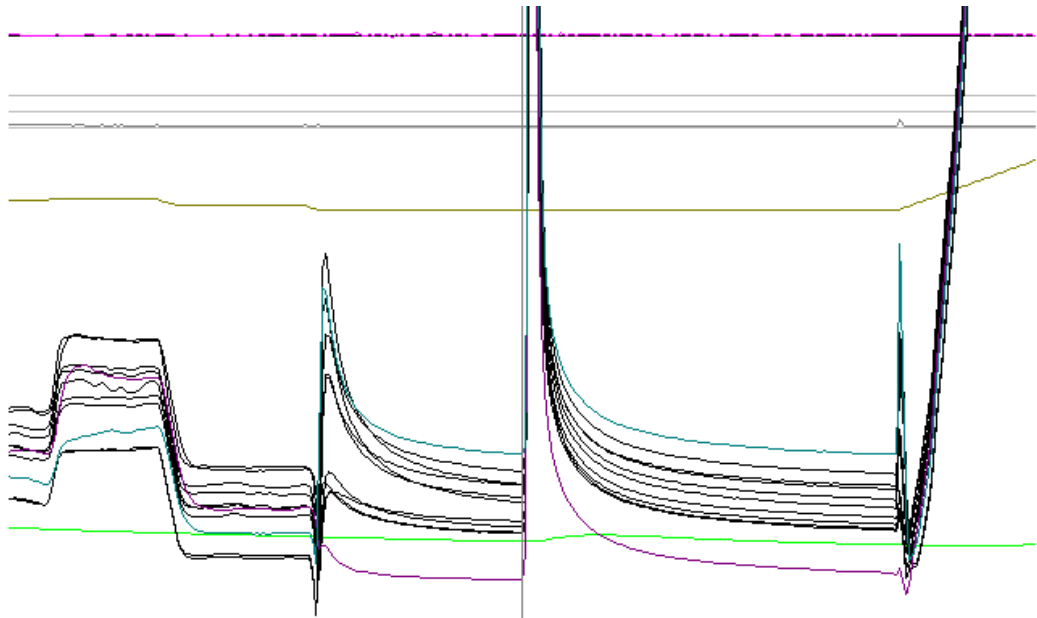
**Sensors 1-11:** The temperatures, in mK, measured within the probe at locations 50 cm apart, with sensor 1 being the deepest, closest to the bottom of the sensor tube. These sensor temperatures appear as a cluster of 11 lines with nearly the same value (water temperature), until they divide into separate values when the probe enters the sediment. They respond very sharply to the heat pulse, and may be heated by frictional heating on probe penetration and pullout. On this cruise all thermistor sensors worked exceedingly well.



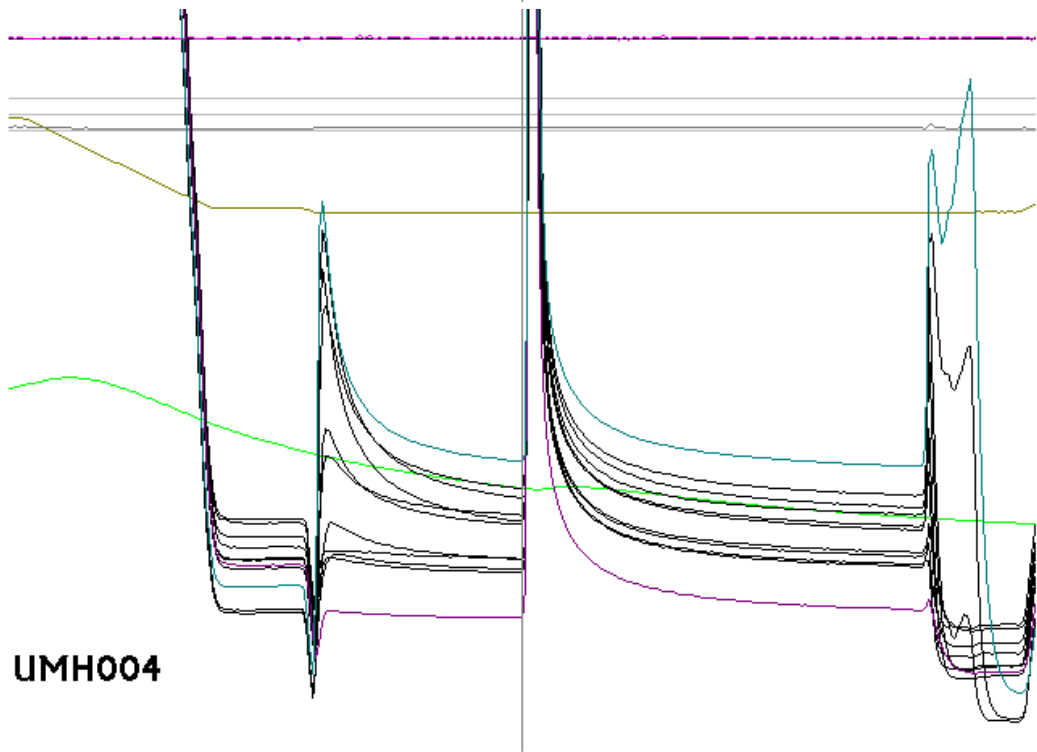
**UMH001**



**UMH002**

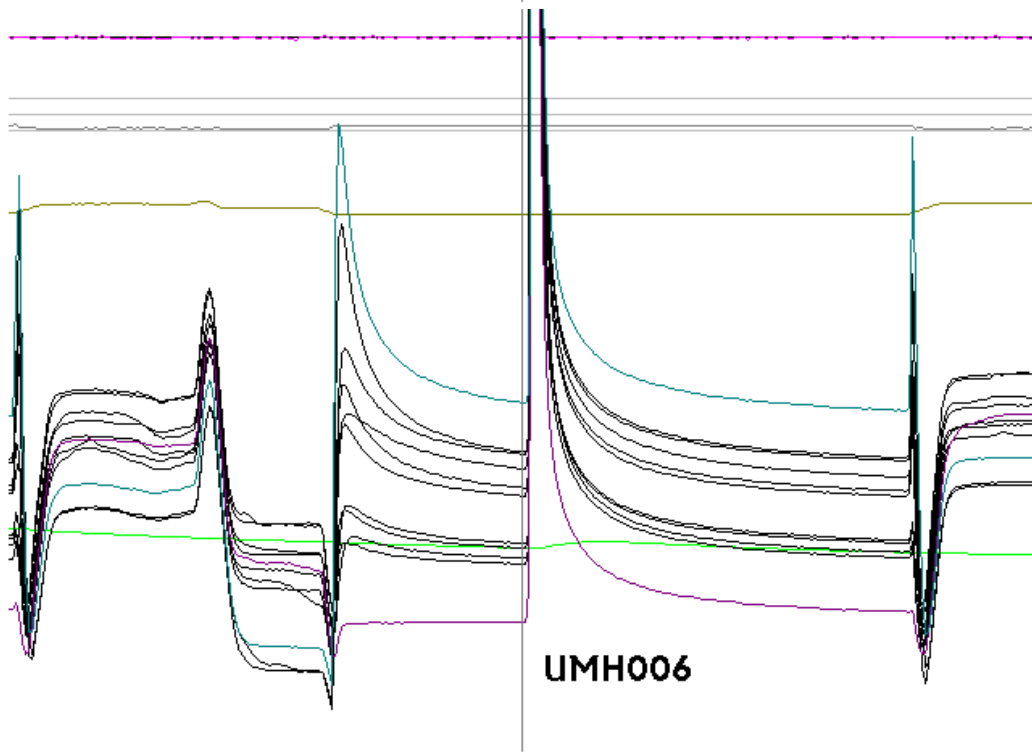
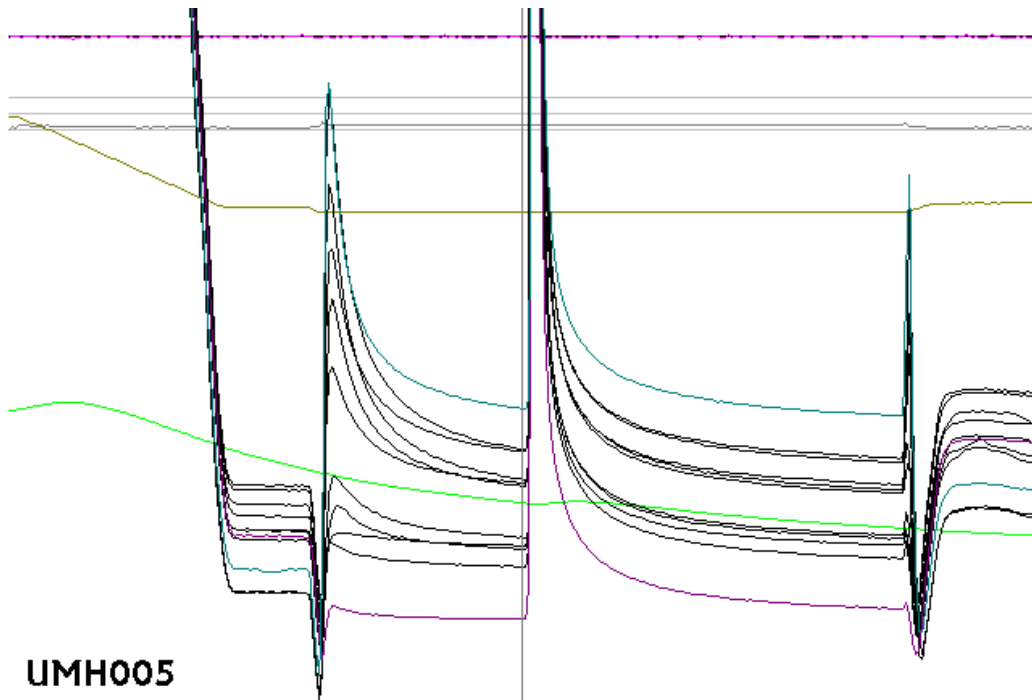


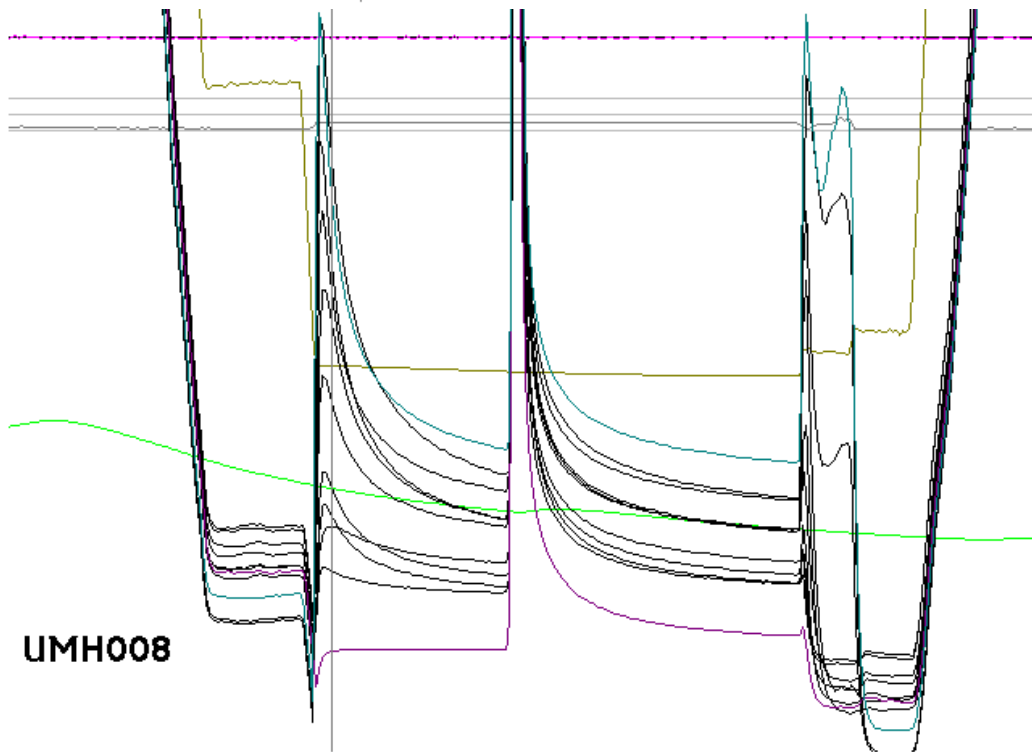
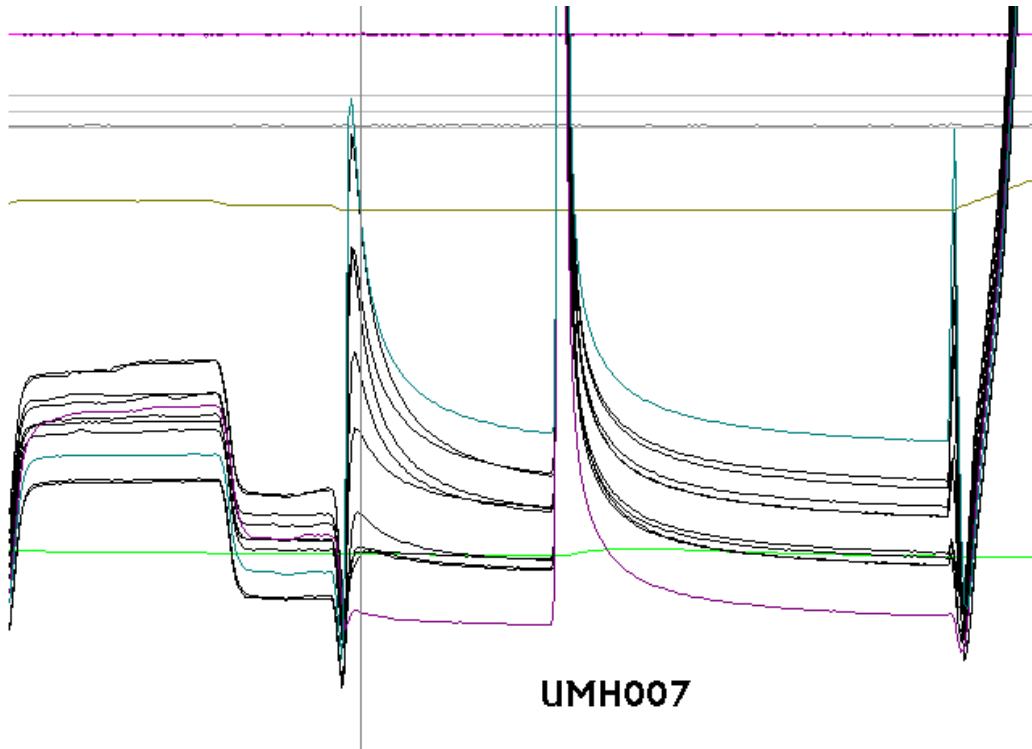
**UMH003**

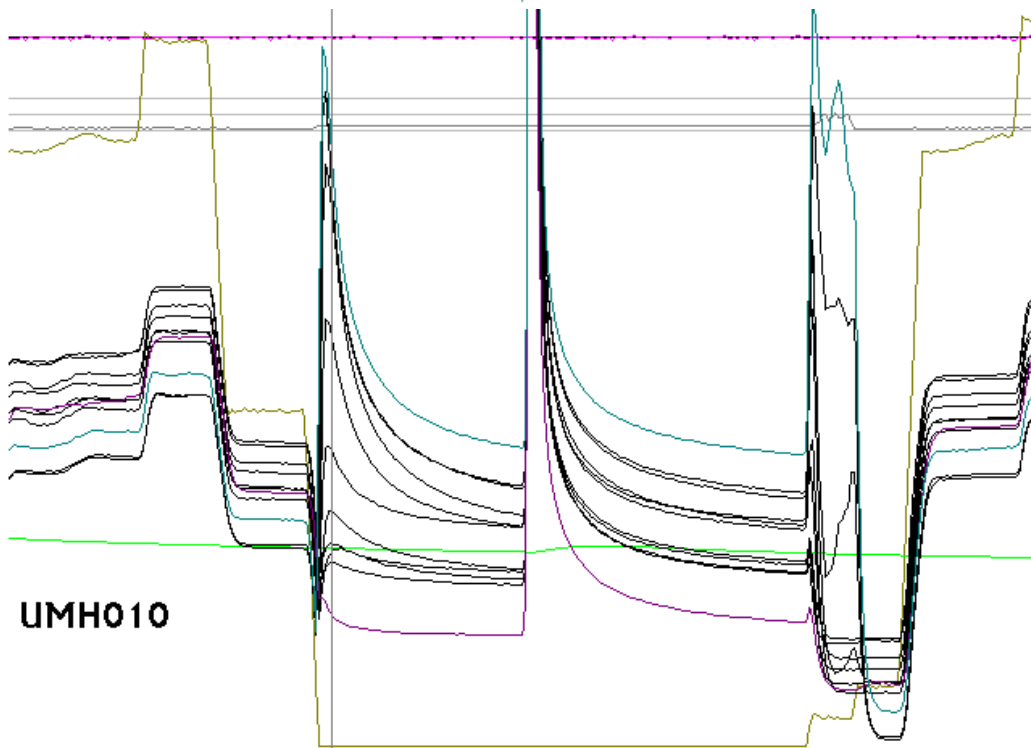
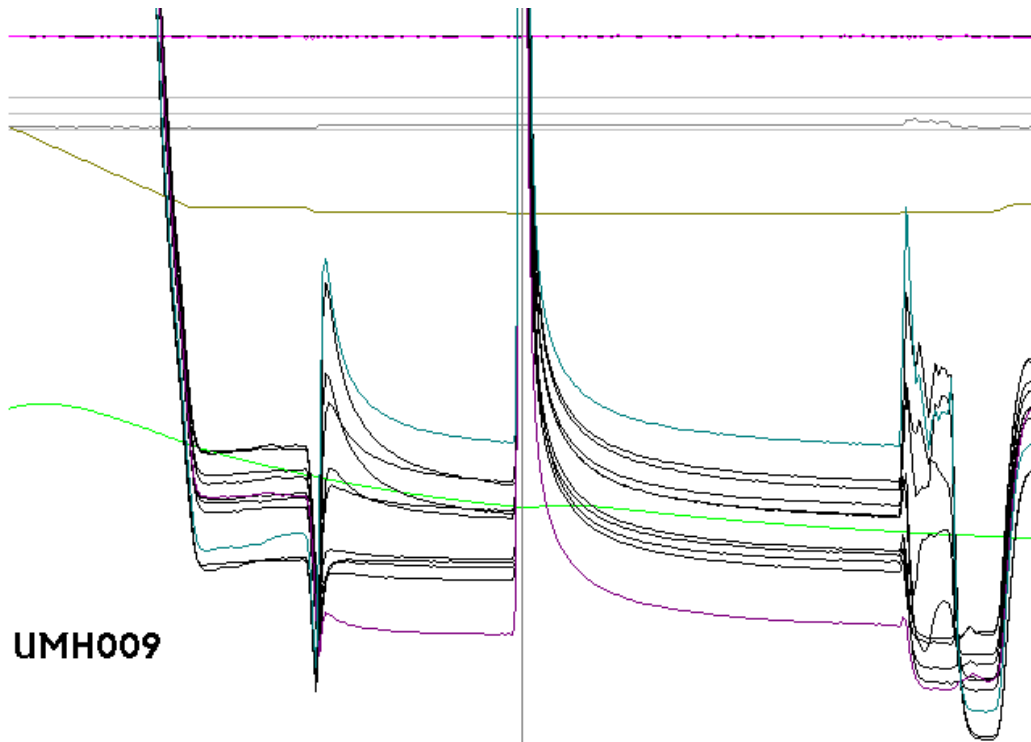


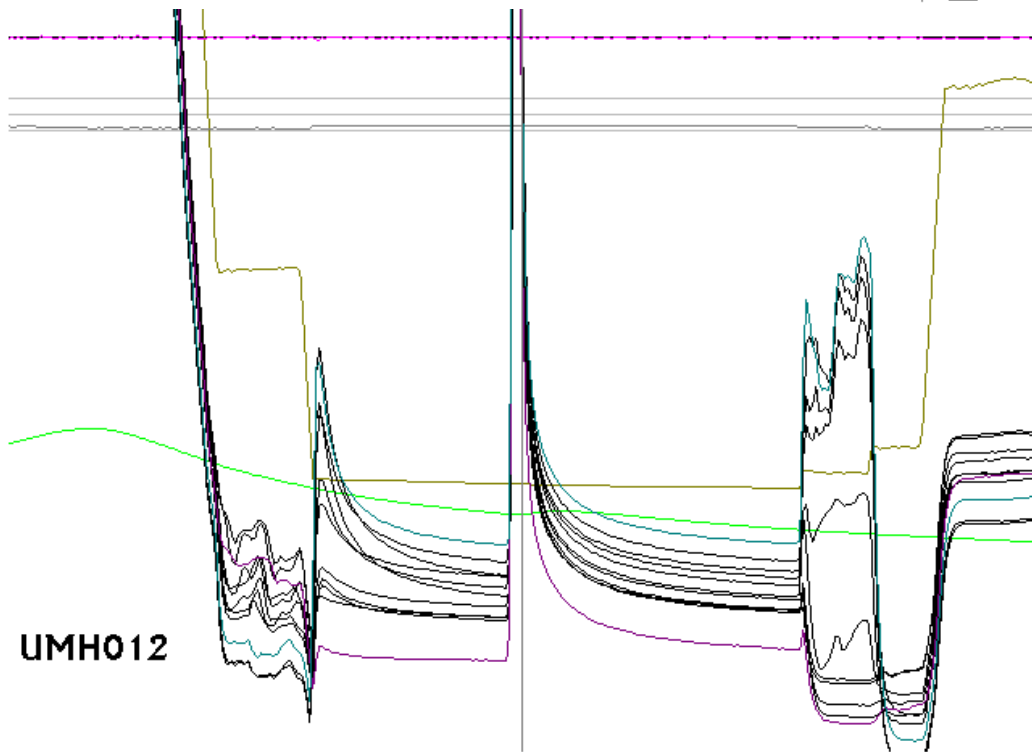
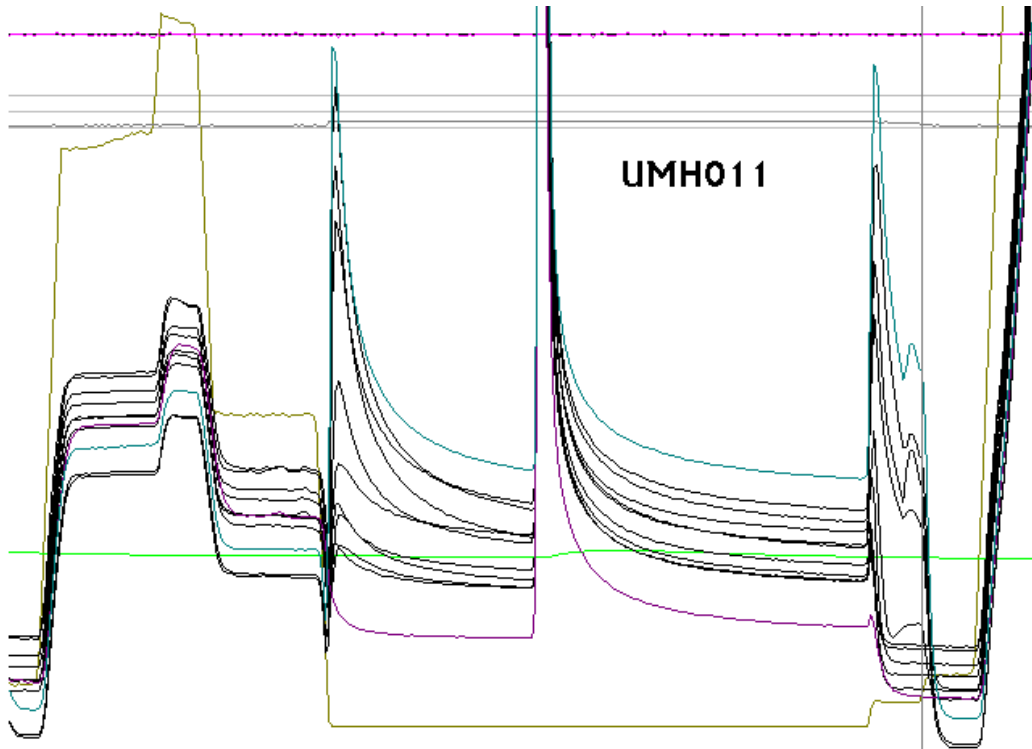
**UMH004**

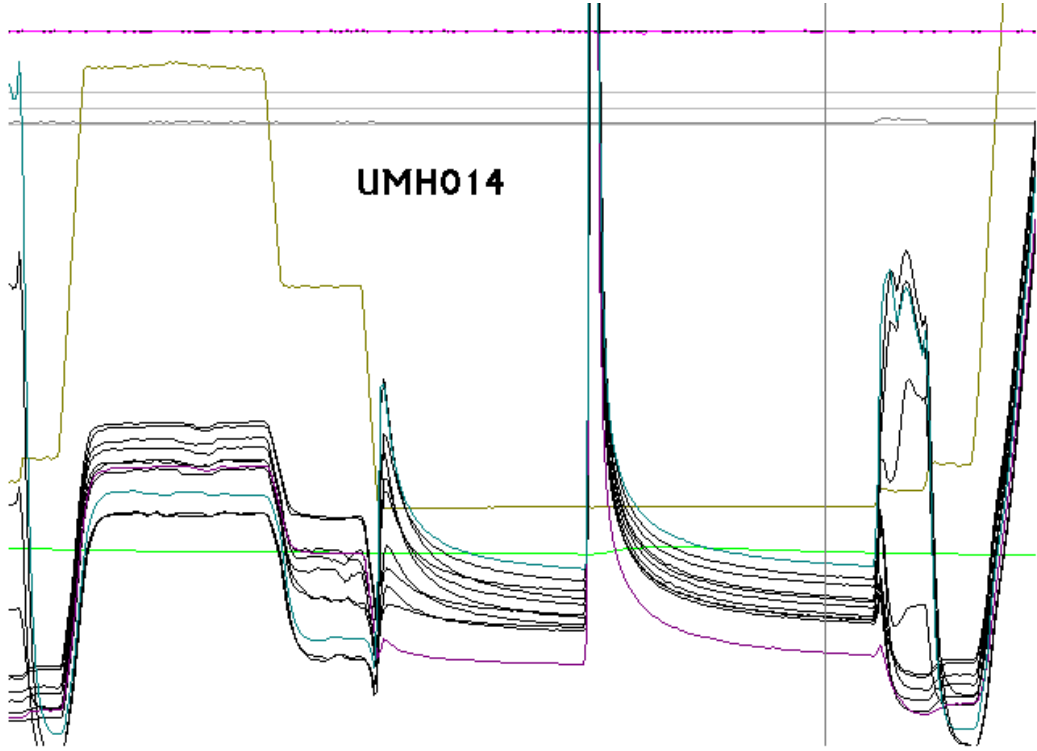
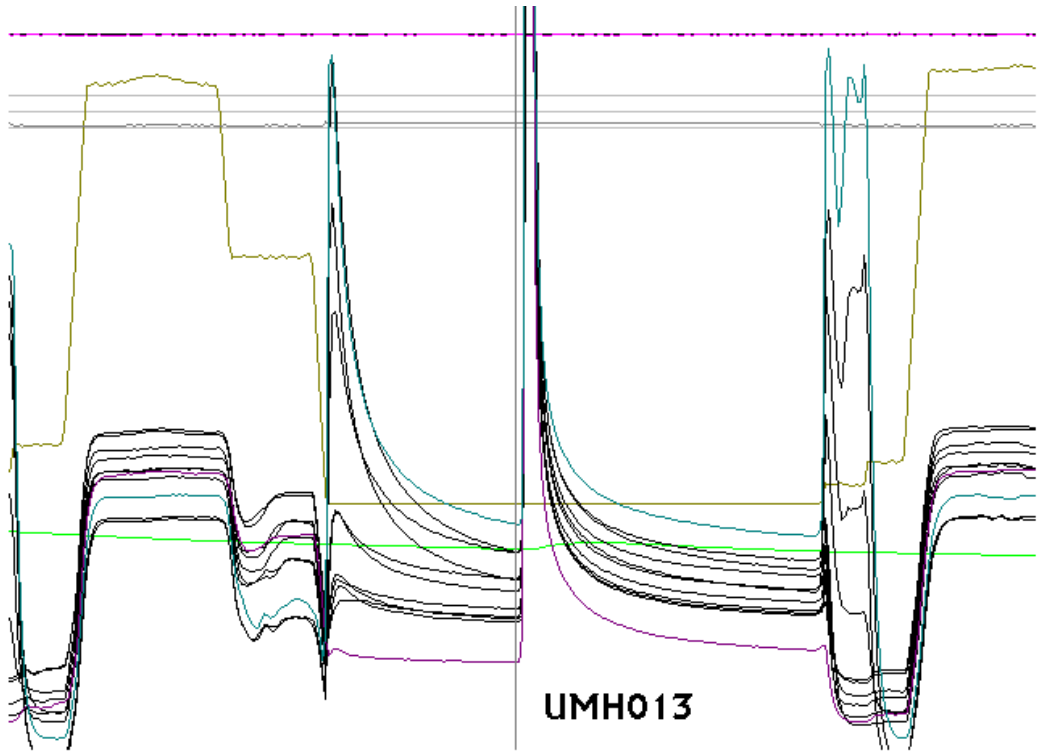




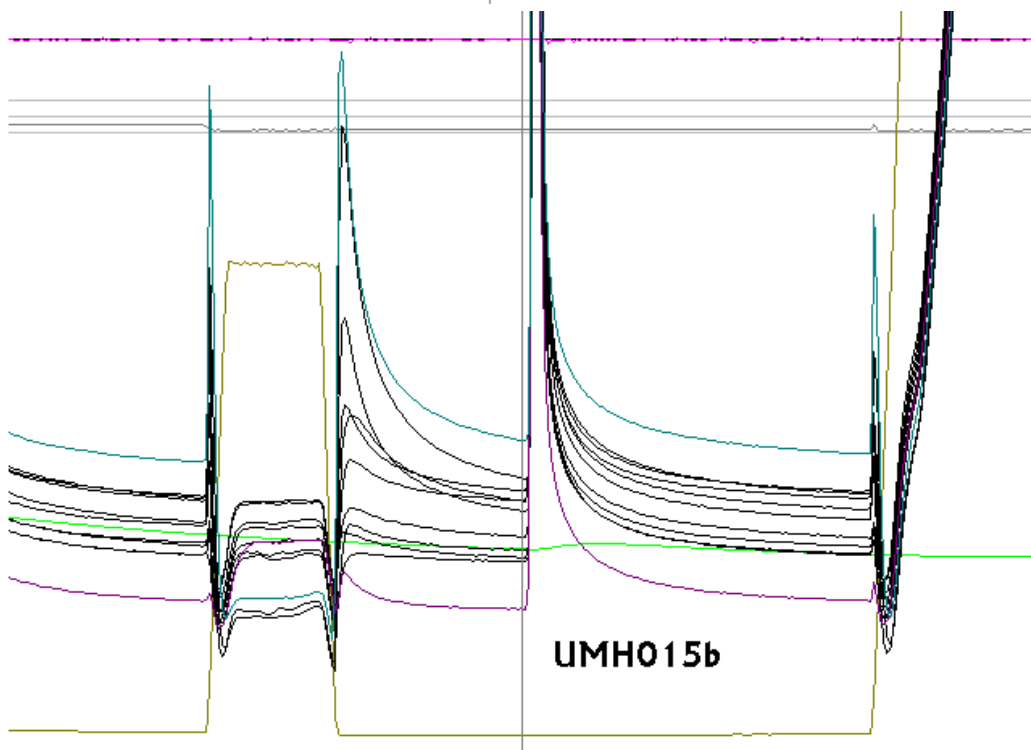
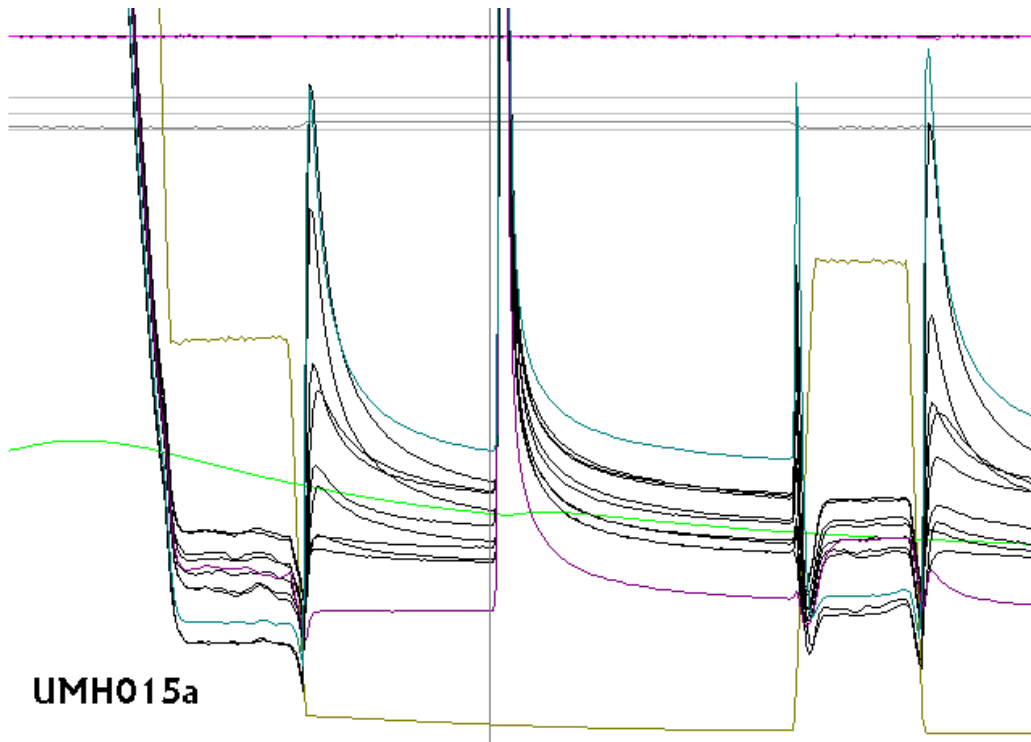


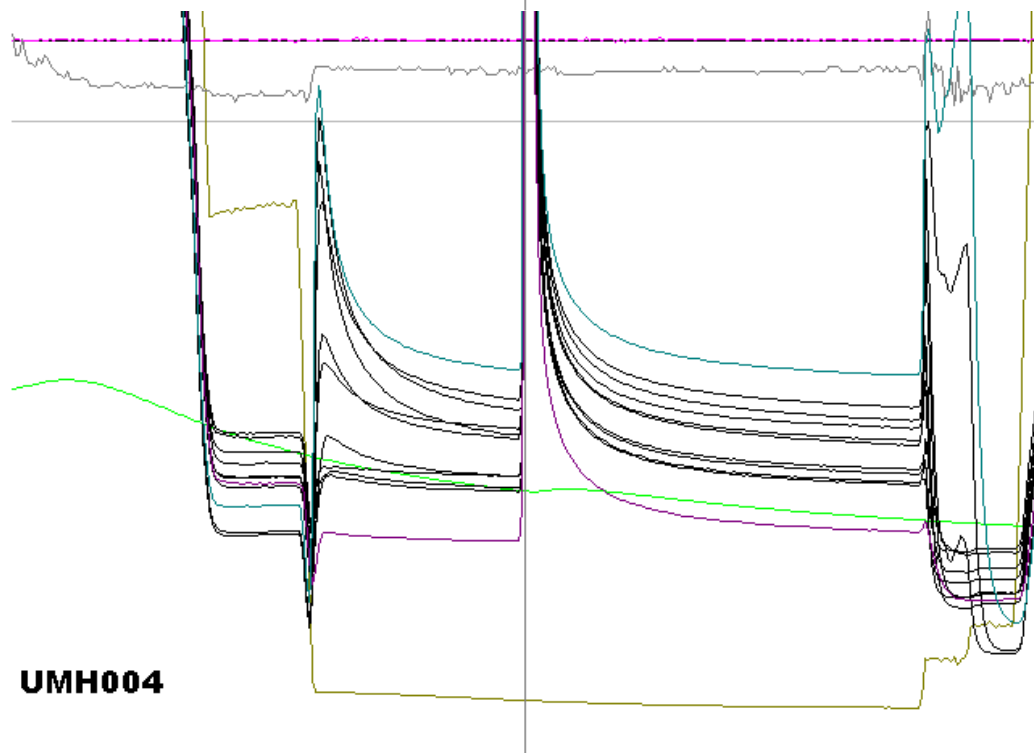
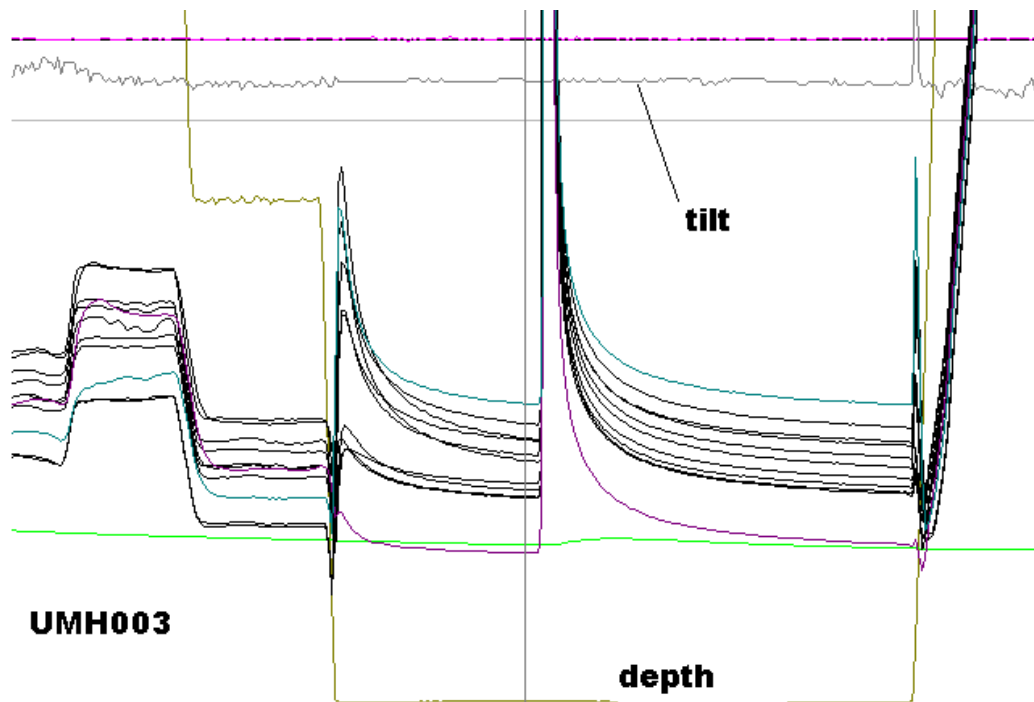


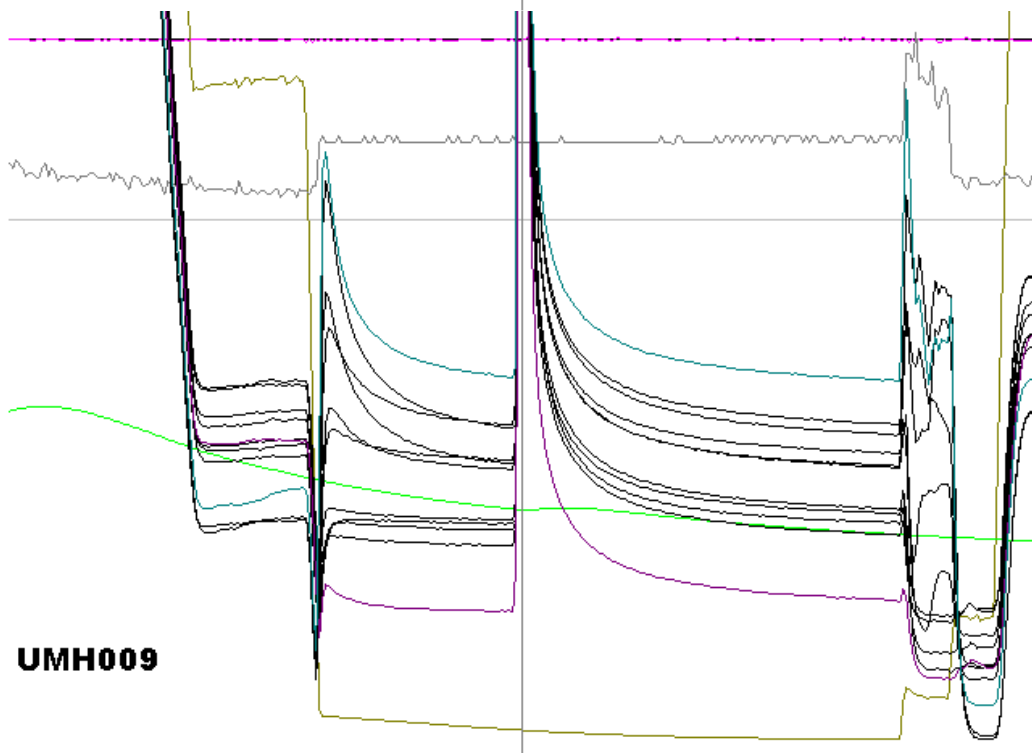
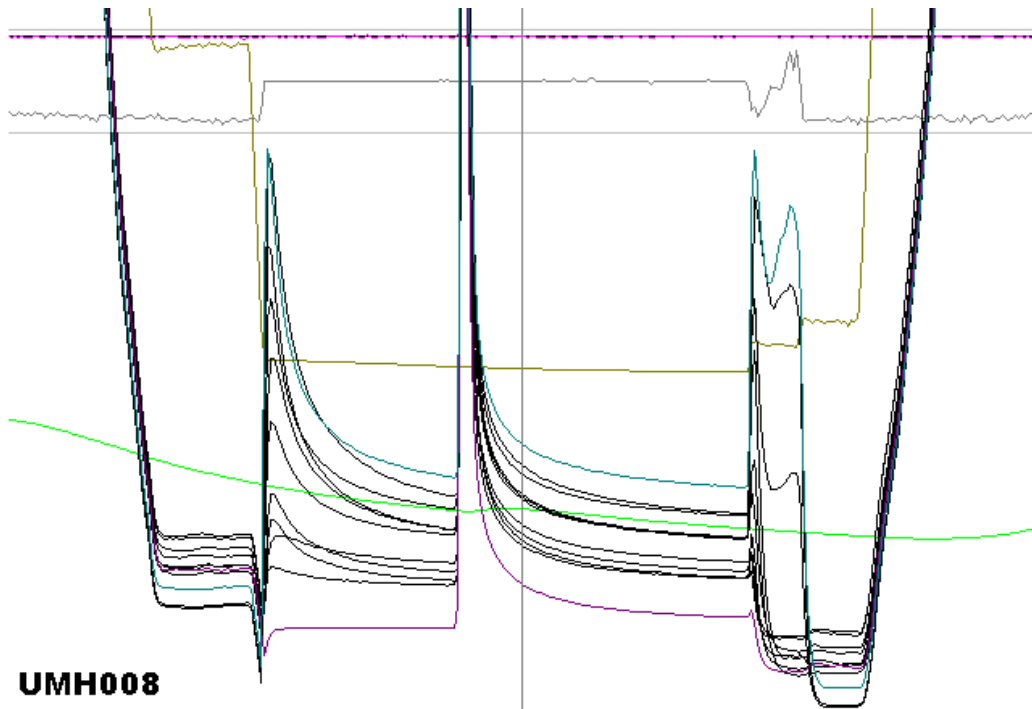


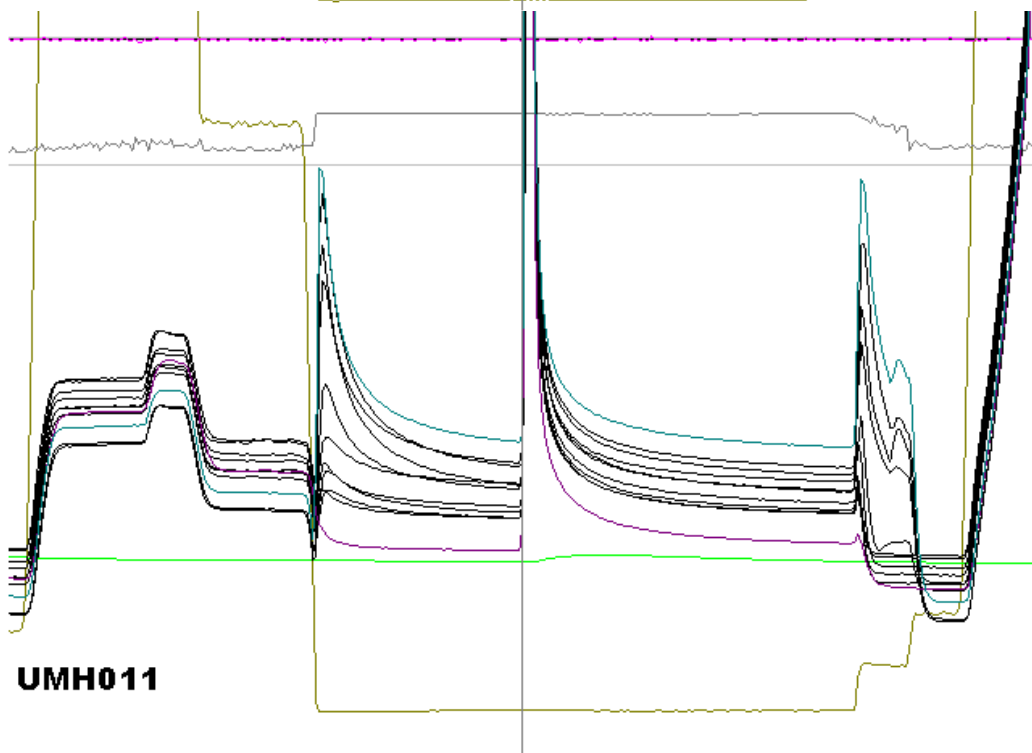
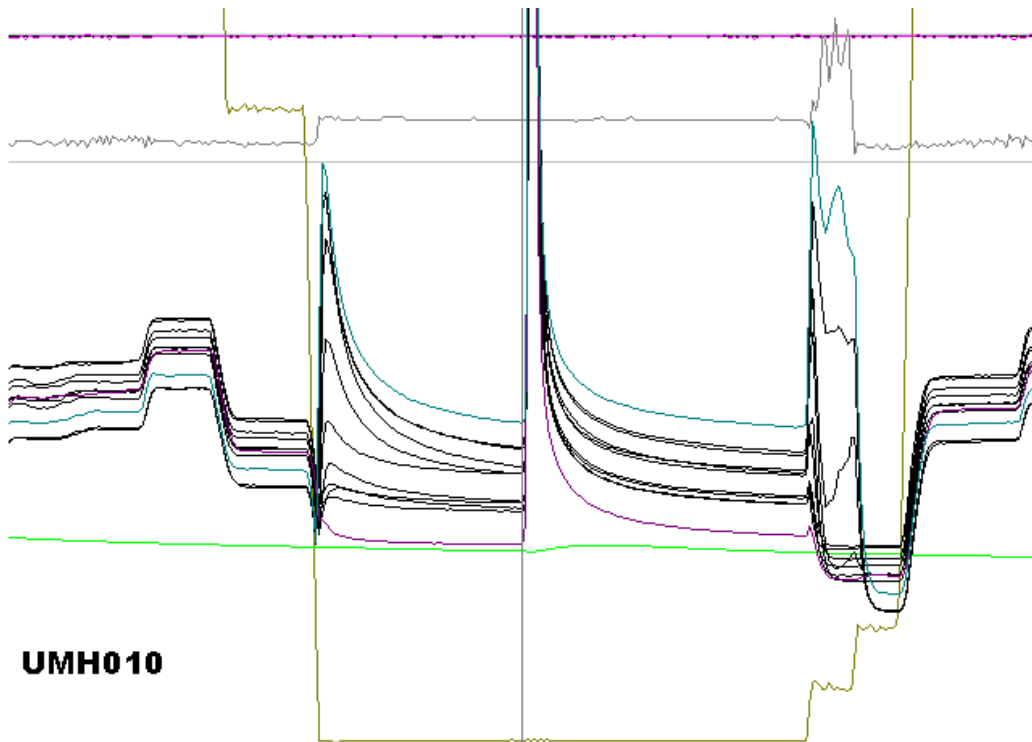


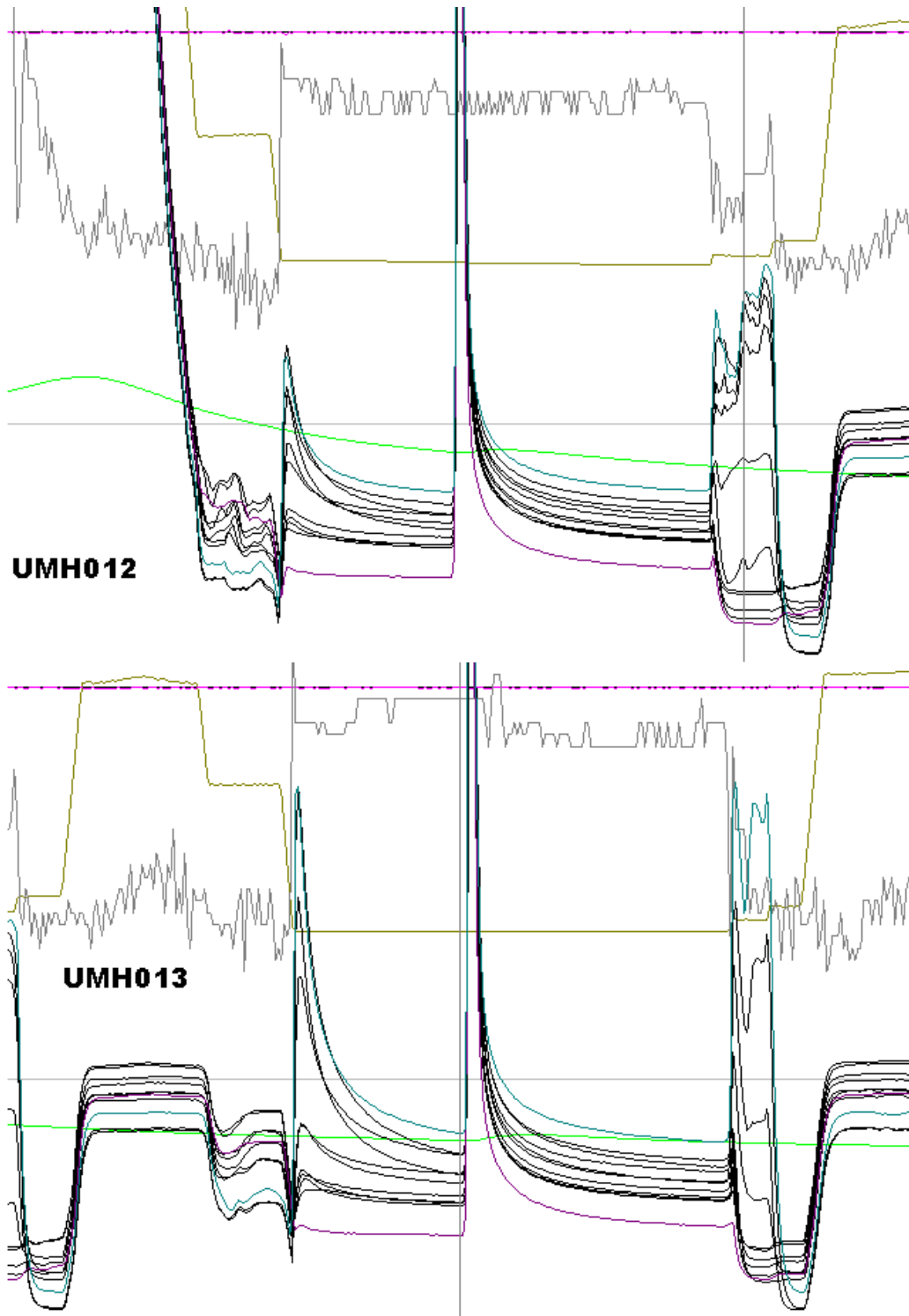




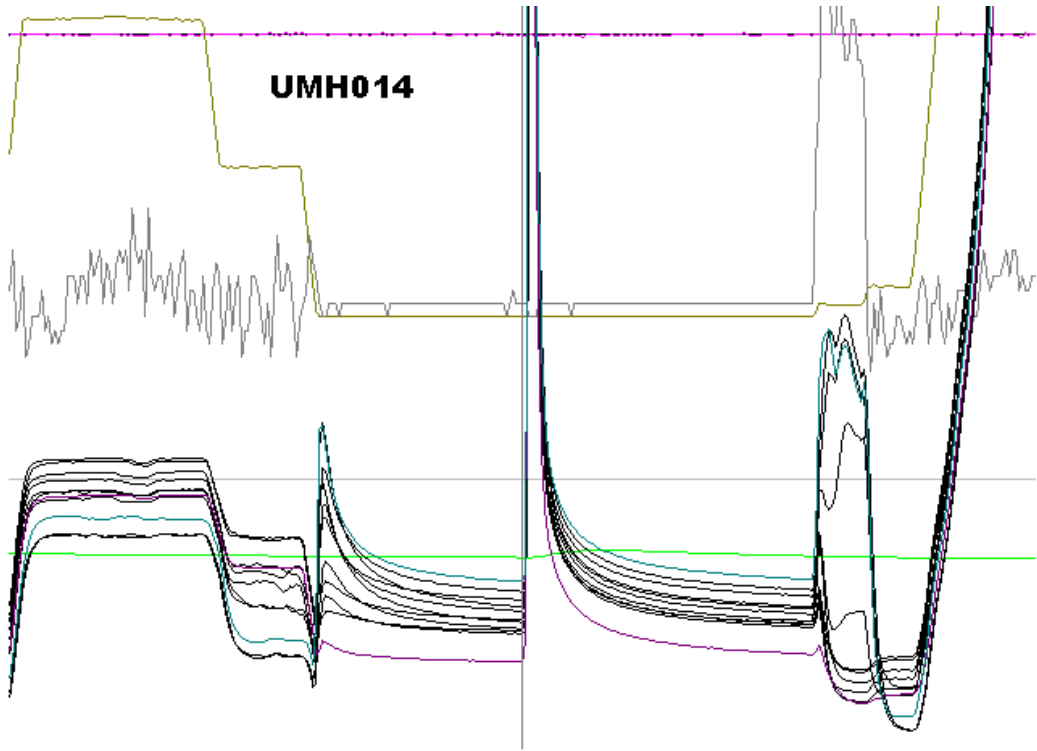












## APPENDIX 2 - DESCRIPTION OF THE DIGITAL HEAT FLOW DATA FILES

On this cruise, the probes recorded the date and time as well as a record of the value sensed by each of the 16 sensors every 10 seconds. Two types of data files are provided with this report, denoted by the file extensions .dat and .pen. The initial file identification is the station number (*e.g.*, UMH001.dat). These files are located on the CD-ROM that accompanies this report.

### **.DAT FILES**

A .raw file was downloaded from the probe each time it came on board after a station, and it was converted to a UMHnnn.dat file, which then could be plotted on the screen. This appendix contains a plot of this file for each station.

### **.PEN FILES**

The .pen files are designed for input into the HFRED data reduction program. Data from the first 12 temperature channels are in decimal numbers (mK units). For this cruise, all sensors were working well, at all sites. The sixth line of this file contains the calibration temperatures for each of the sensors.

## APPENDIX 3 - DETAILED ANALYSIS OF THE HEAT FLOW AT EACH STATION

This appendix contains data analysis for each station. The **\*.out** files and the **\*.r** files for all stations are included on the CD-ROM.

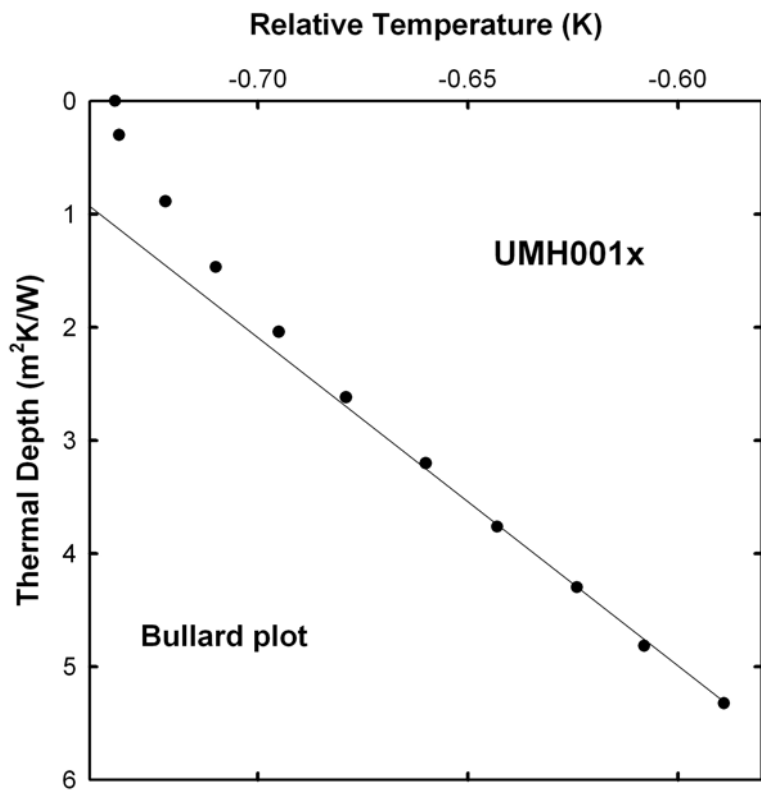
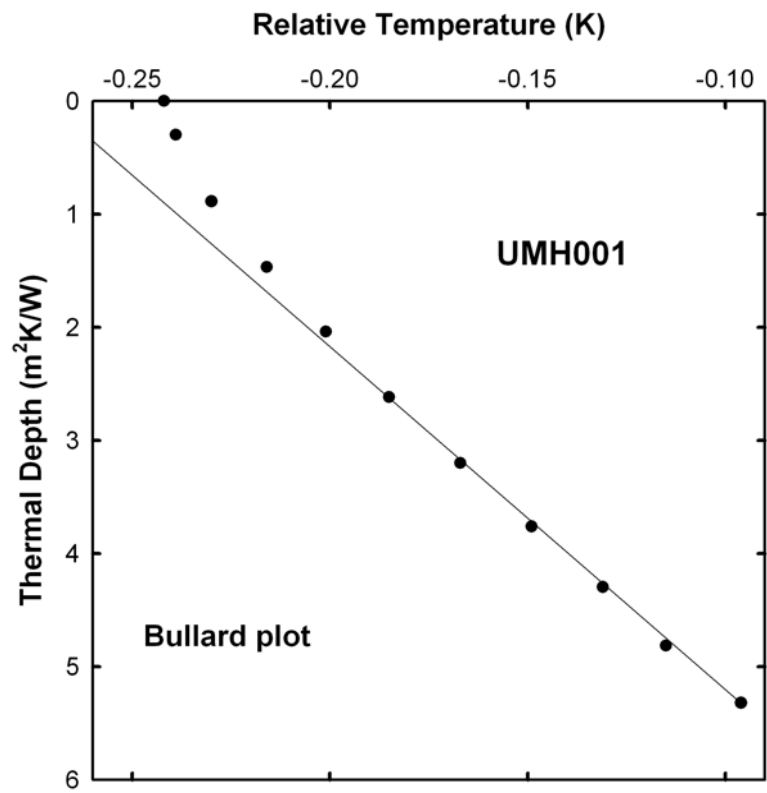
**\*.out file.** Identification and parameter pages. Since normally the bottom water is generally isothermal, the sediment temperature is measured with respect to the water temperature for each sensor. As described in the text, files with an x, y or z used different calibration temperatures.

**\*.r file (one example station).** This page gives parameters and attempts to fit the best straight line to the Bullard plot using various data points, always including the deepest points that are less likely to be disturbed. The bottom column entitled Temp/Depth gives the heat flow, the slope of each line, in  $W/m^2$ .

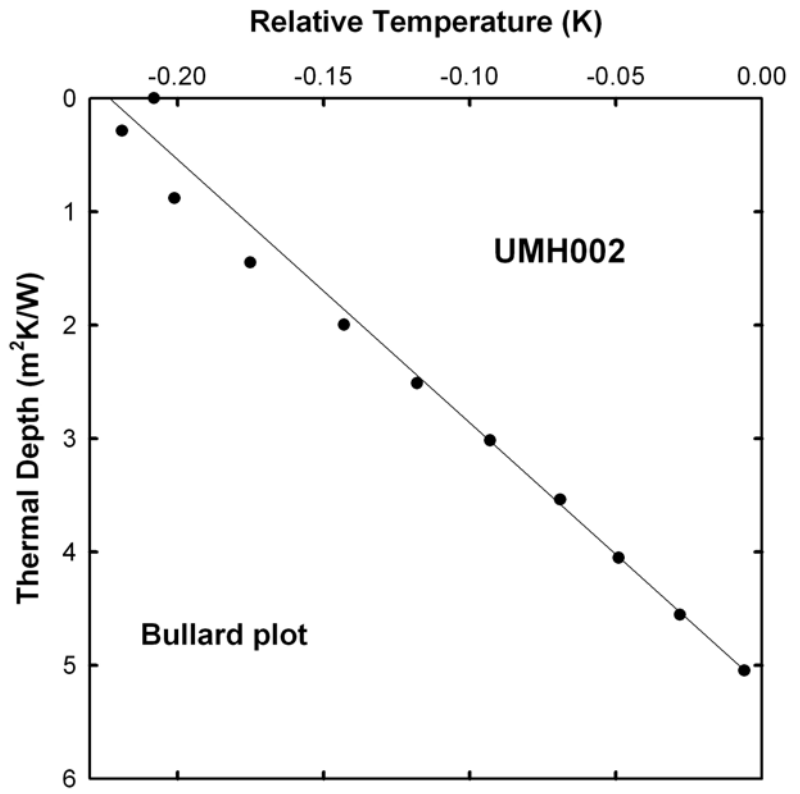
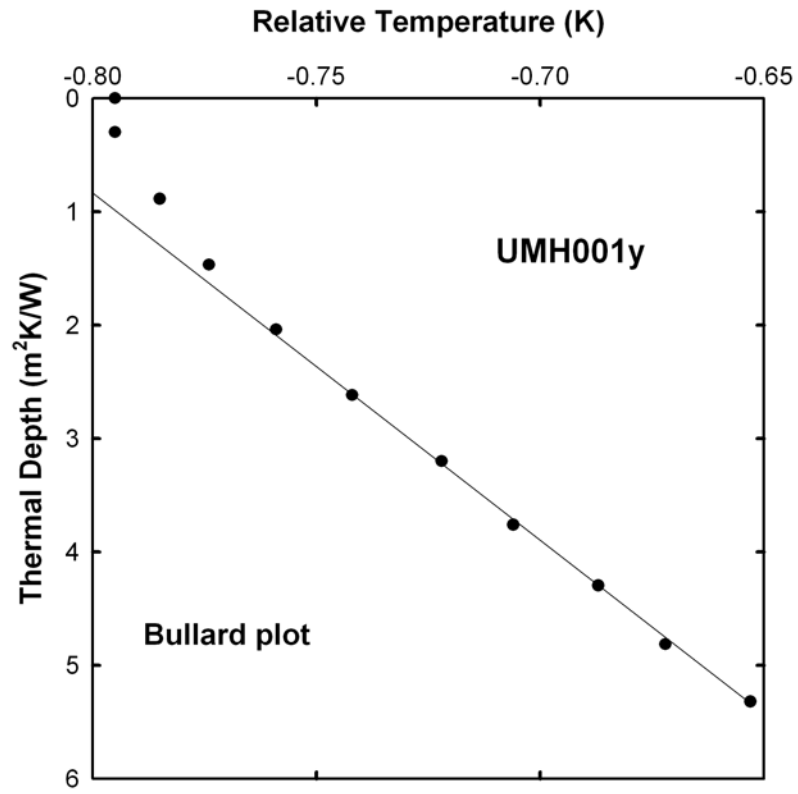
## APPENDIX 4 - BULLARD PLOTS OF DATA IN MS EXCEL

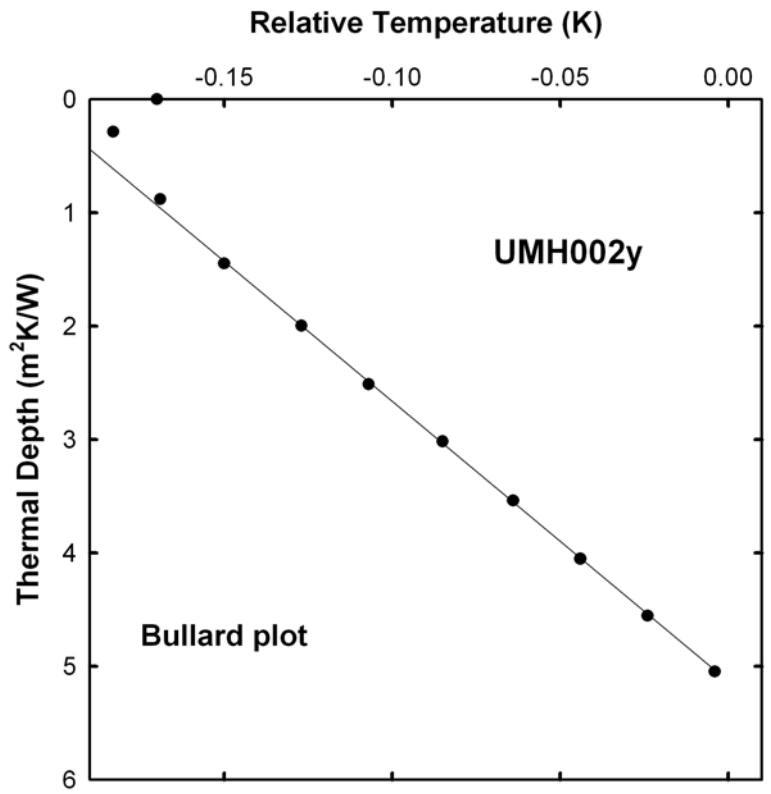
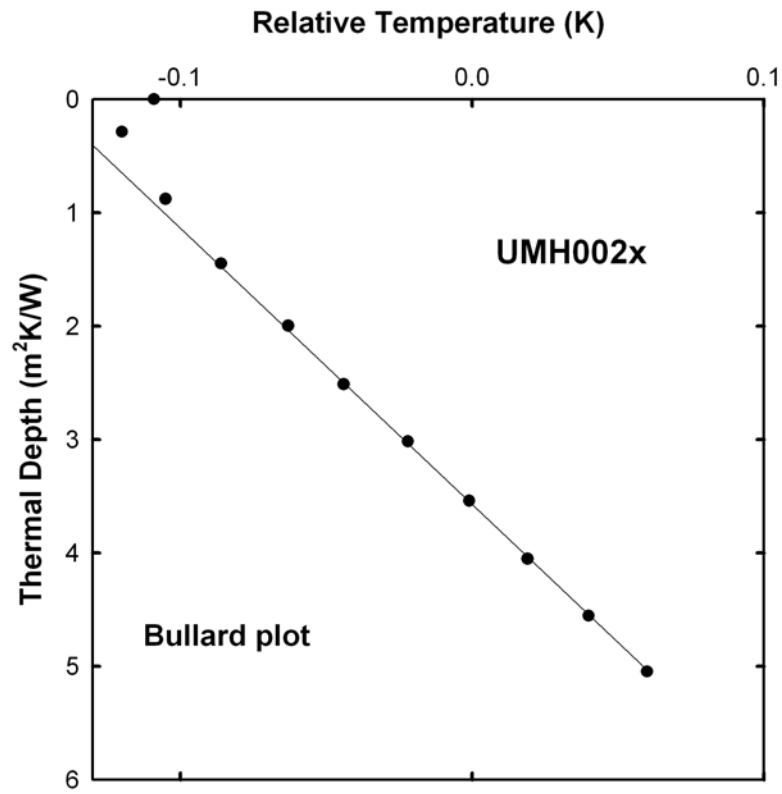
Presentation quality Bullard plots of data are included here for all stations. Each plot in this appendix illustrates the relative temperature as a function of the thermal resistance integrated from the top sensor downward through the sediment. The reciprocal of the slope of the resulting best-fit line is the heat flow (we plot thermal resistance as the vertical parameter because it tracks depth; heat flow is  $\Delta T/\Delta R$ ). Under ideal conditions of a constant vertical heat flow in a conductive regime, with isotropic thermal parameters, this would be a straight line. The thermal conductivity of a depth interval is assumed to be the average of the two values measured at either end of it. The inverse of the slope of the straight line shown in each plot represents the (best fit) heat flow given in Table 2 of this report.

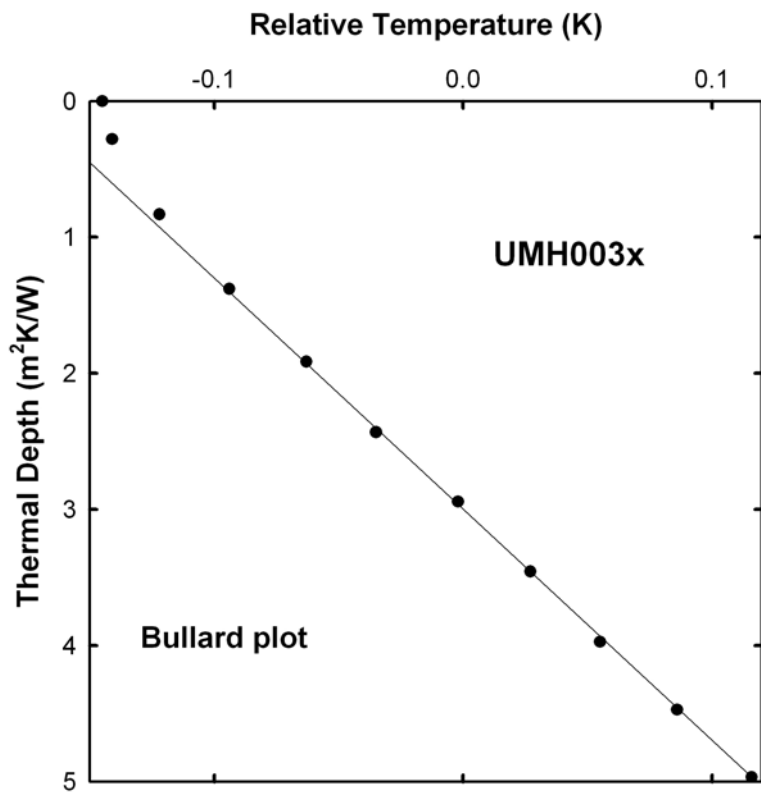
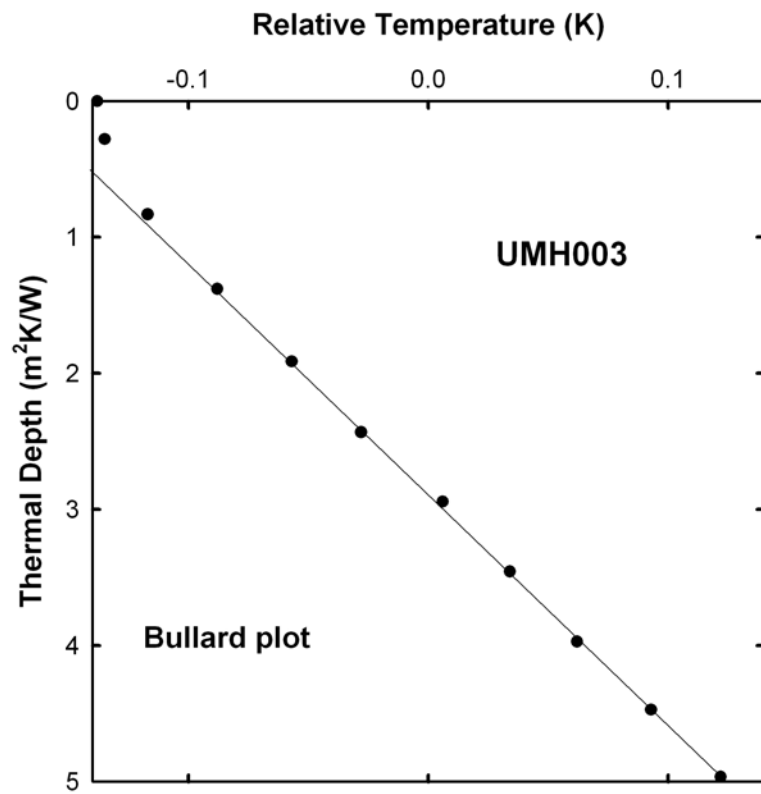
Often the thermal conductivity varies a lot near the water-sediment interface, and one measured value doesn't represent it well. Consequently the data point nearest the surface is most often omitted. When other data don't fit a straight line (indicating constant vertical heat flow), they were also omitted, down to a depth interval of 2.5 m. All of the temperatures are plotted on the Bullard plots.

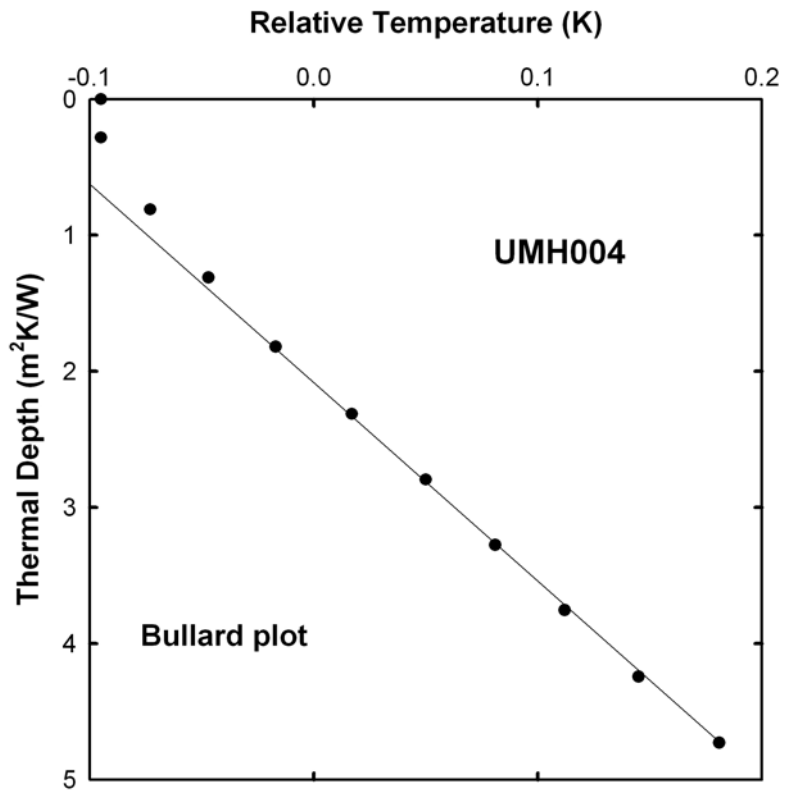
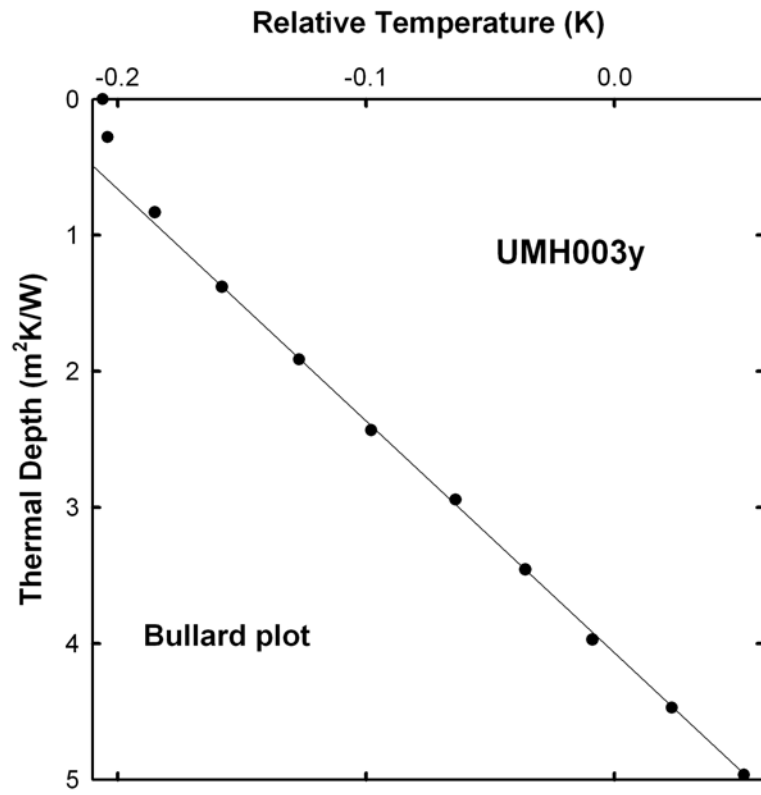


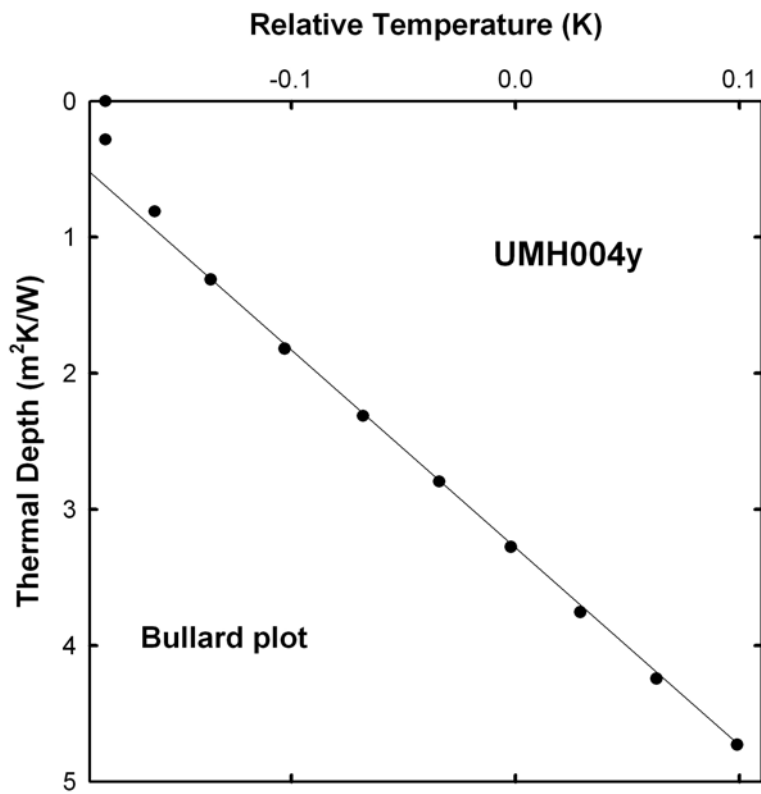
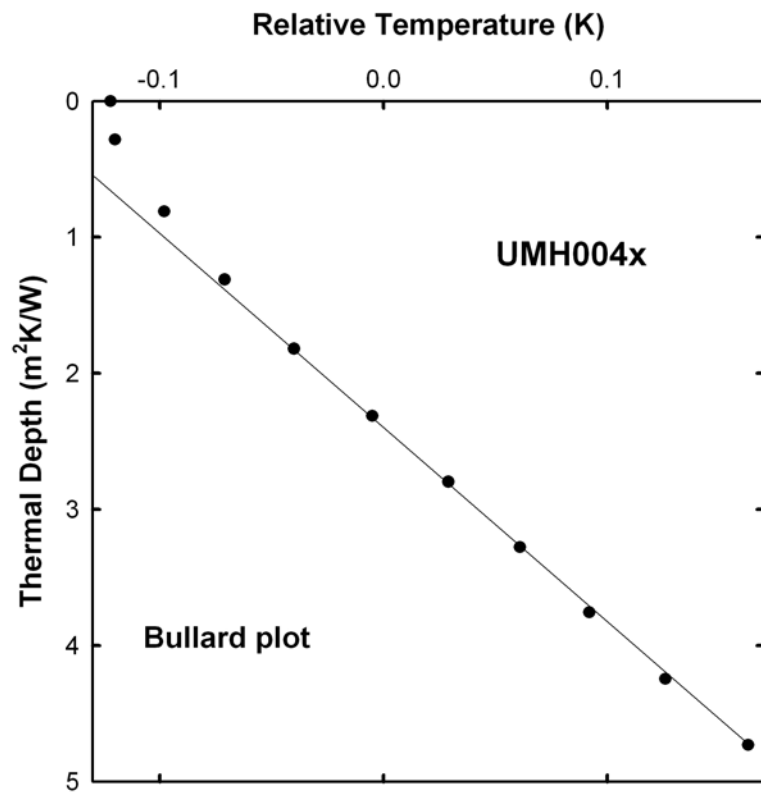




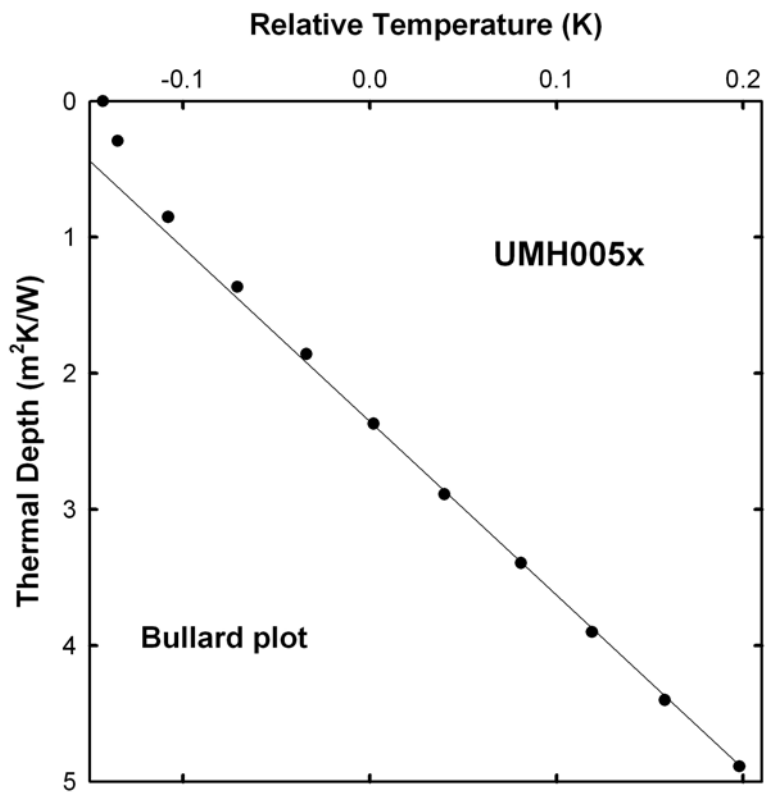
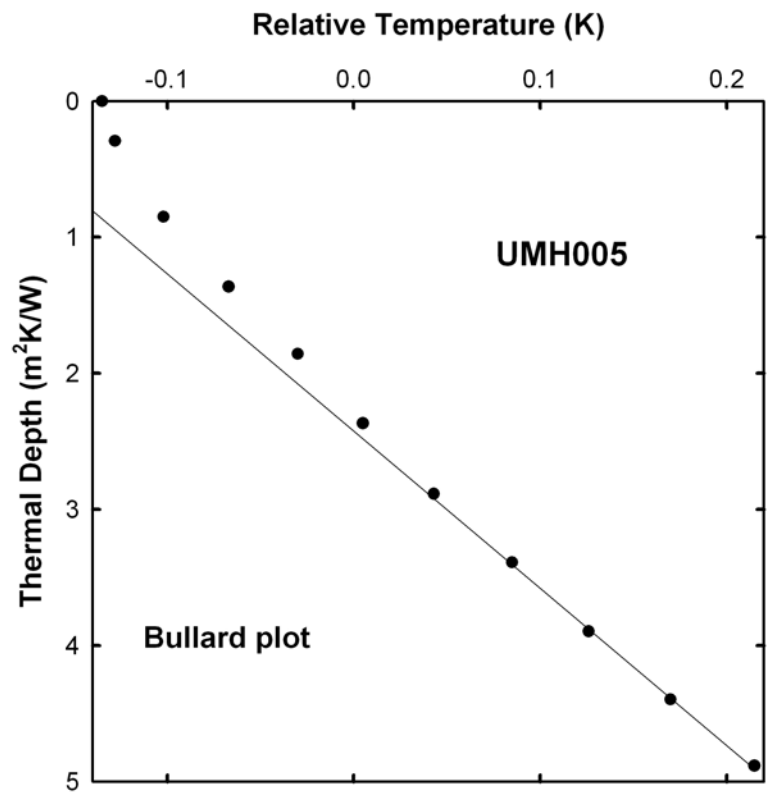


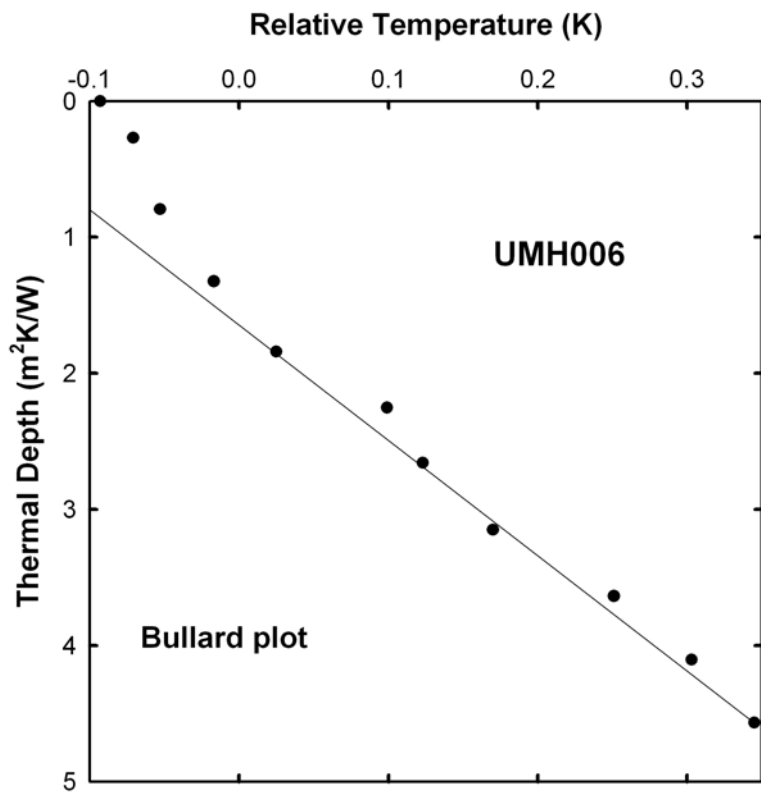
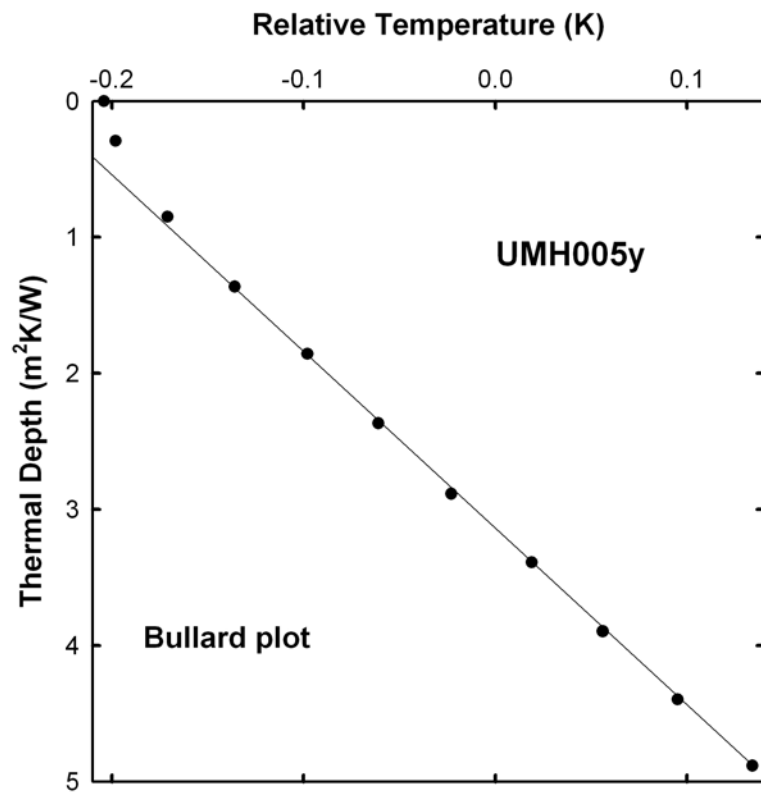


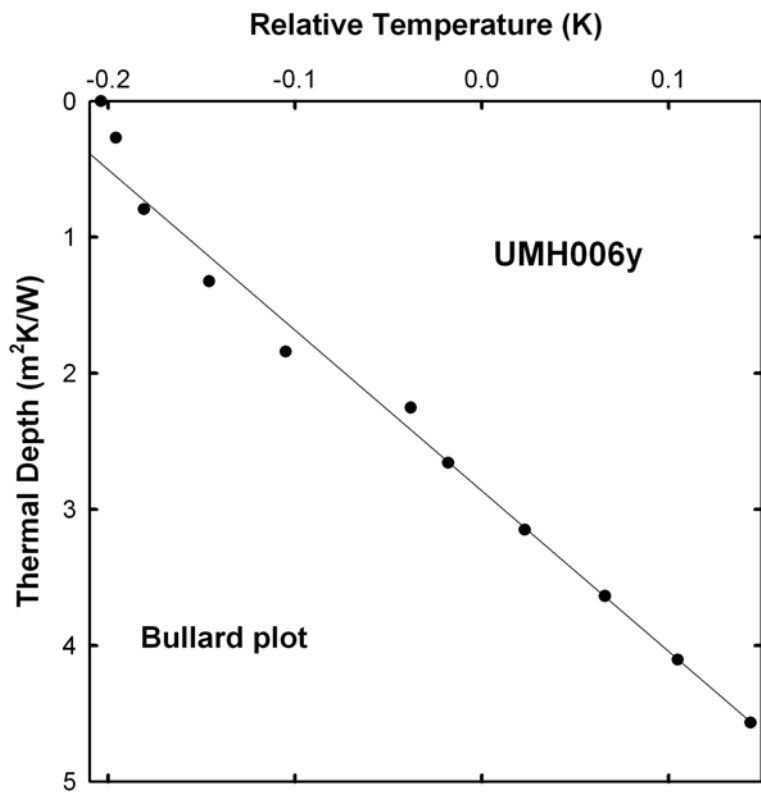
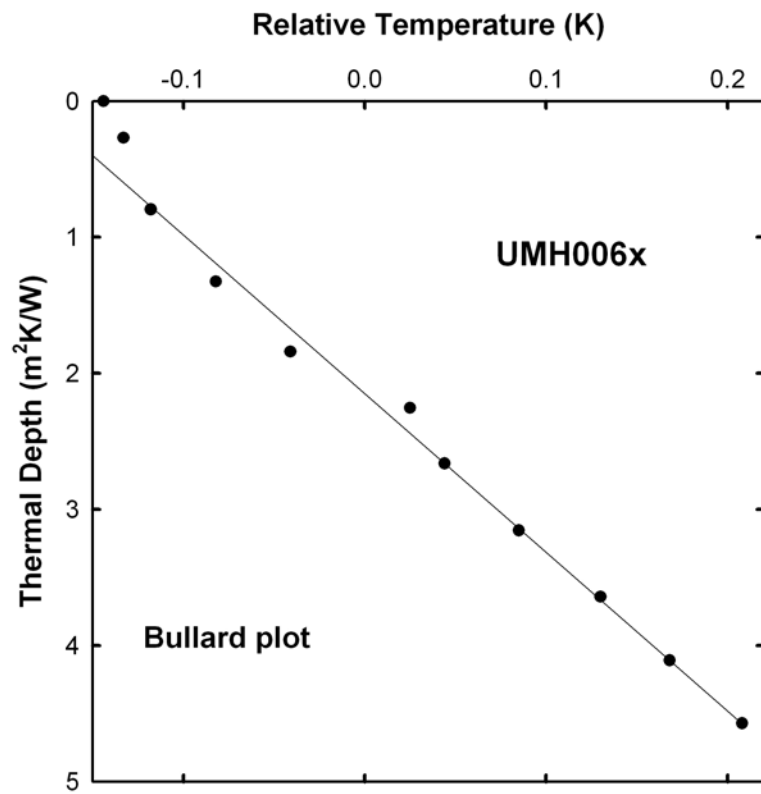


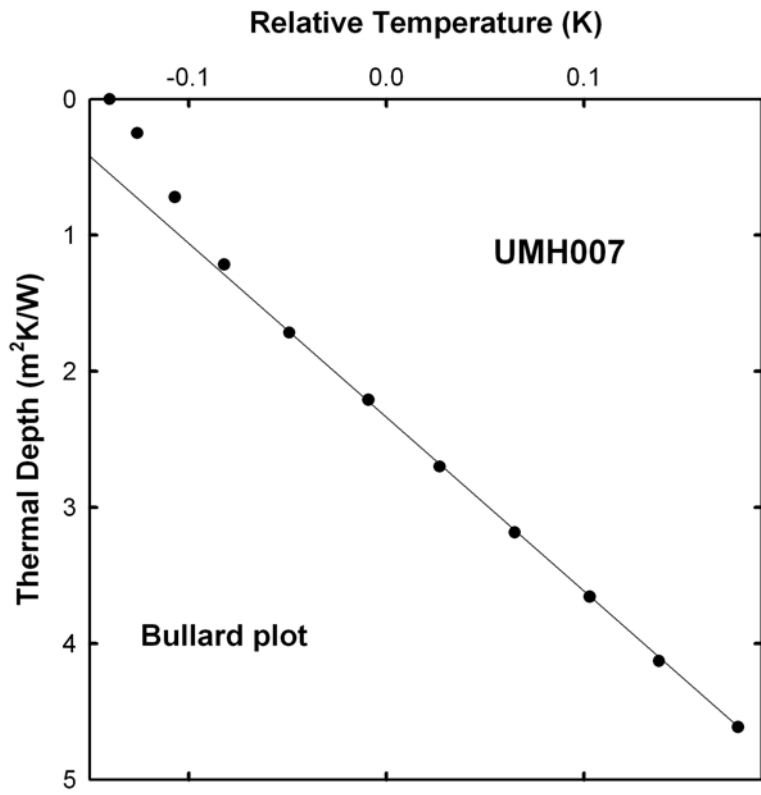
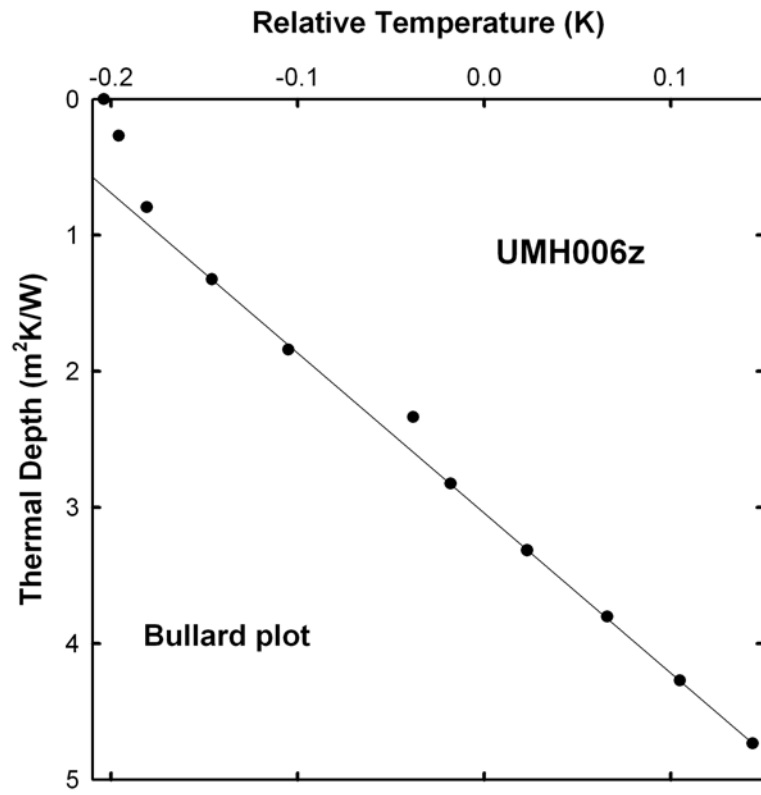


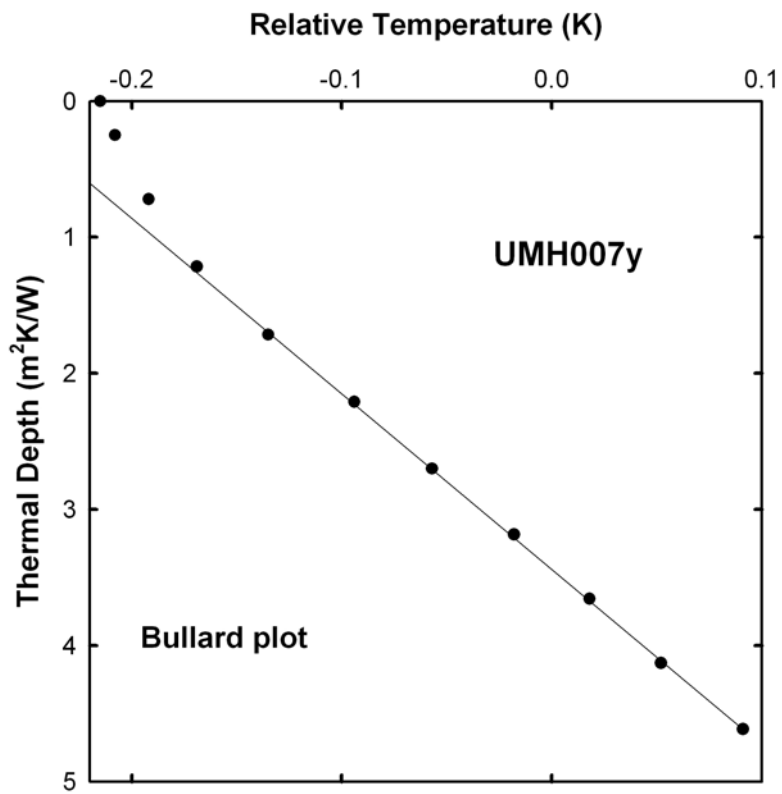
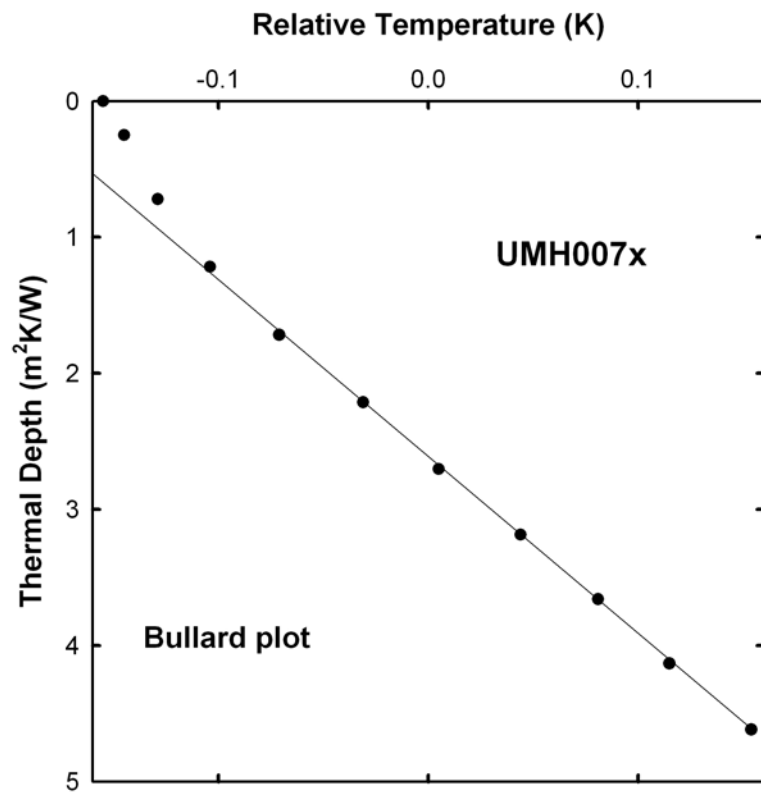




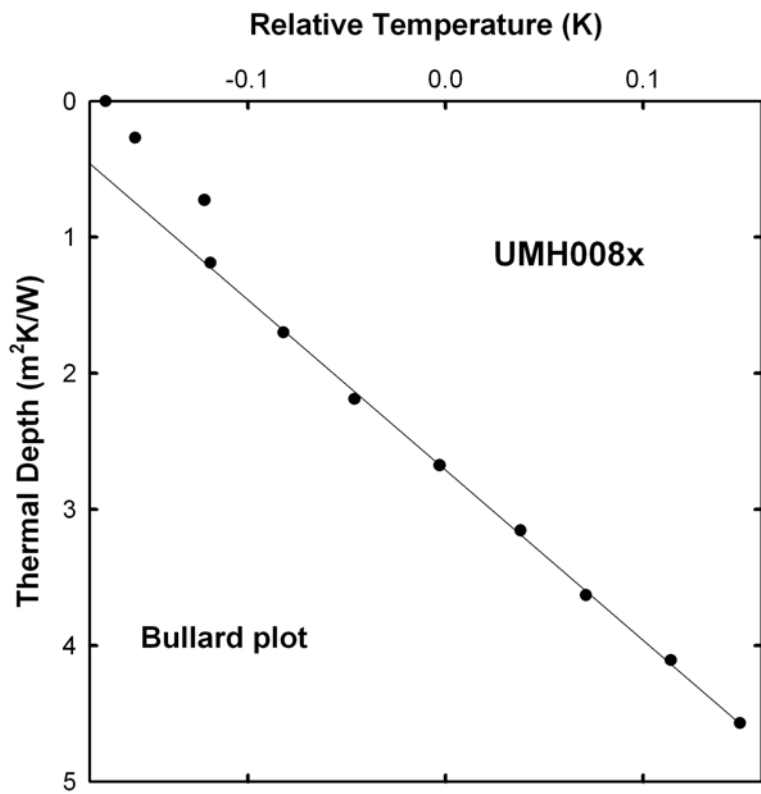
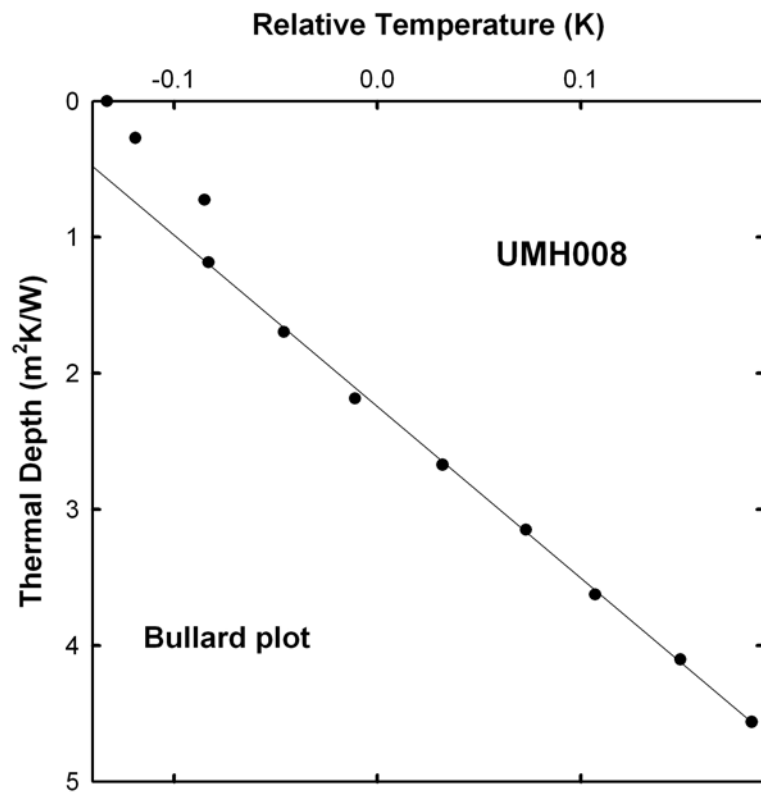


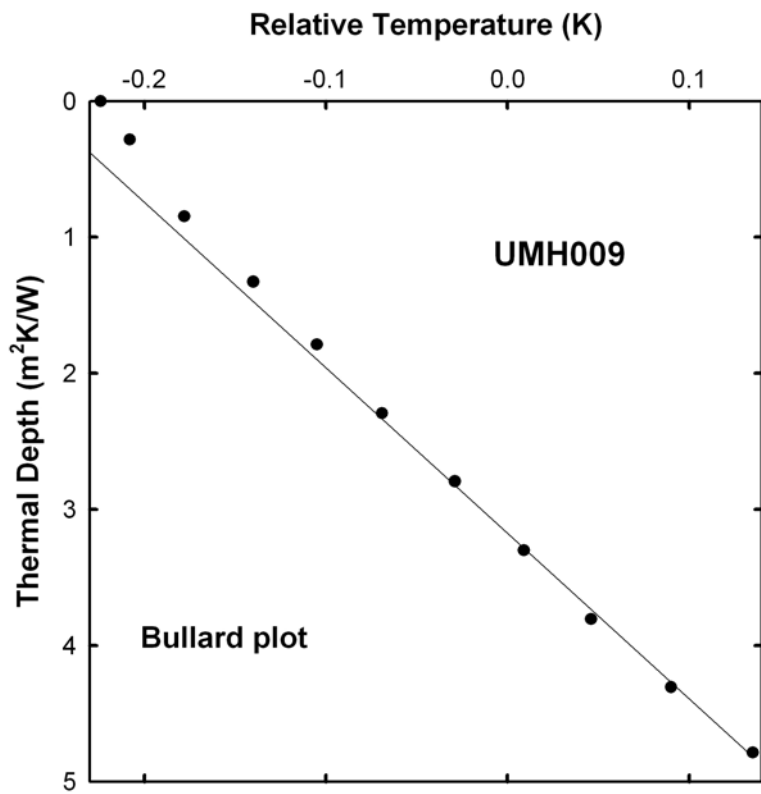
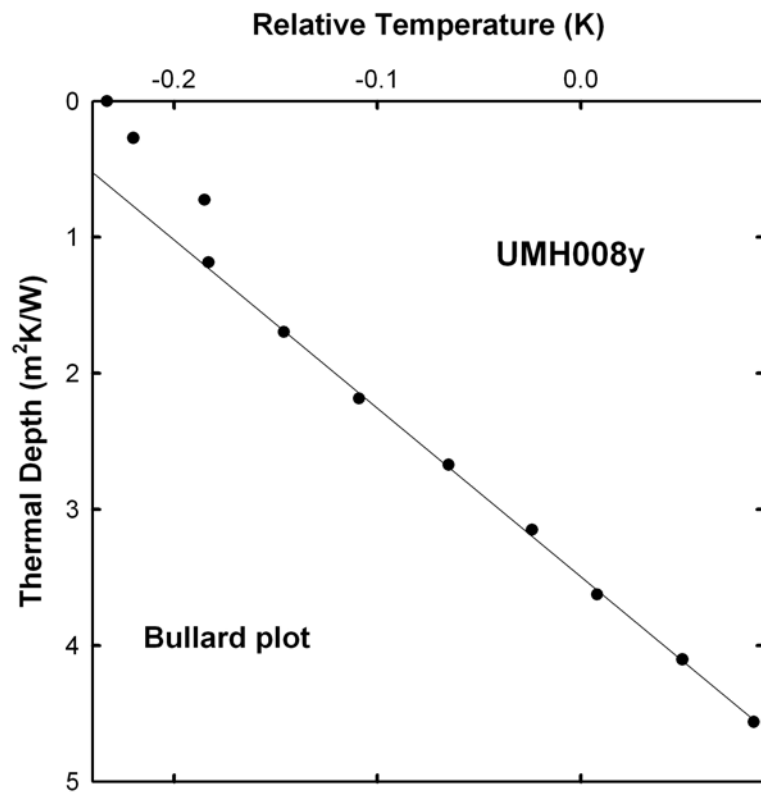


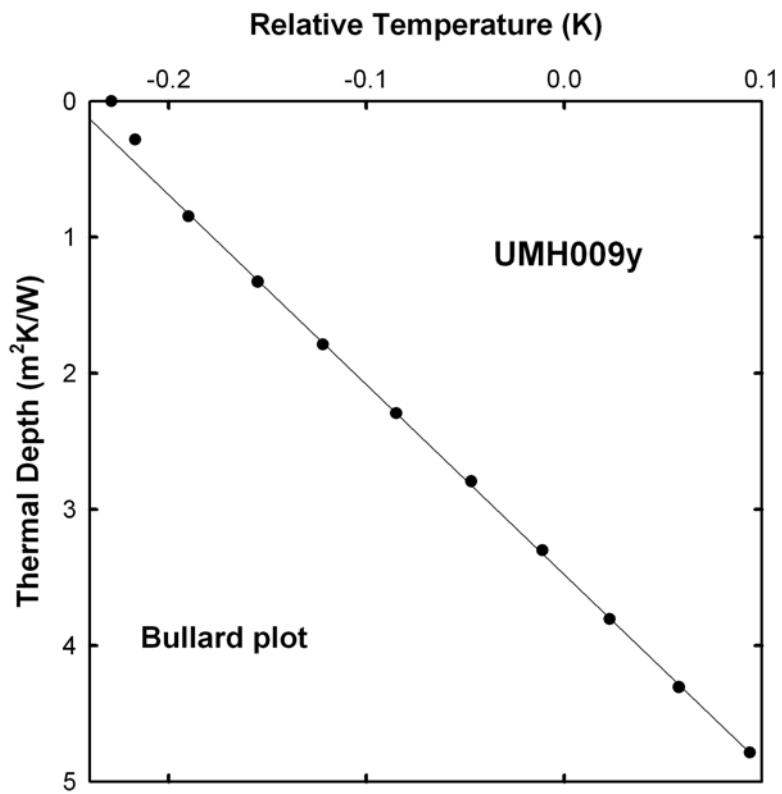
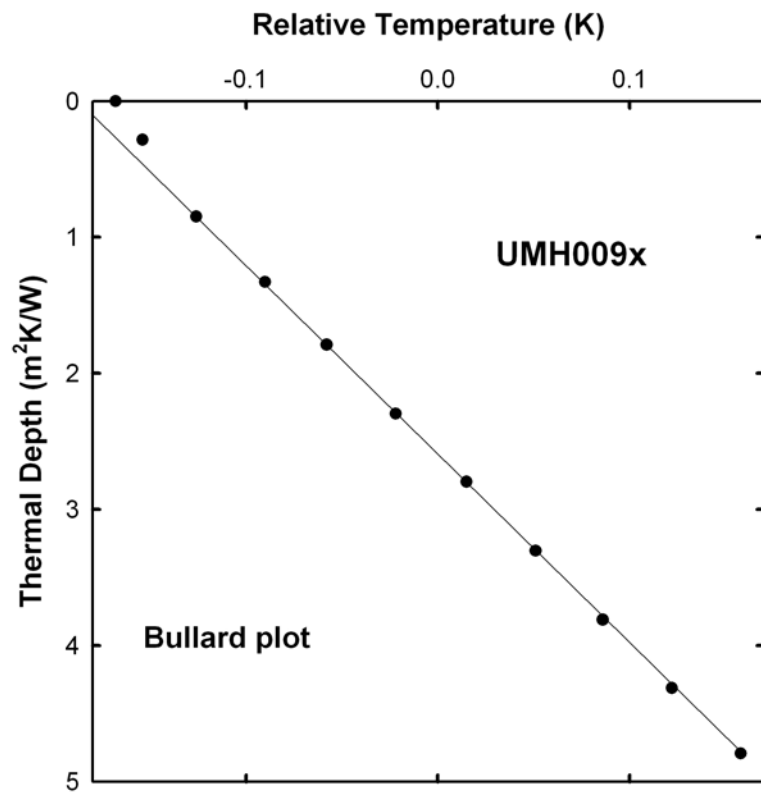


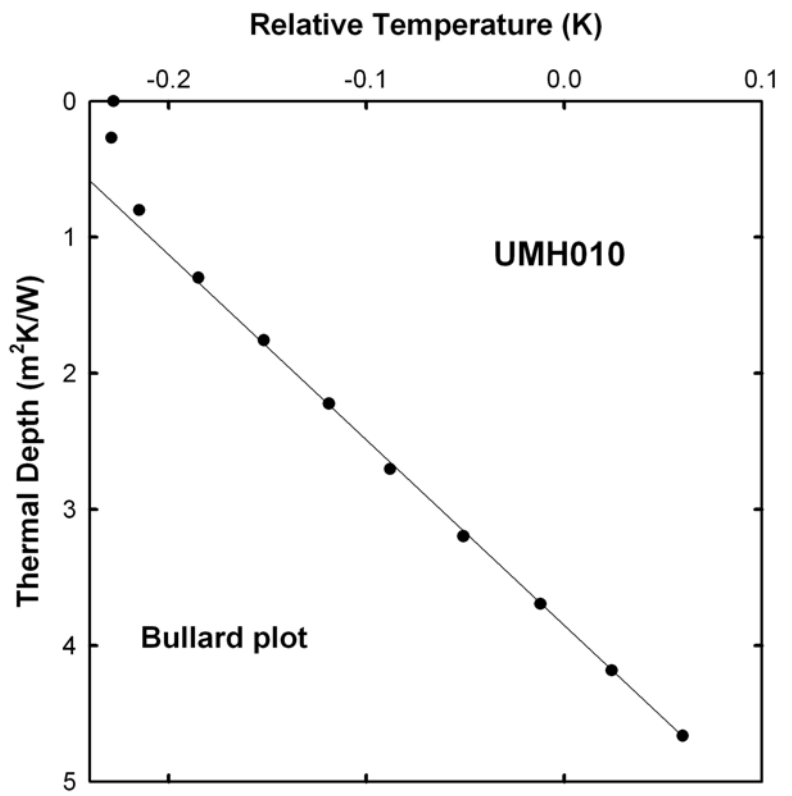
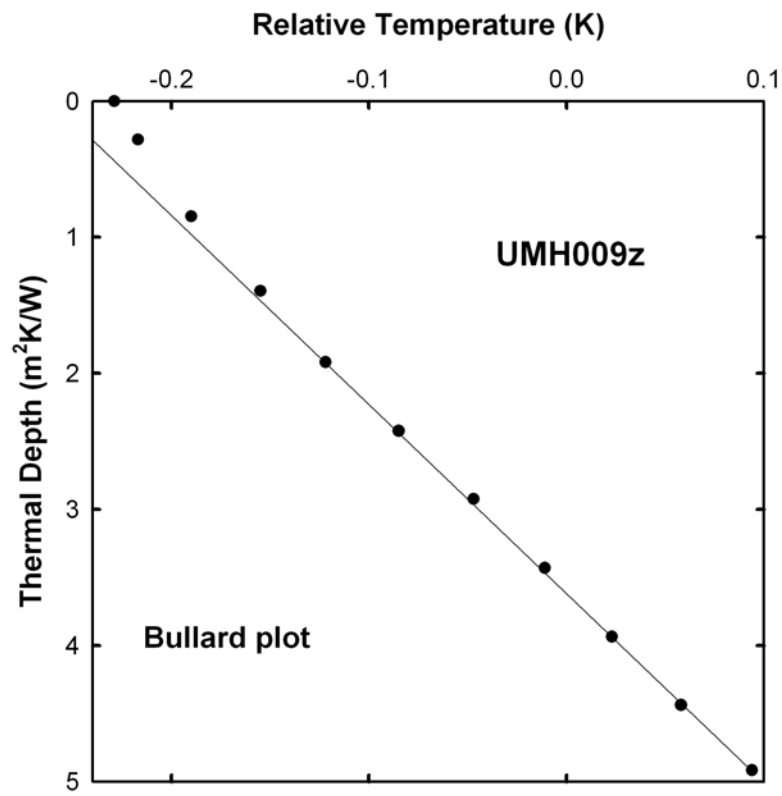


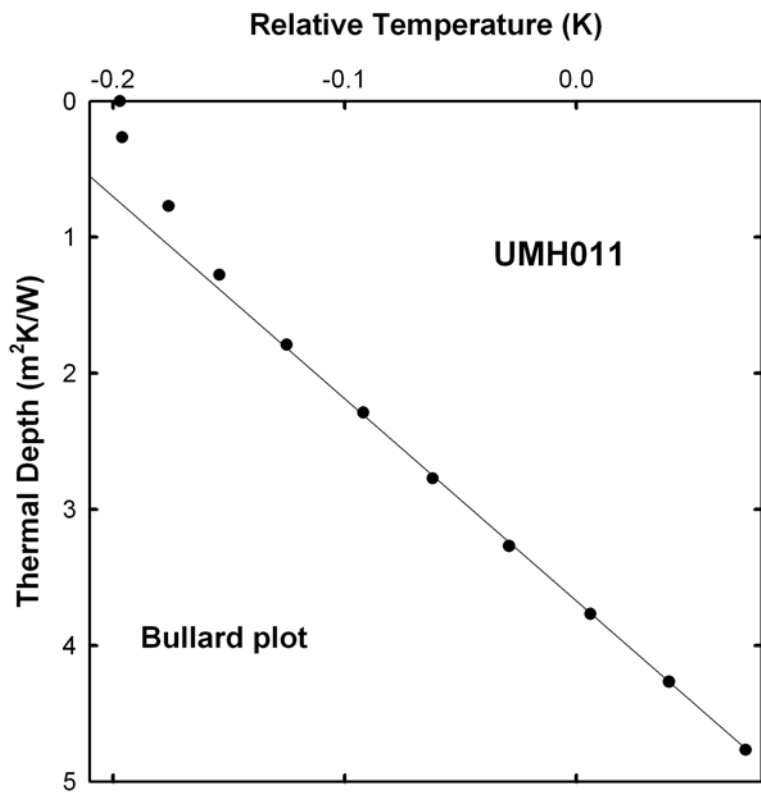
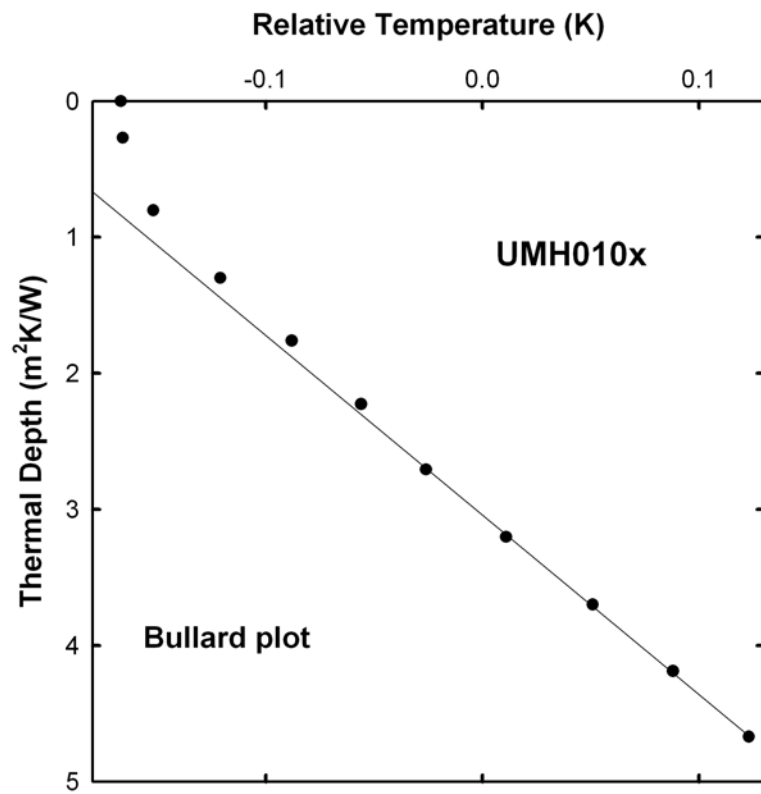


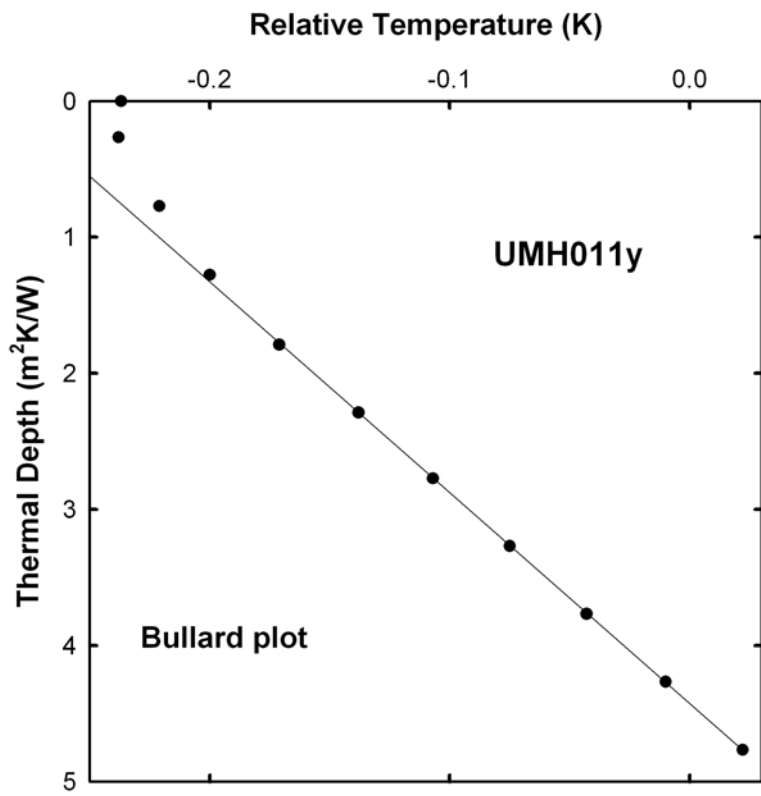
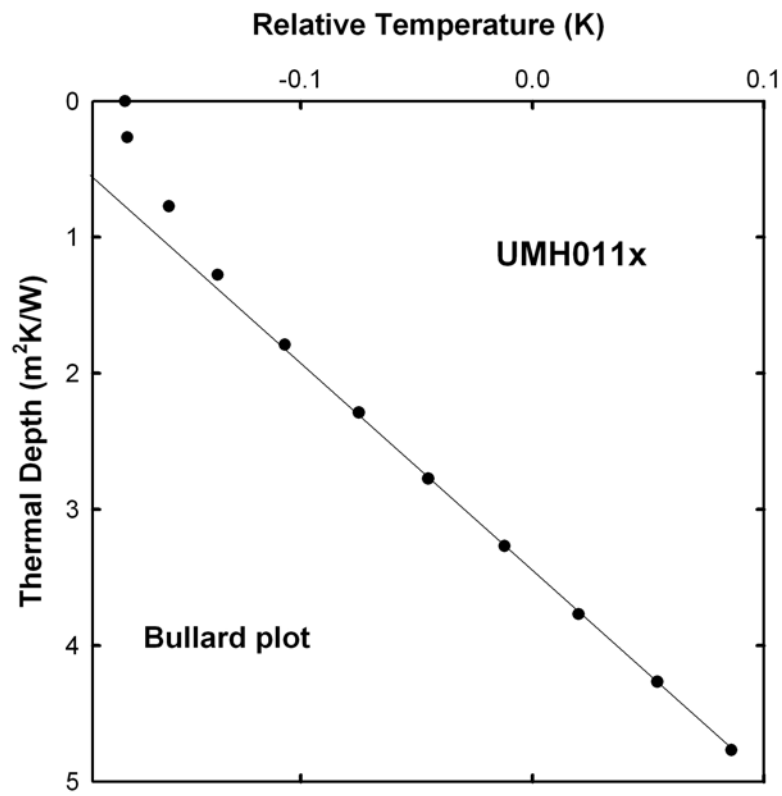




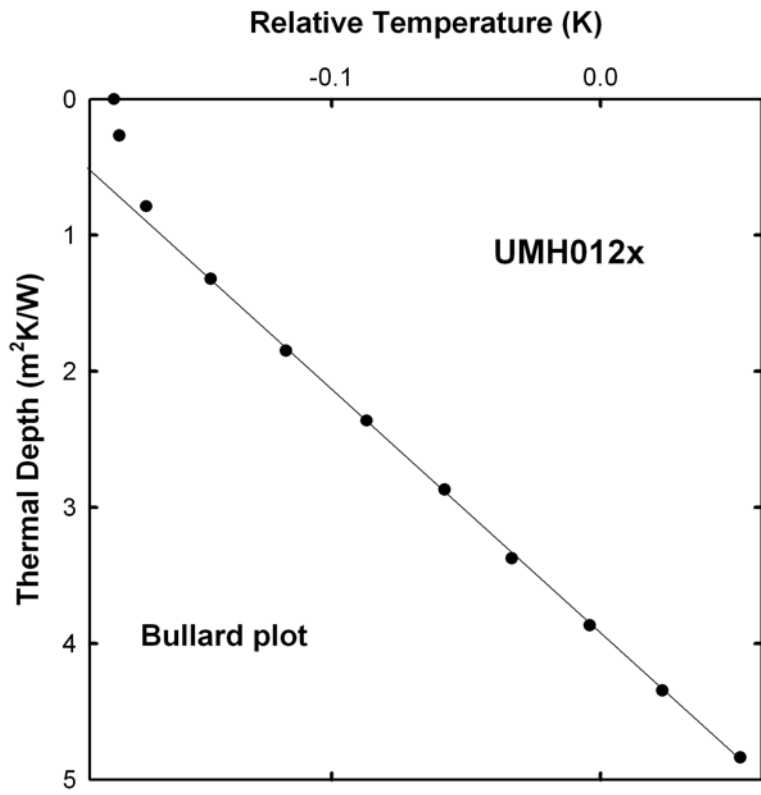
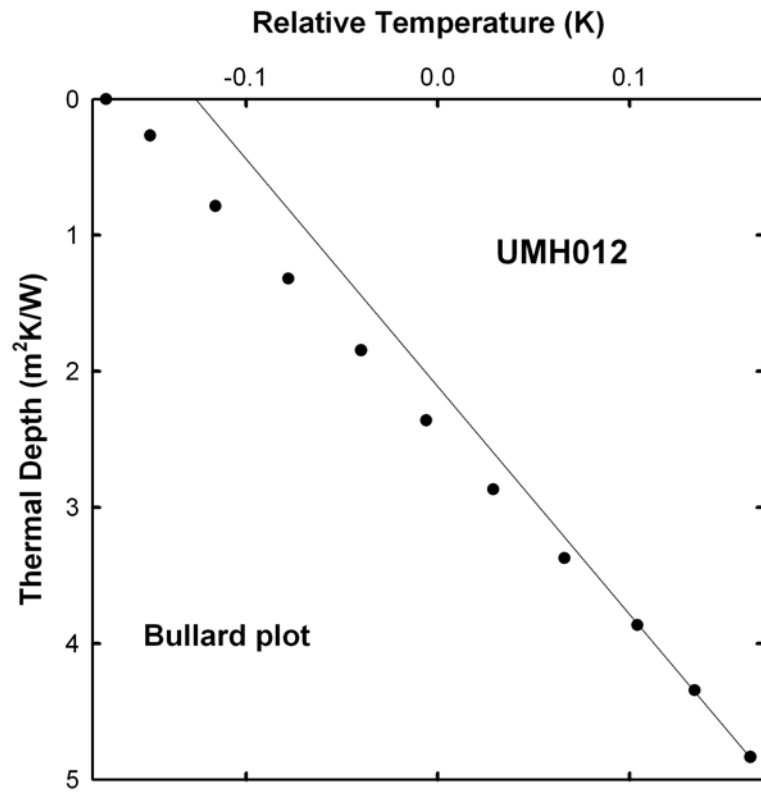


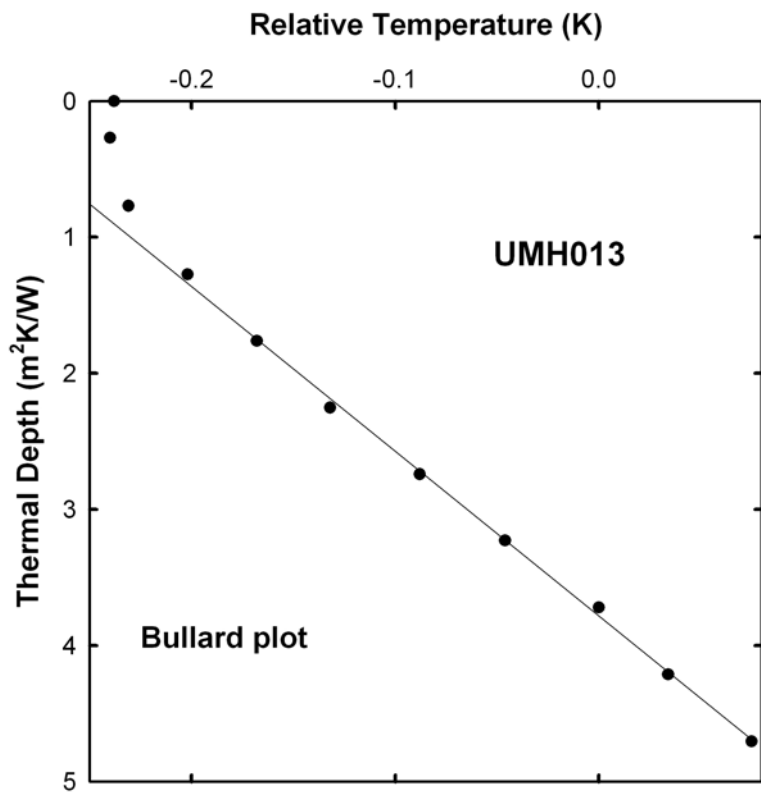
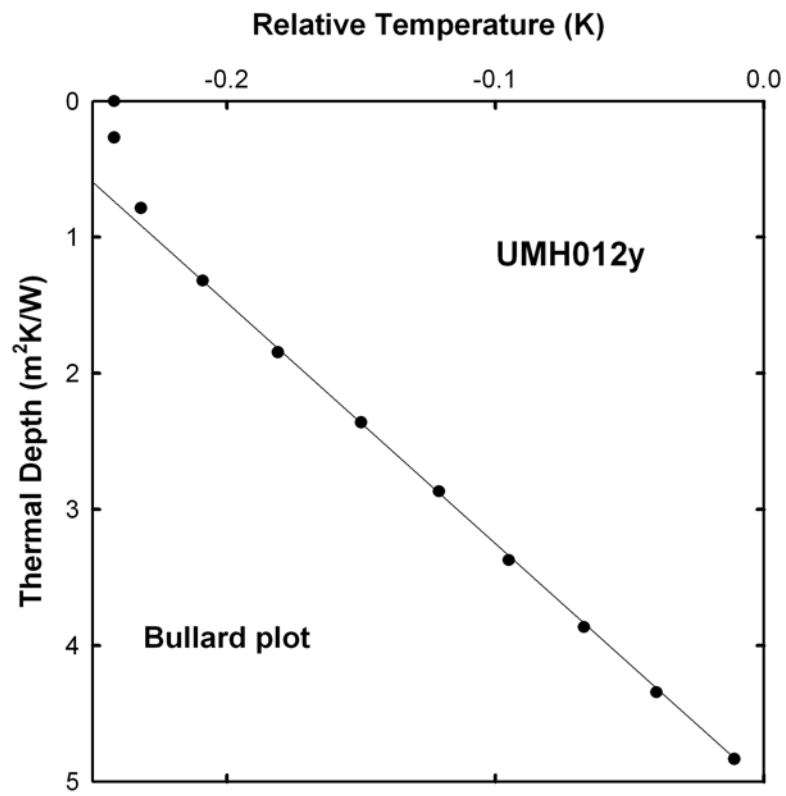


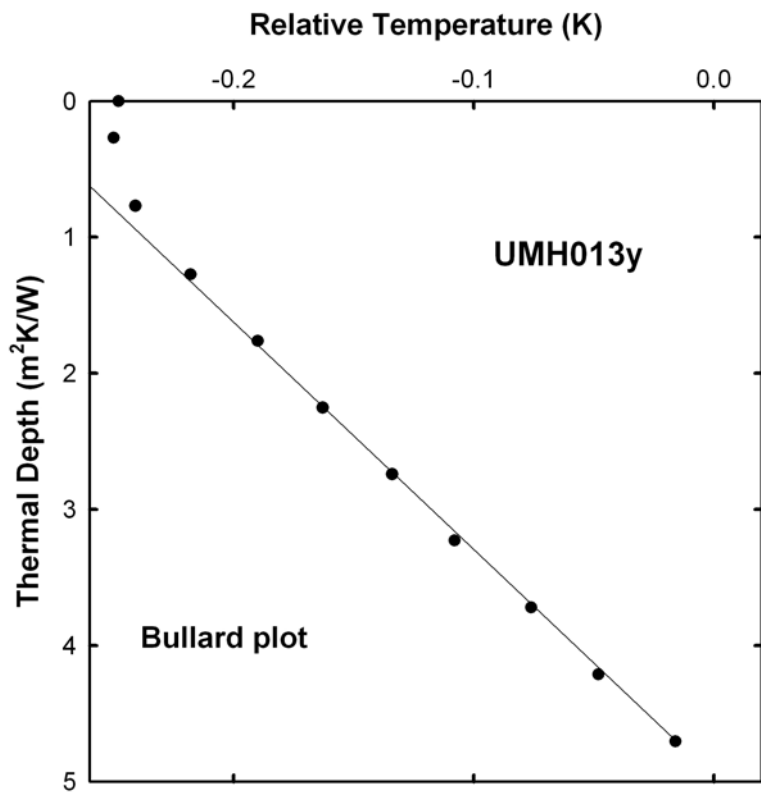
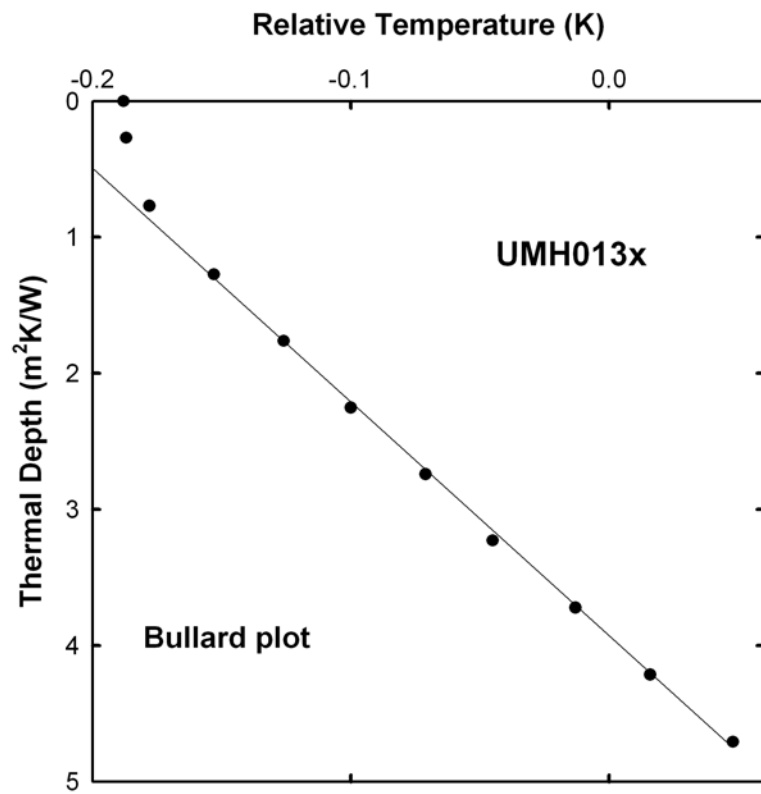


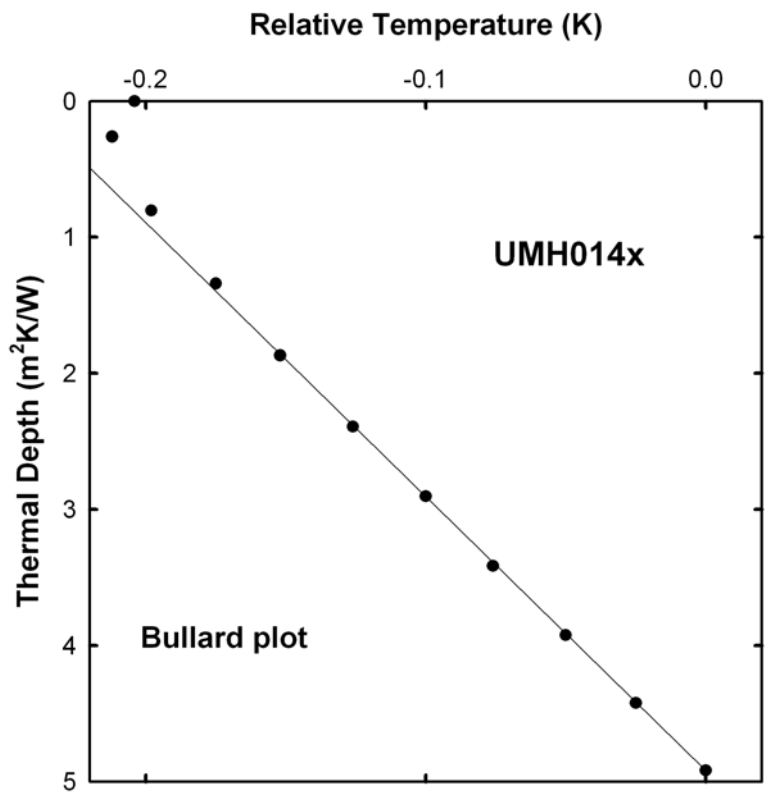
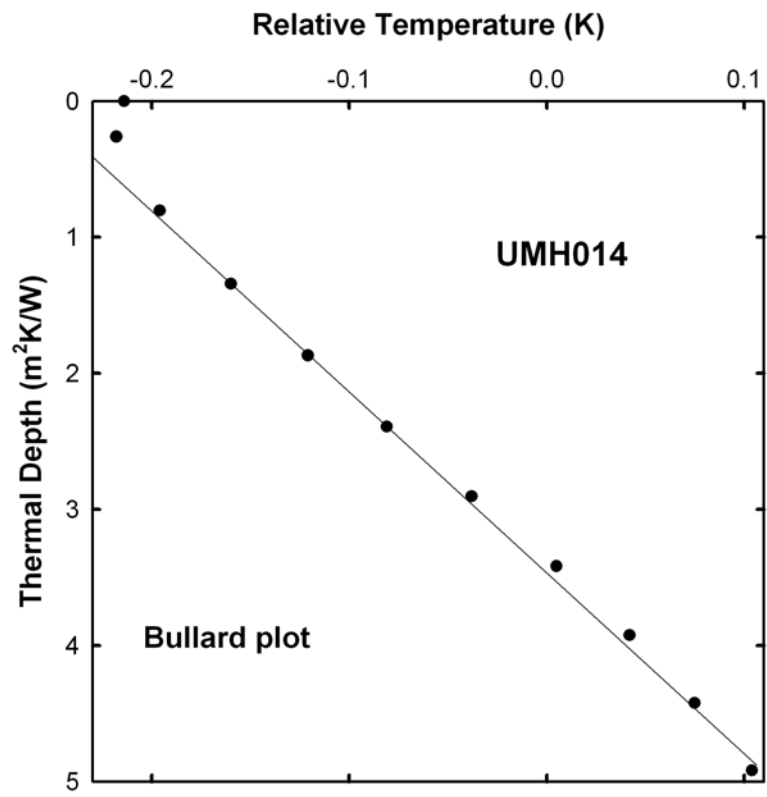


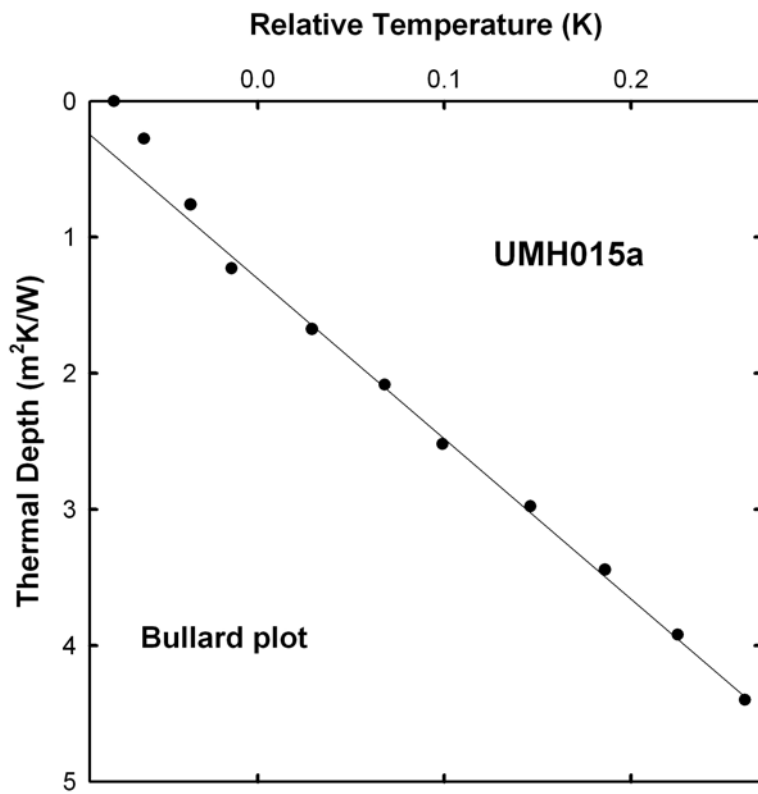
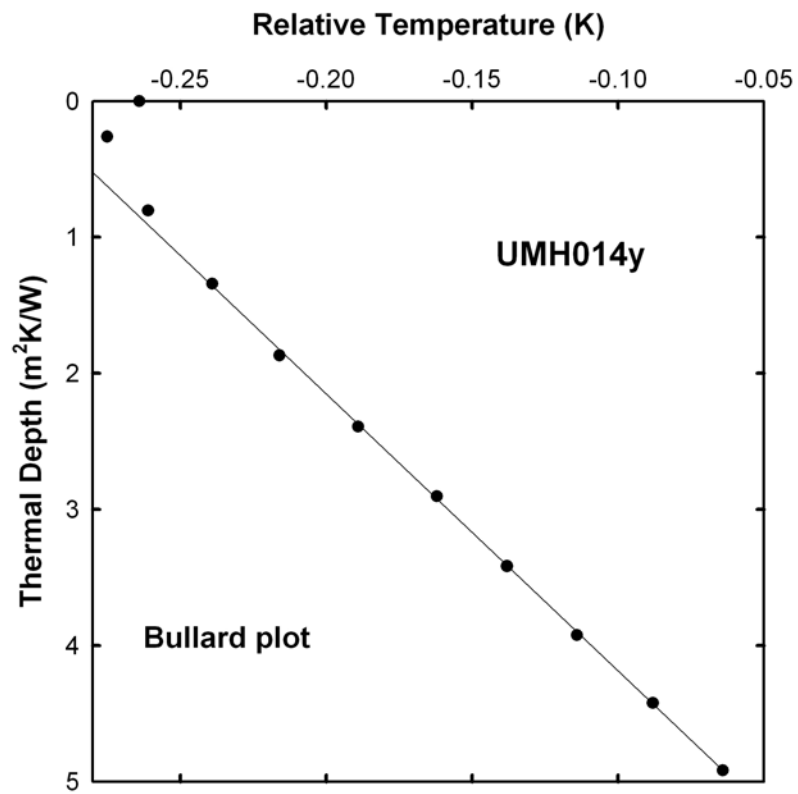


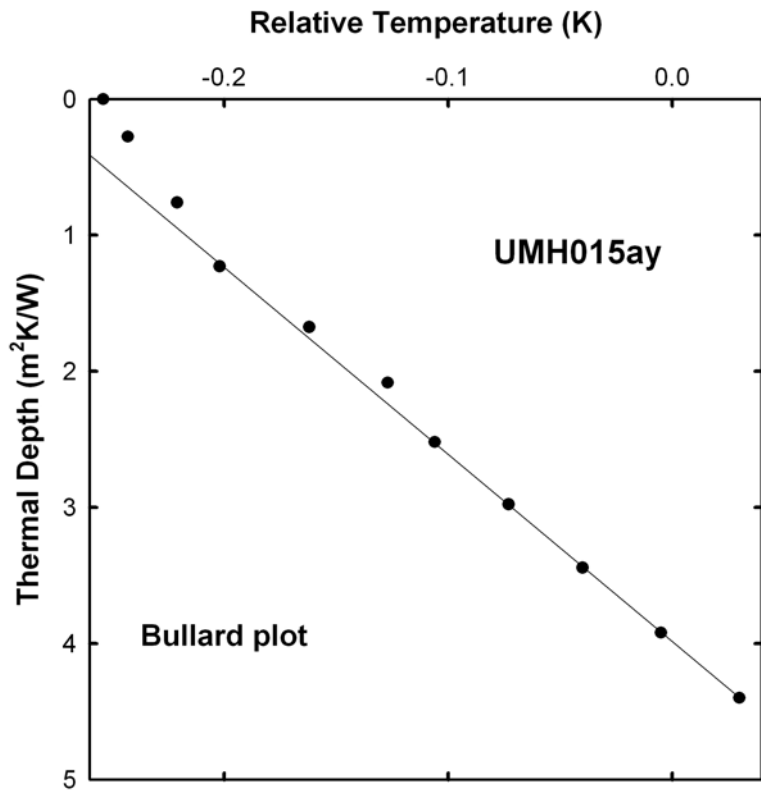
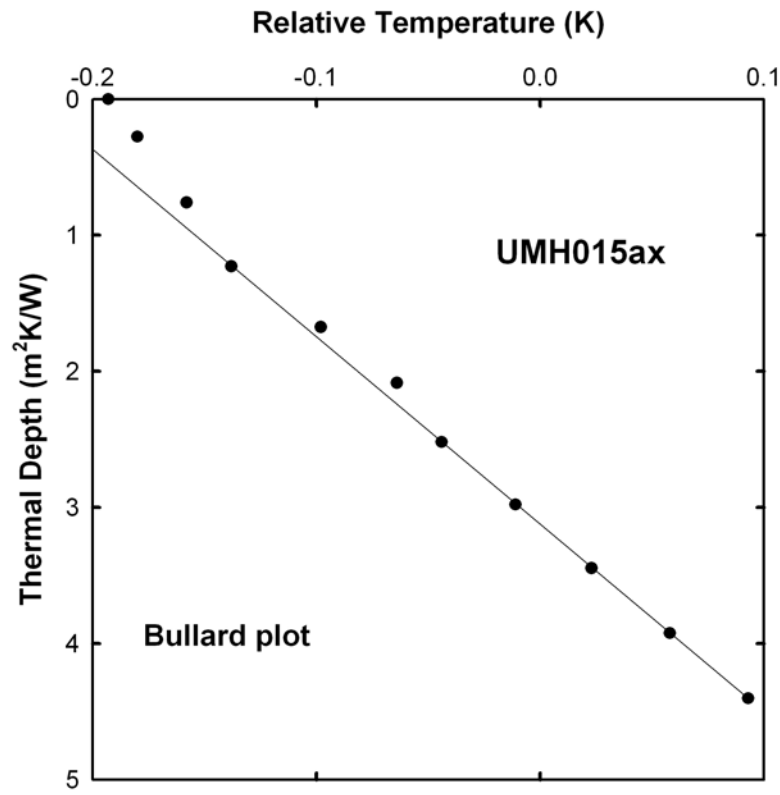




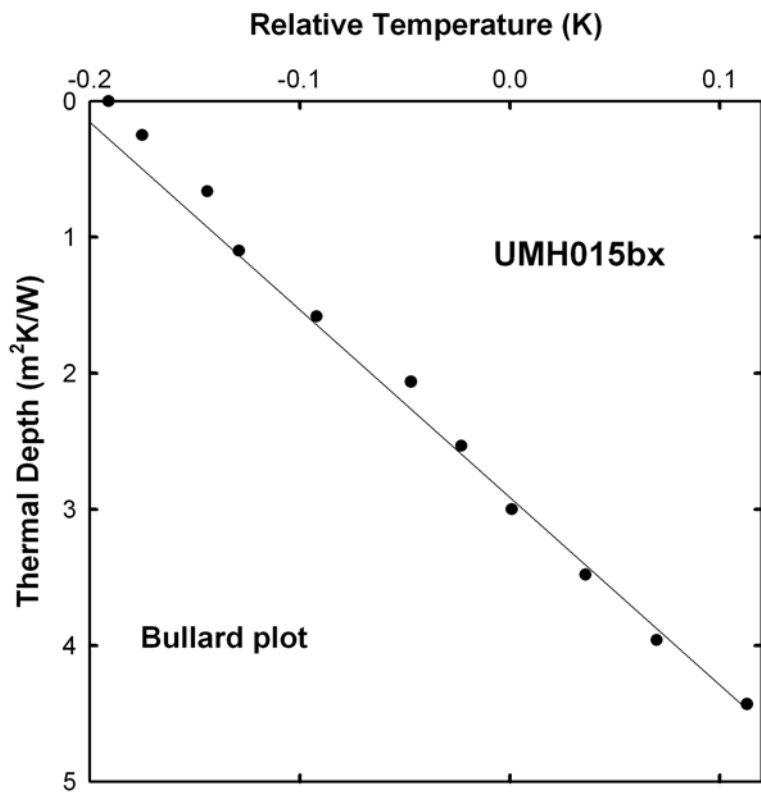
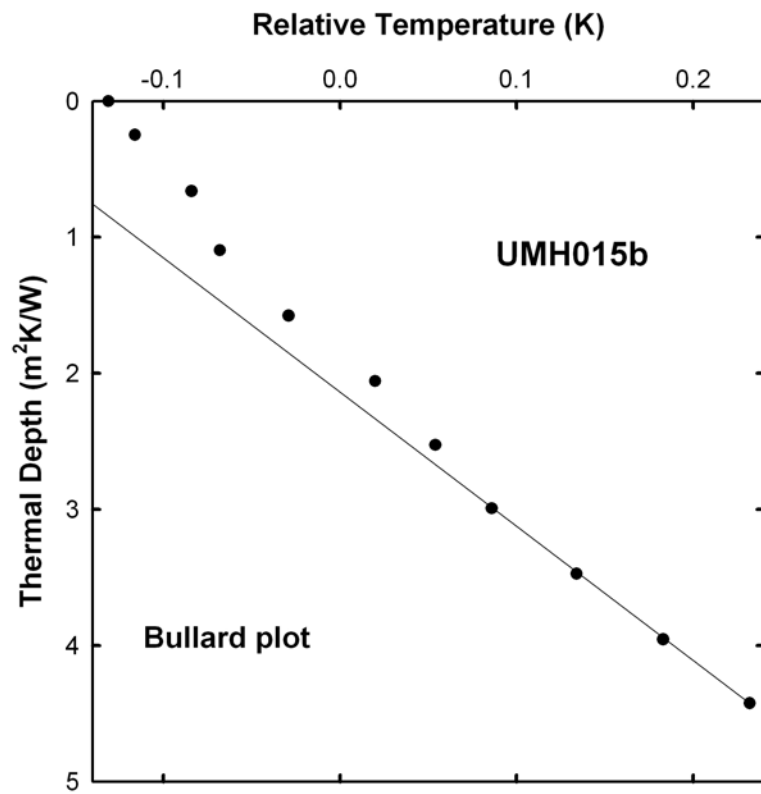


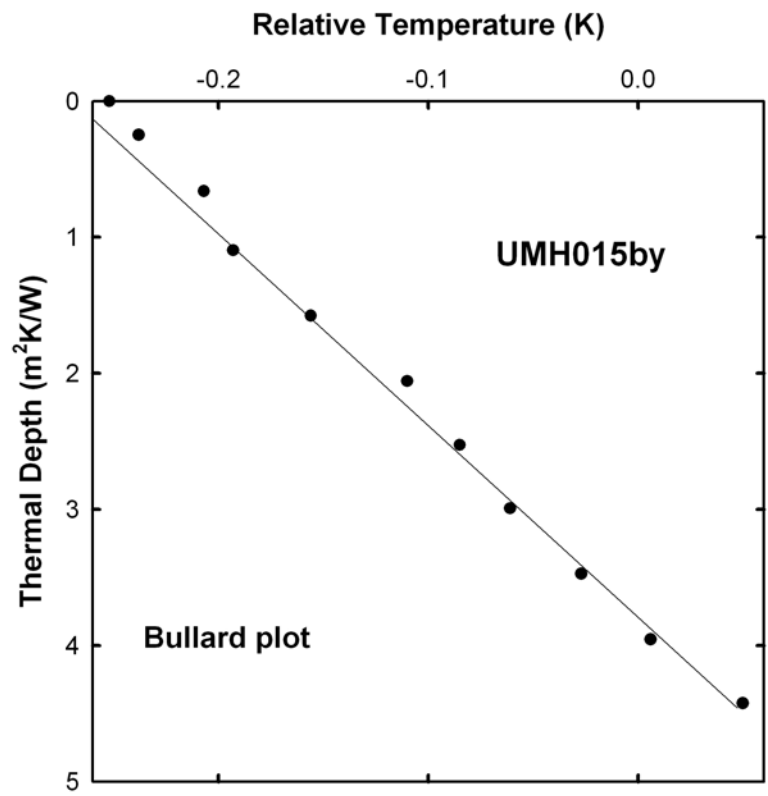












## **National Energy Technology Laboratory**

626 Cochrans Mill Road  
P.O. Box 10940  
Pittsburgh, PA 15236-0940

3610 Collins Ferry Road  
P.O. Box 880  
Morgantown, WV 26507-0880

One West Third Street, Suite 1400  
Tulsa, OK 74103-3519

1450 Queen Avenue SW  
Albany, OR 97321-2198

539 Duckering Bldg./UAF Campus  
P.O. Box 750172  
Fairbanks, AK 99775-0172

Visit the NETL website at:  
[www.netl.doe.gov](http://www.netl.doe.gov)

Customer Service:  
1-800-553-7681

